



VNIVERSITAT E VALÈNCIA

CHEMISTRY DOCTORATE

Unravelling [3+2] cycloaddition reactions
through the Molecular Electron Density
Theory

M^a del Mar Ríos Gutiérrez

Director: Prof. Luis Ramón Domingo Asensi

Departament de Química Orgànica
Universitat de València

January 2018

*To Prof. Bernard Silvi, for developing the
topological analysis of the electron localisation
function in the field of Organic Chemistry*



SUMMARY

After the first classification of [3 +2] cycloaddition (32CA) reactions into *zw-type* and *pr-type* reactions, established in 2014, the structure and reactivity of the most important three-atom-components (TACs) used in 32CA reactions has been completely characterised within the recently proposed Molecular Electron Density Theory (MEDT). Among the huge amount of work developed along the present Ph.D thesis, eight representative publications have been selected and discussed herein, which allowed characterising two new reactivity types as well as consolidating the original *zw-type* reactivity. Thus, depending on the four different electronic structures of TACs, i.e. *pseudodiradical*, *pseudoradical*, carbenoid and zwitterionic, 32CA reactions have been classified into *pdr-*, *pmr-*, *cb-* and *zw-type* reactions. While *pdr-type* 32CA reactions are the fastest, *zw-type* reactions are the slowest. The different electronic structures at the ground state of the reagents account for this reactivity trend and reveal that the reactivity of carbenoid TACs is different. In addition, no TAC can be considered a 1,2-zwitterionic structure as proposed for “1,3-dipoles”. The polar character of the reaction, measured by the global electron density transfer value computed at the transition state structure (TS), affects the four reactivity types in such a manner that the stronger the nucleophilic/electrophilic interactions taking place at the TS, the faster the reaction, and may even change the molecular mechanism according to the Parr functions defined within Conceptual DFT. This MEDT rationalisation of 32CA reactions unravels classical Huisgen’s and Firestone’s mechanistic proposals established in the 60’s. Regardless of the reactivity type and polar character of the reaction, topological analysis of the electron localisation function along one-step 32CA reactions suggests that the bonding changes are not “concerted”, but sequential, thus ruling out the classification of these reactions as “pericyclic”. In the present thesis, the classical theory of 32CA reactions, established in the 60’s of the past century and still prevailing today, is revisited and reinterpreted based on MEDT. A solid new reactivity model for 32CA reactions is established, emphasising that the way that organic chemists conceive organic chemistry demands a contemporary revision aimed towards the analysis of electron density.

ACKNOWLEDGMENTS

First, I wish to express my warmest gratitude to Prof. Luis R. Domingo, my mentor and my role model. Thanks for giving me the opportunity to be able to work under your supervision, for teaching me everything you know, for helping me in every difficulty and for your patience, for offering me the best possible training, for trusting me like nobody else and for guiding me in the life of a scientist. Thanks for making me the scientist I am now.

I am also deeply grateful to Prof. P. Pérez (Chile) for her support and wise advice, for having always a smile and make everything easier. Thanks also for helping me so much and making me feel at home the three times I have been to Chile.

Thanks to Prof. E. Chamorro (Chile) for delighting me with his scientific discussions and vast knowledge; to Prof. S. Emamian (Iran) for his numerous and novel ideas, questions and discussions, as well as to Prof. P. Merino (Spain) for sharing with us ideas, research and some useful scripts. Neither should Prof. A. Djereourou (Algeria), Prof. R. Jasinski (Poland), Prof. F. Mongin (France), Prof. I. M. Ndassa (Cameroon), Prof. P. Ramasami (Mauritius), Prof. B. Silvi (France) and Prof. S.-E. Stiriba (Spain) be forgotten for their valuable collaboration.

I would also like to acknowledge the Ministry of Economy and Competitiveness (MINECO) of the Spanish Government for granting me a pre-doctoral contract co-financed by the European Social Fund (BES-2014-068258) and for the financial support to the investigation carried out in our group through projects CTQ2013-45646-P and CTQ2016-78669-P, which has allowed my doctorate studies at University of Valencia.

And finally, thanks to my best friends Samuel Ceballos and Ana Martínez, my parents and my brother for their unconditional support and advice.

“To raise new questions, new possibilities, to regard old problems from a new angle, requires creative imagination and marks real advance in science.”

—Albert Einstein

INDEX OF ACRONYMS

A	electron affinity
AI	azomethine imine
AIM	atoms in molecules
AO	atomic orbital
ASD	atomic spin densities
A-TAC	allylic-type TAC
AY	azomethine ylide
BET	Bonding Evolution Theory
32CA	[3+2] cycloaddition
CDFT	conceptual DFT
CHDE	1,2-cyclohexadiene
CI	carbonyl imine
CNDO	complete neglect of differential overlap
CO	carbonyl oxide
CT	catastrophe theory
CY	carbonyl ylide
3D	three-dimensional
Da	diazoalkane
DA	Diels-Alder
DCE	1,1-dicyanoethylene
DCM	dichloromethane
DFT	Density Functional Theory
DIEM	distortion/interaction energy model
DMAD	dimethyl acetylenedicarboxylate
DNCP	gem-dinitrocyclopropane
DNE	1,1-dinitroethylene
EC	energy cost
ELF	electron localisation function
ERG	electron-releasing group
EWG	electron-withdrawing group
FMO	Frontier Molecular Orbital Theory
GEDT	global electron density transfer

GS	ground state
HF	Hartree-Fock
HMOT	Hückel's Molecular Orbital Theory
HOMO	Highest Occupied Molecular Orbital
HSAB	hard and soft acids and bases
I	ionisation potential
IRC	intrinsic reaction coordinate
LCAO	linear combination of atomic orbitals
LUMO	Lowest Unoccupied Molecular Orbital
MA	methyl acrylate
MCSCF	multi-configuration self-consistent field
MEDT	Molecular Electron Density Theory
MNDO	modified neglect of diatomic overlap
MO	molecular orbital
MOT	Molecular Orbital Theory
NCI	non-covalent interactions
Ni	nitrene
NI	nitrile imine
NO	nitrile oxide
NPA	natural population analysis
NY	nitrile ylide
PCM	polarisable continuum model
P-TAC	propargylic-type TAC
PYZ	pyrazole
QC	quantum chemical
QTAIM	quantum theory of atoms in molecules
RDS	rate-determining step
SCF	self-consistent field
SCRFF	self-consistent reaction field
TAC	three-atom-component
TCE	tetracyanoethylene
TS	transition state structure
TST	Transition State Theory
VBT	Valence Bond Theory

INDEX OF CONTENTS

1. Introduction	1
1.1. Heterocycles	3
1.2. 32CA reactions in the synthesis of five-membered heterocycles	4
1.3. Mechanistic aspects of 32CA reactions	5
1.3.1. Huisgen's and Firestone's mechanistic proposals based on experiment	5
1.3.2. FMO theory study of 32CA reactions	8
1.3.3. QC mechanistic studies of 32CA reactions based on the TST	10
1.3.4. Houk's mechanistic studies based on geometry deformation	12
1.3.5. QC mechanistic studies based on the MEDT	14
2. Objectives	19
3. Results and discussion	23
3.1. 32CA reactions of zwitterionic TACs	25
3.1.1. 32CA reactions between substituted NOs III and MA 5	25
3.1.2. 32CA reactions of Nis IX with ketenes	32
3.1.3. 32CA reactions of Nis IX with strained allenes	41
3.2. 32CA reactions of carbenoid TACs	50
3.2.1. Formal 32CA reactions of carbonyl compounds with nucleophilic carbenoid intermediates generated from carbene isocyanides	50
3.2.2. 32CA reactions of carbenoid NYs I with electrophilic ethylenes	60
3.2.3. <i>Cb-type</i> 32CA reactions of NYs I with electrophilic chiral oxazolidinones	69
3.3. 32CA reactions of <i>pseudoradical</i> TACs	78
3.3.1. 32CA reactions of Das IV with electrophilic ethylenes	78
3.3.2. 32CA reactions of the simplest AI 15	87
4. Conclusions	97
5. Future perspectives	107
6. Appendix	111
7. Theoretical background	145
7.1. QC models	147
7.2. Reactivity models derived from HMOT: the FMO theory and the "pericyclic" mechanism	148

7.3.	Development of computational chemistry and application of the TST	150
7.4.	Application of CDFT reactivity indices to the study of 32CA reactions	151
7.4.1.	Global properties	152
7.4.2.	Local properties	155
7.5.	GEDT	157
8.	Computational methods	161
9.	References	165
10.	Publication copies	201

1. INTRODUCTION

1.1. Heterocycles

Heterocyclic compounds are carbocyclic compounds having at least one heteroatom such as nitrogen, oxygen and sulphur. Heterocycles can be classified into two categories: aliphatic, such as tetrahydrofuran or 4,5-dihydroisoxazole, and aromatic, such as 1,3-thiazole or quinoline (see Figure 1.1).¹ The most common ones are five-membered and six-membered heterocycles.

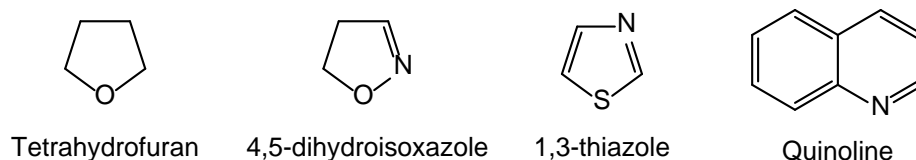


Figure 1.1. Some aliphatic and aromatic heterocycles.

The number, diversity, as well as applications of heterocycles is enormous. They have received a great deal of attention in recent years, particularly owing to their pharmacological as well as synthetic potential.

Nature is the first and the largest producer of heterocycles. Heterocycles like *chlorophylls* and *heme* derivatives are responsible for the colour and texture of nature. Similarly, base pairs found in DNA and RNA, the genetic material of most living organisms, as well as many known natural drugs, such as penicillin, quinine, papaverine, atropine, codeine, morphine etc. are also heterocycles (see Figure 1.2). Three out of twenty natural amino acids contain heterocyclic ring components and likewise many vitamins, e.g. vitamin B series and vitamin C. In addition, the ability of many heterocycles to produce stable metalloheterocycles is of immense biochemical significance (e.g. haemoglobin, chlorophyll, vitamins, enzymes etc.).

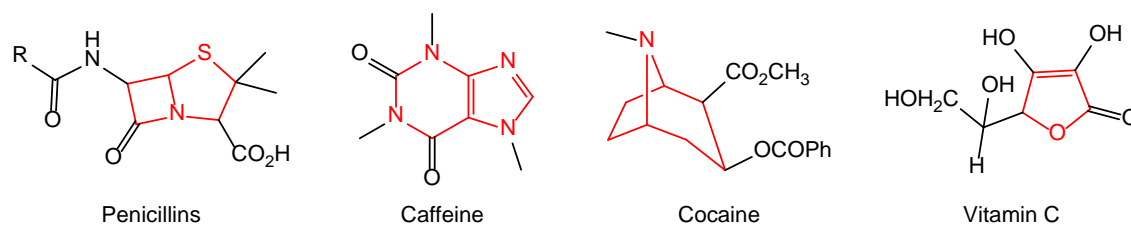


Figure 1.2. Examples of natural heterocyclic compounds.

In conjunction with nature, chemists have artificially synthesised and tailored a great many heterocyclic compounds. Most of today's synthetic drugs, such as rofecoxib, sulphadiazine, diazepam, chlorpromazine, barbiturates etc. as well as a number of useful

1. Introduction

materials like dyes (e.g. indigo blue), luminophores (e.g. acridine orange), pesticides, (e.g. diazinon), herbicides (e.g. paraquat) etc. possess heterocyclic rings (Figure 1.2).²

Heterocycles are chemically more flexible and able to respond to the demands of biochemical systems. Introduction of heteroatoms into a carbocyclic compound makes a spectacular change in its chemistry and renders it synthetically much more attractive. For instance, depending on the pH of the medium, heterocycles may behave as acids or bases, forming anions or cations. Some interact readily with electrophilic reagents, others with nucleophiles, yet others with both. Some are easily oxidised, but resist reduction, while others can be readily hydrogenated but are stable towards the action of oxidising agents. Certain amphoteric heterocyclic systems simultaneously demonstrate all the above mentioned properties. In addition to this, the presence of heteroatoms allows tautomerism in heterocyclic series. Such a versatile reactivity is associated with the special electron distribution within heterocyclic systems.³

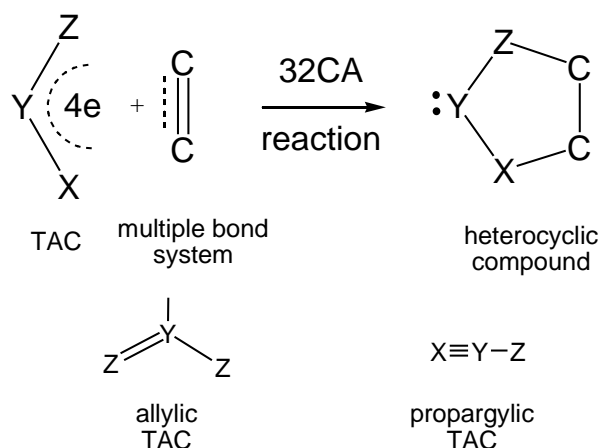
Considering all of the aforementioned aspects, the synthesis of heterocyclic compounds and their derivatives is of significant interest. Various methods currently available for the synthesis of heterocyclic compounds can be grouped into the following three broad categories:

- Modification of existing carbocyclic rings
- Cyclisation processes
- Cycloaddition reactions

Among these three methods, cycloaddition reactions involving two simple components appear to be the most attractive choice for the synthesis of heterocyclic compounds as it provides easy access to them usually with excellent selectivities.⁴ In particular, 32CA reactions are one of the most powerful methods for the synthesis of five-membered heterocycles.⁵

1.2. 32CA reactions in the synthesis of five-membered heterocycles

32CA reactions consist of the addition of a multiple bond system to a TAC, which is a neutral species whose core framework is constituted by three continued nuclei sharing an electron density of $4e$ (see Scheme 1.1). TACs can be geometrically classified into two categories: A-TAC and P-TAC structures;⁶ while A-TACs are bent, P-TACs have a linear structure (see Scheme 1.1).



Scheme 1.1. Construction of five-membered heterocyclic compounds by a 32CA reaction and geometrical classification of TACs.

Although 32CA reactions had been experimentally known since the end of the 19th century, e.g. the 32CA reactions of diazoacetates **1** and diazomethane **2** with C–C multiple bond systems were reported by Büchner and von Pechmann in the 1890s,⁷ they were for the first time recognised for their generality, scope and mechanism by Huisgen in 1961.⁸ The great deal of work and efforts made by Huisgen and co-workers led to the rapid development of these reactions and gave him the name “father” of “1,3-dipolar cycloadditions”, in which a formally zwitterionic molecule (the “1,3-dipole”) undergoes “1,3-addition” of a multiple bond system (the “dipolarophile”).⁹ It is worth mentioning, however, that the concept of “1,3-dipolar cycloadditions” was first suggested in 1938 by Smith.¹⁰

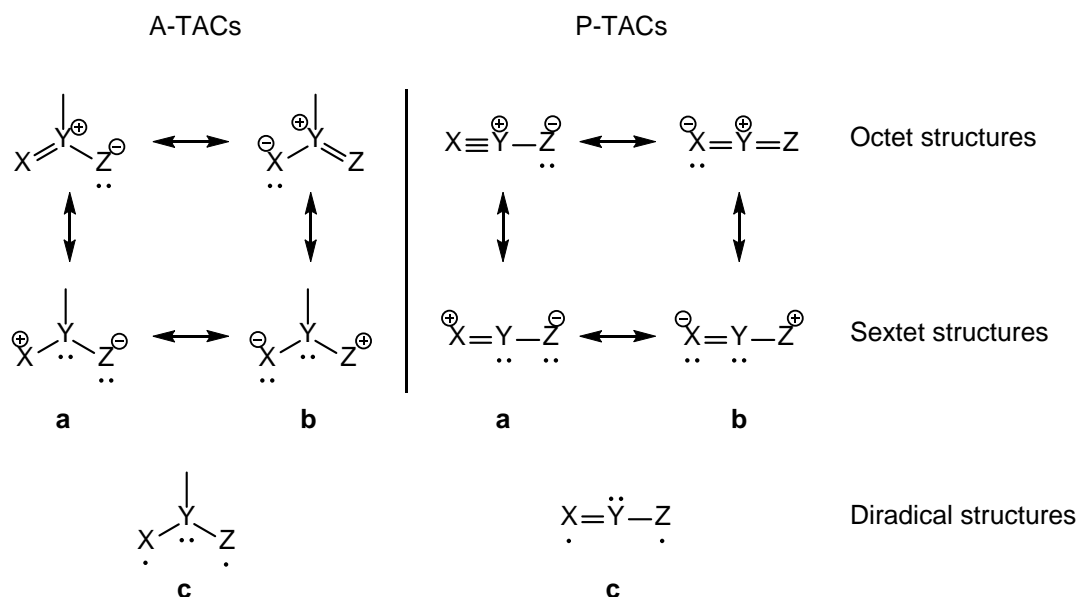
1.3. Mechanistic aspects of 32CA reactions

1.3.1. Huisgen’s and Firestone’s mechanistic proposals based on experiment

Unlike unsaturated hydrocarbon compounds participating in DA reactions, TACs cannot be represented by a single Lewis structure. According to the resonance concept developed by Pauling in 1928¹¹ within the VBT¹² (see Theoretical Background), Huisgen proposed in 1961 that “1,3-dipoles” could be mainly represented by octet and sextet resonance Lewis structures (see Scheme 1.2).⁸ While octet resonance structures were suggested to be the major contributors to the electronic structure of “1,3-dipoles”, the sextet resonance structures symbolised their 1,3-dipolar character and, hence, these species were thus considered “heteroallyl anion” systems whose termini are both nucleophilic and electrophilic (ambivalent).^{6a} On the other hand, in 1968, Firestone proposed that a

1. Introduction

diradical resonance structure **c** equivalent to $\mathbf{a} \leftrightarrow \mathbf{b}$ may usually be accepted as the principal representation of these species (see **c** in Scheme 1.2).¹³ Although this idea was initially criticised by Huisgen, he finally accepted that at the GS some participation of a diradical structure **c** could be conceivable.^{6a}



Scheme 1.2. Resonance Lewis structures used to represent the electronic structure of TACs. Sextet structures account for the “1,3-dipolar” concept.

If the three heavy nuclei are restricted to carbon, nitrogen and oxygen, the TACs shown in Table 1 are obtained.^{6a}

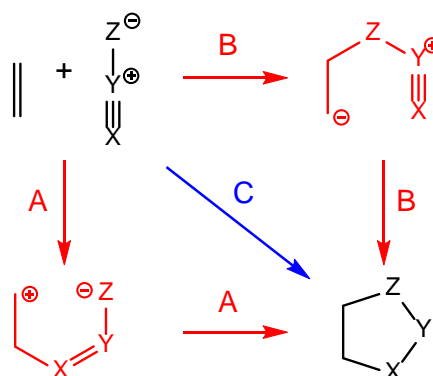
The exponential growth of the new research field of 32CA reactions was intrinsically accompanied by an exhaustive theoretical study of the mechanistic aspects governing the reactivity and selectivity of TACs, which quickly became the subject of a long ranging controversy. In the 1960s, two different models were independently proposed by Huisgen¹⁴ and Firestone.¹³

On the one hand, Huisgen initially proposed that three mechanisms were conceivable: A) the positive end of the TAC may initiate the attack and the negative pole then complete the additions; B) the negative center may be attached first and then the positive end; or C) both charge centers may add at the same time. While routes A and B were suggested to take place via octet 1,2-dipoles, route C was considered to take place via sextet 1,3-dipoles (see Scheme 1.3). Thus, due to the supposed “concerted” nature of mechanism C, Huisgen suggested a “concerted” one-step four-center mechanism in which the two new single bonds are both partially formed in the TS, though in 1963 he

Table 1. TACs consisting of carbon, nitrogen and oxygen nuclei.

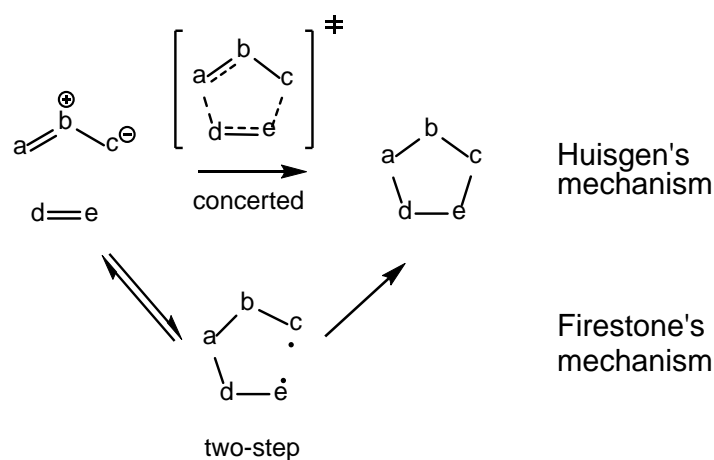
P-TACs		
	Name	Formula
I	Nitrile ylides (NY)	RC-N-CR ₂
II	Nitrile imines (NI)	RC-N-NR
III	Nitrile oxides (NO)	RC-N-O
IV	Diazoalkanes (Da)	N-N-CR ₂
V	Azides	N-N-NR
VI	Nitrous oxide	N ₂ O
A-TACs		
	Name	Formula
VII	Azomethine ylides (AY)	R ₂ C-NR-CR ₂
VIII	Azomethine imines (AI)	R ₂ C-NR-NR
IX	Nitrones (Ni)	R ₂ C-NR-O
X	Azimines	RN-NR-NR
XI	Azoxy compounds	RN-NR-O
XII	Nitro compounds	RNO ₂
XIII	Carbonyl ylides (CY)	R ₂ C-O-CR ₂
XIV	Carbonyl imines (CI)	R ₂ C-O-NR
XV	Carbonyl oxides (CO)	R ₂ C-O-O
XVI	Nitrosimines	RN-O-NR
XVII	Nitrosoxides	RN-O-O
XVIII	Ozone	O ₃

proposed that not necessarily to the same extent (see Scheme 1.3).¹⁴ In accord with this mechanism were the kinetics, the weak effect of solvent polarity on the reaction rates, the high negative activation entropy associated with these bimolecular processes and low activation energies, the general effects of structural variation in the reagents and, most particularly, the strict *cis* nature of the additions.¹⁴

**Scheme 1.3.** Three possible mechanisms proposed by Huisgen for 32CA reactions.

1. Introduction

On the other hand, in 1968, Firestone argued several experimental inconsistencies with respect Huisgen's suggestions about the mechanism, stereospecificity, TAC structure, solvent effects, acetylenic derivatives and orientation of reagents in these cycloaddition reactions, proposing an alternative two-step mechanism via formation of a diradical intermediate (see Scheme 1.4), but yet recognising that a duality of mechanisms may exist.¹³ Note that the idea of diradical intermediates in thermal cycloaddition reactions had been proposed for the DA reaction in 1937 by Kistiakowsky et al.¹⁵ and revived in the '60s by Walling and Peisach,¹⁶ having been also widely suggested for small-ring cycloadditions.¹⁷



Scheme 1.4. Huisgen's and Firestone's proposed mechanisms for 32CA reactions.

Approximately twenty years later, in 1985, while working with Houk on the 32CA reaction of benzonitrile oxide **3** with styrene **4** and methyle acrylate **5**, the observed stereospecificity forced Firestone to finally accept the "concerted" mechanism proposed by Huisgen.¹⁸ Later, in 1986, Huisgen reported the first two-step 32CA cycloaddition,¹⁹ proposing a two-step zwitterionic mechanism in which the rate of rotation around the zwitterionic single bond was competitive with the formation of the second, ring-closing bond. Today, Firestone still supports the stepwise diradical mechanism²⁰ after having gathered many experimental evidence of the presence of diradical species along the reaction path of several cycloaddition reactions, thus accounting for a two-step (non-concerted) mechanism.

1.3.2. FMO theory study of 32CA reactions

Until the mid-1950s, chemistry was dominated by the classical VBT. When this theory lacked accuracy and did not progress, the MOT²¹ became increasingly important (see

Theoretical Background). In order to study the electronic structure of unsaturated hydrocarbon compounds such as ethylene **6** and benzene **7**, Hückel established, in 1930, the simplest approach to MOT used in organic chemistry, known as HMOT,²² in which only valence p_z AOs were used to build MOs. This very simple approach, which is still widely used in organic chemistry nowadays, was employed in the 1960s to establish important organic reactivity models, such as the FMO theory,²³ the Evans' Principle formulated by Dewar,²⁴ and the Woodward and Hoffmann orbital symmetry rules²⁵ and "pericyclic" mechanism,²⁶ for the study of the reactivity in organic chemistry²⁷ (see Theoretical Background).

In 1972, Sustmann applied, for the first time, these precedents to the study of the mechanism of 32CA reactions through semi-empirical computational methods.²⁸ Depending on the relative disposition of the HOMO and LUMO of the reagents in the MO energy diagram, Sustmann classified 32CA reactions into three types: *type-I*, *type-II* and *type-III* (see Figure 1.3).²⁹ In *type-I* (generally referred to as "normal electron demand"), the dominant FMO interaction is that of HOMO_{TAC} with LUMO_{ethylene}; they are accelerated by the presence of ERGs in the TAC and EWGs in the ethylene derivative. In *type-II*, FMO energies of TAC and ethylene derivative are similar, so both are to be considered; adding either an ERG or EWG to the TAC or ethylene derivative can accelerate these reactions. Finally, *type-III* cycloadditions (generally referred to as "inverse electron demand") are dominated by interactions between LUMO_{TAC} and HOMO_{ethylene}; ERGs on the ethylene derivative and EWGs on the TAC will accelerate the reaction. According to this classification, 32CA reactions of AYs **VII** and AIs **VIII** (see Table 1) are typical examples for *type-I*, Nis **IX** normally participate in *type-II*, NO **III** reactions are classified on the borderline to *type-III*, while inorganic TACs such as nitrous oxide **VI** and ozone **XVIII** are common examples participating in *type-III* reactions.^{29,30} It should be emphasised that Sustmann concluded that, though a plethora of data could be explained in a unifying model, molecules are more than HOMOs and LUMOs and, thus, one should not try to overdraw this model based on an oversimplified one-electron treatment of the Hückel type.²⁹

In 1973, Houk calculated a set of FMO energies and coefficients using semi-empirical methods for ten parent and some substituted nitrilium betaines **I-III**, diazonium betaines **IV-VI**, azomethinium betaines **VII-IX** and carbonyl betaines **XIII-XV**, and for a series of substituted alkenes, with the aim of rationalising and predicting relative rates

1. Introduction

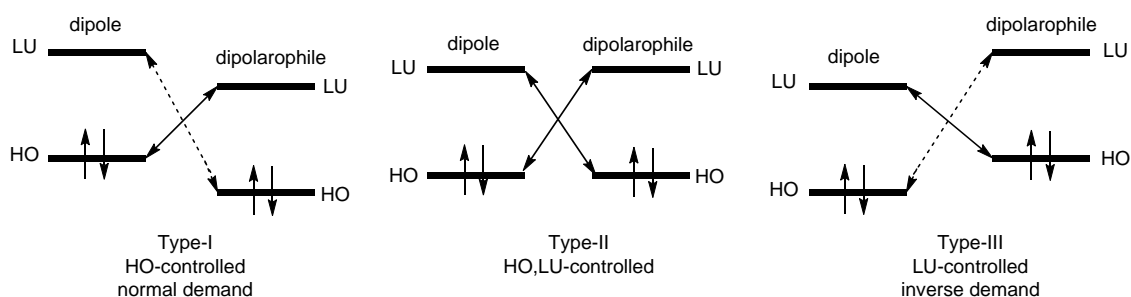


Figure 1.3. Sustainmann's classification of 1,3-dipolar cycloadditions and Houk's terminology.

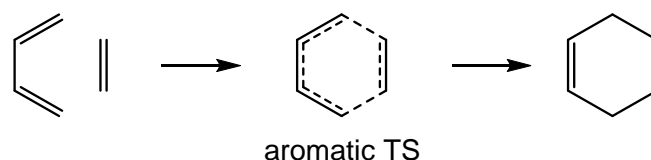
and regioselectivities of 32CA reactions.³¹ He renamed the three Sustainmann's types as HO-controlled (*type-I*), HO,LU-controlled (*type-II*) and LU-controlled (*type-III*) reactions (see Figure 1.3) and, based on these generalised FMOs, provided a qualitative explanation³² for the differential reactivity, regioselectivity and "periselectivity" (i.e. selective formation of one of the "thermally allowed pericyclic" reaction products)³³ phenomena within the framework of qualitative perturbation MOT.³⁴ This FMO theory study led him to confirm the traditional assumed concept of bond formation non-synchronicity.³⁵

1.3.3. QC mechanistic studies of 32CA reactions based on the TST

In the '70s, simultaneously to the study of molecular mechanisms based only on the features of reagents because of the inherent nature of both the perturbation MOT and FMO theories, chemists started the first geometry optimisations of the TSs using QC procedures, which enabled the first studies of molecular mechanisms based on the TST.³⁶

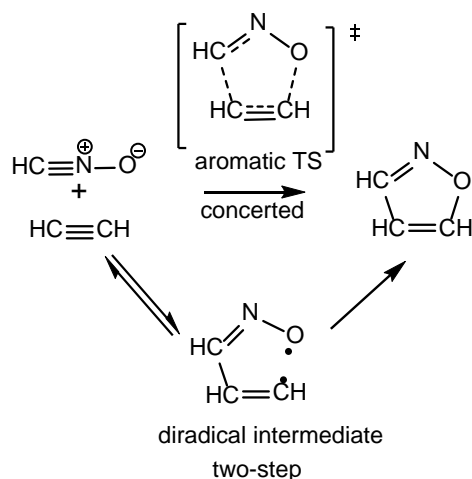
The fact that the orbital symmetry rules established by Woodward and Hoffmann systematised in a very satisfactory manner many experimental observations of cycloaddition reactions, for which the term "no mechanism reaction" was suggested due to the very difficult mechanistic problems they presented,³⁷ caused the "pericyclic mechanism" concept²⁶ to spread like wildfire since its establishment in 1969.³⁸ Accordingly, one-step 32CA reactions were classified as "pericyclic" reactions.

In 1971, Dewar proposed an alternative theoretical model for the rationalisation of the "pericyclic" mechanism.³⁸ Based on a general theory of aromaticity^{24,39} and the analogy between the TS of a "pericyclic" process and the classical hybrid of aromatic structures (see Scheme 1.5), Dewar described the cyclic TSs as being aromatic, nonaromatic, or antiaromatic and related the facility of "pericyclic" reactions to the stability of cyclic TSs relative to open chain analogues (see Theoretical Background).³⁸



Scheme 1.5. Dewar's proposal of aromatic TSs involved in "concerted" processes.

Many QC calculations performed on those dates began the evolution of computational studies on 32CA reactions and provided further material for the debates about the relative merits of different calculations.⁴⁰ For instance, while pioneering *ab initio* calculations by Poppinger⁴¹ on the reaction of fulminic acid **8** with acetylene **9**, an example involving an NO **III**, supported the one-step mechanism with a "concerted aromatic" TS, MNDO calculations predicted a two-step reaction involving a diradical intermediate (see Scheme 1.6).⁴² Later *ab initio* calculations carried out by Komornivki et al. confirmed the previous *ab initio* results, i.e. the TS is asynchronous but "concerted".⁴³ These studies were followed by Hiberty and co-workers,⁴⁴ whose MSCF plus configuration interaction calculations predicted that the stepwise diradical mechanism is favoured. Here, *ab initio* calculations with electron correlation and semiempirical calculations appeared to agree with each other on a stepwise mechanism. However, MCSCF calculations by McDouall et al. showed that the "concerted" one-step mechanism was favoured.⁴⁵ Finally, using high-level calculations, that 32CA reaction was predicted to be "concerted".



Scheme 1.6. Proposed "concerted" and stepwise mechanism for the 32CA reaction between fulminic acid **8** and acetylene **9**.

Therefore, until then there were both experimental and theoretical evidence that 32CA reactions may occur by one-step or stepwise mechanisms. In general, QC theoretical studies of 32CA reactions, based on the characterisation of the stationary points along the

1. Introduction

reaction path, allowed establishing that most of them take place through a one-step mechanism in which the formation of the two single bonds is more or less asynchronous. The strong growth of the “pericyclic mechanism” concept since it was proposed in the 70’s led to the unquestionable classification of one-step 32CA reactions as “pericyclic” reactions.⁴⁶ Today, one-step 32CA reactions remain classified for the majority of chemists as “concerted pericyclic” reactions taking place through “aromatic TSs” for which the Woodward-Hoffmann orbital symmetry rules as well as Dewar’s aromaticity rules explain their allowance.⁴⁷ However, it should be emphasised that although various theoretical derivations for the rules provided by Woodward and Hoffmann were given as alternative rationalising models for “pericyclic” reactions, this mechanism was never demonstrated. Indeed, the presence of stepwise 32CA reactions suggests that Woodward and Hoffmann’s rules are permissive but not obligatory.²⁰

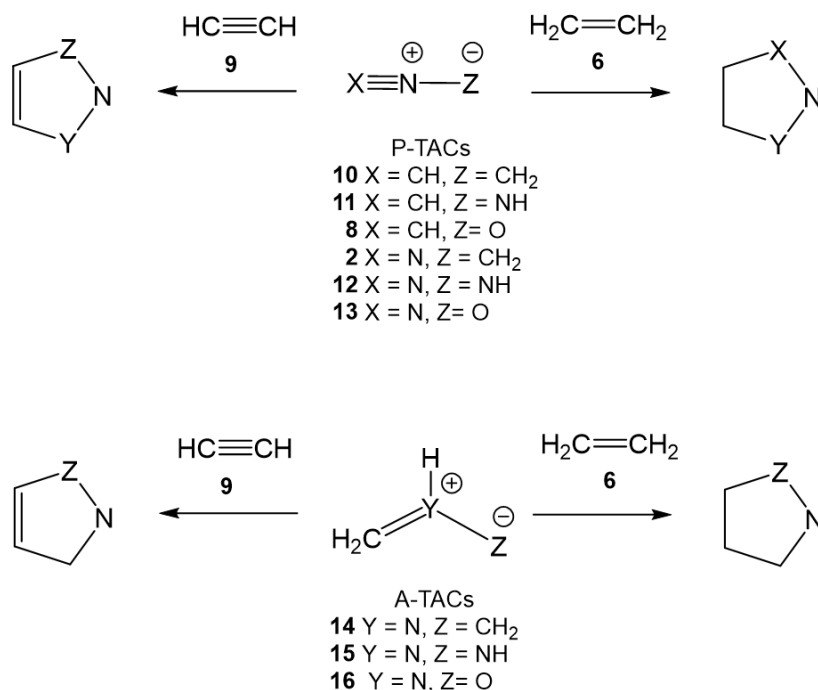
1.3.4. Houk’s mechanistic studies based on geometry deformation

To explain the reactivity of TACs in 32CA reactions, Houk proposed, in 2007, a DIEM⁴⁸ in which, based on Morokuma’s energy decomposition⁴⁹ (see Theoretical Background), the activation barrier is divided into two additive terms (see Eq. [1]): ΔE_d^\ddagger , called *distortion energy*, which is the energy required to distort the reagents into the TS geometries without allowing interaction, and ΔE_i^\ddagger , called *interaction energy*, which in turn consists of several attractive and repulsive forces.

$$\Delta E^\ddagger = \Delta E_d^\ddagger + \Delta E_i^\ddagger \quad (1)$$

The suitability of this reactivity model was checked in 32CA reactions of nine different TACs, six P-TACs **2,8,10-13** and three A-TACs **14-16**, with ethylene **6** and acetylene **9** (see Scheme 1.7).⁴⁸ Houk found that the computed B3LYP/6-31G(d) activation enthalpies correlated very nicely with the distortion energies (see Figure 1.4) and, then, he concluded that *the distortion energy of the reagents towards the TS is the major factor controlling the reactivity differences of TACs*. Thus, when distortion energies are approximately the same, interactions can become the determining factor.

However, this finding, which can be considered a computational assertion of Hammond’s postulate established in 1955,⁵⁰ does not resolve the question why activation energies depend on geometries, which are the result of the distribution of the molecular



Scheme 1.7. The 32CA reactions of nine TACs, **2,8,10-16**, with ethylene **6** and acetylene **9** studied by Houk.

electron density.⁵¹ In addition, the partition of the TS geometry into two separated structures has no physical sense within DFT,⁵² since in this QC model the energy of a system is a functional of the electron density $\rho(\mathbf{r})$ and the external potential, i.e. the nuclei positions. Consequently, the energy of the two separated fragments cannot be correlated with the energy of the TS because each of them loses the external potential created by the other fragment.

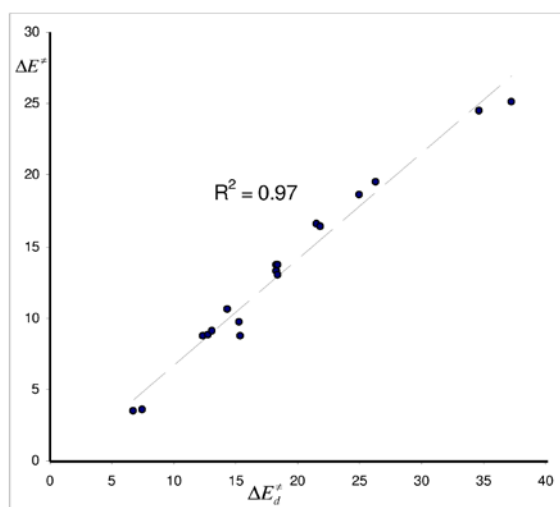


Figure 1.4. Plot of B3LYP/6-31G(d) activation energies vs distortion energies, in kcal·mol⁻¹, for Houk's 32CA reactions of TACs **2,8,10-16** with ethylene **6** and acetylene **9**.

1. Introduction

1.3.5. QC mechanistic studies based on the MEDT

Although several theoretical models based on the analysis of MOs, such as the FMO theory, have been widely used to explain chemical reactivity in organic chemistry, MOs are not physically observable but only mathematical constructs, used to obtain the molecular wavefunction, that cannot be determined by experiment.⁵³ In contrast, the electron density distribution in a molecule or crystal can be experimentally observed by electron diffraction and X-ray crystallography;⁵⁴ and it can also, and often more readily, be obtained from *ab initio* or DFT calculations. Thus, unlike MOs, only electron density is an experimentally accessible scalar field, being responsible for all molecular properties, including the geometry.

Very recently, Domingo proposed a new reactivity theory in organic chemistry, namely the MEDT,⁵⁵ in which changes in the electron density, but not MO interactions as the FMO theory proposed,²³ are responsible for the reactivity of the organic molecules. The proposed MEDT is not only a new model of reactivity in organic chemistry based on the analysis of the molecular electron density, but also rejects those models based on the analysis of MOs, such as the FMO theory.⁵⁵ Although many FMO theory studies numerically give qualitative results that fit experimental observations, this model is conceptually wrong because MOs have no physical reality and then they cannot physically interact. In addition, LUMO is the first unoccupied virtual MO without any participation in the construction of the molecular wavefunction.

Unlike the FMO theory, MEDT focuses on the analysis of the electron density and the energy changes associated with its redistribution along the reaction path. Within MEDT, besides an exhaustive exploration and characterisation of the reaction paths associated with the studied reaction, the CDFT reactivity indices,⁵⁶ as well as QC tools based on the topological analysis of the molecular electron density such as the ELF,⁵⁷ the QTAIM⁵⁸ and the NCI,⁵⁹ are used in order to study the reactivity in organic chemistry.

Since the beginning of this century, the analysis of electron density has been applied to the study of several organic reactions, including 32CA reactions.⁶⁰ These early MEDT studies supposed the beginning of a revolution in the field of organic chemistry, as allowed building a new reactivity model that contributed to the advancement of conceptual chemistry as well as ruling out strongly established concepts such as the “concerted” and “pericyclic” mechanisms for DA reactions.⁶¹ After publishing the first scale of the electrophilicity ω index for a series of organic compounds participating in

DA reactions,⁶² in 2003 Domingo established, for the first time, a reactivity scale for the simplest TACs participating in 32CA reactions within the CDFT (see Table 2 and Theoretical Background).⁶³

Table 2. Global properties and global electrophilicity scale for the most common simple TACs involved in 32CA reactions.

	HOMO	LUMO	μ	η	ω
<i>Strong electrophiles</i>					
Ozone	-0.3352	-0.1846	-0.2599	0.1505	6.10
Nitrosoxide	-0.3000	-0.1415	-0.2207	0.1585	4.18
Nitrosimine	-0.2589	-0.1037	-0.1813	0.1552	2.88
Carbonyl oxide	-0.2420	-0.0889	-0.1655	0.1530	2.43
Nitro compound	-0.3215	-0.0852	-0.2034	0.2363	2.38
Azoxy compound	-0.2812	-0.0551	-0.1682	0.2261	1.70
Carbonyl imine	-0.2055	-0.0603	-0.1329	0.1452	1.65
<i>Moderate electrophiles</i>					
Diazoalkane	-0.2208	-0.0471	-0.1339	0.1737	1.40
Nitrous oxide	-0.3422	-0.0191	-0.1807	0.3231	1.37
Azimine	-0.2393	-0.0329	-0.1361	0.2064	1.22
Nitrone	-0.2279	-0.0241	-0.1260	0.2038	1.06
Carbonyl ylide	-0.1686	-0.0279	-0.0983	0.1407	0.93
<i>Marginal electrophiles (nucleophiles)</i>					
Nitrile oxide	-0.2709	0.0211	-0.1249	0.2919	0.73
Azomethine imine	-0.1912	-0.0069	-0.0990	0.1844	0.72
Azide	-0.2685	0.0287	-0.1199	0.2972	0.66
Nitrile ylide	-0.1661	-0.0075	-0.0868	0.1586	0.65
Azomethine ylide	-0.1489	0.0155	-0.0667	0.1644	0.37
Nitrile imine	-0.2073	0.0589	-0.0742	0.2661	0.28

(a) HOMO and LUMO energies, electronic chemical potential, μ , and chemical hardness, η , are given in atomic units; global electrophilicity, ω , in eV.

Early ELF topological analyses of the electronic structure of the simplest AY **14**⁶⁴ and CY **17**⁶⁵ carried out in 2010 showed that these TACs present a *pseudodiradical* electronic structure (see Figure 1.5).¹ This finding contrasted with the general representation of TACs as 1,2- or 1,3-dipoles proposed by Huisgen, but was quite similar to Firestone's proposal of a diradical Lewis structure. DFT calculations revealed that the 32CA reactions of these TACs present very low activation energies even having a very low polar character.^{64,65} Note that in DA reactions a good correlation between the polar character of a reaction, measured by the GEDT at the TS, and its feasibility was previously established for DA reactions,⁶⁶ in such a manner that the higher the GEDT at the TS, the

¹ In 1960 Errede et al. studied the high chemical reactivity of *p*-xylylene, which was attributed to its *pseudodiradical* character. They defined a *pseudodiradical* as a diamagnetic compound that behaves chemically as if it were a diradical.⁶⁷

1. Introduction

faster the reaction (see Theoretical Background). This finding allowed an early rationalisation of Houk's proposal, since TACs having a *pseudodiradical* character do not require any structural distortion.

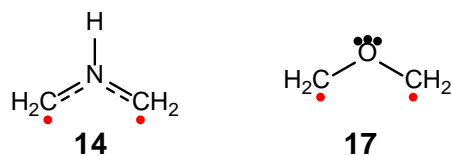
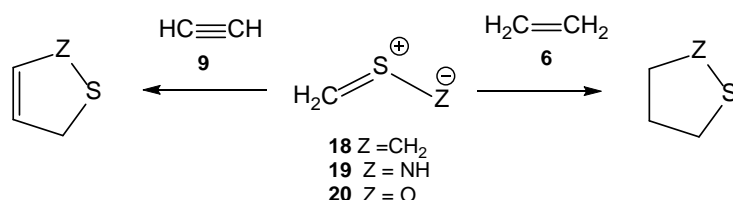


Figure 1.5. *Pseudodiradical* electronic structure of AY **14** and CY **17**.

Based on this finding, the 32CA reactions of TACs **2,8,10-16** (see Scheme 1.7) and three sulphur-centred TACs **18-20** (see Scheme 1.8), equivalent to the parent **XIII-XV** (see Table 1), with ethylene **6** and acetylene **9** were studied in 2014 in order to establish a structure/reactivity relationship.⁵¹ This study allowed establishing a reactivity index, named the *pseudoradical pr* index, for distinguishing TACs possessing a *pseudodiradical* character from the rest and, thus, 32CA reactions were classified into two types (see Figure 1.6): i) *pseudodiradical-type* (*pr-type*) 32CA reactions involving *pseudodiradical* TACs such as AY **14** and CY **17**; and ii) *zwitterionic-type* (*zw-type*) 32CA reactions involving the rest of TACs, for which a 1,2-zwitterionic electronic structure was suggested.⁸ In that study, it was proposed that unlike *pr-type* 32CA reactions, *zw-type* 32CA reactions demand adequate nucleophilic/ electrophilic activations to take place.⁵¹



Scheme 1.8. 32CA reactions of three sulphur-centred TACs, **18-20**, with ethylene **6** and acetylene **9**.

In order to verify this hypothesis, a series of the most common simple TACs used in organic chemistry,^{5b} **2,8,10-12,16** (see Scheme 1.7) and methyl nitronate **16'**, showing low reactivity in 32CA reactions with ethylene **6** and classified as zwitterionic TACs, were further explored,⁶⁸ demonstrating that the electronic activation of both TACs and ethylene derivatives favours the *zw-type* 32CA reactions via a polar mechanism (see Figure 1.7), similarly to the polar model previously established for DA reactions.⁶⁶

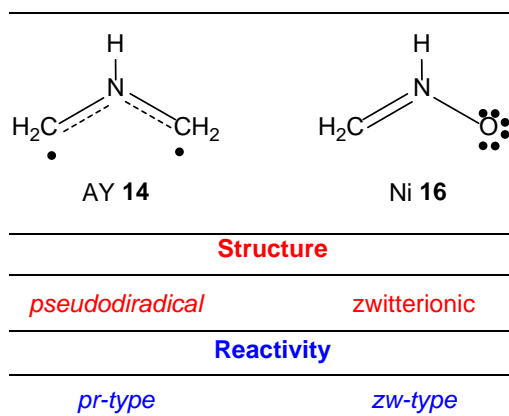


Figure 1.6. First classification of 32CA reactions according to the electronic structure of TACs.

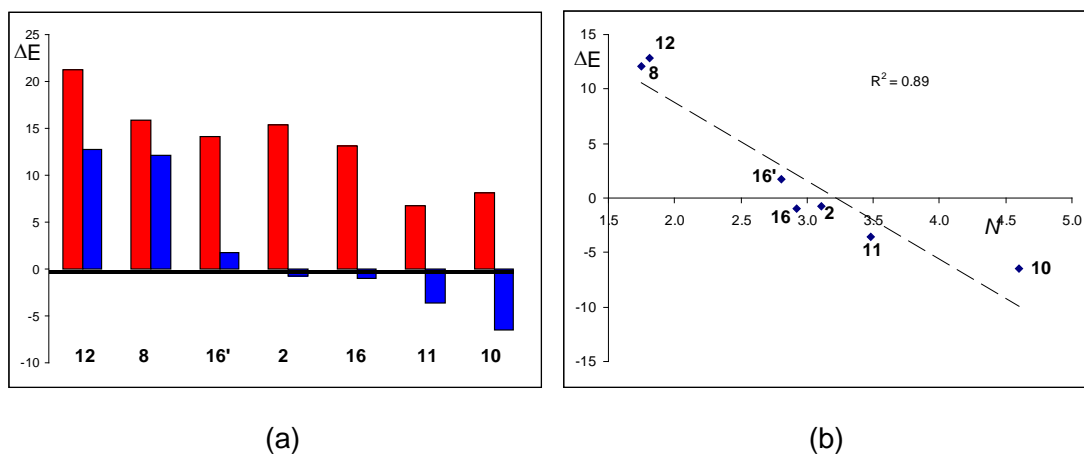


Figure 1.7. (a) activation energies in DCM associated with the 32CA reactions of the non-substituted TACs **2,8,10-12,16** and methyl nitronate **16'** with ethylene **6**, in red, and with electrophilic DCE **21**, in blue; (b) plot of activation energies in DCM associated with the 32CA reactions of the non-substituted TACs **2,8,10-12,16** with DCE **21** vs the nucleophilicity N index of TACs.

2. OBJECTIVES

Although Firestone proposed a diradical resonance Lewis structure as the main contributor to the resonance hybrid of TACs,¹³ today organic chemists represent TACs as 1,2-zwitterionic Lewis structures, according to Huisgen's proposal.⁸

In 2010, ELF topological analysis of the electronic structure of AY **14** and CY **17** revealed that these relevant TACs present a *pseudodiradical* structure.⁶⁴ The high reactivity of these TACs in 32CA reactions was, then, attributed to their *pseudodiradical* character. Thus, in 2014, depending on the observed different reactivity patterns of TACs, 32CA reactions were initially classified into *pr-type* and *zw-type*.⁵¹ Note that the electronic structure of other TACs remained unexplored and, consequently, every TAC without a *pseudodiradical* structure was classified as a zwitterionic TAC.

In this context, three main objectives were conceived to be dealt with in the present thesis:

- 1) To complete the characterisation of the electronic structure of the most important organic TACs used in 32CA reactions, in order to establish a general classification of this significant type of cycloaddition reactions.
- 2) To establish the electronic structural factors governing the reactivity of TACs.
- 3) To shed light onto the molecular mechanisms of 32CA reactions, which in turn, would allow testing the validity of earlier Huisgen's and Firestone's mechanistic proposals.

Derived from the above objectives, several additional aims were established:

- 4) To provide an explanation to the linear trend between activation energies and geometry changes observed by Houk in 32CA reactions.⁴⁸
- 5) To investigate the truthfulness of non-proven assumed classical concepts such as the "pericyclic" mechanism proposed for one-step 32CA reactions. Note that the "pericyclic" mechanism was previously ruled out for DA reactions.⁶¹
- 6) And last, but certainly not least, to demonstrate that a rethinking of organic chemistry by the study of the molecular electron density as a whole, instead of the analysis of individual MOs, is demanded.

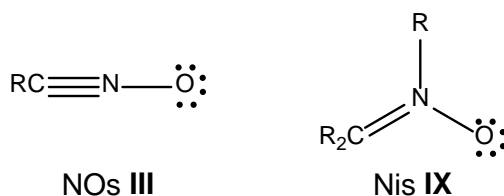
Although along these three years a huge amount of work has been developed by our group resulting in more than thirty-five publications, twenty-two of them being devoted to the study of 32CA reactions, only eight directly related with the objectives of the thesis are presented and discussed herein.

3. RESULTS AND DISCUSSION

In this section, a set of eight selected publications are summarised with the aim of describing the process that allowed meeting the aforementioned objectives. As the original large group of *zw-type* 32CA reactions finally resulted to be composed by three different types, the present section has been divided into three parts corresponding to each type of reactivity except *pr-type* 32CA reactions, which were already characterised before the beginning of the present thesis (see Introduction). These subsections are organised as follows: 3.1) 32CA reactions of zwitterionic TACs, such as NOs **III** and Nis **IX** (see Table 1 in Introduction); 3.2) 32CA reactions of carbenoid TACs, such as NYs **I**; and finally, 3.3) 32CA reactions of *pseudo(mono)radical* TACs, such as Das **IV** and AIs **VIII**.

3.1. 32CA reactions of zwitterionic TACs

Zwitterionic TACs are species containing a multiple bond and non-bonding electron density belonging to a heteroatom (see Scheme 3.1). They are able to participate only in *zw-type* 32CA reactions, which demand adequate nucleophilic/electrophilic activation of the reagents to take place easily. Propargylic NOs **III** and allylic Nis **IX** are typical examples of zwitterionic TACs.



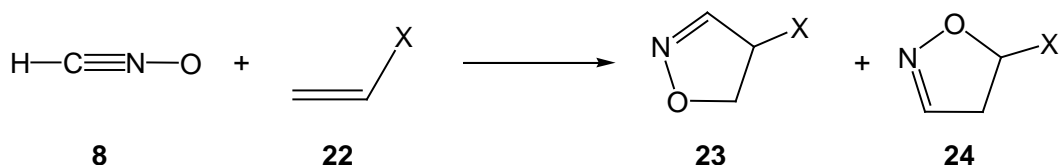
Scheme 3.1. Lewis structures of zwitterionic TACs.

3.1.1. 32CA reactions between substituted NOs **III** and MA **5**⁶⁹

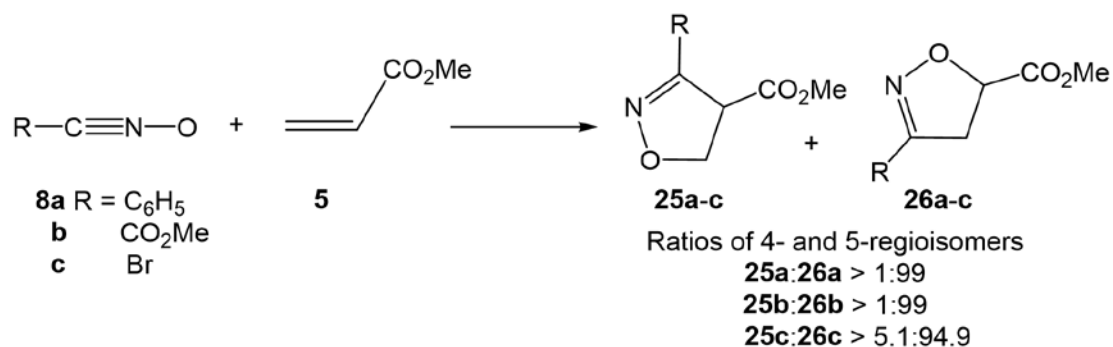
The 32CA reactions of NOs **III** with substituted alkenes is one of the most efficient methods for the synthesis of isoxazolines, which are versatile intermediates for the synthesis of natural products, biologically and medically active compounds,⁷⁰ as well as a variety of functionalities.⁷¹ The 32CA reactions of fulminic acid **8**, the simplest NO **III**, with substituted alkenes **22** may lead to the formation of two regioisomers, the 4- and/or 5-substituted 2-isoxazolines **23** and **24** (see Scheme 3.2).

MA **5** is one of the experimentally most used ethylenes in 32CA reactions.^{5b,72} 32CA reactions between substituted NOs **8a-c** and MA **5** give the 5-substituted isomers **26a-c** with almost complete regioselectivity, the change of substituent R in the TAC having little effect on the regioselectivity of these 32CA reactions (see Scheme 3.3).

3. Results and discussion



Scheme 3.2. 32CA reaction of fulminic acid **8** with substituted alkenes **22** yielding the 4- and/or 5-substituted 2-isoxazolines **23** and **24**.



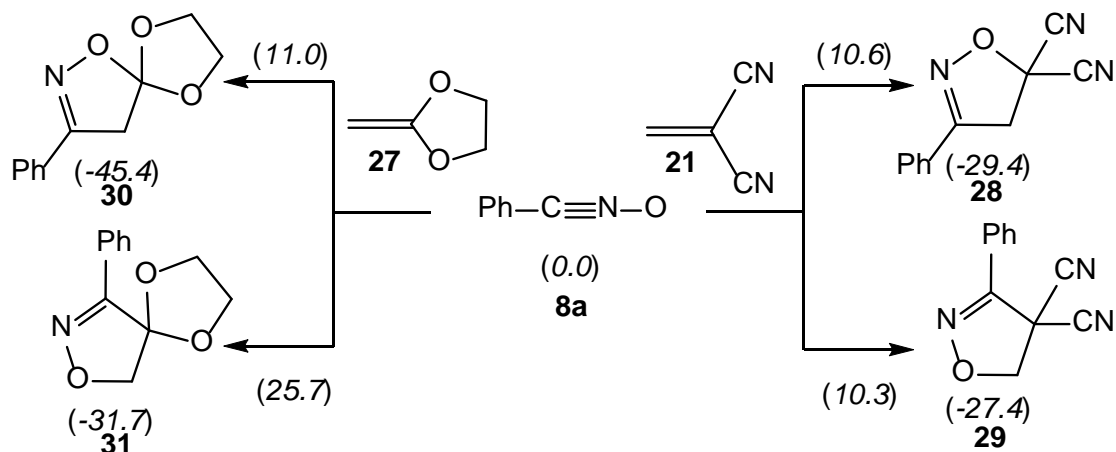
Scheme 3.3. 32CA reaction between substituted NOs **8a-c** and MA **5**.⁷³

The 32CA reactions of NOs **III** with ethylene **6** and acetylene **9** derivatives have been widely analysed within the DFT framework.^{48b,71c,74} Fulminic acid **8** presents a high activation enthalpy towards ethylene **6**, 13.3 kcal·mol⁻¹, and towards acetylene **9**, 13.7 kcal·mol⁻¹ (B3LYP/6-31G(d)).^{48b} Benzonitrile oxide **8a** reacts with electrophilic ethylenes, such as DCE **21** (see Table 3 in Appendix), and nucleophilic ethylenes, such as 2-methylene-1,3-dioxolane **27**, but the regioselectivities of these polar reactions are quite different. While the latter is completely regioselective, yielding 5-isoxazoline **30**, a change in the regioselectivity was observed in the former, which yields a mixture of 4- and 5- isoxazolines **29** and **28** (see Scheme 3.4).^{74j}

NOs **III** are zwitterionic P-TACs participating in *zw-type* 32CA reactions, which demand the nucleophilic activation of the TAC and the electrophilic activation of the ethylene, or vice versa, to take place easily. However, the activation energies associated to the mentioned polar 32CA reactions of benzonitrile oxide **8a** indicate that the electronic activation of the ethylene derivative does not substantially enhance its reactivity (see Scheme 3.4).

Thus, in order to shed light on the participation of NOs **III** in *zw-type* 32CA reactions and how the substitution in the TAC instead in the ethylene derivative could affect the reactivity of NOs **III**, an MEDT⁵⁵ study of the 32CA reactions of the three NOs

given in Scheme 3.3, **8a** (R = Ph), **8b** (R = CO₂Me) and **8c** (R = Br), with electrophilic MA **5** (see Table 3 in Appendix) was carried out through DFT calculations at the B3LYP/6-31g(d) computational level.



Scheme 3.4. 32CA reactions of benzonitrile oxide **8a** with DCE **21** and 2-methylene-1,3-dioxolane **27**, showing different regioselectivities. B3LYP/6-31g(d) gas phase activation energies (in parentheses), relative to the corresponding reagents, are given in kcal·mol⁻¹.

3.1.1.1. Topological analysis of the ELF and NPA of NOs **8** and **8a-c**

According to Lewis's structures, V(C) monosynaptic basins integrating ca. 1e are associated to *pseudoradical* centers, while those integrating ca. 2e in neutral molecules are associated to carbenoid centers. Thus, TACs presenting two *pseudoradical* centers have been classified as *pseudodiradical* TACs, while those presenting only one would be considered as *pseudo(mono)radical* TACs; TACs with a carbenoid center would correspond to carbenoid TACs and, at last, TACs presenting only an A–B multiple bond, i.e. neither *pseudoradical* nor carbenoid centers, have been classified as zwitterionic TACs (see Scheme 3.1). Note, therefore, that the “zwitterionic” term does not refer to any dipolar electronic structure but to the specific bonding pattern (considering no charges) of the principal octet resonance Lewis structure represented by Huisgen for “1,3-dipoles” (see Introduction).

ELF topological analysis of fulminic acid **8** and NOs **8a-c** is shown in Figure 3.1. According to Lewis's bonding model,⁷⁵ the V(O1) monosynaptic basins integrating ca. 5.6e can be associated with three O1 oxygen lone pairs, the V(O1,N2) disynaptic basin integrating ca. 1.8e, with a O1–N2 single bond and the V(N2,C3) disynaptic basin integrating ca. 5.8e, with an N2–C3 triple bond, in agreement with the common bonding pattern represented for NOs **III** (see Figure 3.1). Consequently, the presence of a clear

3. Results and discussion

C3–N2 triple bond indicates that NOs **8** and **8a-c** possess a zwitterionic electronic structure that enables their participation only in *zw-type* 32CA reactions.

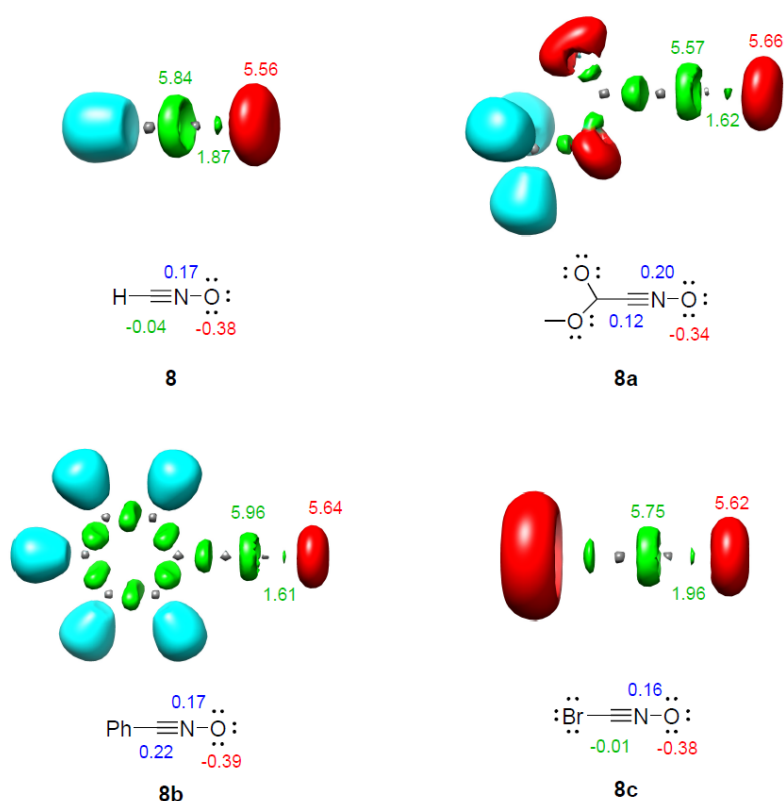


Figure 3.1. ELF localisation domains, together with the most representative valence basin populations, as well as the proposed Lewis structures, together with the natural atomic charges, of NOs **8** and **8a-c**. Negative charges are coloured in red, positive charges in blue and negligible charges in green. ELF valence basin population and natural atomic charges are given in average number of electrons, e.

NPA at NOs **8** and **8a-c** indicated that while the O1 oxygen presents a negative charge of ca. 0.37e, the N2 nitrogen is positively charged by ca. 0.18e. This charge distribution, which is in reasonable agreement with the representation of NOs **III** as 1,2-zwitterionic Lewis structures, is a consequence of the polarisation of the N–O bonding region. Note that the charge distribution obtained by NPA is the consequence of the asymmetric electron density delocalisation resulting from the presence of different nuclei in the molecule, rather than the consequence of resonance Lewis structures.

3.1.1.2. Analysis of the CDFT reactivity indices at the GS of the reagents

CDFT reactivity indices⁵⁶ of NOs **8** and **8a-c** and MA **5**, i.e. the electronic chemical potential μ , the electrophilicity ω index and the nucleophilicity N index, are gathered in Table 3 in Appendix. The electronic chemical potential μ of NO **8a** (R = Ph), -3.83 eV,

is higher than that of MA **5**, -4.31 eV, suggesting that along a polar reaction the GEDT⁶¹ will take place from NO **8a**, acting as the nucleophile, to MA **5**, acting as the electrophile. On the other hand, NOs **8b,c** have electronic chemical potentials similar to that of MA **5** (see Table 3 in Appendix). Consequently, neither of these NOs will have any tendency to transfer electron density towards MA **5**.

According to the electrophilicity⁶² and nucleophilicity⁷⁶ scales, fulminic acid **8** is considered a moderate electrophile, $\omega = 0.73$ eV, and a marginal nucleophile, $N = 1.75$ eV; thus, it is expected that this TAC will not participate in polar reactions. Conversely, NOs **8a-c** are classified as strong electrophiles, $\omega = 1.5 - 1.9$ eV, but as moderate nucleophiles except **8b**, which is classified as a marginal nucleophile (see Table 3 in Appendix). For its part, MA **5** is classified on the borderline of strong electrophiles, $\omega = 1.50$ eV, and as a marginal nucleophile, $N = 1.70$ eV; therefore, it will participate in polar reactions only towards strong nucleophiles.

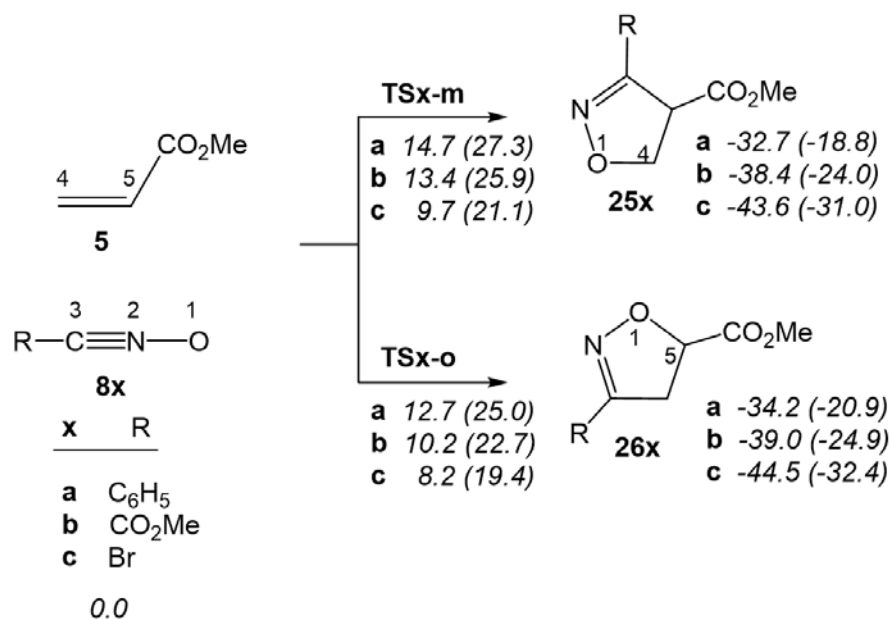
Zw-type 32CA reactions demand the participation of strong nucleophiles, $N > 3.0$ eV, and strong electrophiles, $\omega > 2.0$ eV, to take place easily.⁵¹ Since the pairs of reagents involved in these 32CA reactions do not meet these requirements, it is expected that the corresponding reactions will have a low-polar character, presenting similar activation energies to that involved in the non-polar 32CA reaction between the simplest NO **8** and ethylene **6**.

3.1.1.3. Analysis of the reaction paths of the 32CA reactions between NOs **8a-c** and MA **5**

Due to the non-symmetry of the reagents, the 32CA reactions between NOs **8a-c** and MA **5** can take place along two regioisomeric pathways, the *ortho* and the *meta*, leading to the formation of the 4- and 5-substituted 2-isoxazolines **25a-c** and **26a-c**, respectively (see Scheme 3.5). Analysis of the stationary points involved in the two competitive reaction paths indicates that these 32CA reactions take place through a one-step mechanism.

Some appealing conclusions were drawn from the thermodynamic data given in Scheme 3.5: i) while the activation enthalpy associated with the 32CA reaction involving NO **8a**, 12.7 kcal·mol⁻¹, is similar to that associated with the 32CA reaction between fulminic acid **8** and ethylene **6**, 13.3 kcal·mol⁻¹, those involving NOs **8b** and **8c**

3. Results and discussion



Scheme 3.5. Studied competitive regioisomeric pathways associated with the 32CA reactions between NOs **8a-c** and MA **5**. B3LYP/6-31G(d) relative enthalpies and Gibbs free energies (in parentheses), computed at 25 °C and 1 atm in DCM, are given in kcal·mol⁻¹.

are 3.1 and 5.1 kcal·mol⁻¹ lower. Interestingly, the bromide derivative NO **8c** experiences the faster acceleration; ii) while the 32CA reaction involving NO **8b** is highly *ortho* regioselective, $\Delta\Delta E_{(\text{TS}_o-\text{TS}_m)} = 3.2$ kcal·mol⁻¹, the 32CA reactions involving NOs **8a** and **8c** are moderately *ortho* regioselective, $\Delta\Delta E_{(\text{TS}_o-\text{TS}_m)} = 2.0$ and 1.5 kcal·mol⁻¹; iii) the high exergonic character of these 32CA reactions makes these processes irreversible; and iv) the 32CA reaction involving bromide derivative NO **8c** is kinetically and thermodynamically the most favourable one.

The geometries of the TSs involved in the 32CA reactions of NO **8a-c** with MA **5** (see Figure 3.2) indicated that: i) the more favourable *ortho* TSs are geometrically more asynchronous than the *meta* ones; ii) the C–C and O–C forming bond distances at the more favourable *ortho* TSs indicate that they have a strongly asynchronous character, in which the C–C single bond formation is clearly more advanced than the O–C one; and finally, iii) the most favourable **TS_{c-o}** is the most asynchronous and earliest TS.

In order to evaluate the electronic nature of the 32CA reactions between NOs **8a-c** and MA **5**, the GEDT at the TSs was analysed.⁶¹ The net charge computed at the MA frameworks was found between -0.04e and 0.02e. These negligible GEDT values indicate that these 32CA reactions have a marked non-polar character, which accounts for the high activation energies computed.

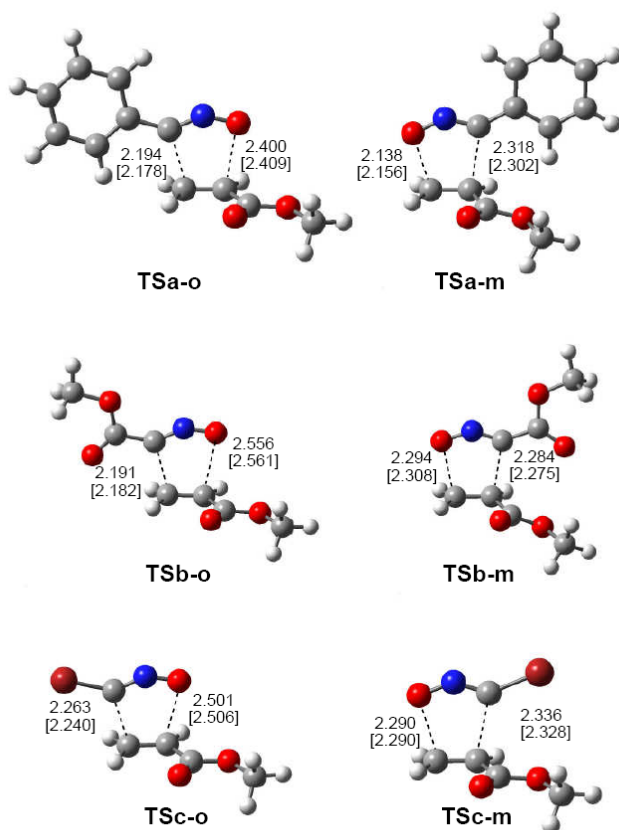


Figure 3.2. B3LYP/6-31G(d) gas phase optimised geometries for the TSs associated with the 32CA reactions between NOs **8a-c** and MA **5**. Distances are given in angstroms, Å, while those in DCM are given in brackets.

3.1.1.4. BET study of the most favourable 32CA reaction between NO **8c** and MA **5**

A BET study of the more favourable *ortho* regioisomeric pathway associated with the non-polar 32CA reaction between NO **8c** and MA **5** (see Table 4 and Scheme 6.1. in Appendix) allowed drawing the following conclusions: i) the IRC associated with the *ortho* regioisomeric reaction path of the 32CA reaction of NO **8c** and MA **5** can be divided in fourteen differentiated phases, a behaviour that clearly indicates that the bonding changes along this one-step mechanism are non-concerted; ii) the reaction begins with the rupture of the N2–C3 triple bond of NO **8c**, similarly to the 32CA reaction between fulminic acid **8** and acetylene **9**;^{60b} iii) the bonding changes in the ethylene framework are more delayed than at the NO framework; iv) formation of the first C3–C4 single bond begins at a distance of ca. 2.00 Å by sharing some non-bonding electron density of the C3 carbon and that of the C4 one. Interestingly, after the formation of this bond, the C3 carbon still displays non-bonding electron density (see Figure 3.3); v) formation of the second O1–C5 single bond begins at the end of the reaction at a distance of ca. 1.78 Å by

3. Results and discussion

donation of non-bonding electron density of the O1 oxygen of the NO framework to the C5 carbon of the MA one (see Figure 3.3), when the first C3–C4 single bond has already reached ca. 94% of its final population (see Table 4 in Appendix); vi) this behaviour makes it possible to establish that this 32CA reaction takes place through a non-concerted *two-stage one-step* mechanism;⁷⁷ v) analysis of the GEDT along the *ortho* reaction path confirms the non-polar character of this 32CA reaction; vi) similarly to the 32CA reaction between fulminic acid **8** and acetylene **9**,^{60b} the bonding changes taking place from the reagents to **TSc-o** are mainly associated to the rupture of the C1–N2 triple bond in NO **8c**. These bonding changes demand an EC of 8.8 kcal·mol⁻¹ from the first point of the reaction path. Consequently, the acceleration found in this 32CA reaction with respect to that between fulminic acid **8** and ethylene **6** can be associated to the presence of the bromide nucleus at the C1 carbon of NO **8c**, which favours the rupture of C1–N2 triple bond in this non-polar process.

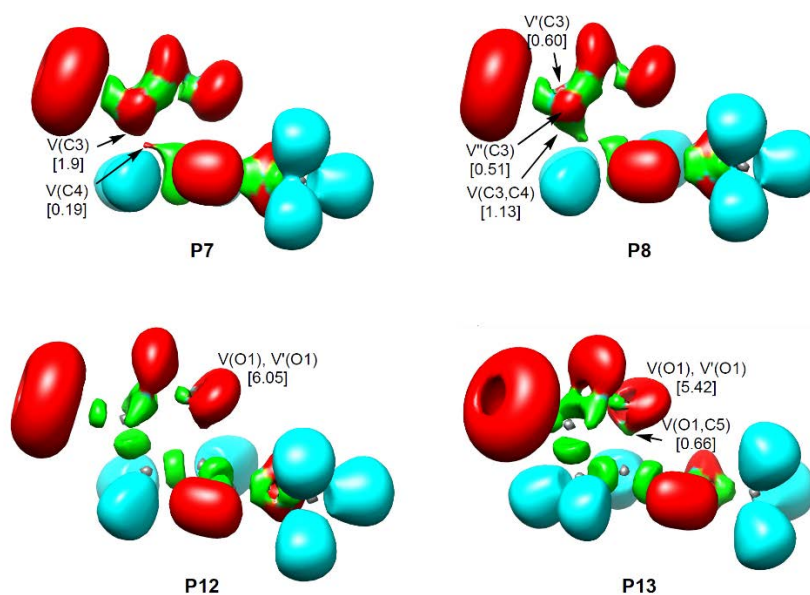
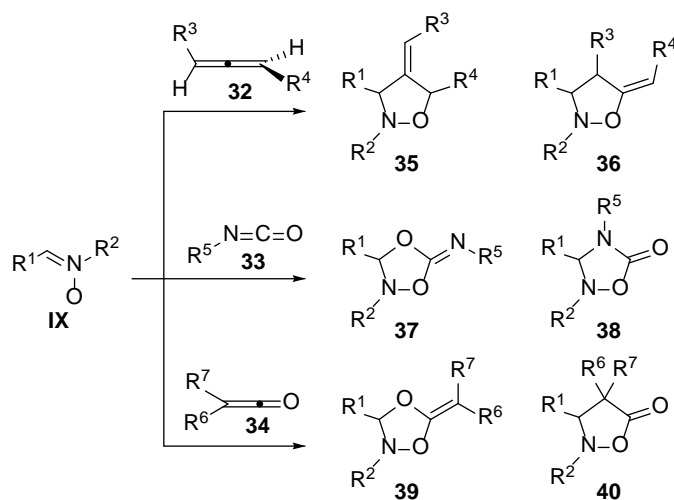


Figure 3.3. ELF localisation domains of the points of the IRC defining the four phases involved in the formation of the new O1–C5 and C3–C4 single bonds along the more favourable *ortho* regioisomeric pathway associated with the *zw*-type 32CA reaction between NO **8c** and MA **5**. The electron populations, in average number of electrons (e), are given in brackets.

3.1.2. 32CA reaction of Nis **IX** with ketenes⁷⁸

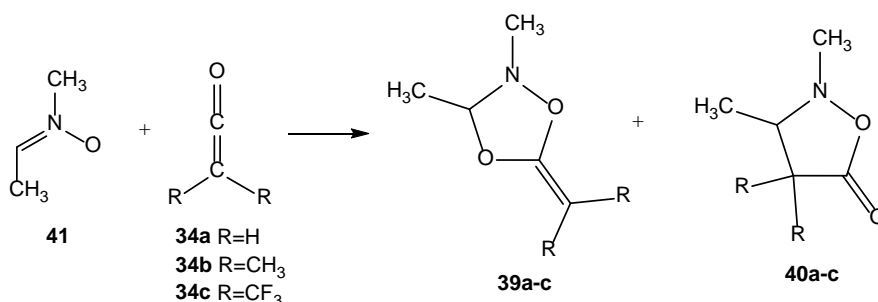
Nis **IX** are zwitterionic A-TACs participating in *zw*-type 32CA reactions. 32CA reactions of Nis **IX** with allenes **32**⁷⁹ and heteroallenes such as isocyanates **33**⁸⁰ and ketenes **34**⁸¹

are of particular interest since they present alternative reaction paths leading to different heterocyclic compounds depending on the allenic part of the system in which the cycloaddition takes place (see Scheme 3.6).



Scheme 3.6. Reactions of Nis **IX** with allenes **32** and heteroallenes **33** and **34**.

Although of synthetic utility, mechanistic studies that allow predicting and interpreting the adducts to be obtained are scarce. In order to understand the *zw*-type reactivity^{51,68} of Nis **IX** towards ketenes **34**, the 32CA reaction of *N*-methyl-*C*-methyl Ni **41** with ketenes **34b** and **34c** yielding dioxazolidines **39b,c** and isoxazolidinones **40b,c** (see Scheme 3.7) were studied within the MEDT⁵⁵ through DFT calculations at the MPWB1K/6-311G(d,p) computational level.



Scheme 3.7. 32CA reactions of Ni **41** with ketenes **34a-c** yielding **39a-c** and **40a-c**.

3.1.2.1. Topological analysis of the ELF and NPA of Nis **16** and **41**

As can be seen in Figure 3.4, Ni **16** presents two V(O1) and V'(O1) monosynaptic basins, integrating a total of 5.91e, and one V(O1,N2) disynaptic basin with a population of 1.39e. This behaviour suggests that the O1–N2 bonding region is strongly polarised towards the O1 oxygen. In addition, the presence of one V(N2,C3) disynaptic basin integrating 3.89e

3. Results and discussion

indicates that the N2–C3 bonding region has a strong double bond character. Consequently, ELF topology of the simplest Ni **16** clearly indicates that this TAC presents a zwitterionic electronic structure that enables its participation in *zw-type* 32CA reactions only.⁵¹

On the other hand, the ELF topology of Ni **41** shows a very similar bonding pattern to that found in the simplest Ni **16**. The ELF valence basin populations have varied very slightly (see Figure 3.4), although in this case the N2–C3 bonding region is characterised by the presence of two disynaptic basins, $V(N2,C3)$ and $V'(N2,C3)$, integrating a total population of 4.09e. Therefore, according to the ELF topological analysis, Ni **41** will also behave as a zwitterionic TAC participating only in *zw-type* 32CA reactions,⁵¹ just as the simplest Ni **16**.

Finally, NPA indicates that neither of these Nis has a 1,2-zwitterionic charge distribution with a negative and a positive charge entirely located at the O1 and N2 centers. Although the O1 oxygen has a high negative charge, $-0.48e$ (**16**) and $-0.53e$ (**41**), the N2 nitrogen presents practically no charge, $-0.06e$ (**16**) and $0.08e$ (**41**).

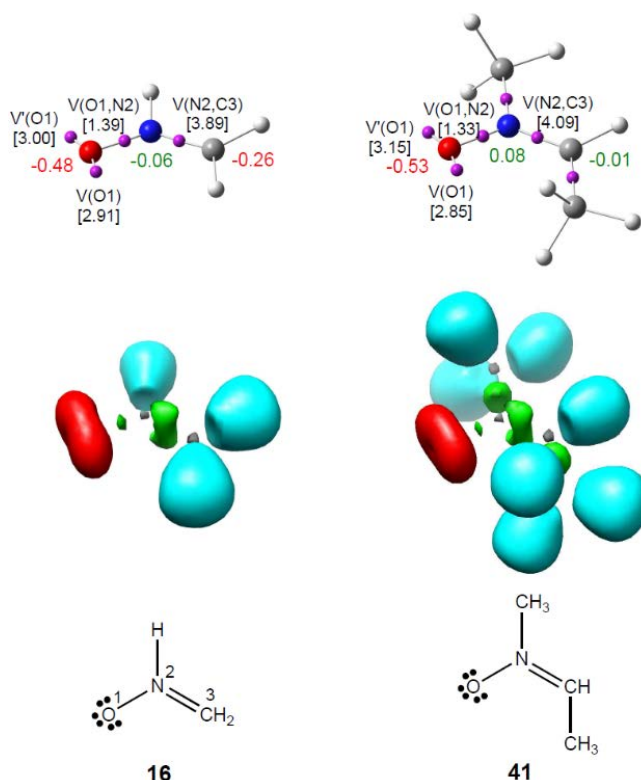


Figure 3.4. ELF valence basin attractors, together with the most representative valence basin populations and natural atomic charges, ELF localisation domains and the proposed Lewis structures of Nis **16** and **41**. Negative charges are coloured in red and negligible charges in green. ELF valence basin populations and natural atomic charges are given in average number of electrons, e.

3.1.2.2. Analysis of the CDFT reactivity indices at the GS of the reagents

CDFT reactivity indices⁵⁶ of Nis **16** and **41** and ketenes **34a-c** are gathered in Table 3 in Appendix. As the electronic chemical potential μ of Ni **41**, -2.95 eV, is higher than that of ketenes **34b,c**, -3.23 and -5.26 eV, the GEDT⁶¹ will flux from the Ni framework, acting as the nucleophile, towards the ketene framework, acting as the electrophile, along polar reactions. On the other hand, according to the electrophilicity⁶² and nucleophilicity⁷⁶ scales, ketene **34b**, $\omega = 1.02$ eV, will behave as a moderate electrophile, ketene **34c**, $\omega = 2.47$ eV, as a strong electrophile and Ni **41**, $N = 3.46$ eV, as a strong nucleophile.

Regarding the local reactivity, analysis of the nucleophilic P_k^- Parr functions⁸² of Ni **41** and the electrophilic P_k^+ Parr functions⁸² of ketenes **34b,c** indicated that the O1 oxygen is the most nucleophilic center of the former and the central C5 carbon the most electrophilic center of the latter, the terminal C6 carbon being electrophilically deactivated (see Figure 3.5). Consequently, analysis of the CDFT reactivity indices⁵⁶ of these Nis and ketenes predicts a complete C=O regio- and chemoselectivity.

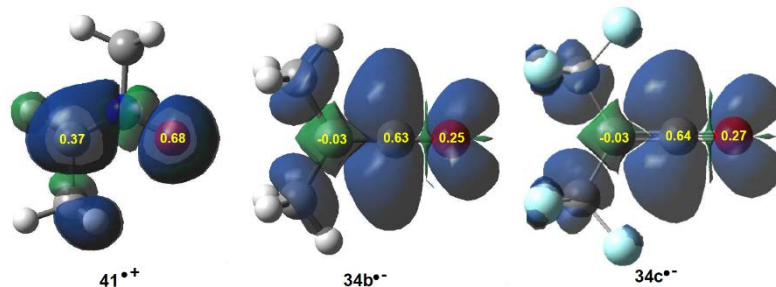


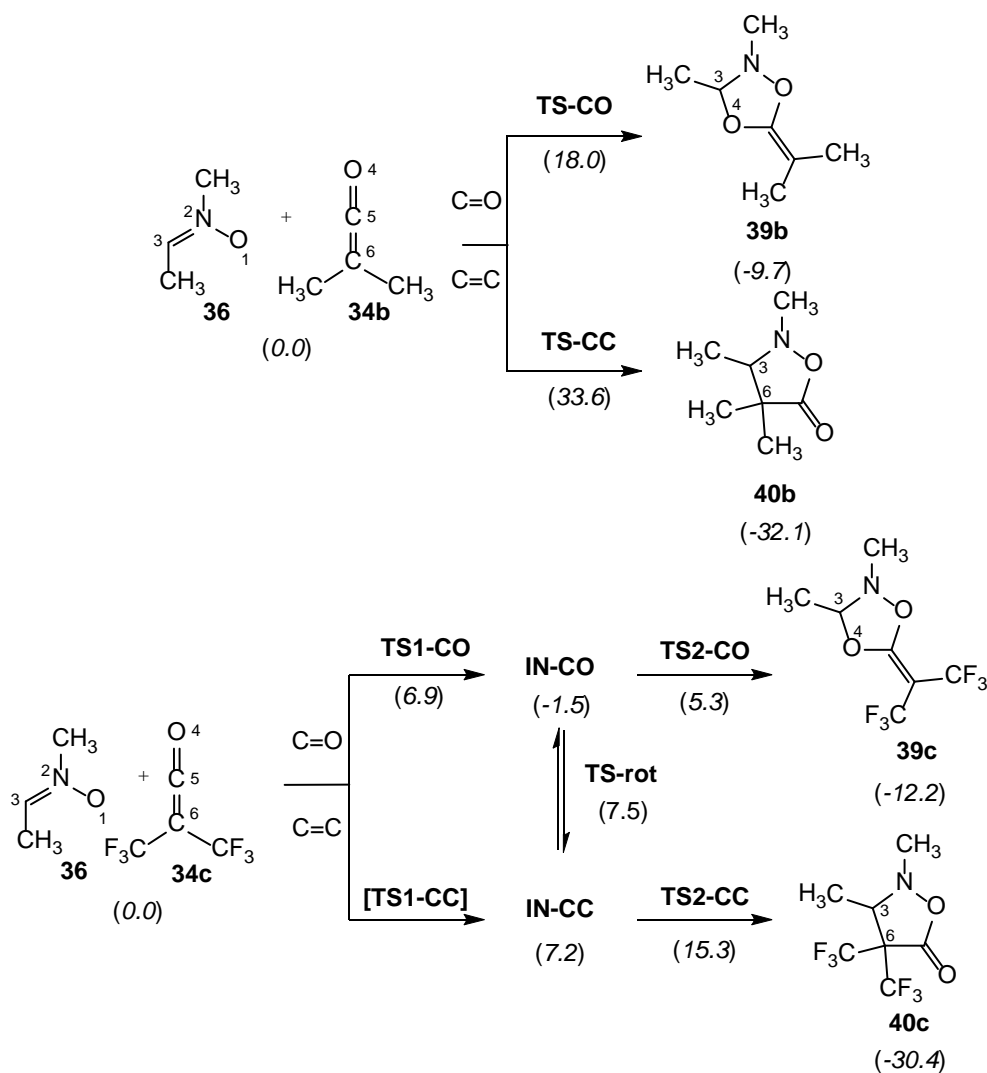
Figure 3.5. 3D representations of the ASD of the radical cation **41**^{•+} and the radical anions **34b,c**^{•-}, together with the nucleophilic P_k^- Parr functions⁸² of Ni **41** and the electrophilic P_k^+ Parr functions⁸² of ketenes **34b,c**.

3.1.2.3. Analysis of the reaction paths of the 32CA reactions between Ni **41** and ketenes **34b,c**

Due to the non-symmetry of both reagents, the 32CA reactions between Ni **41** and ketenes **34b,c** can take place along four competitive chemo- and regioisomeric reaction paths. Due to the predicted high C=O regioselectivity, only the two chemoisomeric pathways associated with the initial nucleophilic attack of the Ni O1 oxygen on the central C5 carbon of ketenes **34b,c** were studied.

3. Results and discussion

As Scheme 3.8 shows, analysis of the stationary points involved in the two reaction paths associated with the two studied 32CA reactions indicates that they take place through different mechanisms; while the 32CA reaction involving ketene **34b** takes place via a one-step mechanism, that involving electrophilic ketene **34c** takes place via a two-step mechanism.



Scheme 3.8. C=O and C=C chemoisomeric pathways associated with the *z,w*-type 32CA reaction between Ni **41** and ketenes **34b,c**. MPWB1K/6-311G(d,p) relative Gibbs free energies (in parentheses), computed at 25 °C and 1 atm in benzene, are given in kcal·mol⁻¹.

Some appealing conclusions were drawn from the Gibbs free energies given in Scheme 3.8 and the Gibbs free energy profile represented in Figure 3.6: i) both 32CA reactions are kinetically very favourable; ii) the 32CA reaction involving ketene **34b** is kinetically completely C=O chemoselective, as **TS-CO** is 15.6 kcal·mol⁻¹ lower in Gibbs free energy than **TS-CC**. However, isoxazolidinone **40b** could become the product of a thermodynamic control under thermal equilibrium conditions as it is more stable than

dioxazolidine **39b**; iii) the 32CA reaction involving ketene **34c** is also completely C=O chemoselective, as **TS2-CO** is 10.5 kcal·mol⁻¹ lower in Gibbs free energy than **TS2-CC**; iv) **IN-CO** and **IN-CC** are two conformers being interconvertible by an O1–C5 single bond rotation implying only 0.3 kcal·mol⁻¹. Consequently, these intermediates connect both chemoisomeric reaction paths. Thus, under thermodynamic control, dioxazolidine **39c** could be converted into the more thermodynamically stable **40c** with an activation energy of 27.5 kcal·mol⁻¹; and finally, v) a comparison between the energy profiles of the 32CA reactions of Ni **41** with ketenes **34b,c** allows obtaining two appealing conclusions: a) the electrophilic activation of the ketene changes the molecular mechanism and activation energies, but it does not change the thermodynamics of the reaction; and b) in both reactions, the ring closure is the step controlling the chemoselectivity.

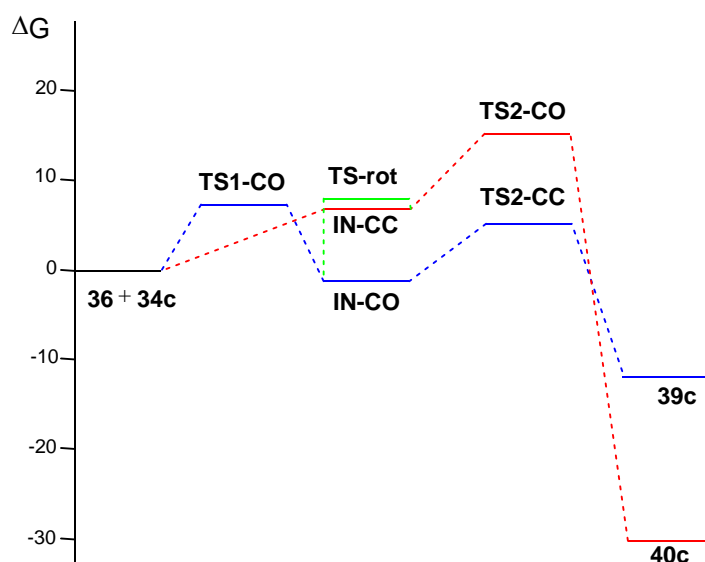


Figure 3.6. MPWB1K/6-311G(d,p) Gibbs free energy profile (ΔG , kcal·mol⁻¹), computed at 25 °C and 1 atm in benzene, of the 32CA reaction between Ni **41** and electrophilic ketene **34c**.

The geometries of the TSs and intermediates involved in the 32CA reactions of Ni **41** with ketenes **34b,c** are displayed in Figure 3.7. The short distance between the O1 and C5 nuclei at both **TS-CO** and **TS-CC** indicates that the O1–C5 single bond is already formed.⁸³ Consequently, these TSs are associated to the formation of the second C3–O4 or C3–C6 single bonds. At **TS1-CO**, the distances between the interacting nuclei indicated that this TS is very early, in clear agreement with its low activation energy. At intermediates **IN-CO** and **IN-CC**, the O1–C5 single bond is already formed, while the distances between the C3 and O4/C6 nuclei suggest still delayed bond formation processes. Finally, at **TS2-CO** and **TS2-CC**, while the length of the O1–C5 single bond

3. Results and discussion

has slightly decreased by 0.1 Å, the distances between the C3 and O4/C6 nuclei have decreased by ca. 0.7 Å.

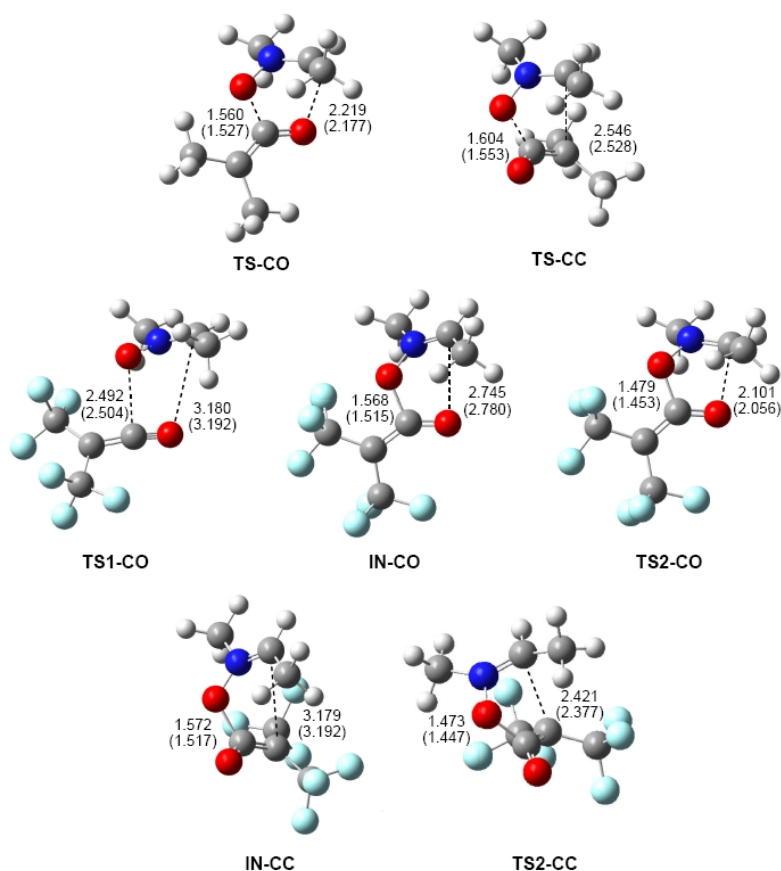


Figure 3.7. MPWB1K/6-311G(d,p) gas phase optimised geometries of the TSs and intermediates involved in the 32CA reaction of Ni **41** with ketenes **34b,c**. Distances are given in angstroms, Å, while those in benzene are given in parentheses.

In order to evaluate the electronic nature of the 32CA reaction of Ni **41** with ketenes **34b,c**, the GEDT at the TSs was analysed.⁶¹ At **TS-CO** and **TS-CC**, the GEDT that takes place from the Ni to the ketene framework is 0.33e and 0.21e, respectively. These high values indicate that these TSs have polar character. On the other hand, at the TSs and intermediates associated with the 32CA reaction of Ni **41** with electrophilic ketene **34c**, the GEDT is 0.05e at **TS1-CO**, 0.45e at **IN-CO**, 0.44e at **IN-CC**, 0.41e at **TS2-CO** and 0.37e at **TS2-CC**, indicating a higher polar character of this reaction due to the higher electrophilic character of ketene **34c**. Analysis of the GEDT is in agreement with the low computed activation energies and confirms that the feasibility of these *zw-type* 32CA reactions depends on their polar character, i.e. the electrophilic character of the ketene.

3.1.2.4. BET study of the 32CA reaction between Ni **41** and ketene **34b**

A BET study of the most favourable reaction path associated with the 32CA reaction between Ni **41** and ketene **34b** (see Table 5 and Scheme 6.2 in Appendix) allowed drawing the following appealing conclusions: i) the corresponding IRC is divided in eight differentiated phases, a behaviour that clearly indicates that the bonding changes along this one-step mechanism are non-concerted; ii) formation of the first O1–C5 single bond begins at a distance of ca. 1.64 Å, by donation of part of the non-bonding electron density of the O1 oxygen of the Ni framework to the C5 carbon of the ketene moiety (see Figure 3.8). Note that the O1 oxygen is the most nucleophilic center of Ni **41** and the C5 carbon corresponds to the most electrophilic center of ketene **34b**; iii) formation of this bond demands the asymmetric depopulation of the O4–C5 bonding region of ketene **34b**. The high GEDT, 0.34e, taking place along this *zw-type* 32CA reaction favours these bonding changes according to the electronic behaviour anticipated by the Parr functions,⁸² which is in agreement with the computed total C=O chemoselectivity; iv) formation of the second C3–O4 single bond begins at a distance of ca. 1.84 Å by donation of part of the non-bonding electron density of the O4 oxygen to the C3 *pseudoradical* center of the Ni framework. This carbon participates with a residual electron density of 0.03e in the formation of the C3–O4 single bond (see Figure 3.8); v) the reaction follows a *two-stage one-step* mechanism⁷⁷ in which the formation of the second C3–O4 bond begins when the first O1–C5 single bond is practically already formed, by up to 89% (see Table 5 in Appendix). This fact also emphasises that the bonding changes in this one-step reaction are non-concerted; vi) the activation energy associated with this 32CA reaction, 9.3 kcal·mol⁻¹, can mainly be associated with the depopulation of the O4–C5 and N2–C3 bonding regions towards the O4 oxygen and the N2 nitrogen, respectively, which is demanded before the donation of the electron density of the O4 oxygen to the C3 carbon; vii) this BET study allowed establishing the molecular mechanism of the *zw-type* 32CA reactions between Nis **IX** and ketenes **34** as a [2n+2n] mechanism,⁸⁴ i.e. only two non-bonding electrons of the oxygen lone pairs of Ni **41**, and two non-bonding electrons of the oxygen lone pairs of ketene **34b**, are mainly involved in the formation of the two C–O single bonds of cycloadduct **39b**.

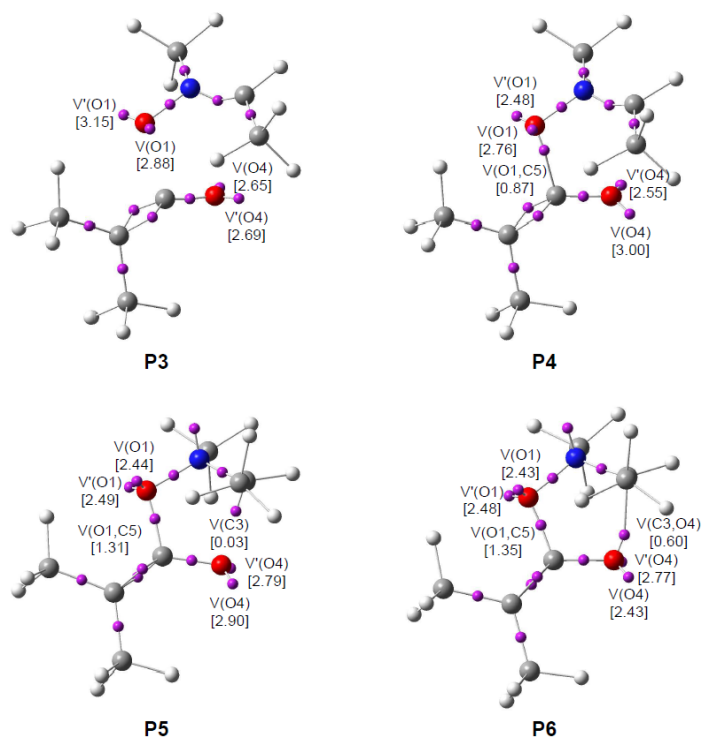


Figure 3.8. ELF attractor positions for the points of the IRC defining the four phases involved in the formation of the O1–C5 and C3–O4 single bonds along the most favourable reaction path associated with the *zw*-type 32CA reaction between Ni **41** and ketene **34b**. The electron populations, in average number of electrons (e), are given in brackets.

3.1.2.5. ELF topological analysis of the stationary points involved in the 32CA reaction involving electrophilic ketene **34c**

Finally, an ELF topological analysis of the electron density distribution of the stationary points involved in the most favourable reaction path associated with the 32CA reaction involving electrophilic ketene **34c** (see Table 6 and Scheme 6.3 in Appendix) allowed obtaining the following conclusions: i) the bonding pattern of **TS1-CO** (see Figure 3.9) resembles that associated with the structures located at the end of *Phase I* of the reaction between Ni **41** and ketene **34b** (see Scheme 6.2 in Appendix), emphasising its earlier character; ii) as expected, at **IN-CO**, while formation of the O1–C5 single bond is very advanced, formation of the C3–O4 single bond has not yet begun; iii) the bonding pattern of **IN-CO** (see Figure 3.9) resembles that of point **P5** of the reaction between Ni **41** and ketene **34b** (see Scheme 6.2 in Appendix). The main difference between **IN-CO** and **P5** is the C3–O4 distance: 2.745 Å at **IN-CO** and 2.329 Å at **P5**. The short C3–O4 distance at **P5** justifies that this species cannot be a stationary point; iv) the bonding pattern of **TS2-CO** (see Figure 3.9) resembles that of **TS-CO** (see Table 5 in Appendix). The only difference is that **TS2-CO** is slightly more advanced than **TS-CO**; and v) the GEDT at

IN-CO and **TS2-CO** is larger than that at **P5** and **TS-CO** due to the higher electrophilic character of ketene **34c** than that of ketene **34b**. The higher polar character of the *zw-type* 32CA reaction between nucleophilic Ni **41** and electrophilic ketene **34c** permits the stabilisation of the zwitterionic intermediate, thus changing the molecular mechanism from a one-step mechanism to a two-step one, but the bonding changes in both 32CA reactions are essentially the same. This similar bonding pattern along the two 32CA reactions supports the non-concerted nature of the *two-stage one-step* mechanism.⁷⁷

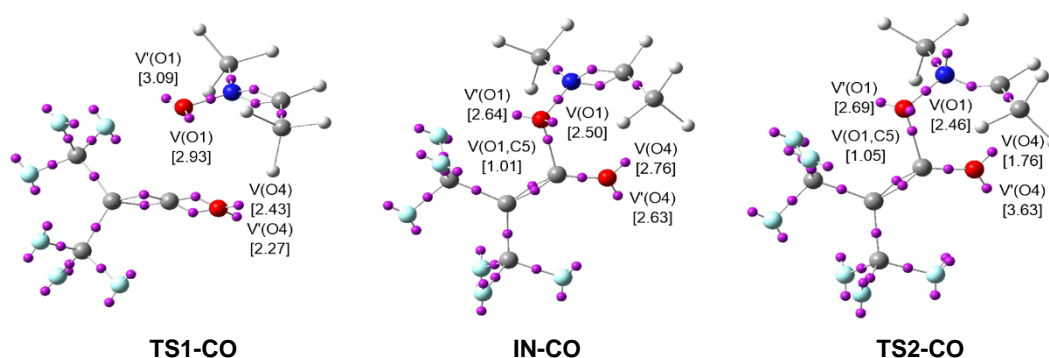


Figure 3.9. ELF attractor positions of the stationary points involved in the most favourable reaction path associated with the *zw-type* 32CA reaction between Ni **41** and ketene **34c**. The electron populations, in average number of electrons (e), are given in brackets.

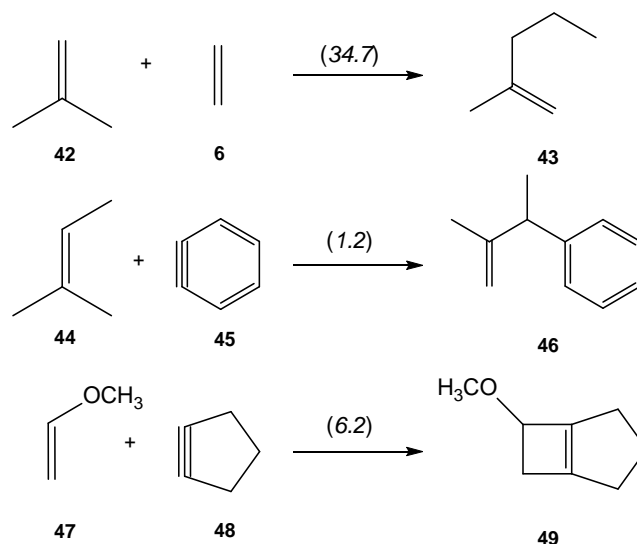
3.1.3. 32CA reaction of Nis IX with strained allenes⁸⁵

The use of strained species such as benzyne **45** and cyclic alkynes such as cyclopentyne **48** in organic synthesis permits their participation in organic reactions in which linear alkynes do not react⁸⁶ (see Scheme 3.9).

An ELF topological analysis of the electronic structure of benzyne **45** made it possible to explain the high reactivity of this strained aromatic alkyne.^{86a} The ELF topology of benzyne **45** showed the presence of two monosynaptic basins, V(C1) and V(C2), integrating 0.64e each one (see Figure 3.10). This electronic characteristic of benzyne **45** allowed associating its reactivity to that of a highly reactive *pseudodiradical* species.^{67,86a}

Unlike arynes and cyclic alkynes, whose structure and reactivity have been widely studied,^{86,87} highly strained allene species have been studied to a much lesser extent. Since

3. Results and discussion



Scheme 3.9. Non-polar reactions of ethylene derivatives and strained species. Activation energies, in parentheses, are given in kcal·mol⁻¹.

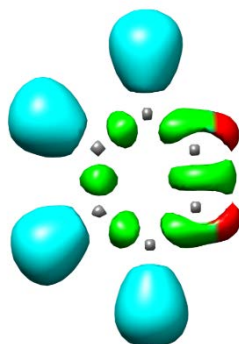
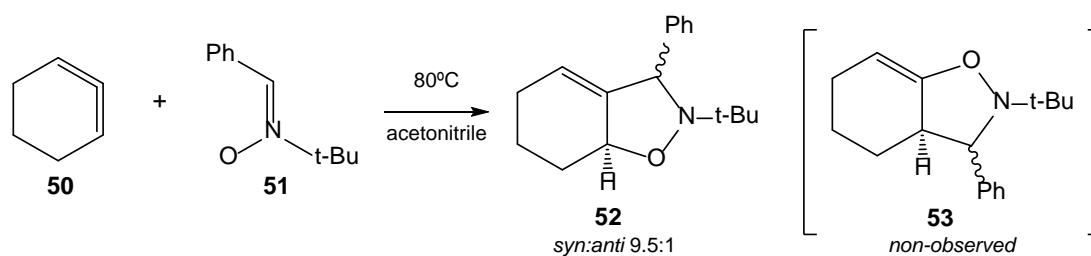


Figure 3.10. ELF localisation domains of benzyne **45**. The two non-bonding V(C1) and V(C2) monosynaptic basins are represented in red.

1966, when Wittig reported, for the first time, the existence of CHDE **50**,⁸⁸ the chemistry of this highly strained species has received little attention especially compared to its aryne and alkyne counterparts.

Very recently, Houk et al. studied experimentally as well as theoretically the 32CA reaction of the *in situ* generated CHDE **50** with Ni **51** participating as the TAC, yielding the two stereoisomeric isoxazolidines **52** (Ph/H *syn:anti* 9.5:1); regioisomeric isoxazolidines **53** were not observed (see Scheme 3.10).⁸⁹

Houk proposed that the predistortion of CHDE **50** into geometries similar to those of the TSs for cycloadditions could be responsible for the low activation energy of these reactions compared with that for the 32CA reaction with the simplest allene **54**.⁸⁹



Scheme 3.10. 32CA reaction of CHDE **50** with Ni **51** yielding the stereoisomeric isoxazolidines **52**.

However, similarly to benzyne **45**,⁸⁶ the strain present at the sp hybridised C5 carbon of CHDE **50** could provide some *pseudoradical* character to the C5 carbon, enabling this compound to experience a different reactivity pattern to that of linear allenes.

These different interpretations about the role of the strain in the reactivity of strained species prompted us to revisit the 32CA reaction of the strained CHDE **50** with Ni **51** within the MEDT.⁵⁵ Thus, in order to understand how the strain modifies the reactivity of CHDE **50** with respect to the non-strained linear allene **54** and how this fact affects the usual *zw-type* reactivity of Nis **IX**, an MEDT⁵⁵ study of the 32CA reaction of Ni **51** with strained CHDE **50** and the simplest allene **54** was performed at the B3LYP/6-311G(d,p) computational level.

3.1.3.1. Topological analysis of the ELF and NPA of linear allene **54** and strained CHDE **50**

As commented, the high reactivity of benzyne **45** was attributed to its *pseudodiradical* character, which was topologically characterised by the presence of two ELF V(C) monosynaptic basins (see Figure 3.10).⁸⁶ However, ELF topological analysis of both allenes **50** and **54** did not show the presence of any V(C) monosynaptic basin (see Figure 3.11). Instead, while the V(C_x,C_y) disynaptic basins associated with the C4–C5 and C5–C6 double bonds are clearly differentiated in the linear allene **54** as they are positioned in two perpendicular molecular planes, they are linked in a singular and twisted manner at strained CHDE **50** due to the slight torsion of the C4=C5=C6 framework. This particular feature found in the strained CHDE **50** suggests that this species will have a different chemical behaviour to that of linear allene **54**, with the participation of the two C–C double bonds of the strained allene in its special reactivity.

3. Results and discussion

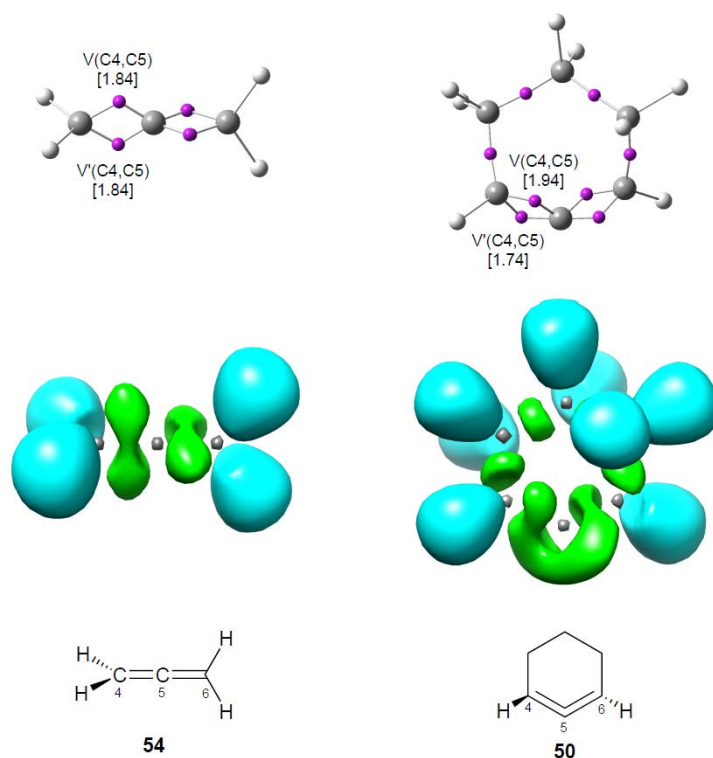


Figure 3.11. ELF valence basin attractors, together with the C4–C5 valence basin populations, in average number of electrons (e), ELF localisation domains and the proposed Lewis structures for allenes **50** and **54**.

3.1.3.2. Analysis of the CDFT reactivity indices at the GS of the reagents

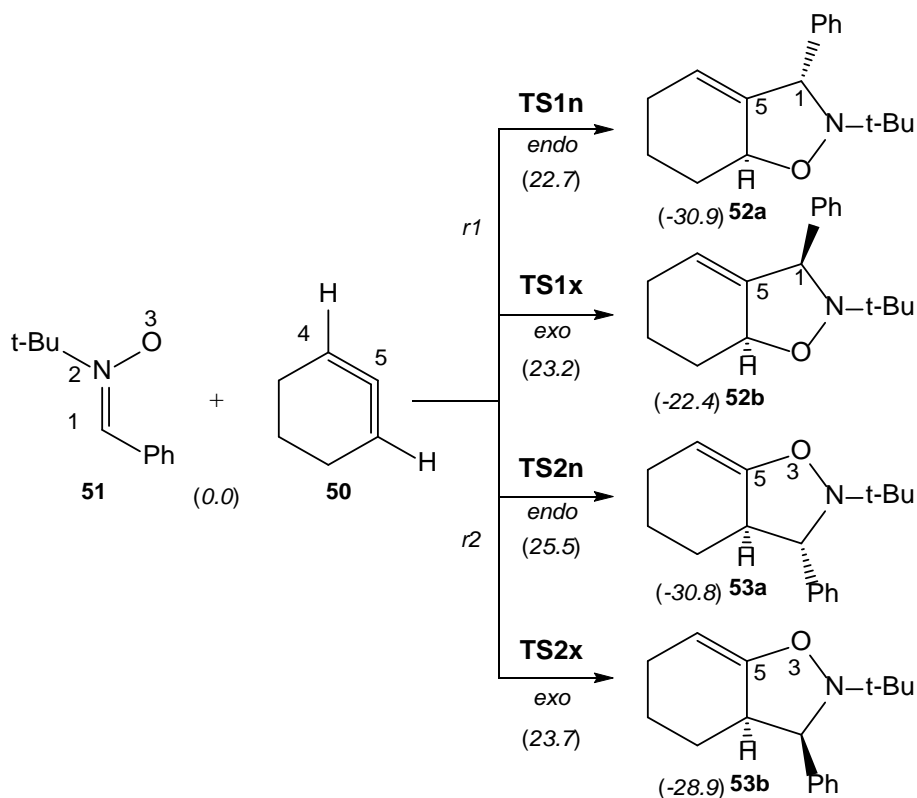
CDFT reactivity indices⁵⁶ of Ni **51** and allenes **50** and **54** are gathered in Table 3 in Appendix. As the electronic chemical potential of Ni **51**, -3.29 eV, is close to that of the simplest allene **54**, -3.30 eV, and only slightly higher than that of CHDE **50**, -3.44 eV, none of the reagents will have any tendency to exchange electron density with the other along these 32CA reactions, suggestive of non-polar reactions.

According to the electrophilicity⁶² and nucleophilicity⁷⁶ scales, Ni **51** is classified as a moderate electrophile, $\omega = 1.26$ eV, and as a strong nucleophile, $N = 3.70$ eV. On the other hand, CDFT reactivity indices of the simplest linear allene **54** are very similar to those of ethylene **6** (see Table 3 in Appendix), thus being classified as a marginal electrophile, $\omega = 0.70$ eV, and on the borderline of marginal nucleophiles, $N = 1.97$ eV. Otherwise, the angular strain of the allene framework in CHDE **50** causes an increase of both the electrophilicity ω and nucleophilicity N indices so that this species is classified as a moderate electrophile, $\omega = 1.24$ eV, and a strong nucleophile, $N = 3.29$ eV. However, in spite of this electrophilic activation with respect to the simplest linear allene **54**, this is not sufficient to favour the GEDT,⁶¹ in clear agreement with the analysis of the global

electronic chemical potentials of the reagents. Consequently, it is expected that the corresponding non-polar 32CA reactions will present high activation barriers.

3.1.3.3. Study of the reaction paths associated with the 32CA reaction of Ni **51** with strained CHDE **50**

Due to the non-symmetry of the two reagents, the 32CA reaction of Ni **51** with strained CHDE **50** can take place along four isomeric reaction paths: one pair of stereoisomeric pathways and one pair of regioisomeric ones. As Scheme 3.11 shows, analysis of the stationary points involved in the four reaction paths indicates that this 32CA reaction takes place through a one-step mechanism.



Scheme 3.11. The four competitive reaction paths associated with the 32CA reaction of Ni **51** with CHDE **50**. B3LYP/6-311G(d,p) relative Gibbs free energies (in parentheses), computed at 80 °C and 1 atm in acetonitrile, are given in kcal·mol⁻¹.

Some appealing conclusions were drawn from Scheme 3.11 and the Gibbs free energy profile represented in Figure 3.12: i) the activation Gibbs free energy associated with the 32CA reaction of Ni **51** with CHDE **50** via **TS1n** is 19.9 kcal·mol⁻¹ lower in energy than that associated with the 32CA reaction of Ni **51** with the simplest allene **54**, 42.6 kcal·mol⁻¹; ii) this 32CA reaction presents a low C1–C5 regioselectivity and a low *endo*

3. Results and discussion

stereoselectivity; iii) the 32CA reaction of Ni **51** with strained CHDE **50** presents an opposed regioselectivity to that found in the reaction with the simplest allene **54**; and finally, iv) the strain present in CHDE **50** does not only affect the kinetics, but also the thermodynamics: while this 32CA reaction is strongly exergonic (**52a**), the most favourable reaction path associated with the 32CA reaction involving the simplest allene **54** is exergonic by only 4.3 kcal·mol⁻¹.

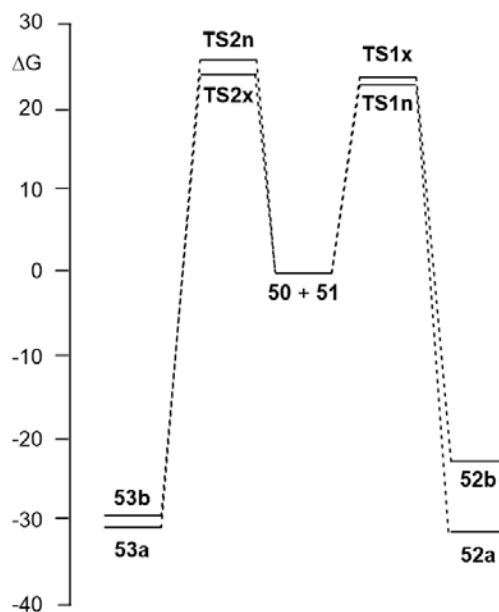


Figure 3.12. B3LYP/6-311G(d,p) Gibbs free energy profile, in kcal·mol⁻¹, of the 32CA reaction of Ni **51** with CHDE **50**.

The geometries of the TSs involved in the 32CA reaction of Ni **51** with CHDE **50** in acetonitrile (see Figure 3.13) indicated that: i) the four TSs correspond to highly asynchronous single bond formation processes, while the two regioisomeric TSs associated with the 32CA reaction of Ni **51** with the simplest allene **54** are hardly asynchronous; ii) the more unfavourable *exo* **TS1x** is slightly more advanced and more asynchronous than *endo* **TS1n**; iii) the formation of the single bond involving the C5 carbon of CHDE **50** is more advanced than that involving the C4 carbon; iv) CHDE **50** approaches Ni **51** perpendicularly, while in the 32CA reaction between Ni **51** and the simplest allene **54**, the two frameworks approach each other in a parallel manner; v) the strain present in CHDE **50** notably modifies the reactivity of this strained cyclic allene when it is compared to that of the simplest allene **54**. Note the different synchronicities and approach modes.

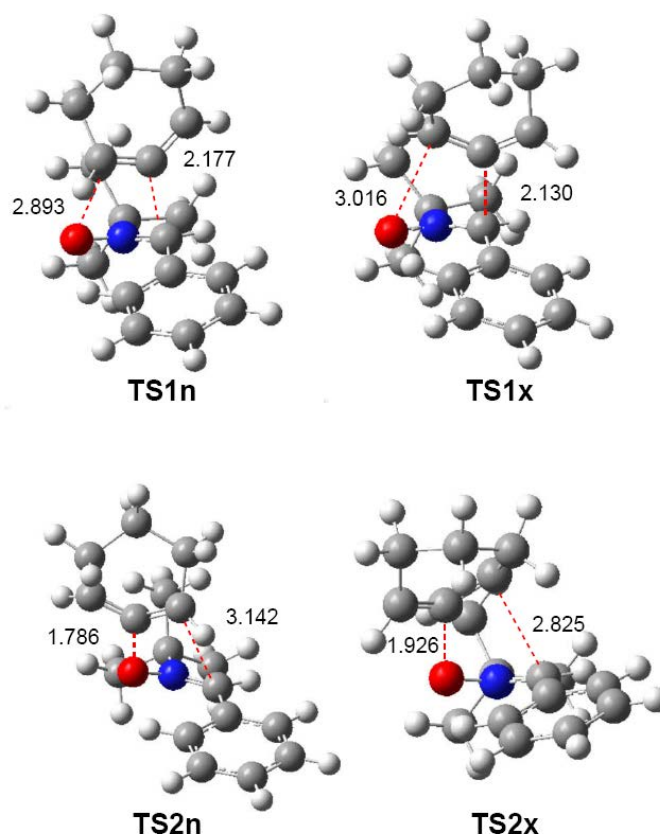


Figure 3.13. B3LYP/6-311G(d,p) optimised geometries in acetonitrile of the TSs involved in the 32CA reaction of Ni **51** with CHDE **50**. Distances are given in angstroms, Å.

The GEDT at the four TSs, which fluxes from the Ni to the CHDE frameworks, is 0.02e at **TS1n**, 0.02e at **TS1x**, 0.02e at **TS2n** and 0.09e at **TS2x**, indicating that this 32CA reaction has a non-polar character,⁶¹ in agreement with the analysis of the CDFT reactivity indices at the GS of the reagents.

3.1.3.4. BET study of the 32CA reaction of Ni **51** with strained allene CHDE **50** and linear allene **54**

BET data are gathered in Tables 7 and 8 in Appendix while simplified representations of the molecular mechanisms arising from the BET study are shown in Schemes 6.4 and 6.5. The BET study of the 32CA reaction of Ni **51** with strained allene CHDE **50** (see Table 8 and Scheme 6.5 in Appendix) allowed drawing the following appealing conclusions: i) the IRC of the most favourable *endo/rl* reaction path is divided in ten differentiated phases related to the disappearance or creation of valence basins, emphasising the non-concerted nature of the bonding changes along the reaction; ii) the reaction begins with the depopulation of the allenic C4–C5–C6 bonding region of strained CHDE **50** in order

3. Results and discussion

to permit the creation of a *C5 pseudoradical* center (see Scheme 6.5 in Appendix). Due to the strain present in CHDE **50**, this electronic change demands a relatively low EC of $8.3 \text{ kcal}\cdot\text{mol}^{-1}$ (see Table 8 in Appendix), which is $15.1 \text{ kcal}\cdot\text{mol}^{-1}$ lower than that demanded for the creation of the first *pseudoradical* center at the Ni framework in the reaction involving the simplest allene **54** (see Table 7 in Appendix); iii) thus, the relatively low activation energy found in this non-polar 32CA reaction, $8.5 \text{ kcal}\cdot\text{mol}^{-1}$, can be mainly associated to the creation of a *pseudoradical* center at the C5 carbon of strained allene CHDE **50**; iv) once this *C5 pseudoradical* center is formed in the allenic framework, the subsequent rupture of the C1–N2 double bond of the Ni fragment and creation of the C1 *pseudoradical* center has an unappreciable EC, $0.1 \text{ kcal}\cdot\text{mol}^{-1}$ (see Table 8 in Appendix). Consequently, once the *C5 pseudoradical* center is created, it induces the easy rupture of the C1–N2 double bond. This reactivity behaviour is characteristic of radical species; v) formation of the first C1–C5 single bond begins at a distance of 1.94 \AA through a C-to-C coupling of two C1 and C5 *pseudoradical* centers⁶¹ (see **P4n** and **P5n** in Figure 3.14). Interestingly, the *C5 pseudoradical* center participates with a high electron density, $0.89e$, in the formation of the new C1–C5 single bond; vi) however, formation of the second O3–C4 single bond begins at a distance of 1.75 \AA by donation of non-bonding electron density of the O1 oxygen present in the Ni framework to the C2 carbon of the allene fragment, similar to previous O–C bond formations⁸³ (see **P8n** and **P9n** in Figure 3.14); and finally, vii) formation of the second O3–C4 single bond takes place at the end of the reaction path once the first C1–C5 single bond has already been formed (see Table 8 in Appendix). This fact allows characterising the molecular mechanism of this 32CA reaction as a non-concerted *two-stage one-step* mechanism⁷⁷ associated to the attack of the *pseudoradical* allenic C5 carbon of CHDE **50** onto the C1 carbon of Ni **51** which, after the complete C1–C5 single bond formation, experiences a rapid ring-closure process.

A comparative analysis of the BET studies of the non-polar 32CA reactions between Ni **51** and allenes **50** and **54** made it possible to explain the high reactivity of strained cyclic allene CHDE **50**. The non-polar 32CA reaction between Ni **51** and the simplest allene **54** begins with the rupture of the Ni C1–N2 double bond (see Figure 3.15a and Scheme 6.4 in Appendix). However, a completely different scenario was

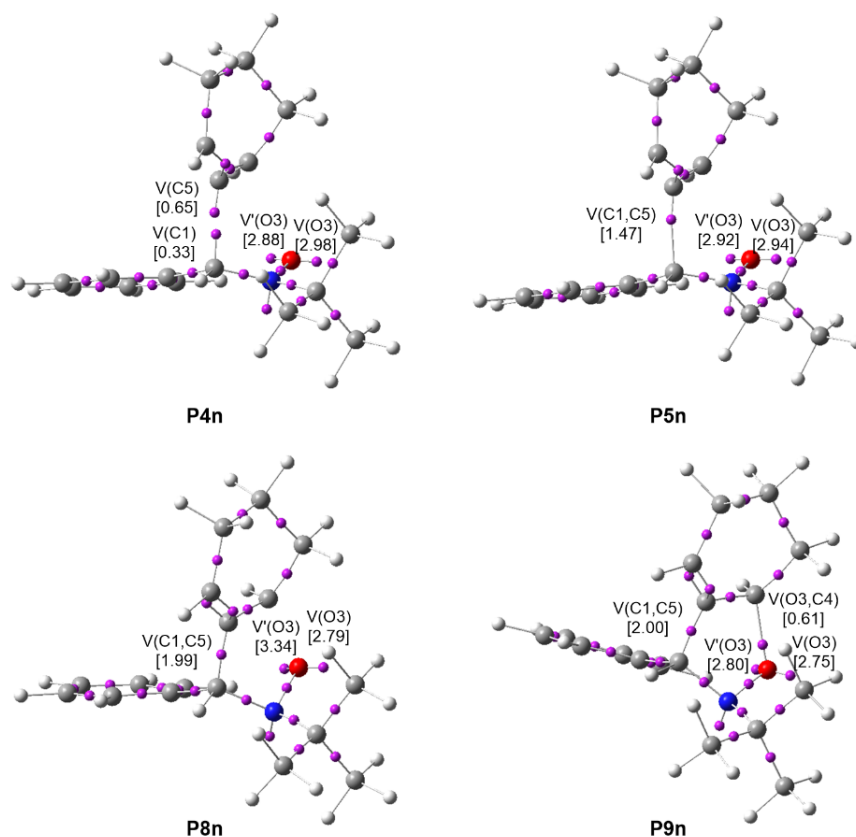


Figure 3.14. ELF attractor positions for the points of the IRC defining the four phases involved in the formation of the C1–C5 and O3–C4 single bonds along the most favourable *endo/r1* reaction path associated with the 32CA reaction between Ni **51** and strained allene CHDE **50**. The electron populations, in average number of electrons (e), are given in brackets.

found along the non-polar 32CA reaction between Ni **51** and strained allene CHDE **50**; at the beginning of the reaction, CHDE **50** becomes a *pseudoradical* species⁶⁷ (see Figure 3.15b and Scheme 6.5 in Appendix), which explains the high reactivity of strained allenes in cycloaddition reactions.⁹⁰ Consequently, we can conclude that, from an MEDT⁵⁵ perspective, the geometrical predistortion of the strained allene CHDE **50** is not responsible for the high reactivity of this species as previously proposed,⁸⁹ but the change of reactivity of the strained CHDE **50**, which, with a relatively low EC of 8.3 kcal·mol⁻¹, behaves as a radical species rather than an ethylene derivative, as occurs in the case of linear allene **54**. The present MEDT⁵⁵ study allowed establishing that the radical character of CHDE **50** acquired at the beginning of the reaction notably favours the corresponding non-polar *zw-type* 32CA reaction.

3. Results and discussion

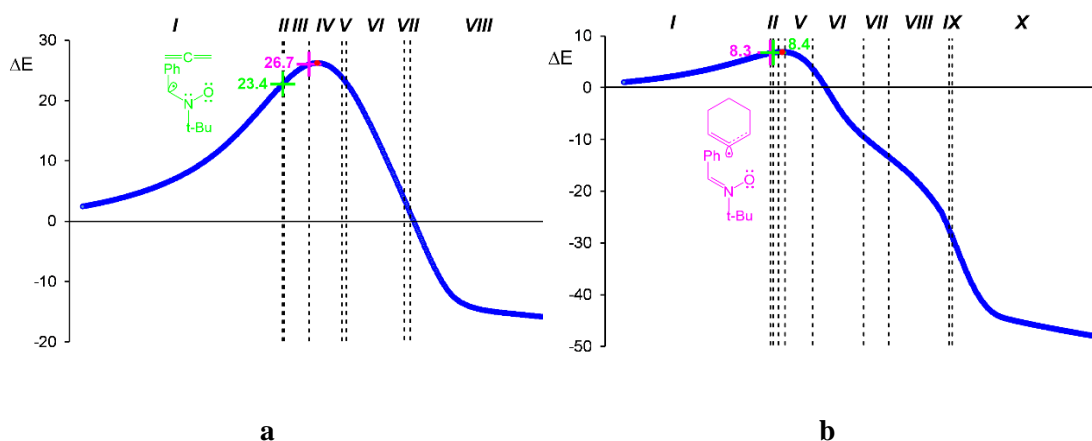
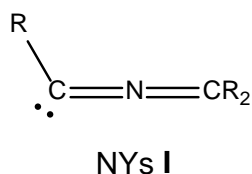


Figure 3.15. Relative energy (ΔE , in $\text{kcal}\cdot\text{mol}^{-1}$) variations along the IRC associated with a) the regioisomeric *r1* reaction path of the 32CA reaction between Ni **51** and the simplest allene **54** and b) the most favourable *endo/r1* reaction path of the 32CA reaction between Ni **51** and strained allene CHDE **50**. Black dashed lines separate the topological phases along the IRC, the red point indicates the position of the TS and the green and magenta lines show the relative position of the points of the IRC associated with the formation of the C1 and C5 *pseudoradical* centers, respectively. Relative energies are given with respect to the separated reagents, while the ECs are relative to the corresponding molecular complexes.

3.2. 32CA reactions of carbenoid TACs

Carbenoid TACs are species containing a carbenoid center, i.e. a neutral carbon presenting a non-bonding electron density of ca. $2e$ (see Scheme 3.12). They are able to participate in *cb-type* 32CA reactions with electrophilic ethylene derivatives presenting an EWG group. Propargylic NYs **I** are a typical example of carbenoid TACs.

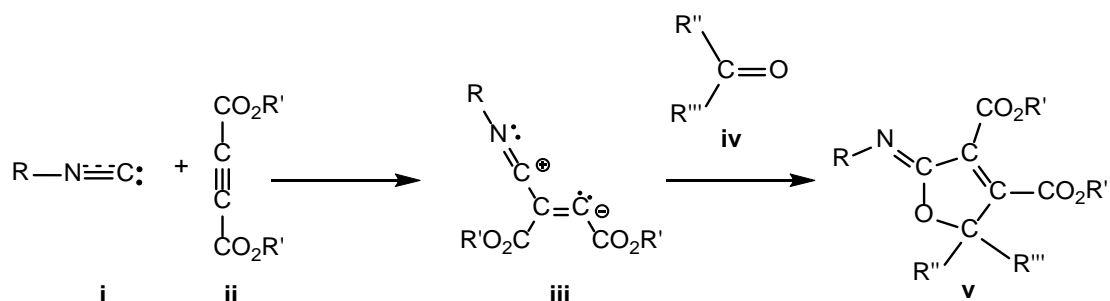


Scheme 3.12. Lewis structure of carbenoid TACs.

3.2.1. Formal 32CA reactions of carbonyl compounds with nucleophilic carbenoid intermediates generated from carbene isocyanides⁸⁴

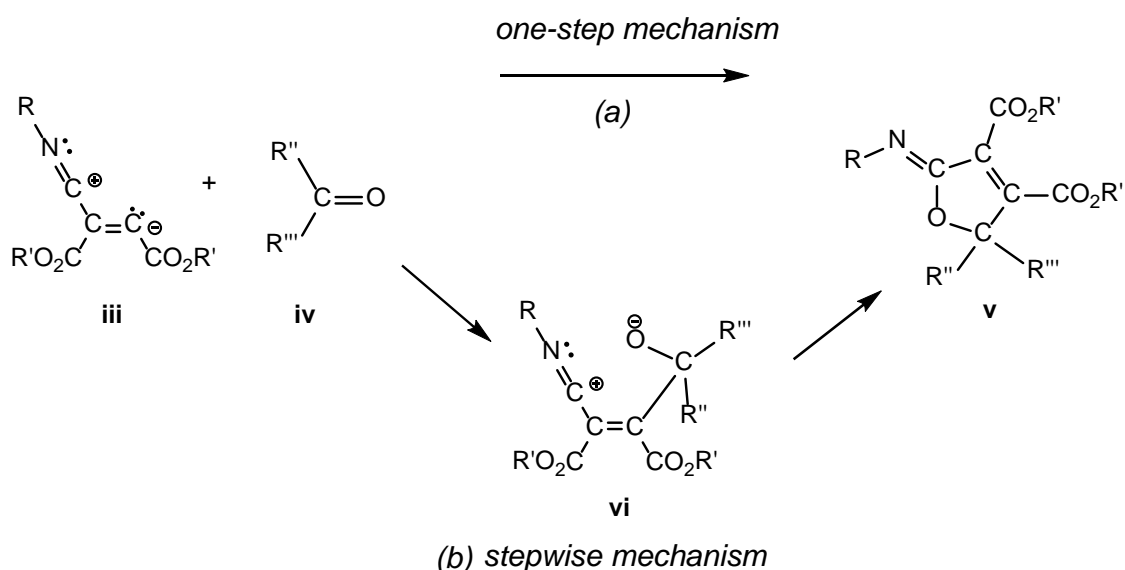
Carbene isocyanides **i** are essential building blocks in modern organic chemistry,⁹¹ and it has been reported that these species nucleophilically attack dialkyl acetylenedicarboxylates **ii** yielding zwitterionic species **iii**, which act as crucial

intermediates. These reactive intermediates are readily trapped by several kinds of electrophilic carbon molecules⁹² such as aldehydes,^{92b} ketones,^{92c,d} esters,^{92e} and sulfonylimines,⁹³ even carbon dioxide.⁹⁴ When electrophilic molecules are carbonyl derivatives **iv**, the reaction products are 2-imino-furan derivatives **v** (see Scheme 3.13).



Scheme 3.13. Multicomponent domino reaction between carbene isocyanides **i**, acetylenedicarboxylates **ii** and carbonyl derivatives **iv**.

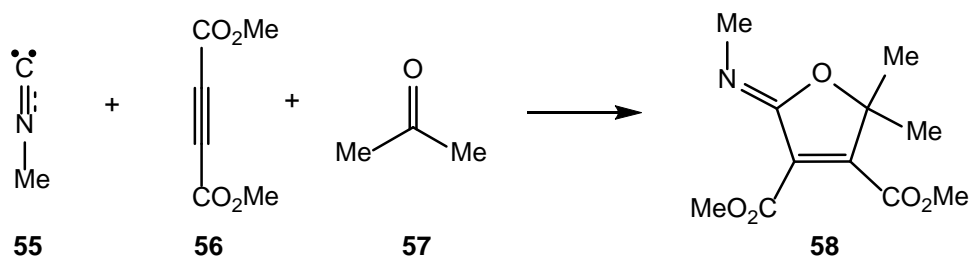
The second step of this domino process was associated with a “1,3-dipolar” cycloaddition reaction, for which two mechanisms were proposed^{92b-d} (see Scheme 3.14): i) a one-step mechanism in which the C–C and C–O bonds are formed in a single step but asynchronously,^{92d} and ii) a stepwise mechanism in which a new zwitterionic intermediate **vi** is formed through the nucleophilic attack of zwitterionic intermediate **iii** on carbonyl derivative **iv**; the subsequent cyclisation in this intermediate will yield 2-imino-furan derivative **v**.^{92c}



Scheme 3.14. Proposed mechanisms for the “1,3-dipolar” cycloadditions of intermediate **iii** with carbonyl derivatives **iv**.

3. Results and discussion

Due to the high reactivity evidenced by intermediate **iii** and the significance of the formation of 2-imino-furans **v** through these reactions involving a large diversity of carbonyl derivatives **iv**,^{92b-e,94} an MEDT⁵⁵ study of the multicomponent domino reaction between methyl isocyanide **55**, DMAD **56** and acetone **57** yielding 2-imino-furan **58**, as a model, was performed at the MPWB1K/6-311G(d,p) computational level (see Scheme 3.15)



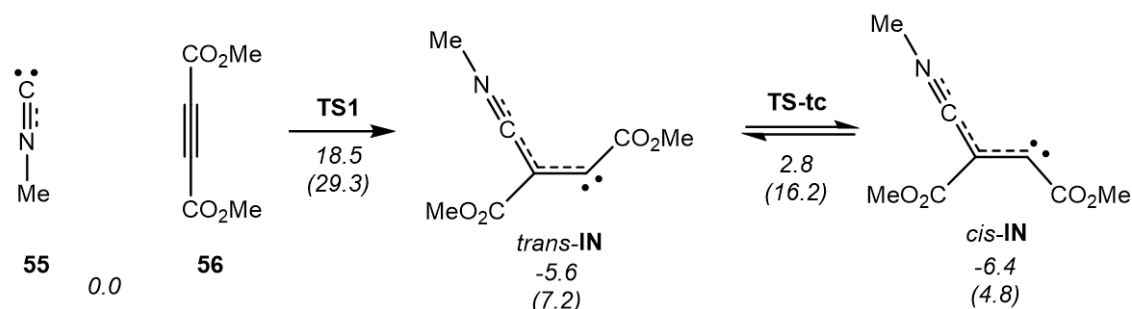
Scheme 3.15. Selected reaction model for the multicomponent domino reaction between isocyanides **i**, acetylenedicarboxylate derivatives **ii** and carbonyl compounds **iv**.

3.2.1.1. Study of the energy profile of the multicomponent reaction between methyl isocyanide **55**, DMAD **56** and acetone **57**

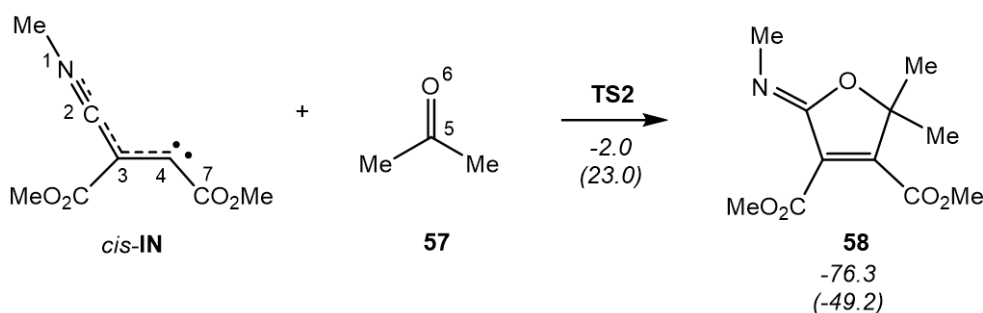
The multicomponent reaction between methyl isocyanide **55**, DMAD **56** and acetone **57** yielding 2-imino-furan **58** is a domino process that comprises two consecutive addition reactions (see Scheme 3.16). The first one is the nucleophilic attack of carbene methyl isocyanide **55** on one of the two electrophilic acetylenic carbons of DMAD **56** to yield intermediate *trans*-**IN**, which, after isomerisation to intermediate *cis*-**IN**, attacks acetone **57** along the second addition reaction.

Some interesting conclusions were drawn from the thermodynamic data given in Scheme 3.16 and the Gibbs free energy profile represented in Figure 3.16: i) the first nucleophilic attack of carbene isocyanide **55** on DMAD **56** is the RDS of this domino process; ii) intermediate *trans*-**IN** quickly isomerises, via **TS-tc**, to *cis*-**IN**, which is 2.4 kcal·mol⁻¹ more stable and whose *cis* disposition is required for the following cycloaddition reaction with acetone **57** to occur; iii) the activation Gibbs free energy of the cycloaddition reaction of intermediate *cis*-**IN** with acetone **57** via **TS2** is 6.3 kcal/mol lower than that of the RDS of the domino process via **TS1**; iv) the strong exergonic character of the cycloaddition reaction between *cis*-**IN** and acetone **57** makes this process irreversible; and v) although the formation of intermediate *cis*-**IN** is slightly endergonic,

a) formation of the carbene intermediate *cis-IN*



b) addition of the carbene intermediate *cis-IN* to acetone **57**



Scheme 3.16. Domino reaction between methyl isocyanide **55**, DMAD **56** and acetone **57**. MPWB1K/6-311G(d,p) relative enthalpies and Gibbs free energies (in parentheses), computed at 25 °C and 1 atm in acetonitrile, with respect to **55**, **56** and **57**, are given in kcal·mol⁻¹.

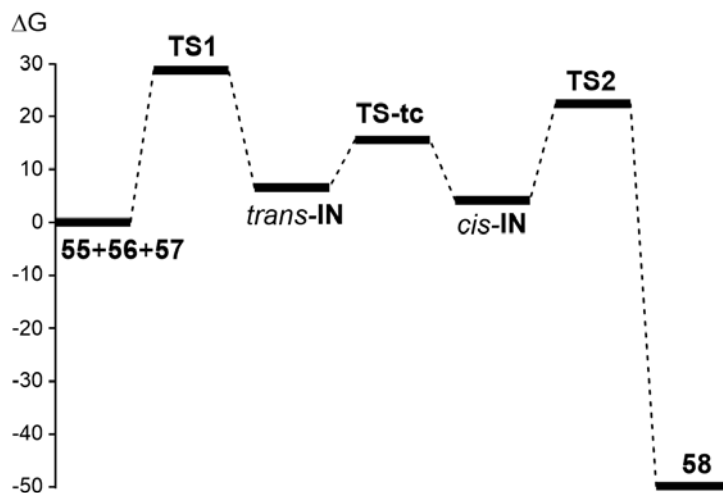


Figure 3.16. MPWB1K/6-311G(d,p) Gibbs free energy profile (ΔG , in kcal·mol⁻¹), computed at 25 °C and 1 atm in acetonitrile, of the domino reaction between methyl isocyanide **55**, DMAD **56** and acetone **57**.

3. Results and discussion

as soon as it is formed it is quickly and irreversibly captured by acetone **57** yielding 2-imino-furan **58**. Accordingly, the multicomponent reaction between isocyanide **55**, DMAD **56** and acetone **57** is kinetically and thermodynamically very favourable.

The geometries of the TSs involved in the domino reaction between methyl isocyanide **55**, DMAD **56** and acetone **57** in acetonitrile are displayed in Figure 3.17. The IRC from **TS2** towards the final 2-imino-furan **58** indicated that the second reaction of this multicomponent process is associated with a *two-stage one-step* mechanism⁷⁷ in which the C4–C5 single bond is completely formed before the formation of the second C2–O6 single bond starts (see later). This finding allowed ruling out the proposed two-step mechanism for the second addition reaction. In addition, this IRC also showed that the carbonyl C5–O6 bond of acetone **57** approaches to intermediate *cis*-**IN** in the C2–C3–C4 plain, in which the two C4–C5 and C2–O6 single bonds will be formed (see **TS2** in Figure 3.17). This approach mode is different to that demanded in “1,3-dipolar” cycloadditions, in which the “dipolarophile” approaches above the plain of the “1,3-dipole”.

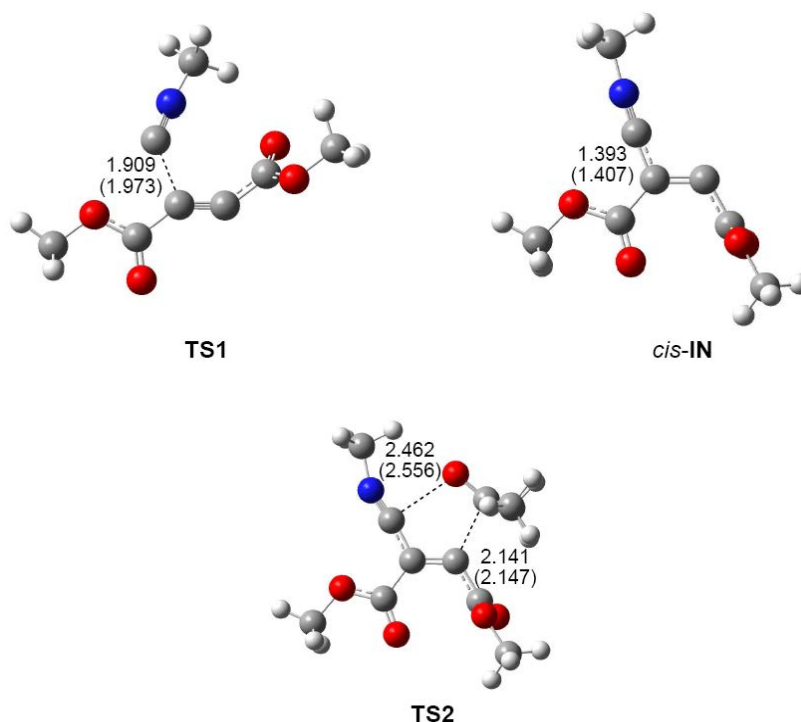


Figure 3.17. MPWB1K/6-311G(d,p) gas phase optimised geometries of the most important stationary points involved in the domino reaction between methyl isocyanide **55**, DMAD **56** and acetone **57**. Distances are given in angstroms, Å, while those in acetonitrile are given in parentheses.

Finally, the computed GEDT⁶¹ values, 0.26e at **TS1**, 0.62e at *trans*-**IN** and 0.26e at **TS2**, emphasised the high polar nature of the domino reaction between methyl isocyanide **55**, DMAD **56** and acetone **57**.

3.2.1.2. Analysis of the CDFT reactivity indices at the GS of the reagents and intermediate *cis*-**IN**

CDFT reactivity indices⁵⁶ of the species involved in the domino reaction between methyl isocyanide **55**, DMAD **56** and acetone **57** are gathered in Table 3 in Appendix. The electronic chemical potential of carbene isocyanide **55**, -3.90 eV, is higher than that of DMAD **56**, -5.01 eV, indicating that along a polar reaction the GEDT⁶¹ will flux from the carbene isocyanide framework, acting as the nucleophile, towards the acetylene one, acting as the electrophile. In the same way, the higher electronic chemical potential of intermediate *cis*-**IN**, -3.58 eV, than that of acetone **57**, -3.72 eV, suggests that along the subsequent cycloaddition reaction, the GEDT will flux towards the ketone framework.

According to the electrophilicity⁶² and nucleophilicity⁷⁶ scales, methyl isocyanide **55** is classified on the borderline of moderate electrophiles and as a marginal nucleophile, $\omega = 0.66$ eV and $N = 0.77$ eV, while DMAD **56** is classified as a strong electrophile and as a marginal nucleophile $\omega = 1.40$ eV and $N = 0.91$ eV. In spite of the strong electrophilic character of DMAD **56**, the low nucleophilic character of isocyanide **55** accounts for the high activation energy associated with the nucleophilic addition of isocyanide **55** to DMAD **2** (see above). *cis*-**IN**, $\omega = 1.06$ eV and $N = 3.80$ eV, is classified on the borderline of strong electrophiles and as a strong nucleophile. Finally, acetone **57**, $\omega = 0.77$ eV and $N = 2.16$ eV, behaves as a moderate electrophile and a moderate nucleophile. Thus, the low electrophilic character of acetone **57** demands its electrophilic activation in order to participate in polar reactions.

Regarding the local reactivity, analysis of the nucleophilic P_k^- Parr functions⁸² of carbene isocyanide **55** and *cis*-**IN** (see Figure 3.18) showed that the C2 carbon of isocyanide **55** and the C4 carbon of intermediate *cis*-**IN** are the most nucleophilic centers of these species. On the other hand, analysis of the electrophilic P_k^+ Parr functions⁸² of DMAD **56** indicated that the acetylene C3 and C4 carbons are ca. twice as electrophilically activated as the carbonyl carbons. Finally, acetone **57** presents its electrophilic activation at the carbonyl carbon. Consequently, the most favourable

3. Results and discussion

electrophile-nucleophile interaction along the nucleophilic attack of carbene isocyanide **55** on DMAD **56** will take place between the C2 carbon of isocyanide **55** and the C3 or C4 carbons of DMAD **56**. Likewise, the most favourable bond formation along the nucleophilic attack of intermediate *cis*-**IN** on acetone **57** will take place between the C4 carbon of the former and the electrophilic carbon of the latter.

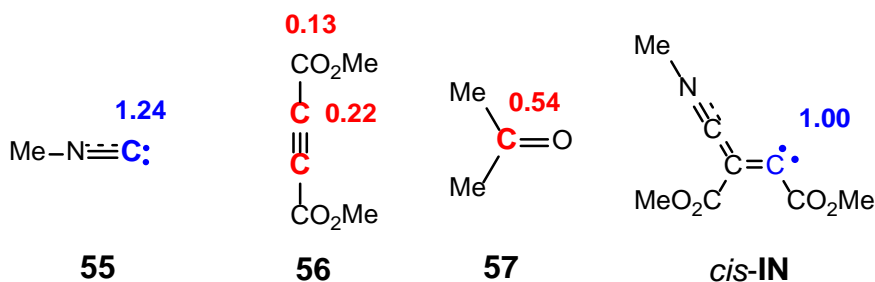


Figure 3.18. Nucleophilic P_k^- Parr functions, in blue, and electrophilic P_k^+ Parr functions, in red,⁸² of methyl isocyanide **55**, DMAD **56**, acetone **57** and intermediate *cis*-**IN**.

Thus, analysis of the CDFT reactivity indices of the species involved in the model domino reaction between methyl isocyanide **55**, DMAD **56**, acetone **57** made it possible to explain the experimentally observed reactivity in the multicomponent reaction between carbene isocyanides **i**, acetylenedicarboxylates **ii** and carbonyl derivatives **iv**.

3.2.1.3. BET study of the domino reaction between methyl isocyanide **55**, DMAD **56** and acetone **57**

BET data are gathered in Tables 9 and 10 in Appendix, while simplified representations of the molecular mechanisms arising from the BET study are shown in Schemes 6.6 and 6.7. From the BET study of this domino reaction, the following conclusions were drawn: i) along the nucleophilic attack of methyl isocyanide **55** on DMAD **56**, the C2–C3 bond is formed with a high electron density, 2.55e, at a distance of 1.90 Å, by donation of the electron density of the carbene C2 center to one of the two acetylenic carbons of DMAD **56** (see Figure 3.19); ii) as the consequence of the depopulation of the acetylenic C3–C4 triple bond, a new V(C4) monosynaptic basin appears at the C4 carbon with an initial population of 0.52e. This V(C4) monosynaptic basin reaches 2.06e at intermediate *cis*-**IN**; iii) along the nucleophilic attack of *cis*-**IN** on acetone **57**, formation of the C4–C5 single bond begins at a distance of 2.14 Å through by donation of the electron density of the carbenoid C4 center of *cis*-**IN** to the carbonyl C5 carbon of acetone **57** (see Figure 3.20); iv) formation of the third C2–O6 single bond begins at the end of the cycloaddition

path at a distance of 1.75 Å by donation of part of the non-bonding electron density of the carbonyl O6 oxygen to the C2 carbon (see Figure 3.20); and finally, v) formation of the C2–O6 single bond begins after the almost complete formation of the C4–C5 one by above 98% (see Table 10 in Appendix), characterising the mechanism of the cycloaddition reaction as a non-concerted *two-stage one-step* mechanism.⁷⁷

Both, analysis of the atomic movements of the *cis*-**IN** and acetone **57** molecules along the IRC associated with the cycloaddition step and the corresponding BET analysis, indicated that the N1–C2 triple bond and C3–C4 double bond regions of intermediate *cis*-**IN** do not actively participate in the cycloaddition reaction, as expected in a “1,3-dipole” participating in a “1,3-dipolar” cycloaddition, but the carbenoid C4 carbon and the carbonyl O6 oxygen. Consequently, this cycloaddition should be classified as a [2n+2n], in which only two lone pairs are involved, instead of a [4π+2π], as proposed in a “1,3-dipolar” cycloaddition.⁴⁶

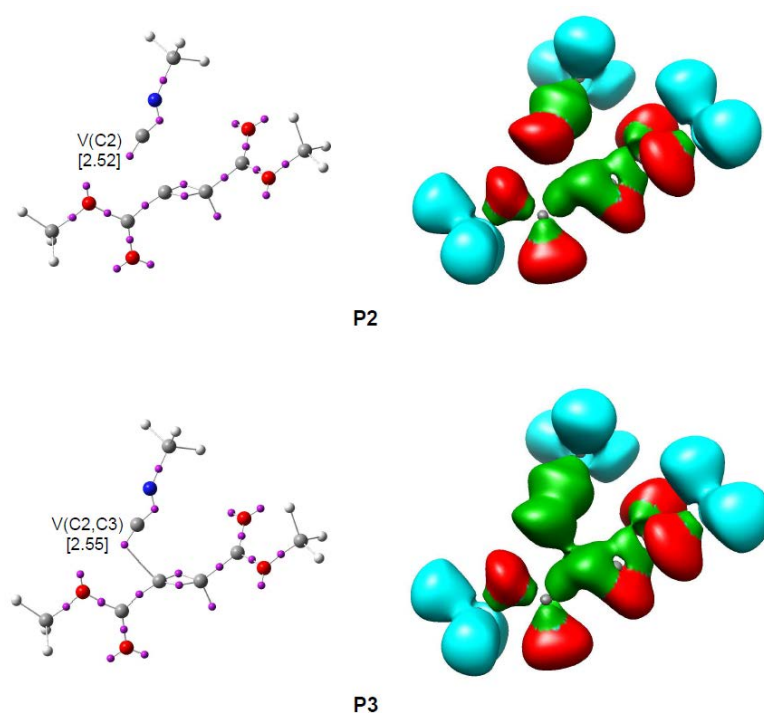


Figure 3.19. ELF basin attractor positions and localisation domains for the most relevant points along the IRC associated with the formation of the C2–C3 single bond along the nucleophilic addition of methyl isocyanide **55** to DMAD **56**. Disynaptic basins are coloured in green and monosynaptic basins in red. The electron populations, in average number of electrons (e), are given in brackets.

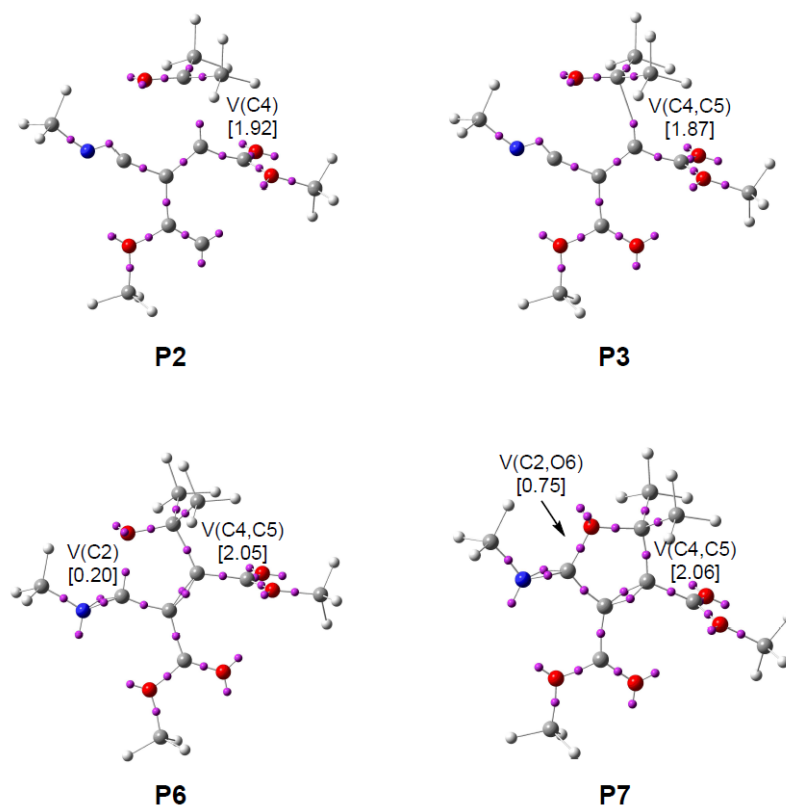
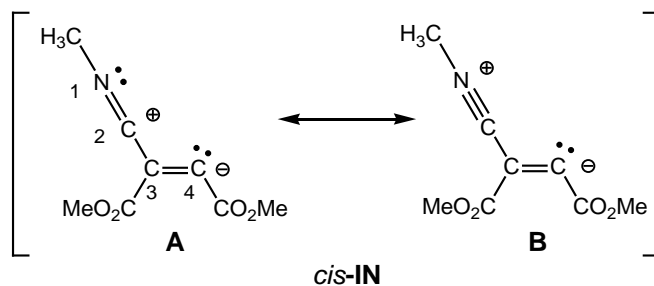


Figure 3.20. ELF attractor positions for the most relevant points along the IRC associated with the formation of the C4–C5 and C2–O6 single bonds along the cycloaddition reaction of intermediate *cis*-**IN** with acetone **57**. The electron populations, in average number of electrons (e), are given in brackets.

3.2.1.4. The electronic structure of intermediate *cis*-**IN** and the origin of the high reactivity of carbonyl compounds towards this intermediate

At first, intermediate *cis*-**IN** can be represented by either of the resonance Lewis structures, **A** and **B**, given in Scheme 3.17. Experimental chemists represent *cis*-**IN** by means of the 1,3-zwitterionic structure **A**, since it justifies the participation of *cis*-**IN** in a 32CA reaction with carbonyl derivatives **iv**.



Scheme 3.17. Lewis structures representing zwitterionic intermediate *cis*-**IN**.

Both NPA and ELF analyses of the electronic structure of the intermediate *cis*-**IN** yielded a different representation for this intermediate (see Figure 3.21). In spite of the zwitterionic character of intermediate *cis*-**IN**, the high reactivity of this intermediate towards carbonyl compounds **iv** could not be related to its zwitterionic character but rather to the singlet carbenoid character of the C4 carbon that grants a high nucleophilic character to this molecule.

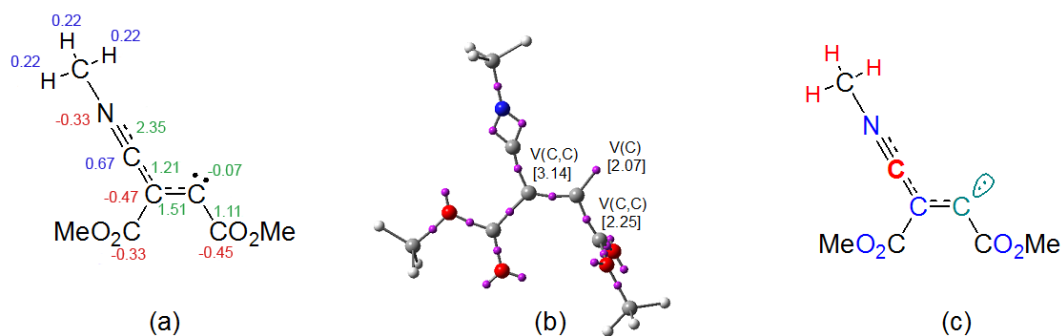


Figure 3.21. Representation of the electronic structure of carbenoid intermediate *cis*-**IN** based on (a) NPA, (b) ELF and (c) the mixture of both analyses. Green values in (a) indicate the bond order of the corresponding bond.

MEP of *cis*-**IN** showed that the highest positive region corresponds to the methyl substituent present in the isocyanide framework (see Figure 3.22a). The MEP of **TS2** showed that along the nucleophilic attack of *cis*-**IN** on acetone **57**, the GEDT that takes place in this polar process gives rise to an increase of electron density at the carbonyl oxygen, in agreement with the Parr functions.⁸² This feature, which is unfavourable in a non-catalysed nucleophilic addition to carbonyl compounds, is favoured in **TS2** by the presence of the positively charged methyl group, which electrostatically stabilises the negative charge developed at the carbonyl oxygen (see Figure 3.22b).

Although some weak interactions between the carbonyl oxygen and the methyl isocyanide framework were revealed by NCI,⁵⁹ no hydrogen bond interaction was observed. Consequently, the high reactivity of intermediate *cis*-**IN** towards carbonyl derivatives **iv** is due to two specific features: i) the carbenoid character of the sp^2 hybridised C4 carbon more than the negative charge on a carbanionic center, and ii) the special geometric disposition of the alkyl substituents in isocyanides **i** that electrostatically favours the GEDT along the nucleophilic attack of these nucleophilic carbenoid intermediates **iii** on carbonyl compounds **iv**.

3. Results and discussion

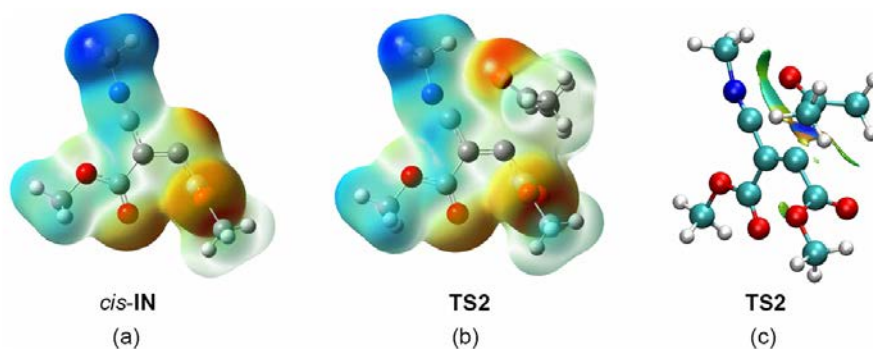
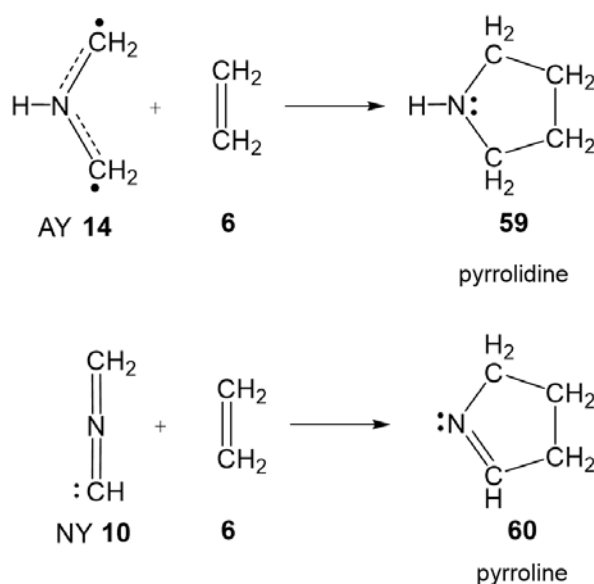


Figure 3.22. MEP of carbenoid intermediate *cis*-IN (a) and TS2 (b), and NCI at TS2 (c).

3.2.2. 32CA reactions of NYs I with electrophilic ethylenes⁹⁵

Pyrrolidine **59** and pyrroline **60** are five-membered heterocyclic compounds, containing only one nitrogen nucleus in their core framework, of great pharmaceutical importance.⁹⁶ These compounds can easily be synthesised by a 32CA reaction of AY **14**, an A-TAC, or NY **10**, a P-TAC, with ethylene **6** (see Scheme 3.18).



Scheme 3.18. 32CA reactions of the simplest AY **14** and NY **10** with ethylene **6**.

The simplest AY **14** is one of the most reactive TACs participating in 32CA reactions with ethylene **6**. Topological analysis of the ELF of AY **14** made it possible to establish its *pseudodiradical* character (see the four V(C) monosynaptic basins at the two carbons of AY **14** in Figure 3.23), which allows its participation in *pdr*-type 32CA reactions.⁶⁴

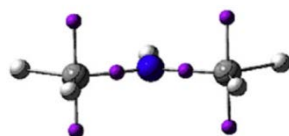
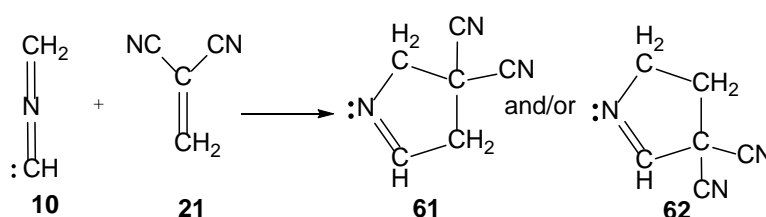


Figure 3.23. ELF attractor positions at AY **14**.

However, the electronic structure and reactivity of NY **10** remained unexplored. In order to characterise the electronic structure of NY **10** and its reactivity, the 32CA reactions of NY **10** with ethylene **6** and DCE **21** were studied within MEDT⁵⁵ at the MPWB1K/6-31G(d) computational level (see Schemes 3.18 and 3.19).



Scheme 3.19. 32CA reaction of NY **10** with DCE **21** yielding pyrrolines **61** and/or **62**.

3.2.2.1. Topological analysis of the ELF and NPA of NY **10**

ELF topology of the simplest NY **10** reveals a different electronic structure to that of AY **14**, which has a *pseudodiradical* Lewis structure (see Figure 3.23). Interestingly, the C1 carbon presents a V(C1) monosynaptic basin integrating 1.95e, which can be related to a non-bonding sp^2 hybridised lone pair (see the red V(C1) monosynaptic basin in Figure 3.24). In addition, NPA of C1 indicates that this carbon practically presents a null charge. This behaviour, together with the slight negative charge of the C3 carbon, $-0.22e$, as well as the presence of two V(C1,N2) and V(N2,C3) disynaptic basins integrating 4.00e and 3.50e, suggests an allenic structure with a strong carbenoid character (see Figure 3.24), instead of the commonly accepted propargylic structure.

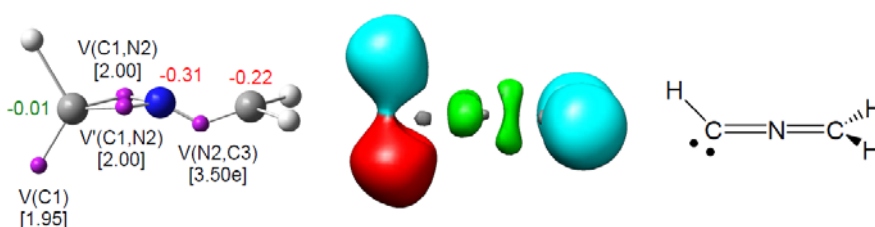


Figure 3.24. ELF valence basin attractors, together with the valence basin populations and natural atomic charges, ELF localisation domains and the proposed carbenoid Lewis structure of NY **10**. Negative charges are coloured in red and negligible charges in green. ELF valence basin population and natural atomic charges are given in average number of electrons, e.

3. Results and discussion

3.2.2.2. Analysis of the CDFT reactivity indices at the GS of the reagents

CDFT reactivity indices⁵⁶ of NY **10**, ethylene **6** and DCE **21** are gathered in Table 3 in Appendix. The electronic chemical potential of NY **10**, -2.90 eV, is considerably higher than that of DCE **21**, -5.64 eV, indicating that along a polar reaction with DCE **21** the GEDT⁶¹ will flux from the NY framework towards the electrophilic ethylene one. Note that the similar electronic chemical potentials of NY **10** and ethylene **6**, -3.37 eV, suggests that ethylene **6** will hardly participate in a polar reaction with NY **10**.

According to the electrophilicity⁶² and nucleophilicity⁷⁶ scales, the simplest NY **10**, $\omega = 0.77$ eV and $N = 3.50$ eV, is classified as a marginal electrophile and a strong nucleophile, DCE **21**, $\omega = 2.82$ eV and $N = 0.65$ eV, as a strong electrophile and a marginal nucleophile, while ethylene **6** cannot participate in polar reactions (see Table 3 in Appendix). Thus, analysis of the global reactivity indices indicates that NY **10** will participate as the nucleophilic species in the polar 32CA reaction with electrophilic DCE **21**.

Regarding the local reactivity, analysis of the nucleophilic P_k^- Parr functions⁸² at the simplest NY **10** indicated that the carbenoid C1 carbon is the most nucleophilic center of this species, although the C3 carbon also presents a strong nucleophilic activation (see Figure 3.25). On the other hand, the electrophilic P_k^+ Parr functions⁸² of DCE **21** indicate that the non-substituted C4 carbon is the most electrophilic center of this electrophilic ethylene. Therefore, the most favourable electrophile-nucleophile interaction along the nucleophilic attack of NY **10** on DCE **21** will take place between the most nucleophilic center of the nucleophile NY **10**, the carbenoid C1 carbon, and the most electrophilic center of the electrophile DCE **21**, the C4 carbon.

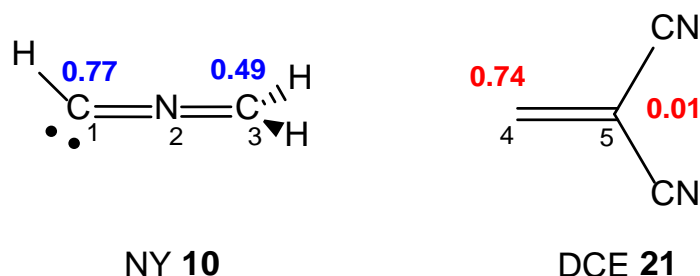
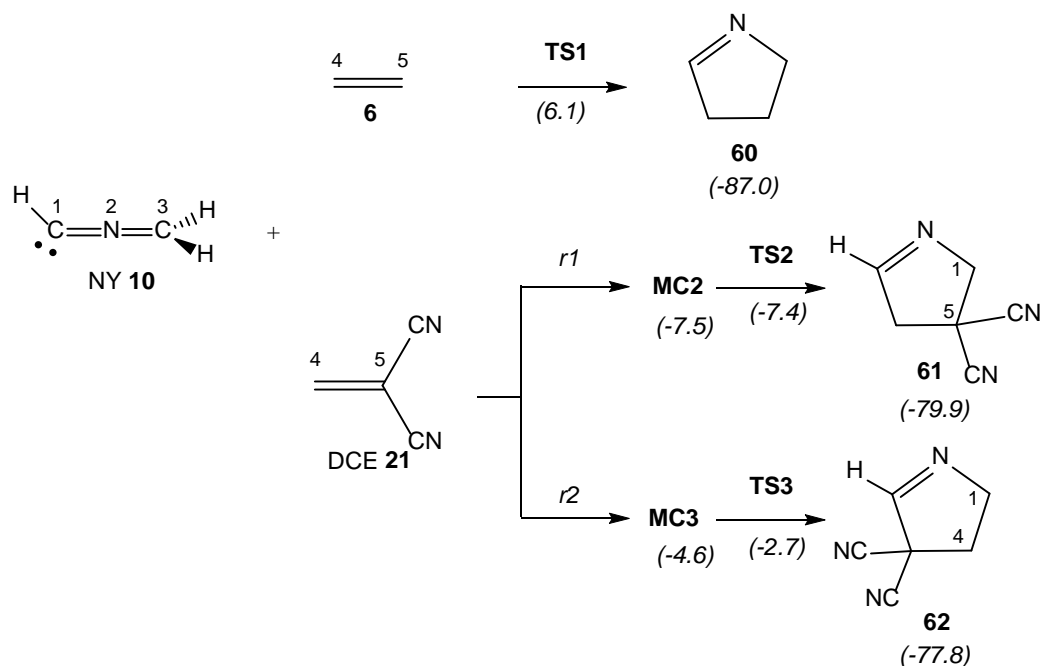


Figure 3.25. Nucleophilic P_k^- Parr functions of NY **10**, in blue, and electrophilic P_k^+ Parr functions,⁸² in red, of DCE **21**.

3.2.2.3. Analysis of the reaction paths associated with the 32CA reactions of NY **10** with ethylene **6** and DCE **21**

Due to the symmetry of ethylene **6**, the 32CA reaction involving ethylene **6** can take place only through one single reaction path, while the non-symmetry of both reagents in the 32CA reaction involving DCE **21** causes this reaction to take place through two regioisomeric pathways. As Scheme 3.20 shows, analysis of the stationary points involved in these 32CA reactions indicates that they take place through a one-step mechanism.



Scheme 3.20. 32CA reactions of NY **10** with ethylene **6** and DCE **21**. MPWB1K/6-31G(d) gas phase relative electronic energies, in kcal·mol⁻¹, are given with respect to the separated reagents.

While the 32CA reaction of NY **10** with ethylene **6** presents a relatively low activation energy, 6.1 kcal·mol⁻¹, the most favourable regioisomeric TS associated with the polar 32CA reaction of NY **10** with DCE **21** is found 7.4 kcal·mol⁻¹ below the separated reagents, the reaction being completely regioselective as **TS2** is 4.7 kcal·mol⁻¹ below **TS3**. Both 32CA reactions are strongly exothermic. Note that the activation energy of the non-polar 32CA reaction is ca. 7.5 kcal·mol⁻¹ higher than that of the *pdr*-type 32CA reaction of the simplest AY **14** with ethylene **6** and ca. 4.3 kcal·mol⁻¹ lower than that of the *zw*-type 32CA reaction of the simplest Ni **16** with ethylene **6**, emphasising the different reactivity of NY **10**.

3. Results and discussion

Some appealing conclusions were obtained from the geometries of the TSs involved in the 32CA reactions of NY **10** with ethylene **6** and DCE **21** (see Figure 3.26): i) the long distances between the interacting nuclei at the three TSs indicated that these TSs appear very early; ii) at **TS2** and **TS3**, the difference between the lengths of the two forming bonds showed that they correspond to asynchronous TSs; iii) the most favourable **TS2** is more asynchronous; and iv) the shortest C–C distance at both TSs corresponds to the C–C bond formation at the most electrophilic β -conjugated carbon of DCE **21**, i.e. the electrophilic species controls the asynchronicity of the formation of the two new C–C single bonds.

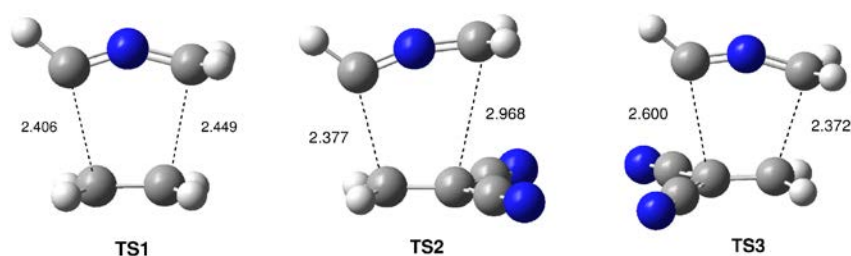


Figure 3.26. MPWB1K/6-31G(d) gas phase optimised geometries of the TSs involved in the 32CA reaction of NY **10** with ethylene **6** and DCE **21**. Distances are given in angstroms, Å.

In order to evaluate the electronic nature of the 32CA reaction of NY **10** with ethylene **6** and DCE **21**, the GEDT at the TSs was analysed.⁶¹ At **TS1**, there is a slight GEDT from the NY to the ethylene one, 0.11e. This GEDT value can be considered as some delocalisation of the electron density of the highly nucleophilic NY **10** into the ethylene fragment, instead of a GEDT process associated with a polar process. Conversely, there is a clear GEDT taking place from the nucleophilic NY **10** to the electrophilic DCE **21**, 0.24e (**TS2**) and 0.25e (**TS3**), in agreement with a polar 32CA reaction and thereby with the lower activation energies found for the 32CA reaction with DCE **21** than that associated with the low-polar process with ethylene **6**.

3.2.2.4. BET study of the 32CA reactions of NY **10** with ethylene **6** and DCE **21**

A BET study of the 32CA reaction between NY **10** and ethylene **6** (see Table 11 and Scheme 6.8 in Appendix) allowed drawing the following conclusions: i) the IRC is divided in six differentiated phases related to the disappearance or creation of valence basins, emphasising the non-concerted nature of the bonding changes along the reaction; ii) formation of two new C–C single bonds takes place in an almost asynchronous manner

at the beginning of the last phase, but with different electron populations (see Figure 3.27); iii) formation of the C1–C4 single bond begins at a distance of 2.01 Å by donation of the non-bonding electron density present at the sp^2 hybridised C1 carbon of NY **10** to the *pseudoradical* C4 carbon created at ethylene **6** along the reaction path (see Figure 3.27); iv) this bonding pattern demands the depopulation of the C1 non-bonding electron density present in NY **10** in order to achieve the C–C formation with ethylene **6**; v) formation of the C3–C5 single bond begins at a distance of 2.04 Å through the C-to-C coupling of two C3 and C5 *pseudoradical* centers⁶¹ (see Figure 3.27); vi) in this low-polar reaction, the two C4 and C5 *pseudoradical* centers generated in the ethylene framework come mainly from the depopulation of the C4–C5 double bond region of ethylene **6**.

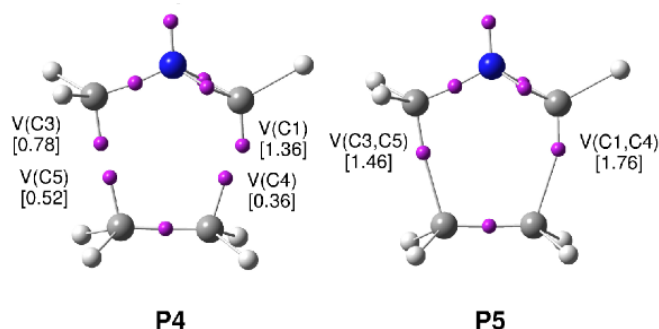


Figure 3.27. ELF attractor positions for the points of the IRC defining the two phases involved in the formation of the C1–C4 and C3–C5 single bonds along the 32CA reaction of NY **10** with ethylene **6**. The electron populations, in average number of electrons (e), are given in brackets.

A BET study of the more favourable *rl* regioisomeric path associated with the 32CA reaction between NY **10** and DCE **21** (see Table 12 and Scheme 6.9 in Appendix) allowed drawing the following conclusions: i) the IRC is divided in nine differentiated phases; ii) formation of the two new C–C single bonds takes place at two well differentiated phases of the reaction; iii) formation of the first C1–C4 single bond begins at a distance of ca. 2.15 Å by donation of the non-bonding electron density belonging to the C1 carbon of NY **10** to the β -conjugated C4 carbon of the DCE moiety (see Figure 3.28); iv) formation of the second C3–C5 single bond begins in the last phase at a distance of ca. 2.19 Å through the C-to-C coupling of the two C3 and C5 *pseudoradical* centers⁶¹ (see Figure 3.28); v) this polar 32CA reaction presents a *two-stage one-step* mechanism,⁷⁷ in which formation of the second C3–C5 begins after the almost complete formation of the first C1–C4 single bond by above 97% (see Table 12 in Appendix).

3. Results and discussion

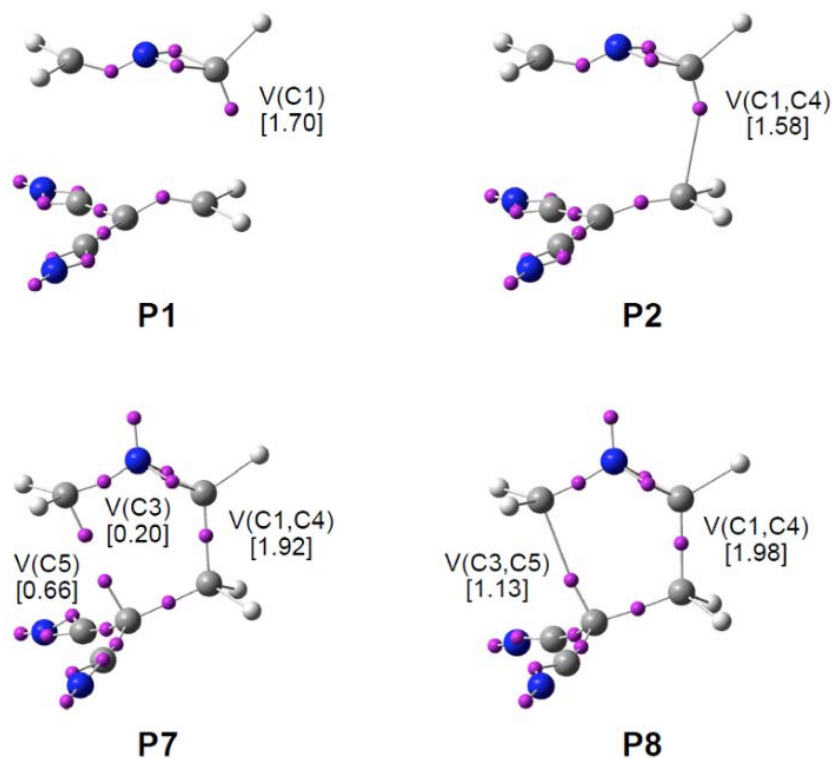


Figure 3.28. ELF attractor positions for the points of the IRC defining the four phases involved in the formation of the C1-C4 and C3-C5 single bonds along the more favourable *r1* regioisomeric pathway associated with 32CA reaction of NY **10** with DCE **21**. The electron populations, in average number of electrons (e), are given in brackets.

A BET study of the less favourable *r2* regioisomeric path associated with the 32CA reaction between NY **10** and DCE **21** (see Table 13 and Scheme 6.10 in Appendix) allowed drawing the following conclusions: i) the IRC is divided in eight differentiated phases; ii) formation of the two C-C single bonds takes place in a more synchronous manner; iii) formation of the first C3-C4 single bond begins at a distance of ca. 2.08 Å through the C-to-C coupling of the two *pseudoradical* centers⁶¹ generated at the C3 carbon of NY **10** and at the C4 carbon of DCE **21** in previous phases (see Figure 3.29); iv) formation of the second C1-C5 single bond begins at the last phase at a distance of ca. 1.96 Å by sharing the non-bonding electron density coming from the C1 carbon of NY **10** and that of a C5 *pseudoradical* center generated at the DCE framework in the previous phase (see Figure 3.29).

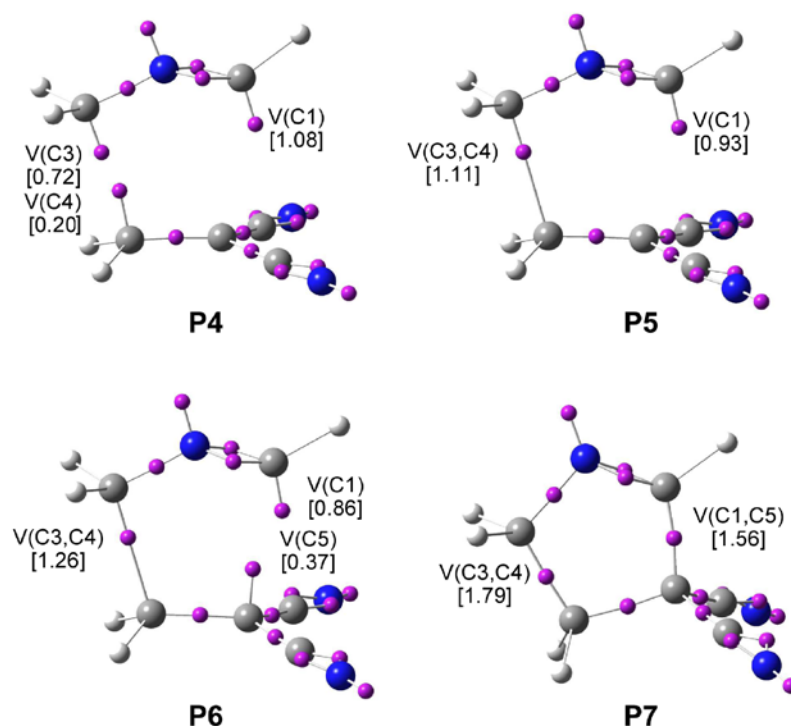


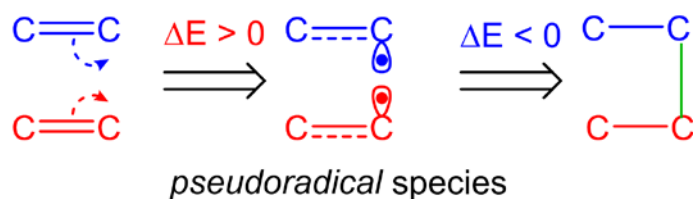
Figure 3.29. ELF attractor positions for the points of the IRC defining the four phases involved in the formation of the C1–C5 and C3–C4 single bonds along the less favourable r_2 regioisomeric pathway associated with 32CA reaction of NY **10** with DCE **21**. The electron populations, in average number of electrons (e), are given in brackets.

3.2.2.5. A new C–C bond formation model involving neutral sp^2 hybridised carbon lone pairs

In 2014, based on the ELF topological analysis of the bonding changes along organic reactions, Domingo proposed a model for the formation of C–C single bonds involving multiple bond systems.⁶¹ This model is characterised by three sequential events related to the sharing of non-bonding electron density (see Scheme 3.21): i) depopulation of the C–C multiple bonds in the two reactant species; ii) creation of two *pseudoradical* centers at the two interacting carbons; and iii) C-to-C coupling of these *pseudoradical* centers yielding the formation of the new C–C single bond. The last event takes place in the short distance range of 2.0 – 1.9 Å, with an initial electron density of ca. 1.0e. In polar reactions, these *pseudoradical* centers appear at the most nucleophilic and electrophilic centers of the two molecules.⁶¹

3. Results and discussion

C-C bond formation involving multiple bond systems



Scheme 3.21. Model for the formation of C–C single bonds involving multiple bond systems by sharing non-bonding electron density.

ELF topological analysis of the C–C single bond formation along the two regioisomeric pathways associated with the polar 32CA reaction of NY **10** with DCE **21** made it possible to characterise two different models for the C–C bond formation along these 32CA reactions. Along the less favourable *r2* reaction path, formation of the first C–C single bond takes place through the C-to-C coupling of two *pseudoradical* centers generated along the reaction at the C3 carbon of NY **10** and at the β -conjugated carbon of DCE **21** (see Scheme 3.21), which is the usual bond formation process involving unsaturated species.⁶¹ Conversely, along the more favourable *r1* regioisomeric reaction path, formation of the first C–C single bond begins by donation of the non-bonding electron density of the C1 carbenoid center of NY **10** to the β -conjugated carbon of DCE **21** (see Figure 3.30). Note that along both regioisomeric paths, the C–C bond formation at the β -conjugation position is more advanced than at the α position; i.e. the asynchronicity in the C–C single bond formation is controlled by the electrophile DCE **21**.⁹⁵

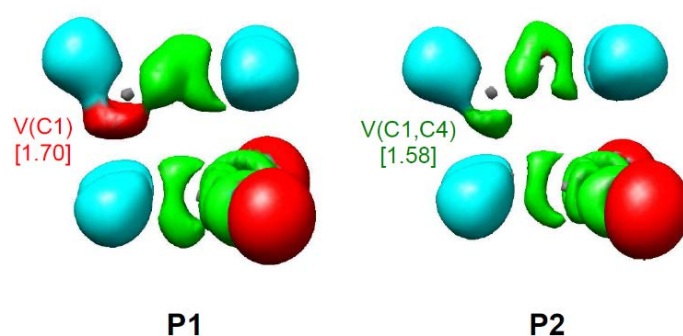
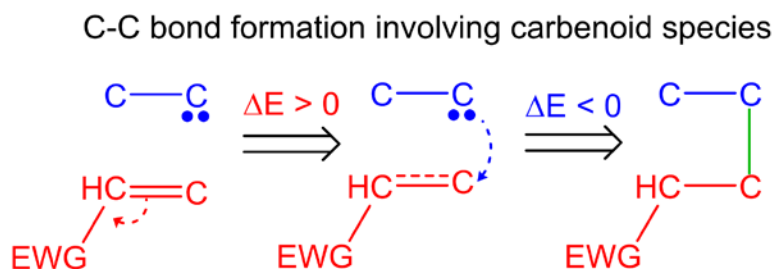


Figure 3.30. ELF localisation domains of the selected points of the IRC, **P1** and **P2**, defining the two phases involved in the formation of the C1–C4 single bond. The electron populations, in average number of electrons (e), are given in brackets.

The carbenoid electronic structure of the simplest NY **10**, different from the *pseudodiradical* structure of AYs **VII** and the zwitterionic structure of Nis **IX**, as well as its reactivity in 32CA reactions, made it possible to introduce not only a new model for the formation of C–C single bonds involving carbenoid species (see Scheme 3.22), but also a new type of 32CA reaction, namely carbenoid-type (*cb-type*) reaction, whose feasibility, similar to *zw-type* 32CA reactions, also depends on its polar character.

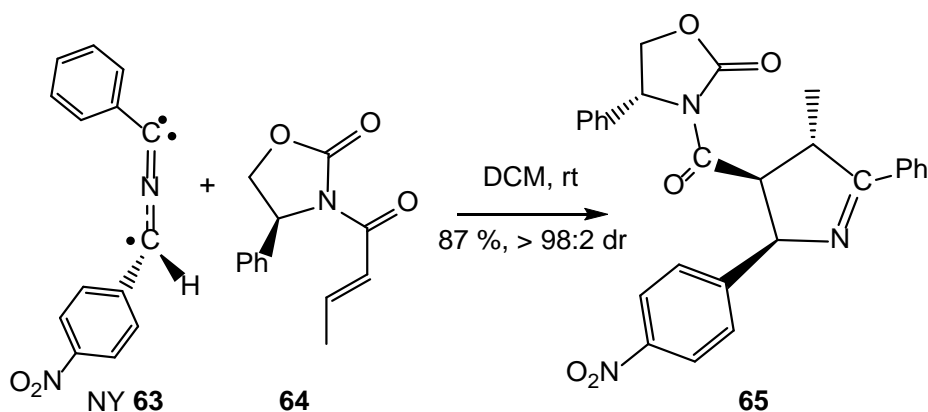


Scheme 3.22. Model for the formation of C–C single bonds involving carbenoid species by donation of non-bonding electron density.⁹⁵

3.2.3. 32CA reactions of NYs **I** with electrophilic chiral oxazolidinones⁹⁷

The previous MEDT⁵⁵ study of the 32CA reactions of the simplest NY **10** with ethylene **6** and electrophilic DCE **21**⁹⁵ allowed establishing the *cb-type* mechanism within 32CA reactions, which, similar to *zw-type* reactions, is also favoured by the nucleophilic/electrophilic interactions taking place along polar processes.

In 2009, Sibi et al.⁹⁸ showed that the 32CA reaction of NY **63** with electrophilic ethylene **64**, possessing a chiral auxiliary, takes place in high yield and stereoselectivity (see Scheme 3.23).



Scheme 3.23. 32CA reaction of NY **63** with chiral oxazolidinone **64** yielding pyrrolines **65**.

3. Results and discussion

In order to characterise experimental *cb-type* 32CA reactions, an MEDT⁵⁵ study of the 32CA reaction of NY **63** with 3-((*E*)-but-2-enoyl)oxazolidin-2-one **64** yielding pyrroline **65**, experimentally studied by Sibi et al.,⁹⁸ was performed at the MPWB1K/6-31G(d) computational level. To this end, the molecular mechanism, as well as the regio- and *endo/exo* stereoselectivity of the 32CA reaction of NY **63** with the non-chiral oxazolidinone **67** was first studied (see Scheme 3.23). Then, the *syn/anti* facial diastereoselectivity along the most favourable reaction path of the 32CA reaction of NY **63** with chiral oxazolidinone **64** was analysed.

3.2.3.1. Topological analysis of the ELF and NPA of NY **63**

ELF topological analysis of the experimental NY **63** showed a similar bonding pattern to that of the simplest NY **10**,⁹⁵ i.e. a linear allenic structure rather than a linear propargylic one with a carbenoid center at the C1 carbon, but also suggesting, interestingly, that the C3 carbon of NY **63** has a *pseudoradical* character (see Figure 3.31).

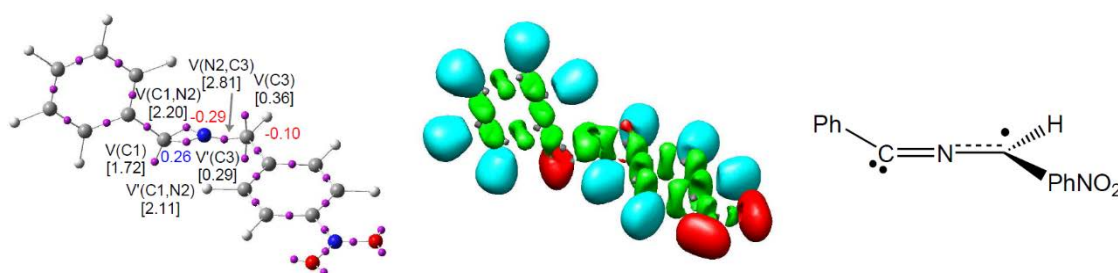


Figure 3.31. ELF valence basin attractors, together with the most representative valence basin populations and natural atomic charges, ELF localisation domains and the proposed carbenoid Lewis structure of NY **63**. Negative charges are coloured in red and positive charges in blue. ELF valence basin population and natural atomic charges are given in average number of electrons, e.

NPA of NY **63** indicated that the presence of the phenyl and aryl substituents at the C1 and C3 carbons decreases the electron density of these centers with respect to those in the simplest NY **10**.⁹⁵ Just as in NY **10**, the charge distribution at NY **63** does not agree with the common representation of NYs **I** as 1,2-zwitterionic charged structures with the negative charge gathered at the C1 carbon and the positive one at the N2 nitrogen. Note that the N2 nitrogen is negatively charged by $-0.29e$, while the C1 carbon gathers a low negative charge of $-0.10e$.

3.2.3.2. Analysis of the CDFT reactivity indices at the GS of the reagents

CDFT reactivity indices⁵⁶ of NY **63** and oxazolidinones **64** and **66** are gathered in Table 3 in Appendix. The electronic chemical potential μ of experimental NY **63**, -3.86 eV, is higher than that of oxazolidinones **64** and **67**, -4.07 and -4.28 eV, indicating that along polar reactions the GEDT⁶¹ will flux from the NY framework, acting as the nucleophile, towards the oxazolidinone one, acting as the electrophile.

According to the electrophilicity⁶² and nucleophilicity⁷⁶ scales, NY **63**, $\omega = 2.33$ eV and $N = 3.67$ eV, is classified as a strong electrophile but remains a strong nucleophile as the simplest NY **10** (see Table 3 in Appendix), oxazolidinone **67**, $\omega = 1.56$ eV and $N = 1.90$ eV, is classified on the borderline of strong electrophiles and as a moderate nucleophile, and chiral oxazolidinone **64**, $\omega = 1.50$ eV and $N = 2.30$ eV, is slightly less electrophilic and more nucleophilic than **67**. Thus, the presence of the nitro group in NY **63** hardly affects its reactivity as nucleophile towards electrophilic oxazolidinones **64** and **67**, which will present similar reactivity in polar processes towards strong nucleophiles.

Regarding the local reactivity, analysis of the nucleophilic P_k^- Parr functions⁸² of NY **63** indicated that the carbenoid C1 carbon is the most nucleophilic center of this species, while the electrophilic P_k^+ Parr functions⁸² of oxazolidinones **64** and **67** indicated that the β -conjugated C5 carbon is the most electrophilic center of these molecules (see

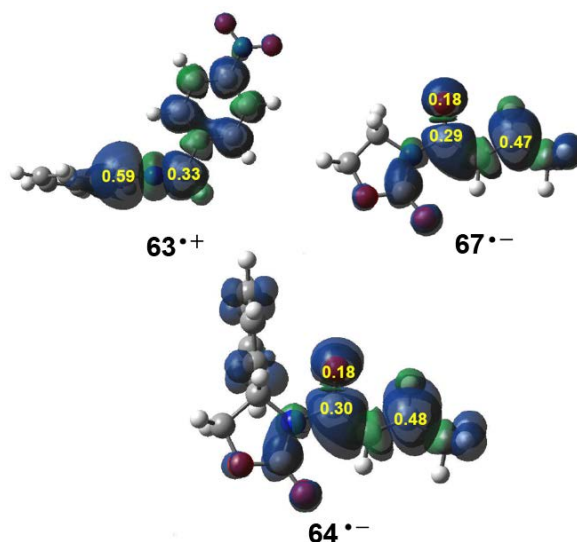


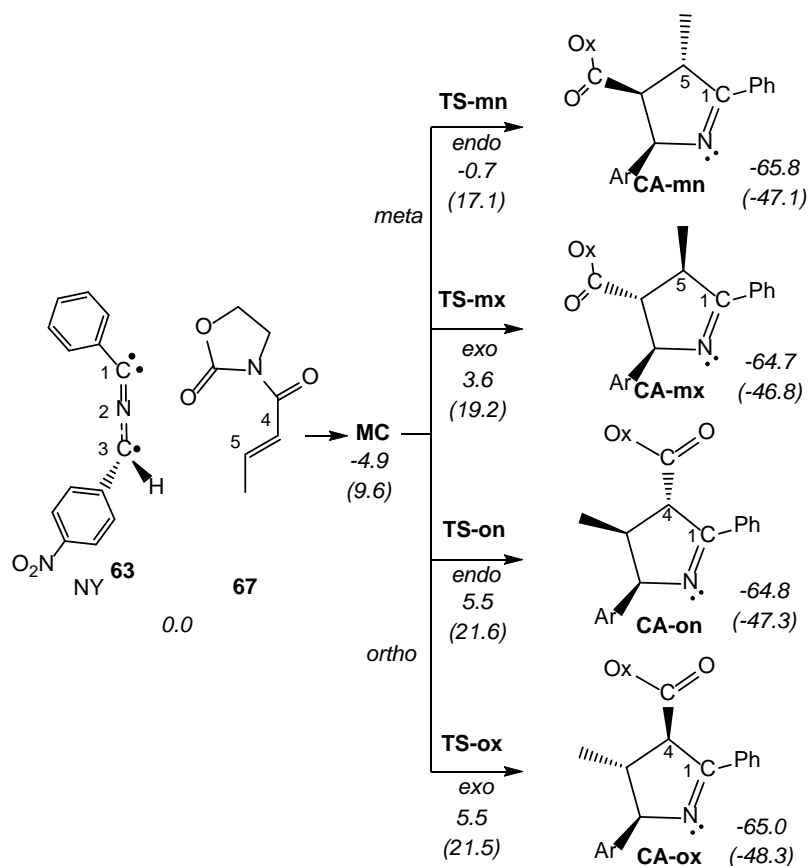
Figure 3.32. 3D representations of the ASD of the radical cation **63**^{•+} and the radical anions **64**^{•-} and **67**^{•-}, together with the nucleophilic P_k^- Parr functions⁸² of NY **63** and the electrophilic P_k^+ Parr functions⁸² of oxazolidinones **64** and **67**.

3. Results and discussion

Figure 3.32). Consequently, the most favourable electrophile-nucleophile interaction along the polar 32CA reactions of NY **63** with oxazolidinones **64** and **67** will take place between the most nucleophilic center of NY **63**, the carbenoid C1 carbon, and the most electrophilic center of oxazolidinones **64** and **67**, the β -conjugated C5 carbon, in clear agreement with the experimental outcomes.

3.2.3.3. Study of the reaction paths associated with the 32CA reaction of NY **63** with oxazolidinone **67**

Due to the non-symmetry of both reagents, the 32CA reaction between NY **63** and the non-chiral oxazolidinone **67** can take place through four competitive reaction paths. As Scheme 3.24 shows, analysis of the stationary points involved in the four reaction paths indicates that this 32CA reaction takes place along a one-step mechanism.



Scheme 3.24. Competitive *meta/ortho* regio- and *endo/exo* stereoisomeric reaction paths associated with the 32CA reaction between NY **63** and the non-chiral oxazolidinone **67**. MPWB1K/6-31G(d) relative enthalpies and Gibbs free energies (in parentheses), computed at 25 °C and 1 atm in DCM, are given in kcal·mol⁻¹.

Some appealing conclusions were drawn from the thermodynamic data given in Scheme 3.24: i) the activation enthalpy associated with this 32CA reaction is $4.2 \text{ kcal}\cdot\text{mol}^{-1}$, via the most favourable **TS-mn**; ii) this 32CA reaction is completely *endo* stereoselective, as **TS-mn** is $4.3 \text{ kcal}\cdot\text{mol}^{-1}$ lower in energy than **TS-mx**, and completely *meta* regioselective, as **TS-mn** is $6.2 \text{ kcal}\cdot\text{mol}^{-1}$ lower in energy than **TS-ox**; iii) these behaviours are in complete agreement with the experimental results in which only the *meta/endo* cycloadduct **65** is obtained; iv) the strong exergonic character of these 32CA reactions makes them irreversible.

The geometries of the TSs involved in the four competitive reaction paths (see Figure 3.33) indicated that: i) the TSs related to the more favourable *meta* reaction paths are more asynchronous than those related to the *ortho* ones; ii) at the TSs associated with the *meta* reaction paths, the C–C bond formation involving the carbenoid C1 carbon and the β -conjugated position of oxazolidinone **67** is more advanced than the other, in clear agreement with the analysis of the Parr functions;⁸² iii) at the synchronous *ortho* TSs, the C–C bond formation involving the carbenoid C1 carbon is slightly more advanced than that at the β -conjugated position of oxazolidinone **67**; iv) in DCM, the 32CA reaction becomes slightly more asynchronous.⁹⁹

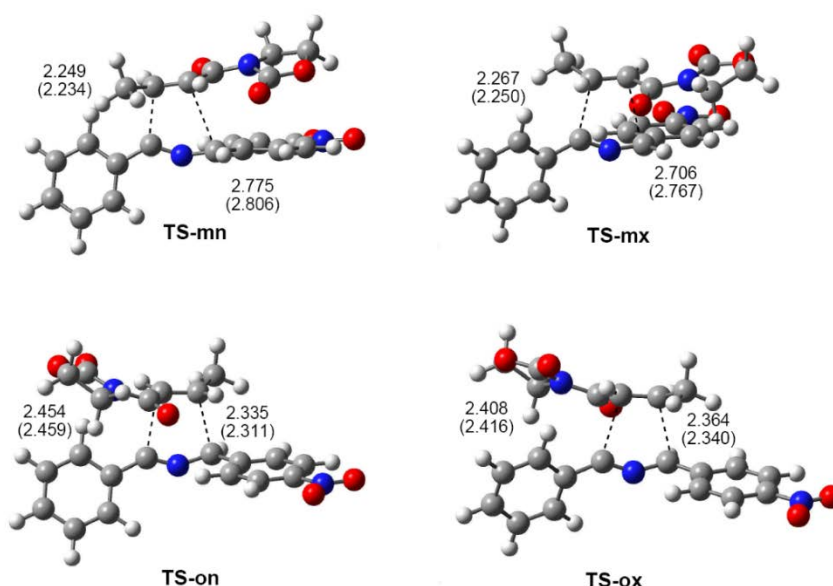


Figure 3.33. MPWB1K/6-31G(d) gas phase optimised geometries of the TSs involved in the 32CA reaction of NY **63** with the oxazolidinone **67**. Distances are given in angstroms, Å, while those in DCM are given in parentheses.

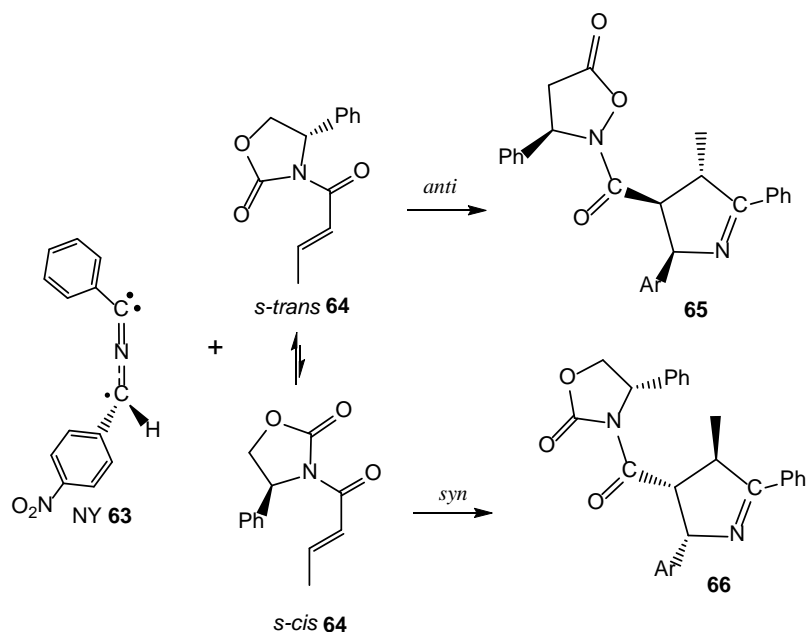
The GEDT⁶¹ fluxing from NY **63** toward oxazolidinone **67** at the gas phase TSs is $0.20e$ at **TS-mn**, $0.19e$ at **TS-mx**, $0.18e$ at **TS-on** and $0.16e$ at **TS-ox**, indicating that this 32CA

3. Results and discussion

reaction has some polar character. The GEDT at the more favourable *meta* TSs is slightly higher than that at the *ortho* ones, and slightly lower than that computed at the *meta* TS associated with the 32CA reaction between the simplest NY **10** and DCE **21** (0.24e).⁹⁵

3.2.3.4. Study of the *anti/syn* facial diastereoselectivity along the *meta/endo* approach mode of NY **63** towards chiral oxazolidinone **64**

The chiral character of oxazolidinone **64** makes that the approach of NY **63** towards the two diastereotopic faces of the former could result in two different pyrrolines. Due to the high *meta/endo* selectivity found in the 32CA reaction of non-chiral oxazolidinone **67**, only the *anti* and *syn* approaches of NY **63** to the diastereotopic faces of **64**, yielding pyrrolines **65** and **66**, were studied (see Scheme 3.25). The geometries of the two distereoisomeric TSs and their relative energies are displayed in Figure 3.34.



Scheme 3.25. *Anti/syn* diastereoisomeric reaction paths along the *meta/endo* reactive approach mode of NY **63** towards the *s-trans* and *s-cis* conformations of chiral oxazolidinone **64**.

The relative energies in DCM showed that *anti* **TS-mna** is 5.8 kcal·mol⁻¹ lower in energy than *syn* **TS-mns** (see Figure 3.34), the reaction presenting complete diastereoselectivity, in total agreement with the experimental outcomes. At **TS-mna**, the phenyl substituent in chiral oxazolidinone **64** is located away from NY **63**, not causing any steric hindrance. Although the phenyl substituent in the most favourable *s-trans* conformation of chiral oxazolidinone **64** prevents the *syn* approach of NY **63**, the C–N single bond rotation in oxazolidinone **64** makes it possible that the phenyl substituent could also be located away

from NY **63**. However, this steric demand makes chiral oxazolidinone **64** adopt the more unfavourable *s-cis* conformation, thus increasing the relative energy of **TS-mns**.

The lengths of the forming bonds at **TS-mna** and **TS-mns** are close to those found at **TS-mn** (see Figure 3.34), indicating that the inclusion of the phenyl substituent in oxazolidinone **67**, resulting in oxazolidinone **64**, does not excessively modify the TS geometries since in both TSs the phenyl substituent is located away from NY **63**.

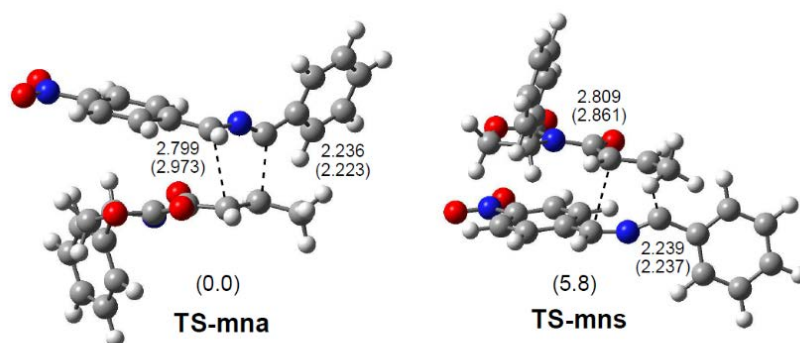


Figure 3.34. MPWB1K/6-31G(d) gas phase optimised geometries of the *anti/syn* diastereoisomeric TSs involved in the *meta/endo* reaction paths associated with the 32CA reaction of NY **63** with chiral oxazolidinone **64**. Distances are given in angstroms, Å, while relative energies, in parentheses, are given in kcal·mol⁻¹. Distances in DCM are also given in parentheses.

3.2.3.5. BET study of the 32CA reaction of NY **63** with oxazolidinone **67**

A BET study of the most favourable *meta/endo* reaction path associated with the 32CA reaction between NY **63** and oxazolidinone **67** (see Table 14 and Scheme 6.11) allowed drawing the following conclusions: i) the IRC associated with the *meta/endo* reaction path is topologically characterised by ten differentiated phases. Consequently, this 32CA reaction is a non-concerted process; ii) formation of the first C1–C5 single bond begins at a distance of 2.04 Å by donation of the non-bonding electron density belonging to the carbenoid C1 center of NY **63** to the β -conjugated position of the oxazolidinone moiety (see **P7** in Figure 3.35).⁹⁵ This behaviour, which is similar to that found in the 32CA reaction between the simplest NY **10** and DCE **21**, characterises the *cb-type* mechanism; iii) formation of the second C3–C4 single bond begins at a distance of 2.05 Å through the C-to-C coupling of two C3 and C4 *pseudoradical* centers⁶¹ generated along the IRC (see **P8** and **P9** in Figure 3.35); iv) formation of the C3–C4 single bond begins when the C1–C5 single bond is almost completely formed, by ca. 97% (see Table 14 in Appendix).

3. Results and discussion

This behaviour characterises the reaction mechanism as a non-concerted *two-stage one-step* mechanism;⁷⁷ and finally, v) the changes in electron density required to reach the TS, which are mainly associated to the depopulation of the C4–C5 double bond, present a low EC of 5.0 kcal·mol⁻¹ (see Table 14 in Appendix) as a consequence of the electrophilic character of oxazolidinone **67**.

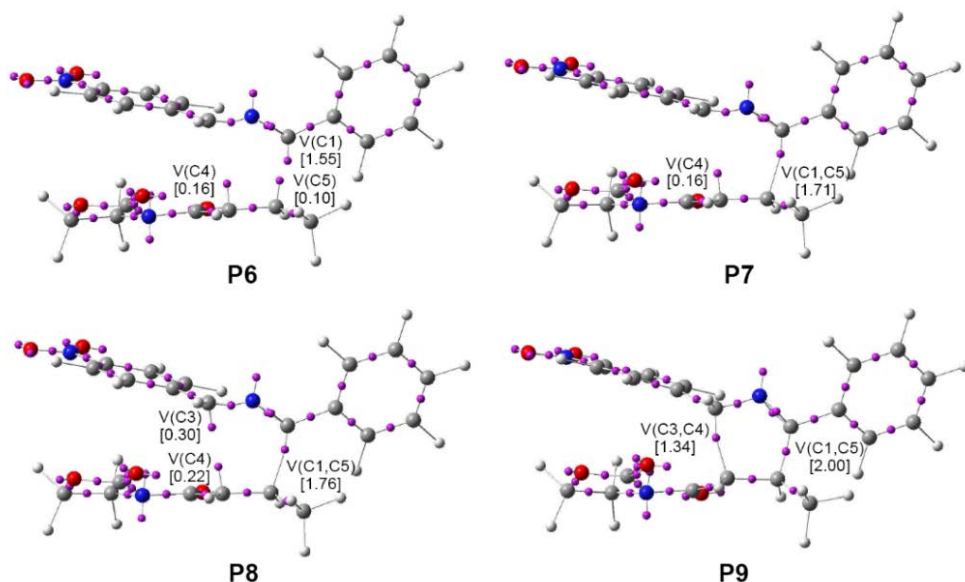


Figure 3.35. ELF attractor positions for the points of the IRC defining the four phases involved in the formation of the C1–C5 and C3–C4 single bonds along the *meta/endo* reaction path associated with the 32CA reaction of NY **63** with oxazolidinone **67**. The electron populations, in average number of electrons (e), are given in brackets.

3.2.3.6. NCI topological analysis of the origin of the *endo* and *anti* selectivities in the 32CA reactions of NY **63** with oxazolidinones **64** and **67**

A detailed analysis of the geometries of the *meta* TSs showed that while the oxazolidinone ring of **64** is positioned away from the aryl substituent at **TS-mx**, the former ring is precisely above the aryl substituent and parallel at the *endo* TSs (see Figure 3.36). This geometrical arrangement allows generating some type of favourable electronic interactions between the oxazolidinone and the aryl groups, justifying the preference of *endo* **TS-mn** over *exo* **TS-mx**. As at the *ortho* TSs the phenyl ring of oxazolidinone **64** is positioned orthogonally to the molecular plane, any interaction with the oxazolidinone ring is prevented. Consequently, favourable interactions are only feasible along the *meta/endo* reactive pathway.

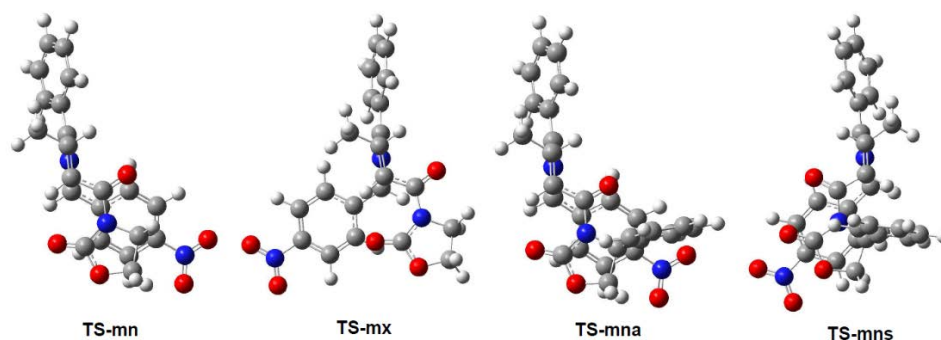


Figure 3.36. Top view of the geometries of **TS-mn**, **TS-mx**, **TS-mna** and **TS-mns**.

NCI topological analysis indicated that, although weak attractive VdW interactions are appreciable in the TSs associated with the more favourable *meta* regioisomeric pathways (see Figure 3.37), the stronger VdW interactions taking place between the oxazolidinone ring of **64** and **67** and the aryl group of NY **63** along the *meta/endo* approach could be responsible for the total stereoselectivity experimentally found in the 32CA reactions of NY **63** with oxazolidinone **64**.⁹⁸ In addition, these VdW interactions can reinforce the regioselectivity resulting from the most favourable nucleophilic/ electrophilic interaction, thus accounting for the high energy difference between **TS-mn** and **TS-on**, 6.2 kcal·mol⁻¹. Interestingly, despite the similar NCI profiles of the *anti/syn* diastereoisomeric

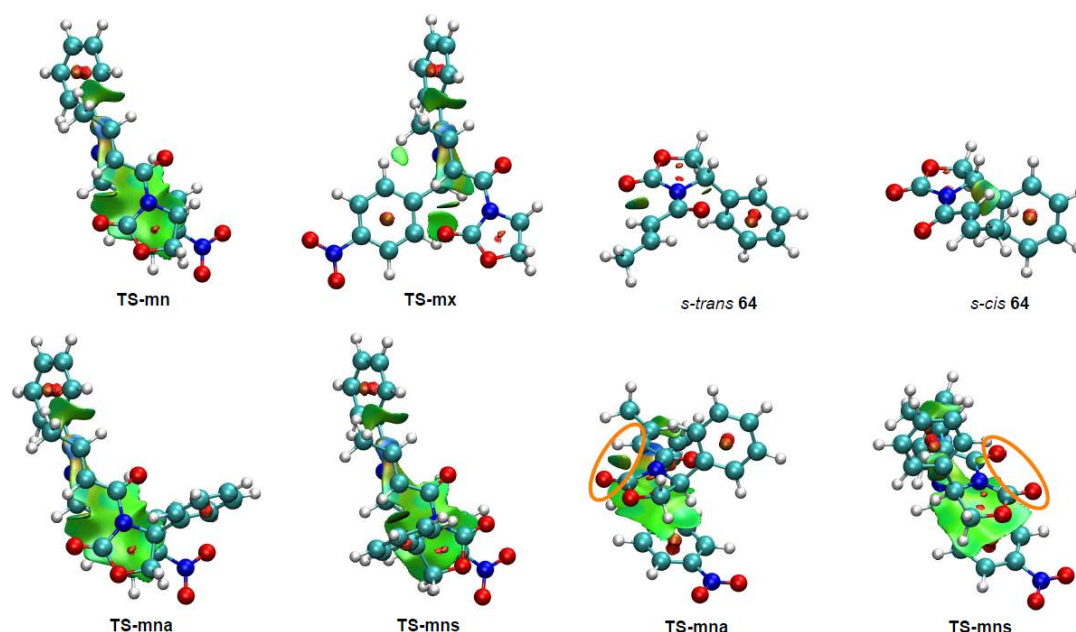


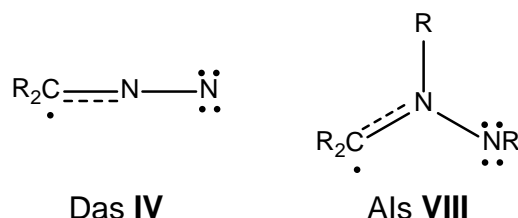
Figure 3.37. NCI gradient isosurfaces of the *meta endo/exo* TSs associated with the 32CA reaction of NY **63** with oxazolidinone **67**, of the *syn/anti* TSs of the *meta/endo* pathway related to the 32CA reaction involving chiral oxazolidinone **64** and of the *s-trans* and *s-cis* conformations of **64**.

3. Results and discussion

meta/endo TSs, the presence of a hydrogen-bond between the α -hydrogen and the carbonyl oxygen of the oxazolidinone ring in oxazolidinone *s-trans* **64** appears to be responsible for the high *anti* diastereoisomeric excess experimentally obtained in the 32CA reaction of NY **63** with oxazolidinone **64**.

3.3. 32CA reactions of *pseudoradical* TACs

Pseudoradical TACs are species containing one single *pseudoradical* center (see Scheme 3.26). They are able to participate in *pmr-type* 32CA reactions, which take place moderately without the necessity of strong electrophilic ethylenes. Propargylic Das **IV** and allylic AIs **VIII** are typical examples of *pseudoradical* TACs.

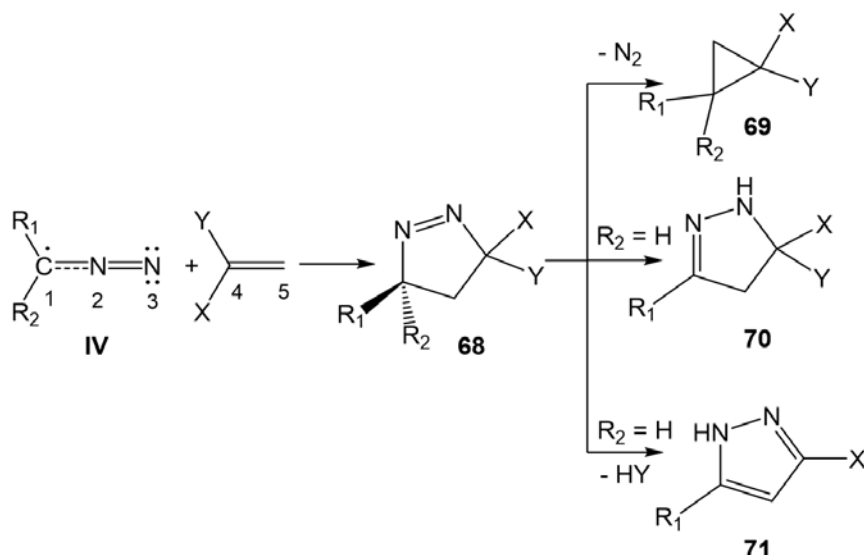


Scheme 3.26. Lewis structures of *pseudoradical* TACs.

3.3.1. 32CA reactions of Das **IV** with electrophilic ethylenes¹⁰⁰

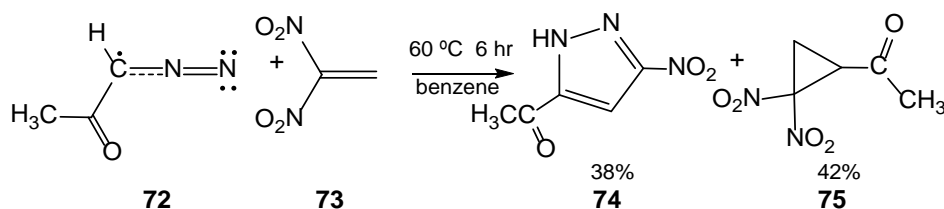
After the cycloadditions of diazoacetates **1** and diazomethane **2** toward C–C multiple bonds were reported by Büchner and von Pechmann in the 1890s,⁷ numerous 32CA reactions of Das **IV** have been described. In contrast to many TACs, which are generated as transient species in the reaction medium, mono- and di-substituted Das **IV** have been extensively prepared and isolated in pure form.^{5b}

1-Pyrazolines **68** resulting from a 32CA reaction between Das **IV** and electrophilic ethylenes can experience different subsequent transformations, depending on the electronic nature of the substituents present both reagents. As shown in Scheme 3.27, cyclopropanes **69**, 2-pyrazolines **70** or PYZs **71** can be obtained via the extrusion of the nitrogen molecule, tautomerisation or HY elimination at the resulting 1-pyrazolines **68**, respectively.



Scheme 3.27. Transformation of 1-pyrazolines **68** into cyclopropanes **69**, 2-pyrazolines **70** or PYZs **71** when appropriate substitutions are present in Das **IV** and in the ethylene derivative.

Recently, Ivanova et al.¹⁰¹ experimentally studied some 32CA reactions of various Das **IV** containing an α -hydrogen with DNE **73**, an electrophilic ethylene. Thus, when diazoacetate **72**, 1-diazopropan-2-one, was treated with DNE **73** in benzene at 60 °C for 6 hr, a mixture of PYZ **74** and DNCP **75** was obtained in 38% and 42% yields, respectively (see Scheme 3.28).¹⁰¹



Scheme 3.28. Generation of PYZ **74** and DNCP **75** via the 32CA reaction of Da **72** with DNE **73** experimentally studied by Ivanova et al..¹⁰¹

In order to understand this complex process, an MEDT⁵⁵ study of the domino reaction of Da **72** with DNE **73** yielding PYZ **74** and DNCP **75**, experimentally reported by Ivanova et al.,¹⁰¹ was carried out using quantum chemical procedures at the B3LYP/6-31G(d,p) computational level.

3.3.1.1. Topological analysis of the ELF and NPA of the simplest Da **2** and experimental Da **72**

As can be seen in Figure 3.38, ELF topology of the simplest Da **2** shows the presence of two monosynaptic basins at the sp^2 hybridised C1 carbon, V(C1) and V'(C1), integrating

3. Results and discussion

a total population of 1.04e, being associated with a C1 *pseudoradical* center; one V(C1,N2) disynaptic basin, integrating 3.06e, characterising a partial C1–N2 double bond; two disynaptic basins, V(N2,N3) and V'(N2,N3), integrating 1.80e each one, which suggest an N2–N3 double bond; and two monosynaptic basins, V(N3) and V'(N3), with a total electron density of 3.90e, associated with two lone pairs at the N3 nitrogen.

On the other hand, ELF topology of the experimental Da **72** shows a very similar electronic structure to that found in the simplest Da **2** (see Figure 3.38). In this TAC, the two monosynaptic basins, V(C1) and V'(C1), present a population of 0.50e each one, while the C1–N2–N3 bonding region shows a similar bonding pattern to that in Da **2**. The only topological difference between the two Das is that at Da **72** the non-bonding electron density associated to the N3 nitrogen is represented by one single V(N3) monosynaptic basin integrating 3.76e. Consequently, ELF topology of the experimental Da **72** and simplest Da **2** indicates that these TACs do not present a *pseudodiradical*,⁵¹ nor a carbenoid⁹⁵ nor a zwitterionic⁵¹ electronic structure that would enable them to participate in *pdr*-, *cb*- or *zw*-type 32CA reactions,^{51,95} but have a *pseudoradical* structure.

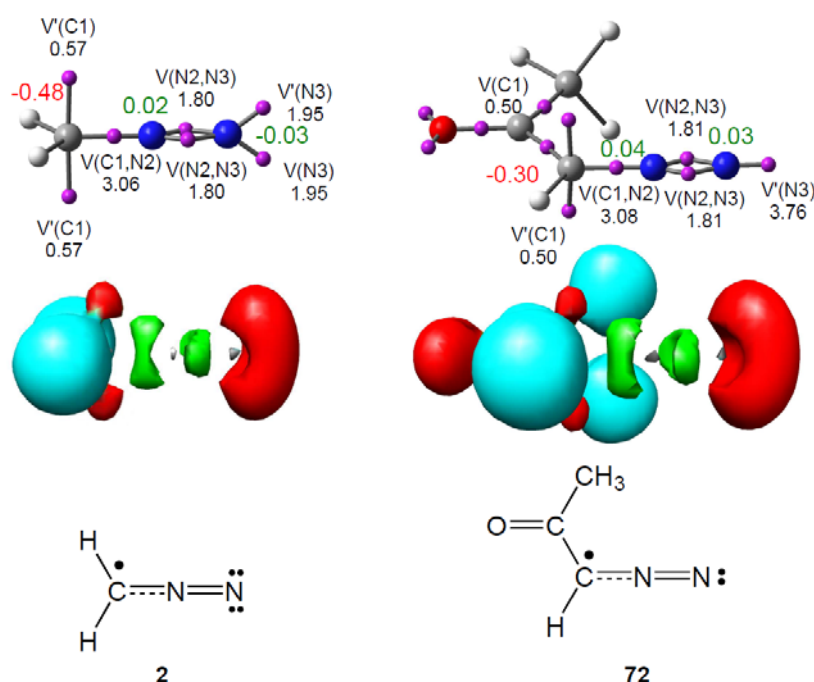


Figure 3.38. ELF valence basin attractors, together with the valence basin populations and natural atomic charges, ELF localisation domains and the proposed *pseudoradical* Lewis structures of Das **2** and **72**. Negative charges are coloured in red and negligible charges in green. ELF valence basin population and natural atomic charges are given in average number of electrons, e.

Finally, NPA did not allow characterising any 1,2-zwitterionic structure for these two Das. While the C1 carbon has a high negative charge, the nitrogen nuclei have negligible

charges (see Figure 3.38). These findings disagree with the commonly accepted Lewis structure of Das **IV** represented by a 1,2-zwitterionic structure.

3.3.1.2. Analysis of the CDFT reactivity indices at the GS of the reagents

CDFT reactivity indices⁵⁶ of Das **2** and **72** and DNE **73** are gathered in Table 3 in Appendix. The electronic chemical potential μ of Da **72**, -4.40 eV, is higher than that of DNE **73**, -5.98 eV. Consequently, along a polar 32CA reaction of Da **72** with DNE **73**, the GEDT⁶¹ will flux from Da **72**, acting as the nucleophile, toward electrophilic DNE **73**.

According to the electrophilicity⁶² and nucleophilicity⁷⁶ scales, the simplest Da **2**, $\omega = 1.40$ eV and $N = 3.11$ eV, is classified on the borderline of strong electrophiles and as a strong nucleophile, Da **72**, $\omega = 2.07$ eV and $N = 2.39$ eV, as a strong electrophile and as a moderate nucleophile and DNE **73**, $\omega = 3.56$ eV and $N = 0.62$ eV, as a strong electrophile and as a marginal nucleophile.

The low *pseudodiradical pr* indices⁵¹ of P-TACs Das **2** and **72**, 0.66 and 0.51 (see Table 3 in Appendix), indicate that, in spite of their *pseudoradical* structure, they will not be able to participate in *pdr-type* 32CA reactions.⁵¹ This analysis is in clear agreement with the previous ELF topological analysis as well as with the high activation energy found in the 32CA reaction between the simplest Da **2** and ethylene **6**, 15.4 kcal·mol⁻¹.⁶⁸

Regarding the local reactivity, analysis of the nucleophilic P_k^- Parr functions⁸² at the reactive sites of Da **72** indicated that the C1 carbon is the most nucleophilic center (see Figure 3.39). On the other hand, the electrophilic P_k^+ Parr functions⁸² at the reactive sites of DNE **73** indicated that the most electrophilic center is the C5 carbon. Therefore, the most favourable electrophile-nucleophile interaction along the nucleophilic attack of Da **72** onto DNE **73** in a polar process will take place between the most nucleophilic center of Da **72**, the C1 carbon, and the most electrophilic center of DNE **73**, the C4 carbon. This prediction is in complete agreement with the experimental outcomes¹⁰¹ favouring the formation of 1-pyrazoline **76** which, in turn, participates in the subsequent reactions to generate PYZ **74** and DNCP **75** (see Schemes 3.28 and 3.29).

3. Results and discussion

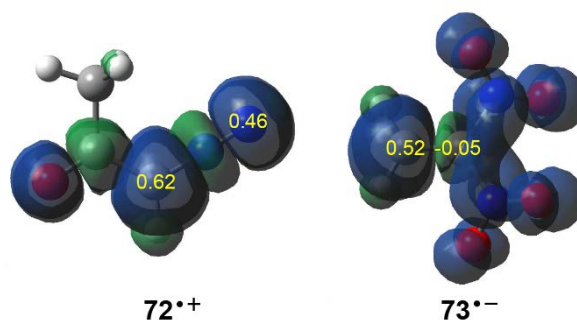
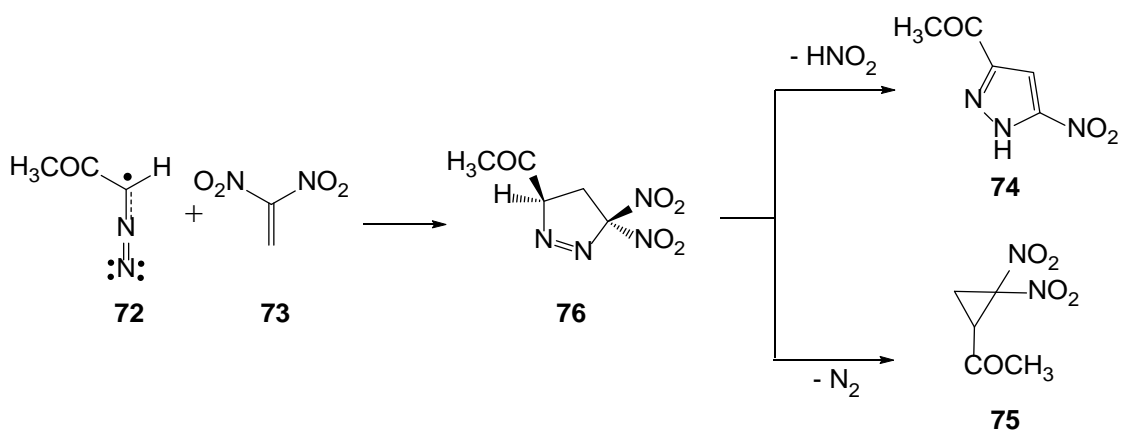


Figure 3.39. 3D representations of the ASD of the radical cation $72^{\bullet+}$ and the radical anion $73^{\bullet-}$, together with the nucleophilic P_k^- Parr functions⁸² of Da **72** and the electrophilic P_k^+ Parr functions⁸² of DNE **73**.

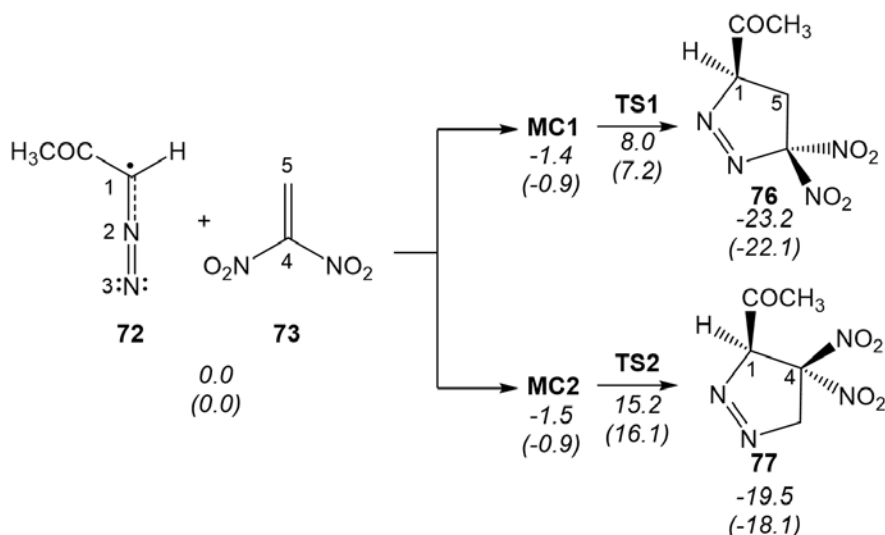
3.3.1.3. Study of the domino reaction between Da **72** and DNE **73** giving PYZ **74** and DNCP **75**

The reaction between Da **72** and DNE **73** giving PYZ **74** and DNCP **75** is a domino process that comprises several consecutive reactions. The first one is a 32CA reaction between Da **72** and DNE **73** yielding 1-pyrazoline **76** (see Scheme 3.29). Then, **76** may experience two competitive reactions: i) a tautomerisation and the subsequent loss of nitrous acid to yield PYZ **74**; or ii) the extrusion of a nitrogen molecule and a ring closure resulting in DNCP **75** (see Scheme 3.29).



Scheme 3.29. Domino reactions between Da **72** and DNE **73** yielding PYZ **74** and DNCP **75**.

Due to the non-symmetry of both reagents, two regioisomeric approach modes of the reagents, i.e. the initial formation of the C1–C5 or C1–C4 single bonds, are feasible along the 32CA reaction between Da **72** and DNE **73**, yielding 1-pyrazolines **76** and/or **77**, respectively (see Scheme 3.30). Analysis of the stationary points involved in the two regioisomeric paths indicated that this 32CA reaction takes place through a one-step mechanism.



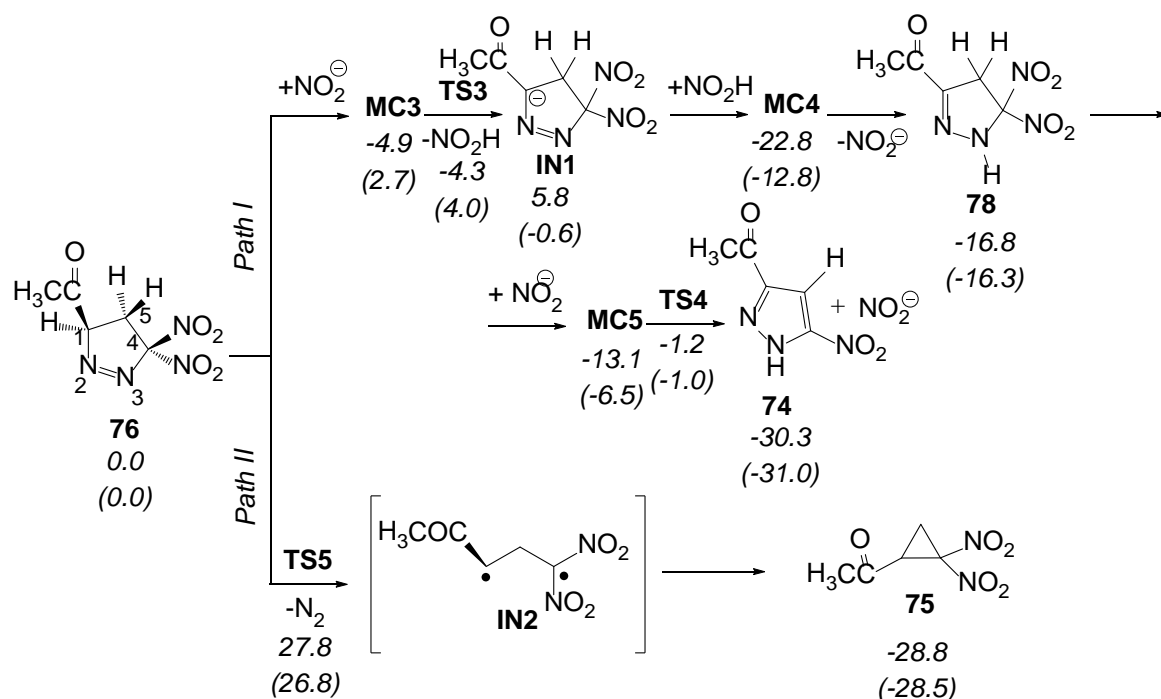
Scheme 3.30. 32CA reaction between Da **72** and DNE **73**. B3LYP/6-31G(d,p) relative electronic energies, in gas phase and in benzene (in parentheses), are given in kcal·mol⁻¹.

Some appealing conclusions were drawn from the energy results given in Scheme 3.30: i) the activation energy associated with the more favourable **TS1**, 9.5 kcal·mol⁻¹, is 6.0 kcal·mol⁻¹ lower in energy than that associated with the 32CA reaction of the simplest Da **72** with ethylene **6**; 15.4 kcal·mol⁻¹,⁶⁸ ii) this 32CA reaction is completely C1–C5 regioselective, in clear agreement with the experimentally observed regioselectivity (see Scheme 3.29); and iii) the strong exothermic character of this reaction makes the formation of 1-pyrazolines **76** and **77** irreversible. Consequently, 1-pyrazoline **76** is obtained under kinetic control of the reaction.

Next, 1-pyrazoline **76** can participate in the competitive reaction paths *I* and *II* (see Scheme 3.31). Along *Path I*, this species first tautomerises to 2-pyrazole **78**, which by the loss of nitrous acid yields PYZ **74**, while along *Path II*, the thermal extrusion of a nitrogen molecule yields the final DNCP **75** in a straightforward manner.

The tautomerisation along *Path I* is a thermodynamically controlled acid/base process. The first step consists of the H1 proton abstraction by the nitrite anion acting as a base yielding anionic intermediate **IN1** with a very low activation energy, 0.6 kcal·mol⁻¹. The subsequent proton transfer from nitrous acid to the N3 nitrogen has no activation energy. Thus, conversion of 1-pyrazoline **76** into 2-pyrazoline **78** is thermodynamically very favourable. This finding is in agreement with the experimental observation that in 32CA reactions of Das **IV** containing an α -hydrogen, 2-pyrazolines **70** are obtained as a reaction product (see 2-pyrazolines **70** in Scheme 3.27). Due to the relative acidic character of the H5 hydrogen of 2-pyrazoline **78**, the corresponding proton abstraction

3. Results and discussion



Scheme 3.31. Proposed reaction paths for the conversion of 1-pyrazoline **76** into PYZ **74** and DNCP **75**. B3LYP/6-31G(d,p) relative energies, in gas phase and in benzene (in parentheses), are given in kcal·mol⁻¹.

process from C5 by the nitrite anion presents a low activation energy, 11.9 kcal·mol⁻¹. Finally, subsequent loss of the nitrite anion to yield PYZ **74** has no activation energy; i.e. the IRC from **TS4** towards the products showed that the extrusion of nitrite anion takes place in the same elementary step after complete proton abstraction.

Along *Path II*, the thermal extrusion of the nitrogen molecule at 1-pyrazoline **76** takes place via **TS5** with a high activation energy, 27.8 kcal·mol⁻¹, but despite this, this unimolecular process is not entropically unfavourable. The IRC from **TS5** to products discontinues at diradical species **IN2**. However, full optimisation of this species yielded the final DNCP **75** in a straightforward manner. Finally, the strong exothermic character of the formation of DNCP **75**, as well as PYZ **74**, makes these domino reactions irreversible.

Gas phase optimised geometries of the TSs involved in the domino reaction between Da **72** and DNE **73** are given in Figure 3.40. From the geometries of the two TSs associated with the 32CA reaction, some appealing conclusions were drawn: i) the more favourable **TS1** is associated with a highly asynchronous bond formation process; ii) this 32CA reaction takes place via a *two-stage one-step* mechanism⁷⁷ (see below). Thus, **TS1** is associated with the nucleophilic attack of the C1 carbon of Da **72** on the β -conjugated

position of DNE **73**, in clear agreement with the analysis of the Parr functions;⁸² and iii) at the two regioisomeric TSs, the single bond formation involving the most electrophilic center of DNE **73**, the C5 carbon, is more advanced than that involving the C4 carbon.

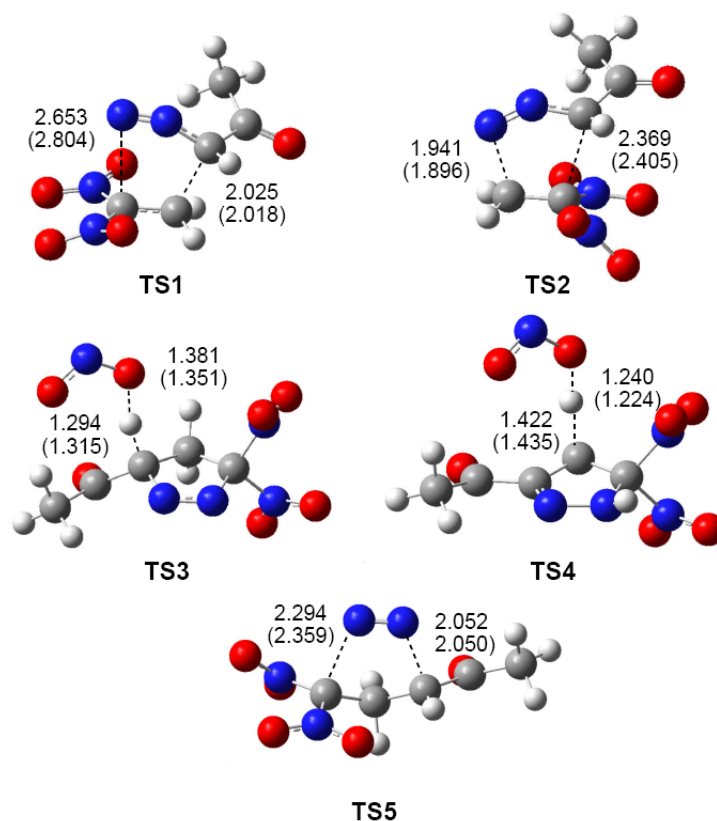


Figure 3.40. B3LYP/6-31G(d,p) gas phase optimised geometries of the TSs involved in the domino reaction between Da **72** and DNE **73** (see Schemes 3.30 and 3.31). Distances are given in angstroms, Å, while those in benzene are given in parentheses.

The polar nature of the 32CA reaction between Da **72** and DNE **73** was analysed by computing the GEDT⁶¹ at the corresponding TSs. The GEDT that fluxes from the Da moiety toward the electrophilic ethylene one is 0.34e at **TS1** and 0.24e at **TS2**. These high values indicate that this 32CA reaction has a strong polar character, due to the high electrophilicity of DNE **73**, in clear agreement with the relatively low activation energy associated with this 32CA reaction, 9.4 kcal·mol⁻¹.

3.3.1.4. BET study of the 32CA reaction between Da **72** and DNE **73**

A BET study along the more favourable C1–C5 regioisomeric pathway associated with the 32CA reaction between Da **72** and DNE **73** (see Table 15 and Scheme 6.12 in Appendix) allowed obtaining the following conclusions: i) the reaction path can be divided in ten differentiated phases associated with the creation or disappearance of

3. Results and discussion

valence basins; ii) formation of the first C1–C5 single bond begins at a distance of ca. 2.01 Å, through the C-to-C coupling of two C1 and C5 *pseudoradical* centers (see Section 3.2.2.5 and Figure 3.41);⁶¹ iii) while the V(C1) monosynaptic basin was already present at Da **72**, the V(C5) monosynaptic basin is formed at the DNE **73** framework along the reaction path, promoted by a high GEDT;¹⁰² iv) a different behaviour is found for the formation of the second N3–C4 single bond. Formation of the N3–C4 single bond begins at the very short distance of ca. 1.69 Å by sharing the non-bonding electron density of a carbon C4 *pseudoradical* center and part of that related to the N3 nitrogen (see Figure 3.41); v) formation of the second N3–O4 single bond begins when the first C1–C5 single bond is already formed by up to 97% (see Table 15 in Appendix), indicating that this 32CA reaction takes place through a *two-stage one-step* mechanism;⁷⁶ and vi) formation of the first C1–C5 single involves the most nucleophilic center of Da **72**, the C1 carbon, and the most electrophilic center of DNE **73**, the C4 carbon, a behaviour anticipated by the analysis of the electrophilic and nucleophilic Parr functions.⁸²

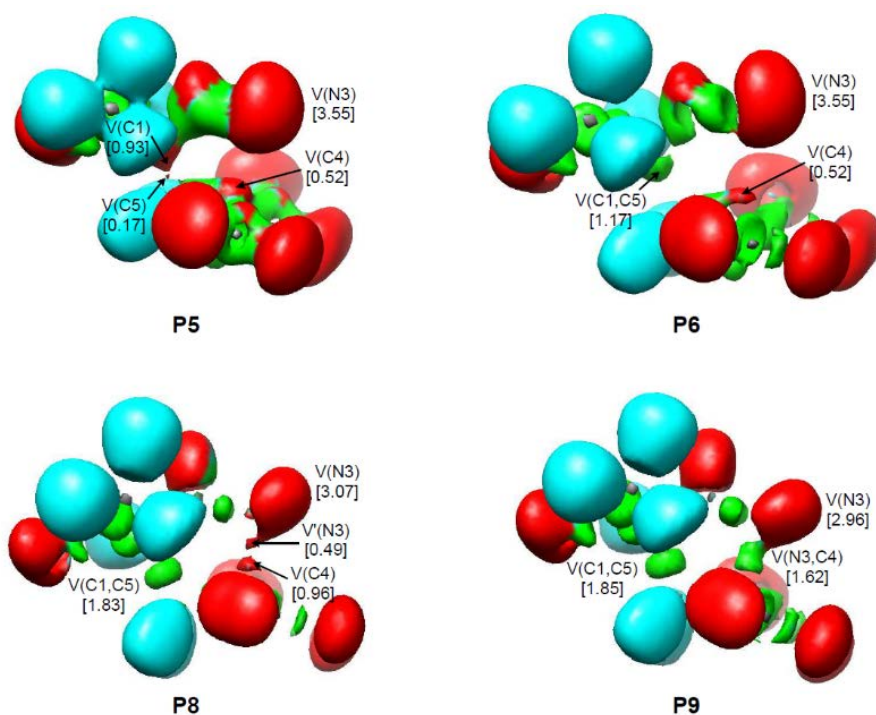


Figure 3.41. ELF localisation domains the points of the IRC defining the four phases involved in the formation of the C1–C5 and N3–C5 single bonds along the IRC path associated with the 32CA reaction between Da **72** and DNE **73**. The electron populations, in average number of electrons (e), are given in brackets.

3.3.2. 32CA reactions of the simplest AI 15¹⁰³

AY 14, AI 15 and Ni 16 constitute a series of three $\text{CH}_2=\text{NH}-\text{X}$ ($\text{X} = \text{CH}_2, \text{NH}, \text{O}$) A-TACs in which the terminal X nucleus changes along the C, N, and O elements of the second arrow (see Figure 3.42). In this short series of TACs, the activation energy associated with the 32CA reactions with ethylene 6 increases as the electronegativity of the nucleus X increases in the order $\text{C} < \text{N} < \text{O}$ (see Figure 3.42).⁵¹ Interestingly, while the simplest AY 14 has a *pseudodiradical* electronic structure,⁶⁴ Ni 16 has a zwitterionic one.⁸³ This behaviour causes these two TACs to have a different reactivity in non-polar 32CA reactions with ethylene 6 (see Figure 3.42). As the activation energy of the 32CA reaction of AI 15 with ethylene 6 is $8.7 \text{ kcal}\cdot\text{mol}^{-1}$, it is expected that both its structure and reactivity will be different.

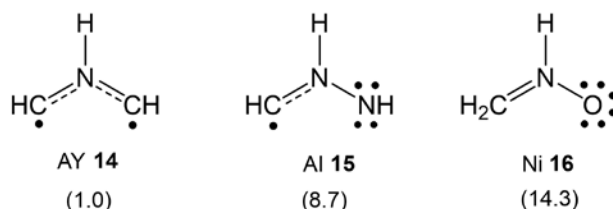
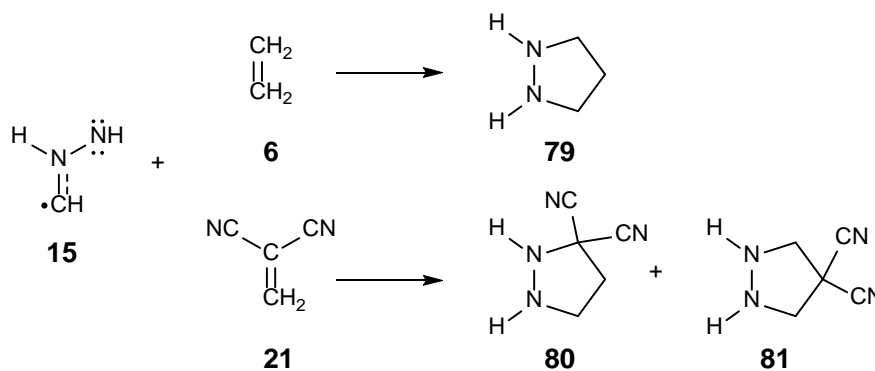


Figure 3.42. Series of $\text{CH}_2=\text{NH}-\text{X}$ ($\text{X} = \text{CH}_2, \text{NH}, \text{O}$) A-TACs 14–16. In parentheses, MPWB1K/6-311G(d) activation energies with respect to the corresponding molecular complexes, in $\text{kcal}\cdot\text{mol}^{-1}$, associated with the non-polar 32CA reactions with ethylene 6.

Thus, considering that the simplest AI 15 has a different activation energy towards ethylene 6 from that shown by AY 14 and Ni 16, two TACs with a different electronic structure, an MEDT⁵⁵ study of the 32CA reactions of the simplest AI 15 with ethylene 6 and the strongly electrophilic DCE 21, was herein carried out at the MPWB1K/6-311G(d) computational level in order to establish the structure and reactivity of this TAC (see Scheme 3.32).



Scheme 3.32. 32CA reactions of AI 15 with ethylene 6 and DCE 21.

3. Results and discussion

3.3.2.1. Topological analysis of the ELF and NPA of AI 15

ELF topological analysis of the simplest AI **15** showed the presence of two V(C1) and V'(C1) monosynaptic basins integrating a total population of 0.62e, two V(C1,N2) and V(N2,N3) disynaptic basins integrating 2.95e and 2.09e, respectively, and one V(N3) monosynaptic basin integrating 3.53e. These ELF basins can be related, according to the Lewis's bonding model, to a C1 *pseudoradical* center, a partial C1–N2 double bond, an N2–N3 single bond and two N3 non-bonding lone pairs (see the proposed Lewis structure of AI **15** in Figure 3.43). Consequently, ELF topological analysis of the electronic structure of the simplest AI **15** indicates that this TAC does not have the electronic structure of any of the three representative *pseudodiradical*, carbenoid and zwitterionic TACs, but a *pseudoradical* electronic structure, similar to its propargylic counterpart, the simplest Da **2**.

On the other hand, NPA showed that the three heavy nuclei belonging to this TAC present negative charges: $-0.30e$ (C1), $-0.18e$ (N2) and $-0.54e$ (N3), while the hydrogen nuclei gather the positive charges. This charge distribution is in complete disagreement with the commonly accepted 1,2-zwitterionic structure given for AIs **VIII** in which a positive charge and a negative charge are entirely located at the N2 and N3 nitrogens (see Figure 3.43).^{6a,8}

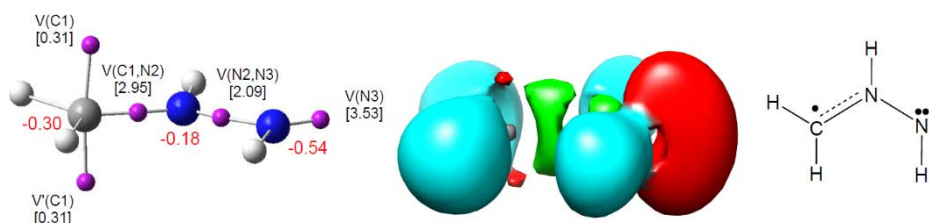


Figure 3.43. ELF valence basin attractors, together with the valence basin populations and natural atomic charges, ELF localisation domains and the proposed Lewis structure of AI **15**. ELF valence basin population and natural atomic charges, in red, are given in average number of electrons, e.

Thus, the different electronic structure of AI **15** with respect to *pseudodiradical*, carbenoid and zwitterionic structures justifies the different reactivity of this TAC (see Figure 3.42), and therefore, the establishment of a new reactivity model in 32CA reactions.

3.3.2.2. Analysis of the CDFT reactivity indices at the GS of the reagents

As shown in Table 3 in Appendix, the electronic chemical potential μ of AI **15**, -2.70 eV, is higher than that of ethylene **6** and DCE **21**. Consequently, along polar 32CA reactions, the GEDT⁶¹ will take place from AI **15** toward ethylene **6** or DCE **21**; however, note that ethylene **6** has no tendency to participate in polar processes.¹⁰⁴

According to the electrophilicity⁶² and nucleophilicity⁷⁶ scales, the simplest AI **15**, $\omega = 0.72$ eV and $N = 3.92$ eV, is classified as a marginal electrophile and as a strong nucleophile. Consequently, while DCE **21** participates only as a strong electrophile in polar 32CA reactions (see Table 3 in Appendix), AI **15** will participate only as a strong nucleophile. Given the strong nucleophilic character of AI **15** and the strong electrophilic character of DCE **21**, it is expected that the 32CA reaction between AI **15** and DCE **21** will have a high polar character. On the other hand, the low *pseudoradical pr* index of AI **15** (lower than 1.00),⁵¹ 0.78, indicated that this TAC will not present a *pdr-type* reactivity in 32CA reactions.

Regarding the local reactivity, analysis of the nucleophilic P_k^- Parr functions⁸² at the reactive sites of AI **15** indicated that both the C1 carbon and the N3 nitrogen are nucleophilically activated, the latter more than the former despite the *pseudoradical* character of the C1 carbon (see Figure 3.44). Note that at the propargylic counterpart of AI **15**, Da **2**, the most nucleophilic center is the *pseudoradical* carbon center.¹⁰⁰ Therefore, the most favourable electrophile-nucleophile interaction along the nucleophilic attack of AI **15** on DCE **21** in a polar process will take place between the most nucleophilic center of AI **15**, the N3 nitrogen, and the most electrophilic center of DCE **21**, the C4 carbon (see Figure 3.44).

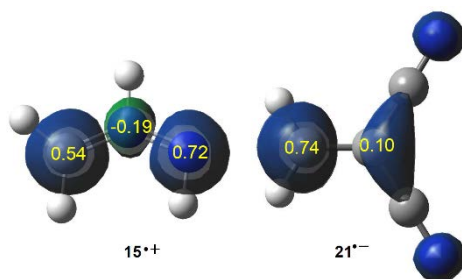
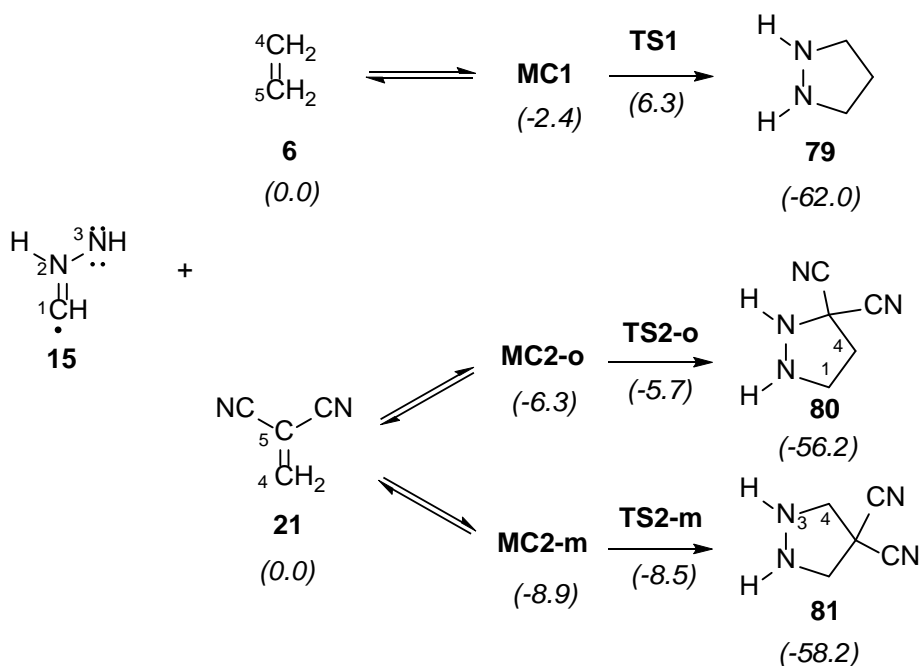


Figure 3.44. 3D representations of the ASD of the radical cation **15**^{•+} and the radical anion **21**^{•-}, together with the nucleophilic P_k^- Parr functions⁸² of AI **15** and the electrophilic P_k^+ Parr functions⁸² of DCE **21**.

3. Results and discussion

3.3.2.3. Study of the reaction paths associated with the 32CA reactions of AI **15** with ethylene **6** and DCE **21**

Due to the symmetry of ethylene **6**, only one reaction path is feasible for the 32CA reaction of AI **15** with ethylene **6**. Conversely, due to the non-symmetry of both AI **15** and DCE **21**, the corresponding polar 32CA reaction can take place along two regioisomeric reaction paths. As Scheme 3.33 shows, analysis of the stationary points involved in the two reactions indicates that these 32CA reactions take place through a one-step mechanism.



Scheme 3.33. 32CA reactions of AI **15** with ethylene **6** and DCE **21**. MPWB1K/6-311G(d) gas phase relative energies (in parentheses) are given in kcal·mol⁻¹.

Some appealing conclusions were drawn from the energy results given in Scheme 3.33 and the energy profile represented in Figure 3.45: i) the activation energy for the non-polar 32CA reaction between AI **15** and ethylene **6** is 8.7 kcal·mol⁻¹; ii) the activation energy of the polar reaction with DCE **21** via the more favourable **TS2-m**, 0.4 kcal·mol⁻¹, is 8.3 kcal·mol⁻¹ lower than that of the non-polar reaction involving ethylene **6**; iii) the polar 32CA reaction is highly regioselective, **TS2-o** being 2.8 kcal·mol⁻¹ above **TS2-m**; and iv) the strong exothermic character of these reactions makes the formation of pyrazolidines **79**, **80** and **81** irreversible.

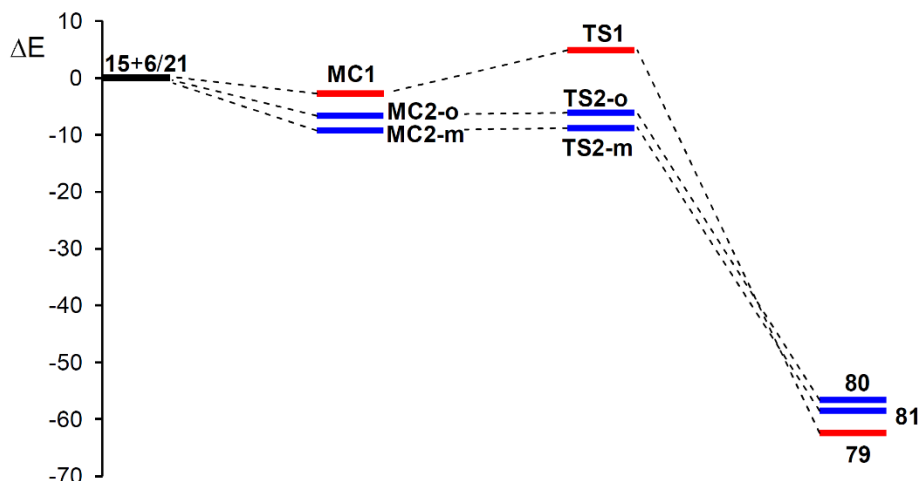


Figure 3.45. MPWB1K/6-311G(d) energy profile (ΔE , in $\text{kcal}\cdot\text{mol}^{-1}$) of the 32CA reaction of AI **15** with ethylene **6**, in red, and with DCE **21**, in blue.

The geometries of the TSs involved in the 32CA reactions of AI **15** with ethylene **6** and DCE **21** are displayed in Figure 3.46. Some appealing conclusions were obtained: i) despite the geometrical symmetry of **TS1**, the distances between the interacting nuclei suggest an asynchronous bond formation process in which the C1–C5 bond formation is more advanced than the N3–C4 one;¹⁰⁰ ii) **TS2-m** and **TS2-o** correspond to highly asynchronous single bond formation processes in which the formation at the β -conjugated position of DCE **21** is more advanced than that at the α one; iii) the more favourable **TS2-m** is more advanced and more asynchronous than **TS2-o**; and iv) the more favourable **TS2-m** is associated to the two-center interaction between the most nucleophilic center of AI **15** and the most electrophilic center of DCE **21**, in complete agreement with the analysis of the Parr functions⁸² (see Section 3.3.2.2).

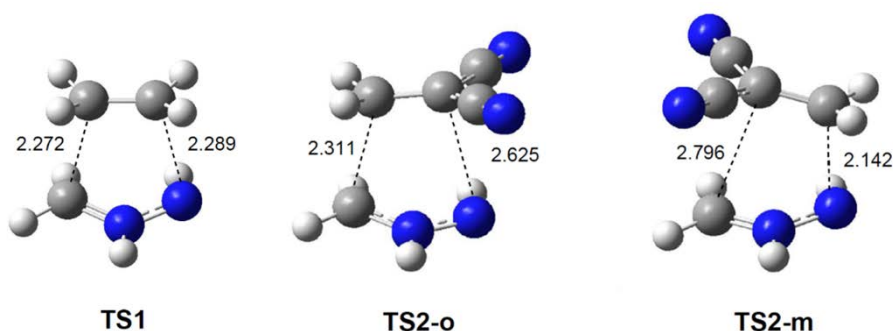


Figure 3.46. MPWB1K/6-311G(d) gas phase optimised geometries of the TSs associated with the 32CA reactions of AI **15** with ethylene **6** and DCE **21**. Distances are given in angstroms, Å.

The GEDT that fluxes from the AI moiety towards the ethylene one is 0.10e at **TS1**, 0.25e at **TS2-o** and 0.27e at **TS2-m**, indicating that while the 32CA reaction with ethylene **6**

3. Results and discussion

has a low polar character, that involving DCE **21** has a high polar character, in clear agreement with the analysis of the CDFT reactivity indices (see Section 3.3.2.2). These results account for the large decrease of the activation energy of the polar 32CA reaction involving DCE **21** with respect to the non-polar 32CA reaction involving ethylene **6**.

3.3.2.4. BET study of the 32CA reaction of AI **15** with ethylene **6**

A BET study of the non-polar 32CA reaction of AI **15** with ethylene **6** (see Table 16 and Scheme 6.13 in Appendix) allowed drawing the following conclusions: i) the corresponding IRC is divided in nine differentiated phases, a behaviour that clearly indicates that the bonding changes along this one-step mechanism are non-concerted; ii) there is no bonding region between the terminal interacting nuclei at **TS1**; iii) the moderate activation energy associated with this reaction, $8.7 \text{ kcal}\cdot\text{mol}^{-1}$, can be mainly associated with the rehybridisation of the C1 *pseudoradical* carbon from sp^2 to sp^3 ; iv) formation of the first C1–C5 single bond begins at a distance of ca. 2.03 \AA through the C-to-C coupling of two C1 and C5 *pseudoradical* centers⁶¹ (see **P5** and **P6** in Figure 3.47); v) interestingly, while the C5 *pseudoradical* center is generated along the reaction path through the depopulation of the C4–C5 double bond of ethylene **6**, the C1 *pseudoradical* center is already present at the simplest AI **15** (see Figure 3.47);

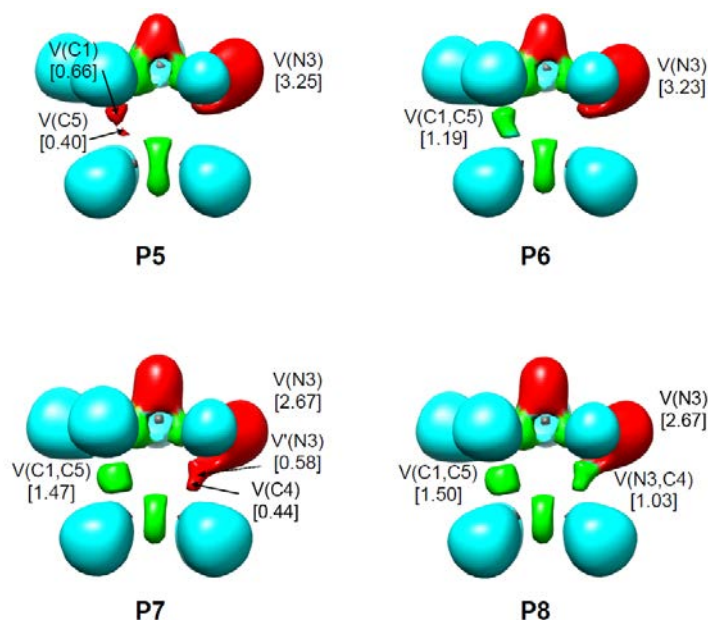


Figure 3.47. ELF localisation domains of the points of the IRC defining the four phases involved in the formation of the C1–C5 and N3–C4 single bonds along the non-polar 32CA reaction between AI **15** and ethylene **6**. The electron populations, in average number of electrons (e), are given in brackets.

vi) formation of the second N3–C4 single bond begins at a distance of ca. 1.92 Å by sharing non-bonding electron density of the N3 nitrogen and that of the C4 *pseudoradical* (see **P7** and **P8** in Figure 3.47); vii) formation of this C–N single bond is thus different to that found in the ketene-imine Staudinger reaction in which the first C–N single bond is formed by donation of the non-bonding electron density of the imine nitrogen to the ketene carbonyl carbon;¹⁰⁵ and viii) the present BET study allows characterising the molecular mechanism of this non-polar 32CA reaction as a $[2n+2\tau]$ process. Note that, in 1931, first Pauling¹⁰⁶ and later Slater^{12a} proposed that the C–C bonding region of ethylene **6** can be represented by two equivalent bonds named τ bonds.

3.3.2.5. ELF topological analysis of the C–C and N–C bond formation processes along the polar 32CA reaction between AI **15** and DCE **21**. Understanding the role of the GEDT.

From the ELF topological analysis along both regioisomeric reaction paths (see Tables 17 and 18, and Schemes 6.14 and 6.15 in Appendix) the following conclusions were drawn: i) formation of the first single bond involves the most electrophilic center of DCE **21**, the C4 carbon (see Figure 3.48); ii) formation of the C–C single bond begins at distances of ca. 2.14 Å (*meta*) and 2.05 Å (*ortho*) through the C-to-C coupling of two C1 and C4/C5 *pseudoradical* centers⁶¹ (see **P1-o** and **P2-o** in Figure 3.48); iii) interestingly, while along the more favourable *meta* pathway the two C1 and C5 *pseudoradical* centers are created as the reaction progresses, the C1 *pseudoradical* center is already present at *ortho* **MC2-o**; iv) while along the more favourable *meta* pathway the C5 *pseudoradical* center created at the DCE framework participates more than the C1 one created at the AI moiety in the C–C bond formation process, along the *ortho* pathway the C1 *pseudoradical* center already present at **MC2-o** contributes more; v) conversely, the N–C bond formation takes place differently along both reaction paths. Formation of the N–C single bond begins at distances of 1.81 Å (*meta*) and 1.84 Å (*ortho*) by donation of part of the non-bonding electron density of the N3 nitrogen to the C4 carbon along the *meta* pathway (see **P1-m** and **P2-m** in Figure 3.48) or by sharing non-bonding electron density of the N3 nitrogen and that of the C5 *pseudoradical* center along the *ortho* pathway; vi) the polar 32CA reaction between AI **15** and DCE **21** proceeds through a *two-stage one-step* mechanism⁷⁷ in which the formation of the second bond begins when the first one is already formed by above 94% (see Tables 17 and 18 in Appendix), in agreement with the

3. Results and discussion

high asynchronicity predicted from the geometry analysis; vii) the bonding patterns of **TS2-o** and **TS2-m** are very similar to those of the corresponding MCs and, accordingly, the very low energy barriers relative to the corresponding MCs, 0.6 (**TS2-o**) and 0.4 (**TS2-m**) kcal·mol⁻¹, can mainly be associated with a slight electron density reorganisation within the molecular system; viii) therefore, these very low activation energies can be the consequence of the GEDT taking place at the polar TSs, which favours the polar 32CA reaction through an electronic stabilisation of the entire molecular system controlled by the electrophilic framework; ix) the energy difference between **TS2-o** and **TS2-m**, 2.8 kcal·mol⁻¹, is likely to be associated to the higher stability of the electron density distribution at **TS2-m** than that at the *pseudoradical* structure of **TS2-o**.

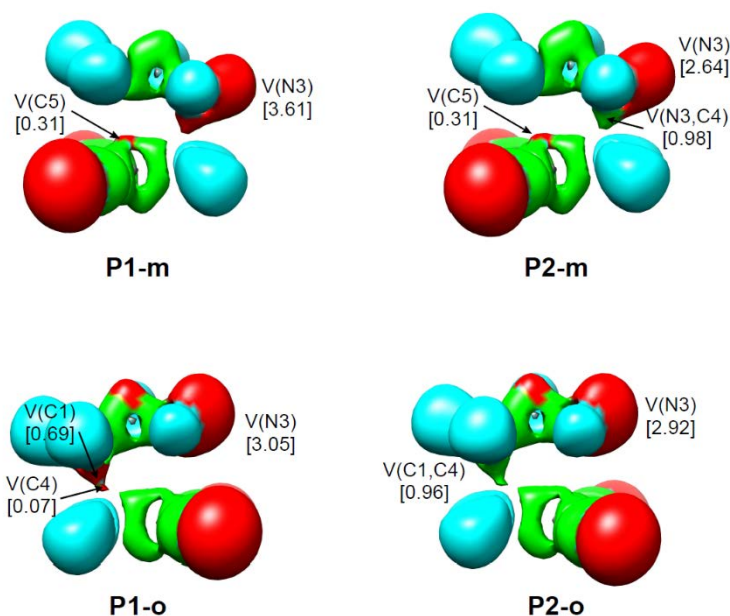


Figure 3.48. ELF localisation domains of the points of the IRC defining the four phases involved in the formation of the first N3–C5 (*meta*) and C1–C4 (*ortho*) single bonds along the two regioisomeric reaction paths associated with the polar 32CA reaction between AI **15** and DCE **21**. The electron populations, in average number of electrons (e), are given in brackets.

A comparative analysis between both BET and ELF studies made it possible to understand the role of the GEDT in the polar process. Some appealing conclusions emerged from this comparative analysis: i) while along the non-polar 32CA reaction involving ethylene **6** and the less favourable *ortho* pathway of the polar 32CA reaction involving DCE **21**, the most favourable interaction is that involving the C1 *pseudoradical* center, along the more favourable *meta* pathway of the polar 32CA reaction it is that involving the most nucleophilic and electrophilic centers of the reagents; ii) thus, while the non-polar cycloaddition and the *ortho* reaction path of the polar reaction begins with

the initial formation of the C–C single bond, the *meta* reaction path of the polar reaction begins with the initial formation of the N–C single bond. Consequently, both mechanisms are different; iii) formation of the new single bonds is slightly asynchronous in the non-polar reaction but highly asynchronous in the polar reaction; iv) unlike polar Diels–Alder reactions and polar *zw-type* 32CA reactions, in which the GEDT favours the bonding changes at the reagents, i.e. the rupture of the double bonds,¹⁰² in the polar 32CA reaction between AI **15** and DCE **21**, the GEDT provokes an electronic stabilisation of the entire molecular system controlled by the electrophilic framework, decreasing the activation energies from 8.7 kcal·mol⁻¹ (**TS1**) to 0.4 (**TS2-o**) and 3.2 (**TS2-m**) kcal·mol⁻¹. This behaviour is similar to that found in the polar 32CA reaction between NY **10** and DCE **21**.⁹⁵

Consequently, the GEDT taking place at the polar 32CA involving DCE **21** does not only decrease the activation energy associated with the non-polar 32CA reaction involving ethylene **6**, but also modifies the molecular mechanism of the polar reaction.

4. CONCLUSIONS

Since the beginning of the present century, there has been a growing interest in explaining the chemical reactivity arising from the analysis of the changes of the electron density along a reaction path.^{60a,107} In this context, in 2016, Domingo proposed the MEDT⁵⁵ as a new reactivity theory in Organic Chemistry, which establishes that the feasibility for the changes in the electron density along a reaction path, but not MO interactions, is responsible for the reactivity of organic molecules.

In the present thesis, the 32CA reactions have been tackled based on MEDT, allowing us to unravel the classical vision of 32CA reactions widely discussed since the 60's, as well as revisiting related theories and concepts also established in the past century.

Recent MEDT studies devoted to the 32CA chemistry, those presented herein being among them, have allowed establishing a very good correlation between the electronic structure of TACs and their reactivity. Accordingly, depending on the electronic structure of the TAC, i.e. *pseudodiradical* (such as AY **14**), *pseudoradical* (such as AI **15**), carbenoid (such as NY **10**) or zwitterionic (such as Ni **16**), 32CA reactions have been classified into *pseudodiradical-type* (*pdr-type*),⁵¹ *pseudoradical-type* (*pmr-type*),¹⁰³ carbenoid-type (*cb-type*)⁹⁵ and zwitterionic-type (*zw-type*)⁵¹ reactions (see Figure 4.1). The reactivity trend decreases in the order *pseudodiradical* > carbenoid \approx *pseudoradical* > zwitterionic,¹⁰³ in such a manner that while *pdr-type* 32CA reactions take place easily through early TSs, *zw-type* 32CA reactions demand adequate nucleophilic/electrophilic

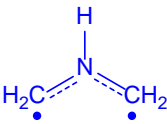
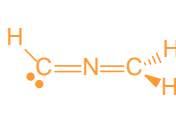
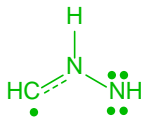
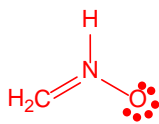
			
Azomethine ylide	Nitrile ylide	Azomethine imine	Nitron
Structure			
<i>pseudodiradical</i>	carbenoid	<i>pseudoradical</i>	zwitterionic
Reactivity			
<i>pdr-type</i>	<i>cb-type</i>	<i>pmr-type</i>	<i>zw-type</i>
Activation Energies			
1.0	7.4	7.7	14.3

Figure 4.1. Electronic structure of TACs and proposed reactivity types in 32CA reactions. MPWB1K/6-311G(d) gas phase activation energies of the non-polar 32CA reactions between the simplest four representative TACs and ethylene **6**, relative to the corresponding molecular complexes, are given in kcal·mol⁻¹.

4. Conclusions

activations to take place.⁵¹ Note that the polar character of the reaction influences the four reactivity types, i.e. the stronger the nucleophilic/electrophilic interactions taking place at the TSs, the faster the reaction.¹⁰² It is also worth mentioning that although substitution may change the electronic structure of the simplest TAC parents,¹⁰⁸ the structure/reactivity relationship is maintained.

Figure 4.2 explains the origin of the reactivity trend in non-polar 32CA reactions. The two *pseudoradical* centers present in symmetric *pseudodiradical* TACs favour the synchronous C–C single bond formation process through a homolytic rupture of the C–C double bond of the ethylene framework (see Figure 4.2). This behaviour accounts for the high reactivity of azomethine and carbonyl ylides **14** and **15**, as they already present the two *pseudoradical* centers demanded for the C–C single bond formation⁶¹ in such a manner that they are already prepared to react. However, this behaviour is not feasible in *pmr-type* 32CA reactions; non-symmetric *pseudoradical* TACs such as AI **15** and Das **2** are not able to induce an effective symmetric electron density depopulation of the C–C bonding region in the ethylene framework because they do not have the second *pseudoradical* center demanded for the formation of the second new single bond (see Figure 4.1). Finally, as the multiple bond present in zwitterionic TACs has to be broken beforehand, *zw-type* 32CA reactions demand the highest EC, which is lowered by the polarity of the reaction.

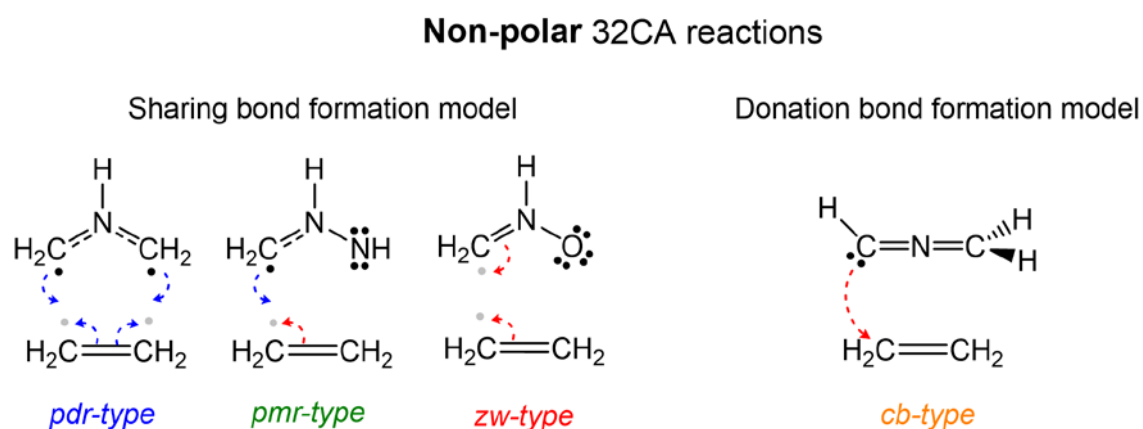


Figure 4.2. Bonding changes associated with the formation of the new C–C single bonds along the four types of non-polar 32CA reactions.

It should be emphasised that the reactivity of carbenoid TACs participating in *cb-type* 32CA reactions is completely different to that of the other three types of TACs. In the 32CA reactions involving carbenoid TACs, formation of the first C–C single bond takes place by donation of the non-bonding electron density of the carbenoid center to an

electrophilic carbon,^{84,95} while in the non-polar 32CA reactions involving the other three types of TACs, formation of the first C–C single bond takes place by the C-to-C coupling of two *pseudoradical* centers generated at the interacting carbons⁶¹ (see Figure 4.2).

On the other hand, polar 32CA reactions begin by the two-center interaction between the most nucleophilic center of the nucleophile and the most electrophilic center of the electrophile,¹⁰⁹ a behaviour anticipated by the analysis of the Parr functions.⁸² In general, TACs participate as the nucleophilic component in polar 32CA reactions. Thus, analysis of the nucleophilic Parr functions of *pseudoradical* and zwitterionic TACs indicates that the terminal heteroatom is usually their most nucleophilic center. In these cases, ELF topological analysis of the bonding changes along the most favourable reaction path reveals that the reaction begins by donation of part of the non-bonding electron density of the most nucleophilic center of the TAC to the most electrophilic carbon of the ethylene derivative.^{69,78,83,103} Consequently, polar *pmr-type* and *zw-type* 32CA reactions follow a molecular mechanism similar to that of *cb-type* 32CA reactions (see Figure 4.3). This behaviour plays an important role in the regioselectivity of these reactions and asserts the relevance of the analysis of the CDFT indices at the GS of the reagents in the study of the reactivity in 32CA reactions.⁵⁶

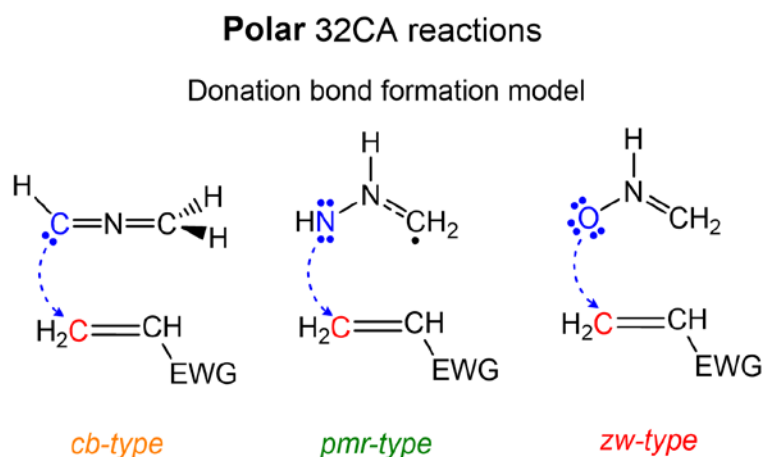


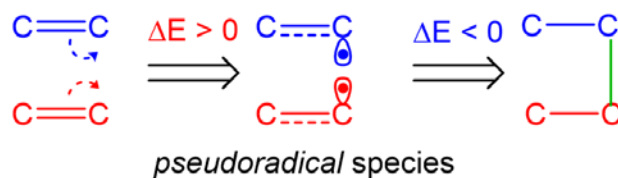
Figure 4.3. Bonding changes associated with the formation of the first new single bond along polar 32CA reactions.

In this sense, from the analysis of the bonding changes along polar *zw-type*, *cb-type* and *pmr-type* 32CA reactions, a new model for the formation of C–X (X=C, N, O) single bonds by donation of non-bonding electron density has been established (see Figure 4.4). Note that while the sharing model demands the homolytic rupture of multiple bonds, the donation mechanism demands the initial depopulation of the β -conjugated carbon of the

4. Conclusions

substituted ethylene, a feature only possible when strong EWG groups, such as $-\text{CHO}$ or $-\text{NO}_2$, are present at the α -position.

a) C-C bond formation involving multiple bonds



b) C-X bond formation involving lone pairs

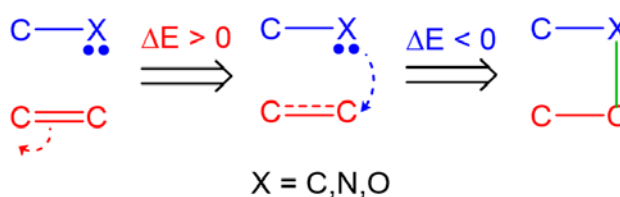


Figure 4.4. Two models for the formation of C–X (X=C, N, O) single bonds.

This MEDT rationalisation of 32CA reactions revives, but also unravels, the classical controversy between Huisgen's¹⁴ and Firestone's¹³ mechanistic proposals.

Regarding the electronic structure of TACs, analysis of their electron density distribution, i.e. bonding pattern, reveals that while zwitterionic TACs correspond to Huisgen's proposal,¹⁴ *pseudodiradical* TACs correspond to Firestone's one.¹³ However, it should be emphasised that NPA of the charge distribution of TACs suggests that they are neither 1,3- nor 1,2- zwitterionic-charged structures with full charge separation¹⁴ and, therefore, our conception of zwitterionic TACs, which does not consider charges but just a bonding pattern, slightly differs from Huisgen's definition of "1,3-dipoles".

Regarding their mechanistic proposals, when two reagents undergo either a polar or non-polar 32CA reaction, there are three different conformational approach modes: one through a one-step mechanism, **A**, and other two giving intermediates that must experience a single bond rotation for the subsequent bond formation, **B** and **C** (see Figure 4.5). In non-polar 32CA reactions, i.e. the reagents are neither strong nucleophiles nor strong electrophiles, these intermediates are diradical (Firestone); conversely, in polar 32CA reactions, i.e. one reagent is a strong nucleophile and the other one is a strong electrophile, these intermediates have a zwitterionic nature (Huisgen).

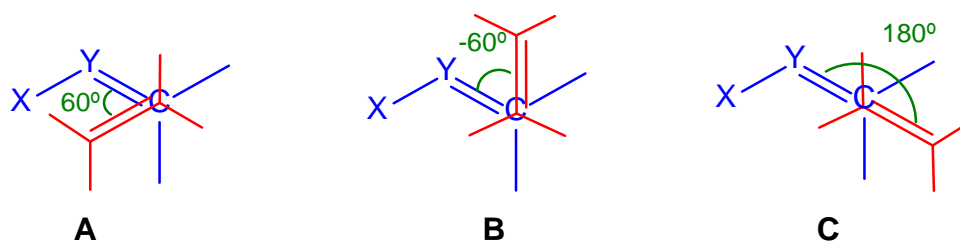


Figure 4.5. Conformational approach modes of the ethylene, in red, to the TACs, in blue, yielding one-step mechanisms (**A**) and stepwise ones (**B** and **C**).

Generally, the one-step approach mode **A** presents lower activation energy than the stepwise approach modes **B** and **C** and, consequently, the stepwise reaction paths are not competitive. However, if both diradical or zwitterionic intermediates are sufficiently stabilised, they could be intercepted or undergo rotation at the ethylene, and then the reaction could lose its stereospecificity. On the other hand, ELF topological analysis of one-step reaction paths type **A** demonstrates that neither non-polar nor polar one-step processes are “concerted”, but the bonding changes are sequential, thus ruling out the “pericyclic” mechanism proposed by Woodward and Hoffmann.²⁶ Polarity increases the asynchronicity of the bond formation in cycloaddition reactions⁶⁶ in such a way that most polar 32CA reactions take place through a non-concerted *two-stage one-step* mechanism;⁷⁷ further stabilisation of a feasible zwitterionic intermediate could change the mechanism to a two-step one, but the sequential bonding changes remain essentially the same.

Finally, our reactivity model for 32CA reactions, based on the analysis of the electron density, allows a rationalisation of Houk’s DIEM,⁴⁸ based on distortion energies; i.e. the feasibility of a 32CA reaction is not controlled by the distortion required to reach the TS (Hammond’s postulate)⁵⁰ but by the semblance of the electronic structure of the TAC to that demanded for the formation of new single bonds, causing an earlier and less energetic TS (see Figure 4.6 in which the activation energies of the non-polar 32CA reactions of twelve different TACs, six A-TACs and six P-TACs, with ethylene **6** are represented with respect to a percentage of reaction progress proportional to the ethylene C–C length). Thus, the position of the TS, i.e. its early or advanced character, is determined by the electronic structure of the TAC (see Figures 4.1 and 4.2) together with the non-polar or polar electronic nature of the reaction.

4. Conclusions

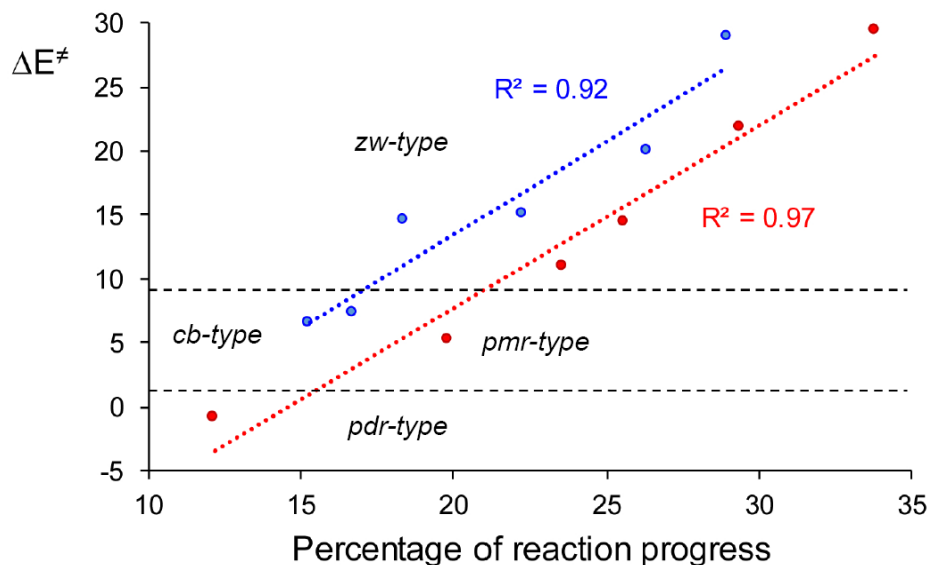


Figure 4.6. Plot of activation energies, in kcal·mol⁻¹, relative to the separated reagents, vs the percentage of reaction progress calculated as $[(d(C-C)_{TS} - d(C-C)_{Ethylene}) / (d(C-C)_{CA} - d(C-C)_{Ethylene})] \times 100$, for twelve non-polar 32CA reactions of six P-TACs, in blue, and six A-TACs, in red, with ethylene **6**.

Some appealing conclusions can be drawn from Figure 4.6: i) only A-TACs can participate in *pdr-type* and *pmr-type* 32CA reactions, unless substitution is able to change the parent electronic structures; ii) only P-TACs can participate in *cb-type* 32CA reactions; iii) non-polar *cb-type* and *pmr-type* 32CA reactions present similar activation energies, though they follow different molecular mechanisms; iv) linear P-TACs present a parallel trend, but with higher activation energies, with respect to that associated with bent A-TACs.

In the present thesis, the classical theory of 32CA reactions,^{5a} established in the 60's of the past century and still prevailing today,⁴⁶ is revisited and reinterpreted based on the MEDT.⁵⁵ A solid new reactivity model for 32CA reactions is established, while the “pericyclic” mechanism and the DIEM, which have been widely used for their rationalisation, are ruled out, emphasising that the way that organic chemists conceive organic chemistry demands a contemporary revision aimed towards the analysis of the electron density.

“In all affairs it’s a healthy thing now and then to hang a question mark on the things you have long taken for granted.”

–Bertrand Russel

5. FUTURE PERSPECTIVES

Despite our recent exhaustive work developed in the field of 32CA reactions, other features still demand further investigation in order to achieve a complete understanding of these relevant cycloaddition reactions.

On the one hand, it is well-established that the GEDT⁶¹ taking place along a polar cycloaddition reaction decreases the corresponding activation energies, either by favouring the bonding changes or simply by an electronic stabilisation of the molecular system.^{61,95,102,103} Unlike DA reactions, which have been classified into non-polar (N-DA), polar (P-DA) and ionic (I-DA) reactions depending on the electronic nature of the reagents,⁶⁶ 32CA reactions lack a clear systematisation of the polar and non-polar mechanisms due to the aforementioned diversity of four different types of TACs (see Figure 4.1 in Conclusions). Therefore, future work will be focused on how the GEDT affects the four types of 32CA reactions.

On the other hand, the partners of P-TACs and A-TACs have shown to present a notably different reactivity in 32CA reactions; i.e. the corresponding trend of activation energies associated with P-TACs, though parallel to that associated with A-TACs, appears to be energetically higher due to the linear structure of P-TACs (see Figure 4.6 in Conclusions). Note, for instance, the different reactivity of the NO **8** / Ni **16** (C–N–O) and Da **2** / Al **15** (C–N–N) partners. Consequently, in this context, our future research will focus on why and how the linearity of P-TACs causes them to be less reactive than bent A-TACs.

Finally, it is worth emphasising that the characterisation of the electronic structure of TACs, which permits the identification of the reactivity types in 32CA reactions, is only possible through a first topological analysis of the ELF of TACs. Most organic chemists do not have adequate computational resources to perform such analyses. In this sense, we are currently designing a way to predict the electronic structure of TACs directly without ELF calculations.

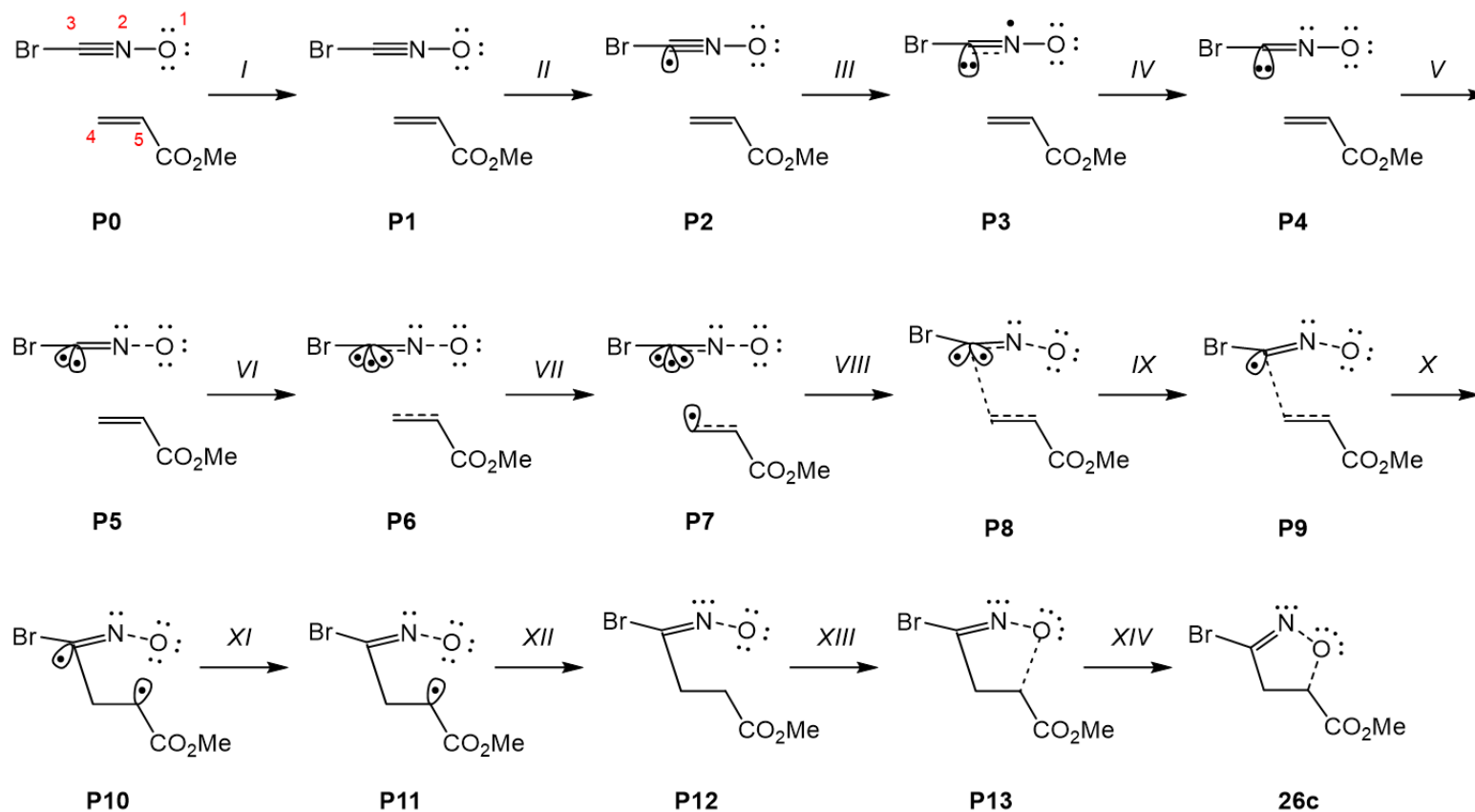
6. APPENDIX

Table 3. B3LYP/6-31G(d) electronic chemical potential, μ , chemical hardness, η , electrophilicity, ω , and nucleophilicity, N , in eV, of the TACs and ethylene/acetylene derivatives discussed, as well as the *pseudodiradical pr* index of NY **10**, AY **14**, Das **2** and **72** and AI **15**.

Reactants	μ	η	ω		N		<i>pr</i>
DNE 73	-5.98	5.03	3.56	strong	0.62	marginal	
DCE 21	-5.64	5.65	2.82	strong	0.65	marginal	
Ketene 34c (R = CF ₃)	-5.26	5.62	2.47	strong	1.05	marginal	
NY 63	-3.86	3.20	2.33	strong	3.67	strong	
Da 72	-4.40	4.66	2.07	strong	2.39	moderate	0.51
NO 8b (R = CO ₂ Me)	-4.69	5.76	1.91	strong	1.55	marginal	
oxazolidinone 67	-4.28	5.88	1.56	strong	1.90	marginal	
oxazolidinone 64	-4.07	5.51	1.50	moderate	2.30	moderate	
MA 5	-4.31	6.23	1.50	moderate	1.70	marginal	
NO 8c (R = Br)	-4.15	5.82	1.48	moderate	2.06	moderate	
NO 8a (R = Ph)	-3.83	5.03	1.46	moderate	2.78	moderate	
Da 2	-3.64	4.73	1.40	moderate	3.11	strong	0.66
DMAD 56	-5.01	8.95	1.40	moderate	0.91	marginal	
Ketene 34a (R = H)	-3.76	5.57	1.27	moderate	2.58	moderate	
Ni 51	-3.29	4.27	1.26	moderate	3.70	strong	
CHDE 50	-3.44	4.77	1.24	moderate	3.29	strong	
<i>cis</i> - IN	-3.58	6.03	1.06	moderate	3.80	strong	
Ni 16	-3.43	5.55	1.06	moderate	2.92	moderate	
Ketene 34b (R = Me)	-3.23	5.08	1.02	moderate	3.35	strong	
Ni 41	-2.95	5.42	0.80	marginal	3.46	strong	
NY 10	-2.90	5.45	0.77	marginal	3.50	strong	0.64
Acetone 57	-3.72	9.02	0.77	marginal	2.16	moderate	
Ethylene 6	-3.37	7.77	0.73	marginal	1.86	marginal	
NO 8	-3.40	7.94	0.73	marginal	1.75	marginal	
AI 15	-2.70	5.02	0.72	marginal	3.92	strong	0.78
Allene 54	-3.30	7.72	0.70	marginal	1.97	marginal	
Methyl isocyanide 55	-3.90	11.46	0.66	marginal	0.77	marginal	
Acetylene 9	-3.53	11.34	0.55	marginal	1.20	marginal	
AY 14	-1.82	4.47	0.37	marginal	5.07	strong	1.13

Table 4. ELF valence basin populations of the IRC points, **P1** – **P13**, defining the fourteen phases characterising the molecular mechanism of the more favourable pathway associated with the polar *zw*-type 32CA reaction between NO **8c** and MA **5**. The stationary points **TSc-o** and **26c** are also included. Distances are given in angstroms (Å), GEDT values and electron populations in average number of electrons (e), and relative energies in kcal·mol⁻¹.

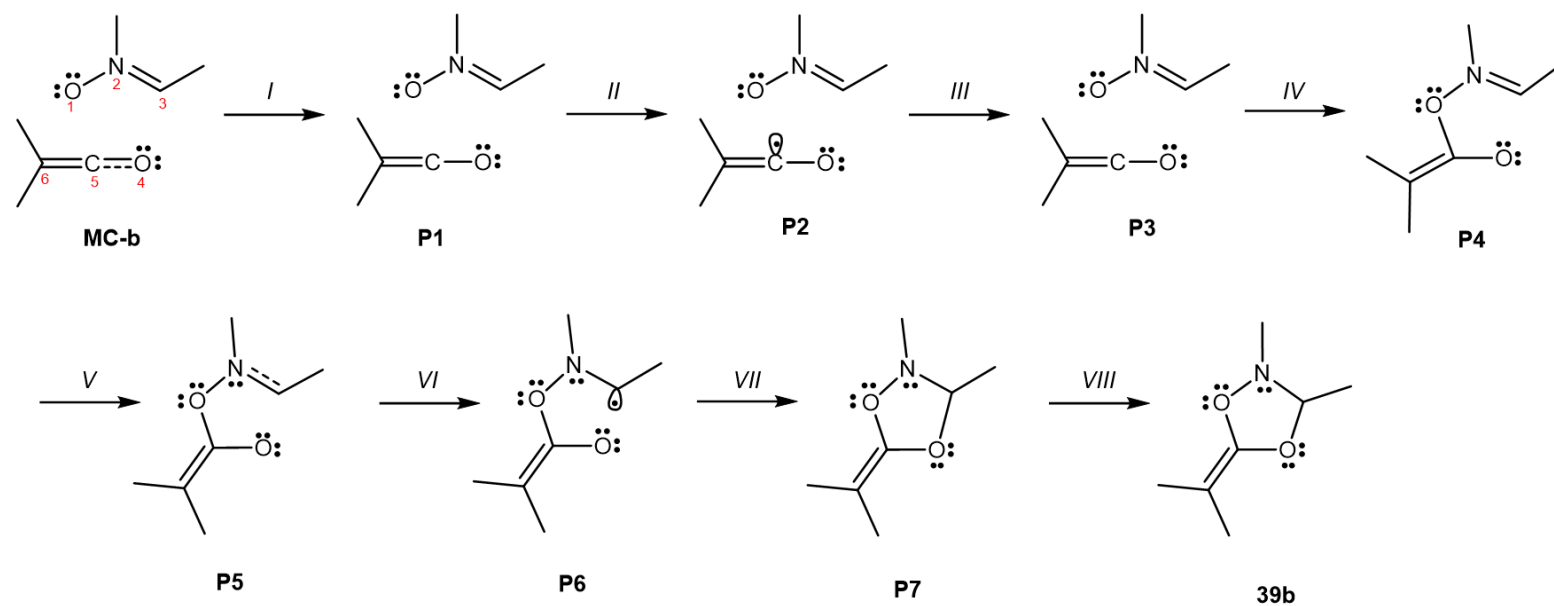
Phases		<i>I</i>	<i>II</i>	<i>III</i>	<i>IV</i>	<i>V</i>	<i>VI</i>	<i>VII</i>	<i>VIII</i>	<i>IX</i>	<i>X</i>	<i>XI</i>	<i>XII</i>	<i>XIII</i>	<i>XIV</i>		
Catastrophes		<i>C</i>	<i>F</i> [†]	<i>F</i> [†]	<i>C</i>	<i>C</i> [†]	<i>C</i> [†]	<i>F</i> [†]	<i>C</i>	<i>F</i>	<i>F</i> [†]	<i>F</i>	<i>F</i>	<i>F</i> [†]			
Points	8c 5	P0	P1	P2	P3	P4	P5	P6	P7	P8	P9	P10	P11	P12	P13	26c	TSc-o
d(C3–C4)		3.698	3.024	2.973	2.563	2.300	2.269	2.204	2.089	1.997	1.859	1.797	1.764	1.562	1.559	1.504	2.263
d(O1–C5)		3.531	2.950	2.924	2.694	2.523	2.505	2.462	2.390	2.332	2.240	2.193	2.166	1.789	1.776	1.470	2.501
ΔE		0.0	2.0	2.3	6.3	8.8	8.8	8.7	7.1	4.6	-1.5	-5.1	-7.3	-30.8	-31.5	-45.3	8.8
GEDT		0.01	0.02	0.03	0.04	0.02	0.01	-0.01	-0.04	-0.06	-0.10	-0.11	-0.12	-0.22	-0.23	-0.28	0.01
V(O1,N2)	1.96	1.61	1.59	1.59	1.50	1.46	1.44	1.44	1.42	1.40	1.34	1.30	1.30	1.07	1.05	0.90	1.46
V(N2)					0.76	1.86	1.90	2.02	2.17	2.30	2.44	2.49	2.52	2.77	2.77	2.91	1.91
V(N2,C3)	5.75	6.42	1.36	2.21	2.13	1.51	1.48	1.46	1.40	1.39	1.36	1.39	1.85	1.77	1.77	1.70	1.48
V'(N2,C3)			5.05	4.20	2.27	1.71	1.67	1.59	1.52	1.49	1.94	1.90	1.91	1.76	1.75	1.69	1.66
V(C4,C5)		1.70	1.73	1.69	1.69	3.20	3.20	3.14	2.89	2.73	2.55	2.40	2.33	2.04	2.04	1.95	3.20
V'(C4,C5)		1.70	1.71	1.70	1.69	1.63											
V(O1)	5.62	2.84	2.98	2.97	2.85	2.84	2.86	2.87	2.81	2.81	2.85	2.88	2.81	3.27	2.70	2.54	2.85
V'(O1)		2.83	2.75	2.76	2.83	2.78	2.79	2.79	2.79	2.77	2.77	2.77	2.81	2.78	2.72	2.55	2.79
V(C3)				0.01	1.44	1.74	0.73	0.68	0.63	0.60	0.55	0.53					0.73
V'(C3)							1.03	0.61	0.75								1.03
V''(C3)								0.54	0.52	0.51							
V(C4)									0.19								
V(C5)												0.05	0.09				
V(O1,C5)															0.66	1.21	
V(C3,C4)										1.13	1.38	1.47	1.53	1.89	1.90	2.01	



Scheme 6.1. Simplified representation of the molecular mechanism of the polar *zW*-type 32CA reaction between NO **8c** and MA **5** by Lewis structures arising from the topological analysis of the ELF along the more favourable reaction path.

Table 5. ELF valence basin populations of the IRC points, **P1** – **P7**, defining the eight phases characterising the molecular mechanism of the most favourable pathway associated with the *zw*-type 32CA reaction between Ni **41** and ketene **34b**. The stationary points **MC-b**, **TS-CO** and **39b** are also included. Distances are given in angstroms (Å), GEDT values and electron populations in average number of electrons (e), and relative energies in kcal·mol⁻¹.

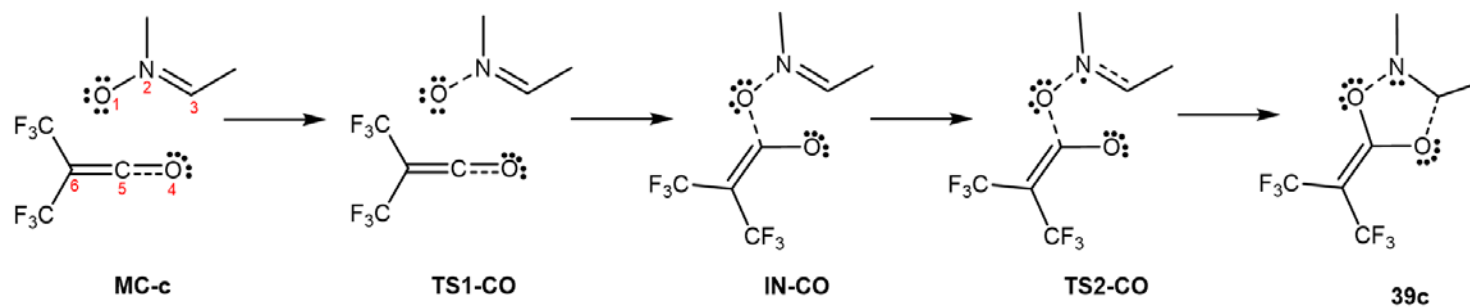
Phases	<i>I</i>	<i>II</i>	<i>III</i>	<i>IV</i>	<i>V</i>	<i>VI</i>	<i>VII</i>	<i>VIII</i>		
Catastrophes	<i>C</i>	<i>CF</i>	<i>F</i>	<i>C</i> [†]	<i>F</i> [†]	<i>F</i> [†]	<i>C</i> [†]			
Points	MC-b	P1	P2	P3	P4	P5	P6	P7	39b	TS-CO
d(O1–C5)	3.046	2.284	1.797	1.786	1.644	1.611	1.463	1.445	1.367	1.560
d(C3–C4)	3.256	2.762	2.552	2.544	2.389	2.329	1.914	1.838	1.420	2.219
ΔE	0.0	2.7	7.0	7.1	8.6	9.0	4.5	1.4	-22.7	9.3
GEDT	0.01	0.09	0.28	0.28	0.34	0.34	0.24	0.21	0.10	0.33
V(O1,N2)	1.48	1.43	1.35	1.35	1.26	1.24	1.10	1.10	0.99	1.18
V(N2)						0.96	1.91	2.01	2.35	1.31
V(N2,C3)	1.90	1.95	3.79	3.80	3.94	3.04	2.37	2.26	1.91	2.78
V'(N2,C3)	1.89	1.84								
V(O4,C5)	1.32	2.52	2.32	2.30	2.14	2.08	1.77	1.75	1.53	1.96
V'(O4,C5)	1.38									
V(C5,C6)	2.08	2.11	2.11	2.11	2.08	2.08	2.06	2.06	2.00	
V'(C5,C6)	2.09	2.11	2.08	2.07	2.03	2.01	1.96	1.97	2.05	
V(O1)	2.95	2.93	2.89	2.88	2.48	2.52	2.44	2.43	2.58	2.47
V'(O1)	3.04	3.07	3.09	3.15	2.76	2.71	2.49	2.48	2.41	2.65
V(C5)			0.02							
V(C3)							0.03			
V(O4)	2.45	2.55	2.65	2.65	3.00	3.04	2.90	2.77	2.34	3.08
V'(O4)	2.48	2.57	2.69	2.69	2.55	2.50	2.79	2.43	2.40	2.54
V(O1,C5)					0.87	0.90	1.31	1.35	1.51	1.05
V(C3,O4)								0.60	1.32	



Scheme 6.2. Simplified representation of the molecular mechanism of the *zw*-type 32CA reaction between Ni **41** and ketene **34b** by Lewis structures arising from the topological analysis of the ELF along the most favourable reaction path.

Table 6. ELF valence basin populations of the stationary points involved in the most favourable pathway associated with the *zw-type* 32CA reaction between Ni **41** and ketene **34c**. Distances are given in angstroms (Å), GEDT values and electron populations in average number of electrons (e), and relative energies in kcal·mol⁻¹.

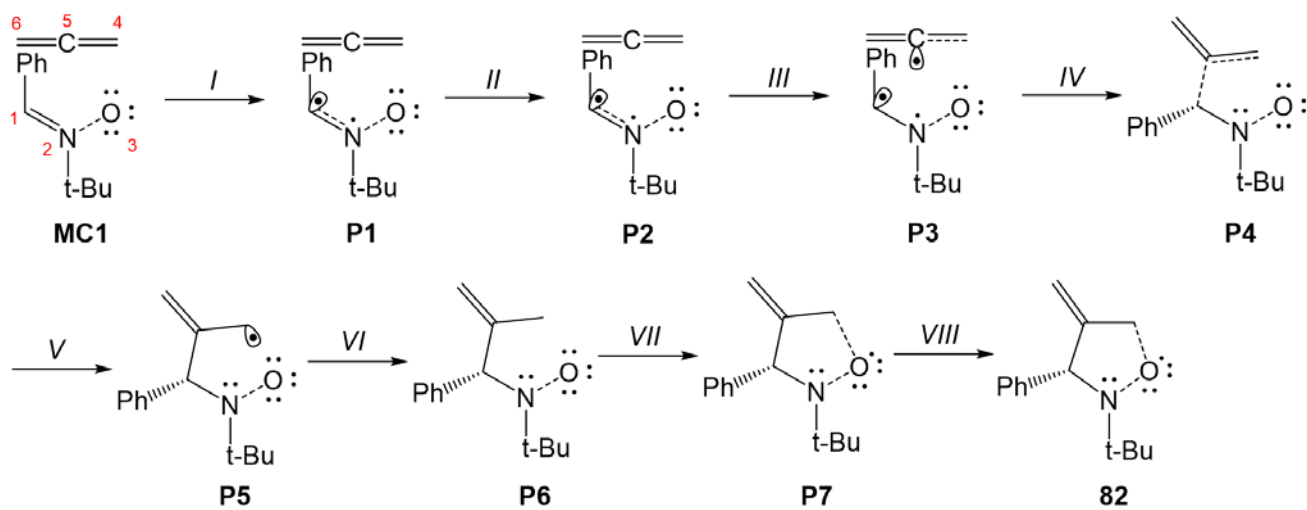
	MC-c	TS1-CO	IN-CO	TS2-CO	39c
d(O1–C5)	2.647	2.492	1.568	1.479	1.339
d(C3–O4)	3.204	3.180	2.745	2.101	1.436
ΔE	0.0	-1.0	-6.4	-1.8	-23.7
GEDT	0.03	0.05	0.45	0.42	0.19
V(O1,N2)	1.48	1.44	1.29	1.21	1.00
V(N2)				1.08	2.34
V(N2,C3)	1.87	1.88	1.90	2.93	1.93
V'(N2,C3)	1.93	1.91	1.92		
V(O4,C5)	1.51	1.52	2.35	2.27	1.66
V'(O4,C5)	1.49	1.46			
V(O1)	2.91	2.93	2.50	2.46	2.26
V'(O1)	3.05	3.09	2.64	2.69	2.52
V(C5)					
V(C3)					
V(O4)	2.32	2.43	2.76	1.76	4.58
V'(O4)	2.36	2.27	2.63	3.63	
V(O1,C5)			1.01	1.05	1.65
V(C3,O4)					1.33
V(C5,C6)	2.05	2.08	2.09	2.04	1.99
V'(C5,C6)	2.08	2.03	1.94	2.01	2.00



Scheme 6.3. Electronic structure of the stationary points involved in the most favourable pathway associated with the polar *zw*-type 32CA reaction between Ni **41** and ketene **34c** by Lewis structures arising from the topological analysis of the ELF.

Table 7. ELF valence basin populations of the IRC points, **P1** – **P7**, defining the eight phases characterising the molecular mechanism of the more favourable pathway associated with the 32CA reaction between Ni **51** and the simplest allene **54**. The stationary points **MC1**, **TS1** and isoxazolidine **82** are also included. Distances are given in angstroms (Å), GEDT values and electron populations in average number of electrons (e), and relative energies in kcal·mol⁻¹.

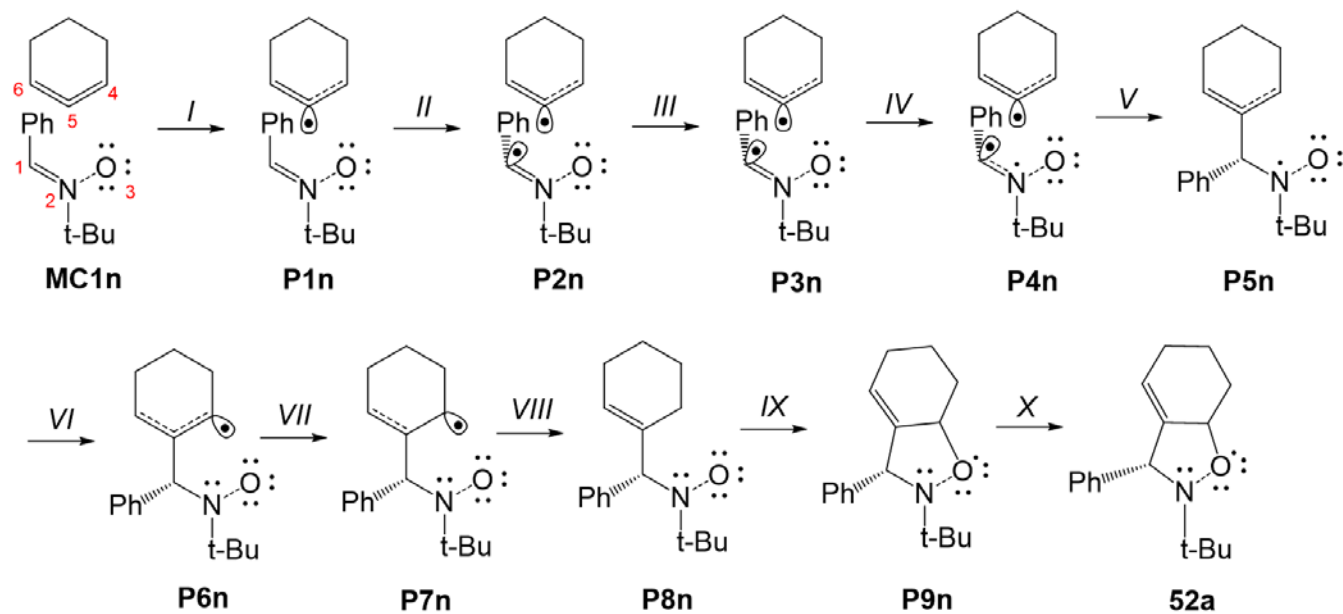
Phases			<i>I</i>	<i>II</i>	<i>III</i>	<i>IV</i>	<i>V</i>	<i>VI</i>	<i>VII</i>	<i>VIII</i>		
Catastrophes			$[F^\ddagger]_2$		<i>C</i>	F^\ddagger	<i>C</i>	F^\ddagger	<i>F</i>	C^\ddagger		
Points	51	54	MC1	P1	P2	P3	P4	P5	P6	P7	82	TS1
d(C1–C5)			5.265	2.297	2.292	2.122	1.909	1.885	1.601	1.586	1.527	2.070
d(O3–C4)			4.120	2.307	2.304	2.220	2.109	2.095	1.804	1.764	1.438	2.195
ΔE			0.0	23.4	23.5	26.7	24.4	23.6	4.1	1.7	-16.9	26.2
GEDT			0.00	-0.04	-0.04	-0.01	0.06	0.06	0.23	0.25	0.29	0.00
V(C1,N2)	3.81		3.88	2.88	2.89	2.50	2.21	2.17	1.93	1.94	1.87	2.41
V(N2)				0.83	0.83	1.24	1.66	1.72	2.16	2.17	2.31	1.36
V(N2,O3)	1.42		1.36	1.31	1.31	1.24	1.15	1.16	1.01	0.99	0.93	1.23
V(C4,C5)		1.84	1.84	1.86	3.55	3.03	2.61	2.54	2.20	2.17	2.05	2.92
V'(C4,C5)		1.85	1.88	1.72								
V(C5,C6)		1.84	1.85	1.87	1.88	1.87	1.86	1.85	1.81	1.83	1.78	1.88
V'(C5,C6)		1.85	1.86	1.82	1.83	1.80	1.75	1.75	1.76	1.75	1.76	1.77
V(C1)				0.28	0.28	0.44						0.50
V(C5)						0.51						0.60
V(O3)	2.99		3.03	2.90	2.90	2.91	2.82	2.85	3.39	2.68	2.51	2.86
V'(O3)	3.02		2.93	2.97	2.96	2.91	2.90	2.89	2.76	2.69	2.55	2.94
V(C4)								0.13				
V(C1,C5)							1.44	1.47	1.88	1.90	1.99	
V(O3,C4)										0.76	1.26	



Scheme 6.4. Simplified representation of the molecular mechanism of the 32CA reaction between Ni **51** and the simplest allene **54** by Lewis structures arising from the topological analysis of the ELF along the more favourable reaction path.

Table 8. ELF valence basin populations of the IRC points, **P1n – P9n**, defining the ten phases characterising the molecular mechanism of the most favourable pathway associated with the 32CA reaction between Ni **51** and strained allene CHDE **50**. The stationary points **MC1n**, **TS1n** and *endo* isoxazolidine **52a** are also included. Distances are given in angstroms (Å), GEDT values and electron populations in average number of electrons (e), and relative energies in kcal·mol⁻¹.

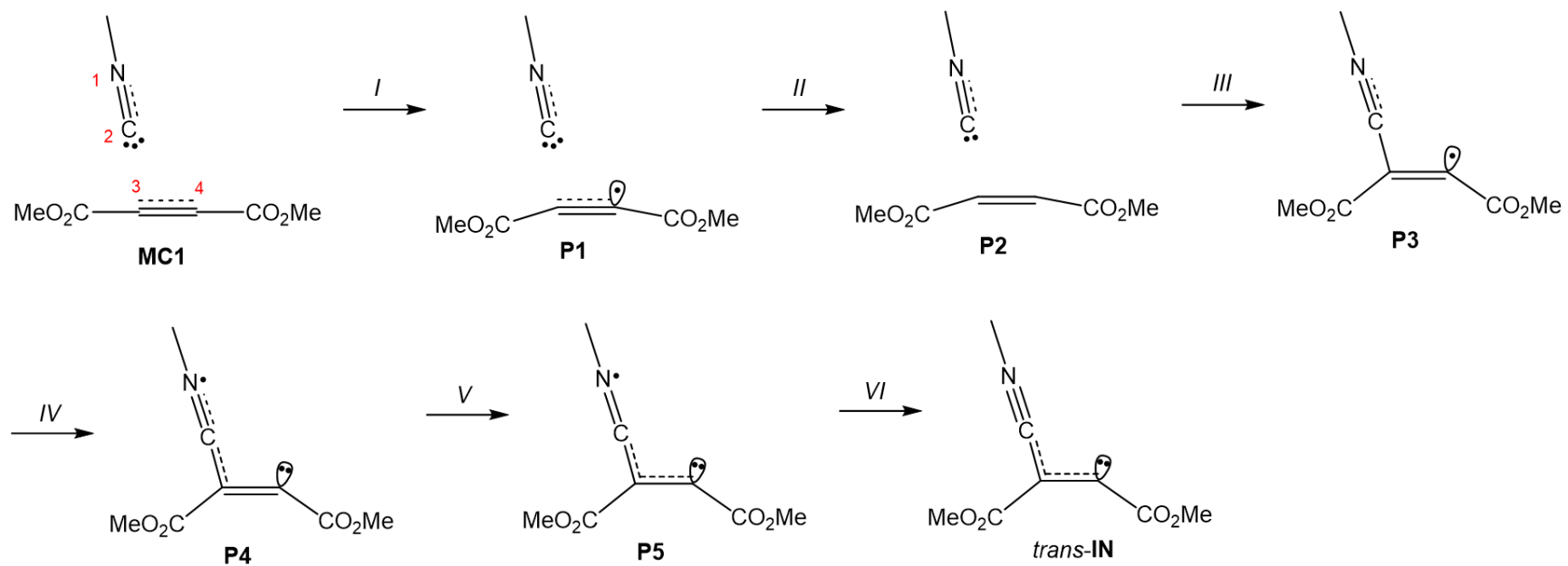
Phases			<i>I</i>	<i>II</i>	<i>III</i>	<i>IV</i>	<i>V</i>	<i>VI</i>	<i>VII</i>	<i>VIII</i>	<i>IX</i>	<i>X</i>		
Catastrophes			<i>F</i> [†]	<i>F</i> [†]	<i>F</i> [†]	<i>C</i>	<i>C</i>	<i>F</i> [†]	<i>C</i> [†]	<i>F</i>	<i>C</i> [†]			
Points	51	50	MC1n	P1n	P2n	P3n	P4n	P5n	P6n	P7n	P8n	P9n	52a	TS1n
d(C1–C5)			5.658	2.317	2.295	2.249	2.203	1.943	1.593	1.562	1.524	1.522	1.522	2.225
d(O3–C4)			4.290	2.762	2.753	2.737	2.720	2.641	2.424	2.252	1.779	1.752	1.421	2.726
ΔE			0.0	8.3	8.4	8.5	8.5	5.2	-7.9	-11.8	-29.3	-29.7	-51.6	8.5
GEDT			0.01	0.04	0.04	0.04	0.03	-0.01	-0.10	-0.14	-0.27	-0.28	-0.33	0.03
V(C1,N2)	3.81		3.87	3.83	3.60	3.61	2.82	2.28	1.90	1.87	1.85	1.85	1.87	3.61
V(N2)							0.80	1.36	1.78	1.90	2.21	2.21	2.37	
V(N2,O3)	1.42		1.39	1.35	1.33	1.33	1.33	1.27	1.20	1.14	0.97	0.95	0.89	1.33
V(C4,C5)		1.73	3.65	3.29	3.26	3.22	3.13	2.94	2.64	2.48	2.23	2.20	2.07	3.17
V'(C4,C5)		1.91												
V(C5,C6)		1.97	1.96	1.98	1.98	3.53	3.49	3.46	3.39	1.85	1.81	1.81	1.85	3.50
V'(C5,C6)		1.74	1.72	1.63	1.62					1.55	1.74	1.75	1.78	
V(C1)					0.24	0.29	0.33							0.32
V(C5)				0.41	0.46	0.55	0.65							0.61
V(O3)	2.99		3.01	3.02	2.87	2.97	2.98	2.94	2.91	2.97	2.79	2.75	2.48	2.97
V'(O3)	3.02		2.93	2.86	2.98	2.88	2.88	2.92	2.94	2.92	3.34	2.80	2.54	2.89
V(C4)									0.10	0.27				
V(C1,C5)								1.47	1.91	1.97	1.99	2.00	1.97	
V(O3,C4)												0.61	1.31	



Scheme 6.5. Simplified representation of the molecular mechanism of the 32CA reaction between Ni **51** and strained allene CHDE **50** by Lewis structures arising from the topological analysis of the ELF along the most favourable reaction path.

Table 9. ELF valence basin populations of the IRC points, **P1** – **P5**, defining the six phases characterising the molecular mechanism associated with the addition reaction of carbenoid isocyanide **55** to DMAD **56**. The stationary points **MC1**, *trans-**IN*** and *cis-**IN*** are also included. Distances are given in angstroms (Å), while GEDT values and electron populations are given in average number of electrons (e).

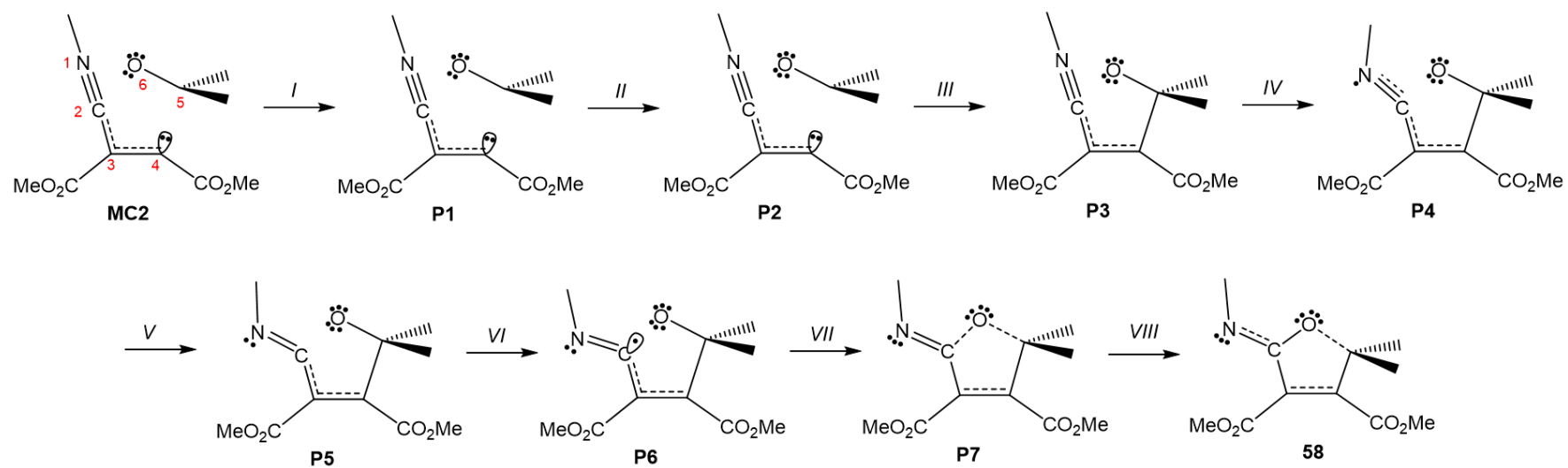
Phases	<i>I</i>	<i>II</i>	<i>III</i>	<i>IV</i>	<i>V</i>	<i>VI</i>		
Points	MC1	P1	P2	P3	P4	P5	<i>trans-IN</i>	<i>cis-IN</i>
d(C2–C3)	3.726	2.282	2.033	1.897	1.551	1.399	1.396	1.393
GEDT	0.00	0.07	0.18	0.27	0.54	0.60	0.62	0.65
V(N1,C2)	3.81	3.15	5.12	5.13	4.71	4.40	5.52	3.19
V'(N1,C2)	1.29	2.00						2.32
V(C3,C4)	2.68	2.37	2.23	2.10	1.73	3.10	3.13	3.14
V'(C3,C4)	2.65	2.48	2.16	2.02	1.74			
V(C2)	2.65	2.58	2.52					
V(C2,C3)				2.55	2.66	2.73	2.71	2.65
V(C4)		0.52	1.06	1.31	1.75	1.90	1.97	2.06
V(N1)					0.66	1.20		



Scheme 6.6. Simplified representation of the molecular mechanism of the addition reaction of carbenoid isocyanide **55** to DMAD **56** by Lewis structures arising from the topological analysis of the ELF along the reaction path.

Table 10. ELF valence basin populations of the IRC points, **P1 – P7**, defining the eight phases characterising the molecular mechanism of the more favourable pathway associated with the 32CA reaction between carbenoid intermediate *cis*-**IN** and acetone **57**. The stationary points **MC2** and **58** are also included. Distances are given in angstroms (Å), while GEDT values and electron populations are given in average number of electrons (e).

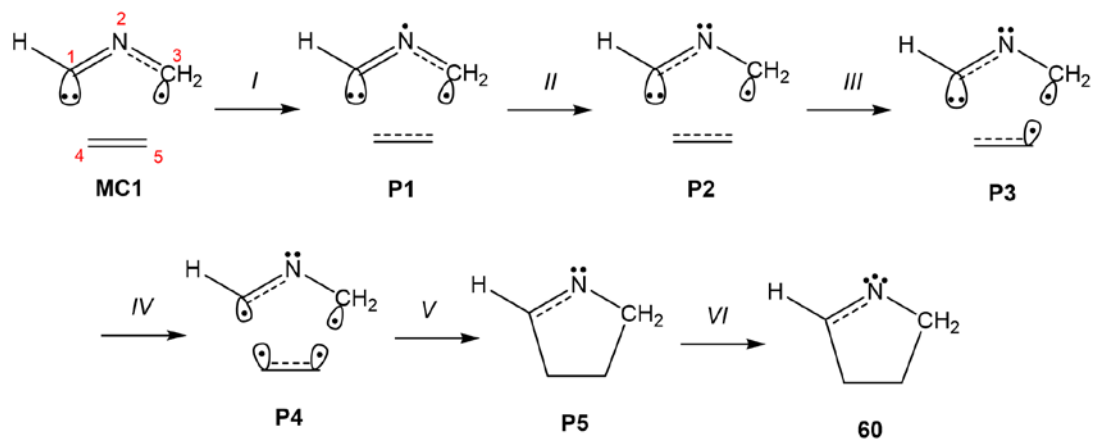
Phases	<i>I</i>	<i>II</i>	<i>III</i>	<i>IV</i>	<i>V</i>	<i>VI</i>	<i>VII</i>	<i>VIII</i>	
Points	MC2	P1	P2	P3	P4	P5	P6	P7	58
d(C4–C5)	3.687	2.798	2.338	2.141	2.070	1.908	1.645	1.578	1.502
d(C2–O6)	3.090	3.007	2.623	2.462	2.412	2.288	1.953	1.746	1.370
GEDT	0.00	0.04	0.16	0.26	0.31	0.40	0.39	0.32	0.19
V(N1,C2)	5.50	1.78	5.48	5.53	4.75	2.14	1.83	1.72	1.64
V'(N1,C2)		3.70				2.09	1.84	1.74	1.63
V(N1)					0.8	1.48	2.26	2.48	2.67
V(C2,C3)	2.60	2.63	2.60	2.59	2.61	2.6	2.47	2.39	2.34
V(C3,C4)	3.17	3.16	3.24	3.27	1.68	1.64	1.71	1.73	1.73
V'(C3,C4)					1.61	1.68	1.68	1.68	1.69
V(O6)	2.64	2.65	2.71	2.85	2.82	2.94	2.92	2.71	2.24
V'(O6)	2.64	2.70	2.77	2.81	2.87	2.96	2.99	2.69	2.52
V(C5,O6)	2.39	2.41	2.23	2.18	2.06	1.77	1.53	1.41	1.43
V(C4)	2.05	2.00	1.92						
V(C4,C5)				1.87	1.89	1.94	2.05	2.06	2.09
V(C2)							0.20		
V(C2,O6)								0.75	1.49



Scheme 6.7. Simplified representation of the molecular mechanism of the 32CA reaction between carbenoid intermediate *cis*-IN and acetone **57** by Lewis structures arising from the topological analysis of the ELF along the more favourable reaction path.

Table 11. ELF valence basin populations of the IRC points, **P1** – **P5**, defining the six phases characterising the molecular mechanism of the *cb-type* 32CA reaction between NY **10** and ethylene **6**. The stationary points **MC1** and pyrroline **60** are also included. Distances are given in angstroms (Å), while GEDT values and electron populations are given in average number of electrons (e).

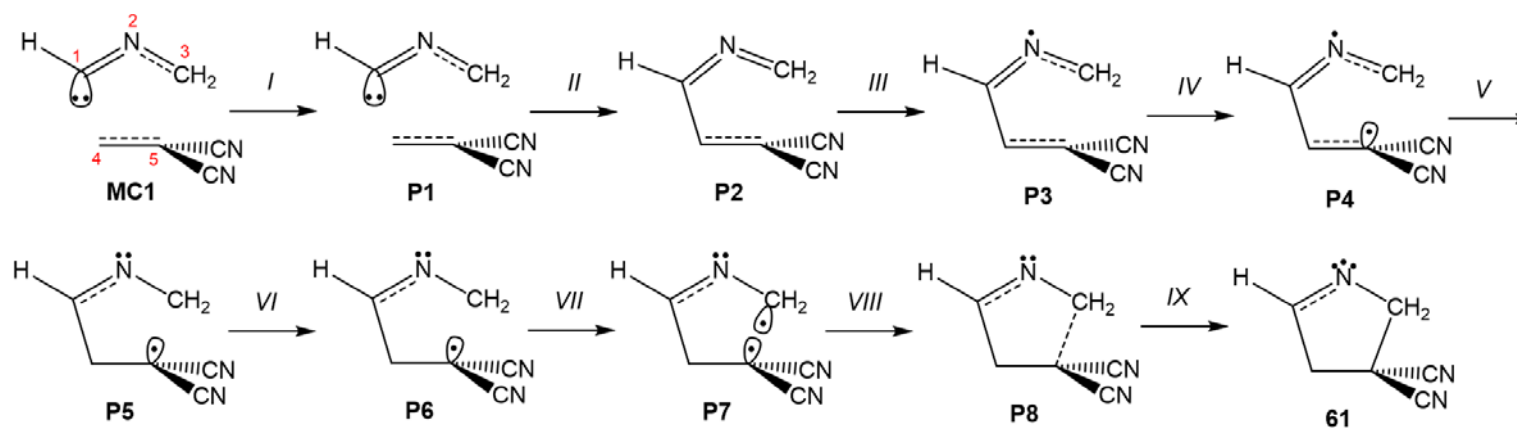
Phases	<i>I</i>	<i>II</i>	<i>III</i>	<i>IV</i>	<i>V</i>	<i>VI</i>	
Catastrophes		F^{\ddagger}	C	F^{\ddagger}	F^{\ddagger}	$[C]_2$	
Points	MC1	P1	P2	P3	P4	P5	60
d(C1–C4)	3.703	2.406	2.324	2.221	2.169	2.009	1.497
d(C3–C5)	3.769	2.449	2.363	2.255	2.202	2.041	1.539
GEDT	0.00	0.10	0.11	0.11	0.11	0.10	0.04
V(C1,N2)	2.03	1.71	1.61	1.52	1.51	1.52	1.48
V'(C1,N2)	2.03	1.88	1.67	1.69	1.68	1.60	1.62
V(N2,C3)	3.25	2.47	2.27	2.09	2.04	1.91	1.70
V(N2)		1.12	1.54	1.95	2.10	2.39	2.71
V(C4,C5)	1.73	1.80	3.30	2.95	2.58	2.22	1.82
V'(C4,C5)	1.74	1.56					
V(C1)	1.95	1.65	1.58	1.47	1.40		
V(C4)					0.30		
V(C1,C4)						1.76	2.00
V(C3)	0.30	0.47	0.57	0.68	0.73		
V(C5)				0.36	0.45		
V(C3,C5)						1.46	1.86



Scheme 6.8. Simplified representation of the molecular mechanism of the *cb-type* 32CA reaction between NY **10** and ethylene **6** by Lewis structures arising from the topological analysis of the ELF along the reaction path.

Table 12. ELF valence basin populations of the IRC points, **P1** – **P8**, defining the nine phases characterising the molecular mechanism of the more favourable pathway associated with the *cb-type* 32CA reaction between NY **10** and DCE **21**. The stationary points **MC2** and pyrroline **61** are also included. Distances are given in angstroms (Å), while GEDT values and electron populations are given in average number of electrons (e).

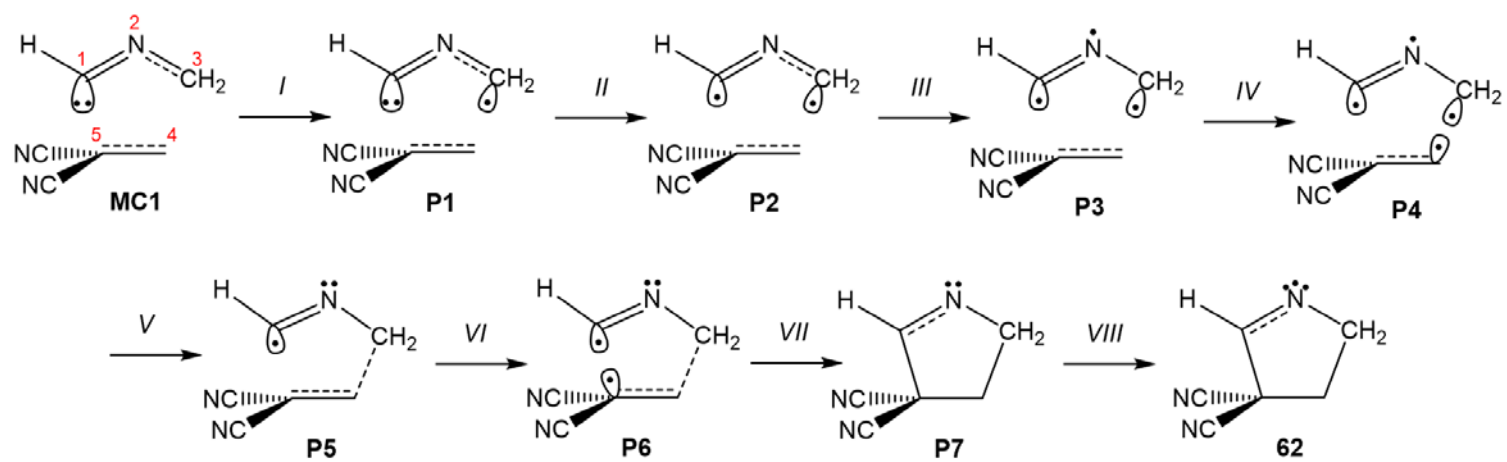
Phases	<i>I</i>	<i>II</i>	<i>III</i>	<i>IV</i>	<i>V</i>	<i>VI</i>	<i>VII</i>	<i>VIII</i>	<i>IX</i>	
Catastrophes	<i>C</i>	<i>C</i>	<i>F[†]</i>	<i>F[†]</i>	<i>C[†]</i>	<i>C</i>	<i>F[†]</i>	<i>C</i>		
Points	MC2	P1	P2	P3	P4	P5	P6	P7	P8	61
d(C1–C4)	2.638	2.367	2.149	1.978	1.900	1.677	1.556	1.536	1.521	1.498
d(C3–C5)	3.034	2.922	2.835	2.772	2.743	2.641	2.489	2.392	2.192	1.560
GEDT	0.14	0.24	0.36	0.46	0.50	0.56	0.53	0.49	0.41	0.19
V(C1,N2)	2.12	2.12	1.99	1.94	1.88	1.66	1.46	1.68	1.44	1.52
V'(C1,N2)	1.86	1.90	1.82	1.70	1.66	1.66	1.67	1.47	1.64	1.56
V(N2)				0.99	1.25	1.85	2.11	2.24	2.36	2.66
V(N2,C3)	3.42	3.43	3.56	2.88	2.71	2.45	2.39	2.16	2.03	1.74
V(C4,C5)	1.67	3.29	3.31	3.14	2.78	2.28	2.24	2.17	2.03	1.77
V'(C4,C5)	1.64									
V(C1)	1.84	1.70								
V(C1,C4)			1.58	1.63	1.68	1.78	1.89	1.92	1.98	2.03
V(C3)								0.20		
V(C5)					0.32	0.45	0.59	0.66		
V'(C5)						0.18				
V(C3,C5)									1.13	1.85



Scheme 6.9. Simplified representation of the molecular mechanism of the *cb*-type 32CA reaction between NY **10** and DCE **21** by Lewis structures arising from the topological analysis of the ELF along the more favourable reaction path.

Table 13. ELF valence basin populations of the IRC points, **P1** – **P7**, defining the eight phases characterising the molecular mechanism of the less favourable pathway associated with the 32CA reaction between NY **10** and DCE **21**. The stationary points **MC3** and pyrroline **62** are also included. Distances are given in angstroms (Å), while GEDT values and electron populations are given in average number of electrons (e).

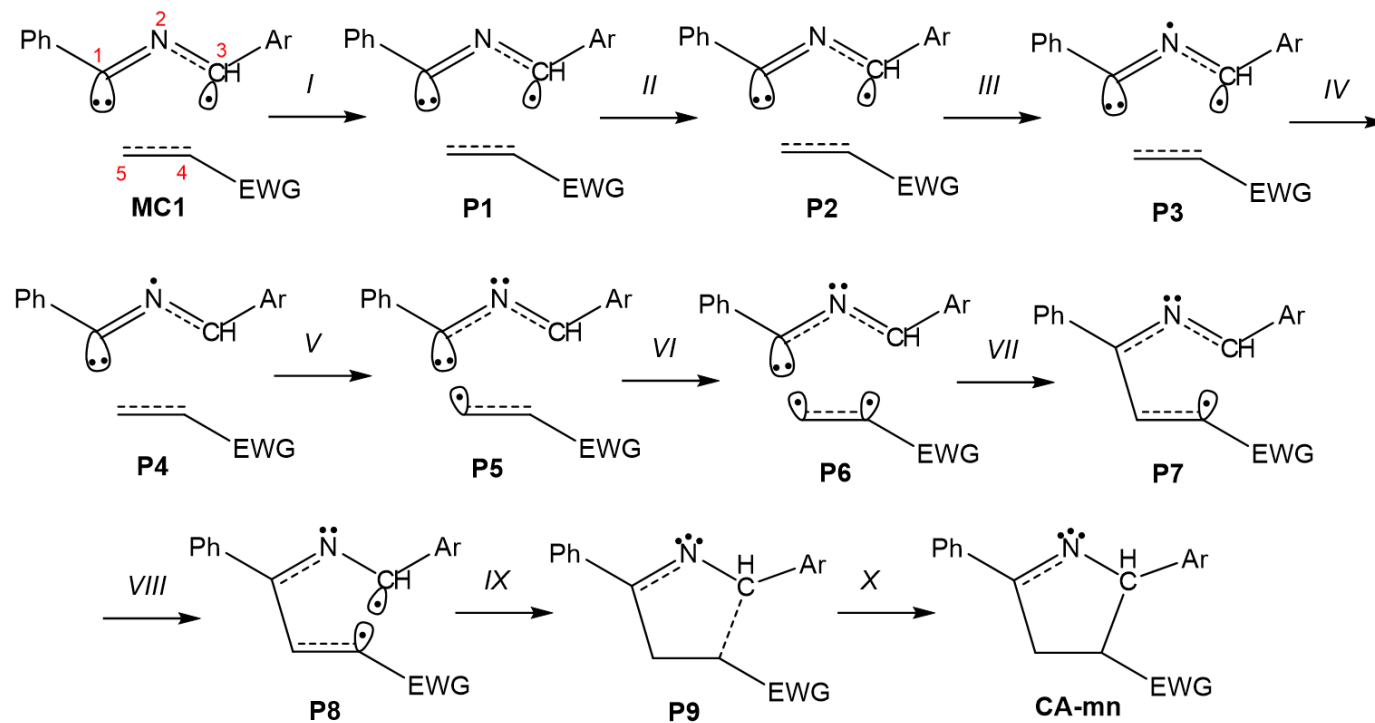
Phases	<i>I</i>	<i>II</i>	<i>III</i>	<i>IV</i>	<i>V</i>	<i>VI</i>	<i>VII</i>	<i>VIII</i>	
Catastrophes		<i>F</i> [†]	<i>C</i>	<i>F</i> [†]	<i>F</i> [†]	<i>C</i>	<i>F</i> [†]	<i>C</i>	
Points	MC3	P1	P2	P3	P4	P5	P6	P7	62
d(C1–C5)	2.899	2.744	2.615	2.530	2.484	2.437	2.388	1.959	1.535
d(C3–C4)	2.978	2.661	2.418	2.255	2.169	2.083	1.998	1.606	1.537
GEDT	0.09	0.16	0.24	0.31	0.35	0.38	0.40	0.30	0.19
V(C1,N2)	2.14	2.18	2.20	2.07	2.03	1.96	1.91	1.74	1.65
V'(C1,N2)	1.95	1.93	1.93	1.83	1.77	1.73	1.66	1.57	1.46
V(N2)				0.85	1.22	1.53	1.80	2.46	2.63
V(N2,C3)	3.38	3.06	3.07	2.46	2.24	2.09	2.00	1.75	1.74
V(C4,C5)	1.61	1.57	3.22	3.23	3.08	2.97	2.57	1.98	1.80
V'(C4,C5)	1.67	1.68							
V(C3)		0.28	0.46	0.61	0.72				
V(C4)					0.20				
V(C3,C4)						1.11	1.26	1.79	1.93
V(C1)	1.77	1.64	1.42	1.22	1.08	0.93	0.86		
V(C5)							0.37		
V(C1,C5)								1.56	1.88



Scheme 6.10. Simplified representation of the molecular mechanism of the *cb*-type 32CA reaction between NY **10** and DCE **21** by Lewis structures arising from the topological analysis of the ELF along the less favourable reaction path.

Table 14. ELF valence basin populations of the IRC points, **P1** – **P9**, defining the ten phases characterising the molecular mechanism of the most favourable pathway associated with the experimental *cb-type* 32CA reaction between NY **63** and oxazolidinone **67**. The stationary points **MC-mn**, **TS-mn** and **CA-mn** are also included. Distances are given in angstroms (Å), GEDT values and electron populations in average number of electrons (e), and relative energies in kcal·mol⁻¹.

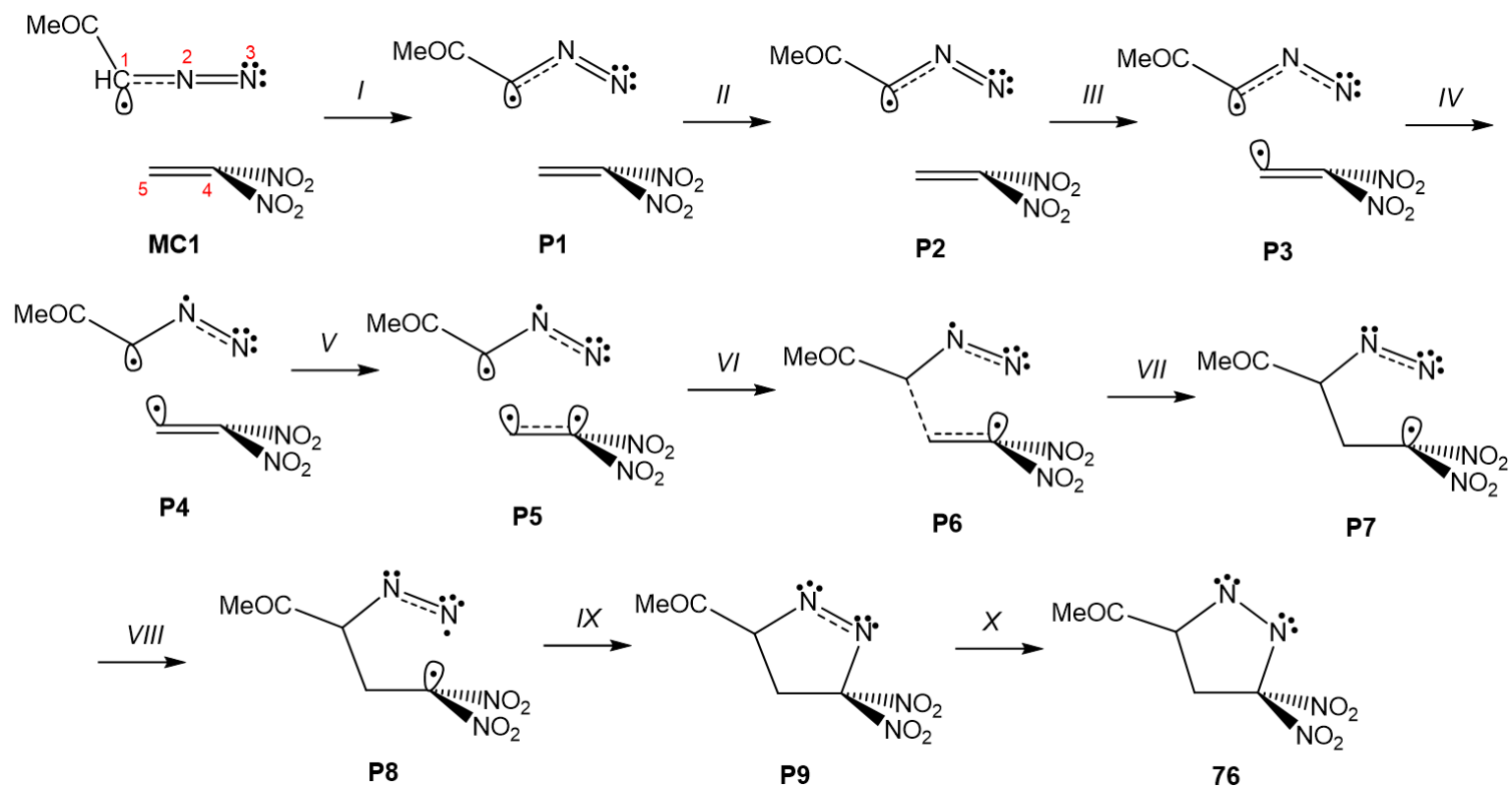
Phases	<i>I</i>	<i>II</i>	<i>III</i>	<i>IV</i>	<i>V</i>	<i>VI</i>	<i>VII</i>	<i>VIII</i>	<i>IX</i>	<i>X</i>		
Catastrophes	<i>F</i>	<i>C</i>	<i>F</i> [†]	<i>F</i>	<i>F</i> [†]	<i>F</i> [†]	<i>C</i>	<i>F</i> [†]	<i>C</i>			
Points	MC-mn	P1	P2	P3	P4	P5	P6	P7	P8	P9	CA-mn	TS-mn
d(C1–C5)	2.870	2.592	2.386	2.340	2.158	2.072	2.058	2.039	1.967	1.563	1.506	2.249
d(C3–C4)	3.178	2.982	2.859	2.835	2.723	2.675	2.666	2.656	2.615	2.037	1.571	2.774
ΔE	0.0	3.1	4.7	5.0	4.9	3.9	3.6	3.2	1.2	-34.3	-63.8	5.2
GEDT	0.05	0.09	0.15	0.17	0.23	0.25	0.26	0.27	0.29	0.15	0.05	0.20
V(C1,N2)	2.30	2.28	2.22	2.05	1.98	1.91	1.90	1.87	1.83	1.46	1.56	2.01
V'(C1,N2)	2.13	2.11	2.14	2.15	1.65	1.45	1.43	1.44	1.42	1.64	1.46	1.81
V(N2,C3)	2.75	2.80	2.90	2.92	2.81	2.71	2.72	2.70	2.34	1.88	2.06	2.62
V(N2)				0.14	1.27	1.61	1.65	1.68	1.87	2.59	2.76	0.91
V(C4,C5)	1.66	1.64	3.26	3.24	3.19	3.04	2.95	2.82	2.67	2.05	1.92	3.21
V'(C4,C5)	1.72	1.73										
V(C1)	1.45	1.44	1.47	1.47	1.44	1.51	1.55					1.43
V(C5)						0.09	0.10					
V(C1,C5)								1.71	1.76	2.00	2.06	
V(C3)	0.35	0.32	0.29	0.30					0.30			0.29
V'(C3)	0.31											
V(C4)							0.16	0.16	0.22			
V(C3,C4)										1.34	1.86	



Scheme 6.11. Simplified representation of the molecular mechanism of the experimental *cb-type* 32CA reaction between NY **63** and oxazolidinone **67** by Lewis structures arising from the topological analysis of the ELF along the most favourable reaction path.

Table 15. ELF valence basin populations of the IRC points, **P1** – **P9**, defining the ten phases characterising the molecular mechanism of the more favourable pathway associated with the 32CA reaction between Da **72** and DNE **73**. The stationary points **MC1** and 1-pyrazoline **76** are also included. Distances are given in angstroms (Å), while GEDT values and electron populations are given in average number of electrons (e).

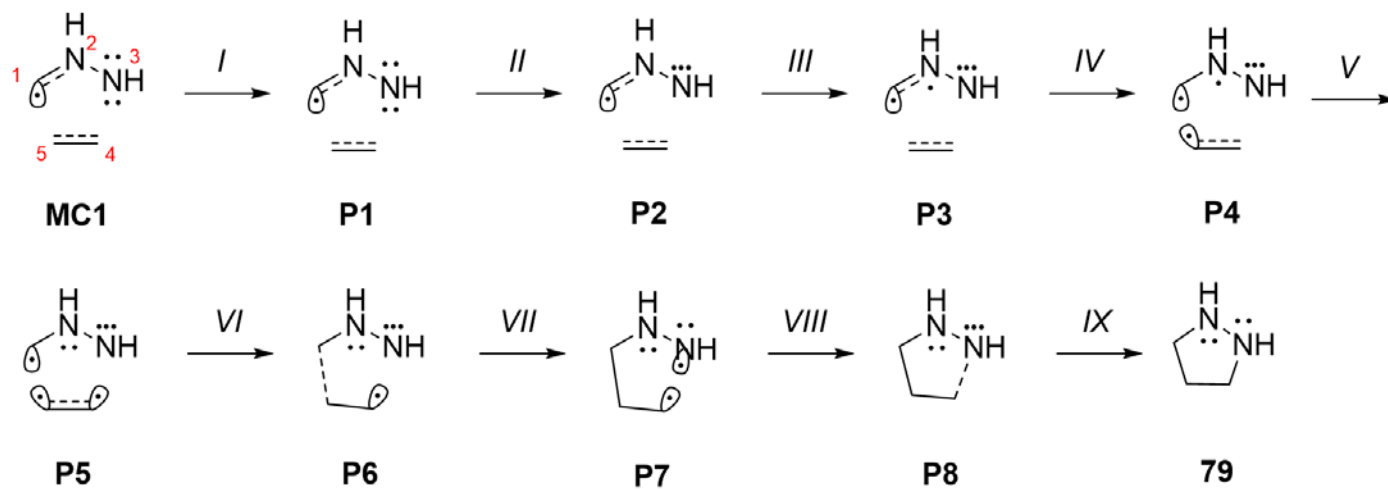
Phases	<i>I</i>	<i>II</i>	<i>III</i>	<i>IV</i>	<i>V</i>	<i>VI</i>	<i>VII</i>	<i>VIII</i>	<i>IX</i>	<i>X</i>	
Catastrophes	<i>C</i>	<i>C</i>	<i>F[†]</i>	<i>F[†]</i>	<i>F[†]</i>	<i>C</i>	<i>C</i>	<i>C[†]</i>	<i>C</i>		
Points	MC1	P1	P2	P3	P4	P5	P6	P7	P8	P9	76
d(C1–C5)	3.295	2.803	2.407	2.076	2.057	2.044	2.006	1.654	1.576	1.567	1.534
d(N3–C4)	3.217	3.001	2.815	2.675	2.667	2.661	2.644	2.371	1.816	1.689	1.503
GEDT	0.02	0.08	0.18	0.32	0.34	0.35	0.38	0.38	0.14	0.06	–0.04
V(C1,N2)	3.07	3.12	3.18	3.42	2.27	2.23	2.15	1.77	1.81	1.83	1.80
V(N2)					1.20	1.24	1.36	2.15	2.54	2.61	2.71
V(N2,N3)	1.79	1.77	1.78	1.64	1.62	1.61	1.58	2.98	2.67	2.64	2.51
V'(N2,N3)	1.88	1.87	1.80	1.75	1.73	1.73	1.73				
V(C4,C5)	1.91	2.00	3.78	3.69	3.66	3.14	3.09	2.54	2.13	2.10	2.04
V'(C4,C5)	1.83	1.76									
V(C1)	0.43	0.51	0.68	0.90	0.92	0.93					
V'(C1)	0.55										
V(C5)				0.14	0.16	0.17					
V(C1,C5)							1.17	1.71	1.83	1.85	1.91
V(N3)	3.76	3.73	3.69	3.56	3.55	3.55	3.54	3.48	3.07	2.96	2.83
V'(N3)									0.49		
V(C4)						0.52	0.55	0.78	0.96		
V(N3,C4)										1.62	1.86



Scheme 6.12. Simplified representation of the molecular mechanism of the 32CA reaction between Da **72** and DNE **73** by Lewis structures arising from the topological analysis of the ELF along the more favourable reaction path.

Table 16. ELF valence basin populations of the IRC points, **P1** – **P8**, defining the nine phases characterising the molecular mechanism of the *pmr*-type 32CA reaction between AI **15** and ethylene **6**. The stationary points **MC1**, **TS1** and **79** are also included. Distances are given in angstroms (Å), GEDT values and electron populations in average number of electrons (e), and relative energies in kcal·mol⁻¹.

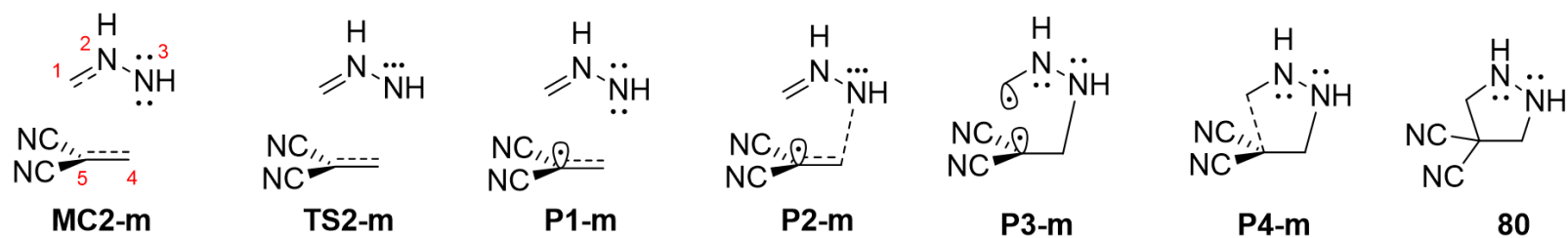
Phases			<i>I</i>	<i>II</i>	<i>III</i>	<i>IV</i>	<i>V</i>	<i>VI</i>	<i>VII</i>	<i>VIII</i>	<i>IX</i>		
Catastrophes			<i>C</i>	<i>C</i>	<i>F[†]</i>	<i>F[†]</i>	<i>F[†]</i>	<i>C</i>	<i>C[†]</i>	<i>C</i>			
Points	15	6	MC1	P1	P2	P3	P4	P5	P6	P7	P8	79	TS1
d(C1–C5)			3.718	2.908	2.311	2.297	2.174	2.091	2.033	1.868	1.849	1.525	2.272
d(N3–C4)			3.337	2.800	2.319	2.307	2.206	2.136	2.086	1.937	1.919	1.463	2.286
ΔE		0.0	-2.4	-1.5	5.2	5.2	4.3	1.3	-2.1	-17.9	-20.1	-62.0	5.3
GEDT			0.01	0.04	0.10	0.10	0.09	0.07	0.05	-0.02	-0.03	-0.13	0.10
V(C1,N2)	2.95		2.97	3.05	3.31	2.55	2.27	2.15	2.07	1.90	1.89	1.75	2.51
V(N2)						0.76	1.22	1.47	1.61	1.94	1.96	2.28	0.84
V(N2,N3)	2.10		2.09	2.07	1.90	1.89	1.78	1.70	1.66	1.56	1.55	1.36	1.87
V(C4,C5)		1.71	1.70	1.67	3.20	3.20	2.96	2.63	2.49	2.19	2.17	1.88	3.18
V'(C4,C5)		1.71	1.69	1.70									
V(C1)	0.31		0.28	0.25	0.50	0.51	0.60	0.66					0.52
V'(C1)	0.31		0.29										
V(N3)	3.53		3.54	3.48	3.32	3.32	3.28	3.25	3.23	2.67	2.67	2.28	3.32
V'(N3)										0.58			
V(C4)								0.21	0.28	0.44			
V(C5)						0.25	0.40						
V(C1,C5)									1.19	1.47	1.50	1.74	
V(N3,C4)											1.03	1.88	



Scheme 6.13 Simplified representation of the molecular mechanism of the *pmr*-type 32CA reaction between AI **15** and ethylene **6** by Lewis structures arising from the topological analysis of the ELF along the reaction path.

Table 17. ELF valence basin populations of the stationary points and some points of the IRC involved in the formation of the new C1–C5 and N3–C4 single bonds along the more favourable pathway associated with the *pmr-type* 32CA reaction between AI **15** and DCE **21**. Distances are given in angstroms (Å), GEDT values and electron populations in average number of electrons (e), and relative energies in kcal·mol⁻¹.

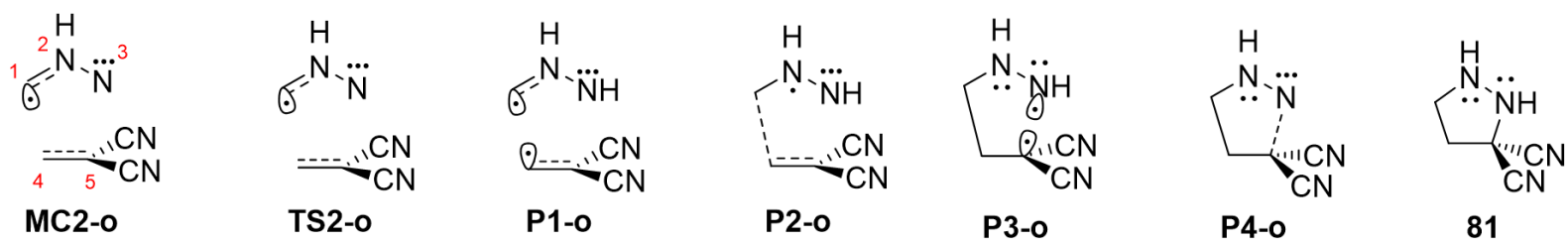
Points	15	21	MC2-m	TS2-m	P1-m	P2-m	P3-m	P4-m	80
d(C1–C5)			2.957	2.796	2.680	2.675	2.318	2.145	1.564
d(N3–C4)			2.462	2.142	1.822	1.810	1.521	1.500	1.441
ΔE		0.0	-8.9	-8.5	-11.1	-11.4	-23.1	-29.5	-58.2
GEDT			0.17	0.27	0.39	0.40	0.34	0.26	0.03
V(C1,N2)	2.95		3.39	3.46	3.64	3.67	2.38	2.19	1.74
V(N2)							1.75	1.78	2.25
V(N2,N3)	2.10		2.02	1.89	1.72	1.70	1.48	1.42	1.38
V(C4,C5)		1.66	1.66	3.26	2.79	2.78	2.18	2.07	1.83
V'(C4,C5)		1.66	1.63						
V(C1)	0.31						0.15		
V'(C1)	0.31								
V(N3)	3.53		3.46	3.40	3.61	2.64	2.32	2.27	2.24
V(C5)					0.31	0.31	0.67		
V(C1,C5)								1.09	1.82
V(N3,C4)						0.98	1.58	1.64	1.73



Scheme 6.14. Electronic structure of the stationary points and simplified representation of the bond formation processes by Lewis structures arising from the topological analysis of the ELF along the more favourable pathway associated with the *pmr*-type 32CA reaction between AI **15** and DCE **21**.

Table 18. ELF valence basin populations of the stationary points and some selected points of the IRC involved in the formation of the new C1–C4 and N3–C5 single bonds along the less favourable pathway associated with the *pmr-type* 32CA reaction between AI **15** and DCE **21**. Distances are given in angstroms (Å), GEDT values and electron populations in average number of electrons (e), and relative energies in kcal·mol⁻¹.

Points	15	21	MC2-o	TS2-o	P1-o	P2-o	P3-o	P4-o	81
d(C1–C4)			2.758	2.311	2.121	2.048	1.556	1.554	1.515
d(N3–C5)			2.752	2.625	2.560	2.536	1.865	1.837	1.474
ΔE		0.0	-6.3	-5.7	-6.5	-7.5	-37.9	-39.2	-56.2
GEDT			0.14	0.25	0.32	0.35	0.14	0.13	-0.01
V(C1,N2)	2.95		2.98	2.97	2.96	2.40	1.78	1.77	1.75
V(N2)						0.61	2.00	2.02	2.26
V(N2,N3)	2.10		2.12	2.15	2.12	2.10	1.58	1.58	1.36
V(C4,C5)		1.66	1.64	3.19	3.15	3.01	1.99	1.99	1.82
V ⁺ (C4,C5)		1.66	1.62						
V(C1)	0.31		0.38	0.53	0.69				
V ⁺ (C1)	0.31								
V(N3)	3.53		3.36	3.17	3.05	2.92	2.62	2.60	2.25
V ⁺ (N3)							0.32		
V(C4)					0.07				
V(C5)							0.72		
V(C1,C4)						0.96	1.81	1.81	1.89
V(N3,C5)								1.06	1.70



Scheme 6.15. Electronic structure of the stationary points and simplified representation of the bond formation processes by Lewis structures arising from the topological analysis of the ELF along the less favourable pathway associated with the polar *pmr*-type 32CA reaction between AI **15** and DCE **21**.

7. THEORETICAL BACKGROUND

7.1. QC models

Since the introduction of the chemical bond concept by Lewis in 1916,⁷⁵ two different QC theories, namely, the VBT¹² and the MOT,²² have been developed as an approach to the resolution of Schrödinger's equation, established in 1926 (see Eq. [2]).¹¹⁰ The information obtained from the resolution of Schrödinger's equation (2) is a wavefunction Ψ , whose square describes the probability distribution of the particles within the molecule, i.e. the molecular electron density, and the total electronic energy E associated with this wavefunction Ψ .

$$H \Psi = E \Psi \quad (\text{Schrödinger equation}) \quad (2)$$

Until the mid-1950s, chemistry was dominated by the classical VBT. However, the computational effort required in classical VBT caused it to be employed in an oversimplified manner. Relevant concepts used in organic chemistry such as hybridisation¹⁰⁶ and resonance¹¹ were developed within VBT. When the early *ab initio* VBT lacked accuracy and did not progress, MOT became increasingly important.

Within MOT, the polyelectronic wavefunction Ψ of Eq. [2] is approximated as an antisymmetrised product of a series of mono-electronic orbitals Ψ_i , named MOs, and spin functions. In turn, these MOs are beforehand obtained by LCAO, which are mathematical functions describing the electron movement in a hydrogen-type AO.¹¹¹ Thus, in MOT, electrons are not assigned to individual bonds between atoms, but they are treated as moving under the influence of the nuclei along MOs in the whole molecule. Similar to the wavefunction Ψ , the square of an MO represents the probability distribution of the electrons of the MO in space. However, it is worth emphasising that the molecular electron density is not obtained from a combination of the electron density of MOs, i.e. the square of the occupied MOs. Consequently, the analysis of individual MOs has no chemical significance as they do not represent the behaviour of the molecular wave function Ψ .

Parallel to the development of the VBT and MOT based on Schrödinger's equation (2), in the '60s of the past century and based on the Hohenberg and Kohn's theorems, a different QC theory to describe the electronic structure of matter, known as DFT,⁵² in which the GS energy of a non-degenerate N -electron system is functional of only the

7. Theoretical background

electron density $\rho(\mathbf{r})$, was established (3). Note that unlike the MOs, electron density is an experimentally accessible scalar field.¹¹²

$$E[\rho(\mathbf{r})] = \int \rho(\mathbf{r})v(\mathbf{r})d\mathbf{r} + F[\rho(\mathbf{r})] \quad (3)$$

In turn, within the DFT framework, the electron density $\rho(\mathbf{r})$ is expressed as the functional derivative of the energy with respect to the external potential, the number of electrons being kept constant:

$$\rho(\mathbf{r}) = \left(\frac{\partial E}{\partial v(\mathbf{r})} \right)_N \quad (4)$$

Thus, DFT calculations imply the construction of an expression of the electron density. Unfortunately, similar to the QC theories based on Schrödinger's equation, neither is the resolution of the functional of the electron density $\rho(\mathbf{r})$ for a complex system computationally feasible. As an approximation, the Kohn–Sham formalism¹¹³ was introduced in analogy to the HF methods (see Eq. [5]). It should be emphasised, then, that Kohn–Sham orbitals were conceived as an instrument to conveniently construct the exact density, which could then be substituted into (a good approximation to) the Hohenberg–Kohn density functional to provide, in turn, the exact (or accurate) total energy: $E = E[\rho(\mathbf{r})]$. Consequently, in the DFT framework, the Kohn–Sham orbitals do not define any wavefunction although they are used to calculate the one-electron density distribution function.¹¹⁴

$$H \Psi_{\text{KS}} = E \Psi_{\text{KS}} \quad (\text{Kohn–Sham equation}) \quad (5)$$

7.2. Reactivity models derived from HMOT: the FMO theory and the “pericyclic” mechanism

In 1952, studying the reactivity of aromatic compounds, Fukui observed that the electron density distribution of the highest occupied π -orbital at the GS correlated well with their reactivity, thus establishing that the position at which the electron density is largest is most readily attacked by electrophilic or oxidising reagents.¹¹⁵ He concluded that unlike other π -electrons, the pair of π -electrons occupying the energetically highest MO, which is referred to as frontier electrons, plays a decisive role in the chemical activation of these hydrocarbon molecules.¹¹⁵

It was in 1964 when Fukui went one-step further and established the FMO theory²³ to study how molecules react with each other. He proposed that *a majority of chemical reactions should take place at the position and in the direction of maximum overlapping of the HOMO (highest occupied MO) and the LUMO (lowest unoccupied MO) of the reacting species*,¹¹⁶ accordingly, the most favourable interaction will take place by overlapping and mixing the two FMOs with the lowest energy separation in such a manner that the rate of reaction is inversely related to the energy gap, and between the centers of the two molecules with the highest MO coefficients. Consequently, within the FMO theory, MOs do not only control the reactivity, but also the regioselectivity.

Meanwhile, based on HMOT, Hoffmann developed in 1963 the extended HMOT,¹¹⁷ which is a semi-empirical QC method that uses the valence ‘s’ AOs additionally to the originally employed valence ‘p_z’ AOs to build MOs. In 1965, based on the symmetry of wavefunctions, Longuet-Higgins and Abrahamson suggested an approach to explain the reaction mechanisms.¹¹⁸ If a molecule has some element of symmetry, the molecular wavefunction must conform^{39g} to that symmetry. They applied this treatment to several simple “pericyclic” reactions of symmetrical molecules, assuming symmetry to be retained throughout, and showed what reactions were allowed or forbidden. A simpler version of this treatment was adopted in 1965 by Woodward and Hoffmann who, based on an analysis of the orbital symmetry of the p_z AOs rather than of symmetry of states, introduced the orbital symmetry rules to explain the stereochemistry, as well as feasibility, in cycloaddition, electrocyclic and sigmatropic reactions.¹¹⁹ It was in 1968 when they generalised the conservation of orbital symmetry “*for every concerted reaction*”.²⁵ Further, in 1969, in a review devoted to the orbital symmetry rules, they defined the concept of “pericyclic” reactions, i.e. “*reactions in which all first-order changes in bonding relationships take place in concert on a closed curve and must obey the selection rules*”.²⁶ The original discussion of cycloaddition, electrocyclic and sigmatropic reactions by Woodward and Hoffmann¹¹⁹ was formulated in terms of the FMO method and later Fukui, in 1971, extended it to the whole range of “pericyclic” processes.^{116g}

For half a century, organic chemists had recognised the possibility that certain reactions and molecular rearrangements might take place by a mechanism involving the “concerted” (simultaneous) cyclic permutation of bonds round a ring of atoms. In the era of the classical electronic theory of Lapworth, Robinson¹²⁰ and Ingold,¹²¹ such mechanisms were proposed for a number of reactions using the current curved arrow

7. Theoretical background

symbolism to represent the displacement of electron pair bonds. However, although the possibility of such processes, which Woodward and Hoffmann²⁶ had termed “pericyclic”, was recognised at an early date through the joint-use of the “concerted” concept¹²² and the proposed electron displacement movement by curved arrows¹²¹, it was only in the 60’s that they became a matter of major concern to organic chemists.

In 1939, Evans and Warhurst¹²³ emphasised the analogy between the delocalised electrons in the cyclic and linear TSs for the DA reaction of butadiene with ethylene and the π system of benzene and hexatriene, respectively. They stated that the additional resonance energy of the cyclic TS over the linear TS should be a factor in favouring the one-step reaction. In 1952, on the basis of an extension of the HMOT and using the perturbation theory, Dewar developed a simple procedure for stating whether a given system is aromatic or not^{39a-f} and established a general theory of aromaticity.^{39g} Later, in 1966,²⁴ Dewar suggested that a “pericyclic” process is formally analogous to the conversion of one Kekulé structure for a cyclic polyene into the other. The TS for the “pericyclic” reaction was thus suggested to be precisely analogous to the hybrid of classical resonance structures in an intermediate “aromatic” structure for the polyene. Dewar related, therefore, the facility of a “pericyclic” reaction to the stability of the cyclic TS relative to an open chain analogue and thus described the cyclic TSs as being aromatic, non-aromatic, or anti-aromatic. This led him to formulate the Evan’s Principle, a rule for predicting the facility of “pericyclic” reactions, which says “*thermal pericyclic reactions take place preferentially via aromatic transition states*”.

In this context, in 1971, Dewar proposed the Evan’s Principle,²⁴ together with the perturbation MO treatment of aromaticity and the derived rules for aromaticity,³⁹ to be a simple theory of “pericyclic” reactions, regarding it either as a satisfactory theoretical basis of the Woodward and Hoffmann rules or as a satisfactory alternative to them.³⁸ He concluded that thermally induced “pericyclic” reactions proceed preferentially via aromatic TSs, whereas their photochemical counterparts lead to products that are formed via anti-aromatic TSs.

7.3. Development of computational chemistry and application of the TST

At the beginning of the past century, some important theories based on experiments, such as the TST,³⁶ were developed in kinetic chemistry, which permitted to establish fundamental concepts used in the study of molecular mechanisms. Within this theory, the

concept of the activation complex or TS enabled the establishment of a relationship between the experimental activation energy¹²⁴ and the energy of the TS associated to an organic reaction.

From the extended HMOT developed by Hoffmann in 1963,¹¹⁷ Pople, Santry and Segal proposed, in 1965 and 1966, one of the first semi-empirical methods in quantum chemistry, namely, the CNDO method.¹²⁵ CNDO/2 is the main version of CNDO and marked the beginning of the development and the application in molecular physics and theoretical chemistry of semi-empirical methods taking into account all valence electrons.

The development of the semi-empirical methods in the late '60s allowed the first molecular geometry optimisations based on QC procedures. Based on TST, Dewar was one of the first in performing molecular geometry optimisations along a reaction path.¹²⁶ Thus, in 1970, Dewar obtained approximate geometries for reactants, TSs and products involved in the Cope rearrangement and electrocyclic processes.¹²⁶

The growth of computation in the two last decades of the 20th century enabled the study of the molecular mechanism of many organic reactions by characterising the stationary points involved in a reaction, i.e. reagents, TSs, intermediates and products. While *ab initio* HF calculations¹²⁷ rendered good geometries, experimental activation energies were overestimated. Consequently, very time-consuming post-HF energy calculations¹²⁷ were demanded to reproduce the experimental values. Alternatively, in the last decades, a series of empiric DFT functionals such as B3LYP,¹²⁸ MPWB1K¹²⁹ and, more recently, M06-2X,¹³⁰ which provide more accurate energies, have been developed, making the study of organic reactions with a computational demand similar to HF calculations possible. Today, these DFT functionals are widely used in the study of the mechanism of organic reactions.

7.4. Application of CDFT reactivity indices to the study of 32CA reactions

Parallel to the development of QC models to approach the Hohenberg-Kohn equation (3),⁵² Parr developed the so-called "CDFT" in the late 1970s and early 1980s.¹³¹ CDFT is a DFT-subfield in which relevant concepts and principles are extracted from electron density, making it possible to understand and predict the chemical behaviour of a molecule. Parr and co-workers, and later a large community of theoretical chemists, were able to give precise definitions for chemical concepts which had already been known and

7. Theoretical background

used for many years in various branches of chemistry, thus providing their calculations with a quantitative use.

7.4.1. Global properties

The main global reactivity indices defined within CDFT are the electronic chemical potential μ and the chemical hardness η , from which the electrophilicity ω index was further obtained by combination of the two former. Then, several proposals for a nucleophilicity N index were developed apart.

7.4.1.1. Electronic chemical potential

In 1983, Parr defined the electronic chemical potential μ as the energy changes of the system with respect to the electron number N at a fixed external potential $v(\mathbf{r})$, i.e. the potential created by the nuclei (see Eq. [6]).¹³² The electronic chemical potential μ is associated with the feasibility of a system to exchange electron density with the environment at the GS.

$$\mu = \left(\frac{\partial E}{\partial N} \right)_{v(\mathbf{r})} \quad (6)$$

Applying the finite difference approximation, the following simple expression is obtained:

$$\mu \approx -\frac{I+A}{2} \quad (7)$$

where I and A are the ionisation potential and the electron affinity of an atom or molecule, respectively. Although a large number of experimental I values for organic molecules can be obtained, a very small number of experimental A values can be found. Using Koopmans' theorem¹³³ and Kohn–Sham's formalism¹¹³ within DFT, these energies can be approached by the frontier HOMO and LUMO energies as I by $-E_{\text{HOMO}}$ and A by $-E_{\text{LUMO}}$. Consequently, the electronic chemical potential μ can be expressed as:

$$\mu \approx \frac{E_{\text{HOMO}} + E_{\text{LUMO}}}{2} \quad (8)$$

Note that this relationship comprises only the FMO energies but not additional physical significance and, therefore, the use of the HOMO and LUMO energies of a molecule to

approach the I and A values in the CDFT is completely different to the analysis of the HOMO–LUMO interactions between two molecules used in the FMO theory.

The identification of the electronic chemical potential μ with the negative of Mulliken electronegativity, $-\chi$, which is a measure of the resistance to electron density loss, offers a way to calculate electronegativity values for atoms and molecules. In this sense, it was an important step forward, as there was no systematic way to evaluate electronegativities for atoms and molecules with the existing scales established by Pauling.¹³⁴

According to the electronegativity equalisation principle, primarily formulated by Sanderson,¹³⁵ “when two or more atoms initially different in electronegativity combine chemically, their electronegativities become equalised in the molecule” through a flux of electron density from the less electronegative atom towards the more electronegative one. This behaviour can be extrapolated to molecules. Thus, the electronic chemical potential μ allows the establishment of the flux direction of the GEDT between two molecules along a polar reaction.⁶¹ Usually, the larger the electronic chemical potential difference, $\Delta\mu$, the larger the GEDT.

7.4.1.2. Chemical hardness

In 1963, Pearson established a classification of Lewis acids and bases into hard and soft.¹³⁶ He proposed that in an acid/base reaction, the most favourable interactions take place between hard/hard or soft/soft pairs, the HSAB principle. Within CDFT, Parr defined, in 1983, a quantitative expression for the chemical hardness η , which can be expressed as the changes of the electronic chemical potential μ of the system with respect to the electron number N at a fixed external potential $v(\mathbf{r})$ (see Eq. [9]).^{132a} Chemical hardness η can be thought as the resistance of a molecule to exchange electron density with the environment.^{132a}

$$\eta = \left(\frac{\partial \mu}{\partial N} \right)_{v(\mathbf{r})} = \left(\frac{\partial^2 E}{\partial N^2} \right)_{v(\mathbf{r})} \quad (9)$$

Applying the finite difference approximation, the following simple expression is obtained:

$$\eta \approx \frac{I-A}{2} \quad (10)$$

7. Theoretical background

which by substitution of I by $-E_{\text{HOMO}}$ and A by $-E_{\text{LUMO}}$ can be expressed as:

$$\eta \approx \frac{E_{\text{LUMO}} - E_{\text{HOMO}}}{2} \quad (11)$$

Usually, the term 1/2 is neglected, so that chemical hardness η is expressed as:

$$\eta \approx E_{\text{LUMO}} - E_{\text{HOMO}} \quad (12)$$

On the other hand, chemical softness S was introduced as the inverse of chemical hardness η (see Eq. [13]).

$$S = \frac{1}{\eta} \quad (13)$$

7.4.1.3. Electrophilicity

In 1999, Parr defined the electrophilicity ω index,¹³⁷ which gives a measure of the energy stabilisation of a molecule when it acquires an additional amount of electron density from the environment (see Eq. [14]).

$$\omega = \frac{\mu^2}{2\eta} \quad (14)$$

The electrophilicity ω index has become a powerful tool for the study of the reactivity of organic molecules participating in polar reactions.¹³⁸ A comprehensive study carried out in 2002 on the electrophilicity of a series of reagents involved in DA reactions allowed establishing a single electrophilicity ω scale.⁶² In 2003, the TACs participating in 32CA reactions were studied using the electrophilicity ω index, allowing a rationalisation of their reactivity in polar processes.⁶³ In 2009, Domingo studied the DA reactions of cyclopentadiene with twelve ethylenes of increased electrophilicity.⁶⁶ For this short series, a good correlation between the computed activation energies and the electrophilicity ω index of these ethylene derivatives was found (see Figure 7.1). In addition, a good correlation between the inverse of the electrophilicity ω index of simple molecules and their expected nucleophilicity was also found. However, this prediction for the nucleophilicity fails for more complex molecules such as captodative ethylenes displaying concurrently both electrophilic and nucleophilic behaviours.^{56b,139}

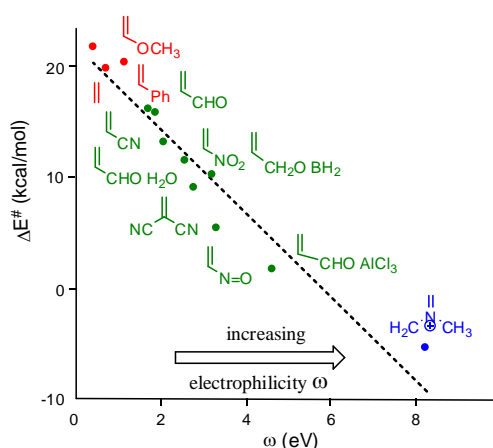


Figure 7.1. Plot of the activation barriers (ΔE^\ddagger) vs the electrophilicity index (ω), $R^2 = 0.92$, for the DA reactions of cyclopentadiene with a substituted ethylene series.

7.4.1.4. Nucleophilicity

While for the electrophilicity ω index only one expression was established, several approaches for the nucleophilicity index were given.^{56b} In 2008, Domingo proposed an empirical (relative) nucleophilicity N index for closed-shell organic molecules¹³⁹ based on the HOMO energies and referred to TCE, which is one of the most electrophilic neutral species (see Eq. [15]).

$$N = E_{\text{HOMO}}(\text{Nucleophile}) - E_{\text{HOMO}}(\text{TCE}) \quad (15)$$

Similar to the electrophilicity scale,⁶² analysis of a series of common nucleophilic species participating in polar organic reactions allowed establishing a single nucleophilic scale.⁷⁶ Several theoretical and experimental studies have evidenced the capability of the nucleophilicity N index to predict the nucleophilic behaviour of simple and complex organic molecules displaying concurrently electrophilic and nucleophilic behaviours.¹⁴⁰ A good correlation between the experimental rate constant for the reactions of a series of 5-substituted indoles with benzhydryl cation¹⁴¹ and the nucleophilicity N index of the former was found.¹⁴⁰

7.4.2. Local properties

Another index that directly comes from CDFT is the electronic Fukui function $f(\mathbf{r})$. In 1984, Parr proposed the $f(\mathbf{r})$ function,¹⁴² named frontier function or Fukui function, for a molecule, which represents the changes in electron density at a point \mathbf{r} with respect to the variation of the number of electrons N at a fixed external potential $v(\mathbf{r})$ (see Eq. [16]).

7. Theoretical background

$$f(\mathbf{r}) = \left(\frac{\partial \rho(\mathbf{r})}{\partial N} \right)_{v(\mathbf{r})} \quad (16)$$

As a first approach, Parr proposed that nucleophilic $f(\mathbf{r})^-$ and electrophilic $f(\mathbf{r})^+$ Fukui functions could approach HOMO and LUMO electron densities, respectively:

$$f(\mathbf{r})^- \approx \rho_{HOMO}(\mathbf{r}) \quad \text{for electrophilic attacks} \quad (17)$$

and

$$f(\mathbf{r})^+ \approx \rho_{LUMO}(\mathbf{r}) \quad \text{for nucleophilic attacks} \quad (18)$$

In this sense, the regioselectivity analysed within the FMO theory and that using Fukui functions based on FMOs is numerically identical, but conceptually completely different; while FMO theory establishes the most favourable MO overlap, CDFT establishes the most favourable nucleophilic/electrophilic interaction in a polar reaction, which depends on the total molecular electron density but not on any specific MO. However, these mathematical expressions did not exactly match with the theoretical concept of the electronic Fukui functions as derived from the CDFT.

In case an amount equivalent to one electron is transferred, the nucleophile becomes a radical cation, while the electrophile becomes a radical anion. Interestingly, analysis of the ASD at the radical cation and the radical anion gives a picture of the distribution of the electron density in the nucleophile and the electrophile when they approach each other along the reaction progress. Based on these observations, in 2014, Domingo proposed the Parr functions $P(\mathbf{r})$,^{82,143} based on the analysis of the ASD at the atom \mathbf{r} of the radical cation and anion of a considered molecule; each ASD gathered at the different atoms of the radical cation and the radical anion provides the local nucleophilic P_k^- and electrophilic P_k^+ Parr functions of the neutral molecule. Note that Parr functions are directly obtained from the analysis of the total electron density⁸² instead of only one selected MO that clearly is not representative of the whole system.

$$P(\mathbf{r})^- = \rho_s^{rc}(\mathbf{r}) \quad \text{for electrophilic attacks} \quad (19)$$

and

$$P(\mathbf{r})^+ = \rho_s^{ra}(\mathbf{r}) \quad \text{for nucleophilic attacks} \quad (20)$$

where $\rho_s^{\text{rc}}(\mathbf{r})$ is the ASD at the \mathbf{r} atom of the radical cation of a considered molecule and $\rho_s^{\text{ra}}(\mathbf{r})$ is the ASD at the \mathbf{r} atom of the radical anion. Each ASD gathered at the different atoms of the radical cation and the radical anion of a molecule provides the local nucleophilic P_k^- and electrophilic P_k^+ Parr functions of the neutral molecule.

A great deal of theoretical work devoted to the study of molecular mechanisms of polar reactions involving non-symmetric reagents has shown that the most favourable reactive channel is that associated with the two-center interaction between the most electrophilic center of the electrophile and the most nucleophilic center of the nucleophile.^{61,63,109} Thus, the local electrophilicity ω_k and local nucleophilicity N_k (see Eq. [21] and [22]), which permit the distribution of the global electrophilicity ω and nucleophilicity N indices at the atomic sites k through the electrophilic P_k^+ and nucleophilic P_k^- Parr functions, respectively, enable the characterisation of the most electrophilic and nucleophilic centers in the molecule, and thus, the prediction of the regio- and chemo- selectivities in polar reactions.

$$\omega_k = \omega \cdot P_k^+ \quad (21)$$

$$N_k = N \cdot P_k^- \quad (22)$$

7.5. GEDT

Numerous theoretical studies have shown that along a polar reaction, there is an electron density transfer from the nucleophilic towards the electrophilic species arising from the electronic chemical potential differences of both reagents. This GEDT⁶¹ can be computed as the sum of the atomic charges (q) of each molecular framework (f) (see Eq. [23]), in such a manner that the larger the GEDT at the TS, the more polar the reaction. Note that the GEDT concept comes from the observation that the electron density transfer taking place from the nucleophile to the electrophile along a polar reaction is not a local process, but a global one involving the two interacting frameworks.

$$\text{GEDT}(f) = \sum_{q \in f} q; \quad f = \text{nucleophile, electrophile} \quad (23)$$

Several studies of cycloaddition reactions allowed establishing a very good correlation between the polar character of the reactions and their feasibility; i.e. the larger the GEDT at the TS, the more polar and thus, faster, the reaction (see Figure 7.2). Therefore, GEDT

7. Theoretical background

accelerates polar reactions through more zwitterionic TSs. This good correlation was quantitatively ascertained in 2002⁶² and 2003,⁶³ indicating that GEDT could be one of the key factors in activation energy.⁶⁶ The GEDT depends on the nucleophilic/electrophilic behaviours of the reagents; the more electrophilic a reagent is and more nucleophilic the other is, the higher the GEDT that usually takes place.¹⁰² Consequently, to analyse the polar character of an organic reaction, 32CA reactions among them, both the electrophilicity ω ⁶² and nucleophilicity N indices^{139,140} of the two reagents should be analysed. Note that analysis of the μ of the reagents provides information only about the direction of the GEDT flux.⁶¹

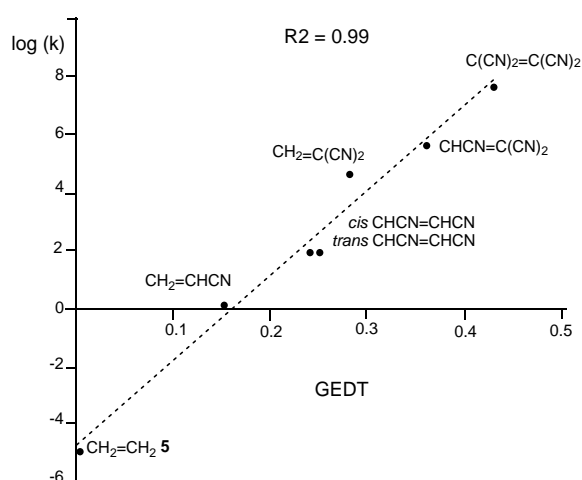


Figure 7.2. Plot of the logarithm of the experimental rate constant k vs the GEDT, in average number of electrons, e , for the DA reactions of cyclopentadiene with ethylene **6** and the cyanoethylene derivatives series; $R^2 = 0.99$.

7.6. QC studies based on the topological analysis of electron density

In spite of the advances made in QC, the characterisation of chemical bonds, and more specifically the breaking/forming processes along a reaction, appeared to be unresolved,¹⁴⁴ hence the unquestionable assumption of concepts such as “concerted” or the self-contradictory “asynchronous concerted” based on hypothesis but not on evidence about how the formation or rupture of bonds along the reaction takes place.

Like many other chemical concepts, chemical bonds are defined in a rather ambiguous manner as they are not observable, but rather belong to a representation of the matter at a microscopic level which is not fully consistent with quantum mechanical principles. To harmonise the chemical description of matter with QC postulates, several mathematical models have been developed. Among them, the theory of dynamical

systems,¹⁴⁵ convincingly introduced by Bader in the early 1960s through the theory of AIM^{58,146} has become a powerful method of analysis. The AIM theory enables a partition of the electron density within the molecular space into basins associated with atoms (see Figure 7.3). The development of the AIM theory was the origin of a significant contribution to conceptual chemistry in the definition of concepts such as the atom inside a molecule or bond critical points.¹⁴⁷ However, as atoms in QTAIM do not overlap, they cannot share electron pairs and therefore, the Lewis's model is not consistent with the description of the matter provided by QTAIM.¹⁴⁸

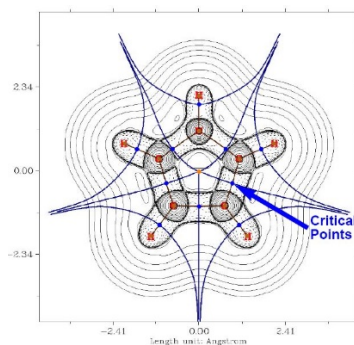


Figure 7.3. QTAM analysis of the electron density of the BF_3 molecule.

Another appealing procedure that provides a more straightforward connection between the electron density distribution and the chemical structure is the QC analysis of the ELF introduced in 1990 by Becke and Edgecombe.⁵⁷ ELF constitutes a useful relative measure of the electron pair localisation characterising the corresponding electron density (see Figure 7.4). In 1991, Silvi and Savin presented the ELF in a very chemical fashion, using its topological analysis as an appealing model of chemical bonding.¹⁴⁹ Thus, the ELF description recovers Lewis's bonding model, providing a very suggestive graphical representation of the molecular system.

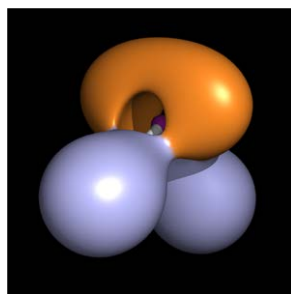


Figure 7.4. ELF basins of the water molecule

The characterisation of the electron density reorganisation to evidence the bonding changes along a reaction path is the most attractive method to characterise a reaction

7. Theoretical background

mechanism.^{60a,107c,150} To perform these analyses quantitatively, the BET, consisting of the joint-use of ELF topology and Thom's CT,¹⁵¹ was proposed by Krokidis et al.¹⁵² in 1997 as a new tool for analysing the electronic changes in chemical processes, being widely applied in the study of different elementary reactions.¹⁵³ This QC methodology makes it possible to establish the nature of the bonding changes associated with the electronic rearrangement along a reaction path and, thus, to understand the molecular mechanism of the reaction.^{60a,107a-c}

Until 2010, only several ways to view and analyse covalent and electrostatic interactions were available. However, analogous methods for NCI were conspicuously missing. Covalent bonds are intuitively represented using conventional Lewis structures⁷⁵ and could be characterised by either the ELF or the AIM theory. Also, purely electrostatic interactions could be analysed using electrostatic potential maps.¹⁵⁴ However, NCI were frequently visualised using distance-dependent contacts, generally without consideration of hydrogen atoms.¹⁵⁵ Hydrogen bonds could be identified from the molecular geometry¹⁵⁶ and from ELF,¹⁵⁷ while grid-based calculations originating from classical force fields were used to model other van der Waals interactions.¹⁵⁸ In 2010, Johnson et al. developed an approach, using the density and its derivatives, that allows simultaneous analysis and visualisation of a wide range of non-covalent interactions types as real space surfaces (see Figure 7.5),⁵⁹ adding an important tool to a chemist's arsenal for the analysis of molecular structure based on electron density.

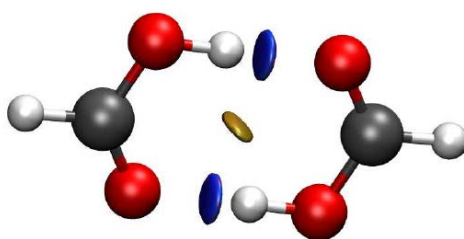


Figure 7.5. NCI analysis of the hydrogen bonds in the acetic acid dimers.

8. COMPUTATIONAL METHODS

A recent analysis about the applicability of the B3LYP¹²⁸ MPWB1K¹²⁹ and M06-2X¹³⁰ functionals in the study of non-polar and polar cycloaddition reactions allowed selecting the two former as the most adequate ones for the study of this type of organic reactions.¹⁰² In addition, several studies have emphasised that the inclusion of diffuse functions¹²⁷ produces no notable changes in the relative energies associated with reactions of species presenting no located charges, such as TACs.¹⁵⁹ Consequently, DFT calculations were performed using the B3LYP or the MPWB1K functionals together with the standard 6-31G(d), 6-311G(d) or 6-311G(d,p) basis sets. Optimisations were carried out using the Berny analytical gradient optimisation method.¹⁶⁰ The stationary points were characterised by frequency computations in order to verify that TSs have one and only one imaginary frequency. The IRC paths¹⁶¹ were traced in order to check and obtain the energy profiles connecting each TS to the two associated minima of the proposed mechanism using the second order González-Schlegel integration method.¹⁶² Solvent effects were taken into account by full optimisation or single-point energy calculations at the gas phase structures using the PCM developed by Tomasi's group¹⁶³ in the framework of the SCRF.¹⁶⁴

The GEDT⁶¹ was computed by the sum of the natural atomic charges (q), obtained by an NPA,¹⁶⁵ of the atoms belonging to each framework (f) at the TSs; i.e. $\text{GEDT}(f) = \sum_{q \in f} q$, where f is the TAC or the ethylene framework. The sign indicates the direction of the electron density flux in such a manner that positive values mean a flux from the considered framework to the other one. CDFT global reactivity indices and Parr functions⁸² were computed using the equations given in the Theoretical Background. All computations were carried out with the Gaussian 09 suite of programs.¹⁶⁶

Topological analysis of the ELF⁵⁷ was performed with the TopMod¹⁶⁷ package using the corresponding monodeterminantal wavefunctions and considering a cubical grid of step size of 0.1 Bohr. For the BET studies,¹⁵² the corresponding reaction paths were followed by performing the topological analysis of the ELF for at least 300 nuclear configurations along the IRC paths. QTAIM⁵⁸ and NCI⁵⁹ studies were performed with the Multiwfn¹⁶⁸ and NCIPLOT¹⁶⁹ programs, respectively, by evaluating the SCF density.

The molecular geometries and ELF basin attractor positions were visualised using the GaussView program,¹⁷⁰ while the representation of the ELF basin isosurfaces and NCI gradient isosurfaces was done by using the UCSF Chimera program,¹⁷¹ at isovalues of 0.7–0.8 a.u., and the VMD program,¹⁷² at an isovalue of 0.5 a.u., respectively.

9. REFERENCES

1. Moss, G. P.; Smith, P. A. S.; Tavernier, D. Glossary of class names of organic compounds and reactive intermediates based on structure. *Pure Appl. Chem.* **1995**, *67*, 1307–1375.
2. (a) Benedlt, D.; Daniel, V. J. Synthesis of 2-methyl-(2)-4-(phenylimino)naphth[2,3-d]oxazol-9-one, a monoimine quinone with selective cytotoxicity toward cancer cells. *Med. Chem.* **1994**, *37*, 710–712; (b) Pereira, E. R.; Sancelme, M; Voldoire, A.; Prudhomme, M. Synthesis and antimicrobial activities of 3-N-substituted-4,5-bis(3-indolyl)oxazo1-2-ones. *Bioorg. Med. Chem. Lett.* **1997**, *7*, 2503–2506.
3. Komeilizadeh, H. Does nature prefer heterocycles? *Iran. J. Pharm. Res.* **2006**, *4*, 229–230.
4. Carruthers, W. *Some Modern Methods of Organic Synthesis*; Cambridge University: Cambridge, UK, **1978**; (b) Carruthers, W. *Cycloaddition Reactions in Organic Synthesis*; Pergamon: Oxford, UK, **1990**.
5. (a) Padwa, A. *1,3-Dipolar Cycloaddition Chemistry*; Wiley-Interscience: New York, NY, USA, **1984**; Vol. 1–2; (b) Padwa, A.; Pearson, W. H. *Synthetic Applications of 1,3-Dipolar Cycloaddition Chemistry Toward Heterocycles and Natural Products*; John Wiley & Sons, Inc.: New York, NY, USA, **2002**; Vol. 59.
6. (a) Huisgen, R. The concerted nature of 1,3-dipolar cycloadditions and the question of diradical intermediates. *J. Org. Chem.* **1976**, *41*, 403–419; (b) Gothelf, K. V.; Jorgensen, K. A. Asymmetric 1,3-dipolar cycloaddition reactions. *Chem. Rev.* **7**, **1998**, *98*, 863–909.
7. (a) Büchner, E. Einwirkung von diazoessigäther auf die aether ungesättigter säuren. *Ber. Dtsch. Chem. Ges.* **1888**, *21*, 2637–2647; (b) Pechmann, H. v. Pyrazol aus acetylen und diazomethan. *Ber. Dtsch. Chem. Ges.* **1898**, *31*, 2950–2951.
8. Huisgen, R. 1,3-dipolar cycloadditions. *Proc. Chem. Soc.* **1961**, *0*, 357–396.
9. (a) Huisgen, R.; Grashey, R.; Sauer, J. *The Chemistry of Alkenes*; Patai, S.; Interscience: London, UK, **1964**; p. 739; (b) Huisgen, R. On the mechanism of 1,3-dipolar cycloadditions. A reply. *J. Org. Chem.* **1968**, *33*, 2291–2297; (c) Huisgen, R.; Sustmann, R.; Bunge, K. 1.3-dipolare cycloadditionen, 65. Zur frage der primären 1.1-Addition bei den cycloadditionen der nitrilium- und diazonium-betaine. *Chem. Ber.* **1972**, *105*, 1324–1339.
10. Smith, L. I. Aliphatic diazo compounds, nitrones, and structurally analogous acompunds. Systems capable of undergoing 1,3-additions. *Chem. Rev.* **1938**, *23*, 193–285.
11. Pauling, L. *The Nature of the Chemical Bond. An Introduction to Modern Structural Chemistry*; Cornell University Press: New York, NY, USA, **1960**.

9. References

12. (a) Slater, J. C. Directed valence in polyatomic molecules. *Phys. Rev.* **1931**, *37*, 481–489; (b) Slater, J. C. Molecular energy levels and valence bonds. *Phys. Rev.* **1931**, *38*, 1109–1144; (c) Pauling, L. The metallic state. *Nature* **1948**, *161*, 1019–1020.
13. Firestone, R. A. On the mechanism of 1,3-dipolar cycloadditions. *J. Org. Chem.* **1968**, *33*, 2285–2290.
14. (a) Huisgen, R. Kinetics and mechanism of 1,3-dipolar cycloadditions. *Angew. Chem. Int. Ed. Engl.* **1963**, *2*, 633–696; (b) Huisgen, R. 1,3-dipolar cycloadditions. Past and future. *Angew. Chem. Int. Ed. Engl.* **1963**, *2*, 565–598.
15. Harkness, J. B.; Kistiakowsky, G. B.; Mears, W. H. J. Studies in gaseous polymerizations. *Chem. Phys.* **1937**, *5*, 682–684.
16. Walling, C.; Peisach, J. Organic reactions under high pressure. IV. The dimerization of isoprene. *J. Am. Chem. Soc.* **1958**, *80*, 5819–5824.
17. (a) Lewis, E. E.; Naylor, M. A. Pyrolysis of polytetrafluoroethylene. *J. Am. Chem. Soc.* **1947**, *69*, 1968–1970; (b) Coyner, E. C.; Hillman, W. S. The thermal dimerization of acrylonitrile. *J. Am. Chem. Soc.* **1949**, *71*, 324–326; (c) Roberts, J. D.; Sharts, C. M. Cyclobutane Derivatives from Thermal Cycloaddition Reactions. *Org. Reactions* **1962**, *12*, 1–56; (d) Barlett, P. D.; Montgomery, L. K.; Seidel, B. Cycloaddition. I. The 1,2-addition of 1,1-dichloro-2,2-difluoroethylene to some dienes. *J. Am. Chem. Soc.* **1964**, *86*, 616–622; (e) Montgomery, L. K.; Schueller, K.; Bartlett, P. D. Cycloaddition. II. Evidence of a biradical intermediate in the thermal addition of 1,1-dichloro-2,2-difluoroethylene to the geometrical isomers of 2,4-hexadiene. *J. Am. Chem. Soc.* **1964**, *86*, 622–628; (f) Barlett, P. D.; Montgomery, L. K. Cycloaddition. III. Kinetics and reactivity in the addition of 1,1-dichloro-2,2-difluoroethylene to dienes. The biradical Mechanism. *J. Am. Chem. Soc.* **1964**, *86*, 628–631; (g) Solomon, W. C.; Dee, L. A. Steric course in cycloaddition of chlorotrifluoroethylene. *J. Org. Chem.* **1964**, *29*, 2790–2791; (h) Cairncross, A.; Blanchard, E. P. Bicyclo[1.1.0]butane chemistry. II. Cycloaddition reactions of 3-methylbicyclo[1.1.0]butanecarbonitriles. The formation of bicyclo[2.1.1]hexanes. *J. Am. Chem. Soc.* **1966**, *88*, 496–504; (i) Skell, P. S.; Woodworth, R. C. Structure of carbene, CH₂. *J. Am. Chem. Soc.* **1956**, *78*, 4496–4497; (j) Scheiner, P. Spin inversion and bond Rotation in 1,3-diradicals. *J. Am. Chem. Soc.* **1966**, *88*, 4759–4760.
18. (a) Houk, K. N.; Firestone, R. A.; Munchausen, L. L.; Mueller, P. H.; Arison, B. H.; García, L. A. Stereospecificity of 1,3-dipolar cycloadditions of p-nitrobenzoxirane to cis- and trans-dideuterioethylene. *J. Am. Chem. Soc.* **1985**, *107*, 7227–7228; (b) Houk, K. N.; Gonsalaz, J.; Li, Y. Pericyclic reaction transition states: passions and punctilios, 1935-1995. *Acc. Chem. Res.* **1995**, *28*, 81–90.

19. (a) Huisgen, R.; Mloston, G.; Langhals, E. The first two-step 1,3-dipolar cycloadditions: interception of intermediate. *J. Org. Chem.* **1986**, *51*, 4085–4087; (b) Huisgen, R.; Mloston, G.; Langhals, E. The first two-step 1,3-dipolar cycloadditions: non-stereospecificity. *J. Am. Chem. Soc.* **1986**, *108*, 6401–6402.
20. Firestone, R. A. The low energy of concert in many symmetry-allowed cycloadditions supports a stepwise-diradical mechanism. *Int. J. Chem. Kinet.* **2013**, *45*, 415–428.
21. Mulliken, R. S. Spectroscopy, molecular orbitals and chemical bonding. *Science* **1967**, *157*, 13–24.
22. (a) Hückel, E. Quantum-theoretical contributions to the benzene problem. I. The electron configuration of benzene and related compounds. *Z. Phys.* **1931**, *70*, 204–286; (b) Hückel, E. Quantum contributions to the benzene problem. II. *Z. Phys.* **1931**, *72*, 310–337; (c) Hückel, E. Quantum contributions to the problem of aromatic and unsaturated compounds. III. *Z. Phys.* **1932**, *76*, 628–648; (d) Coulson, C. A.; O’Leary, B.; Mallion, R. B. *Hückel Theory for Organic Chemists*; Academic Press: London, UK, **1978**.
23. Fukui, K. *Molecular Orbitals in Chemistry, Physics and Biology*; Academic Press: New York, NY, USA, **1964**.
24. Dewar, M. J. S. A molecular orbital theory of organic chemistry-VIII: aromaticity and electrocyclic reactions. *Tetrahedron* **1966**, *22*, 75–92.
25. Woodward, R. B.; Hoffmann, R. The conservation of orbital symmetry. *Acc. Chem. Res.* **1968**, *1*, 17–22.
26. Woodward, R. B.; Hoffmann, R. The conservation of orbital symmetry. *Angew. Chem. Int. Ed.* **1969**, *8*, 781–932.
27. Fleming, I. *Molecular Orbitals and Organic Chemical Reactions*; Wiley: Hoboken, NJ, USA, **2009**.
28. Sustmann, R.; Trill, H. Substituent effects in Diels-Alder additions. *Angew. Chem. Int. Ed. Engl.* **1972**, *11*, 838–840.
29. Sustmann, R. Orbital energy control of cycloaddition reactivity. *Pure Appl. Chem.* **1974**, *40*, 569–593.
30. John, P. R.; Prathapan, S. *Synthesis and Transformations of a Few Nitrogen and Oxygen Heterocycles*; Cochin University of Science & Technology, **2010**. <http://dyuthi.cusat.ac.in/purl/1923>
31. Houk, K. N.; Sims, J.; Duke, R. E.; Strozier, R. W.; George, K. Frontier molecular orbitals of 1,3-dipoles and dipolarophiles. *J. Am. Chem. Soc.* **1973**, *95*, 7287–7301.

9. References

32. Houk, K. N.; Sims, J.; Watts, C. R., Luskus, L. J. The origin of reactivity, regioselectivity, and periselectivity in 1,3-dipolar cycloadditions. *J. Am. Chem. Soc.* **1973**, *95*, 7301–7315.
33. Houk, K. N.; Luskus, L. J.; Bhacca, N. S. Novel double [6+4] cycloaddition of tropone to dimethylfulvene. *J. Am. Chem. Soc.* **1970**, *92*, 6392–6394.
34. (a) Pople, J. A. Molecular orbital perturbation theory. I. A perturbation method based on self-consistent orbitals. *Proc. R. Soc. Lond. A* **1955**, *233*, 233–241; (b) Pople, J. A.; Schofield, P. Molecular orbital perturbation theory. II. Charge displacement and stabilization in conjugated molecules. *Proc. R. Soc. Lond. A* **1955**, *233*, 241–247.
35. (a) Huisgen, R.; Szeimies, G.; Möbius, L. 1.3-Dipolare Cycloadditionen, XXXII. Kinetik der Additionen organischer Azide an CC-Mehrfachbindungen. *Chem. Ber.* **1967**, *100*, 2494–2507; (b) Scheiner, P.; Schomaker, J. H.; Deming, S.; Libbey, W. J.; Nowack G. P. The addition of aryl azides to norbornene. A kinetic investigation. *J. Am. Chem. Soc.* **1965**, *87*, 306–311; (c) Scheitler, P. The addition of aryl azides to unstrained olefins. *Tetrahedron* **1968**, *24*, 349–356; (d) Munk, M. E.; Kim, Y. K. Enamines as dipolarophiles in 1,3-dipolar addition reactions. *J. Am. Chem. Soc.* **1964**, *86*, 2213–2217; (e) Huisgen, R.; Möbius, L.; Szeimies, G. 1.3-dipolare cycloadditionen, XIV: die anlagerung organischer azide an enoläther: orientierung und triazolin-zerfall. *Chem. Ber.* **1965**, *98*, 1138–1152; (f) Huisgen, R.; Szeimies, G. 1.3-Dipolare cycloadditionen, XV: der sterische ablauf der azid-addition an enoläther. *Chem. Ber.* **1965**, *98*, 1153–1158; (g) Ykman, P.; L'Abbe, G.; Smets, G. Reactions of aryl azides with α -keto phosphorus ylides. *Tetrahedron* **1971**, *27*, 845–849; (h) Kirmse, W.; Horner, L. Umsetzung von phenylacetylen mit aziden und diazoverbindungen. *Justus Liebigs Ann. Chem.* **1958**, *614*, 1–3; (i) Sheehan, J. C.; Robinson, C. A. The synthesis of phenyl-substituted triazole analogs of histamine. *J. Am. Chem. Soc.* **1951**, *73*, 1207–1210; (j) Fusco, R.; Bianchetti, G.; Pocar, D. *Gazz. Chim. Ital.* **1961**, *91*, 849–865.
36. Trautz, M. Das gesetz der reaktionsgeschwindigkeit und der gleichgewichte in gasen. Bestätigung der additivität von $Cv-3/2R$. Neue bestimmung der integrationskonstanten und der moleküldurchmesser. *Z. Anorg. Allg. Chem.* **1916**, *96*, 1–28.
37. Doering, W. v. E.; Roth, W. R. The overlap of two allyl radicals or a four-centered transition state in the cope rearrangement. *Tetrahedron* **1962**, *18*, 67–74.
38. Dewar, M. J. S. Aromaticity and pericyclic reactions. *Angew. Chem. Int. Ed. Engl.* **1971**, *10*, 761–776.
39. (a) Dewar, M. J. S. A molecular orbital theory of organic chemistry. I. General principles. *J. Am. Chem. Soc.* **1952**, *74*, 3341–3345; (b) Dewar, M. J. S. A molecular

- orbital theory of organic chemistry. II. The structure of mesomeric systems. *J. Am. Chem. Soc.* **1952**, *74*, 3345–3350; (c) Dewar, M. J. S. A molecular orbital theory of organic chemistry. III. Charge displacements and electromeric substituents. *J. Am. Chem. Soc.* **1952**, *74*, 3350–3353; (d) Dewar, M. J. S. A molecular orbital theory of organic chemistry. IV. Free radicals. *J. Am. Chem. Soc.* **1952**, *74*, 3353–3355; (e) Dewar, M. J. S. A molecular orbital theory of organic chemistry. V. Theories of reactivity and the relationship between them. *J. Am. Chem. Soc.* **1952**, *74*, 3355–3357; (f) Dewar, M. J. S. A molecular orbital theory of organic chemistry. VI. Aromatic substitution and addition. *J. Am. Chem. Soc.* **1952**, *74*, 3357–3363; (g) Dewar, M. J. S. *The Molecular Orbital Theory of Organic Chemistry*; McGraw-Hill: New York, NY, USA, **1969**.
40. (a) Caramella, P.; Houk, K. N.; Domelsmith, L. N. The dichotomy between cycloaddition transition states calculated by semiempirical and ab initio techniques. *J. Am. Chem. Soc.* **1977**, *99*, 4511–4514; (b) Dewar, M. J. S. Multibond reactions cannot normally be synchronous. *J. Am. Chem. Soc.* **1984**, *106*, 209–219.
41. Poppinger, D. Ab initio molecular orbital study of simple 1,3-dipolar reactions. *Aust. J. Chem.* **1976**, *29*, 465–478.
42. Dewar, M. J. S.; Olivella, S.; Rzepa, H. S. Ground states of molecules. 49. MINDO/3 study of the retro-Diels-Alder reaction of cyclohexene. *J. Am. Chem. Soc.* **1978**, *100*, 5650–5659.
43. Komornicki, A.; Goddard, J. D.; Schaefer III, H. F. Reaction of acetylene with fulminic acid. The prototype 1,3-dipolar cycloaddition. *J. Am. Chem. Soc.* **1980**, *102*, 1763–1769.
44. Hiberty, P. C.; Ohanessian, G.; Schlegel, H. B. Theoretical ab initio study of 1,3-dipolar cycloaddition of fulminic acid to acetylene. Support for Firestone's mechanism. *J. Am. Chem. Soc.* **1983**, *105*, 719–723.
45. McDouall, J. J. W.; Robb, M. A.; Niazi, U.; Bernardi, F.; Schlegel, H. B. An MC-SCF study of the mechanisms for 1,3-dipolar cycloadditions. *J. Am. Chem. Soc.* **1987**, *109*, 4642–4648.
46. Carey, F. A.; Sundberg, R. J. *Advanced Organic Chemistry. Part A: Structure and Mechanisms*; Springer: New York, NY, USA, **2007**.
47. Arrieta, A.; de la Torre, M. C.; de Cózar, A.; Sierra, M. A.; Cossío, F. P. Computational chemistry; A useful tool for the chemical synthesis of complex molecules, heterocycles and catalysts. *Synlett.* **2013**, *24*, 535–549.
48. (a) Ess, D. H.; Houk, K. N. Distortion/interaction energy control of 1,3-dipolar cycloaddition reactivity. *J. Am. Chem. Soc.* **2007**, *129*, 10646–10647; (b) Ess, D.

9. References

- H.; Houk, K. N. Theory of 1,3-dipolar cycloadditions: distortion/interaction and frontier molecular orbital models. *J. Am. Chem. Soc.* **2008**, *130*, 10187–10198.
49. (a) Morokuma, K. Molecular orbital studies of hydrogen bonds. III. C=O...H-O Hydrogen bond in H₂CO...H₂O and H₂CO...2H₂O. *J. Chem. Phys.* **1971**, *55*, 1236–1244; (b) Nagase, S.; Morokuma, K. An ab initio molecular orbital study of organic reactions. The energy, charge, and spin decomposition analysed at the transition state and along the reaction pathway. *J. Am. Chem. Soc.* **1978**, *100*, 1666–1672.
50. Hammond, G. S. A correlation of reaction rates. *J. Am. Chem. Soc.* **1955**, *77*, 334–338.
51. Domingo, L. R.; Emamian, S. R. Understanding the mechanisms of [3+2] cycloaddition reactions. The pseudoradical versus the zwitterionic mechanism. *Tetrahedron* **2014**, *70*, 1267–1273.
52. Hohenberg, P.; Kohn, W. Inhomogeneous electron gas. *Phys. Rev.* **1964**, *136*, B864–B871.
53. Scerri, E. R. Have orbitals really been observed? *J. Chem. Educ.* **2000**, *77*, 1492–1494.
54. (a) Coppens, P. *X-ray Charge Densities and Chemical Bonding*; Oxford University Press: New York, NY, USA, **1997**; (b) Koritsanszky, T. S.; Coppens, P. Chemical applications of X-ray charge-density analysis. *Chem. Rev.* **2001**, *101*, 1583–1628.
55. Domingo, L. R. Molecular electron density theory: a modern view of reactivity in organic chemistry. *Molecules*, **2016**, *21*, 1319.
56. (a) Geerlings, P.; De Proft, F.; Langenaeker, W. Conceptual density functional theory. *Chem. Rev.* **2003**, *103*, 1793–1873; (b) Domingo, L. R.; Ríos-Gutiérrez, M.; Pérez, P. *Molecules* **2016**, *21*, 748.
57. Becke, A. D.; Edgecombe, K. E. A simple measure of electron localization in atomic and molecular-systems. *J. Chem. Phys.* **1990**, *92*, 5397–5403.
58. Bader, R. F. W. *Atoms in Molecules. A Quantum Theory*; Clarendon Press: Oxford, UK, **1990**.
59. Johnson, E. R.; Keinan, S.; Mori-Sánchez, P.; Contreras-García, J.; Cohen, A. J.; Yang, W. Revealing noncovalent interactions. *J. Am. Chem. Soc.* **2010**, *132*, 6498–6506.
60. (a) Polo, V.; Andrés, J.; Berski, S.; Domingo, L. R.; Silvi, B. Understanding reaction mechanisms in organic chemistry from catastrophe theory applied to the electron localization function topology. *J. Phys. Chem. A* **2008**, *112*, 7128–7136; (b) Polo, V.; Andrés, J.; Castillo, R.; Berski, S.; Silvi, B. Understanding the

- molecular mechanism of the 1,3-dipolar cycloaddition between fulminic acid and acetylene in terms of the electron localization function and catastrophe theory. *Chem. Eur. J.* **2004**, *10*, 5165–5172; (c) Berski, S.; Latajka, Z. A mechanism of the 1,3-dipolar cycloaddition between the hydrogen nitryl HNO₂ and acetylene HCCH: the electron localization function study on evolution of the chemical bonds. *Chem. Eur. J.* **2011**, *10*, 2378–2389.
61. Domingo, L. R. A new C–C bond formation model based on the quantum chemical topology of electron density. *RSC Adv.* **2014**, *4*, 32415–32428.
 62. Domingo, L. R.; Aurell, M. J.; Pérez, P.; Contreras, R. Quantitative characterization of the global electrophilicity power of common diene/dienophile pairs in Diels-Alder reactions. *Tetrahedron* **2002**, *58*, 4417–4423.
 63. Pérez, P.; Domingo, L. R.; Aurell, M. J.; Contreras, R. Quantitative characterization of the global electrophilicity pattern of some reagents involved in 1,3-dipolar cycloaddition reactions. *Tetrahedron* **2003**, *59*, 3117–3125.
 64. Domingo, L. R.; Chamorro, E.; Pérez, P. Understanding the high reactivity of the azomethine ylides in [3+2] cycloaddition reactions. *Lett. Org. Chem.* **2010**, *7*, 432–439.
 65. Domingo, L. R.; Sáez, J. A. Understanding the electronic reorganization along the nonpolar [3+2] cycloaddition reactions of carbonyl ylides. *J. Org. Chem.* **2011**, *76*, 373–379.
 66. Domingo, L. R.; Sáez, J. A. Understanding the mechanism of polar Diels-Alder reactions. *Org. Biomol. Chem.* **2009**, *7*, 3576–3583.
 67. Errede, L. A.; Hoyt, J. M.; Gregorian, R. S. The chemistry of xylylenes. VII. Some reactions of p-xylylene that occur via cationic intermediates. *J. Am. Chem. Soc.* **1960**, *53*, 5224–5227.
 68. Domingo, L. R.; Aurell, M. J.; Pérez, P. A DFT analysis of the participation of zwitterionic TACs in polar [3+2] cycloaddition reactions. *Tetrahedron*, **2014**, *70*, 4519–4525.
 69. Adjieufack, A. I.; Ndassa, I. M.; Mbadcam, J. K.; Berski, S.; Ríos-Gutiérrez, M.; Domingo, L. R. Understanding the reactivity and regioselectivity of [3+2] cycloaddition reactions between substituted nitrile oxides and methyl acrylate. A molecular electron density theory study. *Int. J. Quantum Chem.* **2017**, *117*, e25451.
 70. (a) Prajapati, S. K.; Shrivastava, S.; Bihade, U.; Gupta, A. K.; Naidu, V. G. M.; Banerjee, U. C.; Babu, B. N. Synthesis and biological evaluation of novel Δ^2 -isoxazoline fused cyclopentane derivatives as potential antimicrobial and anticancer agents. *Med. Chem. Commun.* **2015**, *6*, 839–845; (b) Kumar, K. A.;

9. References

- Govindaraju, M.; Renuka, N.; Kumar, G. V. Isoxazolines: an insight to their synthesis and diverse applications. *J. Chem. Pharm. Res.* **2015**, *7*, 250–257.
71. (a) Grünanger, P.; Vita-Finzi, P. *Isoxazoles, Part I*; Taylor, E. C.; John Wiley & Sons, Inc.: New York, NY, USA, **1991**; p. 417; (b) Curran, D. P. *Advances in Cycloadditions*; JAI Press: Greenwich, CT, USA, **1988**; Vol. 1, p. 280; (c) Jeong, J.; Zong, K.; Choe, J. C. Regioselectivity of 1,3-dipolar cycloadditions of benzonitrile oxide to alkenyl boronic esters: an experimental and computational study. *J. Heterocycl. Chem.* **2017**, *54*, 1007–1014.
72. (a) Bast, K.; Christl, M.; Huisgen, R.; Mack, W. 1,3-Dipolare Cycloadditionen, 73. Relative Dipolarophilen-Aktivitäten bei Cycloadditionen des Benzonitriloxids. *Chem. Ber.* **1973**, *106*, 3312–3344; (b) Schwarz, M. *Dissertation*; Würzburg, Germany, **1993**.
73. Kim, J. N.; Chung, K. H.; Ryu, E. K. Alkali metal fluoride promoted generation of nitrile oxides from hydroximoyl chlorides. *Heterocycles* **1991**, *32*, 477–480.
74. (a) Chiacchio, M. A.; Borrello, L.; Pasquale, G.; Pollicino, A.; Bottino, F. A.; Rescifina, A. Synthesis of functionalized polyhedral oligomeric silsesquioxane (POSS) macromers by microwave assisted 1,3-dipolar cycloaddition. *Tetrahedron* **2005**, *61*, 7986–7993; (b) Domingo, L. R.; Picher, M. T.; Arroyo, P.; Sáez, J. A. 1,3-dipolar cycloadditions of electrophilically activated benzonitrile N-oxides. Polar cycloaddition versus oxime formation. *J. Org. Chem.* **2006**, *71*, 9319–9330; (c) Ponti, A.; Molteni, G. DFT-HSAB prediction of regioselectivity in 1,3-dipolar cycloadditions: behavior of (4-substituted)benzonitrile oxides towards methyl propiolate. *Chem. Eur. J.* **2006**, *12*, 1156–1161; (d) Luft, J. A. R.; Meleson, K.; Houk, K. N. Transition structures of diastereoselective 1,3-dipolar cycloadditions of nitrile oxides to chiral homoallylic alcohols. *Org. Lett.* **2007**, *9*, 555–558; (e) Nishiwaki, N.; Kobiro, K.; Hirao, S.; Sawayama, J.; Saigo, K.; Ise, Y.; Okajima, Y.; Ariga, M. Inverse electron-demand 1,3-dipolar cycloaddition of nitrile oxide with common nitriles leading to 3-functionalized 1,2,4-oxadiazoles. *Org. Biomol. Chem.* **2011**, *9*, 6750–6754; (f) Domingo, L. R.; Aurell, M. J.; Jalal, R.; Esseffar, M. A DFT study of the role of Lewis acid catalysts in the mechanism of the 1,3-dipolar cycloaddition of nitrile imines towards electron-deficient acryloyl derivatives. *Comp. Theor. Chem.* **2012**, *986*, 6–13; (g) Adjieufack, A. I.; Ndassa, I. M.; Mbadcam, J. K.; Ríos-Gutiérrez, M.; Domingo, L. R. Steric interactions controlling the syn diastereofacial selectivity in the [3+2] cycloaddition reaction between acetonitrile oxide and 7-oxanorborn-5-en-2-ones: A molecular electron density theory study. *J. Phys. Org. Chem.* **2017**, *30*, e3710; (h) Sankar, U.; Kumar, Ch. V. S.; Subramanian, V.; Balasubramanian, K. K.; Mahalakshimi, S. Stereo-, regio-, and chemoselective [3+2]-cycloaddition of (2E,4E)-ethyl 5-(phenylsulfonyl)penta-2,4-dienoate with various azomethine ylides, nitrones, and nitrile oxides: synthesis of pyrrolidine, isoxazolidine, and isoxazoline derivatives and a computational study. *J. Org. Chem.* **2016**, *81*, 2340–2354; (i) Jasiński, R.;

- Jasińska, E.; Dresler, E. A DFT computational study of the molecular mechanism of [3+2] cycloaddition reactions between nitroethene and benzonitrile N-oxides. *J. Mol. Model.* **2017**, *23*, 13; (j) Domingo, L. R.; Chamorro, E.; Pérez, P. An analysis of the regioselectivity of 1,3-dipolar cycloaddition reactions of benzonitrile N-oxides based on global and local electrophilicity and nucleophilicity indices. *Eur. J. Org. Chem.* **2009**, 3036–3044; (k) Lin, B.; Yu, P.; He, C. Q.; Houk, K. N. Origins of regioselectivity in 1,3-dipolar cycloadditions of nitrile oxides with alkynylboronates. *Bioorg. Med. Chem.* **2016**, *24*, 4787–4790.
75. Lewis, G. N. The atom and the molecule. *J. Am. Chem. Soc.* **1916**, *38*, 762–785.
76. Jaramillo, P.; Domingo, L. R.; Chamorro, E.; Pérez, P. A further exploration of a nucleophilicity index based on the gas-phase ionization potentials. *J. Mol. Struct. THEOCHEM* **2008**, *865*, 68–72.
77. Domingo, L. R.; Saéz, J. A.; Zaragoza, R. J.; Arnó, M. Understanding the participation of quadricyclane as nucleophile in polar $[2\sigma + 2\sigma + 2\pi]$ cycloadditions toward electrophilic π molecules. *J. Org. Chem.* **2008**, *73*, 8791–8799.
78. Ríos-Gutiérrez, M.; Darù, A.; Tejero, T.; Domingo, L. R.; Merino, P. A molecular electron density theory study of the [3+2] cycloaddition reaction of nitrones with ketenes. *Org. Biomol. Chem.* **2017**, *15*, 1618–1627.
79. (a) Malinina, J.; Tran, T. Q.; Stepanov, A. V.; Gurzhiy, V. V.; Starova, G. L.; Kostikov, R. R.; Molchanov, A. P. [3+2] Cycloaddition reactions of arylallenes with C-(N-arylcarbonyl)- and C,C-bis(methoxycarbonyl)nitrones and subsequent rearrangements. *Tetrahedron Lett.* **2014**, *55*, 3663–3666; (b) Kawai, T.; Kodama, K.-H.; Ooi, T.; Kusumi, T. 1,3-Dipolar addition of nitrones to symmetrically substituted allenes: for the determination of absolute configuration of chiral allenes by NMR spectroscopy. *Tetrahedron Lett.* **2004**, *45*, 4097–4099; (c) Padwa, A.; Kline, D. N.; Koehler, K. F.; Matzinger, M.; Venkatramanan, M. K. Cycloaddition of nitrones with allenes. An example of steric control of regiochemistry. *J. Org. Chem.* **1987**, *52*, 3909–3917.
80. (a) Mo, D.-L.; Pecak, W. H.; Zhao, M.; Wink, D. J.; Anderson, L. L. Synthesis of N-styrenyl amidines from α,β -unsaturated nitrones and isocyanates through CO₂ elimination and styrenyl migration. *Org. Lett.* **2014**, *16*, 3696–3699; (b) Holt J.; Fiksdahl A. Nitropyridyl isocyanates in 1,3-dipolar cycloaddition reactions. *J. Heterocycl. Chem.* **2007**, *44*, 375–379.
81. (a) Celebi-Ölçüm, N.; Lam, Y.-h.; Richmond, E.; Ling, K. B.; Smith, A. D.; Houk, K. N. Pericyclic cascade with chirality transfer: reaction pathway and origin of enantioselectivity of the hetero-Claisen approach to oxindoles. *Angew. Chem. Int. Ed.* **2011**, *50*, 11478–11482; (b) Richmond, E.; Duguet, N.; Slawin, A. M. Z.; Lebl, T.; Smith, A. D. Asymmetric pericyclic cascade approach to spirocyclic oxindoles.

9. References

- Org. Lett.* **2012**, *14*, 2762–2765; (c) Evans, A. R.; Hafiz, M.; Taylor, G. A. Ketene. Part 21. Reactions of heterocumulenes with nitrones. *J. Chem. Soc. Perkin Trans.* **1984**, *1*, 1241–1245.
82. Domingo, L. R.; Pérez, P.; Sáez, J. A. Understanding the local reactivity in polar organic reactions through electrophilic and nucleophilic Parr functions. *RSC Adv.* **2013**, *3*, 1486–1494.
83. Ríos-Gutiérrez, M.; Pérez, P.; Domingo, L. R. A bonding evolution theory study of the mechanism of [3+2] cycloaddition reactions of nitrones with electron-deficient ethylenes. *RSC Adv.* **2015**, *5*, 58464–58477.
84. Ríos-Gutiérrez, M.; Domingo, L. R.; Pérez, P. Understanding the high reactivity of carbonyl compounds towards nucleophilic carbenoid intermediates generated from carbene isocyanides. *RSC Adv.* **2015**, *5*, 84797–84809.
85. Domingo, L. R.; Ríos-Gutiérrez, M.; Pérez, P. A molecular electron density theory study of the [3+2] cycloaddition reaction of nitrones with strained allenes. *RSC Adv.* **2017**, *7*, 26879–26887.
86. (a) Pérez, P.; Domingo, L. R. A DFT study of inter- and intramolecular aryne ene reactions. *Eur. J. Org. Chem.* **2015**, 2826–2834; (b) Domingo, L. R.; Pérez, P.; Contreras, R. π -Strain-induced electrophilicity in small cycloalkynes: a DFT analysis of the polar cycloaddition of cyclopentyne towards enol ethers. *Eur. J. Org. Chem.* **2006**, 498–506.
87. Fernández, I.; Cossío, F. P. Interplay between aromaticity and strain in double group transfer reactions to 1,2-benzyne. *J. Comput. Chem.* **2016**, *37*, 1265–1273.
88. Wittig, G.; Fritze, P. On the intermediate occurrence of 1,2-cyclohexadiene. *Angew. Chem. Int. Ed. Engl.* **1966**, *5*, 846.
89. Barber, J. S.; Styduhar, E. D.; Pham, H. V.; McMahon, T. C.; Houk, K. N.; Garg, N. K. Nitron cycloadditions of 1,2-cyclohexadiene. *J. Am. Chem. Soc.* **2016**, *138*, 2512–2515.
90. (a) Bottini A. T.; Corson, F. P.; Fitzgerald, R.; Frost, K. A. Reactions of 1-halocyclohexenes and methyl substituted 1-halocyclohexenes with potassium t-butoxide. *Tetrahedron* **1972**, *28*, 4883–4904; (b) Christl, M.; Fischer, H.; Arnone, M.; Engels, B. 1-Phenyl-1,2-cyclohexadiene: astoundingly high enantioselectivities on generation in a Doering–Moore–Skattebøl reaction and interception by activated olefins. *Chem. Eur. J.* **2009**, *15*, 11266–11272; (c) Christl, M.; Schreck, M. 1,2,3,5,8,8a-Hexahydronaphthalene from 1,2-cyclohexadiene. *Angew. Chem. Int. Ed. Engl.* **1987**, *26*, 449–451; (d) Moore, W. R.; Moser, W. R. Reaction of 6,6-dibromobicyclo[3.1.0]hexane with methyllithium. Efficient trapping of 1,2-cyclohexadiene by styrene. *J. Org. Chem.* **1970**, *35*, 908–912; (e) Quintana, I.

- Pena, D.; Pérez, D.; Guitian, E. Generation and reactivity of 1,2-cyclohexadiene under mild reaction conditions. *Eur. J. Org. Chem.* **2009**, 5519–5524; (f) Balci, M. J.; Jones, W. M. Chirality as a probe for the structure of 1,2-cycloheptadiene and 1,2-cyclohexadiene. *J. Am. Chem. Soc.* **1980**, *102*, 7607–7608; (g) Tolbert, L. M.; Islam, M. N.; Johnson, R. P.; Loisel, P. M.; Shakespeare, W. C. Carbanion photochemistry: a new photochemical route to strained cyclic allenes. *J. Am. Chem. Soc.* **1990**, *112*, 6416–6417.
91. (a) Dömling, A. Recent developments in isocyanide based multicomponent reactions in applied chemistry. *Chem. Rev.* **2006**, *106*, 17–89; (b) Millich, F. Polymerization of isocyanides. *Chem. Rev.* **1972**, *2*, 101–113; (c) Dömling, A.; Ugi, I. Multicomponent reactions with isocyanides. *Angew. Chem. Int. Ed.* **2000**, *39*, 3168–3210; (d) Gulevich, A. V.; Zhdanko, A. G.; Orru, R. V. A.; Nenajdenko, V. G. Isocyanacetate derivatives: synthesis, reactivity, and application. *Chem. Rev.* **2010**, *110*, 5235–5331; (e) Sadjadi, S.; Heravi, M. M. Recent application of isocyanides in synthesis of heterocycles. *Tetrahedron* **2011**, *67*, 2707–2752; (f) De Moliner, F.; Banfi, L.; Riva, R.; Basso, A. Beyond Ugi and Passerini reactions: multicomponent approaches based on isocyanides and alkynes as an efficient tool for diversity oriented synthesis. *Comb. Chem. High Throughput Screening* **2011**, *14*, 782–810; (g) Sadabad, H. R.; Bazguir, A.; Eskandari, M.; Ghahremanzadeh, R. Pseudo five-component reaction of isocyanides, dialkyl acetylenedicarboxylates, and 2,3-dichloronaphthalene-1,4-dione: a highly diastereoselective synthesis of novel dispiro[furan-2,1'-naphthalene-4',2''-furan] derivatives. *Monatsh. Chem.* **2014**, *145*, 1851–1855; (h) Song, P.; Zhao, L.; Ji, S. Facile synthesis of 4-H-pyran derivatives bearing indole skeleton via [3+3] cyclization of 3-indolyl-3-oxopropanenitriles with dialkyl acetylenedicarboxylates and isocyanides. *Chin. J. Chem.* **2014**, *32*, 381–386; (i) Zhu, T.-H.; Wang, S.-Y.; Tao, Y.-Q.; Wei, T.-Q.; Ji, S.-J. Co(acac)₂/O₂-mediated oxidative isocyanide insertion with 2-aryl anilines: efficient synthesis of 6-amino phenanthridine derivatives. *Org. Lett.* **2014**, *16*, 1260–1263; (j) Gu, Z.-Y., Zhu, T.-H., Cao, J.-J., Xu, X.-P., Wang, S.-Y.; Ji, S.-J. Palladium-catalyzed cascade reactions of isocyanides with enamines: synthesis of 4-aminoquinoline derivatives. *ACS Catal.* **2014**, *4*, 49–52.
92. (a) Nair, V.; Vinoda, A. U.; Abhilasha, N.; Menona, R. S.; Santhia, V.; Varma, R. L.; Vijia, S.; Mathewa, S.; Srinivasb, R. Multicomponent reactions involving zwitterionic intermediates for the construction of heterocyclic systems: one pot synthesis of aminofurans and iminolactones. *Tetrahedron* **2003**, *59*, 10279–10286; (b) Nair, V.; Vinoda, A. U. The reaction of cyclohexyl isocyanide and dimethyl acetylenedicarboxylate with aldehydes: a novel synthesis of 2-aminofuran derivatives. *Chem. Commun.* **2000**, 1019–1020; (c) Ghadari, R.; Hajishaabanha, F.; Mahyari, M.; Shaabani, A.; Khavasi, H. R. An unexpected route toward the synthesis of spiro-benzo[b]acridine-furan derivatives. *Tetrahedron Lett.* **2012**, *53*, 4018–4021; (d) Esmaeili, A. A.; Darbanian, M. Reaction between alkyl isocyanides and dialkyl acetylenedicarboxylates in the presence of N-alkyl isatins: convenient

9. References

- synthesis of γ -spiro-iminolactones. *Tetrahedron* **2003**, *59*, 5545–5548; (e) Shaabani, A.; Rezayan, A. H.; Ghasemi, S.; Sarvary, A. A. A mild and efficient method for the synthesis of 2,5-dihydro-5-imino-2-methylfuran-3,4-dicarboxylates via an isocyanide-based multicomponent reaction. *Tetrahedron Lett.* **2009**, *50*, 1456–1458.
93. Yavari, I.; Djahaniani, H. One-step synthesis of substituted 4,7-bis[alkyl(aryl)imino]-3-oxa-6-thia-1-azaspiro[4.4]nona-1,8-dienes. *Tetrahedron Lett.* **2005**, *46*, 7491–7493.
94. Zhao, L.-L.; Wang, S.-Y.; Xu, X.-P.; Ji, S.-J. Dual 1,3-dipolar cycloaddition of carbon dioxide: two C=O bonds of CO₂ react in one reaction. *Chem. Commun.* **2013**, *49*, 2569–2571.
95. Domingo, L. R.; Ríos-Gutiérrez, M.; Pérez, P. A new model for C–C bond formation processes derived from the molecular electron density theory in the study of the mechanism of [3+2] cycloaddition reactions of carbenoid nitrile ylides with electron-deficient ethylenes. *Tetrahedron* **2016**, *72*, 1524–1532.
96. (a) Bailly, C. Lamellarins, from A to Z: a family of anticancer marine pyrrole alkaloids. *Curr. Med. Chem. AntiCancer Agents* **2004**, *4*, 364–378; (b) Bellina, F.; Rossi, R. Synthesis and biological activity of pyrrole, pyrroline and pyrrolidine derivatives with two aryl groups on adjacent positions. *Tetrahedron* **2006**, *62*, 7213–7256.
97. Domingo, L. R.; Ríos-Gutiérrez, M.; Pérez, P. An MEDT study of the carbenoid-type [3+2] cycloaddition reactions of nitrile ylides with electron-deficient chiral oxazolidinones. *Org. Biomol. Chem.* **2016**, *14*, 10427–10436.
98. Sibi, M. P.; Soeta, T.; Jasperse, C. P. Nitrile ylides: diastereoselective cycloadditions using chiral oxazolidinones without Lewis acid. *Org. Lett.* **2009**, *11*, 5366–5369.
99. Ruiz-López, M. F.; Assfeld, X.; García, J. I.; Mayoral, J. A.; Salvatella, L. Solvent effects on the mechanism and selectivities of asymmetric Diels-Alder reactions. *J. Am. Chem. Soc.* **1993**, *115*, 8780–8787.
100. Domingo, L. R.; Ríos-Gutiérrez, M.; Emamian, S. Understanding the domino reaction between 1-diazopropan-2-one and 1,1-dinitroethylene. A molecular electron density theory study of the [3+2] cycloaddition reactions of diazoalkanes with electron-deficient ethylenes. *RSC Adv.* **2017**, *7*, 15586–15595.
101. Ivanova, O.; Budynina, E. M.; Averina, E. B.; Kuznetsova, T. S.; Grishin, Y. K.; Zefirov, N. S. [3+2] Cycloaddition of diazocarbonyl compounds to 1,1-dinitroethenes: synthesis of functionalized gem-dinitrocyclopropanes. *Synthesis* **2007**, *13*, 2009–2013.

102. Domingo, L. R.; Ríos-Gutiérrez, M.; Pérez, P. How does the global electron density transfer diminish activation energies in polar cycloaddition reactions? A molecular electron density theory study. *Tetrahedron* **2017**, *73*, 1718–1724.
103. Domingo, L. R.; Ríos-Gutiérrez, M. A molecular electron density theory study of the reactivity of azomethine imine in [3+2] cycloaddition reactions. *Molecules* **2017**, *22*, 750.
104. Domingo, L. R.; Chamorro, E.; Pérez, P. Understanding the mechanism of non-polar Diels–Alder reactions. A comparative ELF analysis of concerted and stepwise diradical mechanisms. *Org. Biomol. Chem.* **2010**, *8*, 5495–5504.
105. Domingo, L. R.; Ríos-Gutiérrez, M.; Sáez, J. A. Unravelling the mechanism of the ketene-imine Staudinger reaction. An ELF quantum topological analysis. *RSC Adv.* **2015**, *5*, 37119–37129.
106. Pauling, L. The nature of the chemical bond. Application of results obtained from the quantum mechanics and from a theory of paramagnetic susceptibility to the structure of molecules. *J. Am. Chem. Soc.* **1931**, *53*, 1367–1400.
107. (a) Andrés, J.; Berski, S.; Domingo, L. R.; Polo, V.; Silvi, B. Describing the molecular mechanism of organic reactions by using topological analysis of electronic localization function. *Curr. Org. Chem.* **2011**, *15*, 3566–3575; (b) Andrés, J.; Gracia, L.; González-Navarrete, P.; Safont, V. S. Chemical structure and reactivity by means of quantum chemical topology analysis. *Comp. Theor. Chem.* **2015**, *1053*, 17–30; (c) Andrés, J.; González-Navarrete, P.; Safont, V. Unravelling reaction mechanisms by means of quantum chemical topology analysis. *Int. J. Quantum Chem.* **2014**, *114*, 1239–1252.
108. (a) Domingo, L. R.; Aurell, M. J.; Pérez, P. A mechanistic study of the participation of azomethine ylides and carbonyl ylides in [3+2] cycloaddition reactions. *Tetrahedron* **2015**, *71*, 1050–1057; (b) Hamza-Reguig, A; Bentabed-Ababsa, G.; Domingo, L. R.; Ríos-Gutiérrez, M.; Duval, R. E.; Bach, S.; Roisnel, T.; Mongin, F. A combined experimental and theoretical study of the thermal [3+2] cycloaddition of carbonyl ylides with activated alkenes. *J. Mol. Struct.* **2017**, *1157*, 276–287.
109. Aurell, M. J.; Domingo, L. R.; Pérez, P.; Contreras, R. A theoretical study on the regioselectivity of 1,3-dipolar cycloadditions using DFT-based reactivity indexes. *Tetrahedron* **2004**, *60*, 11503–11509.
110. Schrödinger, E. An ondulatory theory of the mechanics of atoms and molecules. *Phys. Rev. B* **1926**, *28*, 1049–1070.
111. Lennard-Jones, J. E. The electronic structure and the interaction of some simple radicals. *Trans. Faraday Soc.* **1934**, *30*, 70–85.

9. References

112. Matta, C. F.; Gillespie, R. J. Understanding and interpreting molecular electron density distributions. *J. Chem. Educ.* **2002**, *79*, 1141–1152.
113. Kohn, W.; Sham, L. J. Self-consistent equations including exchange and correlation effects. *Phys. Rev. B* **1965**, *140*, A1133–A1138.
114. Contreras, R.; Domingo, L. R.; Silvi, B. *Electron Densities: Population Analysis and Beyond* in *Encyclopedia of Physical Organic Chemistry*; Wang, Z.; Wiley: New York, NY, USA, **2017**; Vol. 4, pp. 2705–2818.
115. Fukui, K.; Yonezawa, T.; Shingu, H. A molecular orbital theory of reactivity in aromatic hydrocarbons. *J. Chem. Phys.* **1952**, *20*, 722–725.
116. (a) Fukui, K. An MO-theoretical illumination for the principle of stereoselection. *Bull. Chem. Soc. Jap.* **1966**, *39*, 498–503; (b) Fukui, K.; Fujimoto, H. Sigma-pi interaction accompanied by stereoselection. *Bull. Chem. Soc. Jap.* **1966**, *39*, 2116–2126; (c) Fukui, K.; Fujimoto, H. *Mechanisms of Molecular Migrations*; Interscience: New York, NY, USA, **1969**; Vol. 2, p 118; (d) Fukui, K. *Theory of Orientation and Stereoselection*; Springer-Verlag: Heidelberg, Germany, **1970**; (e) Salem, L. Orbital interactions and reaction paths. *Chem. Brit.* **1969**, *5*, 449; (f) Fukui, K.; Fujimoto, H. An MO-theoretical interpretation of the nature of chemical reactions. II. The governing principles. *Chem. Brit.* **1969**, *42*, 3399–3409; (g) Fukui, K. Recognition of stereochemical paths by orbital interaction. *Acc. Chem. Res.* **1971**, *4*, 57–64.
117. Hoffmann, R. An extended Hückel theory. I. Hydrocarbons. *J. Chem. Phys.* **1963**, *39*, 1397–1412.
118. Longuet-Higgins, H. C.; Abrahamson, E. W. The electronic mechanism of electrocyclic reactions. *J. Am. Chem. Soc.* **1965**, *87*, 2045–2046.
119. (a) Woodward, R. B.; Hoffmann, R. Stereochemistry of electrocyclic reactions. *J. Am. Chem. Soc.* **1965**, *87*, 395–397; (b) Hoffmann, R.; Woodward, R. B. Orbital symmetries and endo-exo relationships in concerted cycloaddition reactions. *J. Am. Chem. Soc.* **1965**, *87*, 4388–4389; (c) Hoffmann, R.; Woodward, R. Orbital symmetries and orientational effects in a sigmatropic reaction. *J. Am. Chem. Soc.* **1965**, *87*, 4389–4390.
120. (a) Robinson, R. Quatrieme Conseil de la Inst. Chim. Solvay **1931**, 423; (b) *Outline of an Electrochemical Theory of Organic Reactions*; The Institute of Chemistry of Great Britain and Ireland, **1931**.
121. Ingold, C. K. Principles of an electronic theory of organic reactions. *Chem. Rev.* **1934**, *15*, 225–274.

122. Lewis, G. N. *Valence and the Structure of Atoms and Molecules*; Chemical catalog Co., Inc.: New York, NY, USA, **1923**; p. 113.
123. (a) Evans, M. G.; Warhurst, E. The activation energy of diene association reactions. *Trans. Faraday Soc.* **1938**, *34*, 614–624; (b) Evans, M. G. The activation energies of reactions involving conjugated systems. *Trans. Faraday Soc.* **1939**, *35*, 824–834.
124. Arrhenius, S. A. Über die dissociationswärme und den einfluß der temperatur auf den dissociationsgrad der elektrolyte. *Z. Phys. Chem.* **1889**, *4*, 96–116.
125. (a) Pople, J. A.; Santry, D. P.; Segal, G. A. Approximate self-consistent molecular orbital theory. I. Invariant procedures. *J. Chem. Phys.* **1965**, *43*, S129–S135; (b) Pople J. A.; Segal, G. A. Approximate self-consistent molecular orbital theory. II. Calculations with complete neglect of differential overlap. *J. Chem. Phys.* **1965**, *43*, S136–S151; (c) Pople J. A.; Segal, G. A. Approximate self-consistent molecular orbital theory. III. CNDO results for AB₂ and AB₃ systems. *J. Chem. Phys.* **1966**, *44*, 3289–3296; (d) Santry, D. P.; Segal, G. A. Approximate self-consistent molecular orbital theory. IV. Calculations on molecules including the elements sodium through chlorine. *J. Chem. Phys.* **1967**, *47*, 158–174; (e) Pople, J. A.; Beveridge, D. L.; Dobosh, P. A. Approximate self-consistent molecular-orbital theory. V. Intermediate neglect of differential overlap. *J. Chem. Phys.* **1967**, *47*, 2026–2033; (f) Pople, J. A.; Beveridge, D. L. *Approximate Molecular Orbital Theory*; McGraw-Hill: New York, NY, USA, **1970**.
126. (a) Brown, A.; Dewar, M. J. S.; Schoeller, W. MINDO[modified intermediate neglect of differential overlap]/2 study of the Cope rearrangement. *J. Am. Chem. Soc.* **1970**, *92*, 5516–5517; (b) Dewar, M. J. S.; Kirschner, S. MINDO[modified intermediate neglect of differential overlap]/2 study of aromatic (“allowed”) electrocyclic reactions of cyclopropyl and cyclobutene. *J. Am. Chem. Soc.* **1971**, *93*, 4290–4291; (c) Dewar, M. J. S.; Kirschner, S. MINDO[modified intermediate neglect of differential overlap]/2 study of antiaromatic (“forbidden”) electrocyclic processes. *J. Am. Chem. Soc.* **1971**, *93*, 4291–4292; (d) Dewar, M. J. S.; Kirschner, S. Classical and nonclassical potential surfaces. Significance of antiaromaticity in transition states. *J. Am. Chem. Soc.* **1971**, *93*, 4292–4294.
127. Hehre, W. J.; Radom, L.; Schleyer, P. v. R.; Pople, J. A. *AB INITIO Molecular Orbital Theory*; Wiley: New York, NY, USA, **1986**.
128. (a) Becke, A. D. Density-functional thermochemistry. The role of exact exchange. *J. Chem. Phys.* **1993**, *98*, 5648–5652; (b) Lee, C.; Yang, W.; Parr, R. G. Development of the Colle-Salvetti correlation-energy formula into a functional of the electron density. *Phys. Rev. B* **1988**, *37*, 785–789.
129. Zhao, Y.; Truhlar, G. D. Hybrid meta density functional theory methods for thermochemistry, thermochemical kinetics, and noncovalent interactions: the

9. References

- MPW1B95 and MPWB1K models and comparative assessments for hydrogen bonding and van der Waals interactions. *J. Phys. Chem. A* **2004**, *108*, 6908–6918.
130. Zhao, Y.; Truhlar, D. G. The M06 suite of density functionals for main group thermochemistry, thermochemical kinetics, noncovalent interactions, excited states, and transition elements: two new functionals and systematic testing of four M06-class functionals and 12 other functionals. *Theor. Chem. Acc.* **2008**, *120*, 215–241.
131. Parr, R. G.; Yang, W. Density-functional theory of the electronic structure of molecules. *Annu. Rev. Phys. Chem.* **1995**, *46*, 701–728.
132. (a) Parr, R. G.; Pearson, R. G. Absolute hardness: companion parameter to absolute electronegativity. *J. Am. Chem. Soc.* **1983**, *105*, 7512–7516; (b) Parr, R. G.; Yang, W. *Density Functional Theory of Atoms and Molecules*; Oxford University Press: New York, NY, USA, **1989**.
133. Koopmans, T. Über die Zuordnung von Wellenfunktionen und Eigenwerten zu den Einzelnen Elektronen Eines Atoms. *Physica* **1933**, *1*, 104–113.
134. (a) Pauling, L. The nature of the chemical bond. IV. The energy of single bonds and the relative electronegativity of atoms. *J. Am. Chem. Soc.* **1932**, *54*, 3570–3582; (b) Pauling, L.; Sherman, J. A quantitative discussion of bond orbitals. *J. Am. Chem. Soc.* **1937**, *59*, 1450–1456.
135. (a) Sanderson, R. T. Partial charges on atoms in organic compounds. *Science* **1955**, *121*, 207–208; (b) Sanderson, R. T. *Chemical Bonds and Bond Energy*, 2nd ed.; Academic Press: New York, NY, USA, **1976**; (c) Chattaraj, P. K.; Lee, H.; Parr, R. G. DFT-based quantitative prediction of regioselectivity: cycloaddition of nitrilimines to methyl propiolate. *J. Am. Chem. Soc.* **1991**, *113*, 1855–1856; (d) Gázquez, J. L. *Chemical Hardness*; Springer-Verlag: Berlin, Germany, **1993**.
136. (a) Pearson, R. G. Hard and soft acids and bases. *J. Am. Chem. Soc.* **1963**, *85*, 3533–3539; (b) Pearson, R. G. Acids and bases. *Science* **1966**, *151*, 172–177; (c) Pearson, R. G.; Songstad, J. Application of the principle of hard and soft acids and bases to organic chemistry. *J. Am. Chem. Soc.* **1967**, *89*, 1827–1836.
137. Parr, R. G.; Szentpály, L. v.; Liu, S. Electrophilicity index. *J. Am. Chem. Soc.* **1999**, *121*, 1922–1924.
138. Pérez, P.; Domingo, L. R.; Aizman, A.; Contreras, R. *The Electrophilicity Index in Organic Chemistry*, in *Theoretical Aspects of Chemical Reactivity*; Elsevier: New York, NY, USA, **2007**; Vol. 19.

139. Domingo, L. R.; Chamorro, E.; Pérez, P. Understanding the reactivity of captodative ethylenes in polar cycloaddition reactions. A theoretical study. *J. Org. Chem.* **2008**, *73*, 4615–4624.
140. Domingo, L. R.; Pérez, P. The nucleophilicity N index in organic chemistry. *Org. Biomol. Chem.* **2011**, *9*, 7168–7175.
141. Lakhdar, S.; Westermaier, M.; Terrier, F.; Goumont, R.; Boubaker, T. O.; Mayr, H. Nucleophilic reactivities of indoles. *J. Org. Chem.* **2006**, *71*, 9088–9095.
142. Parr, R. G.; Yang, W. Density functional approach to the frontier-electron theory of chemical reactivity. *J. Am. Chem. Soc.* **1984**, *106*, 4049–4050.
143. Chamorro, E.; Pérez, P.; Domingo, L. R. On the nature of Parr functions to predict the most reactive sites along organic polar reactions. *Chem. Phys. Lett.* **2013**, *582*, 141–143.
144. Sutcliffe, B. T. The development of the idea of a chemical bond. *Int. J. Quantum Chem.* **1996**, *58*, 645–655.
145. Abraham, R. H.; Shaw, C. D. *Dynamics: The Geometry of Behavior*; Addison-Wesley: Redwood City, CA, USA, **1992**.
146. Bader, R. F. W. Molecular fragments or chemical bonds. *Acc. Chem. Res.* **1975**, *8*, 34–40.
147. (a) Bader, R. F. W.; Anderson, S. G.; Duke, A. J. Quantum topology of molecular charge distributions. I. *J. Am. Chem. Soc.* **1979**, *101*, 1389–1395; (b) Bader, R. F. W.; Nguyendang, T. T.; Tal, Y. Quantum topology of molecular charge distributions. II. Molecular structure and its change. *J. Chem. Phys.* **1979**, *70*, 4316–4329.
148. Silvi, B.; Alikhani, M. E.; Lepetit, C.; Chauvin, R.; *Chapter 1. Topological Approaches of the Bonding*, In *Applications of Topological Methods in Molecular Chemistry, Challenges and Advances in Computational Chemistry and Physics in Conceptual Chemistry*; Leszczynski, J.; Springer: Berlin, Germany, **2016**.
149. (a) Savin, A.; Becke, A. D.; Flad, J.; Nesper, R.; Preuss, H.; Schnering, H. G. v. A new look at electron localization. *Angew. Chem. Int. Ed.* **1991**, *30*, 409–412; (b) Silvi, B.; Savin, A. Classification of chemical bonds based on topological analysis of electron localization functions. *Nature* **1994**, *371*, 683–686; (c) Savin, A.; Silvi, B.; Colonna, F. Topological analysis of the electron localization function applied to delocalized bonds. *Can. J. Chem.* **1996**, *74*, 1088–1096; (d) Savin, A.; Nesper, R.; Wengert, S.; Fassler, T. F. ELF: the electron localization function. *Angew. Chem. Int. Ed.* **1997**, *36*, 1808–1832.

9. References

150. Berski, S.; Andrés, J.; Silvi, B.; Domingo, L. R. The joint use of catastrophe theory and electron localization function to characterize molecular mechanisms. A density functional study of the Diels-Alder reaction between ethylene and 1,3-butadiene. *J. Phys. Chem. A* **2003**, *107*, 6014–6024.
151. (a) Thom, R. *Structural Stability and Morphogenesis: An Outline of a General Theory of Models*; Westview Press: Boulder, CO, USA, **1976**; (b) Woodcock, A. E. R.; Poston, T. *A Geometrical Study of Elementary Catastrophes*; Springer: Berlin, Germany, **1974**; (c) Gilmore, R. *Catastrophe Theory for Scientists and Engineers*; Courier Corporation: North Chelmsford, MA, USA, **1981**.
152. Krokidis, X.; Noury, S.; Silvi, B. Characterization of elementary chemical processes by catastrophe theory. *J. Phys. Chem. A* **1997**, *101*, 7277–7282.
153. (a) Krokidis, X.; Goncalves, V.; Savin, A.; Silvi, B. How malonaldehyde bonds change during proton transfer. *J. Phys. Chem. A* **1998**, *102*, 5065–5073; (b) Fourre, I.; Silvi, B.; Chaquin, P.; Savin, A. Electron localization function comparative study of ground state, triplet state, radical anion, and cation in model carbonyl and imine compounds. *J. Comput. Chem.* **1999**, *20*, 897–910; (c) Chesnut, D. B.; Bartolotti, L. J. The pair density description of aromaticity in some substituted cyclopentadienyl systems: a comparison of AIM and ELF bonding descriptors. *Chem. Phys.* **2000**, *257*, 175–181; (d) Fuster, F.; Sevin, A.; Silvi, B. Topological analysis of the electron localization function (ELF) applied to the electrophilic aromatic substitution. *J. Phys. Chem. A* **2000**, *104*, 852–858; (e) Chamorro, E.; Santos, J. C.; Gómez, B.; Contreras, R.; Fuentealba, P. The bonding nature of some simple sigmatropic transition states from the topological analysis of the electron localization function. *J. Phys. Chem. A* **2002**, *106*, 11533–11539; (f) Chaquin, P.; Scemama, A. Theoretical study of the electrocyclization product of butadiyne: structure, stability and possible formations. *Chem. Phys. Lett.* **2004**, *394*, 244–249; (g) Polo, V.; González-Navarrete, P.; Silvi, B.; Andrés, J. An electron localization function and catastrophe theory analysis on the molecular mechanism of gas-phase identity S_N2 reactions. *Theor. Chem. Acc.* **2008**, *120*, 341–349; (h) Salinas-Olvera, J. P.; Gómez, R. M.; Cortés-Guzman, F. Structural evolution: mechanism of olefin insertion in hydroformylation reaction. *J. Phys. Chem. A* **2008**, *112*, 2906–2912; (i) Ndassa, I. M.; Silvi, B.; Volatron, F. Understanding reaction mechanisms in organic chemistry from catastrophe theory: ozone addition on benzene. *J. Phys. Chem. A* **2010**, *114*, 12900–12906; (j) Gillet, N.; Chaudret, R.; Contreras-García, J.; Yang, W. T.; Silvi, B.; Piquemal, J. P. Coupling quantum interpretative techniques: another look at chemical mechanisms in organic reactions. *J. Chem. Theory Comput.* **2012**, *8*, 3993–3997.
154. Honig, B.; Nicholls, A. Classical electrostatics in biology and chemistry. *Science* **1995**, *268*, 1144–1149.

155. (a) Word, J. M.; Lovell, S. C.; LaBean, T. H.; Taylor, H. C.; Zalis, M. E.; Presley, B. K.; Richardson, J. S.; Richardson, D. C. Visualizing and quantifying molecular goodness-of-fit: small-probe contact dots with explicit hydrogen atoms. *J. Mol. Biol.* **1999**, *285*, 1711–1733; (b) Davis, I. W.; Leaver-Fay, A.; Chen, V. B.; Block, J. N.; Kapral, G. J.; Wang, X.; Murray, L. W.; Arendall III, W. B.; Snoeyink, J.; Richardson, J. S.; Richardson, D. C. MolProbity: all-atom contacts and structure validation for proteins and nucleic acids. *Nucleic Acids Res.* **2007**, *35*, W375–W383; (c) Sobolev, V.; Sorokine, A.; Prilusky, J.; Abola, E. E.; Edelman, M. Automated analysis of interatomic contacts in proteins. *Bioinformatics* **1999**, *15*, 327–332.
156. McDonald, I. K.; Thornton, J. M. Satisfying hydrogen bonding potential in protein. *J. Mol. Biol.* **1994**, *238*, 777–793.
157. Alikhani, M. E.; Fuster, F.; Silvi, B. What can tell the topological analysis of ELF on hydrogen bonding? *Struct. Chem.* **2005**, *16*, 203–210.
158. Cramer III, R. D.; Patterson, D. E.; Bunce, J. D. Comparative molecular field analysis (CoMFA). 1. Effect of shape on binding of steroids to carrier proteins. *J. Am. Chem. Soc.* **1988**, *110*, 5959–5967.
159. Rhyman, L.; Jhaumeer-Laulloo, S.; Domingo, L. R.; Joule, J. A.; Ramasami, P. Computational assessment of 1,3-dipolar cycloaddition of nitrile oxides with ethane and [60]fullerene. *Heterocycles* **2012**, *84*, 719–735.
160. (a) Schlegel, H. B. Optimization of equilibrium geometries and transition structures. *J. Comput. Chem.* **1982**, *3*, 214–218; (b) Schlegel, H. B. *Modern Electronic Structure Theory*; Yarkony, D. R.; World Scientific Publishing: Singapore, **1994**.
161. Fukui, K. Formulation of the reaction coordinate. *J. Phys. Chem.* **1970**, *74*, 4161–4163.
162. (a) González, C.; Schlegel, H. B. Reaction path following in mass-weighted internal coordinates. *J. Phys. Chem.* **1990**, *94*, 5523–5527; (b) González, C.; Schlegel, H. B. Improved algorithms for reaction path following: higher-order implicit algorithms. *J. Chem. Phys.* **1991**, *95*, 5853–5860.
163. (a) Tomasi, J.; Persico, M. Molecular interactions in solution: an overview of methods based on continuous distributions of the solvent. *Chem. Rev.* **1994**, *94*, 2027–2094; (b) Simkin, B. Y.; Sheikhet, I. I. *Quantum Qhemical and Statistical Theory of Solutions: a Computational Approach*; Ellis Horwood: London, UK, **1995**.
164. (a) Cancès, E.; Mennucci, B.; Tomasi, J. A new integral equation formalism for the polarizable continuum model: theoretical background and applications to isotropic

9. References

- and anisotropic dielectrics. *J. Chem. Phys.* **1997**, *107*, 3032–3041; (b) Cossi, M.; Barone, V.; Cammi, R.; Tomasi, J. Ab initio study of solvated molecules: a new implementation of the polarizable continuum model. *J. Chem. Phys. Lett.* **1996**, *255*, 327–335; (c) Barone, V.; Cossi, M.; Tomasi, J. Geometry optimization of molecular structures in solution by the polarizable continuum model. *J. Comput. Chem.* **1998**, *19*, 404–417.
165. (a) Reed, A. E.; Weinstock, R. B.; Weinhold, F. Natural population analysis. *J. Chem. Phys.* **1985**, *83*, 735–746; (b) Reed, A. E.; Curtiss, L. A.; Weinhold, F. Intermolecular interactions from a natural bond orbital, donor-acceptor viewpoint. *Chem. Rev.* **1988**, *88*, 899–926.
166. Frisch, M. J.; Trucks, G. W.; Schlegel, H. B.; Scuseria, G. E.; Robb, M. A.; Cheeseman, J. R.; Scalmani, G.; Barone, V.; Mennucci, B.; Petersson, G. A.; Nakatsuji, H.; Caricato, M.; Li, X.; Hratchian, H. P.; Izmaylov, A. F.; Bloino, J.; Zheng, G.; Sonnenberg, J. L.; Hada, M.; Ehara, M.; Toyota, K.; Fukuda, R.; Hasegawa, J.; Ishida, M.; Nakajima, T.; Honda, Y.; Kitao, O.; Nakai, H.; Vreven, T.; Montgomery, J., J. A.; Peralta, J. E.; Ogliaro, F.; Bearpark, M.; Heyd, J. J.; Brothers, E.; Kudin, K. N.; Staroverov, V. N.; Keith, T.; Kobayashi, R.; Normand, J.; Raghavachari, K.; Rendell, A.; Burant, J. C.; Iyengar, S. S.; Tomasi, J.; Cossi, M.; Rega, N.; Millam, J. M.; Klene, M.; Knox, J. E.; Cross, J. B.; Bakken, V.; Adamo, C.; Jaramillo, J.; Gomperts, R.; Stratmann, R. E.; Yazyev, O.; Austin, A. J.; Cammi, R.; Pomelli, C.; Ochterski, J. W.; Martin, R. L.; Morokuma, K.; Zakrzewski, V. G.; Voth, G. A.; Salvador P.; Dannenberg, J. J.; Dapprich, S.; Daniels, A. D.; Farkas, O.; Foresman, J. B.; Ortiz, J. V.; Cioslowski, J.; Fox, D. J. *Gaussain 09, Revision D.01*; Gaussian, Inc.: Wallingford, CT, USA, **2013**.
167. Noury, S.; Krokidis, X.; Fuster, F.; Silvi, B. Computational tools for the electron localization function topological analysis. *Comput. Chem.* **1999**, *23*, 597–604.
168. Lu, T.; Chen, F. Multiwfn: a multifunctional wavefunction analyser. *J. Comput. Chem.* **2012**, *33*, 580–592.
169. Contreras-García, J.; Johnson, E. R.; Keinan S.; Chaudret, R.; Piquemal, J.-P.; Beratan, D. N.; Yang, W. NCIPLLOT: a program for plotting noncovalent interaction regions. *J. Chem. Theory Comput.* **2011**, *7*, 625–632.
170. Dennington, R.; Keith, T.; Millam, J. *GaussView, version 3*; Shawnee Mission: Kansas, KS, USA, **2009**.
171. Pettersen, E. F.; Goddard, T. D.; Huang, C. C.; Couch, G. S.; Greenblatt, D. M.; Meng, E. C.; Ferrin, T. E. UCSF Chimera—A visualization system for exploratory research and analysis. *J. Comput. Chem.* **2004**, *25*, 1605–1612.
172. Humphrey, W.; Dalke, A.; Schulten, K. VMD – Visual molecular dynamics. *J. Mol. Graphics* **1996**, *14*, 33–38.

“The only source of knowledge is experience.”

—Albert Einstein

RESUMEN EN CASTELLANO

Introducción

Los compuestos heterocíclicos son especies carbocíclicas que contienen al menos un heteroátomo, como nitrógeno, oxígeno o azufre. Se pueden clasificar en dos categorías: alifáticos, como el tetrahidrofurano o el 4,5-dihidroisoxazol, y aromáticos, como el 1,3-tiazol o la quinolina. Los más comunes son de cinco o seis miembros. El número, diversidad y aplicaciones de los compuestos heterocíclicos son enormes. En los últimos años, han recibido una gran atención, particularmente debido a su potencial tanto farmacológico como sintético.

Las reacciones de cicloadición intermoleculares son una de las mejores opciones para sintetizar compuestos heterocíclicos, por su facilidad sintética dando generalmente excelentes selectividades. En particular, las reacciones de cicloadición [3+2] (32CA) son uno de los métodos más poderosos para la síntesis de compuestos heterocíclicos de cinco miembros.

Las reacciones 32CA consisten en la adición de un sistema con enlaces múltiples a un componente triatómico (TAC), que es una especie neutra cuya estructura principal está constituida por tres núcleos continuos que comparten una densidad electrónica de $4e$. Los TACs pueden clasificarse geoméricamente en dos categorías: estructuras de tipo alílico (A-TAC) y de tipo propargílico (P-TAC); mientras que los A-TACs están doblados, los P-TACs tienen una estructura lineal.

Aunque las reacciones 32CA se conocían experimentalmente desde finales del siglo XIX, fueron reconocidas por Huisgen por primera vez en 1961 por su generalidad, aplicación y mecanismo. El gran trabajo y esfuerzo de Huisgen y colaboradores en este campo condujeron al rápido desarrollo de estas reacciones y le consagraron como el “padre” de las “cicloadiciones 1,3-dipolares”.

A diferencia de los hidrocarburos insaturados que participan en las reacciones de Diels-Alder (DA), los TACs no pueden ser representados por una única estructura de Lewis. De acuerdo con el concepto de resonancia desarrollado por Pauling en 1928 dentro de la Teoría del Enlace de Valencia (VBT), Huisgen propuso en 1961 que los TACs podrían representarse principalmente mediante estructuras resonantes octeto y sexteto de Lewis. Mientras que las estructuras de resonancia octeto eran las principales contribuyentes a la estructura electrónica de los TACs, las estructuras de resonancia

sexteto mostraban un carácter “1,3-dipolar” y, por tanto, estas especies se denominaron “1,3-dipolos” con ambas terminaciones siendo tanto nucleofílicas como electrofílicas (especies ambivalentes). Por otra parte, en 1968, Firestone propuso, como representación principal de estas especies, una estructura de resonancia diradical equivalente a las estructuras resonantes zwitteriónicas. Aunque esta idea fue inicialmente criticada por Huisgen, éste finalmente aceptó una cierta participación de esta estructura diradical en el híbrido de resonancia.

En cuanto al mecanismo, Huisgen propuso inicialmente tres mecanismos: A) el extremo positivo del TAC inicia el ataque y el polo negativo completa la adición; B) el centro negativo puede actuar primero y luego el positivo; o C) ambos centros cargados pueden actuar al mismo tiempo. Si bien sugirió que las rutas A y B tendrían lugar a través de los octetos 1,2-dipolares, consideró que la ruta C tenía lugar a través de los sextetos 1,3-dipolares. Por tanto, debido a la naturaleza supuestamente “concertada” del mecanismo C, Huisgen sugirió un mecanismo “concertado” a cuatro centros en un solo paso, en el que los dos nuevos enlaces sencillos están parcialmente formados en el estado de transición (TS), aunque en 1963 propuso que no necesariamente en la misma medida.

Por otro lado, en 1968, Firestone expuso varias inconsistencias experimentales sobre el mecanismo, la estereoespecificidad, la estructura de los TACs y de los derivados de etileno y acetilénicos, el efecto solvente y la orientación de los reactivos que propuso Huisgen para estas reacciones de cicloadición, proponiendo un mecanismo alternativo en dos etapas a través de la formación de un intermedio diradical, pero reconociendo que podía existir una dualidad de mecanismos.

En esas fechas, diversos cálculos basados en la química cuántica permitieron el comienzo de los estudios computacionales sobre las reacciones 32CA. Hasta entonces había evidencias tanto teóricas como experimentales de que las reacciones 32CA pueden transcurrir por mecanismos de uno o varios pasos. En general, los estudios teóricos de reacciones 32CA, basados en la caracterización de los puntos estacionarios a lo largo del camino de reacción, permitieron establecer que la mayoría de ellas tienen lugar a través de un mecanismo de un solo paso en el que la formación de los dos enlaces sencillos es más o menos asíncrona. La gran aceptación que tuvo el concepto de “mecanismo pericíclico” desde que se propuso en los años 70 condujo a la clasificación de las reacciones 32CA de un solo paso como reacciones “pericíclicas” incuestionablemente. Hoy en día, las reacciones 32CA de un solo paso siguen clasificadas para la mayoría de los químicos como “reacciones pericíclicas concertadas” que tienen lugar a través de “TSs

aromáticos” y que se explican por las reglas de simetría orbital de Woodward-Hoffmann, así como las reglas de aromaticidad de Dewar. Sin embargo, debe señalarse que aunque varias derivaciones teóricas de las reglas establecidas por Woodward y Hoffmann se propusieron como modelos alternativos de racionalización de las reacciones “pericíclicas”, este mecanismo nunca se demostró.

Para explicar la reactividad de los TACs en las reacciones 32CA, Houk propuso, en 2007, el modelo energético de distorsión/interacción (DIEM) en el que la barrera de activación se divide en dos términos aditivos: la energía de distorsión, que es la energía necesaria para distorsionar los reactivos hasta la geometría del TS sin permitir interacción entre ellos, y la energía de interacción, que consiste, a su vez, en varias fuerzas atractivas y repulsivas. La idoneidad de este modelo de reactividad se verificó en las reacciones 32CA de nueve TACs diferentes, seis P-TAC y tres A-TAC, con etileno y acetileno. Houk encontró que las entalpías de activación se correlacionaban muy bien con las energías de distorsión, concluyendo que la energía de distorsión de los reactivos hacia el TS es el factor principal que controla las diferencias de reactividad de los TACs. Cuando las energías de distorsión son aproximadamente las mismas, las interacciones pueden convertirse en el factor determinante.

Sin embargo, este hallazgo, que puede considerarse una afirmación computacional del postulado de Hammond establecido en 1955, no resuelve la pregunta de por qué las energías de activación dependen de las geometrías, que son el resultado de la distribución de la densidad electrónica molecular. Además, la partición de la geometría del TS en dos estructuras separadas no tiene sentido físico dentro de la Teoría del Funcional de la Densidad (DFT), ya que en este modelo químico-cuántico la energía de un sistema es función de la densidad electrónica y el potencial externo, es decir, las posiciones nucleares. Por tanto, la energía de los dos fragmentos separados no puede correlacionarse con la energía del TS porque cada uno de ellos pierde el potencial externo creado por el otro fragmento.

Aunque varios modelos teóricos basados en el análisis de orbitales moleculares (MO), como la teoría de los orbitales moleculares frontera (FMO), se han usado ampliamente para explicar la reactividad en química orgánica, los MOs no son físicamente observables, sino sólo construcciones matemáticas, que no pueden determinarse experimentalmente, utilizadas para obtener la función de onda molecular. Por el contrario, la distribución de la densidad electrónica en una molécula o cristal puede observarse experimentalmente mediante difracción de electrones y cristalografía de rayos

X; de hecho, puede obtenerse también a partir de cálculos *ab initio* o DFT, y con frecuencia más fácilmente que los MOs. Por tanto, a diferencia de los MOs, sólo la densidad electrónica, que es responsable de todas las propiedades moleculares, incluida la geometría, es un escalar accesible experimentalmente.

Recientemente, Domingo ha propuesto una nueva teoría de reactividad en química orgánica, la Teoría de la Densidad Electrónica Molecular (MEDT), según la cual los cambios en la densidad electrónica a lo largo de una reacción, y no las interacciones entre MOs como propone la teoría FMO, son los responsables de la reactividad de las moléculas orgánicas. La MEDT no es solo un nuevo modelo de reactividad en química orgánica basado en el análisis de la densidad electrónica molecular, sino que también descarta los modelos basados en el análisis de MOs, como la teoría FMO. Aunque muchos estudios teóricos que aplican la teoría FMO dan resultados numéricamente cualitativos que se ajustan a las observaciones experimentales, dicho modelo es conceptualmente incorrecto porque los MOs no tienen realidad física y por tanto no pueden interactuar físicamente. Además, el LUMO es el primer MO virtual no ocupado sin ninguna participación en la construcción de la función de onda molecular.

A diferencia de la teoría FMO, la MEDT se centra en el análisis de la densidad electrónica y los cambios energéticos asociados con su redistribución a lo largo del camino de reacción. En los análisis llevados a cabo dentro la MEDT, además de una exhaustiva exploración y caracterización de los caminos de reacción correspondientes a la reacción estudiada, se utilizan los índices de reactividad definidos en la DFT conceptual (CDFT), así como herramientas químico-cuánticas basadas en el análisis topológico de la densidad electrónica molecular como la función de localización electrónica (ELF), la Teoría Cuántica de Átomos en Moléculas (QTAIM) y las interacciones no-covalentes (NCI), para estudiar la reactividad en química orgánica.

Desde el comienzo de este siglo, el análisis de la densidad electrónica se ha aplicado al estudio de varias reacciones orgánicas, incluidas las reacciones 32CA. Estos primeros estudios MEDT supusieron el comienzo de una revolución en el campo de la química orgánica, permitiendo la construcción de un nuevo modelo de reactividad que contribuyó al avance de la química conceptual así como a descartar conceptos fuertemente establecidos tales como los mecanismos “concertados” y “pericíclicos” para las reacciones de DA.

Objetivos

Aunque Firestone propuso una estructura resonante de Lewis diradical como el principal contribuyente al híbrido de resonancia de los TACs, en la actualidad los químicos orgánicos representan los TACs como estructuras de Lewis 1,2-zwitteriónicas, de acuerdo con la propuesta de Huisgen.

En 2010, el análisis topológico de la ELF de la estructura electrónica de los iluros de azometino y carbonilo reveló que estos TACs presentan una estructura pseudodiradical. La alta reactividad de estos TACs en reacciones 32CA se atribuyó, por tanto, a su carácter pseudodiradical. Así, en 2014, dependiendo de los diferentes patrones de reactividad observados, las reacciones 32CA se clasificaron inicialmente en tipo pr (pseudodiradical) y tipo zw (zwitteriónico). Nótese que la estructura electrónica de otros TACs siguió estando inexplorada y, en consecuencia, cualquier TAC que no tuviera una estructura pseudodiradical fue clasificado como un TAC zwitteriónico.

En este contexto, tres fueron los principales objetivos que nos propusimos:

- 1) Completar la caracterización de la estructura electrónica de los TAC orgánicos más importantes utilizados en las reacciones 32CA, con el fin de establecer una clasificación general de este importante tipo de reacciones de cicloadición.
- 2) Establecer los factores estructurales electrónicos que rigen la reactividad de los TACs.
- 3) Esclarecer los mecanismos moleculares de las reacciones 32CA, lo que, a su vez, permitiría probar la validez de las anteriores propuestas mecanísticas de Huisgen y Firestone.

De los objetivos anteriores derivaron varios objetivos adicionales:

- 4) Proporcionar una explicación de la tendencia lineal entre las energías de activación y los cambios de geometría observados por Houk en las reacciones 32CA.
- 5) Investigar la veracidad de los conceptos clásicos supuestamente no demostrados, como el mecanismo "pericíclico" propuesto para las reacciones 32CA en un paso. Hay que considerar que el mecanismo "pericíclico" se descartó previamente para las reacciones de DA.
- 6) Y, por último, demostrar que la química orgánica necesita replantearse en base al estudio de la densidad electrónica molecular como un todo, en lugar del análisis individual de MOs.

Si bien a lo largo de estos tres años el grupo ha desarrollado una gran cantidad de trabajo, resultando en más de treinta y cinco publicaciones, veintidós de ellas dedicadas al estudio de las reacciones 32CA, solo ocho directamente relacionadas con los objetivos de la tesis se han presentado y discutido en la presente tesis doctoral.

Metodología

Un análisis reciente sobre la aplicabilidad de los funcionales B3LYP, MPWB1K y M06-2X en el estudio de reacciones de cicloadición no polares y polares permitió seleccionar los dos primeros como los más adecuados para el estudio de este tipo de reacciones orgánicas. Además, varios estudios han demostrado que la inclusión de funciones difusas no produce cambios notables en las energías relativas asociadas a reacciones de especies que no presentan cargas localizadas, como los TACs. Por tanto, los cálculos DFT se realizaron usando los funcionales B3LYP o MPWB1K junto con las basis sets estándar 6-31G(d), 6-311G(d) o 6-311G(d, p). Las optimizaciones se llevaron a cabo utilizando el método de optimización del gradiente analítico de Berny. Los puntos estacionarios se caracterizaron por cálculos de frecuencia para verificar que los TSs tenían una y sólo una frecuencia imaginaria. Se trazaron las trayectorias de la coordenada de reacción intrínseca (IRC) para verificar y obtener los perfiles de energía que conectan cada TS con los dos mínimos asociados del mecanismo propuesto, utilizando el método de integración González-Schlegel de segundo orden. Los efectos del disolvente se tuvieron en cuenta mediante optimización completa o lectura energética en las estructuras optimizadas en fase gas, usando el modelo continuo polarizable (PCM) desarrollado por el grupo de Tomasi en el marco del campo de reacción auto-consistente (SCRF).

La transferencia global de densidad electrónica (GEDT) se calculó como la suma de las cargas atómicas naturales (q), obtenidas por un análisis de las poblaciones naturales (NPA), de los átomos que pertenecen a cada estructura (f) en los TS; es decir, $GEDT(f) = \sum_{q \in f} q$, donde f es el TAC o el etileno. El signo indica la dirección del flujo de densidad electrónica, de tal forma que valores positivos significan un flujo desde la estructura considerada hacia la otra. Los índices globales de reactividad definidos en la CDFT y las funciones Parr se calcularon usando las ecuaciones publicadas en *Molecules* 2016, 21, 748. Todos los cálculos se llevaron a cabo con el paquete de programas Gaussian 09.

El análisis topológico de la ELF se realizó con el programa TopMod usando las funciones de onda monodeterminantes correspondientes y considerando una cuadrícula

cúbica de 0.1 Bohr de tamaño. Para los estudios BET, se siguieron las trayectorias de reacción correspondientes realizando el análisis topológico de la ELF para al menos 300 configuraciones nucleares a lo largo de las trayectorias del IRC. Los estudios QTAIM y NCI se realizaron con los programas Multiwfn y NCIPLOT, respectivamente, mediante la evaluación de la densidad SCF.

Las geometrías moleculares y las posiciones de los atractores de los basines de la ELF se visualizaron usando el programa GaussView, mientras que las representaciones de las isosuperficies de los basines de la ELF y las isosuperficies de gradiente del NCI se realizaron utilizando el programa UCSF Chimera, con isovalores de 0.7-0.8 a.u. y el programa VMD, con un isovalor de 0.5 a.u., respectivamente.

Conclusiones

Desde el comienzo del presente siglo, ha habido un creciente interés en explicar la reactividad química a partir del análisis de los cambios de la densidad electrónica a lo largo del camino de reacción. En este contexto, en 2016, Domingo propuso la MEDT como una nueva teoría de reactividad en Química Orgánica, que establece que los cambios en la densidad electrónica a lo largo del camino de reacción, y no las interacciones entre MOs, son los responsables de la reactividad de las moléculas orgánicas.

En la presente tesis, se ha abordado el estudio de las reacciones 32CA basándonos en la MEDT, lo cual nos ha permitido revisar la visión clásica de las reacciones 32CA, ampliamente discutidas desde los años 60, así como las teorías y conceptos relacionados. Los recientes estudios MEDT dedicados a las reacciones 32CA, entre ellos los que se incluyen en la presente tesis doctoral, han permitido establecer una muy buena correlación entre la estructura electrónica de los TACs y su reactividad. Así, dependiendo de la estructura electrónica del TAC, es decir, pseudodiradical, pseudoradical, carbenoide o zwitteriónica, las reacciones 32CA se han clasificado en reacciones de tipo pseudodiradical (tipo pdr), tipo pseudoradical (tipo pmr), tipo carbenoide (tipo cb) y tipo zwitteriónico (tipo zw). La tendencia de reactividad disminuye en el orden pseudodiradical > carbenoide \approx pseudoradical > zwitterionic, de forma que mientras que las reacciones 32CA de tipo pdr tienen lugar fácilmente a través de TSs tempranos, las reacciones 32CA de tipo zw requieren una adecuada activación nucleofílica/ electrofílica para tener lugar. El carácter polar de la reacción influye en los cuatro tipos de reactividad,

es decir, cuanto más intensas sean las interacciones nucleofílicas/ electrofílicas que tienen lugar en los TSs, más rápidas serán las reacciones. También hay que señalar que aunque la sustitución puede cambiar la estructura electrónica de los TACs más simples, la relación entre la estructura y la reactividad se mantiene.

Las características electrónicas de los distintos tipos de estructuras de TACs explican el origen de la tendencia de reactividad en las reacciones 32CA no polares. Los dos centros pseudodiradicales presentes en los TAC pseudodiradicales simétricos favorecen un proceso de formación de enlace simple C-C sincrónico a través de una ruptura homolítica del doble enlace C-C del etileno. Este comportamiento explica la alta reactividad de los iluros de azometino y carbonilo, puesto que ya presentan los dos centros pseudoradicales necesarios para la formación del enlace sencillo C-C, de forma que ya están preparados para reaccionar. Sin embargo, este comportamiento no es posible en las reacciones 32CA de tipo pmr; los TACs pseudoradicales no simétricos no pueden inducir una desdoblación simétrica del doble enlace C-C del etileno efectiva, ya que no tienen el segundo centro pseudoradical requerido para la formación del segundo enlace sencillo. Por último, como el enlace múltiple presente en los TACs zwitteriónicos tiene que romperse primero, las reacciones 32CA de tipo zw exigen el coste energético más alto, que puede reducirse por la polaridad de la reacción.

La reactividad de los TAC carbenoides que participan en las reacciones 32CA de tipo cb es completamente diferente a la de los otros tres tipos de TACs. En las reacciones 32CA en las que participan TACs carbenoides, la formación del primer enlace sencillo C-C tiene lugar mediante la donación de la densidad electrónica no enlazante del centro carbenoide a un carbono electrofílico, mientras que en las reacciones 32CA no polares en las que participan los otros tres tipos de TACs, la formación del primer enlace sencillo C-C tiene lugar mediante el acoplamiento de dos centros pseudoradicales generados en los átomos de carbono que están interaccionando.

Por otro lado, las reacciones polares 32CA comienzan por la interacción a dos centros entre el centro más nucleofílico del nucleófilo y el centro más electrofílico del electrófilo, comportamiento que se anticipa por el análisis de las funciones de Parr. En general, los TACs participan como nucleófilos en las reacciones 32CA polares. Así, el análisis de las funciones de Parr nucleofílicas de los TACs pseudoradicales y zwitteriónicos indica que el heteroátomo terminal es normalmente su centro más nucleofílico. En estos casos, el análisis topológico de la ELF de los cambios de enlace a lo largo del camino de reacción más favorable revela que la reacción comienza por la

donación de parte de la densidad electrónica no enlazante del centro más nucleofílico del TAC al carbono más electrofílico del derivado de etileno. Por tanto, las reacciones 32CA polares de tipo pmr y zw siguen un mecanismo molecular similar al de las reacciones 32CA de tipo cb. Este comportamiento juega un papel importante en la regioselectividad de estas reacciones y soporta la relevancia del análisis de los índices de la CDFT en el estado fundamental de los reactivos en el estudio de la reactividad en reacciones 32CA.

En este sentido, a partir del análisis de los cambios de enlace a lo largo de las reacciones 32CA polares de tipo zw, cb y pmr, se ha establecido un nuevo modelo para la formación de enlaces simples C-X (X = C, N, O) por donación de densidad electrónica no enlazante. Mientras que el modelo por compartición exige la ruptura homolítica de enlaces múltiples, el mecanismo por donación exige la despoblación inicial del carbono β -conjugado del etileno sustituido, un hecho que solo es posible cuando hay grupos fuertemente atractores de electrones, como -CHO o -NO₂, en la posición α .

Esta racionalización MEDT de las reacciones 32CA revive, pero también aclara, la clásica controversia entre las propuestas mecanísticas de Huisgen y Firestone.

En cuanto a la estructura electrónica de los TACs, el análisis de su distribución de densidad electrónica, es decir, el patrón de enlaces, revela que mientras que los TACs zwitteriónicos corresponden a la propuesta de Huisgen, los TACs pseudodiradicales corresponden a la propuesta de Firestone. Sin embargo, el NPA de la distribución de cargas de los TACs sugieren que no son estructuras 1,3- ni 1,2-zwitteriónicas con una separación de cargas total y, por lo tanto, nuestra concepción de TACs zwitteriónicos, que no considera cargas sino solo un patrón de enlaces, difiere ligeramente de la definición de Huisgen de "1,3-dipolos".

En cuanto a sus propuestas mecanísticas, cuando dos reactivos experimentan una reacción 32CA polar o no polar, hay tres modos de aproximación conformacionales diferentes: uno a través de un mecanismo de un paso y otros dos que dan lugar a intermedios que deben experimentar una rotación a través del enlace sencillo para la formación del siguiente enlace. En reacciones 32CA no polares, es decir, los reactivos no son nucleófilos fuertes ni electrófilos fuertes, estos compuestos intermedios son diradicales (Firestone); por el contrario, en reacciones 32CA polares, es decir, un reactivo es un nucleófilo fuerte y el otro es un electrófilo fuerte, estos intermedios tienen una naturaleza zwitteriónica (Huisgen).

En general, el modo de aproximación en una etapa presenta una energía de activación más baja que los modos de aproximación por etapas y, por tanto, los caminos de reacción por etapas no son competitivos. Sin embargo, si ambos intermedios diradicales o zwitteriónicos están lo suficientemente estabilizados, podrían interceptarse o experimentar rotación en el etileno, y entonces la reacción podría perder su estereoespecificidad. Por otro lado, el análisis topológico de la ELF a lo largo de caminos de reacción de un paso demuestra que ni los procesos polares ni los no-polares en una etapa son “concertados”, sino que los cambios de enlace son secuenciales, descartando así el mecanismo “pericíclico” propuesto por Woodward y Hoffmann. La polaridad aumenta la asincronicidad de la formación de los nuevos enlaces sencillos en reacciones de cicloadición, de tal forma que la mayoría de las reacciones 32CA polares tienen lugar a través de un mecanismo no concertado de dos etapas en un solo paso; la estabilización adicional de un intermediario zwitteriónico viable podría cambiar el mecanismo a uno de dos pasos, pero los cambios de enlace secuenciales siguen siendo esencialmente los mismos.

Finalmente, nuestro modelo de reactividad para reacciones 32CA, basado en el análisis de la densidad electrónica, permite una racionalización del DIEM de Houk, basado en energías de distorsión; es decir, la viabilidad de una reacción 32CA no está controlada por la distorsión requerida para alcanzar el TS (postulado de Hammond) sino por la similitud de la estructura electrónica del TAC a la requerida para la formación de los nuevos enlaces simples, que hace que el TS sea menos energético y más temprano. Por lo tanto, la posición del TS, es decir, su carácter temprano o avanzado, está determinada por la estructura electrónica del TAC junto con la naturaleza electrónica polar o no polar de la reacción.

En la presente tesis doctoral, la clásica teoría sobre reacciones 32CA, establecida en los años 60 del siglo pasado y que aún prevalece hoy día, se ha revisitado y reinterpretado basándonos en la MEDT. Se ha establecido un nuevo y sólido modelo de reactividad para las reacciones 32CA, mientras que el mecanismo “pericíclico” y el DIEM, que han sido ampliamente utilizados para su racionalización, se descartan, enfatizando que la forma en que los químicos orgánicos conciben la química orgánica necesita una revisión contemporánea basada en el análisis de la densidad electrónica.

En resumen, después de la primera clasificación de las reacciones 32CA en reacciones de tipo zw y pr, establecidas en el año 2014, la estructura y reactividad de los TACs más

importantes utilizados en las reacciones 32CA ha sido completamente caracterizado en base a la MEDT propuesta recientemente. Entre la gran cantidad de trabajo desarrollado a lo largo de la presente tesis doctoral, se han seleccionado y discutido ocho publicaciones representativas, que permitieron caracterizar dos nuevos tipos de reactividad y consolidar la reactividad original de tipo zw. Así, dependiendo de las cuatro estructuras electrónicas diferentes de los TACs, es decir, pseudodiradical, pseudoradical, carbenoide y zwitteriónica, las reacciones 32CA se han clasificado en reacciones de tipo pdr, pmr, cb y zw. Mientras que las reacciones 32CA de tipo pdr son las más rápidas, las reacciones de tipo zw son las más lentas. Las diferentes estructuras electrónicas en el estado fundamental de los reactivos explican esta tendencia de reactividad y revelan que la reactividad de los TACs carbenoides es diferente. Además, ningún TAC puede considerarse una estructura 1,2-zwitteriónica, tal y como se propone para los “1,3-dipolos”. El carácter polar de la reacción, medido por el valor de la GEDT calculado en la estructura del TS, afecta a los cuatro tipos de reactividad, de tal forma que cuanto más fuertes sean las interacciones nucleofílicas / electrofílicas que tienen lugar en el TS, más rápida es la reacción, e incluso puede cambiar el mecanismo molecular de acuerdo con las funciones de Parr definidas dentro de la CDFT. Esta racionalización basada en la MEDT de las reacciones 32CA esclarece las propuestas mecanísticas de Huisgen y Firestone establecidas en los años 60. Independientemente del tipo de reactividad y el carácter polar de la reacción, el análisis topológico de la ELF a lo largo de las reacciones 32CA que tienen lugar en un solo paso sugiere que los cambios de enlace no son “concertados” sino secuenciales, descartando así la clasificación de estas reacciones como “pericíclicas”. En la presente tesis doctoral, la teoría clásica de las reacciones 32CA, establecida en los años 60 del siglo pasado y que aún prevalece en la actualidad, es revisitada y reinterpretada en base a la MEDT. Se establece un nuevo y sólido modelo de reactividad para las reacciones 32CA, enfatizando que la visión actual de la química orgánica necesita replantearse en base al análisis de la densidad electrónica.

10. PUBLICATION COPIES

RESEARCH ARTICLE

Steric interactions controlling the *syn* diastereofacial selectivity in the [3 + 2] cycloaddition reaction between acetonitrile oxide and 7-oxanorborn-5-en-2-ones: A molecular electron density theory study

A. I. Adjieufack¹ | I.M. Ndassa² | J. Ketcha Mbadcam¹ | M. Ríos-Gutiérrez³ | L.R. Domingo³ 

¹Physical and Theoretical Chemistry Laboratory, Faculty of Science, University of Yaoundé I, Yaoundé, Cameroon

²Department of Chemistry, High Teacher Training College, University of Yaoundé I, Yaoundé, Cameroon

³Department of Organic Chemistry, University of Valencia, Burjassot, Valencia, Spain

Correspondence

Luis R. Domingo, Department of Organic Chemistry, University of Valencia, Dr. Moliner 50, 46100 Burjassot, Valencia, Spain. Ibrahim M. Ndassa, Department of Chemistry, High Teacher Training College, University of Yaoundé I, P.O. Box 47, Yaoundé, Cameroon.
Email: domingo@utopia.uv.es

Funding information

MINECO and EUROPEAN Social fund, Grant/Award Number: (CTQ2016-78669-P) and (BES-2014-068258).

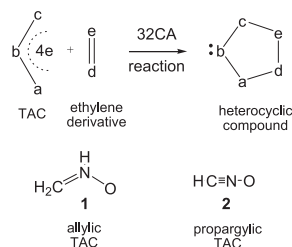
A Molecular Electron Density Theory study of the *zw*-type 32CA reactions of acetonitrile oxide (NO) with two 7-oxanorborn-5-en-2-ones (ONBs) has been performed at the DFT B3LYP/6-31G(d) computational level. These cycloadditions proceed through one-step mechanisms with high activation energies and present low *para* regio and complete *syn* diastereofacial selectivities. While the non-polar character of these *zw*-type 32CA reactions, which is the consequence of the insufficient electrophilic activation of ONBs, according to the analysis of the conceptual DFT reactivity indices, accounts for the high activation energies, and low *para* regioselectivity, NCI topological analyses at the *anti/syn* pairs of *para* TSs reveal that the steric hindrance encountered between the NO framework and the ONB side containing the carbonyl group along the *anti* approach mode is responsible for the complete *syn* diastereofacial selectivity.

1 | INTRODUCTION

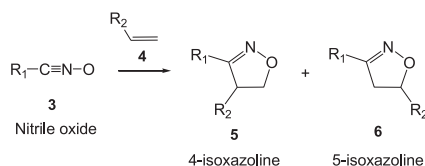
[3 + 2] Cycloaddition (32CA) reactions have emerged as a powerful synthetic tool for the construction of five-membered heterocyclic compounds^[1] after the great effort made by Huisgen and coworkers.^[2] 32CA reactions are bimolecular in nature and involve the 1,3-addition of an ethylene derivative to a three-atom-component (TAC), leading to the formation of five-membered heterocycles (see Scheme 1). TACs can be structurally classified into two categories: allylic type (A-TAC) and propargylic type (P-TAC) structures.^[3] While A-TACs such as nitron 1 are bent, P-TACs such as nitrile oxide (NO) 2 have a linear structure (see Scheme 1).

Many TACs are readily available and react with a variety of multiple bond systems in a highly regioselective and stereoselective manner.^[2] Weygand's group was the first to perform the first 32CA reaction between NOs 3 and olefins 4.^[4] Huisgen later categorised NOs 3 as members of a broader class of TACs able to undergo 32CA reactions.^[5] In particular, the 32CA reactions of NOs 3 with asymmetric alkenes 4 lead to the formation of 4-isoxazoline 5 and 5-isoxazoline 6 mixtures (Scheme 2), which are versatile intermediates for the synthesis of natural products and biologically, medically active compounds.^[6]

Very recently, Domingo has proposed a new reactivity theory in organic chemistry, the Molecular Electron Density Theory (MEDT),^[7] in which changes in the electron density



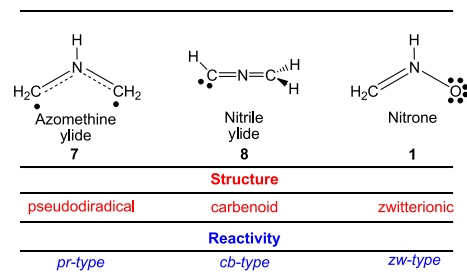
SCHEME 1 Construction of 5-membered heterocyclic compounds by a 32CA reaction and classification of TACs by structure



SCHEME 2 32CA reactions of NOs **3** with alkenes **4** yielding regiosomeric 4- and 5-isoxazolines **5** and **6**

along an organic reaction, and not molecular orbital (MO) interactions, are responsible for the molecular organic reactivity. Note that MOs are not physical observables but only mathematical constructs that cannot be experimentally determined,^[8] and therefore, they cannot physically interact with each other, as the Frontier Molecular Orbital^[9] theory proposed. Within MEDT, besides a deep exploration and characterisation of the reaction paths associated with the studied reaction, analysis of the conceptual density functional theory (CDFT) reactivity indices,^[10,11] as well as quantum chemical tools based on the topological analysis of the electron density such as the electron localisation function^[12] (ELF), quantum theory of atoms in molecules,^[13] and noncovalent interaction^[14] (NCI), are used to study the reactivity in organic chemistry.

Several theoretical studies devoted to the study of the reactivity of TACs participating in 32CA reactions performed within the MEDT have allowed establishing a useful classification of these cycloaddition reactions into *pseudoradical*-type (*pr*-type, typically an azomethine ylide **7**),^[15] *carbenoid*-type (*cb*-type, typically a nitrile ylide **8**),^[16] and *zwitterionic*-type (*zw*-type, typically a nitron **1**)^[15] reactions (Scheme 3), depending on the electronic structure of the TAC. Unlike *pr*-type 32CA reactions, which take place quickly even through non-polar TSs,^[15] the feasibility of *cb*-type and *zw*-type 32CA reactions depends on the polar character of the reactions, ie, the nucleophilic character of the TAC and the electrophilic character of the ethylene derivative, or vice versa.^[15,16] In general, NOs **3** are neither good nucleophiles nor electrophiles and only react with strongly electrophilically or nucleophilically activated multiple bond derivatives in polar *zw*-type 32CA reactions.^[15–17]

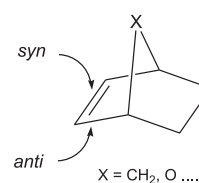


SCHEME 3 Electronic structure of TACs and the proposed reactivity types in 32CA reactions

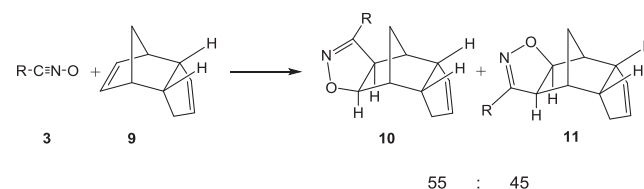
Norbornene derivatives are attacked by a variety of reagents preferentially from the *syn* face of the double bond (see Scheme 4).^[18] The preferred *syn* attack has been attributed to different stereo-electronic effects such as steric effects, torsional effects, “nonequivalent orbital extension,” or Huisgen’s factor “*x*,”^[18–20] which, according to Houk, arises from enforced staggering of allylic bonds in norbornene and not from nonequivalent orbital extension or hyperconjugative interactions.^[18]

In 2004, Namboothiri et al^[21] reported the experimental chemoselective and stereoselective 32CA reactions of NOs **3** with dicyclopentadiene **9** and its derivatives. In that work, the approach of NO **3b** (R = CH₃) takes place exclusively from the *syn* face of the dicyclopentadiene moiety providing a mixture of regioisomers **10** and **11** in an approximate 55:45 ratio (see Scheme 5). Computational studies at *ab initio* and DFT levels of theory were in good agreement with the experimental outcomes.

Very recently, Tajabadi et al^[22] performed a DFT study about the regioselectivity and diastereofacial selectivity in the 32CA reactions between NOs **3** and 1-substituted 7-



SCHEME 4 *Syn* and *anti* stereoisomeric attacks on the 2 diastereotopic faces of norbornene derivatives

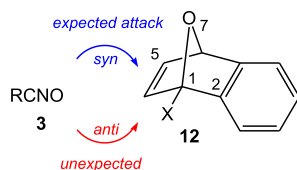


SCHEME 5 Exclusive chemoselective *syn* attacks of NOs **3** on dicyclopentadiene **9**

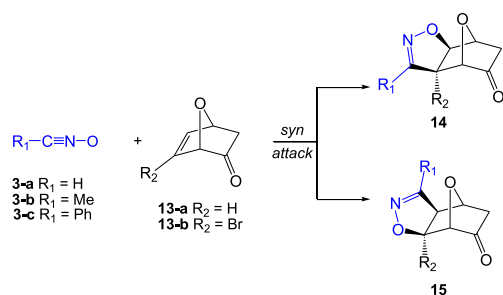
oxanorborn-5-enes (ONBs) **12** (see Scheme 6), finding that the reactions are *syn* diastereofacial and regioselective, and suggested that they could be classified as *pr*-type 32CA reactions taking place through a low asynchronous one-step mechanism with non-polar character. The classification of this 32CA reaction as a *pr*-type 32CA reaction was totally erroneous, as NOs **3** are zwitterionic TACs participating in *zw*-type 32CA reactions (see later).^[17] Indeed, the non-polar character of the studied reactions accounted for the high computed activation energies, a behaviour typical of non-polar *zw*-type 32CA reactions.

Although the chemistry of NOs **3** with a huge variety of bicyclic compounds containing multiple bonds has been widely investigated, the reactivity of these TACs towards 2-substituted 7-oxanorborn-5-en-2-ones **13** has only been superficially explored since the 1990, when Plumet et al.^[23,24] experimentally studied the 32CA reactions of NOs **3-b,c** with ONBs **13-a,b** (Scheme 7) giving the corresponding *syn* adducts exclusively with excellent yields.^[23]

Herein, to understand the *zw*-type reactivity of NOs **3** towards ONBs **13**, as well as to explain the origin of the regioselectivity and diastereofacial selectivity experimentally obtained by Plumet et al.,^[23] an MEDT study of the 32CA reactions of NO **3-b** with ONBs **13-a,b** was performed using DFT methods at the B3LYP/6-31G(d) computational level. To this end, after characterising of the electronic structure of NOs **3-a,b** through the topological analysis of the ELF^[12] and the analysis of the reactivity indices defined within the CDFT,^[10,11] the reaction paths associated to both 32CA reactions and NCI taking place in the transition state



SCHEME 6 Expected exclusive *syn* attack of NOs **3** on ONBs **12**



SCHEME 7 32CA reactions of NOs **3** with ONBs **13-a,b** yielding regioisomeric *syn* adducts **14** and **15**

structures (TSs) are explored and characterised. Moreover, the possible electronic effect of the bromine substituent of ONB **13-b** on the molecular mechanism and the reaction rate of the 32CA reaction involving the simplest ONB **13-a** will be also discussed.

2 | COMPUTATIONAL METHODS

All geometry optimisations and energy calculations were performed with the Gaussian 3.0 suite of programs.^[25] The geometries of the reactants and TSs were fully optimised through DFT calculations using the B3LYP^[26,27] functional together with the standard 6-31G(d) basis set.^[28] The stationary points were characterised by frequency calculations to verify the number of imaginary frequencies (zero for local minimum and one for TSs). The intrinsic reaction coordinate paths^[29] were traced to check the energy profiles connecting each TS to the two associated minima of the proposed mechanism using the second-order González-Schlegel integration method.^[30,31] Natural atomic charges were obtained through a natural population analysis (NPA) within the natural bond orbital method.^[32,33] Solvent effects of benzene in the single-point energy calculations were taken into account using the polarisable continuum model developed by Tomasi's group^[34,35] in the framework of the self-consistent reaction field (SCRF).^[36,37] Electron localisation function^[12] calculations were performed with the TopMod^[38] program using the corresponding B3LYP/6-31G(d) monodeterminantal wavefunctions over a grid spacing of 0.1 au, and ELF localisation domains were obtained for an ELF value of $\eta = 0.75$. Noncovalent interaction^[14] was computed with the NCIPLLOT program^[39,40] by evaluating the Self-Consistent Field (SCF) density and using the methodology previously described.

Conceptual density functional theory provides different indices to rationalise and understand chemical structure and reactivity.^[10,11] The global electrophilicity index,^[41] ω , is given by the following expression, $\omega = (\mu^2/2\eta)$, in terms of the electronic chemical potential, μ , and the chemical hardness, η . Both quantities may be approached in terms of the one-electron energies of the frontier molecular orbitals HOMO and LUMO, ϵ_H and ϵ_L , as $\mu \approx (\epsilon_H + \epsilon_L)/2$ and $\eta \approx (\epsilon_L - \epsilon_H)$, respectively.^[42,43] The empirical (relative) nucleophilicity index,^[44,45] N , based on the HOMO energies obtained within the Kohn-Sham scheme,^[46] is defined as $N = E_{\text{HOMO}}(\text{Nu}) - E_{\text{HOMO}}(\text{TCE})$, where tetracyanoethylene (TCE) is the reference, because it presents the lowest HOMO energy in a long series of molecules already investigated in the context of polar organic reactions. This choice allows handling conveniently a nucleophilicity scale of positive values. Nucleophilic P_k^- and electrophilic P_k^+ Parr functions,^[47] which allow for the characterisation of the

nucleophilic and electrophilic centres of a molecule, were obtained through the analysis of the Mulliken atomic spin density (ASD) of the corresponding radical cations or anions, by single-point energy calculations over the optimised neutral geometries.

3 | RESULTS AND DISCUSSION

The present MEDT study has been divided into 4 sections: (1) in Section 3.1, an ELF topological analysis and an NPA of NOs **3-a,b** are performed to characterise their electronic structure; (2) in Section 3.2, an analysis of the CDFT reactivity indices at the ground state of the reagents involved in the two 32CA reactions under study, ie, NO **3-b** and ONBs **13-a,b**, is performed; (3) in Section 3.3, the reaction paths associated to both 32CA reactions are explored and characterised, and energy- and geometry-related aspects of the corresponding stationary points are discussed; and finally, (4) in Section 3.4, the origin of the *syn* diastereofacial selectivity experimentally reported is explained in terms of NCI.

3.1 | ELF topological analysis and NPA of NOs **3-a,b**

As the reactivity of TACs can be correlated with their electronic structure,^[15,16] an ELF topological analysis of the simplest NO **3-a** and acetonitrile oxide **3-b** was first performed to characterise the electronic structure of these TACs and thus to predict their reactivity in 32CA reactions. The representation of attractor positions of the ELF valence basins, as well as ELF electron populations, natural atomic charges obtained by a NPA, and the Lewis structures arising of the ELF topological analysis for NOs **3-a,b**, are shown in Figure 1.

ELF topological analysis of the simplest NO **3-a** shows the presence of one V(O1) monosynaptic basin integrating 5.56e, which, according to the Lewis bonding model, can be related to three non-bonding O1 oxygen lone pairs, and two disynaptic basins, V(O1,N2) and V(N2,C3), with electron populations of 2.06e and 5.65e, which correspond to an O1–N2 single bond and an N2–C3 triple bond (see the ELF-based Lewis structure of NO **3-a** in Figure 1). Consequently, ELF topological analysis of the electronic structure of the simplest NO **3-a** indicates that this TAC will be able to participate only in *zw-type* 32CA reactions. Note that according to the Lewis structures, V(C) monosynaptic basins integrating *ca.* 1e are associated to *pseudoradical* centres,^[48,49] while those integrating *ca.* 2e in neutral molecules are associated to a carbenoid centres.^[50] TACs presenting two *pseudoradical* centres have been classified as *pseudodiradical* TACs,^[15] while those presenting a carbenoid centre have been classified as carbenoid TACs.^[16] Finally, TACs that present neither *pseudoradical* nor carbenoid centres have been classified as zwitterionic TACs.^[15]

When the ELF topology of NO **3-b** is analysed, some topological differences with respect to the ELF topological characteristics of the simplest NO **3-a** are found. Three monosynaptic basins, V(O1), V'(O1), and V''(O1), integrating a total population of 5.73e, appear around the O1 oxygen atom, related to the three non-bonding O1 oxygen lone pairs. Likewise, while the V(O1,N2) disynaptic basin characterising the O1–N2 single bond integrates an electron population of 1.61e, three V(N2,C3), V'(N2,C3) and V''(N2,C3) disynaptic basins are observed in the N2–C3 bonding region with a total integration of 6.18e, thus being associated to an N2–C3 triple bond. The increase of the electron density at the O1 oxygen, together the depopulation of the O1–N2 bonding region, with respect to the ELF populations

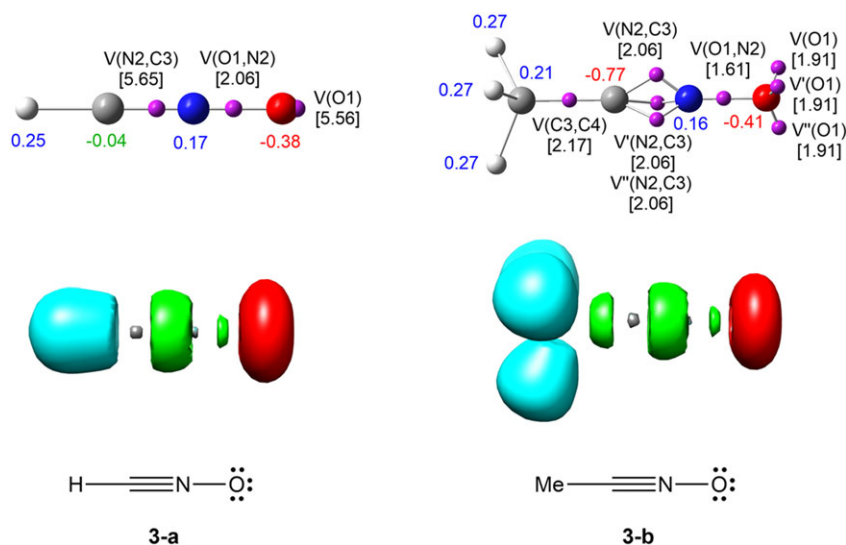


FIGURE 1 Representation of electron localisation function (ELF) attractors and valence basin populations, in e, natural atomic charges (negative in red, positive in blue, and neutral in green), ELF localisation domains, and the proposed Lewis structures for NOs **3-a,b**

at the simplest NO **3-a**, is suggestive of a notable polarisation of the O1–N2 single bond towards the adjacent O1 oxygen atom. This polarisation, as well as the increase of the electron density in the N2–C3 bonding region, is the consequence of the electron-releasing effect of the methyl group of NO **3-b**. However, note that despite these topological differences, the ELF-based Lewis structures of both NOs are very similar (see the ELF-based Lewis structure of NO **3-b** in Figure 1), thus allowing characterising the *zw-type* reactivity of NO **3-b** in 32CA reactions.

After the establishment of the bonding pattern of NOs **3-a,b** based on the ELF topological analysis, the charge distribution at both NOs was analysed. The natural atomic charges, obtained through an NPA, are shown in Figure 1. As can be observed, while the O1 oxygen presents a considerable negative charge, $-0.38e$ (**3-a**) and $-0.41e$ (**3-b**), the N2 nitrogen is slightly positively charged, $0.17e$ (**1-a**) and $0.16e$ (**1-b**). However, note that the most positively charged atoms at both NOs correspond to the hydrogen atoms with positive charges of $0.25e$ (**3-a**) and $0.27e$ (**3-b**), and that the most negatively charged atom at NO **3-b** is the methyl carbon with a negative charge of $-0.77e$. These charge distributions are in complete disagreement with the commonly accepted 1,2-zwitterionic structure in which a positive charge and a negative charge are entirely located at the N2 nitrogen and O1 oxygen atoms, respectively.

Thus, unlike NPA, which reveals that these TACs do not have a 1,2-zwitterionic Lewis structure, ELF topological analysis of the electron density of NOs **3-a,b** makes it possible to establish a bonding pattern concordant with the commonly accepted Lewis structure associated with them and which is characteristic of TACs participating in *zw-type* 32CA reactions.

3.2 | Analysis of the CDFT reactivity indices

Studies devoted to polar organic reactions have shown that the analysis of the reactivity indices defined within CDFT^[10,11] is a powerful tool to understand the reactivity in polar cycloadditions. Global CDFT indices, namely, the electronic chemical potential, μ ; chemical hardness, η ; electrophilicity, ω ; and nucleophilicity, N , in eV, of NOs **3-a,b**, ONBs **13-a,b**, and ethylene **18**

TABLE 1 B3LYP/6-31G(d) electronic chemical potential, μ ; chemical hardness, η ; electrophilicity, ω ; and nucleophilicity, N , in eV, of NOs **3-a,b**, ONBs **13-a,b**, and ethylene **18**

Compound	μ	η	ω	N
NO 3-b	-2.90	7.66	0.55	2.40
Ethylene 18	-3.37	7.77	0.73	1.86
NO 3-a	-3.40	7.94	0.73	1.75
ONB 13-a	-3.57	5.44	1.17	2.84
ONB 13-b	-3.83	5.36	1.37	2.62

electrophilicity, ω ; and nucleophilicity, N , at the ground state of the reagents involved in these 32CA reactions are given in Table 1.

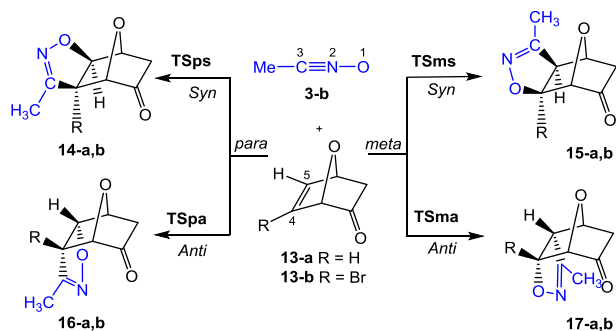
The electronic chemical potential μ of NO **3-b**, -2.90 eV, is higher than that of ONBs **13-a**, -3.57 eV, and **13-b**, -3.83 eV, which indicates that along polar reactions, the global electron density transfer (GEDT)^[51] would take place from the NO framework towards the ONB one.

Along a polar reaction, there is an electron density transfer from the nucleophilic to the electrophilic species, which is measured by the GEDT^[51] value computed at the TS of the reaction; the larger the GEDT at the TS, the more polar the reaction. Note that the GEDT concept comes from the observation that the electron density transfer taking place from the nucleophile to the electrophile along a polar reaction is not a local process, but a global one involving the two interacting frameworks^[51] and depending on the electrophilic/nucleophilic interactions taking place between them.

The electrophilicity ω and nucleophilicity N indices of NO **3-a**, $\omega = 0.73$ and $N = 1.75$ eV, allow its classification as a marginal electrophile and a marginal nucleophile based on the electrophilicity^[52]/nucleophilicity^[53] scales. Substitution of the terminal hydrogen by a methyl group decreases the electrophilicity of NO **3-b** to $\omega = 0.55$ eV and increases its nucleophilicity to $N = 2.40$ eV, being classified as a marginal electrophile and a moderate nucleophile. Note that most zwitterionic TACs are strong nucleophiles.^[17]

Polar cycloaddition reactions require the participation of good electrophiles and good nucleophiles.^[15–17,54] Ethylene **18** is one of the poorest electrophilic, $\omega = 0.73$ eV, and nucleophilic, $N = 1.86$ eV, species involved in cycloaddition reactions, being classified as a marginal electrophile and a marginal nucleophile. Consequently, ethylene **18** cannot participate in polar reactions.^[55] In the simplest ONB **13-a**, both the electrophilicity ω and N nucleophilicity indices considerably increase, $\omega = 1.17$ and $N = 2.84$ eV, being classified as a moderate electrophile and a moderate nucleophile. Substitution of the C4-H hydrogen atom of ONB **13-a** by a bromine one (see Scheme 8 for atom numbering) increases the electrophilicity and decreases the nucleophilicity of ONB **13-b**, $\omega = 1.37$ eV and $N = 2.62$ eV, by *ca.* 0.2 eV, which is not notable enough to enhance its reactivity towards NO **3-b**, thus remaining classified as a moderate electrophile and a moderate nucleophile. Therefore, no significant electronic difference between **13-a** and **13-b**, and thus between their reactivity towards NO **3-b**, is expected.

In polar cycloaddition reactions involving the participation of non-symmetric reagents, the most favourable reactive channel is that involving the initial two-centre interaction between the most electrophilic centre of the electrophile and the most nucleophilic centre of the nucleophile.^[47] To determinate the most electrophilic and nucleophilic centres of the species participating in a given reaction, Domingo



SCHEME 8 Competitive regioisomeric and diastereofacial isomeric channels associated with the 32CA reactions between NO **3-b** and ONBs **13-a,b**

et al^[47] proposed the nucleophilic P_k^- and electrophilic P_k^+ Parr functions, derived from the changes of spin electron density reached via the GEDT process from the nucleophile to the electrophile, as a powerful tool for the study of the local reactivity in polar processes. Accordingly, the nucleophilic P_k^- Parr functions of NO **3-b** and the electrophilic P_k^+ Parr functions of ONBs **13-a,b** (Figure 2) were analysed to characterise the most electrophilic and nucleophilic centres of the species involved in these 32CA reactions and, thus, to explain the expected regioselectivity in a polar reaction.

Analysis of the nucleophilic P_k^- Parr functions at NO **3-b** indicates that the O1 oxygen is the most nucleophilic centre with a maximum value of $P_k^- = 0.68$, being more than twice as nucleophilically activated than the C3 carbon, $P_k^- = 0.30$. At this oxygen atom, the value of the local nucleophilicity N_k index is 1.63 eV. On the other hand, analysis of the electrophilic P_k^+ Parr functions of ONBs **13-a,b** shows that the C5 carbon of these species is the most electrophilic centre, $P_k^+ = 0.38$ (**13-a**) and 0.40 (**13-b**), with local electrophilicity ω_k values of 0.44 and 0.52 eV respectively, while the adjacent alkene C4 carbon is poorly electrophilically activated, $P_k^+ = 0.13$ (**13-a**) and 0.14 (**13-b**). The large differences between the electrophilic P_k^+ Parr functions of the C4 and C5 carbons suggest that, in the case of being polar, these 32CA reactions would present a high regioselectivity. In addition, a notable electrophilic activation of the carbonyl carbon, $P_k^+ = 0.31$ (**13-a**) and 0.27 (**13-b**), which is not involved in the considered 32CA reactions, is observed.

Consequently, the most favourable nucleophile/electrophile interaction along a polar 32CA reaction of NO **3-b** with

ONBs **13-a,b** would take place between the most nucleophilic centre of NO **1-b**, the O1 oxygen, and the most electrophilic centre of ONBs **13-a,b**, the C5 carbon.^[47]

3.3 | Study of the reaction paths associated to the 32CA reactions between NO **3** and ONBs **13-a,b**

Because of the non-symmetric of both reagents and the chiral character of ONBs **13-a,b**, four reactive channels are possible for these 32CA reactions; two regioisomeric pathways, named *meta* and *para*, related to the relative position of the nitrile oxide O1 oxygen with respect to the carbonyl group in the 6-membered ring of the bicyclic ONBs, and two stereoisomeric pathways, *syn* and *anti*, corresponding to the approach of NO **3-b** towards the two diastereotopic faces of ONBs **13-a,b** (Scheme 8).

Analysis of the stationary points involved in the reaction paths associated with the 32CA reactions between NO **3-b** and ONBs **13-a,b** indicates that these cycloaddition reactions take place through a one-step mechanism. Consequently, the reagents, NO **3-b** and ONBs **13-a,b**, four TSs, **TSms-a,b**, **TSma-a,b**, **TSps-a,b**, and **TSpa-a,b**, and four cycloadducts, **14-a,b**, **15-a,b**, **16-a,b**, and **17-a,b**, were located and characterised for each one of the two 32CA reactions (Scheme 8). Total and relative energies, in gas phase and in benzene, of the stationary points involved in the 32CA reactions of NO **3-b** with ONBs **13-a,b** are given in Table 2.

The gas phase activation energies associated with the four competitive channels are 10.5 (**TSps-a**), 13.8 (**TSpa-a**), 11.0 (**TSms-a**), and 17.4 kcal·mol⁻¹ (**TSma-a**) for the 32CA reaction of NO **1-b** with ONB **13-a**, and 10.7 (**TSps-b**), 15.1 (**TSpa-b**), 12.3 (**TSms-b**), and 18.7 kcal·mol⁻¹ (**TSma-b**) for the 32CA reaction involving ONB **13-b**, both reactions being strongly exothermic by between 47 and 51 kcal·mol⁻¹. Some appealing conclusions can be drawn from these energy results: (1) The 32CA reactions of NO **3-b** with ONBs **13-a,b** present high activation energies, since none of the reagents is neither a strong nucleophile nor a strong electrophile. Note that the activation energy associated with the 32CA reaction of the simplest NO **3-a**, a poor nucleophile, with ethylene **18**, a marginal electrophile, is 11.4 kcal·mol⁻¹,^[16] (2) Interestingly, while *syn* TSs present similar activation energies than that associated with the 32CA between the

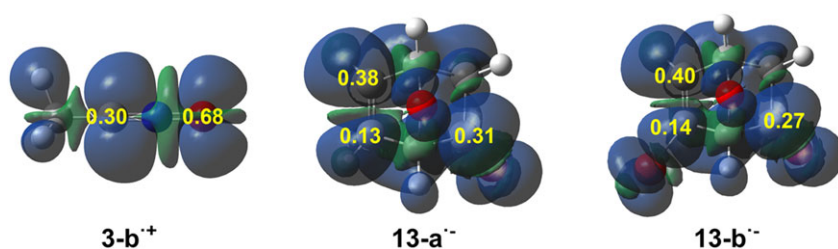


FIGURE 2 Three-dimensional representations of the atomic spin density of radical cation **3-b**⁺ and radical anions **13-a,b**⁻, together with the nucleophilic P_k^- Parr functions of NO **3-b** and the electrophilic P_k^+ Parr functions of ONBs **13-a,b**

TABLE 2 B3LYP/6-31G (d) total (E, in au) and relative^a (ΔE , in kcal·mol⁻¹) energies, in gas phase and in benzene, of the stationary points involved in the 32CA reactions between NO **3-b** and ONBs **13-a,b**

	Gas Phase		Benzene	
	E	ΔE	E	ΔE
3-b	-207.899238		-207.902713	
13-a	-382.629956		-382.635147	
TSps-a	-590.512496	10.5	-590.519217	11.7
TSpa-a	-590.507128	13.8	-590.513001	15.6
TSms-a	-590.511681	11.0	-590.518483	12.2
TSma-a	-590.501488	17.4	-590.508892	18.2
14-a	-590.609845	-50.6	-590.617257	-49.8
15-a	-590.607725	-49.3	-590.614357	-48.0
16-a	-590.608397	-49.7	-590.616025	-49.0
17-a	-590.603950	-46.9	-590.611423	-46.2
13-b	-2953.732859		-2953.737908	
TSps-b	-3161.615025	10.7	-3161.621167	12.1
TSpa-b	-3161.608055	15.1	-3161.613311	17.1
TSms-b	-3161.612520	12.3	-3161.619525	13.4
TSma-b	-3161.602252	18.7	-3161.609608	19.5
14-b	-3161.713249	-50.9	-3161.719991	-49.8
15-b	-3161.712064	-50.2	-3161.717905	-48.5
16-b	-3161.713134	-50.9	-3161.720414	-50.1
17-b	-3161.709768	-48.7	-3161.716899	-47.9

^aRelative to the separated reagents NO **3-b** and ONBs **13-a,b**.

simplest NO **3-a** and ethylene **18**, those associated with the *anti* TSs are higher, suggesting some type of unfavourable interactions along the *anti* approach mode of NO **3-b** towards ONBs **13-a,b**; (3) both 32CA reactions are thermodynamically irreversible. Consequently, *syn* cycloadducts are the product of kinetic control; (4) in gas phase, the 32CA reaction with ONB **13-a** presents a poor *para* regioselectivity, as **TSps-a** is only 0.5 kcal·mol⁻¹ lower in energy than **TSms-a**, and a high *syn* diastereofacial selectivity, as **TSps-a** is 3.3 kcal·mol⁻¹ below **TSpa-a**; (5) in the 32CA reaction involving ONB **13-b**, both *para* regioselectivity and *syn* diastereofacial selectivity increase to 1.6 and 4.4 kcal·mol⁻¹, respectively, making the reaction moderately *para* regioselective and completely *syn* diastereofacially selective, in total agreement with the experimental outcomes;^[23] (6) in spite of the increase of the selectivities, the use of ONB **13-b** produces no significant energy differences with respect to the energy profile of the 32CA reaction involving the simpler ONB **13-a**, as expected according to the previous analysis of the CDFT reactivity indices (see Section 3.2).

Solvent effects of benzene increase activation and reaction energies very slightly, by between 1 and 2 kcal·mol⁻¹,

because of a slight better solvation of the reagents than TSs and cycloadducts (Table 2).^[56] Consequently, the low *para* regioselectivity and total *syn* diastereofacial selectivity found in gas phase remain practically unchanged in the presence of benzene.

To investigate how thermal corrections can modify the relative electronic energies and selectivities, thermodynamic calculations for the 32CA reaction between NO **3-b** and ONB **13-a** in benzene at 25°C and 1 atm were performed. Enthalpies, entropies and Gibbs free energies, and the relative ones are given in Table 3. Inclusion of thermal corrections to the electronic energies did not significantly change the relative enthalpies; while relative activation enthalpies remained almost unchanged, relative reaction enthalpies were slightly decreased by *ca.* 3.0 kcal·mol⁻¹. Inclusion of entropies to enthalpies strongly increased relative Gibbs free energies by between 12 and 13 kcal·mol⁻¹ because of the unfavourable entropies associated with this bimolecular process, the reaction being exergonic by between 17 and 18 kcal·mol⁻¹, and irreversible. Analysis of the Gibbs free energies indicates that the 32CA reaction between NO **3-b** and ONB **13-a** remains low *para* regioselective and completely *syn* diastereofacial selective.

Thorough studies have permitted to establish good correlations between the polar character of the reactions and their feasibility.^[15-17,54] To evaluate the electronic nature of the 32CA reaction between NO **3-b** and ONBs **13-a,b**, the GEDT was analysed.^[51] The GEDT of a reaction is computed by the sum of the natural atomic charges of the atoms belonging to each framework at the corresponding TSs; the sign indicating the direction of the electron density flux in such a manner that positive values mean a flux from the considered framework to the other one. Reactions with GEDT values near 0.0e correspond to non-polar processes, whereas values higher than 0.2e correspond to polar processes.

The GEDT that fluxes from the NO framework towards the ONB one at the TSs associated with the 32CA reaction between NO **3-b** and ONB **13-a** is 0.03e at **TSps-a**, 0.01e at **TSpa-a**, 0.01e at **TSms-a**, and 0.03e at **TSma-a**, while that at the TSs associated with the 32CA reaction involving ONB **13-b** is 0.07e at **TSps-b**, 0.06e at **TSpa-b**, 0.05e at **TSms-b**, and 0.03e at **TSma-b**. These negligible GEDT values indicate that these *zw-type* 32CA reactions have a marked non-polar character,^[15-17,54] which is the consequence of the low electrophilic character of both ONBs **13-a,b** (see Section 3.2) and, accordingly, accounts for the computed high activation energies.

The geometries of the TSs involved in the 32CA reaction of NO **3-b** with ONBs **13-a,b** are displayed in Figure 3. At the *para* TSs, the distances between the two O1 and C5, and the two C3 and C4 interacting atoms are 2.323 and 2.291 Å at **TSps-a**, 2.336 and 2.248 Å at **TSpa-a**, 2.257 and 2.288 Å at **TSps-b**, and 2.261 and 2.281 Å at **TSpa-b**.

TABLE 3 B3LYP/6-31G(d) enthalpies (H, in au), entropies (S, in cal·mol⁻¹·K⁻¹) and Gibbs free energies (G, in au), and the relative^a ones (ΔH in kcal·mol⁻¹, ΔS in cal·mol⁻¹·K⁻¹, and ΔG in kcal·mol⁻¹), in benzene and computed at 25°C and 1 atm, for the stationary points involved in the 32CA reaction between NO **3-b** and ONB **13-a**

	H	ΔH	S	ΔS	G	ΔG
3-b	-207.847051		67.4		-207.879092	
13-a	-382.517197		76.5		-382.553560	
TSps-a	-590.345597	11.7	103.0	-41.0	-590.394534	23.9
TSpa-a	-590.339323	15.6	99.2	-44.8	-590.386463	29.0
TSms-a	-590.344933	12.1	103.1	-40.9	-590.393923	24.3
TSma-a	-590.335440	18.1	101.8	-42.2	-590.383802	30.7
14-a	-590.439449	-47.2	94.5	-49.4	-590.484360	-32.4
15-a	-590.436342	-45.2	93.8	-50.2	-590.480886	-30.3
16-a	-590.438161	-46.4	94.7	-49.3	-590.483142	-31.7
17-a	-590.433478	-43.4	94.8	-49.1	-590.478531	-28.8

^aRelative to the separated reagents NO **3-b** and ONB **13-a**.

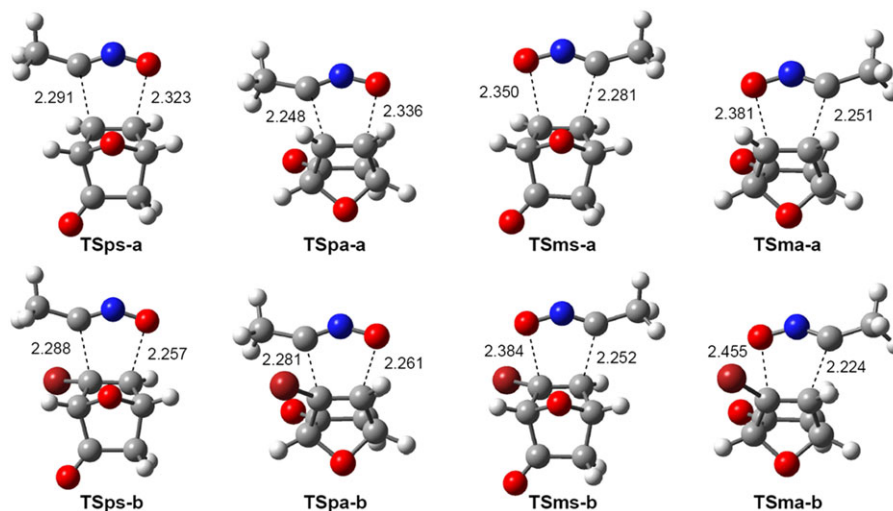


FIGURE 3 B3LYP/6-31G(d) gas phase geometries for the TSs involved in the *zw*-type 32CA reaction between NO **3-b** and ONBs **13-a,b**. Distances are given in Angstroms

On the other hand, at the *meta* TSs, the distances between the two O1 and C4, and the two C3 and C5 atoms are 2.350 and 2.281 Å at **TSms-a**, 2.381 and 2.251 Å at **TSma-a**, 2.384 and 2.252 Å at **TSmb-b**, and 2.455 and 2.224 Å at **TSma-b**. It has been well established that the formation of C–C single bonds takes place in the short distance range of *ca.* 1.9–2.0 Å,^[51] while several studies have shown that the formation of C–O single bonds begins at shorter distances, *ca.* 1.7 Å.^[57] Thus, these geometrical parameters suggest asynchronous bond formation processes initialised by a C3–C4 two-centre interaction. It should be emphasised that the presence of the bromine atom slightly increases the asynchronicity in general, resulting in the distance between the O1 and C5 atoms being slightly shorter at the *para* **TSps-b** and **TSpa-b**. This behaviour is in disagreement with the previous analysis of

the Parr functions, which gives the NO O1 oxygen and the ONB C5 atoms as the most nucleophilic and the most electrophilic centres of the reagents, respectively. This discordance is the consequence of the non-polar character of these *zw*-type 32CA reactions (see above). Note that, as aforementioned, Parr functions are useful for the study of the local reactivity in polar cycloaddition reactions.^[47]

3.4 | Origin of the *syn* diastereofacial selectivity along the 32CA reactions between NO **3-b** and ONBs **13-a,b**

As has been commented, experimental and as well as theoretical evidence reveal that the 32CA reactions of NO **3-b** with ONBs **13-a,b** are poorly *para* regioselective and completely

syn diastereofacially selective. While the low regioselectivity is the consequence of the non-polar character of these *zw*-type 32CA reactions (see Section 3.3), Non-covalent interactions (NCIs) taking place at the TSs could be responsible for the total diastereofacial selectivity. Thus, NCI topological analysis of the electron density of the *para* pairs of *syn/anti* TSs associated with the 32CA reaction involving the simpler ONB **13-a** was performed. The corresponding NCI gradient isosurfaces are shown in Figure 4.

NCI topological analysis of **TSps-a** and **TSpa-a** shows that there is a small green surface between the NO N2 nitrogen and the ONB oxygen atom at **TSps-a**; a notably more extended green surface appears between the entire NO framework and the ONB side containing the carbonyl group at **TSpa-a**. NCI green colour is usually associated to weak favourable or non-favourable Van der Waals (VdW) interactions. Given that **TSpa-a** is 3.3 kcal·mol⁻¹ more unfavourable than **TSps-a**, this extended green surface corresponds to non-favourable VdW interactions taking place between the NO and the ONB H–C–C–O frameworks as a consequence of the steric hindrance developed along the *anti* approach of the NO to the unsaturated system.

To evaluate the favourable/non-favourable nature of the noncovalent VdW interaction appearing at **TSps-a**, an analysis of the NCIs taking place at the *para* TSs associated with the 32CA reaction of NO **3-b** with 7,7-dimethylnorbornene

19, having a bulky C7 isopropyl group, was then performed. In this 32CA reaction, **TSps-19** is 1.2 kcal·mol⁻¹ above **TSpa-19**, thus indicating that along the *para* regioisomeric channel, the *anti* approach mode becomes more favoured than the *syn* one. This change in the facial diastereoselectivity could be caused by the unfavourable steric hindrance encountered between the NO framework and the norbornene 7-methyl substituent at **TSps-19**. As can be observed from the corresponding NCI surfaces shown in Figure 4, while the extended green NCI surface related to unfavourable VdW interactions remains exactly unaltered at **TSpa-19**, the green surface present at **TSps-19** between the NO N2 nitrogen and the norbornene 7-methyl substituent is larger than that comprising the ONB oxygen at **TSps-a**, thus confirming that the VdW surface appearing at the *para/syn* TSs also corresponds to non-favourable steric interactions.

Consequently, the *syn* facial diastereoselectivity in 32CA reactions involving ONBs **13-a,b** appears to be exclusively controlled by steric factors taking place at the corresponding TSs, stronger at the *anti* TSs than at the *syn* ones, and not by torsional effects, “nonequivalent orbital extension,” or Huisgen's factor “*x*,”^[18–20] which arises from enforced staggering of allylic bonds in norbornene, as has been proposed.^[18] In fact, it should be emphasised that these classical observations are based on geometry changes, which are the consequence of the electron density redistribution demanded for the subsequent bond formations, and not the cause of the facial approach mode preference. Note that the C3–C4–C–H dihedral angles at **TSps-19** and **TSpa-19**, 49.4 and –87.9, are in disagreement with the preference for the *anti* TS according to Huisgen's factor “*x*,”^[19,20] while the *syn* facial diastereoselectivity slightly increases along the *meta* regioisomeric channel associated with the reaction involving ONB **13-b** as a consequence of the extra steric hindrance provoked by the bromine lone pairs along the *anti* approach of NO **3-b**.

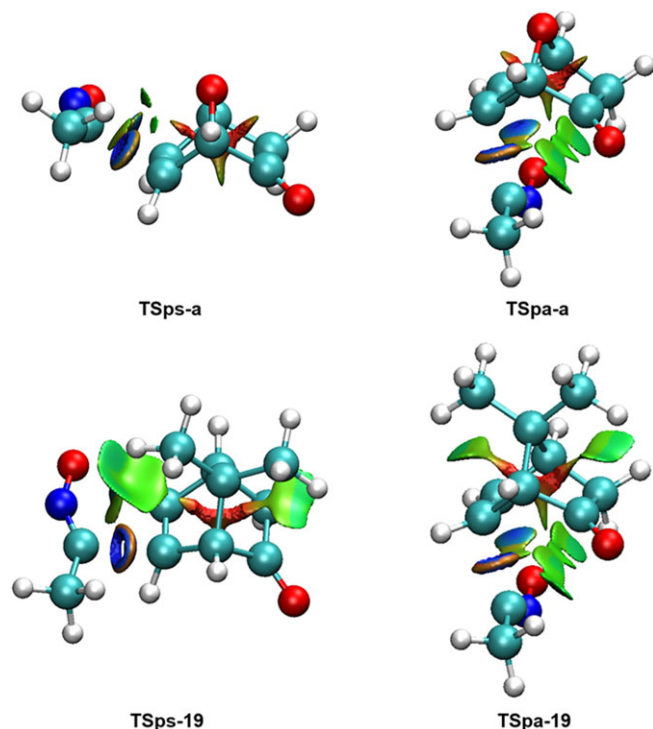


FIGURE 4 NCI gradient isosurfaces, represented at an isovalue of 0.5 au, of the TSs involved in the *para syn/anti* isomeric channels associated with the 32CA reactions between NO **3-b** and ONB **13-a** or 7,7-dimethylnorbornene **19**

4 | CONCLUSIONS

The 32CA reactions of NO **3-b** with ONBs **13-a,b** have been theoretically studied within the MEDT at the DFT B3LYP/6-31G(d) computational level.

ELF topological analysis of the electron density of NOs **3-a,b** permits to establish a bonding pattern concordant with the commonly accepted Lewis structures, although the corresponding charge distribution reveals that these TACs have no 1,2-zwitterionic Lewis structure, confirming that these TACs will participate in *zw*-type 32CA reactions controlled by nucleophile/electrophile interactions taking place along the reaction.

Analysis of the CDFT reactivity indices allows classifying NO **3-b** as a moderate nucleophile and ONBs **13-a,b** as

moderate electrophiles. Consequently, despite the electronic chemical potential differences, a low GEDT along these *zw*-type 32CA reactions is expected. No significant reactivity differences between ONBs **13-a** and **13-b** provoked by the presence of the bromine atom at ONB **13-b** are anticipated.

Analysis of the two *zw*-type 32CA reactions of NO **3-b** with ONBs **13-a,b** shows that four competitive one-step reaction channels related to the *para/meta* regio- and *syn/anti* diastereofacial approaches are feasible. Both cycloadditions present relatively high activation energies as well as low *para* regioselectivity and complete *syn* diastereofacial selectivity, in agreement with the experimental outcomes. Formation of the corresponding *syn* cycloadducts is strongly exothermic, being obtained by kinetic control.

Analysis of the geometries of the TSs suggests asynchronous bond formation processes initialised by the two-centre interaction between the C3 and C4 carbons. This behaviour is in disagreement with the analysis of the Parr functions as a consequence of the non-polar character of these *zw*-type 32CA reactions, evidenced by the negligible GEDT values computed at the corresponding TSs. In general, the presence of the bromine atom at ONB **13-b** slightly increases the asynchronicities.

Finally, while the non-polar character of these *zw*-type 32CA reactions accounts for the high activation energies and low *para* regioselectivity, NCI topological analyses at two *para anti/syn* pairs of TSs reveal that the steric hindrance encountered between the NO framework and the ONB side containing the carbonyl group along the *anti* approaches are responsible for the complete *syn* diastereofacial selectivity.

ACKNOWLEDGEMENTS

Adjieufack, Ndassa, and Mbadcam are grateful the Ministry of Higher Education of the Republic of Cameroon to finance the project with modernization research allowance. The authors also thank the University of Yaoundé I and High Teacher Training College (Cameroon) for infrastructural facilities. This research was also supported by the Ministry of Economy and Competitiveness (MINECO) of the Spanish Government (CTQ2016-78669-P). Ríos-Gutiérrez thanks the Spanish MINECO for a predoctoral contract cofinanced by the European Social Fund (BES-2014-068258).

REFERENCES

- [1] J. Sauer, *Angew. Chem. Int. Ed. Engl.* **1967**, *6*, 16.
- [2] A. Padwa (Ed), *1,3-Dipolar Cycloaddition Chemistry*, Vol. 1 & 2, Wiley Interscience, New York **1984**.
- [3] K. V. Gothelf, K. A. Jorgensen, *Chem. Rev.* **1998**, *98*, 863.
- [4] C. Weygand, E. Bauer, *Justus Liebigs Ann. Chem.* **1927**, *459*, 123.
- [5] R. Huisgen, *Proc. Chem. Soc.* **1961**, 357.
- [6] S. Kobayashi, K. A. Jorgensen, *Cycloaddition Reactions in Organic Synthesis*, Wiley-VCH, Weinheim, Germany **2002**.
- [7] L. R. Domingo, *Molecules* **2016**, *21*, 1319.
- [8] E. R. Scerri, *J. Chem. Educ.* **2000**, *77*, 1492.
- [9] K. Fukui, *Molecular Orbitals in Chemistry Physics and Biology*, New York **1964**.
- [10] P. Geerlings, F. De Proft, W. Langenaeker, *Chem. Rev.* **2003**, *103*, 1793.
- [11] L. R. Domingo, M. Ríos-Gutiérrez, P. Pérez, *Molecules* **2016**, *21*, 748.
- [12] A. D. Becke, K. E. Edgecombe, *J. Chem. Phys.* **1990**, *92*, 5397.
- [13] R. F. W. Bader, *Atoms in Molecules. A Quantum Theory*, Clarendon Press, Oxford, U.K **1990**.
- [14] E. R. Johnson, S. Keinan, P. Mori-Sanchez, J. Contreras-Garcia, J. Cohen, A. W. Yang, *J. Am. Chem. Soc.* **2010**, *132*, 6498.
- [15] L. R. Domingo, S. R. Emamian, *Tetrahedron* **2014**, *70*, 1267.
- [16] L. R. Domingo, M. Ríos-Gutiérrez, P. Pérez, *Tetrahedron* **2016**, *72*, 1524.
- [17] L. R. Domingo, M. J. Aurell, P. Pérez, *Tetrahedron* **2014**, *70*, 4519.
- [18] N. G. Rondan, M. N. Paddon-Row, P. Caramella, J. Mareda, P. H. Mueller, K. N. Houk, *J. Am. Chem. Soc.* **1982**, *104*, 4974.
- [19] R. Huisgen, P. H. J. Ooms, M. Mingin, N. L. Allinger, *J. Am. Chem. Soc.* **1980**, *102*, 3951.
- [20] R. Huisgen, *Pure Appl. Chem.* **1981**, *53*, 171.
- [21] I. N. N. Namboothiri, N. Rastogi, B. Ganguly, S. M. Mobin, M. Cojocaru, *Tetrahedron* **2004**, *60*, 1453.
- [22] J. Tajabadi, M. Bakavoli, M. Gholizadeh, H. Eshghi, M. Izadyar, *RSC Adv.* **2015**, *5*, 38489.
- [23] O. Arjona, A. de Dios, R. F. de la Pradilla, A. Mallo, A. Plumet, *Tetrahedron* **1990**, *46*, 8179.
- [24] O. Arjona, C. Dominguez, R. F. de la Pradilla, A. Mallo, C. Manzano, J. Plumet, *J. Org. Chem.* **1989**, *54*, 5883.
- [25] M. J. Frisch, G. W. Trucks, H. B. Schlegel, G. E. Scuseria, M. A. Robb, J. R. Cheeseman, J. A. Montgomery Jr., T. Vreven, K. N. Kudin, J. C. Burant, J. M. Millam, S. S. Iyengar, J. Tomasi, V. Barone, B. Mennucci, M. Cossi, G. Scalmani, N. Rega, G. A. Petersson, H. Nakatsuji, M. Hada, M. Ehara, K. Toyota, R. Fukuda, J. Hasegawa, M. Ishida, T. Nakajima, Y. Honda, O. Kitao, H. Nakai, M. Klene, X. Li, J. E. Knox, H. P. Hratchian, J. B. Cross, V. Bakken, C. Adamo, J. Jaramillo, R. Gomperts, R. E. Stratmann, O. Yazyev, A. J. Austin, R. Cammi, C. Pomelli, J. W. Ochterski, P. Y. Ayala, K. Morokuma, G. A. Voth, P. Salvador, J. J. Dannenberg, V. G. Zakrzewski, S. Dapprich, A. D. Daniels, M. C. Strain, O. Farkas, D. K. Malick, A. D. Rabuck, K. Raghavachari, J. B. Foresman, J. V. Ortiz, Q. Cui, A. G. Baboul, S. Clifford, J. Cioslowski, B. B. Stefanov, G. Liu, A. Liashenko, P. Piskorz, I. Komaromi, R. L. Martin, D. J. Fox, T. Keith, M. A. Al-Laham, C. Y. Peng, A. Nanayakkara, M. Challacombe, P. M. W. Gill, B. Johnson, W. Chen, M. W. Wong, C. Gonzalez, J. A. Pople, *Gaussian 03, revision A.1*, Gaussian, Inc., Wallingford, CT **2003**.
- [26] A. D. Becke, *J. Chem. Phys.* **1993**, *98*, 5648.
- [27] C. Lee, W. Yang, R. G. Parr, *Phys. Rev. B* **1988**, *37*, 785.

- [28] W. J. Hehre, L. Radom, P. V. R. Schleyer, J. Pople, *Ab initio Molecular Orbital Theory*, Wiley, New York **1986**.
- [29] K. Fukui, *J. Phys. Chem.* **1970**, *74*, 4161.
- [30] C. González, H. B. Schlegel, *J. Phys. Chem.* **1990**, *94*, 5523.
- [31] C. González, H. B. Schlegel, *J. Chem. Phys.* **1991**, *95*, 5853.
- [32] A. E. Reed, R. B. Weinstock, F. Weinhold, *J. Chem. Phys.* **1985**, *83*, 735.
- [33] A. E. Reed, L. A. Curtiss, F. Weinhold, *Chem. Rev.* **1988**, *88*, 899.
- [34] J. Tomasi, M. Persico, *Chem. Rev.* **1994**, *94*, 2027.
- [35] B. Y. Simkin, I. Sheikhet, *Quantum Chemical and Statistical Theory of Solutions—Computational Approach*, Ellis Horwood, London **1995**.
- [36] E. Cancès, B. Mennucci, J. Tomasi, *J. Chem. Phys.* **1997**, *107*, 3032.
- [37] M. Cossi, V. Barone, R. Cammi, J. Tomasi, *Chem. Phys. Lett.* **1996**, *255*, 327.
- [38] S. Noury, K. Krokidis, F. Fuster, B. Silvi, *Comput. Chem.* **1999**, *23*, 597.
- [39] J. R. Lane, J. Contreras-García, J.-P. Piquemal, B. J. Miller, H. G. Kjaergaard, *J. Chem. Theory Comput.* **2013**, *9*, 3263.
- [40] J. Contreras-García, E. R. Johnson, S. Keinan, R. Chaudret, J.-P. Piquemal, D. N. Beratan, W. Yang, *J. Chem. Theory Comput.* **2011**, *7*, 625.
- [41] R. G. Parr, L. von Szentpaly, S. Liu, *J. Am. Chem. Soc.* **1999**, *121*, 1922.
- [42] R. G. Parr, R. G. Pearson, *J. Am. Chem. Soc.* **1983**, *105*, 7512.
- [43] R. G. Parr, W. Yang, *Density Functional Theory of Atoms and Molecules*, Oxford University Press, New York **1989**.
- [44] L. R. Domingo, E. Chamorro, P. Pérez, *J. Org. Chem.* **2008**, *73*, 4615.
- [45] L. R. Domingo, P. Pérez, *Org. Biomol. Chem.* **2011**, *9*, 7168.
- [46] W. Kohn, L. Sham, *J. Phys. Rev.* **1965**, *140*, 1133.
- [47] L. R. Domingo, P. Pérez, J. A. Sáez, *RSC Adv.* **2013**, *3*, 1486.
- [48] L. R. Domingo, E. Chamorro, P. Pérez, *Lett. Org. Chem.* **2010**, *7*, 432.
- [49] L. R. Domingo, J. A. Sáez, *J. Org. Chem.* **2011**, *76*, 373.
- [50] M. Ríos-Gutiérrez, L. R. Domingo, P. Pérez, *RSC Adv.* **2015**, *5*, 84797.
- [51] L. R. Domingo, *RSC Adv.* **2014**, *4*, 32415.
- [52] L. R. Domingo, M. J. Aurell, P. Pérez, R. Contreras, *Tetrahedron* **2002**, *58*, 4417.
- [53] P. Jaramillo, L. R. Domingo, E. Chamorro, P. Pérez, *J. Mol. Struct.: THEOCHEM* **2008**, *865*, 68.
- [54] L. R. Domingo, J. A. Sáez, *Org. Biomol. Chem.* **2009**, *7*, 3576.
- [55] L. R. Domingo, E. Chamorro, P. Pérez, *Eur. J. Org. Chem.* **2009**, 3036.
- [56] W. Benchouk, S. M. Mekelleche, B. Silvi, M. J. Aurell, L. R. Domingo, *J. Phys. Org. Chem.* **2011**, *24*, 611.
- [57] M. Ríos-Gutiérrez, P. Pérez, L. R. Domingo, *RSC Adv.* **2015**, *5*, 58464.

SUPPORTING INFORMATION

Additional Supporting Information may be found online in the supporting information tab for this article.

How to cite this article: Adjieufack AI, Ndassa IM, Ketcha Mbadcam J, Ríos-Gutiérrez M, Domingo LR. Steric interactions controlling the *syn* diastereofacial selectivity in the [3 + 2] cycloaddition reaction between acetonitrile axide and 7-oxanorborn-5-en-2-ones: A molecular electron density theory study. *J Phys Org Chem.* 2017:e3710. <https://doi.org/10.1002/poc.3710>



Cite this: *Org. Biomol. Chem.*, 2017, **15**, 1618

A molecular electron density theory study of the [3 + 2] cycloaddition reaction of nitrones with ketenes†

Mar Ríos-Gutiérrez,^a Andrea Darù,^b Tomás Tejero,^b Luis R. Domingo*^a and Pedro Merino*^b

The [3 + 2] cycloaddition (32CA) reaction between nitrones and ketenes has been studied within the Molecular Electron Density Theory (MEDT) at the Density Functional Theory (DFT) MPWB1K/6-311G(d,p) computational level. Analysis of the conceptual DFT reactivity indices allows the explanation of the reactivity, and the chemo- and regioselectivity experimentally observed. The particular mechanism of this 32CA reaction involving low electrophilic ketenes has been elucidated by using a bonding evolution theory (BET) study. It is determined that this reaction takes place in one kinetic step only but in a non-concerted manner since two stages are clearly identified. Indeed, the formation of the second C–O bond begins when the first O–C bond is already formed. This study has also been applied to predict the reactivity of nitrones with highly electrophilic ketenes. Interestingly, this study predicts a switch to a two-step mechanism due to the higher polar character of this zw-type 32CA reaction. In both cases, BET supports the non-concerted nature of the 32CA reactions between nitrones and ketenes.

Received 19th December 2016,

Accepted 16th January 2017

DOI: 10.1039/c6ob02768g

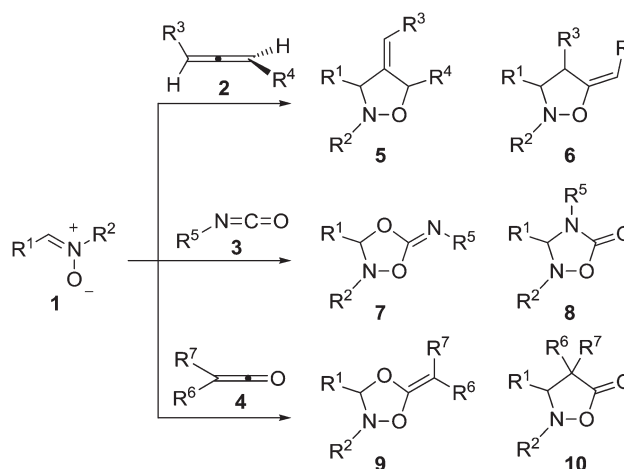
rsc.li/obc

1. Introduction

Since the first examples gathered by Irvin in 1938,¹ demonstrating that nitrones are capable of undergoing 1,3-additions, the [3 + 2] cycloaddition (32CA) reaction of nitrones with alkenes² has been widely used as a key step for the synthesis of heterocycles and natural products.³ The ready availability and ease of use of nitrones,⁴ the tuneability of the reaction by using chiral Lewis acids⁵ and the high efficiency of this transformation⁶ combine to make this reaction a powerful method for heterocyclic synthesis.⁷ Of particular interest are cycloadditions with allenes **2**⁸ and heteroallenes such as isocyanates **3**⁹ and ketenes **4**,¹⁰ which present alternative reaction paths

leading to different heterocyclic compounds depending on the allenic part of the system in which the cycloaddition takes place (Scheme 1).

Despite this synthetic utility, mechanistic studies that allow the interpretation and prediction of the adducts to be obtained with allenes or heteroallenes showing different alternatives like **2–4** are scarce. The reaction of the simplest nitrone **1a** ($R^1, R^2 = H$) with the simplest allene **2** ($R^3, R^4 = H$) was computationally studied and it was determined that the reaction follows a stepwise mechanism.¹¹ Very recently, we



Scheme 1 Reactions of nitrones with allenes and heteroallenes.

^aDepartment of Organic Chemistry, University of Valencia, Dr. Moliner 50, E-46100 Burjassot, Valencia, Spain. E-mail: domingo@utopia.uv.es; <http://www.luisrdomingo.com>

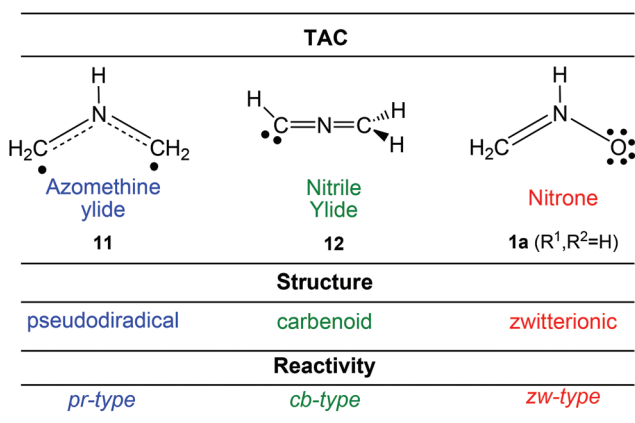
^bLaboratorio de Síntesis Asimétrica, Instituto de Síntesis Química y Catálisis Homogénea (ISQCH), Universidad de Zaragoza-CSIC, Zaragoza 50009, Spain. E-mail: pmerino@unizar.es; <http://www.pmerino.com>

† Electronic supplementary information (ESI) available: BET characterisation of the molecular mechanism of the zw-type 32CA reaction between nitrone **1b** and ketene **4b**. ELF topological analysis of the stationary points involved in the most favourable reactive channel associated with the 32CA reaction of nitrone **1b** with electrophilic ketene **4c**. Tables with the MPWB1K/6-311G(d,p) total and relative electronic energies, in the gas phase and in benzene, and enthalpies, entropies and Gibbs free energies, and the relative ones, computed at room temperature and 1 atm in benzene, for the stationary points involved in the 32CA reactions between nitrone **1b** and ketenes **4b,c**. See DOI: 10.1039/c6ob02768g

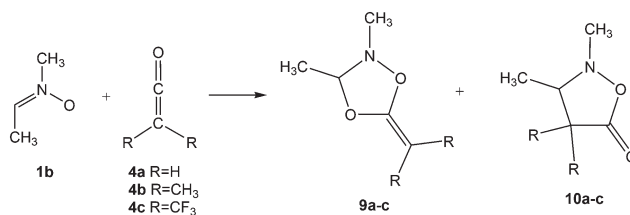
observed the same preference for a stepwise mechanism in the reaction with isocyanates.¹² Houk and co-workers studied the reaction between *N*-aryl nitrones and alkylarylketenes giving rise to a “pericyclic” cascade with chirality transfer.¹³ However, their study only referred to a particular process in which it was suggested that the first cycloaddition step between the nitron and the ketene is a one-step reaction but highly asynchronous.

Several Density Functional Theory¹⁴ (DFT) studies carried out within the Molecular Electron Density Theory (MEDT)¹⁵ devoted to the study of the reactivity of three-atom-components (TACs) participating in 32CA reactions have allowed the establishment of a useful classification of this class of cycloaddition reactions depending on the electronic structure and behaviour of the TAC into pseudodiradical-type (*pr*-type, typically an azomethine ylide **11**),¹⁶ carbenoid-type (*cb*-type, typically a nitrile ylide **12**)¹⁷ and zwitterionic-type (*zw*-type, typically a nitron **1a**)¹⁶ reactions (Scheme 2). The feasibility of the *zw*-type 32CA reactions depends on the polar character of the reactions, *i.e.* the nucleophilic character of the nitrones and the electrophilic character of the ethylene derivatives, or *vice versa*. In general, nitrones are good nucleophiles that react with electron-deficient alkenes.¹⁸

In order to understand the *zw*-type reactivity^{16,18} of nitrones towards ketenes, the 32CA reaction of nitron **1b** ($R^1, R^2 = \text{Me}$) with ketenes **4b** and **4c** yielding cycloadducts (CAs) **9b,c** and **10b,c** are herein studied within the MEDT through DFT calculations at the MPWB1K/6-311G(d,p) computational level (see Scheme 3). The chemoselectivity associated with the 32CA reactions of nitron **1b** with the C=O and C=C double bonds of ketenes **4b** and **4c** is first studied. Then, a Bonding Evolution Theory¹⁹ (BET) analysis of the most favourable chemoisomeric channel associated with the 32CA reaction of nitron **1b** with ketene **4b** is carried out in order to understand the mechanism of these *zw*-type reactions. Finally, an ELF comparative analysis of the TSs and intermediate related to the most favourable channel associated with the 32CA reaction of nitron **1b** with ketene **4c** is performed.



Scheme 2 Electronic structure of TACs and the proposed reactivity types in 32CA reactions.



Scheme 3 32CA reactions of nitron **1b** with ketenes **4a–c** yielding cycloadducts **9a–c** and **10a–c**.

2. Computational methods

DFT calculations were performed using the MPWB1K functional²⁰ together with the 6-311G(d,p) basis set.²¹ Optimisations were carried out using the Berny analytical gradient optimization method.²² The stationary points were characterised by frequency computations in order to verify that TSs have one and only one imaginary frequency. The IRC paths²³ were traced in order to check the energy profiles connecting each TS to the two associated minima of the proposed mechanism using the second order González–Schlegel integration method.²⁴ The solvent effects of benzene were taken into account by full optimization of the gas phase structures at the MPWB1K/6-311G(d,p) computational level using the polarisable continuum model (PCM) developed by Tomasi’s group²⁵ in the framework of the self-consistent reaction field (SCRF).²⁶ The values of enthalpies, entropies and Gibbs free energies in benzene were calculated with the standard statistical thermodynamics at 25 °C and 1 atm.²¹ The electronic structures of the stationary points were characterised by a natural population analysis (NPA),²⁷ and by the electron localisation function (ELF)²⁸ topological analysis of the electron density. All computations were carried out with the Gaussian 09 suite of programs.²⁹ ELF studies were performed with the TopMod³⁰ program using the corresponding MPWB1K/6-311G(d,p) monodeterminantal wavefunctions. For the BET study, the corresponding reaction channel was followed by performing the topological analysis of the ELF for 862 nuclear configurations along the IRC path. ELF calculations were computed over a grid spacing of 0.1 a.u. for each structure and ELF basin isosurfaces were obtained for an ELF value of 0.75 a.u.

Conceptual DFT (CDFT) provides different indices to rationalise and understand chemical structure and reactivity.³¹ The global electrophilicity index,³² ω , is given by the following expression, $\omega = (\mu^2/2\eta)$, in terms of the electronic chemical potential μ and the chemical hardness η . Both quantities may be approached in terms of the one-electron energies of the frontier molecular orbitals HOMO and LUMO, ϵ_H and ϵ_L , as $\mu = (\epsilon_H + \epsilon_L)/2$ and $\eta = (\epsilon_L - \epsilon_H)$, respectively.³³ The global nucleophilicity index,³⁴ N , based on the HOMO energies obtained within the Kohn–Sham scheme,³⁵ is defined as $N = E_{\text{HOMO}}(\text{Nu}) - E_{\text{HOMO}}(\text{TCE})$, where tetracyanoethylene (TCE) is the reference because it presents the lowest HOMO energy in a long series of molecules already investigated in the context of polar organic reactions. The electrophilic P_k^+ and nucleophilic P_k^- Parr

functions,³⁶ which allow for the characterisation of the electrophilic and nucleophilic centers of a molecule, were obtained through the analysis of the Mulliken atomic spin density (ASD) of the radical cation of nitrene **1b** and the radical anion of ketenes **4a** and **4c**, by single-point energy calculations from the optimised neutral geometries.

3. Results and discussion

The present MEDT study is organised as follows: in section 3.1, an analysis of the electronic structure of nitrenes **1a,b** is performed in order to understand the *zw*-type reactivity of **1b** in 32CA reactions. Section 3.2 contains an analysis of the CDFT reactivity indices of the reagents involved in the 32CA reactions of nitrene **1b** with ketenes **4b,c**. In section 3.3, the potential energy surfaces (PESs) associated with the chemoisomeric channels associated with the 32CA reactions of nitrene **1b** with ketenes **4b,c** are explored and characterised. Section 3.4 discusses a BET study characterising the bonding changes, as well as the energies related to those changes, along the most favourable reaction channel associated with the 32CA reaction of nitrene **1b** with ketene **4b**. And finally, in section 3.5, a comparative ELF topological analysis of the TSs and intermediate involved in the most favourable reaction channel associated with the 32CA reaction of nitrene **1b** with electrophilic ketene **4c** is performed.

3.1. ELF topological analysis of the electronic structure of nitrenes **1a,b**

As commented in the Introduction part, the reactivity of TACs can be correlated with their electronic structure.^{16,17} Thus, an ELF topological analysis of the simplest nitrene **1a** and nitrene **1b** was first performed in order to characterise the electronic structure of these TACs. The representation and attractor positions of ELF valence basins, as well as ELF electron populations, natural atomic charges and the Lewis structures arising from the ELF topological analysis for nitrenes **1a,b** are shown in Fig. 1.

The ELF topology of the simplest nitrene **1a** permits the establishment of the Lewis structure of this TAC (see Fig. 1). As can be seen, nitrene **1a** presents two $V(O1)$ and $V'(O1)$ monosynaptic basins, integrating a total of $5.91e$, and one $V(O1,N2)$ disynaptic basin with a population of $1.39e$. This behaviour suggests that the O1–N2 bonding region is strongly polarised towards the O1 oxygen atom. In addition, the presence of one $V(N2,C3)$ disynaptic basin integrating $3.89e$ indicates that the N2–C3 bonding region has a strong double bond character. Consequently, the ELF topology of the simplest nitrene **1a** clearly indicates that this TAC is able to participate only in *zw*-type 32CA reactions, as it neither presents a pseudodiradical³⁷ nor a carbenoid¹⁷ electronic structure that would enable it to participate in *pr*- or *cb*-type 32CA reactions.^{16,17}

On the other hand, the ELF topology of nitrene **1b** shows a very similar bonding pattern to that found in the simplest nitrene **1a**. Indeed, the substitution of the hydrogen atoms bound to the N2 nitrogen and C3 carbon by a methyl group is

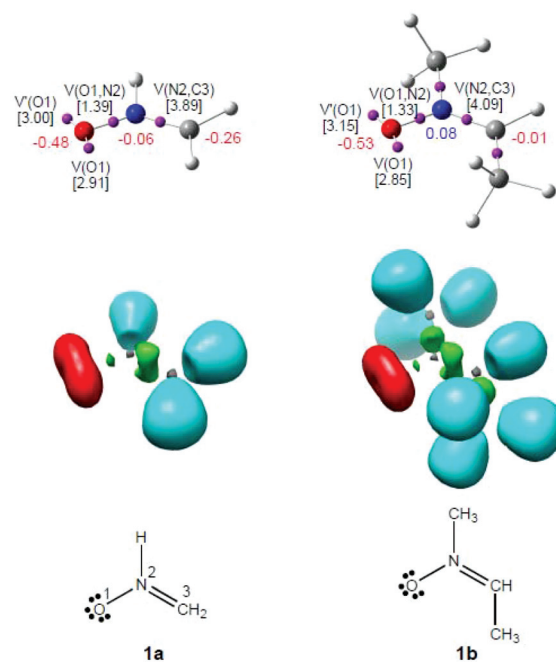


Fig. 1 Representation of ELF attractors and valence basin populations, in *e*, natural atomic charges (negative in red and positive in blue), ELF valence basins and proposed Lewis structures for nitrenes **1a,b**.

expected to produce no significant electronic changes. The ELF valence basin populations have varied very slightly (see Fig. 1), although in this case the N2–C3 bonding region is characterised by the presence of two disynaptic basins, $V(N2,C3)$ and $V'(N2,C3)$, integrating a total population of $4.09e$. Therefore, according to the ELF topological analysis, nitrene **1b** will behave as a zwitterionic TAC participating only in *zw*-type 32CA reactions such as the simplest nitrene **1a**.¹⁶

Although the ELF topological analysis of nitrenes **1a** and **1b** allows the establishment of a bonding pattern in these TACs, NPA indicates that neither nitrene has zwitterionic charge distribution. Note that although the O1 oxygen has a high negative charge, $-0.48e$ (**1a**) and $-0.53e$ (**1b**), the N2 nitrogen presents practically no charge, $-0.06e$ (**1a**) and $0.08e$ (**1b**). Moreover, the C3 carbon appears negatively charged at nitrene **1a**, $-0.26e$, while at nitrene **1b** it presents a null charge, $-0.01e$.

Thus, although ELF topological analysis provides a bonding pattern concordant with the commonly accepted Lewis structures of nitrenes **1a,b**, the NPA is completely in disagreement with the representation of their electronic structure as a 1,2-zwitterionic structure. Nevertheless, ELF topological characterisation of the electron density distribution at these nitrenes accounts for their *zw*-type reactivity.

3.2 Analysis of the CDFT reactivity indices of the reagents involved in the 32CA reactions of nitrene **1b** with ketenes **4b,c**

Studies devoted to polar organic reactions have shown that the analysis of the reactivity indices defined within the CDFT^{31d,38} is a powerful tool to understand the reactivity in polar cycloadditions. Global DFT indices, namely, the electronic chemical

potential, μ , chemical hardness, η , electrophilicity, ω , and nucleophilicity, N , at the ground state of the reagents involved in these 32CA reactions are given in Table 1.

The electronic chemical potential of nitrene **1b**, -2.95 eV, is higher than that of ketenes, -3.23 (**4b**) and -5.26 (**4c**) eV, indicating that along polar reactions the global electron density transfer (GEDT)³⁹ will flux from the nitrene framework towards the ketene one.

Along a polar reaction, there is an electron density transfer from the nucleophilic to the electrophilic species, which is measured by the GEDT³⁹ value computed at the TS of the reaction; the larger the GEDT at the TS, the more polar the reaction. Note that the GEDT concept comes from the observation that the electron density transfer taking place from the nucleophile to the electrophile along a polar reaction is not a local process, but a global one involving the two interacting frameworks³⁹ and depending on the electrophilic/nucleophilic interactions taking place between them.

The electrophilicity ω and nucleophilicity N indices of the simplest nitrene **1a** are 1.06 eV and 2.92 eV, being classified as a moderate electrophile and on the borderline of strong nucleophiles within the electrophilicity⁴⁰ and nucleophilicity⁴¹ scales. Inclusion of the two electron-releasing (ER) methyl groups at the N2 and C3 atoms of the simplest nitrene **1a** decreases the electrophilicity ω index of nitrene **1b** to 0.80 eV and increases its nucleophilicity N index to 3.46 eV. Consequently, nitrene **1b** will behave as a strong nucleophile participating in *zw*-type 32CA reactions.¹⁸

On the other hand, the electrophilicity ω and nucleophilicity N indices of the simplest ketene **4a** are 1.27 eV and 2.58 eV, being classified as a moderate electrophile and nucleophile. Inclusion of the two ER methyl groups at the terminal C6 carbon of ketene **4a** decreases the electrophilicity ω index of ketene **4b** to 1.02 eV and increases its nucleophilicity N index to 2.58 eV. Thus, ketene **4b** will behave as a moderate electrophile and a strong nucleophile. Regarding ketene **4c**, inclusion of the two electron-withdrawing (EW) trifluoromethyl (CF₃) groups at the terminal C6 carbon of ketene **4a** notably increases the electrophilicity ω index to 2.47 eV and decreases the nucleophilicity N index to 1.05 eV. Therefore, ketene **4c** will behave as a strong electrophile and a marginal nucleophile. This early analysis of the CDFT global reactivity indices suggests that, as expected, the *zw*-type 32CA reaction of nitrene **1b** with the more electrophilic ketene **4c** will be more favourable than that with ketene **4b**.

Table 1 B3LYP/6-31G(d) electronic chemical potential, μ , chemical hardness, η , electrophilicity, ω , and nucleophilicity, N , in eV, of nitrenes **1a,b** and ketenes **4a–c**

	μ	η	ω	N
4c	-5.26	5.62	2.47	1.05
4a	-3.76	5.57	1.27	2.58
1a	-3.43	5.55	1.06	2.92
4b	-3.23	5.08	1.02	3.35
1b	-2.95	5.42	0.80	3.46

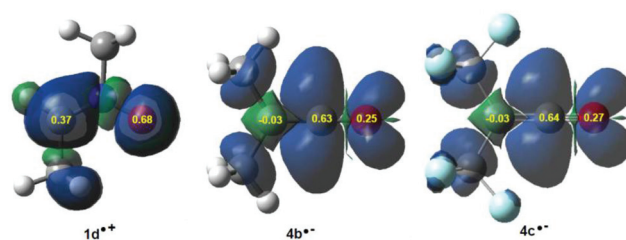


Fig. 2 3D representations of the ASD of the radical cation **1b**^{•+} and the radical anions **4b,c**^{•-}, together with the nucleophilic P_k^- Parr functions of nitrene **1b** and the electrophilic P_k^+ Parr functions of ketenes **4b,c**.

In polar cycloaddition reactions involving the participation of non-symmetric reagents, the most favourable reactive channel is that involving the initial two-center interaction between the most electrophilic center of the electrophile and the most nucleophilic center of the nucleophile. Recently, Domingo *et al.* proposed the electrophilic P_k^+ and nucleophilic P_k^- Parr functions³⁶ derived from the changes of spin electron density reached *via* the GEDT process from the nucleophile to the electrophile as powerful tools in the study of the local reactivity in polar processes. Accordingly, the nucleophilic P_k^- Parr functions of nitrene **1b** and the electrophilic P_k^+ Parr functions of ketenes **4b,c** were analysed in order to characterise the most electrophilic and nucleophilic centers of the species involved in these 32CA reactions and, thus, to explain the regio- and chemoselectivity experimentally observed (see Fig. 2).

Analysis of the nucleophilic P_k^- Parr functions of nitrene **1b** indicates that the O1 oxygen, $P_k^- = 0.68$, is twice as nucleophilically activated as the C3 carbon, $P_k^- = 0.37$, while the electrophilic P_k^+ Parr functions of ketenes **4b,c** indicate that the central C5 carbon is the most electrophilic center of these molecules, $P_k^+ = 0.63$ (**4b**) and 0.64 (**4c**). Consequently, the most favourable electrophile–nucleophile interaction along the polar *zw*-type 32CA reactions of nitrene **1b** with ketenes **4b,c** will take place between the most nucleophilic center of nitrene **1b**, the O1 oxygen atom, and the most electrophilic center of ketenes **4b,c**, the central C5 carbon, in clear agreement with the regioselectivity experimentally reported first by Taylor⁴² and further by Houk.¹³

On the other hand, analysis of the electrophilic P_k^+ Parr functions of ketenes **4b,c** also indicates that while the ketene O4 oxygen atom presents some electrophilic activation, $P_k^+ = 0.25$ (**4b**) and 0.27 (**4c**), the terminal C6 carbon is slightly electrophilically deactivated, $P_k^+ = -0.03$. This means that along the *zw*-type 32CA reaction of nitrene **1b** with ketenes **4b,c**, the terminal carbon does not participate in the reaction, and thereby, this *zw*-type 32CA reaction will present a complete C=O chemoselectivity.

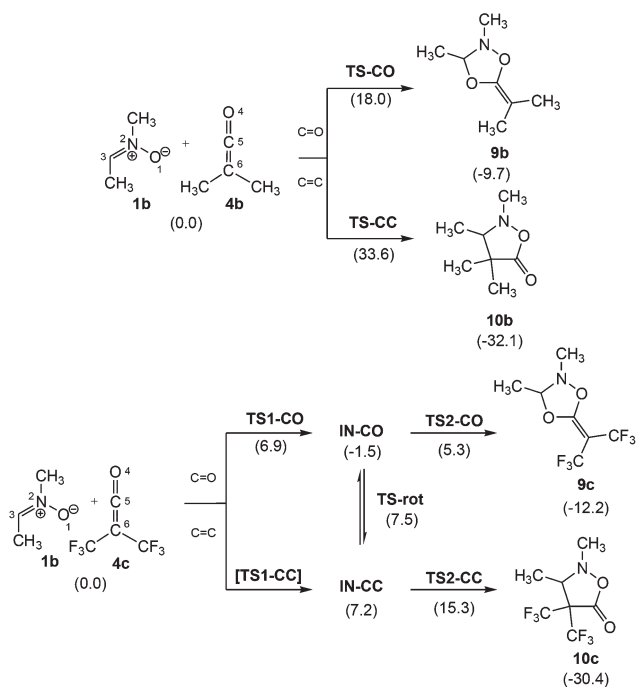
3.3. Analysis of the PESs of the 32CA reactions of nitrene **1b** with ketenes **4b,c**

Due to the non-symmetry of both the reagents, the 32CA reactions between nitrene **1b** and ketenes **4b,c** can take place through four competitive reaction channels, which are related

to the chemoisomeric attacks of nitrene **1b** on the C=O and C=C double bonds of ketenes **4b,c**, and with the two regioisomeric approach modes of nitrene **1b** towards each one of the two double bonds of ketenes **4b,c**. Due to the high regioselectivity predicted by the analysis of the electrophilic P_k^+ and nucleophilic P_k^- Parr functions, only the two chemoisomeric channels associated with the initial nucleophilic attack of the nitrene O1 oxygen on the central C5 carbon of ketenes **4b,c** were studied.

Interestingly, analysis of the PESs associated with the two 32CA reactions indicates that they take place through different mechanisms; the 32CA reaction between nitrene **1b** and ketene **4b** takes place *via* a one-step mechanism, while that of nitrene **1b** with electrophilic ketene **4c** takes place *via* a two-step mechanism (see Scheme 4). Total and relative energies, in the gas phase and benzene, as well as total and relative enthalpies, entropies and Gibbs free energies in benzene, of the stationary points involved in the 32CA reactions between nitrene **1b** and ketenes **4b,c** are given in the ESI.†

The activation Gibbs free energy of the 32CA reaction between nitrene **1b** and ketene **4b** presents a low value, 18.8 kcal mol⁻¹, the reaction being exergonic, -9.7 kcal mol⁻¹ (**9b**) (see relative Gibbs free energies in Scheme 4). Analysis of the relative Gibbs free energies of TS-CO and TS-CC indicates that this 32CA is kinetically completely chemoselective, as TS-CC is 15.6 kcal mol⁻¹ higher in Gibbs free energy than TS-CO. However, the formation of CA **10b** is thermodynamically more favourable than **9b**. Consequently, while CA **9b** is the product of a kinetic control, CA **10b** could become



Scheme 4 C=O and C=C chemoisomeric channels associated with the zw-type 32CA reaction between nitrene **1b** and ketenes **4b,c**. Relative Gibbs free energies, in kcal mol⁻¹, are given in parentheses.

the product of a thermodynamic control under thermal equilibrium conditions.

The PES associated with the 32CA reaction between nitrene **1b** and electrophilic ketene **4c** is more complex. In order to understand the reaction mechanism, the Gibbs free energy profiles of the two competitive channels are depicted in Fig. 3. Analysis of these energy profiles allows one to reach some appealing conclusions: (i) the nucleophilic attack of nitrene **1b** to ketene **4c** *via* TS1-CO has an activation Gibbs free energy of 6.9 kcal mol⁻¹; (ii) the activation Gibbs free energy associated with the ring closure from IN-CO *via* TS2-CO is 6.8 kcal mol⁻¹, and 8.1 kcal mol⁻¹ from IN-CC *via* TS2-CC; (iii) this reaction is completely chemoselective, as TS2-CO is 10.5 kcal mol⁻¹ lower in Gibbs free energy than TS2-CC; (iv) formation of CAs **9c** and **10c** is exergonic by 12.2 and 30.4 kcal mol⁻¹, respectively; (v) interestingly, IN-CO and IN-CC are two conformers being interconvertible by a O1-C5 single bond rotation implying only 0.3 kcal mol⁻¹. Consequently, these intermediates connect both chemoisomeric channels. Thus, under thermodynamic control, CA **9c** could be converted into the more thermodynamically stable **10c** with an activation energy of 27.5 kcal mol⁻¹; and finally, (vi) a comparison between the energy profiles of the 32CA reactions of nitrene **1b** with ketenes **4b,c** allows one to reach two appealing conclusions: (a) the electrophilic activation of the ketene changes the molecular mechanism and activation energies, but it does not change the thermodynamics of the reaction; and (b) in both reactions, the ring closure is the step controlling the chemoselectivity.

The geometries of the TSs and intermediates involved in the 32CA reactions of nitrene **1b** with ketenes **4b,c** are given in Fig. 4. At the TSs associated with the 32CA reaction of nitrene **1b** with ketene **4b**, the distances between the two O1 and C5, and the two C3 and O4/C6 interacting atoms are: 1.560 Å and 2.219 Å at TS-CO and 1.604 Å and 2.546 Å at TS-CC, respectively. The short distance between the O1 and C5 atoms at both

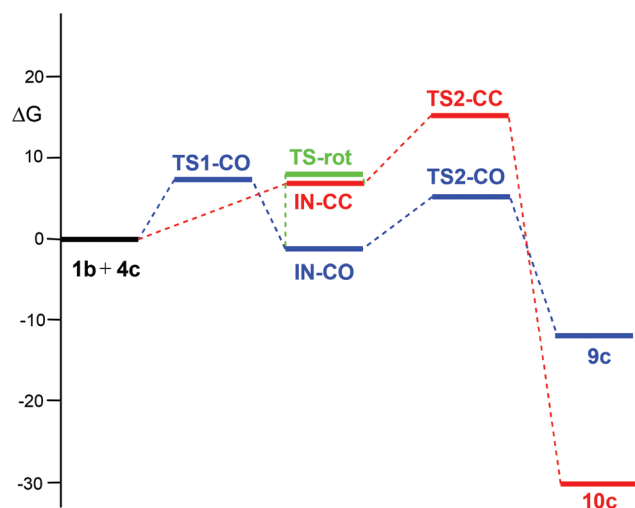


Fig. 3 MPWB1K/6-311G(d,p) Gibbs free energy profile (ΔG , kcal mol⁻¹), in benzene, of the 32CA reaction between nitrene **1b** and electrophilic ketene **4c**.

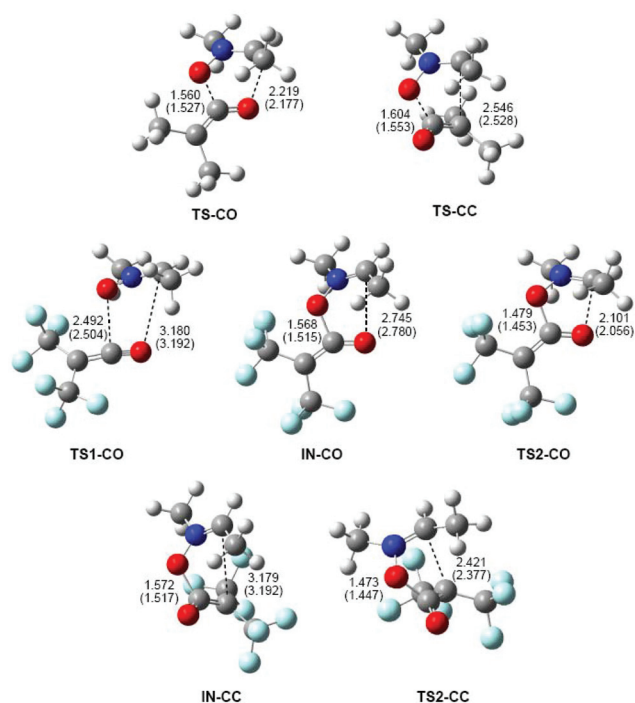


Fig. 4 Geometries of the TSs and intermediates involved in the 32CA reaction of nitrone **1b** with ketenes **4b,c**. Lengths are given in Angstroms. Values in parentheses are associated with the lengths in benzene.

TSs indicates that the O1–C5 single bond is already formed.⁴³ Consequently, these TSs can be associated with the formation of the second C3–O4 or C3–C6 single bonds.

At **TS1-CO**, related to the nucleophilic attack of the nitrone O1 oxygen atom on the C5 carbon of ketene **4c**, the distances between the O1 and C5, and the C3 and O4 atoms are 2.492 and 3.180 Å. These distances are coherent with an early-transition state, in clear agreement with its null activation energy. At intermediates **IN-CO** and **IN-CC**, the lengths of the O1–C5 single bonds are 1.568 and 1.572 Å, respectively, while the distances between the C3 and O4/C6 atoms are 2.745 and 3.179 Å. Finally, at the TSs associated with the ring closure along the two reaction paths, the lengths of the formed O1–C5 single bonds are 1.479 Å (**TS2-CO**) and 1.473 Å (**TS2-CC**), while the distances between the C3 and O4/C6 atoms are 2.101 (**TS2-CO**) and 2.421 (**TS2-CC**) Å, respectively.

Inclusion of benzene in the optimisations does not significantly modify the geometries of the TSs (see Fig. 4). The changes in distances in the gas phase and in benzene are found between 0.05 and 0.01 Å. In general, the distances between the O1 and C5, and the C3 and O4/C6 atoms are shorter in benzene as a consequence of the solvent stabilisation of the corresponding species. Only at **TS1-CO** and intermediates, are the distances between the non-bound atoms slightly increased.

Thorough studies have made it possible to establish good correlations between the polar character of the reactions and their feasibility.⁴⁴ In order to evaluate the electronic nature of

the 32CA reaction of nitrone **1b** with ketenes **4b,c**, the GEDT was analysed. The GEDT of a reaction is computed by the sum of the natural atomic charges of the atoms belonging to each framework at the corresponding TSs; the sign indicates the direction of the electron density flux in such a manner that positive values mean a flux from the considered framework to the other one. Reactions with GEDT values near 0.0e correspond to non-polar processes, whereas values higher than 0.2e correspond to polar processes. Thus, at **TS-CO** and **TS-CC** associated with the 32CA reaction nitrone **1b** with ketene **4b**, the GEDT that takes place from the nitrene to the ketene framework is 0.21e and 0.33e, respectively. These values indicate that these TSs have some polar character. At the TSs and intermediates associated with the 32CA reaction nitrene **1b** with electrophilic ketene **4c**, the GEDT that takes place from the nitrene to the ketene framework is 0.05e at **TS1-CO**, 0.45e at **IN-CO**, 0.44e at **IN-CC**, 0.41e at **TS2-CO** and 0.37e at **TS2-CC**. From these GEDT values some appealing conclusions can be drawn: (i) the negligible GEDT found at **TS1-CO** is a consequence of the earlier character of this TSs; (ii) a high GEDT is found at the corresponding intermediates, ca. 0.45e emphasising the zwitterionic character of these species; (iii) a decrease of the GEDT is found at the TSs associated with the ring closure step as a consequence of a retrodonation process; (iv) the GEDT along the two chemoisomeric channels presents similar values, in spite of the energy differences. This behaviour supports the global character of the electron density transfer from the nucleophilic to the electrophilic framework; and (v) the GEDT at **TS2-CO** and **TS2-CC** presents higher values than that at **TS-CO** and **TS-CC** as a consequence of the higher electrophilic character of ketene **4c**, $\omega = 2.47$ eV, than ketene **4b**, $\omega = 1.02$ eV.

Analysis of the GEDT along the two competitive reaction paths associated with these reactions is in agreement with the low computed activation energies and confirms the *zw*-type character of these 32CA reactions, in which the feasibility of the reaction depends on the electrophilic character of the ketene.

3.4. BET characterisation of the molecular mechanism of the *zw*-type 32CA reaction between nitrene **1b** and ketene **4b**

When trying to achieve a better understanding of bonding changes in organic chemical reactions, the so-called BET¹⁹ has proved to be a very useful methodological tool.⁴⁵ BET applies Thom's catastrophe theory (CT) concepts⁴⁶ to the topological analysis of the gradient field of the ELF²⁸ along the reaction coordinate. Several theoretical studies have shown that the topological analysis of the ELF offers a suitable framework for the study of the changes of electron density. This methodological approach is used as a valuable tool to understand the bonding changes along the reaction path and, consequently, to establish the nature of the electronic rearrangement associated with a given molecular mechanism.⁴⁷

Recently, a BET study of the bonding changes along the *zw*-type 32CA reactions of nitrene **1a** with ED acrolein **13** was carried out in order to understand the O–C and C–C bond

formation processes and to determine the molecular mechanism of these *zw*-type 32CA processes.⁴³ On the other hand, a recent BET study of the molecular mechanism of the ketene–imine Staudinger reaction⁴⁸ permitted one to characterise the participation of the C–C double bond of the ketene in the second step of this reaction. Herein, in order to understand the participation of the O–C double bond of ketenes, a BET study of the most favourable reaction channel associated with the 32CA reaction between nitronne **1b** and ketene **4b** is performed with the aim of characterising the molecular mechanism of 32CA reactions involving ketenes. The complete BET study is reported in the ESI.† The equivalence between the topological characterisation of the different phases and the associated chemical process is given in Table 2.

Some appealing conclusions can be drawn from this BET study: (i) the IRC associated with the 32CA reaction of nitronne **1b** with ketene **4b** is divided in eight differentiated phases. A behaviour that clearly indicates that the bonding changes along this one-step mechanism are non-concerted; (ii) formation of the first O1–C5 single bond takes place at a C–O distance of 1.64 Å, by the donation of some electron density of the O1 oxygen lone pairs of the nitronne to the C5 carbon atom of the ketene moiety. Note that the O1 oxygen is the most nucleophilic center of nitronne **1b** and the C5 carbon corresponds to the most electrophilic center of ketene **4b** (see the chemical process taking place in *phase V* in Table 2, and the V(O1,C5) disynaptic basin in **P4** in Fig. 5); (iii) formation of this bond demands the asymmetric depopulation of the O4–C5 bonding region of ketene **4b**. The large GEDT, 0.34e, taking place along this *zw*-type 32CA reaction favours these bonding changes according to the electronic behaviour anticipated by the Parr functions, which is in agreement with the chemoselectivity experimentally observed; (iv) formation of the second C3–O4 single bond takes place at a C–O distance of 1.84 Å by the donation of some of the electron density of the O4 oxygen lone pairs to the C3 *pseudoradical* center of the nitronne framework (see the chemical process taking place in *phase VIII* in Table 2, and the V(C3,O4) disynaptic basin in **P7** in Fig. 5). This carbon participates with a residual electron density of 0.03e in the formation of the C3–O4 single bond; (v) the reaction follows a *two-stage one-step* mechanism⁴⁹ in which

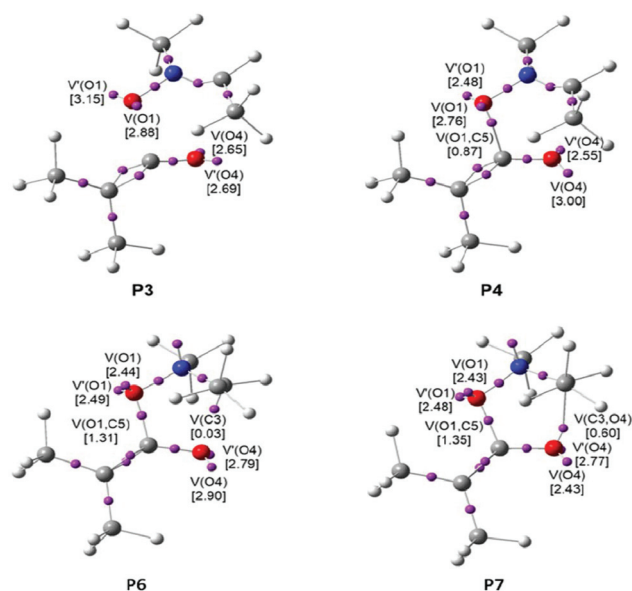


Fig. 5 ELF attractor positions for the points of the IRC defining phases IV, V, VII and VIII involved in the formation of the O1–C5 and C3–O4 single bonds along the most favourable reactive channel associated with the *zw*-type 32CA reaction between nitronne **1b** and ketene **4b**. The electron populations, in e, are given in brackets.

the formation of the second C3–O4 one begins when the first O1–C5 single bond is practically already formed. This fact also emphasises that the bonding changes in this one-step reaction are non-concerted processes; (vi) the activation energy associated with this 32CA reaction, 9.3 kcal mol^{−1}, can be mainly associated with the depopulation of the O4–C5 and N2–C3 bonding regions towards the O4 oxygen and the N2 nitrogen, respectively, which is demanded before the donation of the electron density of the O4 oxygen to the C3 carbon; (vii) the present BET study allows the establishment of the molecular mechanism of the *zw*-type 32CA reactions between nitronnes and ketenes as a [2*n*,2*n*] mechanism,⁵⁰ *i.e.* only two non-bonding electrons of the oxygen lone pairs of nitronne **1b** and two non-bonding electrons of the oxygen lone pairs of ketene **4b** are mainly involved in the formation of the two C–O single bonds in CA **9b**.

Table 2 Sequential bonding changes along the *zw*-type 32CA reaction between nitronne **1b** and ketene **4b**, showing the equivalence between the topological characterisation of the different phases and the associated chemical process

Phases	$d(\text{O1-C5})$	$d(\text{C3-O4})$	ΔE	GEDT	Topological characterisation	Chemical process
a I–IV	$3.04 \geq d > 1.79$	$3.26 \geq d > 2.39$	8.6	≤ 0.34	Depopulation of the V(O4,C5) disynaptic basin	Depopulation of the O4–C5 bonding region
b V	$1.64 \geq d > 1.61$	$2.39 \geq d > 2.33$	9.0(0.4)	0.34	Formation of the V(O1–C5) disynaptic basin	Formation of the O1–C5 single bond
c VI	$1.61 \geq d > 1.46$	$2.33 \geq d > 1.91$	4.5(−4.5)	≤ 0.34	Depopulation of the V(N2,C3) disynaptic basin and the formation of the V(N2) monosynaptic basin	Rupture of the N2–C3 double bond and the formation of the N2 nitrogen lone pair
d VII	$1.46 \geq d > 1.44$	$1.91 \geq d > 1.84$	1.7(−3.1)	≤ 0.24	Formation of the non-bonding V(C3) monosynaptic basin	Formation of the C3 <i>pseudoradical</i> center
e VIII	$1.44 \geq d \geq 1.37$	$1.84 \geq d \geq 1.42$	−22.7(−24.1)	≤ 0.21	Formation of the V(C3–O4) disynaptic basin	Formation of the C3–O4 single bond

3.5. ELF topological analysis of the stationary points involved in the most favourable reactive channel associated with the 32CA reaction of nitrone **1b** with electrophilic ketene **4c**

In order to understand how the EW substitution in the ketene can modify the molecular mechanism of the *zw*-type 32CA reaction of nitrones with electrophilic ketenes, the bonding patterns of the stationary points involved in the most favourable reactive channel associated with the 32CA reaction of nitrone **1b** with electrophilic ketene **4c** were characterised by ELF topological analysis. ELF topological analysis is reported in the ESI.†

Some appealing conclusions can be obtained from this ELF topological analysis: (i) at **TS1-CO**, no bonding change with respect to **MC-c** is observed. The bonding pattern of **TS1-CO** resembles that associated with the structures located at the end of *phase I* of the reaction between nitrone **1b** and ketene **4b**, emphasising its earlier character; (ii) as expected, at **IN-CO**, while the formation of the O1–C5 single bond is very advanced, the formation of the C3–O4 single bond has not yet begun; (iii) the bonding pattern of **IN-CO** resembles that of point **P5** of the reaction between nitrone **1b** and ketene **4b**. The main difference between **IN-CO** and **P5** is the C3–O4 distance: 2.745 Å at **IN-CO** and 2.329 Å at **P5**. The short C3–O4 distance at **P5** justifies that this species is not a stationary point in the PES of the 32CA reaction between nitrone **1b** and ketene **4b**; (iv) the bonding pattern of **TS2-CO** resembles that of **TS-CO**. The only difference is that **TS2-CO** is slightly more advanced than **TS-CO**; and (v) the GEDT at **IN-CO** and **TS2-CO** is larger than that at **P5** and **TS-CO** as a consequence of the higher electrophilic character of ketene **4c** than ketene **4b**. The higher polar character of the *zw*-type 32CA reaction between nitrone **1b** and electrophilic ketene **4c** permits the stabilisation of the zwitterionic intermediate, thus changing the molecular mechanism from a one-step mechanism to a two-step one, but the bonding changes in both 32CA reactions are essentially the same. This similar bonding pattern along the two 32CA reactions makes it possible to establish the non-concerted nature of the *two-stage one-step* mechanism.⁴⁹

4. Conclusions

A comprehensive MEDT study of the reaction between nitrones and ketenes has been carried out using DFT methods at the MPWB1K/6-311G(d,p) computational level. ELF analysis of nitrones confirmed their electronic structure as TACs participating in *zw*-type 32CA reactions although NPA clearly shows that the common representation as 1,2-zwitterions is incorrect. The analysis of CDFT reactivity indices of nitrones and ketenes correctly predicts the experimentally observed complete C=O regio- and chemoselectivities. A detailed analysis of the PES corresponding to the reaction between nitrones and non-electrophilically activated ketenes indicates that the reaction follows a *two-stage one-step* mechanism in which the formation of the second bond takes place once the first one is almost

completely formed. No significant changes are observed by the inclusion of solvent effects. Analysis of the thermodynamic data indicates that while the initial 32CA reaction of the nitrone towards the ketene C–O double bond is kinetically regio- and chemoselectively controlled, the products resulting from the addition of the ketene C–C double bond can be obtained under thermal equilibrium conditions, in clear agreement with the experimental outcomes.

A complete BET study confirms the non-concerted nature of the reaction identifying the mechanism as a [2n,2n] process, *i.e.* only two non-bonding electrons of the oxygen lone pairs of the nitrone and two non-bonding electrons of the oxygen lone pairs of the ketene are mainly involved in the formation of the two C–O single bonds. Finally, an ELF topological analysis of the electron density distribution of the stationary points involved in the most favourable reactive channel associated with the 32CA reaction involving electrophilic ketenes predicts a switch of mechanism from *two-stage one-step* to two-step. Despite the change of mechanism, the bonding pattern is the same for the two reactions, thus the present computational study confirms the non-concerted nature of the cycloaddition between nitrones and ketenes.

Acknowledgements

This research was supported by the Spanish MINECO (FEDER CTQ2016-78669-P and CTQ2016-76155-R), and the Government of Aragón (Grupos Consolidados, E.10). M. R.-G. thanks MINECO for a pre-doctoral contract co-financed by the European Social Fund (BES-2014-068258). The authors thankfully acknowledge the resources from the supercomputers “Memento” and “Cierzo”, technical expertise and assistance provided by BIFI-ZCAM (Universidad de Zaragoza, Spain).

References

- 1 L. Irvin, *Chem. Rev.*, 1938, **23**, 193–285.
- 2 P. N. Confalone and E. M. Huie, *Org. React.*, 1988, **36**, 1–174.
- 3 J. N. Martin and R. C. F. Jones, in *Synthetic Applications of 1,3-Dipolar Cycloaddition Chemistry toward Heterocycles and Natural Products*, ed. A. Padwa and W. H. Pearson, Wiley, Chichester, United Kingdom, 2002, vol. 59, pp. 1–81.
- 4 (a) P. Merino, in *Science of Synthesis*, ed. D. Bellus and A. Padwa, George Thieme, Stuttgart, 2004, vol. 27, pp. 511–580; (b) P. Merino, in *Science of Synthesis*, ed. E. Schaumann, George Thieme, Stuttgart, 2011, vol. 2010/4, pp. 325–403.
- 5 (a) S. Kanemasa, *Synlett*, 2002, 1371–1387; (b) S. Kanemasa, in *Synthetic Applications of 1,3-Dipolar Cycloaddition Chemistry toward Heterocycles and Natural Products*, ed. A. Padwa and W. H. Pearson, Wiley, Chichester, United Kingdom, 2002, vol. 59, pp. 755–815; (c) D. A. Evans, F. Kleinbeck and M. Rüping, in *Asymmetric Synthesis -*

- The Essentials*, ed. M. Christmann and S. Bräse, Wiley-VCH, Weinheim, 2006, pp. 72–77.
- 6 K. Rück-Braun, T. H. E. Freysoldt and F. Wierschem, *Chem. Soc. Rev.*, 2005, **34**, 507–516.
- 7 (a) J. Revuelta, S. Cicchi, A. Goti and A. Brandi, *Synthesis*, 2007, 485–504; (b) A. Brandi, F. Cardona, S. Cicchi, F. M. Cordero and A. Goti, *Chem. – Eur. J.*, 2009, **15**, 7808–7821; (c) M. Frederickson, *Tetrahedron*, 1997, **53**, 403–425; (d) K. V. Gothelf, in *Cycloaddition Reactions in Organic Synthesis*, ed. S. Kobayashi and K. A. Jorgensen, Wiley-VCH, Inc., New York, 2002, pp. 211–247.
- 8 (a) J. Malinina, T. Q. Tran, A. V. Stepanov, V. V. Gurzhiy, G. L. Starova, R. R. Kostikov and A. P. Molchanov, *Tetrahedron Lett.*, 2014, **55**, 3663–3666; (b) T. Kawai, K.-H. Kodama, T. Ooi and T. Kusumi, *Tetrahedron Lett.*, 2004, **45**, 4097–4099; (c) A. Padwa, D. N. Kline, K. F. Koehler, M. Matzinger and M. K. Venkatraman, *J. Org. Chem.*, 1987, **52**, 3909–3917.
- 9 (a) D.-L. Mo, W. H. Pecak, M. Zhao, D. J. Wink and L. L. Anderson, *Org. Lett.*, 2014, **16**, 3696–3699; (b) J. Holt and A. Fiksdahl, *J. Heterocycl. Chem.*, 2007, **44**, 375–379.
- 10 (a) N. Celebi-Oelcuem, Y.-h. Lam, E. Richmond, K. B. Ling, A. D. Smith and K. N. Houk, *Angew. Chem., Int. Ed.*, 2011, **50**, 11478–11482; (b) E. Richmond, N. Duguet, A. M. Z. Slawin, T. Lebl and A. D. Smith, *Org. Lett.*, 2012, **14**, 2762–2765; (c) A. R. Evans, M. Hafiz and G. A. Taylor, *J. Chem. Soc., Perkin Trans. 1*, 1984, 1241–1245.
- 11 K. Kavitha and P. Venuvanalingam, *J. Chem. Soc., Perkin Trans. 2*, 2002, 2130–2139.
- 12 A. Darù, D. Roca-López, T. Tejero and P. Merino, *J. Org. Chem.*, 2016, **81**, 673–680.
- 13 E. Richmond, K. B. Ling, N. Duguet, L. B. Manton, N. Çelebi-Ölçüm, Y.-H. Lam, S. Alsancak, A. M. Z. Slawin, K. N. Houk and A. D. Smith, *Org. Biomol. Chem.*, 2015, **13**, 1807–1817.
- 14 P. Hohenberg and W. Kohn, *Phys. Rev.*, 1964, **136**, B864–B871.
- 15 L. R. Domingo, *Molecules*, 2016, **21**, 1319.
- 16 L. R. Domingo and S. R. Emamian, *Tetrahedron*, 2014, **70**, 1267–1273.
- 17 L. R. Domingo, M. Ríos-Gutiérrez and P. Pérez, *Tetrahedron*, 2016, **72**, 1524–1532.
- 18 L. R. Domingo, M. J. Aurell and P. Pérez, *Tetrahedron*, 2014, **70**, 4519–4525.
- 19 X. Krokidis, S. Noury and B. Silvi, *J. Phys. Chem. A*, 1997, **101**, 7277–7282.
- 20 Y. Zhao and D. G. Truhlar, *J. Phys. Chem. A*, 2004, **108**, 6908–6918.
- 21 W. J. Hehre, L. Radom, P. v. R. Schleyer and J. A. Pople, *Ab initio Molecular Orbital Theory*, Wiley, New York, 1986.
- 22 (a) H. B. Schlegel, *J. Comput. Chem.*, 1982, **3**, 214–218; (b) *Modern Electronic Structure Theory*, ed. H. B. Schlegel and D. R. Yarkony, World Scientific Publishing, Singapore, 1994.
- 23 K. Fukui, *J. Phys. Chem.*, 1970, **74**, 4161–4163.
- 24 (a) C. González and H. B. Schlegel, *J. Phys. Chem.*, 1990, **94**, 5523–5525; (b) C. González and H. B. Schlegel, *J. Chem. Phys.*, 1991, **95**, 5853–5860.
- 25 (a) J. Tomasi and M. Persico, *Chem. Rev.*, 1994, **94**, 2027–2094; (b) B. Y. Simkin and I. Sheikhet, *Quantum Chemical and Statistical Theory of Solutions– Computational Approach*, Ellis Horwood, London, 1995.
- 26 (a) E. Cances, B. Mennucci and J. Tomasi, *J. Chem. Phys.*, 1997, **107**, 3032–3041; (b) M. Cossi, V. Barone, R. Cammi and J. Tomasi, *Chem. Phys. Lett.*, 1996, **255**, 327–335; (c) V. Barone, M. Cossi and J. Tomasi, *J. Comput. Chem.*, 1998, **19**, 404–417.
- 27 (a) A. E. Reed, R. B. Weinstock and F. Weinhold, *J. Chem. Phys.*, 1985, **83**, 735–746; (b) A. E. Reed, L. A. Curtiss and F. Weinhold, *Chem. Rev.*, 1988, **88**, 899–926.
- 28 A. D. Becke and K. E. Edgecombe, *J. Chem. Phys.*, 1990, **92**, 5397–5403.
- 29 M. J. Frisch, *et al.*, *Gaussian 09, Revision A.02*, Gaussian Inc., Wallingford CT, 2009.
- 30 S. Noury, X. Krokidis, F. Fuster and B. Silvi, *Comput. Chem.*, 1999, **23**, 597–604.
- 31 (a) R. G. Parr and W. Yang, *Annu. Rev. Phys. Chem.*, 1995, **46**, 701–728; (b) H. Chermette, *J. Comput. Chem.*, 1999, **20**, 129–154; (c) F. De Proft and P. Geerlings, *Chem. Rev.*, 2001, **101**, 1451–1464; (d) P. Geerlings, F. De Proft and W. Langenaeker, *Chem. Rev.*, 2003, **103**, 1793–1873; (e) P. W. Ayers, J. S. M. Anderson and L. J. Bartolotti, *Int. J. Quantum Chem.*, 2005, **101**, 520–534; (f) J. L. Gázquez, *J. Mex. Chem. Soc.*, 2008, **52**, 3–10; (g) R. F. Nalewajski, J. Korchowiec and A. Michalak, *Density Functional Theory IV, Topics in Current Chemistry*, Springer, Berlin, Heidelberg, 1996, vol. 183, p. 25; (h) P. Geerlings, S. Fias, Z. Boisdenghien and F. De Proft, *Chem. Soc. Rev.*, 2014, **43**, 4989–5008.
- 32 R. G. Parr, L. von Szentpaly and S. Liu, *J. Am. Chem. Soc.*, 1999, **121**, 1922–1924.
- 33 (a) R. G. Parr and R. G. Pearson, *J. Am. Chem. Soc.*, 1983, **105**, 7512–7516; (b) R. G. Parr and W. Yang, *Density Functional Theory of Atoms and Molecules*, Oxford University Press, New York, 1989.
- 34 (a) L. R. Domingo, E. Chamorro and P. Pérez, *J. Org. Chem.*, 2008, **73**, 4615–4624; (b) L. R. Domingo and P. Pérez, *Org. Biomol. Chem.*, 2011, **9**, 7168–7175.
- 35 W. Kohn and L. J. Sham, *Phys. Rev.*, 1965, **140**, 1133–1138.
- 36 L. R. Domingo, P. Pérez and J. A. Sáez, *RSC Adv.*, 2013, **3**, 1486–1494.
- 37 L. R. Domingo, E. Chamorro and P. Pérez, *Lett. Org. Chem.*, 2010, **7**, 432–439.
- 38 L. R. Domingo, M. Ríos-Gutiérrez and P. Pérez, *Molecules*, 2016, **21**, 748.
- 39 L. R. Domingo, *RSC Adv.*, 2014, **4**, 32415–32428.
- 40 L. R. Domingo, M. J. Aurell, P. Pérez and R. Contreras, *Tetrahedron*, 2002, **58**, 4417–4423.
- 41 P. Jaramillo, L. R. Domingo, E. Chamorro and P. Pérez, *J. Mol. Struct. (THEOCHEM)*, 2008, **865**, 68–72.

- 42 (a) R. Pratt, D. P. Stokes and G. A. Taylor, *J. Chem. Soc., Perkin Trans. 1*, 1975, 498–503; (b) A. F. Gettins, D. P. Stokes and G. A. Taylor, *J. Chem. Soc., Perkin Trans. 1*, 1977, 1849–1855; (c) M. Hafiz and G. A. Taylor, *J. Chem. Soc., Perkin Trans. 1*, 1980, 1700–1705; (d) A. R. Evans, M. Hafiz and G. A. Taylor, *J. Chem. Soc., Perkin Trans. 1*, 1984, 1241–1245; (e) C. P. Falshaw, M. Hafiz and G. A. Taylor, *J. Chem. Soc., Perkin Trans. 1*, 1985, 1837–1843.
- 43 M. Ríos-Gutiérrez, P. Pérez and L. R. Domingo, *RSC Adv.*, 2015, **5**, 58464–58477.
- 44 L. R. Domingo and J. A. Sáez, *Org. Biomol. Chem.*, 2009, **7**, 3576–3583.
- 45 (a) S. Berski, J. Andrés, B. Silvi and L. R. Domingo, *J. Phys. Chem. A*, 2003, **107**, 6014–6024; (b) V. Polo, J. Andrés, S. Berski, L. R. Domingo and B. Silvi, *J. Phys. Chem. A*, 2008, **112**, 7128–7136; (c) J. Andrés, P. González-Navarrete and V. Safont, *Int. J. Quantum Chem.*, 2014, **114**, 1239–1252.
- 46 (a) R. Thom, *Structural Stability and Morphogenesis: An Outline of a General Theory of Models*, Inc., Reading, MA, 1976; (b) A. E. R. Woodcock and T. Poston, *A Geometrical Study of Elementary Catastrophes*, Springer-Verlag, Berlin, 1974; (c) R. Gilmore, *Catastrophe Theory for Scientists and Engineers*, Dover, New York, 1981.
- 47 (a) V. Polo, J. Andrés, R. Castillo, S. Berski and B. Silvi, *Chem. – Eur. J.*, 2004, **10**, 5165–5172; (b) J. C. Santos, J. Andrés, A. Aizman, P. Fuentealba and V. Polo, *J. Phys. Chem. A*, 2005, **109**, 3687–3693; (c) S. Berski, J. Andrés, B. Silvi and L. R. Domingo, *J. Phys. Chem. A*, 2006, **110**, 13939–13947; (d) V. Polo and J. Andrés, *J. Chem. Theory Comput.*, 2007, **3**, 816–823; (e) S. Berski and Z. Ciunik, *Mol. Phys.*, 2015, **113**, 765–781.
- 48 L. R. Domingo, M. Ríos-Gutiérrez and J. A. Sáez, *RSC Adv.*, 2015, **5**, 37119–37129.
- 49 L. R. Domingo, J. A. Saéz, R. J. Zaragozá and M. Arnó, *J. Org. Chem.*, 2008, **73**, 8791–8799.
- 50 M. Ríos-Gutiérrez, P. Pérez and L. R. Domingo, *RSC Adv.*, 2015, **5**, 84797–84809.

PAPER

Cite this: *RSC Adv.*, 2017, 7, 26879

A molecular electron density theory study of the [3 + 2] cycloaddition reaction of nitrones with strained allenes†

Luis R. Domingo, *^a Mar Ríos-Gutiérrez ^a and Patricia Pérez ^b

The [3 + 2] cycloaddition (32CA) reaction of *C*-phenyl-*N*-*tert*-butylnitronone with 1,2-cyclohexadiene (CHDE), a strained allene, has been studied within Molecular Electron Density Theory (MEDT) at the DFT B3LYP/6-311G(d,p) computational level. This non-polar 32CA reaction, which takes place through a non-concerted *two-stage one-step* mechanism, proceeds with a moderate Gibbs free activation energy of 22.7 kcal mol⁻¹, and presents low stereo- and regioselectivities. The reaction begins by the creation of a *pseudoradical* center at the central carbon of the strained allene with a relatively low energy cost, which immediately promotes the formation the first C–C single bond. This scenario is completely different from that of the 32CA reaction involving the simplest allene. The strain present in CHDE changes its reactivity to that characteristic of radical species. Consequently, not distortion as previously proposed, but the radical reactivity type of the strained allene is responsible for the feasibility of this 32CA reaction.

Received 15th February 2017

Accepted 10th May 2017

DOI: 10.1039/c7ra01916e

rsc.li/rsc-advances

1. Introduction

The use of strained species such as benzyne **5** and cyclic alkynes such as cyclopentyne **8** in organic synthesis permits their participation in organic reactions in which linear alkynes do not react (see Scheme 1). Thus, while the non-polar ene reaction between 2-methylpropene **1** and ethylene **2** presents a very high activation energy, 34.7 kcal mol⁻¹,¹ the non-polar ene reaction

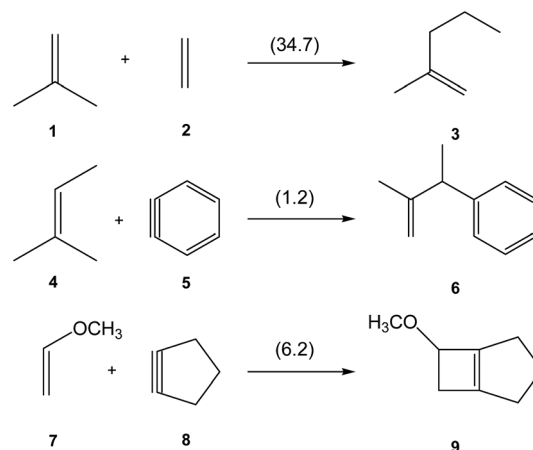
between 2-methylbut-2-en **4** and benzyne **5** has an unappreciable activation energy, 1.2 kcal mol⁻¹.² Similarly, the [2 + 2] cycloaddition between enol ether **7** and cyclopentyne **8** also presents a low activation energy, 6.2 kcal mol⁻¹.³

One appealing procedure that provides a straightforward connection between the electron density distribution and the chemical structure is the quantum chemical analysis of the Becke and Edgecombe's Electron Localisation Function (ELF).⁴ An ELF topological analysis of the electronic structure of benzyne **5** made it possible to explain the high reactivity of this strained aromatic alkyne.² The ELF of benzyne **5** shows the

^aDepartment of Organic Chemistry, University of Valencia, Dr Moliner 50, E-46100 Burjassot, Valencia, Spain. E-mail: domingo@utopia.uv.es; Web: <http://www.luisrdomingo.com>

^bUniversidad Andres Bello, Facultad de Ciencias Exactas, Departamento de Ciencias Químicas, Millennium Nucleus Chemical Processes and Catalysis (CPC), Av. República 498, 8370146, Santiago, Chile

† Electronic supplementary information (ESI) available: Study of the reaction paths associated with the 32CA reaction between nitronone **15** and the simplest allene **18**. BET study of the regioisomeric *r1* reactive channel associated with the 32CA reaction between nitronone **15** and the simplest allene **18** and the *endo/r1* reactive channel associated with the 32CA reaction between nitronone **15** and strained allene CHDE **10**. ELF topological analysis along the *exo/r1* reactive channel associated with the 32CA reaction between nitronone **15** and strained allene CHDE **10**. Theoretical background of the ELF and BET. B3LYP/6-311G(d,p) thermodynamic data. B3LYP/6-311G(d,p) thermodynamic data of the stationary points involved in the 32CA reaction of nitronone **15** with CHDE **10**. Analysis of the dependence of the thermodynamic data of the stationary points involved in the 32CA reaction between nitronone **15** and CHDE **10** with the DFT functional. B3LYP/6-311G(d,p) total and relative energies, in gas phase and in acetonitrile, of the stationary points involved in the 32CA reaction of nitronone **15** with the simplest allene **18** and CHDE **10** and finally, the computed total energies, the only imaginary frequency and Cartesian coordinates, in acetonitrile, of the structures involved in the 32CA reaction between nitronone **15** and strained allene CHDE **10**. See DOI: 10.1039/c7ra01916e



Scheme 1 Non-polar reactions of ethylene and strained species. Activation energies, in parentheses, are given in kcal mol⁻¹.

presence of two monosynaptic basins, $V(C1)$ and $V(C2)$, integrating $0.64e$ each one (see Fig. 1). This electronic characteristic of benzyne **5** allowed associating its reactivity to that of a high reactive *pseudoradical* species.^{2,5} Note that *pseudoradicals* are closed-shell species topologically characterised by the presence of at least one $V(C)$ monosynaptic basin integrating less than $1.0e$ at one carbon atom.⁶

Unlike arynes and cyclic alkynes, whose structure and reactivity have been widely studied,^{1-3,7} highly strained allene species have been studied to a much lesser extent. Since 1966, when Wittig reported, for the first time, the existence of 1,2-cyclohexadiene (CHDE) **10**,⁸ the chemistry of this highly strained species has received little attention especially compared to its aryne and alkyne counterparts. Only some theoretical studies devoted to $[2 + 2]$ ⁹⁻¹³ and $[4 + 2]$ ^{14,15} cycloadditions of CHDE **10** yielding cycloadducts **12** and **14**, respectively, have been reported (see Scheme 2).

Very recently, Houk *et al.* studied experimentally as well as theoretically the $[3 + 2]$ cycloaddition (32CA) reaction of the *in situ* generated CHDE **10** with nitron **15** participating as the three-atom-component (TAC), yielding the two stereoisomeric isoxazolidines **16** (Ph/H *syn*: *anti* 9.5 : 1); regioisomeric isoxazolidines **17** were not observed (see Scheme 3).¹⁶

B3LYP/6-31G(d) calculations for the four competitive channels resulted in a poor stereoselectivity, $\Delta\Delta G^\ddagger = 0.1 \text{ kcal mol}^{-1}$, and a poor regioselectivity, $\Delta\Delta G^\ddagger = 0.7 \text{ kcal mol}^{-1}$.¹⁶ For the stereoisomeric channels giving isoxazolidines **16a**, Ph and H *syn*, and **16b**, Ph and H *anti*, associated with the attack of the C5 carbon of CHDE **10** on the C1 carbon atom of the nitron (see Scheme 4 for atom numbering), two reaction mechanisms were established: (i) a “concerted” mechanism yielding *syn* isoxazolidine **16a**; and (ii) a stepwise mechanism yielding an open-shell diradical intermediate **IN**. From this open-shell intermediate, two competitive reaction channels associated to the ring closures yielding isoxazolidines **16a** and **16b** were characterised (see Scheme 4). Houk proposed that the “concerted” mechanism giving *cis* isoxazolidine **16a** via **TSc** was easily characterised, while the “concerted” *exo* transition state structure (TS) could not be located, suggesting that the “concerted” *exo* reaction was higher in energy. Furthermore, he suggested that the low $\sim 15 \text{ kcal mol}^{-1}$ barrier for these reactions compared with the $>30 \text{ kcal mol}^{-1}$ for the 32CA reaction with the simplest

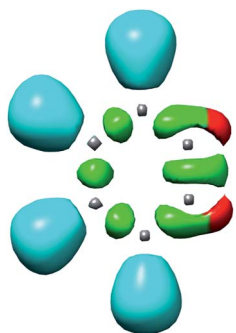
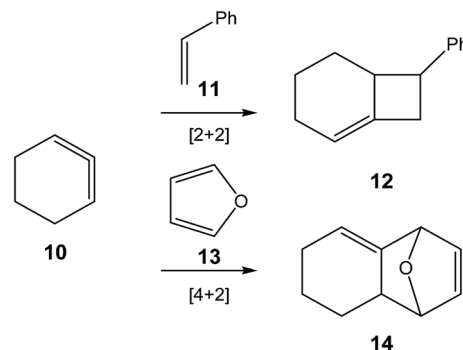


Fig. 1 ELF localisation domains of benzyne **5**. The two non-bonding $V(C1)$ and $V(C2)$ monosynaptic basins are represented in red.



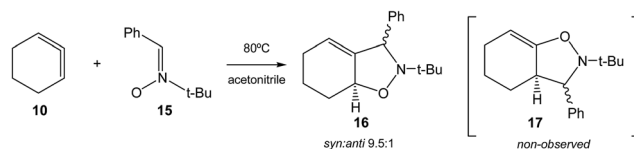
Scheme 2 Cycloaddition reactions of CHDE **10**.

allene **18** can be attributed to the predistortion of CHDE **10** into geometries similar to those of the TSs for cycloadditions.¹⁶

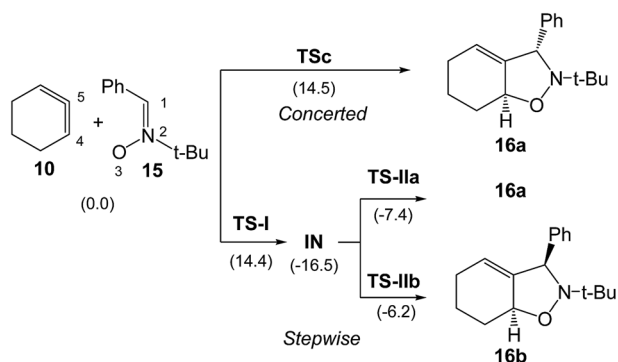
To explain the reactivity of a series of TACs towards ethylene **2** in 32CA reactions, in 2008, Houk introduced the Distortion/Interaction Energy Model (DIEM) in order to interpret the activation energies.^{17,18} He concluded that the distortion energy of the reagents towards the TS is the major factor controlling the reactivity differences of TACs. However, the distortion energy, which is computed through the partition of the TS geometry into two separated structures, has no physical meaning, since within Density Functional Theory (DFT)¹⁹ the energy of a system is a functional of the electron density and the external potential, *i.e.* the nuclei positions. Consequently, the energy of the two separated fragments cannot be correlated with the energy of the TS as each of them loses the external potential created by the other fragment.²⁰

The theoretical study of strained compounds is of special interest for organic chemists as it allows establishing a relationship between structure and reactivity. As aforementioned, Houk proposed that the predistortion of CHDE **10** into geometries similar to those of the TSs for cycloadditions could be responsible for the low activation energy of these reactions.¹⁶ However, similarly to benzyne **5**,² the strain present at the *sp* hybridised C5 carbon of CHDE **10** could provide some *pseudoradical* character to the C5 carbon, enabling CHDE **10** to experience a different reactivity pattern to that of linear allenes, and consequently, the corresponding reaction paths will be non-comparable.

These different interpretations about the role of the strain in the reactivity of strained species prompted us to revisit the 32CA reaction of the strained CHDE **10** with nitron **15** within the recently proposed Molecular Electron Density Theory (MEDT)²¹ (see Scheme 3). The main purpose of the present theoretical



Scheme 3 32CA reaction of CHDE **10** with nitron **15** yielding the stereoisomeric isoxazolidines **16**.¹⁶



Scheme 4 Houk's "concerted" and stepwise mechanisms associated to the formation of the stereoisomeric isoxazolines **16a** and **16b**.¹⁶ B3LYP/6-31G(d) relative Gibbs free energies, in parentheses, are given in kcal mol⁻¹.

study is to understand how the strain modifies the reactivity of CHDE **10** with respect to the non-strained linear allene **18**; this MEDT study provides a different explanation to the one previously reported.¹⁶ Thus, in order to establish the special reactivity of the strained allene CHDE **10**, an MEDT study of the 32CA reaction of nitron **15** with the simplest allene **18** is also performed for comparative analysis. This MEDT study is given in ESI.†

2. Computational methods

DFT calculations were performed using the B3LYP functional^{22,23} together with the 6-311G(d,p) basis set.²⁴ Optimisations were carried out using the Berny analytical gradient optimisation method.^{25,26} The stationary points were characterised by frequency computations in order to verify that TSs have one and only one imaginary frequency. The IRC paths²⁷ were traced in order to check the energy profiles connecting each TS to the two associated minima of the proposed mechanism using the second order González–Schlegel integration method.^{28,29} Solvent effects of acetonitrile were taken into account by full optimisation of the gas phase structures using the polarisable continuum model (PCM) developed by Tomasi's group^{30,31} in the framework of the self-consistent reaction field (SCRf).^{32–34} Enthalpies, entropies and Gibbs free energies in acetonitrile were calculated with standard statistical thermodynamics at 80 °C and 1 atm from the optimised structures in acetonitrile.²⁴ A comparative analysis of the thermodynamic data, obtained by using the MPWB1K,³⁵ ωB97XD³⁶ and M06-2X³⁷ functionals, indicates that the B3LYP and MPWB1K ones are the more adequate to study this non-polar 32CA reaction (see the comparative analysis in ESI†);³⁸ therefore, the B3LYP functional was selected in the present MEDT study to be consistent with previously reported calculations.¹⁶ The global electron density transfer³⁹ (GEDT) is computed by the sum of the natural atomic charges (q), obtained by a natural population analysis (NPA),^{40,41} of the atoms belonging to each framework (f) at the TSs; $\text{GEDT} = \sum q_f$. The sign indicates the direction of the electron density flux in such a manner that positive values mean a flux from the considered framework to the other one. All

computations were carried out with the Gaussian 09 suite of programs.⁴²

ELF studies were performed with the TopMod⁴³ program using the corresponding gas phase B3LYP/6-311G(d,p) mono-determinantal wavefunctions. For the BET study, the corresponding gas phase reaction channel was followed by performing the topological analysis of the ELF for 862 nuclear configurations along the IRC path. ELF calculations were computed over a grid spacing of 0.1 a.u. for each structure and ELF basin isosurfaces were obtained for an ELF value of 0.75.

Conceptual DFT^{44,45} (CDFT) provides different indices to rationalise and understand chemical structure and reactivity. The global electrophilicity index,⁴⁶ ω , is given by the following expression, $\omega = (\mu^2/2\eta)$, in terms of the electronic chemical potential, μ , and the chemical hardness, η . Both quantities may be approached in terms of the one-electron energies of the frontier molecular orbitals HOMO and LUMO, ϵ_H and ϵ_L , as $\mu \approx (\epsilon_H + \epsilon_L)/2$ and $\eta \approx (\epsilon_L - \epsilon_H)$, respectively.^{47,48} The global nucleophilicity index,^{49,50} N , based on the HOMO energies obtained within the Kohn–Sham scheme,⁵¹ is defined as $N = E_{\text{HOMO}}(\text{Nu}) - E_{\text{HOMO}}(\text{TCE})$, where tetracyanoethylene (TCE) is the reference.

3. Results and discussion

The present MEDT study has been divided into four parts: (i) in the first one, an analysis of the CDFT reactivity indices at the ground state (GS) of the reagents involved in the 32CA reactions of nitron **15** with allenes **10** and **18** is performed; (ii) then, the reaction paths associated the 32CA reaction of nitron **15** with CHDE **10** are explored and characterised; (iii) in the third part, a topological analysis of the ELF of the simplest allene **18** and strained CHDE **10** is performed in order to characterise their electronic structures; and (iv) finally, a BET study of the 32CA reaction of nitron **15** with CHDE **10** is carried out in order to establish the origin of the high reactivity of the strained allene CHDE **10**.

3.1. Analysis of the CDFT reactivity indices of nitron **15** and allenes **10** and **18**

Numerous studies devoted to Diels–Alder and 32CA reactions have shown that the analysis of the reactivity indices defined within the CDFT^{44,45} is a powerful tool to understand the reactivity in cycloaddition reactions. Recent MEDT studies have shown that the feasibility of the 32CA reactions involving nitrones depends on the nucleophilic character of these TACs and the electrophilic character of the ethylene derivative.^{52,53} Consequently, an analysis of the CDFT reactivity indices computed in gas phase at the GS of nitron **15** and allenes **10** and **18** was performed to predict their reactivity in 32CA reactions. The global indices, namely, the electronic chemical potential, μ , chemical hardness, η , electrophilicity, ω , and nucleophilicity, N , at the GS of the reagents involved in these 32CA reactions are given in Table 1.

The electronic chemical potential of nitron **15**, $\mu = -3.29$ eV, is close to that of the simplest allene **18**, $\mu = -3.30$ eV, and only slightly higher than that of CHDE **10**, $\mu = -3.44$ eV.

Table 1 B3LYP/6-31G(d) electronic chemical potential (μ), chemical hardness (η), electrophilicity (ω) and nucleophilicity (N), in eV, of nitron 15, allenes 10 and 18, and ethylene 2

	μ	η	ω	N
Nitron 15	-3.29	4.27	1.26	3.70
CHDE 10	-3.44	4.77	1.24	3.29
Ethylene 2	-3.37	7.77	0.73	1.87
Allene 18	-3.30	7.72	0.70	1.97

Thus, none of the reagents will have a tendency to exchange electron density with the other along these 32CA reactions, suggesting non-polar reactions.

Nitron 15 presents an electrophilicity ω index of 1.26 eV and a nucleophilicity N index of 3.70 eV, being classified as a moderate electrophile and as a strong nucleophile according to the electrophilicity⁵⁴ and nucleophilicity⁵⁵ scales. Note that nitrones usually behave as nucleophilic zwitterionic TACs participating in polar 32CA reactions towards electrophilic ethylene derivatives.^{52,53}

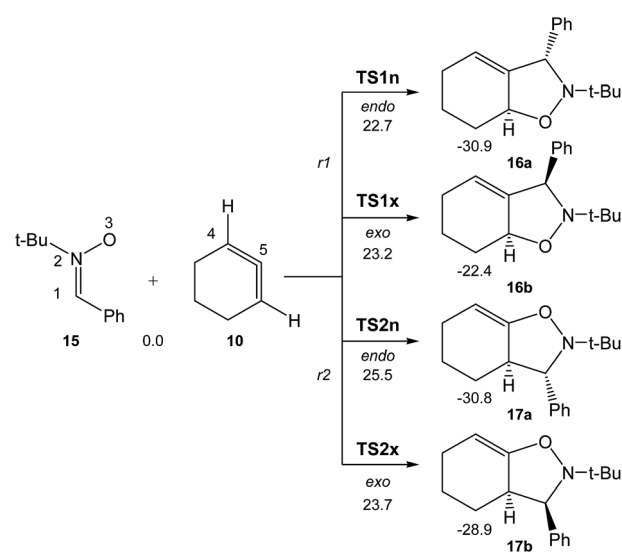
Polar cycloaddition reactions require the participation of good electrophiles and good nucleophiles. Ethylene 2 is one of the poorest electrophilic, $\omega = 0.73$ eV, and nucleophilic, $N = 1.87$ eV, species involved in cycloaddition reactions, being classified as a marginal electrophile and a marginal nucleophile. CDFT reactivity indices of the simplest linear allene 18 are very similar to those of ethylene 2 (see Table 1), thus being also classified as a marginal electrophile and on the borderline between marginal and moderate nucleophiles. Otherwise, the angular strain of the allene framework in CHDE 10 causes an increase of both the electrophilicity ω and nucleophilicity N indices to 1.24 eV and 3.29 eV, respectively, being classified as a moderate electrophile and a strong nucleophile. However, in spite of this electrophilic activation with respect to the simplest linear allene 18, this is not sufficient to favour the GEDT,³⁹ in clear agreement with the analysis of the electronic chemical potentials of the reagents. Consequently, it is expected that the corresponding non-polar 32CA reactions will present high activation barriers (see the 32CA reaction between nitron 15 and the simplest allene 18 in ESI†).

3.2. Study of the reaction paths associated with the 32CA reaction of nitron 15 with CHDE 10

Due to the non-symmetry of the two reagents, the 32CA reaction of nitron 15 with CHDE 10 can take place along four isomeric channels: one pair of stereoisomeric channels and one pair of regioisomeric ones. The regioisomeric channels are related to the initial formation of the C1–C5 single bond, channel *r1*, or to the initial formation of the O3–C5 single bond, channel *r2*, while the *endo* and *exo* stereoisomeric channels are related to the relative position of the allenic H4 hydrogen with respect to the nitron N2 nitrogen, in such a manner that along the *endo* channel this hydrogen atom is far away. This 32CA reaction presents a one-step mechanism; only one TS, **TS1n**, **TS1x**, **TS2n** and **TS2x**, and the corresponding isoxazolidine, **16a**, **16b**, **17a**

and **17b**, were located and characterised along each reactive channel (see Scheme 5). Relative Gibbs free energies in acetonitrile of the stationary points involved in the 32CA reaction of nitron 15 with CHDE 10 are given in Scheme 5, while total thermodynamic data are gathered in Table S5 in ESI.† The Gibbs free energy profile is represented in Fig. 2.

The activation Gibbs free energies associated with the four competitive channels are 22.7 (**TS1n**), 23.2 (**TS1x**), 25.5 (**TS2n**), and 23.7 (**TS2x**) kcal mol⁻¹, the reaction being strongly exergonic, between 22–31 kcal mol⁻¹. Some appealing conclusions can be drawn from these relative energies: (i) the activation Gibbs free energy associated with the 32CA reaction of nitron 15 with CHDE 10 *via* **TS1n** is 19.9 kcal mol⁻¹ lower in energy than that associated with the 32CA reaction of nitron 15 with the simplest allene 18 (see ESI†); (ii) this 32CA reaction presents a low *endo* selectivity as **TS1n** is 0.5 kcal mol⁻¹ lower in energy than **TS1x**; (iii) this 32CA reaction presents a low regioselectivity as **TS2x** is only 1.0 kcal mol⁻¹ higher in energy than **TS1n**; (iv) the 32CA reaction of nitron 15 with CHDE 10 presents an opposed regioselectivity to that found in the reaction with the simplest allene 18 (see ESI†). The most favourable reactive channel corresponds to the initial C1–C5 bond formation; (v) this 32CA reaction is strongly exergonic by 30.9 kcal mol⁻¹ (**16a**). Note that the most favourable reactive channel associated with the 32CA reaction involving the simplest allene 18 is exergonic by only 4.3 kcal mol⁻¹ (see ESI†). Consequently, the strain present in CHDE 10 does not only affect the kinetics, but also the thermodynamics; and finally, (vii) the Gibbs free energy profile corresponding to the *exo/r1* reactive channel in acetonitrile is quite different to that reported by Houk *et al.* in gas phase (see the stepwise mechanism *via* an open-shell intermediate given in Scheme 4 as proposed by Houk,¹⁶ and the one-step mechanism shown in Fig. 2). It is interesting to note that the gas phase B3LYP/6-311G(d,p) IRC from *exo* **TS1x** to *exo*



Scheme 5 The four competitive reactive channels associated with the 32CA reaction of nitron 15 with CHDE 10. B3LYP/6-311G(d,p) relative Gibbs free energies, in acetonitrile, are given in kcal mol⁻¹.

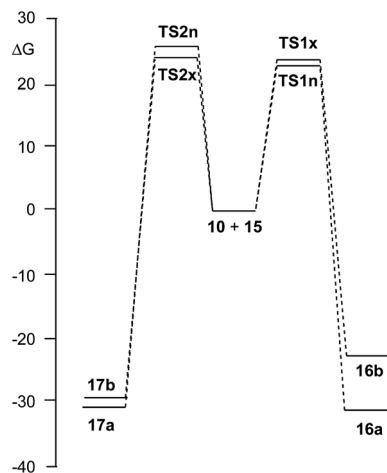


Fig. 2 B3LYP/6-311G(d,p) Gibbs free energy profile, in kcal mol⁻¹, of the 32CA reaction of nitrene **15** with CHDE **10**.

isoxazolidine **16b** discontinues at a species that is not a stationary point; a downhill calculation from this species gives the final *exo* isoxazolidine **16b** in a straightforward manner (see Fig. S10 in ESI[†]).

The optimised geometries of the TSs in acetonitrile involved in the 32CA reaction of nitrene **15** with CHDE **10**, including the distances between the four interacting atoms, are given in Fig. 3. Some appealing conclusions can be drawn from these geometrical parameters: (i) the distances between the interacting atoms at the four TSs indicate that they correspond to highly asynchronous C–C and C–O single bond formation processes;

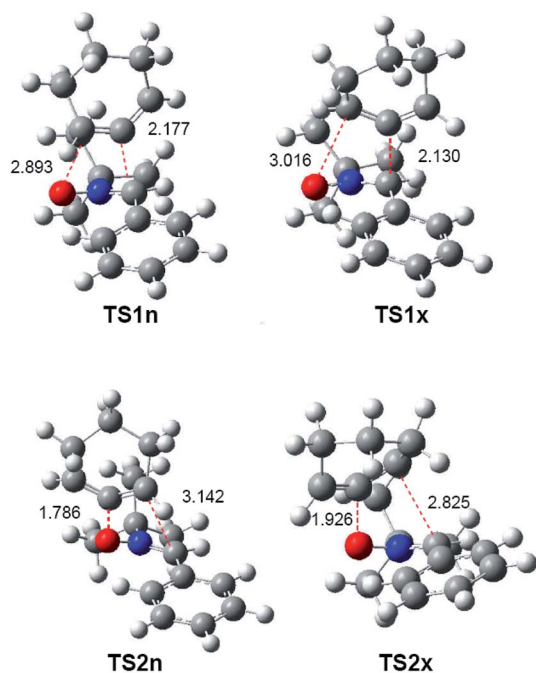


Fig. 3 B3LYP/6-311G(d,p) geometries in acetonitrile of the TSs involved in the 32CA reaction of nitrene **15** with CHDE **10**. Distances are given in angstroms, Å.

(ii) at the two pairs of stereoisomeric TSs associated with the most favourable regioisomeric *r1* channel, the more unfavourable *exo* **TS1x** is slightly more advanced and more asynchronous than *endo* **TS1n**; (iii) at the four TSs, the formation of the single bond involving the C5 atom of CHDE **10** is more advanced than that involving the C4 atom; (iv) CHDE **10** approaches nitrene **15** perpendicularly, while in the 32CA reaction between nitrene **15** and the simplest allene **18**, the two frameworks approach each other in a parallel manner (see Fig. S1 in ESI[†]). These different approach modes emphasise different reactivities; (v) both geometries and relative energies of the four TSs indicate that the strain present in CHDE **10** notably modifies the reactivity of this strained cyclic allene when it is compared to that of the simplest allene **18**. Note that the two regioisomeric TSs associated with the 32CA reaction of nitrene **15** with the simplest allene **18** are poorly asynchronous (see ESI[†]).

In acetonitrile, *endo* **TS1n** and *exo* **TS1x** have a great similitude; they present a similar only imaginary frequency, -297.6918 cm^{-1} (**TS1n**) and -311.8100 cm^{-1} (**TS1x**), with a similar transition vector, $0.86023\text{ B}(\text{C1-C5})$ and $0.25045\text{ B}(\text{C4-O3})$ (**TS1n**) and $0.80798\text{ B}(\text{C1-C5})$ and $0.31925\text{ B}(\text{C4-O3})$ (**TS1x**). The vibration modes of these stereoisomeric TSs are completely different to those of the TSs associated with the 32CA reaction of nitrene **15** with the linear allene **18**, indicating again different reactivities; **TS1n** and **TS1x** are associated to a two-center interaction in which only the C5 carbon of CHDE **10** and the C1 carbon of nitrene **15** participate. In addition, these stereoisomeric channels, which are associated to a non-concerted *two-stage one-step* mechanism,⁵⁶ present analogous IRCs (see Fig. 4). In this mechanism, the formation of the second O3–C4 single bond begins once the first C1–C5 single bond has been completely formed in a single elementary step (see later).

In order to evaluate the polar or non-polar electronic nature of these TSs, the GEDT was analysed.³⁹ The GEDT at the four TSs, which fluxes from the nitrene to the CHDE frameworks, is $0.02e$ at **TS1n**, $0.02e$ at **TS1x**, $0.02e$ at **TS2n** and $0.09e$ at **TS2x**. These negligible values indicate that this 32CA reaction has a non-polar character.

3.3. Topological analysis of the ELF of linear allene **18** and strained CHDE **10**

As commented in the introduction, the high reactivity of benzyne **5** was attributed to its *pseudoradical* character, which was topologically characterised by the presence of two ELF V(C) monosynaptic basins (see Fig. 1).² Consequently, a topological analysis of the ELF of linear allene **18** and strained CHDE **10** was performed in order to characterise their electronic structure. ELF attractors, together with the C4–C5 valence basin populations, ELF localisation domains and the proposed ELF-based Lewis structures are shown in Fig. 5.

ELF topological analysis of both allenes **10** and **18** shows the presence of two V(C4,C5) and V'(C4,C5) disynaptic basins within the C4–C5 bonding region, integrating a total population of $3.68e$ at both allenes, which indicates that the C4–C5 bonding region possesses a strong double bond character (see Fig. 5).

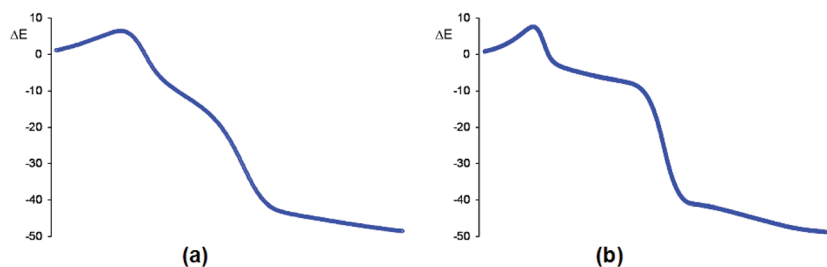


Fig. 4 Relative energy (ΔE , in kcal mol^{-1}) variations along the IRC ($\text{amu}^{1/2} \text{ bohr}$) associated with the *endo/r1* (a) and *exo/r1* (b) reactive channels of the 32CA reaction between nitrone **15** and strained allene CHDE **10** in acetonitrile. Relative energies are given with respect to the separated reagents.

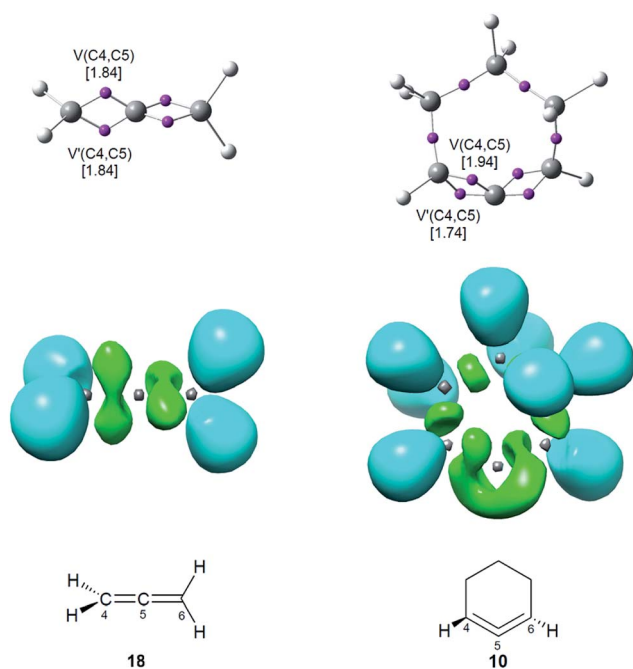


Fig. 5 ELF attractors, together with the C4–C5 valence basin populations, in average number of electrons (e), ELF localisation domains and the proposed Lewis structures for allenes **10** and **18**.

However, the topology of the ELF $V(C_x, C_y)$ disynaptic basins associated with the C4–C5 and C5–C6 bonding regions shows a notable difference at the two structures; while these disynaptic basins are clearly differentiated in the linear allene **18** as they are positioned in two perpendicular molecular planes, they are linked in a singular and twisted manner at strained CHDE **10** due to the slight torsion of the $C1=C2=C3$ framework (see ELF localisation domains in Fig. 5). This particular feature found in the strained CHDE **10** suggests the participation of the two C–C double bonds of the strained allene in the special reactivity of this strained species.

Consequently, although the strained CHDE **10** does not present a *pseudoradical* structure such as benzyne **5** (see Fig. 1), the ELF topological analysis of the C4–C5–C6 bonding region suggests that this species will have a different chemical behaviour to that of linear allene **18**.

3.4. BET study of the 32CA reaction between nitrone **15** and strained allene CHDE **10** yielding *endo* isoxazolidine **16a**

When trying to achieve a better understanding of bonding changes in organic reactions, the so-called BET⁵⁷ has proven to be a very useful methodological tool. This quantum-chemical methodology makes it possible to understand the bonding changes along a reaction path and, thus, to establish the nature of the electronic rearrangement associated with a given molecular mechanism.^{58–60}

Recently, a BET study of the bonding changes along the 32CA reactions of *C*-phenyl-*N*-methyl nitrone **21** with electron-deficient acrolein **22** was carried out in order to understand the molecular mechanism of these 32CA processes.⁶¹ Herein, in order to understand the different reactivity of linear or cyclic strained allenes towards nitrones, a BET study of the molecular mechanism of the most favourable *endo/r1* reaction channel associated with the 32CA reaction between nitrone **15** and strained allene CHDE **10** is performed; the complete BET study is discussed in ESI†. The characterisation of the molecular mechanism of the 32CA reaction of nitrone **15** with the simplest linear allene **18** is also carried out with the aim of rationalising the origin of the differences between the reactivity of both allenes (see ESI†). The attractor positions of the ELF basins for the points involved in the bond formation processes are shown in Fig. 6.

Some appealing conclusions can be drawn from this BET study: (i) the IRC of the *endo/r1* reactive channel is divided in ten differentiated phases related to the disappearance or creation of valence basins, emphasising the non-concertedness of the reaction; (ii) the reaction begins with the depopulation of the allenic C4–C5–C6 bonding region of the strained CHDE **10** in order to permit the creation of a C5 *pseudoradical* center. Due to the strain present in CHDE **10**, this electronic change demands a moderate energy cost of $8.3 \text{ kcal mol}^{-1}$ (see Table S3 in ESI†), which is $15.1 \text{ kcal mol}^{-1}$ lower than that demanded for the creation of the first *pseudoradical* center at the nitrone **15** in the reaction involving the simplest allene **18** (see Table S2 in ESI†); (iii) thus, the moderate activation energy found in this non-polar 32CA reaction, $8.5 \text{ kcal mol}^{-1}$, can be mainly associated to the creation of a *pseudoradical* center at the C5 carbon of strained allene CHDE **10**; (iv) once the C5 *pseudoradical* center is formed in the allenic framework, the subsequent rupture of the C1–N2 double bond of the nitrone fragment and creation of the

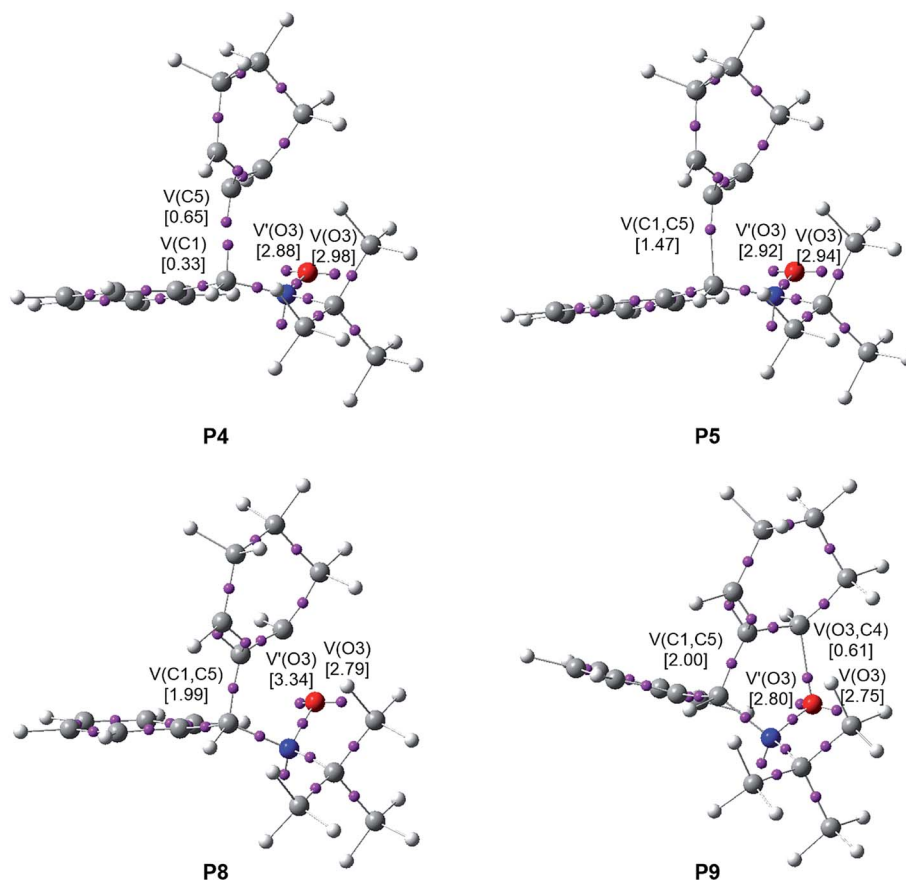


Fig. 6 ELF attractor positions for the points of the IRC involved in the formation of the C1–C5 and O3–C4 single bonds along the most favourable *endo/r1* reactive channel associated with the 32CA reaction between nitrone **15** and strained allene CHDE **10**. The electron populations, in e, are given in brackets.

C1 *pseudoradical* center has an unappreciable energy cost, 0.1 kcal mol⁻¹. Consequently, once the C5 *pseudoradical* center is created, it induces the easy rupture of the C1–N2 double bond (see Table S3 in ESI[†]). This reactivity behaviour is characteristic of radical species. (v) Formation of the first C1–C5 single bond begins at a C1–C5 distance of 1.94 Å through a C-to-C coupling of two C1 and C5 *pseudoradical* centers (see **P4** and **P5** in Fig. 6).³⁹ Interestingly, the C5 *pseudoradical* center participates with a high electron density, 0.89e, in the formation of the new C1–C5 single bond; (vi) however, formation of the second O3–C4 single bond begins at an O3–C4 distance of 1.75 Å through the donation of the electron density of one of the two O3 oxygen lone pairs of the nitrone framework to the C2 carbon atom of the allene fragment, similar to previous O–C bond formations,⁶¹ (see **P8** and **P9** in Fig. 6); and (vii) formation of the second O3–C4 single bond takes place at the end of the reaction path once the first C1–C5 single bond has already reached 99% of its population present at *endo* isoxazolidine **16a**. This fact allows characterising the molecular mechanism of this 32CA reaction as a non-concerted *two-stage one-step* mechanism⁵⁶ associated to the attack of the *pseudoradical* allenic C5 carbon of CHDE **10** on the C1 carbon of the nitrone which, after the complete C1–C5 single bond formation, experiences a rapid ring-closure process.

A comparative analysis of the BET studies of the non-polar 32CA reactions between nitrone **15** and allenes **10** and **18** makes it possible to explain the high reactivity of strained cyclic allene CHDE **10**. The bonding changes along the non-polar 32CA reaction between nitrone **15** and the simplest allene **18** are very similar to those along the less favourable *ortho/endo* regioisomeric channel associated with the low-polar 32CA reaction of nitrone **21** with electron-deficient acrolein **22**, which begins with the rupture of the nitrone C1–N2 double bond.⁶¹ The lower activation energy associated with the reaction involving acrolein **22** can be related to the slight GEDT, which favours the rupture of the double bonds in the nitrone and ethylene frameworks involved in this 32CA reaction.⁶¹ However, a completely different scenario is found along the non-polar 32CA reaction between nitrone **15** and strained allene CHDE **10**.

At the beginning of the reaction, a *pseudoradical* center is created at the central C5 carbon of the strained allene CHDE **10** with an energy cost of 8.3 kcal mol⁻¹. Interestingly, once this C5 *pseudoradical* center reaches a population of 0.89e, the subsequent bonding changes take place very easily (see the shortness of *phases II–IV* in the reaction involving CHDE **10** in Fig. S5[†] in contrast to their extension in the reaction involving the linear allene **18** in Fig. S2[†]). This behaviour indicates that, at the beginning of the reaction, CHDE **10** becomes a *pseudoradical*

species,⁵ which explains the high reactivity of strained allenes in cycloaddition reactions.^{9–15}

These findings clearly reveal that the bonding changes demanded to reach the corresponding TSs are completely different and, consequently, they are neither electronically nor geometrically comparable.

4. Conclusions

The 32CA reaction of nitrene **15** with the strained allene CHDE **10** giving isoxazolidines **16** and **17** has been studied within MEDT at the DFT B3LYP/6-311G(d,p) computational level in order to explain the higher reactivity of CHDE **10** with respect to linear allenes.

This 32CA reaction can take place along two pairs of regio- and stereoisomeric reaction channels. In acetonitrile, this reaction presents a low activation Gibbs free energy, 22.7 kcal mol⁻¹, as well as low *endo* stereo- and regioselectivities. The non-polar character of the reaction measured by the GEDT at the TSs agrees with the analysis of the CDFT reactivity indices carried out at the GS of the reagents.

Analysis of the geometries of the *endo* and *exo* stereoisomeric TSs associated with the more favourable *r1* regioisomeric channels indicates that they are related to highly asynchronous C–C and C–O single bond formation processes. Analysis of the IRCs associated to these TSs in acetonitrile clearly permits to establish that this 32CA reaction takes place through a non-concerted *two-stage one-step* mechanism initialised by the attack of the central C5 carbon of CHDE **10** on the C1 carbon of nitrene **15**.

BET analysis of the most favourable *endo/r1* reactive channel allows establishing the molecular mechanism of the 32CA reaction of nitrene **15** with strained allene CHDE **10**. At the beginning of the reaction, a *pseudoradical* center with a population of 0.89*e* is created at the central C5 carbon of the strained allene framework with a moderate energy cost of 8.3 kcal mol⁻¹, which induces the formation of the C1 *pseudoradical* center at the nitrene moiety, demanded for the formation of the first C1–C5 single bond through a two-center interaction. Formation of the second O3–C4 single bond takes place at the end of the reaction path when the first C1–C5 single bond is almost completely formed. This behaviour supports the mechanism of this 32CA reaction as a non-concerted *two-stage one-step* one.

This mechanism is completely different to that associated with the 32CA reaction involving the simplest linear allene **18**, which begins with the rupture of the C1–N2 double bond of the nitrene framework in order to create the C1 *pseudoradical* center required for the formation of the first C1–C5 single bond. This bonding change demands an energy cost of 23.4 kcal mol⁻¹, justifying the high activation energy associated to this non-polar process, 26.2 kcal mol⁻¹.

Consequently, when comparing the mechanisms of the 32CA reactions of nitrene **15** with allenes **10** and **18** characterised from an MEDT perspective, we can conclude that the geometrical predistortion of strained allene CHDE **10** is not responsible for the high reactivity of this species as previously proposed,¹⁶

but a change of reactivity of the strained CHDE **10**, which behaves as a radical species rather than an ethylene derivative, as occurs in the case of linear allene **18**. It is worth mentioning that while the *pseudoradical* character of a species can be correlated with a molecular strain, the energy associated with the geometrical distortion of a relaxed species cannot give any information about its electronic structure.

Acknowledgements

This work has been supported by the Ministry of Economy and Competitiveness (MINECO) of the Spanish Government, project CTQ2016-78669-P, Fondecyt (Chile) grants 1140341, Millennium Nucleus Chemical Processes and Catalysis (CPC) project No. 120082, and the Universidad Andres Bello (UNAB) by grant DI-793-15/R. Prof L. R. D. thanks FONDECYT for continuous support through Cooperación Internacional. Finally, M. R.-G. also thanks MINECO for a pre-doctoral contract co-financed by the European Social Fund (BES-2014-068258).

References

- 1 L. R. Domingo, M. J. Aurell and P. Pérez, *Org. Biomol. Chem.*, 2014, **12**, 7581–7590.
- 2 P. Pérez and L. R. Domingo, *Eur. J. Org. Chem.*, 2015, 2826–2834.
- 3 L. R. Domingo, P. Pérez and R. Contreras, *Eur. J. Org. Chem.*, 2006, 498–506.
- 4 A. D. Becke and K. E. Edgecombe, *J. Chem. Phys.*, 1990, **92**, 5397–5403.
- 5 L. A. Errede, J. M. Hoyt and R. S. Gregorian, *J. Am. Chem. Soc.*, 1960, **53**, 5224–5227.
- 6 L. R. Domingo, E. Chamorro and P. Pérez, *Lett. Org. Chem.*, 2010, **7**, 432–439.
- 7 I. Fernandez and F. P. Cossio, *J. Comput. Chem.*, 2016, **37**, 1265–1273.
- 8 G. Wittig and P. Fritze, *Angew. Chem., Int. Ed. Engl.*, 1966, **5**, 846.
- 9 A. T. Bottini, L. L. Hilton and J. Plott, *Tetrahedron*, 1975, **31**, 1997–2001.
- 10 M. Christl, H. Fischer, M. Arnone and B. Engels, *Chem.–Eur. J.*, 2009, **15**, 11266–11272.
- 11 M. Christl and M. Schreck, *Angew. Chem., Int. Ed. Engl.*, 1987, **26**, 449–451.
- 12 W. R. Moore and W. R. Moser, *J. Org. Chem.*, 1970, **35**, 908–912.
- 13 I. Quintana, D. Pena, D. Perez and E. Guitian, *Eur. J. Org. Chem.*, 2009, 5519–5524.
- 14 M. Balci and W. M. Jones, *J. Am. Chem. Soc.*, 1980, **102**, 7607–7608.
- 15 L. M. Tolbert, M. N. Islam, R. P. Johnson, P. M. Loiselle and W. C. Shakespeare, *J. Am. Chem. Soc.*, 1980, **112**, 6416–6417.
- 16 J. S. Barber, E. D. Styduhar, H. V. Pham, T. C. McMahon, K. N. Houk and N. K. Garg, *J. Am. Chem. Soc.*, 2016, **138**, 2512–2515.
- 17 D. H. Ess and K. N. Houk, *J. Am. Chem. Soc.*, 2007, **129**, 10646–10647.

- 18 D. H. Ess and K. N. Houk, *J. Am. Chem. Soc.*, 2008, **130**, 10187–10198.
- 19 P. Hohenberg and W. Kohn, *Phys. Rev.*, 1964, **136**, B864–B871.
- 20 L. R. Domingo, M. Ríos-Gutiérrez, M. Duque-Noreña, E. Chamorro and P. Pérez, *Theor. Chem. Acc.*, 2016, **135**, 160.
- 21 L. R. Domingo, *Molecules*, 2016, **21**, 1319.
- 22 A. D. Becke, *J. Chem. Phys.*, 1993, **98**, 5648–5652.
- 23 C. Lee, W. Yang and R. G. Parr, *Phys. Rev. B: Condens. Matter Mater. Phys.*, 1988, **37**, 785–789.
- 24 W. J. Hehre, L. Radom, P. V. R. Schleyer and J. A. Pople, *Ab initio Molecular Orbital Theory*, Wiley, New York, 1986.
- 25 H. B. Schlegel, *J. Comput. Chem.*, 1982, **3**, 214–218.
- 26 H. B. Schlegel, in *Modern Electronic Structure Theory*, ed. D. R. Yarkony, World Scientific Publishing, Singapore, 1994.
- 27 K. Fukui, *J. Phys. Chem.*, 1970, **74**, 4161–4163.
- 28 C. González and H. B. Schlegel, *J. Phys. Chem.*, 1990, **94**, 5523–5527.
- 29 C. González and H. B. Schlegel, *J. Chem. Phys.*, 1991, **95**, 5853–5860.
- 30 B. Y. Simkin and I. Sheikhet, *Quantum Chemical and Statistical Theory of Solutions – A Computational Approach*, Ellis Horwood, London, 1995.
- 31 J. Tomasi and M. Persico, *Chem. Rev.*, 1994, **94**, 2027–2094.
- 32 M. Cossi, V. Barone, R. Cammi and J. Tomasi, *Chem. Phys. Lett.*, 1996, **255**, 327–335.
- 33 E. Cancès, B. Mennucci and J. Tomasi, *J. Chem. Phys.*, 1997, **107**, 3032–3041.
- 34 V. Barone, M. Cossi and J. Tomasi, *J. Comput. Chem.*, 1998, **19**, 404–417.
- 35 Y. Zhao and G. D. Truhlar, *J. Phys. Chem. A*, 2004, **108**, 6908–6918.
- 36 J.-D. Chai and M. Head-Gordon, *Phys. Chem. Chem. Phys.*, 2008, **10**, 6615–6620.
- 37 Y. Zhao and D. G. Truhlar, *Theor. Chem. Acc.*, 2008, **120**, 215–241.
- 38 L. R. Domingo, M. Ríos-Gutiérrez and P. Pérez, *Tetrahedron*, 2017, **73**, 1718–1724.
- 39 L. R. Domingo, *RSC Adv.*, 2014, **4**, 32415–32428.
- 40 A. E. Reed, L. A. Curtiss and F. Weinhold, *Chem. Rev.*, 1988, **88**, 899–926.
- 41 A. E. Reed, R. B. Weinstock and F. Weinhold, *J. Chem. Phys.*, 1985, **83**, 735–746.
- 42 M. J. Frisch, G. W. Trucks, H. B. Schlegel, G. E. Scuseria, M. A. Robb, J. R. Cheeseman, G. Scalmani, V. Barone, B. Mennucci, G. A. Petersson, H. Nakatsuji, M. Caricato, X. Li, H. P. Hratchian, A. F. Izmaylov, J. Bloino, G. Zheng, J. L. Sonnenberg, M. Hada, M. Ehara, K. Toyota, R. Fukuda, J. Hasegawa, M. Ishida, T. Nakajima, Y. Honda, O. Kitao, H. Nakai, T. Vreven, J. A. Montgomery Jr, J. A., J. E. Peralta, F. Ogliaro, M. Bearpark, J. J. Heyd, E. Brothers, K. N. Kudin, V. N. Staroverov, T. Keith, R. Kobayashi, J. Normand, K. Raghavachari, A. Rendell, J. C. Burant, S. S. Iyengar, J. Tomasi, M. Cossi, N. Rega, J. M. Millam, M. Klene, J. E. Knox, J. B. Cross, V. Bakken, C. Adamo, J. Jaramillo, R. Gomperts, R. E. Stratmann, O. Yazyev, A. J. Austin, R. Cammi, C. Pomelli, J. W. Ochterski, R. L. Martin, K. Morokuma, V. G. Zakrzewski, G. A. Voth, P. Salvador, J. J. Dannenberg, S. Dapprich, A. D. Daniels, O. Farkas, J. B. Foresman, J. V. Ortiz, J. Cioslowski and D. J. Fox, *Gaussian 09, Gaussian 09 D.01*, Gaussian, Inc, Wallingford CT, 2013.
- 43 S. Noury, X. Krokidis, F. Fuster and B. Silvi, *Comput. Chem.*, 1999, **23**, 597–604.
- 44 P. Geerlings, F. De Proft and W. Langenaeker, *Chem. Rev.*, 2003, **103**, 1793–1873.
- 45 L. R. Domingo, M. Ríos-Gutiérrez and P. Pérez, *Molecules*, 2016, **21**, 748.
- 46 R. G. Parr, L. von Szentpaly and S. Liu, *J. Am. Chem. Soc.*, 1999, **121**, 1922–1924.
- 47 R. G. Parr and R. G. Pearson, *J. Am. Chem. Soc.*, 1983, **105**, 7512–7516.
- 48 R. G. Parr and W. Yang, *Density Functional Theory of Atoms and Molecules*, Oxford University Press, New York, 1989.
- 49 L. R. Domingo, E. Chamorro and P. Pérez, *J. Org. Chem.*, 2008, **73**, 4615–4624.
- 50 L. R. Domingo and P. Pérez, *Org. Biomol. Chem.*, 2011, **9**, 7168–7175.
- 51 W. Kohn and L. J. Sham, *Phys. Rev. [Sect.] B*, 1965, **140**, 1133–1138.
- 52 L. R. Domingo and S. R. Emamian, *Tetrahedron*, 2014, **70**, 1267–1273.
- 53 L. R. Domingo, M. J. Aurell and P. Pérez, *Tetrahedron*, 2014, **70**, 4519–4525.
- 54 L. R. Domingo, M. J. Aurell, P. Pérez and R. Contreras, *Tetrahedron*, 2002, **58**, 4417–4423.
- 55 P. Jaramillo, L. R. Domingo, E. Chamorro and P. Pérez, *J. Mol. Struct.: THEOCHEM*, 2008, **865**, 68–72.
- 56 L. R. Domingo, J. A. Saéz, R. J. Zaragoza and M. Arnó, *J. Org. Chem.*, 2008, **73**, 8791–8799.
- 57 X. Krokidis, S. Noury and B. Silvi, *J. Phys. Chem. A*, 1997, **101**, 7277–7282.
- 58 J. Andrés, P. González-Navarrete and V. Safont, *Int. J. Quantum Chem.*, 2014, **114**, 1239–1252.
- 59 S. Berski, J. Andrés, B. Silvi and L. R. Domingo, *J. Phys. Chem. A*, 2003, **107**, 6014–6024.
- 60 V. Polo, J. Andrés, S. Berski, L. R. Domingo and B. Silvi, *J. Phys. Chem. A*, 2008, **112**, 7128–7136.
- 61 M. Ríos-Gutiérrez, P. Pérez and L. R. Domingo, *RSC Adv.*, 2015, 58464–58477.

CrossMark
click for updatesCite this: *RSC Adv.*, 2015, 5, 84797

Understanding the high reactivity of carbonyl compounds towards nucleophilic carbenoid intermediates generated from carbene isocyanides

Mar Ríos-Gutiérrez,^a Luis R. Domingo^{*a} and Patricia Pérez^b

The high reactivity of carbonyl compounds towards the carbenoid intermediate *cis*-IN, generated *in situ* by the addition of methyl isocyanide to dimethyl acetylenedicarboxylate (DMAD), has been investigated at the MPWB1K/6-311G(d,p) computational level by using Molecular Electron-Density Theory (MEDT). This multicomponent (MC) reaction is a domino process that comprises two sequential reactions: (i) the formation of a nucleophilic carbenoid intermediate *trans*-IN; and (ii) the nucleophilic attack of *cis*-IN on the carbonyl compound, resulting in the formation of the final 2-iminofuran derivative. The present MEDT study establishes that the high nucleophilic character and the electronic structure of the carbenoid intermediate, *cis*-IN, together with the specific approach mode of the carbonyl C=O double bond during the nucleophilic attack of the sp² hybridised carbenoid C4 center of *cis*-IN on the carbonyl C5 carbon of acetone, enables the formation of the C4–C5 single bond with a very low activation enthalpy, 3.3 kcal mol⁻¹, without any external electrophilic activation of the carbonyl group, and the subsequent ring closure through the downhill formation of the C–O single bond. The Bonding Evolution Theory (BET) study for the formation of the 2-iminofuran allows characterisation of the mechanism as a [2n + 2n] cycloaddition, ruling out the proposed 1,3-dipolar cycloaddition mechanism.

Received 5th August 2015
Accepted 14th September 2015

DOI: 10.1039/c5ra15662a

www.rsc.org/advances

Introduction

Carbene isocyanides **I** are essential building blocks in modern organic chemistry,¹ and it has been reported that these species nucleophilically attack dialkyl acetylenedicarboxylates **II** yielding zwitterionic species **III**, which act as crucial intermediates. These reactive intermediates are readily trapped by several kinds of electrophilic carbon molecules² such as aldehydes,³ ketones,⁴ esters,⁵ and sulfonylimines,⁶ and even carbon dioxide.⁷ When the electrophilic molecules are carbonyl derivatives **IV**, the reaction products are 2-iminofuran derivatives **V** (see Scheme 1). Polyfunctionalised furans are versatile synthetic starting materials for the preparation of a great variety of heterocyclic and acyclic compounds,⁸ and especially 2,5-disubstituted furan-3,4-dicarboxylates, which are very important starting materials in the synthesis of natural products containing tetrahydrofuran rings.⁹

This multicomponent (MC) reaction is a domino process that comprises two consecutive reactions: (i) a nucleophilic attack of the carbene isocyanides **I** on the

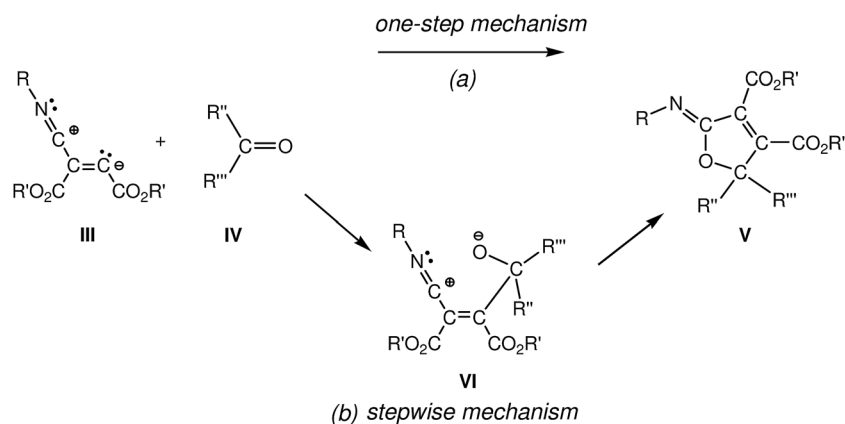
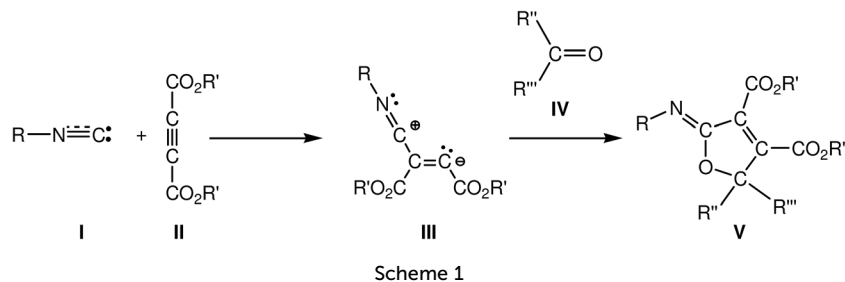
acetylenedicarboxylates **II**, yielding the proposed zwitterionic intermediates **III**; and (ii) the quick capture of these intermediates by a carbonyl derivative **IV** yielding the 2-iminofuran derivatives **V**. This last step has been associated with a 1,3-dipolar cycloaddition reaction in which the zwitterionic intermediate **III** participates as the 1,3-dipole and the carbonyl derivative acts as the dipolarophile.^{3,4}

For this 1,3-dipolar cycloaddition reaction two mechanisms have been proposed (see Scheme 2): (i) a one-step mechanism in which the C–C and C–O bonds are formed in a single step but asynchronously;^{4a} and (ii) a stepwise mechanism in which a new zwitterionic intermediate **VI** is formed through the nucleophilic attack of the zwitterionic intermediate **III** on the carbonyl derivative **IV**; the subsequent cyclisation of this intermediate will yield the 2-iminofuran derivative **V**.^{4b}

Due to the high reactivity evidenced by the intermediate **III** and the significance of the formation of the 2-iminofurans **V** through these MC reactions involving a large diversity of carbonyl derivatives **IV**,^{3–5,7} a Density Functional Theory (DFT) study of the MC reaction between methyl isocyanide **1**, DMAD **2** and acetone **3** yielding 2-iminofuran **4** is performed herein, using Molecular Electron-Density Theory (MEDT) to explain this high reactivity (see Scheme 3). The proposed MEDT, in which the changes in the electron-density and not molecular orbital interactions are considered responsible for reactivity in organic chemistry, uses quantum chemical tools based on the analysis

^aUniversidad de Valencia, Facultad de Química, Departamento de Química Orgánica, Dr Moliner 50, E-46100 Burjassot, Valencia, Spain. E-mail: domingo@utopia.uv.es; Web: <http://www.luisrdomingo.com>

^bUniversidad Andrés Bello, Facultad de Ciencias Exactas, Departamento de Ciencias Químicas, Av. República 230, 8370146, Santiago, Chile



Scheme 2 Proposed mechanisms for the 1,3-dipolar cycloadditions of intermediate III with carbonyl derivatives IV.

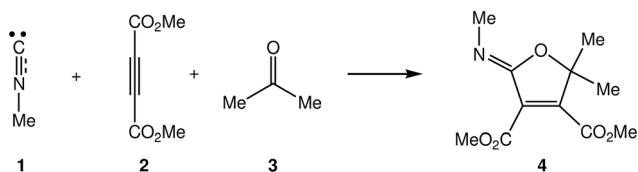
of electron-density, such as the conceptual DFT reactivity indices¹⁰ and the topological Electron Localisation Function¹¹ (ELF) analysis of the changes in the molecular electron-density along the reaction path, in order to establish the molecular mechanism of an organic reaction.

To this end, a theoretical study at the MPWB1K/6-311G(d,p) computational level, in which a combination of (i) the exploration and characterisation of the potential energy surfaces (PESs) associated with the selected domino reaction, (ii) the analysis of the reactivity indices derived from the conceptual DFT for the ground state of the reagents and (iii) the Bonding Evolution Theory¹² (BET) analysis of the two consecutive reactions, was carried out. Three unresolved questions will be answered: (i) what is the electronic structure of the intermediate **III** formed in these domino reactions?; (ii) what is the origin of the high reactivity of the carbonyl compounds **IV** in these MC reactions?; and finally, (iii) what is the mechanism of the

cycloaddition step? As these questions cannot be experimentally resolved, our theoretical study provides valuable information about these MC reactions.

Computational methods

Several studies have shown that the B3LYP functional¹³ is relatively accurate for providing kinetic data, although the reaction exothermicities are underestimated.¹⁴ Truhlar's group has proposed some functionals, such as the MPWB1K functional,¹⁵ which gives good results for combinations of thermochemistry, thermochemical kinetics and other weak interactions. Therefore, in this study the MPWB1K functional was selected together with the standard 6-31G(d) basis set.¹⁶ The optimisations were carried out using the Berny analytical gradient optimisation method.¹⁷ The stationary points were characterised by frequency computations in order to verify that the TSs have one and only one imaginary frequency. The IRC paths¹⁸ were traced in order to check the energy profiles connecting each TS to the two associated minima in the proposed mechanism using the second order González-Schlegel integration method.¹⁹ Solvent effects were taken into account by full optimisation of the gas phase structures at the MPWB1K/6-311G(d,p) level using the polarisable continuum model (PCM) developed by Tomasi's group²⁰ in the framework of the self-consistent reaction field (SCRFF).²¹ The integral equation formalism variant is the SCRFF method used in this work. Several polar solvents such as dichloromethane, benzene and acetonitrile have been used in



Scheme 3 Selected reaction model for the MC reaction of iso-cyanides **I**, acetylenedicarboxylate derivatives **II** and carbonyl compounds **IV**.

these MC reactions. Acetonitrile was selected for the solvent effect calculations since it was used in the reactions of a benzo [b]acridine-6,11-dione acting as the carbonyl derivative.^{4b} The values of enthalpy, entropy and Gibbs free energy in acetonitrile were calculated with the standard statistical thermodynamics at 25 °C and 1 atm.¹⁶ No scaling factor in the thermodynamic calculations was used. The electronic structures of stationary points were characterised by natural bond orbital (NBO) analysis.²²

Conceptual DFT²³ provides different indices to rationalize and understand chemical structure and reactivity.¹⁰ In this sense, the global electrophilicity index,²⁴ ω , is given by the following expression, $\omega = (\mu^2/2\eta)$, in terms of the electronic chemical potential μ and the chemical hardness η . Both quantities may be approached in terms of the one-electron energies of the frontier molecular orbitals HOMO and LUMO, ε_H and ε_L , as $\mu \approx (\varepsilon_H + \varepsilon_L)/2$ and $\eta \approx (\varepsilon_L - \varepsilon_H)$, respectively.²⁵ The empirical (relative) nucleophilicity index,²⁶ N , based on the HOMO energies obtained within the Kohn–Sham scheme,²⁷ is defined as $N = E_{\text{HOMO}}(\text{Nu}) - E_{\text{HOMO}}(\text{TCE})$, where tetracyanoethylene (TCE) is the reference because it presents the lowest HOMO energy in a long series of molecules already investigated in the context of polar organic reactions. This choice allows convenient handling of a nucleophilicity scale of positive values. Nucleophilic P_k^- and electrophilic P_k^+ Parr functions²⁸ were obtained through the analysis of the Mulliken atomic spin density of the corresponding radical cations or anions.

The characterisation of the electron-density reorganisation to evidence the bonding changes along a reaction path is the most attractive method to characterise a reaction mechanism.²⁹ To perform these analyses quantitatively, the BET,¹² consisting of the joint-use of ELF topology and Thom's catastrophe theory³⁰ (CT), proposed by Krokidis *et al.*,¹² is a new tool for analysing the electronic changes in chemical processes. BET has been applied to different elementary reactions,³¹ allowing the molecular mechanism to be established. The ELF topological analysis, $\eta(r)$,³² was performed with the TopMod program³³ using the corresponding MPWB1K/6-311G(d,p) monodeterminantal wavefunctions of the selected structures of the IRC. Non-covalent interactions (NCIs) were computed using the methodology previously described.³⁴ All computations were carried out with the Gaussian 09 suite of programs.³⁵

Results and discussion

The present theoretical study has been divided into four parts: (i) first, the PESs associated with the domino reaction between isocyanide **1**, DMAD **2** and acetone **3** yielding 2-iminofuran **4** are explored and characterised; (ii) then, an analysis of the DFT reactivity indices for the ground state of the reagents involved in this domino process is carried out; (iii) next, a BET study of the two consecutive reactions is performed in order to characterise the molecular mechanism; and finally, (iv) the electronic structure of the intermediate *cis*-**IN** as well as the origin of the high reactivity of carbonyl compounds in these MC reactions are discussed.

(i) Study of the PESs of the MC reaction between methyl isocyanide **1**, DMAD **2** and acetone **3**

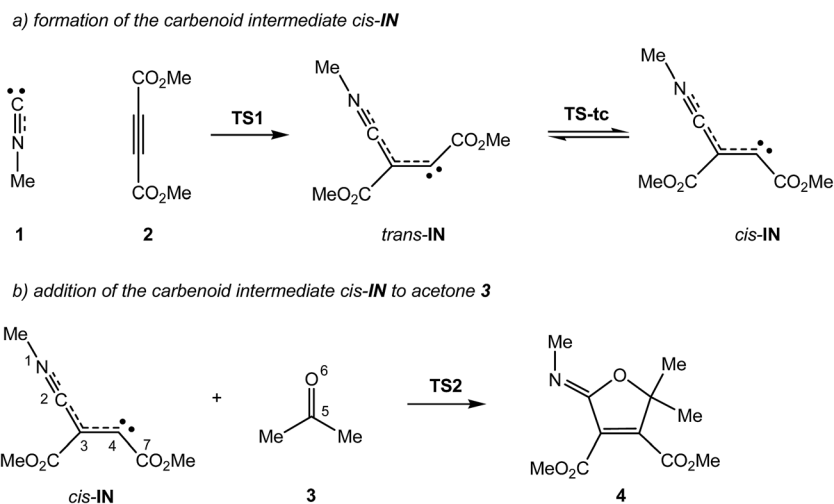
The MC reaction between methyl isocyanide **1**, DMAD **2** and acetone **3** to yield 2-iminofuran **4** is a domino reaction that comprises two addition reactions (see Scheme 4). The first one is the nucleophilic attack of the carbene methyl isocyanide **1** on one of the two electrophilic acetylenic carbon atoms of DMAD **2** to yield the intermediate *trans*-**IN**, which after isomerisation to the intermediate *cis*-**IN** attacks acetone **3**. The total and relative electronic energies of the stationary points involved in the two consecutive processes of the MC reaction between isocyanide **1**, DMAD **2** and acetone **3** are given in Table 1.

The activation energy associated with the nucleophilic attack of carbene methyl isocyanide **1** on DMAD **2**, *via* **TS1**, presents a high value, 17.4 kcal mol⁻¹, with the formation of the intermediate *trans*-**IN** being slightly exothermic, -0.4 kcal mol⁻¹. This intermediate, which presents a *trans* disposition of the two carboxylate groups, undergoes a sp²-sp-sp² rehybridisation process at the C4 carbon *via* **TS-tc** with an estimated activation energy of 9.4 kcal mol⁻¹ to yield *cis*-**IN**, which is 1.4 kcal mol⁻¹ lower in energy than *trans*-**IN**. It is noteworthy that the *cis* rearrangement of the two carboxylate groups at *cis*-**IN** is required for the subsequent addition of acetone **3** followed by the concomitant ring closure. From this intermediate, the formation of 2-iminofuran **4** takes place through the nucleophilic attack of *cis*-**IN** on acetone **3**, followed by a downhill C–O bond formation. This nucleophilic attack *via* **TS2** presents a very low activation energy, 4.1 kcal mol⁻¹, the cycloaddition being strongly exothermic by 88.3 kcal mol⁻¹.

The activation and reaction energies associated with **TS1** and **TS2**, and 2-iminofuran **4**, decrease by 1 kcal mol⁻¹ and 6 kcal mol⁻¹, respectively, when the solvent effects of acetonitrile are considered. On the contrary, the activation and reaction energies associated with **TS-tc**, and *trans*-**IN** and *cis*-**IN**, increase by between 5–7 kcal mol⁻¹. This behaviour is a consequence of the higher solvation of the intermediates *trans*-**IN** and *cis*-**IN** than of the reagents, TSs, and the final product for this MC reaction.

The relative and non-relative enthalpies, entropies and Gibbs free energies of the stationary points involved in the domino reaction between methyl isocyanide **1**, DMAD **2** and acetone **3** are displayed in Table 2. The Gibbs free energy profile including both consecutive processes is graphically represented in Fig. 1. Inclusion of the thermal corrections in the electronic energies does not significantly change the relative enthalpies of the stationary points involved in this MC reaction; those of **TS1**, **TS-tc** and *cis*-**IN** remain almost unchanged but those of *trans*-**IN**, **TS2** and **4** slightly increase by 1–5 kcal mol⁻¹. Inclusion of the entropies in the enthalpies increases the relative Gibbs free energies by between 11 and 33 kcal mol⁻¹, due to the unfavourable entropy associated with this bimolecular reaction.

Thus, the activation Gibbs free energy associated with the first nucleophilic attack of isocyanide **1** on DMAD **2**, *via* **TS1**, is 29.3 kcal mol⁻¹, the formation of the intermediate *trans*-**IN** being endergonic by 7.2 kcal mol⁻¹. The following conversion of *trans*-**IN** into *cis*-**IN** presents an activation Gibbs free energy of



Scheme 4 Domino reaction between methyl isocyanide 1, DMAD 2 and acetone 3.

Table 1 MPWB1K/6-311G(d,p) total (E , in au) and relative^a electronic energies (ΔE , in kcal mol⁻¹), in the gas phase and in acetonitrile, of the stationary points involved in the domino reaction between 1, 2 and 3

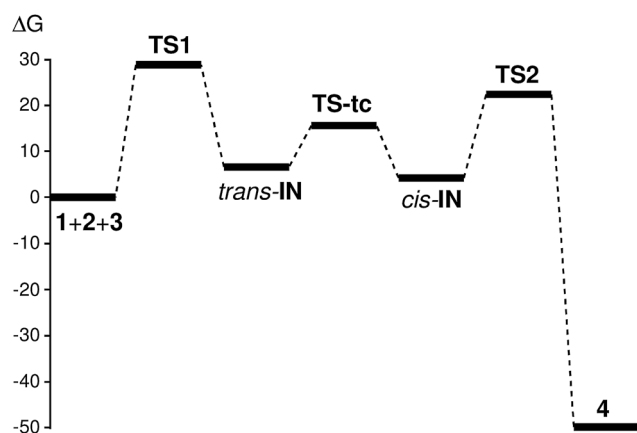
	Gas phase		Acetonitrile	
	E	ΔE	E	ΔE
1	-132.674951		-132.681758	
2	-532.962501		-532.971986	
3	-193.098437		-193.104691	
TS1	-665.609778	17.4	-665.624629	18.3
<i>trans</i> -IN	-665.638068	-0.4	-665.664217	-6.6
TS-tc	-665.622520	9.4	-665.649492	2.7
<i>cis</i> -IN	-665.639621	-1.4	-665.666500	-6.6
TS2	-858.744588	-5.5	-858.765118	-4.2
4	-858.876561	-88.3	-858.888753	-81.8

^a Relative to 1, 2 and 3.Table 2 MPWB1K/6-311G(d,p) enthalpies (H , in au), entropies (S , in cal mol⁻¹ K⁻¹) and Gibbs free energies (G , in au), and relative^a enthalpies (ΔH , in kcal mol⁻¹), entropies (ΔS , in cal mol⁻¹ K⁻¹) and Gibbs free energies (ΔG , in kcal mol⁻¹), at 25 °C and 1 atm in acetonitrile, of the stationary points involved in the domino reaction between 1, 2 and 3

	H	ΔH	S	ΔS	G	ΔG
1	-132.630638		58.298		-132.658324	
2	-532.841793		104.873		-532.891597	
3	-193.013050		71.406		-193.046960	
TS1	-665.442939	18.5	127.102	-36.1	-665.503299	29.3
<i>trans</i> -IN	-665.481317	-5.6	120.401	-42.8	-665.538495	7.2
TS-tc	-665.467932	2.8	118.198	-45.0	-665.524063	16.2
<i>cis</i> -IN	-665.482621	-6.4	125.618	-37.6	-665.542277	4.8
TS2	-858.488597	-2.0	150.779	-83.8	-858.560201	23.0
4	-858.607120	-76.3	143.575	-91.0	-858.675303	-49.2

^a Relative to 1, 2 and 3.

9.0 kcal mol⁻¹ (TS-tc), the conversion being exergonic by 2.4 kcal mol⁻¹. Finally, the cycloaddition reaction of *cis*-IN with acetone 3 via TS2 yields 2-iminofuran 4 with an activation Gibbs

Fig. 1 Gibbs free energy profile (ΔG , in kcal mol⁻¹) of the domino reaction between methyl isocyanide 1, DMAD 2 and acetone 3.

free energy of 23.0 kcal mol⁻¹. The formation of the final cycloadduct 4 is strongly exergonic by 49.2 kcal mol⁻¹.

Some interesting conclusions can be drawn from the Gibbs free energy profile presented in Fig. 1: (i) the first nucleophilic attack of carbene isocyanide 1 on DMAD 2 is the rate-determining step (RDS) of this domino process; (ii) the intermediate *trans*-IN quickly isomerises to *cis*-IN, which is 2.4 kcal mol⁻¹ more stable and whose *cis* disposition is required for the following cycloaddition reaction with acetone 3 to occur; (iii) the activation Gibbs free energy of the cycloaddition reaction of the intermediate *cis*-IN with acetone 3 via TS2 is 6.3 kcal mol⁻¹ lower than that of the RDS of the domino process via TS1; (iv) the strong exergonic character of the cycloaddition reaction between *cis*-IN and acetone 3 makes this process irreversible; and (v) although the formation of the intermediate *cis*-IN is slightly endergonic, as soon as it is formed it is quickly and irreversibly captured by acetone 3 yielding 2-iminofuran 4. Accordingly, the MC reaction between isocyanide 1, DMAD 2 and acetone 3 is kinetically and thermodynamically very favourable.

The geometries of the TSs involved in the domino reaction between methyl isocyanide **1**, DMAD **2** and acetone **3** in acetonitrile are shown in Fig. 2. At **TS1**, associated with the nucleophilic addition of methyl isocyanide **1** to DMAD **2**, the length of the C2–C3 forming bond is 1.973 Å, while at the intermediates *trans*-**IN** and *cis*-**IN** the length of the formed C2–C3 single bond is 1.407 Å. At **TS2**, associated with the cycloaddition reaction of *cis*-**IN** with acetone **3**, the lengths of the C4–C5 and C2–O6 forming bonds are 2.147 and 2.556 Å. The IRC from **TS2** towards the final 2-iminofuran **4** indicates that the second reaction of this MC process is associated with a *two-stage one-step* mechanism³⁶ in which the C4–C5 single bond is completely formed before the formation of the second C2–O6 single bond starts (see later). In addition, this IRC also shows that the carbonyl C5–O6 bond of acetone **3** approaches the intermediate *cis*-**IN** in the C2–C3–C4 plain, in which the two C4–C5 and C2–O6 single bonds will be formed (see **TS2** in Fig. 2). This approach mode is different to that demanded in 1,3-dipolar cycloadditions, in which the dipolarophile approaches over the plain of the 1,3-dipole.

The electronic nature of the nucleophilic addition reaction of carbene isocyanide **1** with DMAD **2**, as well as the cycloaddition reaction of the intermediate *cis*-**IN** with acetone **3**, were analysed by computing the global electron-density transfer (GEDT).³⁷ The natural atomic charges, obtained through a natural population analysis (NPA), were shared between the two frameworks involved in these addition reactions. Thus, the GEDT that fluxes from the carbene isocyanide framework towards the acetylene derivative during the first reaction is 0.26e at **TS1** and 0.62e at *trans*-**IN**, indicating that during the nucleophilic addition of isocyanide **1** to DMAD **2** there is an increase of the GEDT until the maximum value is reached with the formation of the C2–C3 single bond at the intermediate *trans*-

IN. On the other hand, the GEDT that fluxes from the intermediate *cis*-**IN** to the ketone framework during the second process is 0.26e at **TS2**, showing the polar character of the cycloaddition reaction between *cis*-**IN** and acetone **3**. The GEDT values calculated for both reactions emphasise the polar nature of the MC reaction between methyl isocyanide **1**, DMAD **2** and acetone **3**.

(ii) Analysis of the global and local DFT reactivity indices for the ground state of the reagents and of intermediate *cis*-**IN**

Studies devoted to polar organic reactions have shown that the analysis of the reactivity indices defined within conceptual DFT¹⁰ is a powerful tool to understand the reactivity in polar cycloadditions. The global DFT indices, namely, the electronic chemical potential μ , chemical hardness η , global electrophilicity ω and nucleophilicity N , of methyl isocyanide **1**, DMAD **2**, acetone **3** and the intermediate *cis*-**IN** are given in Table 3.

The electronic chemical potential of carbene isocyanide **1**, $\mu = -3.90$ eV, is higher than that of DMAD **2**, $\mu = -5.01$ eV, indicating that for a polar reaction the GEDT³³ will flux from the carbene isocyanide framework towards the electron-deficient acetylene framework. In the same way, the higher electronic chemical potential of the intermediate *cis*-**IN**, $\mu = -3.58$ eV, than that of acetone **3**, $\mu = -3.72$ eV, suggests that for the subsequent cycloaddition reaction between the intermediate *cis*-**IN** and acetone **3**, the GEDT will flux towards the ketone framework.

Methyl isocyanide **1** presents an electrophilicity ω index of 0.66 eV and a nucleophilicity N index of 0.77 eV, being classified on the borderline of moderate electrophiles³⁸ and as a marginal nucleophile.³⁹ Accordingly, carbene isocyanide **1** is considered a weak nucleophile participating in polar reactions and, therefore, a strongly electrophilically activated molecule will be necessary to make the nucleophilic attack of methyl isocyanide **1** feasible.

Polar organic reactions require the participation of good electrophiles and good nucleophiles. Acetylene **5** is one of the poorest electrophilic, $\omega = 0.55$ eV, and nucleophilic, $N = 1.20$ eV, species involved in polar organic reactions, being classified as a marginal electrophile and a marginal nucleophile. Therefore, it cannot participate in polar reactions. The inclusion of two methyl carboxylate groups in the acetylene framework drastically increases the electrophilicity ω index of DMAD **2**, $\omega = 1.40$ eV, being classified as a strong electrophile, and slightly decreases its nucleophilicity N index to $N = 0.91$ eV, remaining

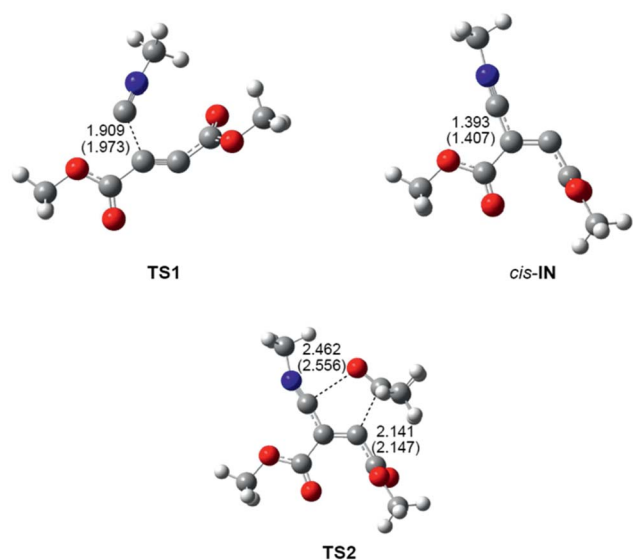


Fig. 2 MPWB1K/6-311G(d,p) geometries of the most important stationary points involved in the domino reaction between methyl isocyanide **1**, DMAD **2** and acetone **3**. Distances are given in Angstroms. Lengths in acetonitrile are given in parentheses.

Table 3 MPWB1K/6-311G(d,p) electronic chemical potential μ , chemical hardness η , global electrophilicity ω and nucleophilicity N , in eV, of methyl isocyanide **1**, DMAD **2**, acetone **3** and intermediate *cis*-**IN**

	μ	η	ω	N
DMAD 2	-5.01	8.95	1.40	0.91
<i>cis</i> - IN	-3.58	6.03	1.06	3.80
Acetone 3	-3.72	9.02	0.77	2.16
Methyl isocyanide 1	-3.90	11.46	0.66	0.77
Acetylene 5	-3.53	11.34	0.55	1.20

classified as a marginal nucleophile. In spite of the strong electrophilic character of DMAD 2, the low nucleophilic character of isocyanide 1 accounts for the high activation energy associated with the nucleophilic addition of isocyanide 1 to DMAD 2 (see above).

Otherwise, the electrophilicity ω and nucleophilicity N indices of the intermediate *cis*-IN, $\omega = 1.06$ eV and $N = 3.80$ eV, allow its classification on the borderline of strong electrophiles and as a strong nucleophile. Acetone 3, which presents an electrophilicity ω index of $\omega = 0.77$ eV and a nucleophilicity N index of $N = 2.16$ eV, will behave as a moderate electrophile and a moderate nucleophile. It is interesting to note that the low electrophilic character of acetone 3 demands its electrophilic activation in order for it to participate in polar reactions.

Recently, the electrophilic P_k^+ and nucleophilic P_k^- Parr functions have been proposed to analyse the local reactivity in polar processes²⁸ involving reactions between a nucleophile–electrophile pair. Accordingly, the electrophilic P_k^+ Parr functions for DMAD 2 and acetone 3, and the nucleophilic P_k^- Parr functions for methyl isocyanide 1 and the intermediate *cis*-IN are analysed (see Fig. 3).

The analysis of the nucleophilic P_k^- Parr functions of carbene isocyanide 1 and *cis*-IN shows that the C2 carbon of isocyanide 1 and the C4 carbon of the intermediate *cis*-IN present the maximum values, $P_k^- = 1.24$ and 1.00, respectively, indicating that these sites are the most nucleophilic centers of these species (see Scheme 4 for atom numbering). From these values two appealing conclusions can be obtained: (i) carbene isocyanide 1 experiences a strong nucleophilic activation at the C2 carbon; and (ii) for the nucleophilic intermediate *cis*-IN, the nucleophilic P_k^- Parr functions are concentrated at the C4 carbon. The strong nucleophilic activation at the C2 carbon of isocyanide 1 is a consequence of the nucleophilic deactivation of the N1 nitrogen atom.

On the other hand, analysis of the electrophilic P_k^+ Parr functions of DMAD 2 indicates that the acetylene C3 and C4 carbons, $P_k^+ = 0.22$, are *ca.* twice as electrophilically activated as the carbonyl carbons, $P_k^+ = 0.13$. Finally, acetone 3 presents its electrophilic activation at the carbonyl carbon atom, $P_k^+ = 0.54$.

Consequently, the most favourable electrophile–nucleophile interaction for the nucleophilic attack of carbene isocyanide 1 on DMAD 2 will take place between the most nucleophilic center of isocyanide 1, the C2 carbon, and the most electrophilic center of DMAD 2, the C3 or C4 carbon. Likewise, the most favourable bond formation for the nucleophilic attack of the

intermediate *cis*-IN on acetone 3 will take place between the most nucleophilic center of the former, the C4 carbon, and the electrophilic carbon atom of acetone 3.

(iii) BET analysis of the domino reaction between methyl isocyanide 1, DMAD 2 and acetone 3

Several theoretical studies have shown that the ELF topological analysis of the changes of electron-density, $\rho(r)$, along a reaction path can be used as a valuable tool to understand the bonding changes along the reaction path, and consequently to establish the molecular mechanisms.²⁹ After an analysis of the electron-density, ELF analysis provides basins of attractors, which are the domains in which the probability of finding an electron pair is maximal.⁴⁰ The spatial points in which the gradient of the ELF has a maximum value are designated as attractors. The basins are classified as core basins and valence basins. The latter are characterised by the synaptic order, *i.e.* the number of atomic valence shells in which they participate. Thus, there are monosynaptic, disynaptic, trisynaptic basins and so on.⁴¹ Monosynaptic basins, labelled V(A), correspond to the lone pairs or non-bonding regions, while disynaptic basins, labelled V(A,B), connect the core of two nuclei A and B and, thus, correspond to a bonding region between A and B. This description recovers the Lewis bonding model, providing a very suggestive graphical representation of the molecular system.

ELF topological analysis of the structures involved in an elementary step mainly allows characterisation of three types of valence basins: (i) protonated basins, V(A,H); (ii) monosynaptic basins, V(A), associated with lone pairs or non-bonding regions; and (iii) disynaptic basins, V(A,B), associated with bonding regions. A set of ELF valence basins topologically characterises a molecular structure. Analysis of changes in the number or type of valence basins of the structures involved along the IRC of the reaction allows the establishment of a set of points, **Pi**, defining the different phases that topologically characterise a molecular mechanism. The further analysis of the different phases characterised by these significant points permits its characterisation.³¹

Herein, a BET study of the MC reaction between isocyanide 1, DMAD 2 and acetone 3 is performed in order to gain insight into how the bonding changes take place during this domino reaction, and thus, to establish the molecular mechanism of the two consecutive reactions.

(iii.a) BET study of the nucleophilic addition reaction of methyl isocyanide 1 with DMAD 2.

The BET study of the nucleophilic addition reaction of the carbene methyl isocyanide 1 to DMAD 2 indicates that this reaction is topologically characterised by six differentiated phases. The population of the most significant valence basins of the selected points of the IRC is included in Table 4. The attractor positions of the ELF for the relevant points along the IRC are shown in Fig. 4, while the basin-population changes along the reaction path are graphically represented in Fig. 5.

Phase I, $3.73 \text{ \AA} \geq d(\text{C2}–\text{C3}) > 2.28 \text{ \AA}$, begins at the molecular complex **MC1**, $d(\text{C2}–\text{C3}) = 3.726 \text{ \AA}$, being a minimum in the PES connecting **TS1** with the separated reagents 1 and 2. The ELF

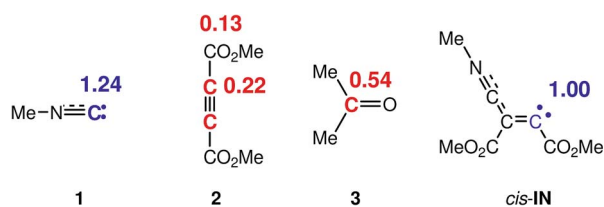


Fig. 3 Nucleophilic P_k^- Parr functions, in blue, and electrophilic P_k^+ Parr functions, in red, in methyl isocyanide 1, DMAD 2, acetone 3 and intermediate *cis*-IN.

Table 4 Valence basin populations N calculated from the ELF analysis of the IRC points, **P1**–**P5**, defining the six phases characterising the molecular mechanism associated with the addition reaction between carbene isocyanide **1** and DMAD **2**. The stationary points **MC1**, *trans*-**IN** and *cis*-**IN** are also included. Distances are given in Å, while the GEDTs that were obtained by NPA are given in e

Phases	I	II	III	IV	V	VI	<i>trans</i> - IN	<i>cis</i> - IN
	MC1	P1	P2	P3	P4	P5		
$d(\text{C2}-\text{C3})$	3.726	2.282	2.033	1.897	1.551	1.399	1.396	1.393
GEDT	0.00	0.07	0.18	0.27	0.54	0.60	0.62	0.65
$V(\text{N1},\text{C2})$	3.81	3.15	5.12	5.13	4.71	4.40	5.52	3.19
$V'(\text{N1},\text{C2})$	1.29	2.00						2.32
$V(\text{C3},\text{C4})$	2.68	2.37	2.23	2.10	1.73	3.10	3.13	3.14
$V'(\text{C3},\text{C4})$	2.65	2.48	2.16	2.02	1.74			
$V(\text{C2})$	2.65	2.58	2.52					
$V(\text{C2},\text{C3})$				2.55	2.66	2.73	2.71	2.65
$V(\text{C4})$		0.52	1.06	1.31	1.75	1.90	1.97	2.06
$V(\text{N1})$					0.66	1.20		

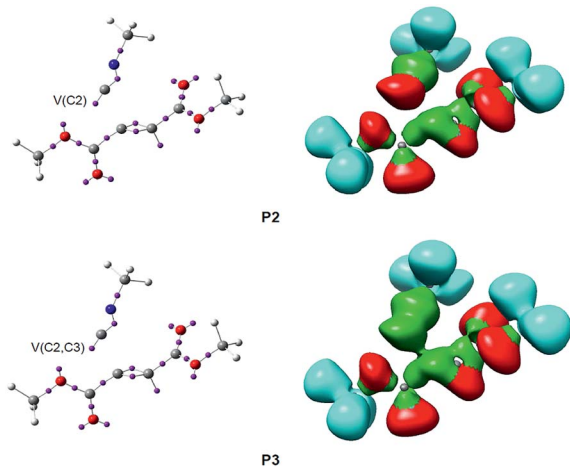


Fig. 4 ELF attractor positions and basins for the most relevant points along the IRC associated with the formation of the C2–C3 single bond during the nucleophilic addition reaction of methyl isocyanide **1** with DMAD **2**. Disynaptic basins are coloured in green and monosynaptic basins are in red.

picture of **MC1** exhibits the topological characteristics of the separated reagents. ELF analysis of **MC1** shows two $V(\text{N1},\text{C2})$ and $V'(\text{N1},\text{C2})$ disynaptic basins with a population of $3.81e$ and $1.29e$, associated with the $\text{N1}\equiv\text{C2}$ triple bond region of the isocyanide framework, and one $V(\text{C2})$ monosynaptic basin integrating for $2.65e$ related to the C2 carbon lone pair. In addition, the ELF topology of **MC1** also shows the presence of two $V(\text{C3},\text{C4})$ and $V'(\text{C3},\text{C4})$ disynaptic basins with populations of $2.41e$ and $2.46e$ belonging to the $\text{C3}\equiv\text{C4}$ triple bond of the acetylene framework.

Phase II, $2.28 \text{ \AA} \geq d(\text{C2}-\text{C3}) > 2.03 \text{ \AA}$, starts at **P1**. The first noticeable topological change along the IRC occurs in this phase; a new $V(\text{C4})$ monosynaptic basin, integrating for $0.53e$, is created at **P1**. The electron-density of this basin mainly proceeds from the depopulation of the $\text{C3}\equiv\text{C4}$ triple bond region until the $V(\text{C3},\text{C4})$ and $V'(\text{C3},\text{C4})$ disynaptic basins reach

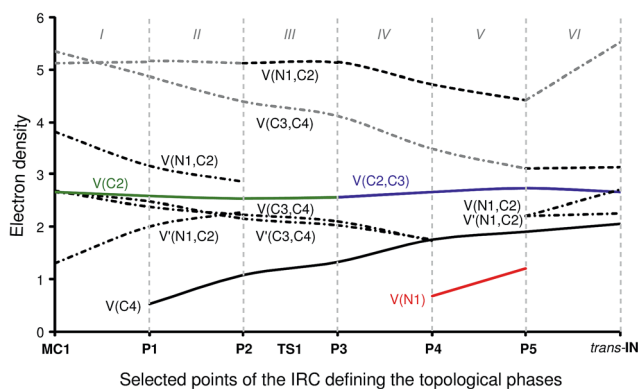


Fig. 5 Graphical representation of the basin population changes during the cycloaddition reaction between methyl isocyanide **1** and DMAD **2**. Point dotted curves in grey represent the sum of disynaptic basins describing a bond region or monosynaptic basins describing lone pairs.

a total population of $4.85e$. Note that the new $V(\text{C4})$ monosynaptic basin is associated with the non-bonding sp^2 hybridised lone pair present at the C4 carbon of the nucleophilic intermediate *cis*-**IN**. On the other hand, the population of the $V(\text{C2})$ monosynaptic basin slightly decreases. The GEDT has increased to a small extent, $0.07e$.

Phase III, $2.03 \text{ \AA} \geq d(\text{C2}-\text{C3}) > 1.90 \text{ \AA}$, begins at **P2**. At this point, the two $V(\text{N1},\text{C2})$ and $V'(\text{N1},\text{C2})$ disynaptic basins present at **MC1** have merged into a new $V(\text{N1},\text{C2})$ disynaptic basin integrating for $5.12e$. This topological change is simply the consequence of electron-density redistribution in the N1–C2 bonding region. In this phase, the TS of the reaction, **TS1**, $d(\text{C2}-\text{C3}) = 1.909 \text{ \AA}$, is found. For this structure, only scanty changes in the electron-density distribution with respect to those found at **P1** are observed with the exception that the population of the $V(\text{C4})$ monosynaptic basin has increased to $1.06e$. The GEDT has increased to $0.18e$.

At phase IV, $1.90 \text{ \AA} \geq d(\text{C2}-\text{C3}) > 1.55 \text{ \AA}$, which begins at **P3**, the most significant topological change along the reaction path takes place. The $V(\text{C2})$ monosynaptic basin present at **P2** is converted into a new $V(\text{C2},\text{C3})$ disynaptic basin with an initial population of $2.55e$ (see **P2** and **P3** in Fig. 4 and the change from $V(\text{C1})$, in green in **P2**, to $V(\text{C2},\text{C3})$, in blue in **P3**, in Fig. 5). In spite of the unexpected position of the $V(\text{C1})$ ELF attractor, the depiction of the valence basins associated with **P3** shows the disynaptic character of the corresponding basin (see **P3** in Fig. 4). This relevant topological change indicates that the formation of the new C2–C3 single bond has already begun at a distance of 1.90 \AA with a high electron-density population. In addition, the $V(\text{C4})$ monosynaptic basin increases its population to $1.31e$ together with the decrease of the total population of the $V(\text{C3},\text{C4})$ and $V'(\text{C3},\text{C4})$ disynaptic basins to $4.12e$, which indicates that the C3–C4 bonding region has just acquired its double bond character. At **P3**, the GEDT is $0.27e$.

Phase V, $1.55 \text{ \AA} \geq d(\text{C2}-\text{C3}) > 1.40 \text{ \AA}$, starts at **P4**. At this point a new $V(\text{N1})$ monosynaptic basin appears with a population of $0.66e$ as a consequence of the depopulation of the $V(\text{N1},\text{C2})$

disynaptic basin to $4.71e$. The electron-density of the $V(C3,C4)$ and $V'(C3,C4)$ disynaptic basins continues to decrease until it reaches a population of $3.47e$, while the $V(C4)$ monosynaptic basin has increased to $1.75e$. The GEDT significantly increases to $0.54e$.

Finally, the extremely short phase VI, $1.40 \text{ \AA} \geq d(C2-C3) \geq 1.39 \text{ \AA}$, begins at **P5** and ends at the nucleophilic intermediate *trans*-IN, $d(C2-C3) = 1.396 \text{ \AA}$. At **P5**, the two $V(C3,C4)$ and $V'(C3,C4)$ disynaptic basins merge into one $V(C3,C4)$ disynaptic basin integrating for $3.10e$, whereas the $V(C4)$ monosynaptic basin has received almost the population of a lone pair, $1.90e$. Besides, while the $V(N1,C2)$ disynaptic basin decreases by $0.31e$, the $V(N1)$ monosynaptic and $V(C2,C3)$ disynaptic basins increase their populations to $1.20e$ and $2.73e$, respectively. At **P5**, the maximum GEDT for the reaction takes place, $0.60e$. From **P5** to *trans*-IN, the most noticeable topological change is the disappearance of the $V(N1)$ monosynaptic basin simultaneously to the significant increase of the population of the $V(N1,C2)$ disynaptic basin to $5.52e$. At *trans*-IN, the $V(C3,C4)$ disynaptic basin presents a population of $3.10e$, indicating that the C3–C4 bonding region is very polarised towards the C2–C3 single bond created at phase IV, which is characterised by one $V(C2,C3)$ disynaptic basin integrating for $2.71e$. Finally, the $V(C4)$ monosynaptic basin associated with the C4 carbon lone pair has a population of $1.97e$. The GEDT computed at *trans*-IN, $0.62e$, is very high.

(iii.b) BET study of the reaction between intermediate *cis*-IN and acetone 3. The study of the nucleophilic attack of the intermediate *cis*-IN on acetone 3 shows that this reaction can be topologically characterised by eight differentiated phases. The populations of the most significant valence basins of the selected points of the IRC are compiled in Table 5. The attractor positions of the ELF for relevant points along the IRC are shown in Fig. 6, while the basin population changes along the reaction path are graphically represented in Fig. 7.

Phase I, $3.69 \text{ \AA} \geq d(C4-C5) > 2.80 \text{ \AA}$ and $3.09 \text{ \AA} \geq d(C2-O6) > 3.00 \text{ \AA}$, begins at the molecular complex **MC2**, $d(C4-C5) = 3.687 \text{ \AA}$ and $d(C2-O6) = 3.090 \text{ \AA}$, which is a minimum in the PES connecting the intermediate *cis*-IN and acetone 3 with the corresponding **TS2**. The ELF picture of **MC2** shows the topological behaviour of the separated reagents. Three disynaptic basins, $V(N1,C2)$, $V(C2,C3)$ and $V(C3,C4)$ integrating for $5.50e$, $2.60e$ and $3.17e$, respectively, can be observed, which are associated with the N1–C2–C3–C4 bonding region of the intermediate *cis*-IN.

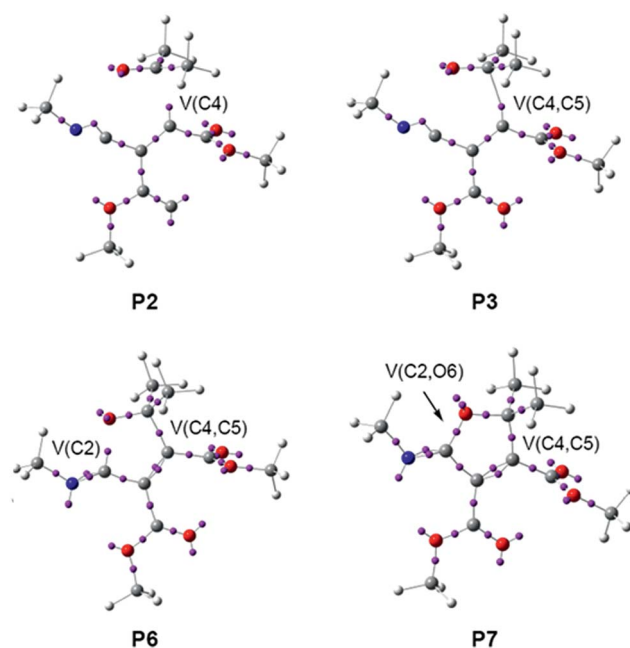


Fig. 6 ELF attractor positions for the most relevant points along the IRC associated with the formation of the C4–C5 and C2–O6 single bonds during the cycloaddition reaction of intermediate *cis*-IN with acetone 3.

Table 5 Valence basin populations N calculated from the ELF analysis of the IRC points, **P1**–**P7**, defining the eight phases characterising the molecular mechanism associated with the cycloaddition reaction between nucleophilic intermediate *cis*-IN and acetone 3. The stationary points **MC2** and **4** are also included. Distances are given in \AA , while the GEDTs obtained by NPA are given in e

Phases	I MC2	II P1	III P2	IV P3	V P4	VI P5	VII P6	VIII P7	4
$d(C4-C5)$	3.687	2.798	2.338	2.141	2.070	1.908	1.645	1.578	1.502
$d(C2-O6)$	3.090	3.007	2.623	2.462	2.412	2.288	1.953	1.746	1.370
GEDT	0.00	0.04	0.16	0.26	0.31	0.40	0.39	0.32	0.19
$V(N1,C2)$	5.50	1.78	5.48	5.53	4.75	2.14	1.83	1.72	1.64
$V'(N1,C2)$		3.70				2.09	1.84	1.74	1.63
$V(N1)$					0.8	1.48	2.26	2.48	2.67
$V(C2,C3)$	2.60	2.63	2.6	2.59	2.61	2.6	2.47	2.39	2.34
$V(C3,C4)$	3.17	3.16	3.24	3.27	1.68	1.64	1.71	1.73	1.73
$V'(C3,C4)$					1.61	1.68	1.68	1.68	1.69
$V(O6)$	2.64	2.65	2.71	2.85	2.82	2.94	2.92	2.71	2.24
$V'(O6)$	2.64	2.70	2.77	2.81	2.87	2.96	2.99	2.69	2.52
$V(C5,O6)$	2.39	2.41	2.23	2.18	2.06	1.77	1.53	1.41	1.43
$V(C4)$	2.05	2.00	1.92						
$V(C4,C5)$				1.87	1.89	1.94	2.05	2.06	2.09
$V(C2)$							0.20		
$V(C2,O6)$								0.75	1.49

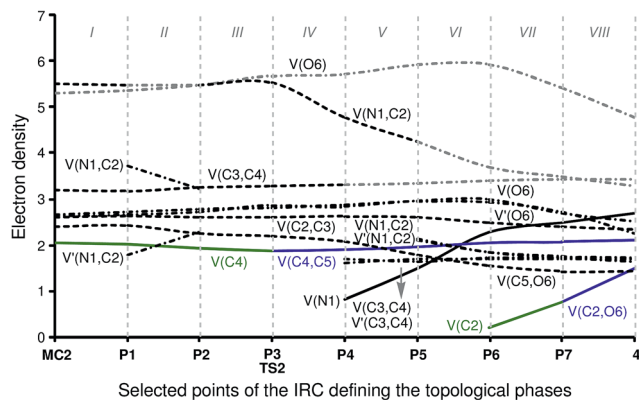


Fig. 7 Graphical representation of the basin population changes during the cycloaddition reaction between nucleophilic intermediate *cis*-IN and acetone **3**. Point dotted curves in grey represent the sum of disynaptic basins describing a bond region or monosynaptic basins describing lone pairs.

The most important characteristic of this framework is the presence of one $V(C4)$ monosynaptic basin with a population of $2.05e$, which is associated with the non-bonding sp^2 hybridised lone pair present on the C4 carbon. On the other hand, the ELF analysis of **MC2** also shows the presence of two monosynaptic basins, $V(O6)$ and $V'(O6)$, with populations of $2.64e$ and $2.64e$, associated with the O6 oxygen lone pairs, and one $V(C5,O6)$ disynaptic basin integrating for $2.39e$ which belongs to the C–O bonding region of acetone **3**. The low population of the C–O bond together with the high population of the oxygen lone pairs indicates that the C–O bond of acetone **3** is very polarised.

Phase II, $2.80 \text{ \AA} \geq d(C4-C5) > 2.33 \text{ \AA}$ and $3.00 \text{ \AA} \geq d(C2-O6) > 2.62 \text{ \AA}$, begins at **P1**. In this phase the most relevant changes imply the splitting of the $V(N1,C2)$ disynaptic basin into two $V(N1,C2)$ and $V'(N1,C2)$ disynaptic basins with populations of $1.78e$ and $3.70e$, and a slight decrease in the population of the $V(C4)$ monosynaptic basin to $2.00e$. The other basins maintain their populations as shown in phase I. On the acetone framework, the population of the $V(C5,O6)$ disynaptic basin is $2.41e$, while the two $V(O6)$ and $V'(O6)$ monosynaptic basins integrate for $2.65e$ and $2.70e$, respectively.

Phase III, $2.34 \text{ \AA} \geq d(C4-C5) > 2.14 \text{ \AA}$ and $2.62 \text{ \AA} \geq d(C2-O6) > 2.46 \text{ \AA}$, begins at **P2**. At this point, the $V(N1,C2)$ and $V'(N1,C2)$ disynaptic basins newly merge into one disynaptic basin $V(N1,C2)$ integrating for $5.58e$, while the population of the $V(C4)$ monosynaptic basin has slightly decreased to $1.92e$ on the *cis*-IN moiety. The populations of the $V(O6)$ and $V'(O6)$ monosynaptic basins slightly increase to $2.71e$ and $2.77e$ for the acetone framework. These changes can be related to the GEDT that fluxes from *cis*-IN to acetone **3** during this polar reaction.

Phase IV, $2.14 \text{ \AA} \geq d(C4-C5) > 2.07 \text{ \AA}$ and $2.46 \text{ \AA} \geq d(C2-O6) > 2.41 \text{ \AA}$, begins at **P3**, which corresponds to the TS of the reaction, **TS2**, $d(C4-C5) = 2.141 \text{ \AA}$ and $d(C2-O6) = 2.462 \text{ \AA}$. At this point, the first most relevant change along the IRC is found; while the $V(C4)$ monosynaptic basin present in *cis*-IN has disappeared, a new $V(C4,C5)$ disynaptic basin, integrating for

$1.87e$, has appeared (see **P2** and **P3** in Fig. 6 and the change from $V(C4)$, in green in **P2**, to $V(C4,C5)$, in blue in **P3**, in Fig. 7). This change indicates that the formation of the new C4–C5 single bond has started at $d(C4-C5) = 2.14 \text{ \AA}$.

Phase V, $2.07 \text{ \AA} \geq d(C4-C5) > 1.91 \text{ \AA}$ and $2.41 \text{ \AA} \geq d(C2-O6) > 2.29 \text{ \AA}$, starts at **P4**. After passing **TS2**, the most important change is the formation of a new $V(N1)$ monosynaptic basin, which integrates for $0.80e$, together with the depopulation of the $V(N1,C2)$ disynaptic basin to $4.75e$. At this point, the $V(C3,C4)$ disynaptic basin present in *cis*-IN splits into two disynaptic basins, $V(C3,C4)$ and $V'(C3,C4)$, integrating for $1.68e$ and $1.61e$, respectively. In addition, the population of the $V(C4,C5)$ disynaptic basin slightly increases to $1.89e$, and the populations of the $V(O6)$ and $V'(O6)$ monosynaptic basins of the acetone framework increase to $2.82e$ and $2.87e$.

Phase VI, $1.91 \text{ \AA} \geq d(C4-C5) > 1.65 \text{ \AA}$ and $2.29 \text{ \AA} \geq d(C2-O6) > 2.14 \text{ \AA}$, starts at **P5**. At this point, the $V(N1,C2)$ disynaptic basin of the intermediate moiety newly splits into two $V(N1,C2)$ and $V'(N1,C2)$ disynaptic basins, which integrate for $2.14e$ and $2.09e$, respectively, while the $V(N1)$ monosynaptic basin reaches a population of $1.48e$. On the acetone moiety, it may be seen that there is a depopulation of the $V(C5,O6)$ disynaptic basin to $1.77e$ and a slight increase of the population of the $V(O6)$ and $V'(O6)$ monosynaptic basins to $2.94e$ and $2.96e$.

The short phase VII, $1.65 \text{ \AA} \geq d(C4-C5) > 1.58 \text{ \AA}$ and $1.95 \text{ \AA} \geq d(C2-O6) > 1.75 \text{ \AA}$, starts at **P6**. At this point, the second relevant topological change along the IRC takes place: a $V(C2)$ monosynaptic basin is created at the C2 carbon, integrating for $0.20e$ (see the $V(C2)$ monosynaptic basin in **P6** in Fig. 6). This change shows the preparation of the intermediate fragment for the subsequent ring closure through the C–O bond formation. In this phase, the population of the $V(C4,C5)$ disynaptic basin increases to $2.05e$ and the population of the $V(N1)$ monosynaptic basin increases to $2.26e$, whereas the populations of the $V(C5,O6)$, $V(N1,C2)$ and $V'(N1,C2)$ disynaptic basins decrease to $1.53e$, $1.83e$ and $1.84e$, respectively, along with the progressing reaction.

Phase VIII, $1.58 \text{ \AA} \geq d(C4-C5) \geq 1.50 \text{ \AA}$ and $1.75 \text{ \AA} \geq d(C2-O6) \geq 1.37 \text{ \AA}$, starts at **P7** and ends at cycloadduct **4**, $d(C4-C5) = 1.502 \text{ \AA}$ and $d(C2-O6) = 1.370 \text{ \AA}$. At this point, the third most relevant change takes place with the formation of a new $V(C2,O6)$ disynaptic basin integrating for $0.75e$ (see the $V(C2,O6)$ disynaptic basin in **P7** in Fig. 6 and the change from $V(C2)$, in green in **P6**, to $V(C2,O6)$, in blue in **P7**, in Fig. 7), while the populations of the $V(O6)$ and $V'(O6)$ monosynaptic basins have slightly decreased to $2.71e$ and $2.69e$. This change indicates that the formation of the second C2–O6 single bond has started at a distance of 1.75 \AA . At 2-iminofuran **4**, the $V(C2,O6)$ disynaptic basin reaches a population of $1.49e$, while the $V(C4,C5)$ disynaptic basin shows a population of $2.09e$. The low population of the $V(C2,O6)$ disynaptic basin indicates a very polarised C2–O6 single bond.

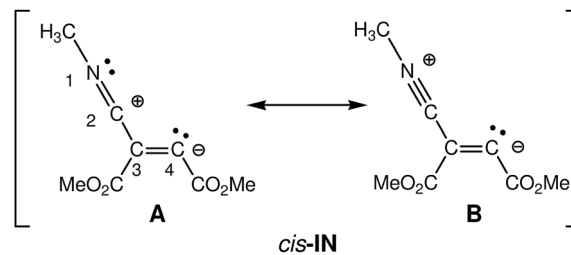
From the BET analysis of this domino reaction some appealing conclusions can be drawn: (i) during the nucleophilic attack of methyl isocyanide **1** on DMAD **2**, the C2–C3 bond is formed at a distance of 1.90 \AA through the donation of the electron-density of the carbene C2 lone pair to one of the two

acetylenic carbons of DMAD 2; (ii) the formation of the new C2–C3 bond takes place with a high electron-density, $2.55e$. Note that this value is higher than that associated with a C–C single bond; (iii) during the nucleophilic attack of isocyanide 1 on DMAD 2, a new $V(C4)$ monosynaptic basin with an initial population of $0.52e$ appears at the C4 carbon as a consequence of the depopulation of the acetylenic C3–C4 bonding region. This $V(C4)$ monosynaptic basin reaches a population of $2.06e$ at the intermediate *cis*-IN, while at the same time the C3–C4 bonding region is depopulated to reach $3.14e$; (iv) during the nucleophilic attack of *cis*-IN on acetone 3, the formation of the C4–C5 single bond begins at a distance of 2.14 \AA through the donation of the electron-density of the carbenoid C4 lone pair of *cis*-IN to the carbonyl C5 carbon of acetone 3; (v) formation of the second C2–O6 single bond takes place at the end of the cycloaddition path at a distance of 1.75 \AA by sharing the electron-density of the $V(C2)$ monosynaptic basin present at the C2 carbon and some of the electron-density of the monosynaptic basins associated with the oxygen O6 lone pairs; (vi) formation of the C2–O6 single bond begins after the complete formation of the C4–C5 bond, characterising the mechanism of the cycloaddition as a non-concerted *two-stage one-step* mechanism;³⁶ and finally (vii) during the cycloaddition step, the $N1 \equiv C2$ triple bond of *cis*-IN becomes a double bond characterised by the presence of two $V(N1, C2)$ and $V'(N1, C2)$ disynaptic basins at 2-iminofuran 4. At the same time, the C2 carbon is rehybridised from sp for *cis*-IN to sp^2 for 2-iminofuran 4 as a consequence of the formation of the C2–O6 single bond. The orthogonal character of the new C2–O6 single bond with respect to the exocyclic $N1-C2$ double bond present in 2-iminofuran 4 indicates that the $N1-C2$ triple bond and C3–C4 double bond regions of the intermediate *cis*-IN do not participate directly in the cycloaddition reaction, as expected in a 1,3-dipole participating in a 1,3-dipolar cycloaddition.

Both analysis of the atomic movements of the *cis*-IN and acetone 3 molecules along the IRC associated with the cycloaddition step and the corresponding BET analysis indicate that the electron-density of the carbenoid C4 carbon and the carbonyl O6 oxygen lone pairs mainly participate in the formation of the C4–C5 and C2–O6 single bonds during the reaction; consequently, this cycloaddition should be classified as $[2n + 2n]$, in which two lone pairs are involved, and not as a $[4\pi + 2\pi]$ 1,3-dipolar cycloaddition.

(iv) What is the electronic structure of intermediate *cis*-IN and the origin of the high reactivity of carbonyl compounds towards this intermediate?

At first, the intermediate *cis*-IN can be represented by either of the Lewis resonant structures A and B given in Scheme 5. Both structures would represent a zwitterionic intermediate in which the negative charge is located at the C4 carbon atom, while the positive charge can be located at the C2 or N1 atoms belonging to the methyl isocyanide framework. Experimental chemists represent *cis*-IN by means of the 1,3-zwitterionic structure A, since it justifies the participation of *cis*-IN in a $[3 + 2]$ cycloaddition towards carbonyl derivatives.



Scheme 5 Lewis structures representing zwitterionic intermediate *cis*-IN.

NPA and ELF analysis of the electronic structure of the intermediate *cis*-IN yield different representations for this intermediate. NPA of *cis*-IN clearly shows the zwitterionic character of this intermediate: while the methyl isocyanide framework is positively charged, the DMAD framework is negatively charged (see Fig. 8a). However, while NPA indicates that the positive charge is mainly located at the C2 carbon, in agreement with Lewis structure A, the results also indicate that the negative charge is mainly located at the C3 carbon and the carboxylate oxygen atoms, the C4 carbon having a negligible negative charge of $-0.07e$.

On the other hand, the ELF topology of *cis*-IN shows the presence of a monosynaptic basin at C4, $V(C4)$, integrating for $2.07e$ (see Fig. 8b). In addition, the C3–C4 double bond regions of the Lewis structures A and B have a noticeable depopulation, $3.14e$. This behaviour can account for the negligible negative charge found at the C4 carbon, $-0.07e$ and thus both Lewis structures, A and B, can be ruled out as representations for the intermediate *cis*-IN.

Consequently, in spite of the zwitterionic character of the intermediate *cis*-IN, it appears that the reactivity of this intermediate towards carbonyl compounds cannot be related to its zwitterionic character but rather to the singlet carbenoid character of the C4 carbon that grants a high nucleophilic character to this molecule (see the C4 carbon in green in Fig. 8c).

In order to explain the high reactivity of acetone 3 towards this intermediate, an analysis of the molecular electrostatic potential (MEP) at *cis*-IN and the corresponding TS2 was also performed (see Fig. 9). The MEP of *cis*-IN allows two appealing conclusions to be reached: (i) around the nucleophilic C4 carbon a low negative electrostatic potential (in red) is found

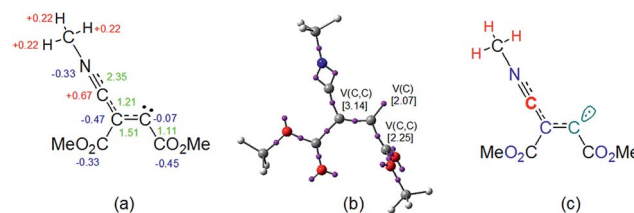


Fig. 8 Electronic representation of the structure of carbenoid intermediate *cis*-IN based on (a) NPA, (b) ELF analysis and (c) the mixture of both analyses. Green values in (a) indicate the bond order of the corresponding bond.

(see Fig. 9a). Note that the carboxylate oxygen atoms show the highest values. This behaviour is in agreement with the unappreciable negative charge found at the C4 atom; (ii) interestingly, the region of MEP with the highest positive value of *cis*-IN corresponds to the methyl substituent present in the isocyanide framework.

The MEP of the carbenoid intermediate *cis*-IN shows the special characteristic of this intermediate that favours the nucleophilic attack on carbonyl derivatives. As can be seen in Fig. 9, the analysis of the MEP of TS2 clearly shows that during the nucleophilic attack of *cis*-IN on acetone 3, the GEDT that takes place in this polar process gives rise to an increase of electron-density of the oxygen carbonyl atom. This feature, which is unfavourable in an uncatalysed nucleophilic addition to carbonyl compounds, is favoured in TS2 by the presence of the positively charged methyl group that electrostatically stabilises the negative charge developed at the carbonyl oxygen atom (see Fig. 9b). Note that during the formation of the first C4–C5 single bond, the GEDT that takes place from *cis*-IN to acetone 3, $0.40e$ at P5, mainly locates the electron-density at the carbonyl oxygen atom (see the integration of the V(O6) and V'(O6) monosynaptic basins at P5 in Table 5).

Finally, in order to rule out a stabilisation of TS2 by a hydrogen bond between the carbonyl oxygen atom and one hydrogen atom of the methyl group, an analysis of the NCI at TS2 was performed. As can be seen in Fig. 9c, although some weak interactions between the carbonyl oxygen atom and the methyl isocyanide framework appear (in green), no hydrogen bond interaction between the carbonyl oxygen and the hydrogen of the methyl group is observed. Note that strong hydrogen bonds appear as a dark turquoise surface. Indeed, the NCI between the carbonyl O6 oxygen atom and the C2 carbon of the isocyanide framework is stronger than that involving the hydrogen of the methyl group, indicating the favourable interaction preceding the C2–O6 single bond formation.

Consequently, we can conclude that the high reactivity of the intermediate *cis*-IN towards carbonyl derivatives is due to two specific features: (i) the carbenoid character of the sp^2 hybridised C4 carbon rather than the negative charge on a carbanionic center and, (ii) the special geometric disposition of the alkyl substituents in isocyanides that electrostatically favours the GEDT during the nucleophilic attack of these carbenoid intermediates on carbonyl compounds.

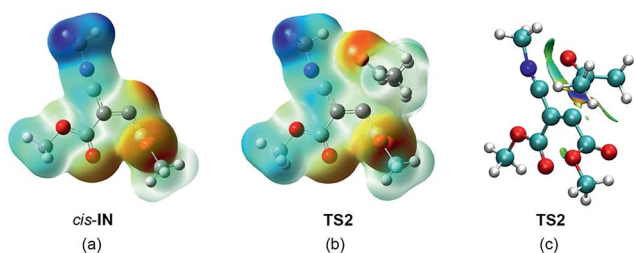


Fig. 9 The MEP of carbenoid intermediate *cis*-IN (a) and TS2 (b), and NCIs for TS2 (c).

Conclusions

The high reactivity of acetone 3 towards the nucleophilic carbenoid intermediate *cis*-IN, generated *in situ* by the addition of methyl isocyanide 1 to DMAD 2, has been studied using DFT methods at the MPWB1K/6-311G(d,p) computational level through the combination of the exploration and characterisation of the PESs associated with this MC reaction and analysis based on the MEDT, consisting of the analysis of the reactivity indices derived from the conceptual DFT at the ground state of the reagents and the BET study for the corresponding reaction paths.

This MC reaction is a domino process that comprises two consecutive reactions: (i) formation of the carbenoid intermediate *trans*-IN, which quickly equilibrates with the thermodynamically more stable *cis*-IN; and (ii) the nucleophilic capture of acetone 3 by the carbenoid intermediate *cis*-IN yielding the formation of the final 2-iminofuran 4.

Analysis of the relative Gibbs free energies in acetonitrile indicates that while the initial nucleophilic attack of the carbene methyl isocyanide 1 on DMAD 2 is the RDS of this MC reaction, once the intermediate *cis*-IN is formed, it quickly and irreversibly captures acetone 3.

Analysis of the DFT reactivity indices for the intermediate *cis*-IN clearly accounts for its high nucleophilic character, entirely at the carbenoid C4 carbon. These behaviours explain the high reactivity of the intermediate *cis*-IN in polar reactions towards electron-deficient carbonyl compounds.

BET analysis of the two reactions involved in this domino process makes it possible to draw some appealing conclusions concerning the bonding changes occurring in this MC reaction: (i) during the nucleophilic attack of isocyanide 1 on DMAD 2, the C2–C3 bond is formed at a distance of 1.90 Å through the donation of the electron-density of the carbene C2 lone pair to one of the two acetylenic carbons of DMAD. Formation of this C2–C3 bond takes place with a high electron-density, $2.55e$; (ii) during the nucleophilic attack of isocyanide 1 on DMAD 2, a new V(C4) monosynaptic basin with an initial population of $0.52e$ appears at the C4 carbon as a consequence of the depopulation of the acetylenic C3–C4 triple bond. This V(C4) monosynaptic basin reaches a population of $2.06e$ for the intermediate *cis*-IN; (iii) during the nucleophilic attack of *cis*-IN on acetone 3, the formation of the C4–C5 single bond begins at a distance of 2.14 Å through the donation of the electron-density of the carbenoid C4 lone pair of *cis*-IN to the carbonyl C5 carbon of acetone 3; (iv) formation of the second C2–O6 single bond takes place at the end of the cycloaddition path at a distance of 1.75 Å by sharing the electron-density of the V(C2) monosynaptic basin present at the C2 carbon and some electron-density of the monosynaptic basins associated with the O6 oxygen lone pairs; and (v) formation of the C2–O6 single bond begins after the complete formation of the C4–C5 bond. This behaviour characterises the mechanism of the cycloaddition as a non-concerted *two-stage one-step* mechanism.³⁶

An analysis of the electronic structure of the intermediate *cis*-IN makes it possible to explain the high reactivity of this

intermediate towards carbonyl derivatives. Two specific features of this intermediate enable this MC reaction: (i) the carbenoid character of the sp^2 hybridised C4 carbon of *cis*-**IN**, rather than the negatively charged carbanionic center as it is represented in the bibliography; and, (ii) the special geometric disposition of the alkyl substituent present in the isocyanide, which electronically stabilises the negative charge gathered at the carbonyl oxygen atom during the nucleophilic attack.

The present MEDT study establishes that the high nucleophilic character of the carbenoid intermediate *cis*-**IN** together with the specific approach mode of the carbonyl C=O double bond during the nucleophilic attack of the sp^2 hybridised carbenoid center of *cis*-**IN** on the carbonyl carbon of acetone **3** make the formation of the C–C single bond with a very low activation enthalpy, 3.3 kcal mol⁻¹, possible, without any external electrophilic activation of the carbonyl group, while the geometric and electronic features of this intermediate favour the subsequent ring closure through the downhill formation of the C–O single bond, thus providing the answers to the three unresolved questions posed concerning the electronic structure of the intermediate involved and the molecular mechanism of these experimentally widely investigated MC reactions.

Finally, both the analysis of the atomic movements of the molecules *cis*-**IN** and acetone **3** along the IRC associated with the cycloaddition step and the corresponding BET analysis allow characterisation of the mechanism of this reaction as a $[2n + 2n]$ cycloaddition in which two lone pairs are involved in the formation of the new C4–C5 and C2–O6 single bonds. These findings make it possible to reject the 1,3-dipolar cycloaddition mechanism for the cycloaddition reactions of carbonyl compounds to these nucleophilic carbenoid intermediates.

Acknowledgements

This work has been supported by the Ministerio de Economía y Competitividad of the Spanish Government, project CTQ2013-45646-P, by FONDECYT through Project 1140341, by the Millennium Nucleus of Chemical Processes and Catalysis (CPC), grant number NC120082 and by DI-UNAB-793-15/R. M. R.-G. thanks the Ministerio de Economía y Competitividad for a pre-doctoral contract co-financed by the European Social Fund (BES-2014-068258).

References

- (a) A. Domling, *Chem. Rev.*, 2006, **106**, 17; (b) F. Millich, *Chem. Rev.*, 1972, **2**, 101; (c) A. Dömling and I. Ugi, *Angew. Chem., Int. Ed.*, 2000, **39**, 3168; (d) A. V. Gulevich, A. G. Zhdanko, R. V. A. Orru and V. G. Nenajdenko, *Chem. Rev.*, 2010, **110**, 5235; (e) S. Sadjadi and M. M. Heravi, *Tetrahedron*, 2011, **67**, 2707; (f) F. de Moliner, L. Banfi, R. Riva and A. Basso, *Comb. Chem. High Throughput Screening*, 2011, **14**, 782; (g) H. R. Sadabad, A. Bazguir, M. Eskandari and R. Ghahremanzadeh, *Monatsh. Chem.*, 2014, **145**, 1851; (h) P. Song, L. Zhao and S. Ji, *Chin. J. Chem.*, 2014, **32**, 381; (i) T.-H. Zhu, S.-Y. Wang, Y.-Q. Tao, T. Q. Wei and S. J. Ji, *Org. Lett.*, 2014, **16**, 12603; (j) Z.-Y. Gu, T.-H. Zhu, J.-J. Cao, X. P. Xu, S. Y. Wang and S. J. Ji, *ACS Catal.*, 2014, **4**, 49.
- (a) V. Nair, A. U. Vinoda, N. Abhilasha, R. S. Menona, V. Santhia, R. L. Varmaa, S. Vijia, S. Mathewa and R. Srinivasb, *Tetrahedron*, 2003, **59**, 10279; (b) V. Nair and A. U. Vinoda, *Chem. Commun.*, 2000, 1019; (c) R. Ghadari, F. Hajishaabanha, M. Mahyari, A. Shaabani and H. R. Khavasi, *Tetrahedron Lett.*, 2012, **53**, 4018; (d) A. A. Esmaili and M. Darbanian, *Tetrahedron*, 2003, **59**, 5545; (e) A. Shaabani, A. H. Rezayan, S. Ghasemi and A. A. Sarvary, *Tetrahedron Lett.*, 2009, **50**, 1456.
- V. Nair and A. U. Vinoda, *Chem. Commun.*, 2000, 1019.
- (a) A. A. Esmaili and M. Darbanian, *Tetrahedron*, 2003, **59**, 5545; (b) R. Ghadari, F. Hajishaabanha, M. Mahyari, A. Shaabani and H. R. Khavasi, *Tetrahedron Lett.*, 2012, **53**, 4018.
- A. Shaabani, A. H. Rezayan, S. Ghasemi and A. A. Sarvary, *Tetrahedron Lett.*, 2009, **50**, 1456.
- I. Yavari and H. Djahaniani, *Tetrahedron Lett.*, 2005, **46**, 7491.
- L.-L. Zhao, S.-Y. Wang, X.-P. Xu and S.-J. Ji, *Chem. Commun.*, 2013, **49**, 2569.
- (a) F. M. Dean, in *Advances in Heterocyclic Chemistry*, ed. A. R. Katritzky, Academic, New York, 1982, vol. 30, p. 167; (b) A. P. Dunlop and F. N. Peters, *The Furans*, Reinhold, New York, 1953; (c) E. J. Corey and X. M. Cheng, *The Logic of Chemical Synthesis*, Wiley, New York, 1989; (d) R. Benassi, in *Comprehensive Heterocyclic Chemistry II*, ed. A. R. Katritzky, C. W. Rees and E. F. V. Scriven, Pergamon, Oxford, 1996, vol. 2, p. 259; (e) S. Onitsuka and H. Nishino, *Tetrahedron*, 2003, **59**, 755; (f) T. Yao, X. Zhang and R. C. Larock, *J. Am. Chem. Soc.*, 2004, **126**, 11164; (g) M. Fan, L. Guo, X. Liu, W. Liu and Y. Liang, *Synthesis*, 2005, 391; (h) C. K. Jung, J. C. Wang and M. J. Krische, *J. Am. Chem. Soc.*, 2004, **126**, 4118; (i) C. Y. Lo, H. Guo, J. J. Lian, F. M. Shen and R. S. Liu, *J. Org. Chem.*, 2002, **67**, 3930.
- W. P. Pei, J. Pei, S. H. Li and X. L. Ye, *Synthesis*, 2000, 2069.
- (a) P. Geerlings, F. de Proft and W. Langenaeker, *Chem. Rev.*, 2003, **103**, 1793; (b) D. H. Ess, G. O. Jones and K. N. Houk, *Adv. Synth. Catal.*, 2006, **348**, 2337.
- A. D. Becke and K. E. Edgecombe, *J. Chem. Phys.*, 1990, **92**, 5397.
- X. Krokidis, S. Noury and B. Silvi, *J. Phys. Chem. A*, 1997, **101**, 7277.
- (a) C. Lee, W. Yang and R. G. Parr, *Phys. Rev. B: Condens. Matter Mater. Phys.*, 1988, **37**, 785–789; (b) A. D. Becke, *J. Chem. Phys.*, 1993, **98**, 5648.
- (a) C. E. Check and T. M. Gilbert, *J. Org. Chem.*, 2005, **70**, 9828; (b) G. O. Jones, V. A. Guner and K. N. Houk, *J. Phys. Chem. A*, 2006, **110**, 1216; (c) G. A. Griffith, I. H. Hillier, A. C. Moralee, J. M. Percy, R. Roig and M. K. Vicent, *J. Am. Chem. Soc.*, 2006, **128**, 13130; (d) M. Ríos-Gutiérrez, P. Pérez and L. R. Domingo, *RSC Adv.*, 2015, **5**, 58464.
- Y. Zhao and D. G. Truhlar, *J. Phys. Chem. A*, 2004, **108**, 6908.
- W. J. Hehre, L. Radom, P. V. R. Schleyer and J. A. Pople, *Ab initio Molecular Orbital Theory*, Wiley, New York, 1986.

- 17 (a) H. B. Schlegel, *J. Comput. Chem.*, 1982, **2**, 214; (b) H. B. Schlegel, in *Modern Electronic Structure Theory*, ed. D. R. Yarkony, World Scientific Publishing, Singapore, 1994.
- 18 K. Fukui, *J. Phys. Chem.*, 1970, **74**, 4161.
- 19 (a) C. González and H. B. Schlegel, *J. Phys. Chem.*, 1990, **94**, 5523; (b) C. González and H. B. Schlegel, *J. Chem. Phys.*, 1991, **95**, 5853.
- 20 (a) J. Tomasi and M. Persico, *Chem. Rev.*, 1994, **94**, 2027; (b) B. Y. Simkin and I. Sheikhet, *Quantum Chemical and Statistical Theory of Solutions-A Computational Approach*, Ellis Horwood, London, 1995.
- 21 (a) E. Cancès, B. Mennucci and J. Tomasi, *J. Chem. Phys.*, 1997, **107**, 3032; (b) M. Cossi, V. Barone, R. Cammi and J. Tomasi, *Chem. Phys. Lett.*, 1996, **255**, 327; (c) V. Barone, M. Cossi and J. Tomasi, *J. Comput. Chem.*, 1998, **19**, 404.
- 22 (a) A. E. Reed, R. B. Weinstock and F. Weinhold, *J. Chem. Phys.*, 1985, **83**, 735; (b) A. E. Reed, L. A. Curtiss and F. Weinhold, *Chem. Rev.*, 1988, **88**, 899.
- 23 (a) R. G. Parr and W. Yang, *Annu. Rev. Phys. Chem.*, 1995, **46**, 701; (b) H. Chermette, *J. Comput. Chem.*, 1999, **20**, 129; (c) F. de Proft and P. Geerlings, *Chem. Rev.*, 2001, **101**, 1451; (d) P. W. Ayers, J. S. M. Anderson and L. J. Bartolotti, *Int. J. Quantum Chem.*, 2005, **101**, 520; (e) J. L. Gázquez, *J. Mex. Chem. Soc.*, 2008, **52**, 3; (f) R. F. Nalewajski, J. Korchowiec and A. Michalak, in *Density Functional Theory IV, Topics in Current Chemistry*, ed. R. Nalewajski, Springer, Berlin, Heidelberg, 1996, vol. 183, p. 25; (g) P. Geerlings, S. Fias, Z. Boisdenghien and F. de Proft, *Chem. Soc. Rev.*, 2014, **43**, 4989.
- 24 R. G. Parr, L. von Szentpaly and S. Liu, *J. Am. Chem. Soc.*, 1999, **121**, 1922.
- 25 (a) R. G. Parr and R. G. Pearson, *J. Am. Chem. Soc.*, 1983, **105**, 7512; (b) R. G. Parr and W. Yang, *Density Functional Theory of Atoms and Molecules*, Oxford University Press, New York, 1989.
- 26 (a) L. R. Domingo, E. Chamorro and P. Pérez, *J. Org. Chem.*, 2008, **73**, 4615; (b) L. R. Domingo and P. Pérez, *Org. Biomol. Chem.*, 2011, **9**, 7168.
- 27 W. Kohn and L. J. Sham, *Phys. Rev.*, 1965, **140**, 1133.
- 28 L. R. Domingo, P. Pérez and J. A. Sáez, *RSC Adv.*, 2013, **3**, 1486.
- 29 (a) S. Berski, J. Andrés, B. Silvi and L. R. Domingo, *J. Phys. Chem. A*, 2003, **107**, 6014; (b) V. Polo, J. Andrés, S. Berski, L. R. Domingo and B. Silvi, *J. Phys. Chem. A*, 2008, **112**, 7128; (c) J. Andrés, P. González-Navarrete and V. S. Safont, *Int. J. Quantum Chem.*, 2014, **114**, 1239; (d) J. Andrés, S. Berski, L. R. Domingo, V. Polo and B. Silvi, *Curr. Org. Chem.*, 2011, **15**, 3566; (e) J. Andrés, L. Gracia, P. González-Navarrete and V. S. Safont, *Comput. Theor. Chem.*, 2015, **1053**, 17.
- 30 (a) R. Thom, *Structural Stability and Morphogenesis: An Outline of a General Theory of Models*, Addison-Wesley Publishing Company, Inc., Reading, MA, 1976; (b) A. E. R. Woodcock and T. Poston, *A Geometrical Study of Elementary Catastrophes*, Spinger-Verlag, Berlin, 1974; (c) R. Gilmore, *Catastrophe Theory for Scientists and Engineers*, Dover, New York, 1981.
- 31 (a) X. Krokidis, V. Goncalves, A. Savin and B. Silvi, *J. Phys. Chem. A*, 1998, **102**, 5065; (b) X. Krokidis, N. W. Moriarty, W. A. Lester and M. Frenklach, *Chem. Phys. Lett.*, 1999, **314**, 534; (c) I. Fourre, B. Silvi, P. Chaquin and A. Sevin, *J. Comput. Chem.*, 1999, **20**, 897; (d) D. B. Chesnut and L. J. Bartolotti, *Chem. Phys.*, 2000, **257**, 175; (e) F. Fuster, A. Sevin and B. Silvi, *J. Phys. Chem. A*, 2000, **104**, 852; (f) E. Chamorro, J. C. Santos, B. Gomez, R. Contreras and P. Fuentealba, *J. Phys. Chem. A*, 2002, **106**, 11533; (g) P. Chaquin and A. Scemama, *Chem. Phys. Lett.*, 2004, **394**, 244; (h) V. Polo, J. Andrés, R. Castillo, S. Berski and B. Silvi, *Chem.-Eur. J.*, 2004, **10**, 5165; (i) V. Polo and J. Andrés, *J. Comput. Chem.*, 2005, **26**, 1427; (j) J. C. Santos, J. Andrés, A. Aizman, P. Fuentealba and V. Polo, *J. Phys. Chem. A*, 2005, **109**, 3687; (k) S. Berski, J. Andrés, B. Silvi and L. R. Domingo, *J. Phys. Chem. A*, 2006, **110**, 13939; (l) V. Polo and J. Andrés, *J. Chem. Theory Comput.*, 2007, **3**, 816; (m) V. Polo, P. Gonzalez-Navarrete, B. Silvi and J. Andrés, *Theor. Chem. Acc.*, 2008, **120**, 341; (n) J. P. Salinas-Olvera, R. M. Gomez and F. Cortes-Guzman, *J. Phys. Chem. A*, 2008, **112**, 2906; (o) I. M. Ndassa, B. Silvi and F. Volatron, *J. Phys. Chem. A*, 2010, **114**, 12900; (p) N. Gillet, R. Chaudret, J. Contreras-Garcia, W. T. Yang, B. Silvi and J. P. Piquemal, *J. Chem. Theory Comput.*, 2012, **8**, 3993.
- 32 (a) A. Savin, A. D. Becke, J. Flad, R. Nesper, H. Preuss and H. G. Vonscherner, *Angew. Chem., Int. Ed.*, 1991, **30**, 409; (b) B. Silvi and A. Savin, *Nature*, 1994, **371**, 683; (c) A. Savin, B. Silvi and F. Colonna, *Can. J. Chem.*, 1996, **74**, 1088; (d) A. Savin, R. Nesper, S. Wengert and T. F. Fassler, *Angew. Chem., Int. Ed. Engl.*, 1997, **36**, 1808.
- 33 S. Noury, X. Krokidis, F. Fuster and B. Silvi, *Comput. Chem.*, 1999, **23**, 597.
- 34 (a) E. R. Johnson, S. Keinan, P. Mori-Sanchez, J. Contreras-Garcia, J. Cohen and A. W. Yang, *J. Am. Chem. Soc.*, 2010, **132**, 6498; (b) J. R. Lane, J. Contreras-Garcia, J.-P. Piquemal, B. J. Miller and H. G. Kjaergaard, *J. Chem. Theory Comput.*, 2013, **9**, 3263; (c) J. Contreras-Garcia, E. R. Johnson, S. Keinan, R. Chaudret, J.-P. Piquemal, D. N. Beratan and W. Yang, *J. Chem. Theory Comput.*, 2011, **7**, 625.
- 35 M. J. Frisch, *et al.*, *Gaussian 09, Revision A.02*, Gaussian Inc, Wallingford, CT, 2009.
- 36 L. R. Domingo, J. A. Saéz, R. J. Zaragoza and M. Arnó, *J. Org. Chem.*, 2008, **73**, 8791.
- 37 L. R. Domingo, *RSC Adv.*, 2014, **4**, 32415.
- 38 L. R. Domingo, M. J. Aurell, P. Pérez and R. Contreras, *Tetrahedron*, 2002, **58**, 4417.
- 39 P. Jaramillo, L. R. Domingo, E. Chamorro and P. Pérez, *J. Mol. Struct.: THEOCHEM*, 2008, **865**, 68.
- 40 A. Savin, *J. Chem. Sci.*, 2005, **117**, 473.
- 41 B. Silvi, *J. Mol. Struct.*, 2002, **614**, 3.



A new model for C–C bond formation processes derived from the Molecular Electron Density Theory in the study of the mechanism of [3+2] cycloaddition reactions of carbenoid nitrile ylides with electron-deficient ethylenes



Luis R. Domingo^{a,*}, Mar Ríos-Gutiérrez^a, Patricia Pérez^b

^aUniversity of Valencia, Department of Organic Chemistry, Dr. Moliner 50, E-46100, Burjassot, Valencia, Spain

^bUniversidad Andrés Bello, Facultad de Ciencias Exactas, Departamento de Ciencias Químicas, Av. República 230, 8370146, Santiago, Chile

ARTICLE INFO

Article history:

Received 17 December 2015

Received in revised form 27 January 2016

Accepted 30 January 2016

Available online 2 February 2016

Keywords:

[3+2] Cycloadditions

Nitrile ylides

Molecular mechanisms

ELF

MEDT

ABSTRACT

The [3+2] cycloaddition (32CA) reactions of the nitrile ylide (NY) with ethylene and with dicyanoethylene (DCE) have been studied using the Molecular Electron Density Theory through DFT calculations at the MPWB1K/6-31G(d) level. The analysis of the electronic structure of NY indicates that it presents a carbenoid structure with an sp^2 lone pair at the carbon atom. While the 32CA reaction with ethylene presents a low activation energy, $6.1 \text{ kcal mol}^{-1}$, the transition state structure associated with the 32CA reaction of NY with DCE is located $7.5 \text{ kcal mol}^{-1}$ below the reagents, the reaction being completely regioselective. The topological analysis of the Electron Localisation Function (ELF) along the reaction path permits to establish a new model for the C–C bond formation characterised by the donation of the electron density of an sp^2 carbon lone pair to the most electrophilic carbon atom of an electron-deficient ethylene. The carbenoid character of NY allows introducing a new type of 32CA reaction, carbenoid type (*cb-type*).

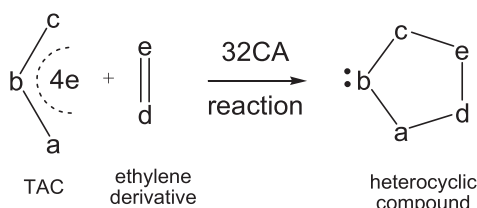
© 2016 Elsevier Ltd. All rights reserved.

1. Introduction

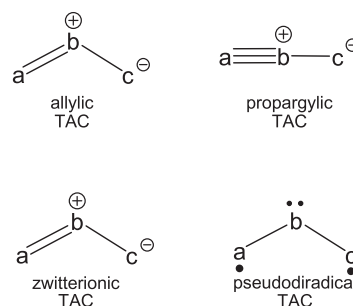
Small ring heterocycles are of great interest in medicinal chemistry,¹ and easily synthesized by a [3+2] cycloaddition (32CA) reaction between a Three Atom-Component (TAC) and an ethylene derivative (see Scheme 1). TACs are species containing four electrons delocalised among three continuous atoms. Substitution of a, b and c in the TAC, and d and e in the ethylene by C, N, O, P or S

atoms has proven to be a powerful synthetic tool in the construction of five-membered heterocyclic compounds.²

TACs can be classified into two categories: allylic type (A-TAC) and propargylic type (P-TAC) structures.³ While A-TACs are bent, P-TACs have a linear structure (see Scheme 2). Depending on their electronic structure, TACs can also be classified as zwitterionic or *pseudodiradical*⁴ TACs. Although the most important TACs such as nitrones and nitrile oxides have a zwitterionic structure, other



Scheme 1. Construction of five-membered heterocyclic compounds by a 32CA reaction.



Scheme 2. Classification of TACs.

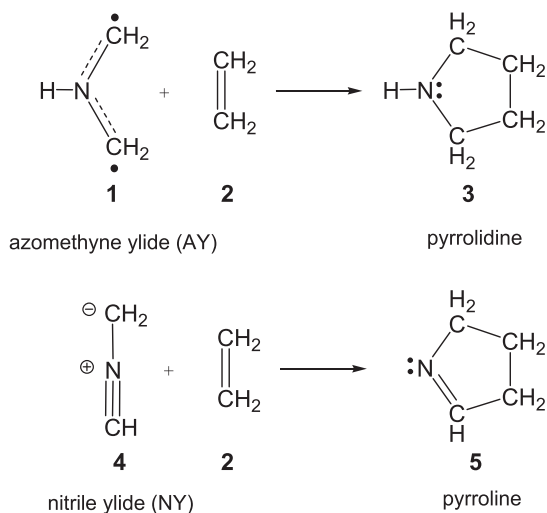
* Corresponding author. E-mail address: domingo@utopia.uv.es (L.R. Domingo).

† Web: www.luisrdomingo.com.

relevant TACs such as carbonyl ylides (CY) and azomethine ylides (AY) have a *pseudoradical* structure⁵ (see Scheme 2).

Based on the electronic structure of the simplest TACs and their reactivity towards ethylene, a useful classification of 32CA reactions into *pseudoradical-type* (*pr-type*) and *zwitterionic-type* (*zw-type*) reactions has recently been proposed.⁴ While TACs with a high *pseudoradical* character participate in *pr-type* 32CA reactions taking place easily through earlier transition state structures (TSs) with a very low polar character, TACs with a high *zwitterionic* character participate in *zw-type* 32CA reactions characterised by favourable nucleophilic/electrophilic interactions at polar TSs.⁴

Pyrrolidine **3** and pyrroline **5** are five-membered heterocyclic compounds containing only one nitrogen atom of great pharmaceutical importance.⁸ These compounds can easily be synthesized by a 32CA reaction of an AY **1**, an A-TAC, or a nitrile ylide (NY) **4**, a P-TAC, with ethylene **2** (see Scheme 3).



Scheme 3. 32CA reactions of the simplest AY **1** and NY **4** with ethylene **2**.

The simplest AY **1**, which has a high *pseudoradical* character,⁴ participates in *pr-type* 32CA reactions towards ethylene **2** with a very low activation energy, below $2.5 \text{ kcal mol}^{-1}$ (see Scheme 3). A topological analysis of the Electron Localisation Function⁹ (ELF) of AY **1** permitted to establish its *pseudoradical* character (see the four V(C) monosynaptic basins at the two carbon atoms of AY **1** in Fig. 1a).⁷ The topological analysis of the ELF of the bonding changes along the reaction path associated with this *pr-type* 32CA reaction showed that the C–C single bond formation takes place synchronously at a distance of 2.10 \AA by a C-to-C coupling of two *pseudoradical* centres, one already present at the carbon atoms of AY **1** and another one generated at each carbon atom of ethylene **2** along the reaction path (see Fig. 1b and c).⁷ The very low activation energy associated with this *pr-type* 32CA reaction was attributed to

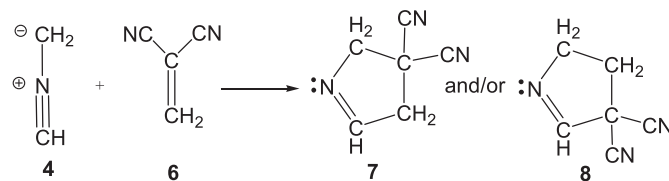
the *pseudoradical* character of AY **1**, which shows a very high reactivity.

In order to highlight the idea that the feasibility for changes in the electron density and not the molecular orbital interactions are responsible of the reactivity of organic molecules,¹⁰ Domingo proposed a new reactivity theory named *Molecular Electron Density Theory* (MEDT).¹¹ Consequently, the molecular reactivity in organic chemistry is studied through a quantum chemical analysis of the changes of the electron density along the reaction path, as well as of the changes in energies required to reach the TS, in order to understand experimental activation energies. Besides the exploration and characterisation of the Potential Energy Surfaces (PES) associated with the studied reaction, within this reactivity model, the organic reactions are studied using quantum chemical tools based on the analysis of the electron density such as conceptual DFT reactivity indices¹² and the topological analysis of the ELF focused on the progress of the bonding changes along the reaction coordinate.

The characterisation of the electron density reorganisation to evidence the bonding changes along a reaction path is the most attractive method to describe a reaction mechanism.¹³ To perform these analyses quantitatively, the Bonding Evolution Theory (BET), consisting of the joint-use of ELF topology and Thom's catastrophe theory¹⁴ (CT), proposed by Krokidis et al.,¹⁵ is a new tool for analysing the electronic changes in chemical processes. BET has been applied to various elementary reactions,^{13,16} allowing the molecular mechanism to be established.

It is worth to mention that Geerlings has recently directed his efforts for reinterpreting the Woodward and Hofmann (WH) rules based on the conceptual DFT, providing orbital-free interpretations of these rules.¹⁷ Previously, Ayers et al. had also explained the WH rules of pericyclic reactions in terms of changes in electron density without the use of other model-dependent concepts.¹⁸

Herein, the 32CA reactions of P-TAC NY **4** with ethylene **2** and with dicyanoethylene (DCE) **6**, a strongly electrophilic ethylene derivative, yielding pyrrolines **5** and **7** and/or **8** are studied within the MEDT through DFT calculations at the MPWB1K/6-31G(d) computational level (see Schemes 3 and 4). A qualitative approach of the BET along these 32CA reactions is performed in order to characterise the molecular mechanisms of these cycloaddition reactions as well as the C–C single bond formation along the reaction.



Scheme 4. 32CA reaction of NY **4** with DCE **6** yielding pyrrolines **7** and/or **8**.

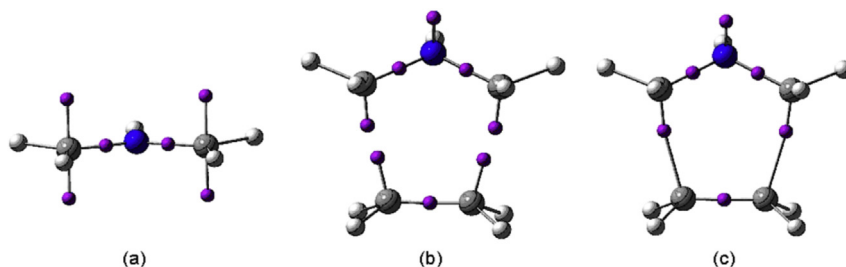


Fig. 1. Positions of the ELF attractors (a) at AY **1**, (b) at a C–C distance of 2.15 \AA and (c) at a C–C distance of 2.10 \AA along the *pr-type* 32CA reaction between AY **1** and ethylene **2**.

2. Computational methods

All stationary points involved in these 32CA reactions were optimised using the MPWB1K hybrid meta functional¹⁹ together with the standard 6-31G(d) basis set.²⁰ This level of theory has shown to have good results for combinations of thermochemistry and thermochemical kinetics in processes including weak interactions.¹⁹ The optimisations were carried out using the Berny analytical gradient optimisation method.²¹ The stationary points were characterised by frequency computations in order to verify that TSs have one and only one imaginary frequency. The intrinsic reaction coordinate (IRC) paths²² were traced in order to check the energy profiles connecting each TS to the two associated minima of the proposed mechanism using the second order González-Schlegel integration method.²³ The electronic structures of stationary points were characterised by the natural bond orbital (NBO) analysis.²⁴

The global electrophilicity index,²⁵ ω , is given by the following expression, $\omega = (\mu^2/2\eta)$, in terms of the electronic chemical potential μ and the chemical hardness η . Both quantities may be approached in terms of the one-electron energies of the frontier molecular orbital HOMO and LUMO, ϵ_H and ϵ_L , as $\mu \approx (\epsilon_H + \epsilon_L)/2$ and $\eta \approx (\epsilon_L - \epsilon_H)$, respectively.²⁶ The empirical (relative) nucleophilicity index,²⁷ N , based on the HOMO energies obtained within the Kohn-Sham scheme,²⁸ is defined as $N = E_{\text{HOMO}}(\text{Nu}) - E_{\text{HOMO}}(\text{TCE})$, where tetracyanoethylene (TCE) is the reference, because it presents the lowest HOMO energy in a long series of molecules already investigated in the context of polar organic reactions. This choice allows conveniently to hand a nucleophilicity scale of positive values. Nucleophilic P_k^- and electrophilic P_k^+ Parr functions²⁹ were obtained through the analysis of the Mulliken atomic spin density of the corresponding radical cations or anions.

The topological analysis of the ELF, $\eta(\mathbf{r})$,⁹ was performed with the TopMod program³⁰ using the corresponding MPWB1K/6-31G(d) monodeterminantal wavefunctions. For the BET studies, the reaction paths were followed using the IRC procedure in mass-weighted internals. Steps of 0.1[amu^{1/2} bohr] along the IRCs were assumed. A total of 200 points along each side of the IRC were chosen for the BET analysis. All computations were carried out with the Gaussian 09 suite of programs.³¹

3. Results and discussion

The present theoretical study has been divided into five parts: i) first, a comparative analysis of the electronic structures of AY **1** and NY **4** is performed; ii) then, an analysis of the conceptual DFT reactivity indices of the reagents involved in the 32CA reactions of NY **4** with ethylene **2** and DCE **6** is given; iii) the PESs associated with these 32CA reactions are explored and characterised; iv) a BET study of the bonding changes along the IRCs of the 32CA reactions of NY **4** with ethylene **2** and DCE **6** is performed in order to characterise the molecular mechanism, and finally, v) a new model for the C–C bond formation is proposed.

3.1. Comparative analysis of the electronic structures of AY **1** and NY **4**

First, a comparative analysis of the electronic structures of AY **1** and NY **4** is performed in order to understand the dissimilar reactivity of these TACs. The representation of ELF attractors, natural atomic charges, obtained through a natural population analysis (NPA), ELF basin pictures and the proposed *pseudodiradical* and carbenoid Lewis structures of AY **1** and NY **4** are shown in Fig. 2.

As has been commented in the introduction section, ELF topology of the simplest AY **1** indicates that this TAC has a *pseudodiradical* Lewis structure. As can be seen, AY **1** presents four V(C)

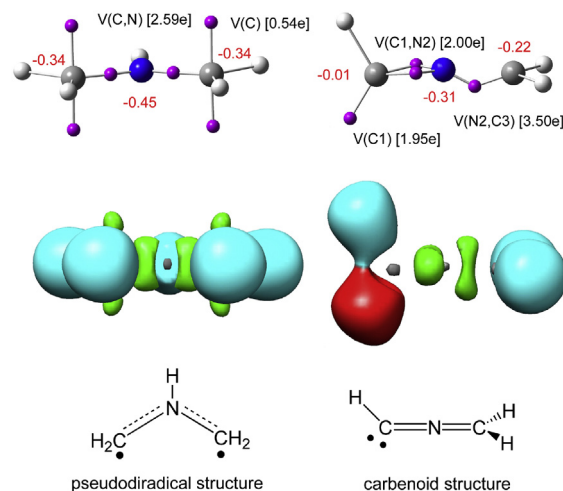


Fig. 2. Representation of ELF attractors and valence basin population, natural charges in red, ELF basin pictures and proposed *pseudodiradical* and carbenoid Lewis structures of AY **1** (Ref. 7) and NY **4** (this work).

monosynaptic basins integrating 0.54e. This picture can be considered as two *pseudoradical* carbons with an sp^2 hybridisation. In addition, the presence of two V(C,N) disynaptic basins integrating 2.59e suggests the complete delocalisation of the lone pair of the N nitrogen atom among the two adjacent carbon atoms.

On the other hand, ELF topology of the simplest NY **4** indicates a different electronic structure than that of AY **1**. Interestingly, the C1 carbon presents a V(C1) monosynaptic basin integrating 1.95e, which can be related to a non-bonding sp^2 hybridised lone pair (see the V(C1) monosynaptic basin in red in the centre of Fig. 2). In addition, NPA of C1 indicates that this carbon practically presents a null charge. This behaviour together with the low negative charge of the C3 carbon suggests an allenic structure instead of a propargylic one with a high carbenoid character (see the carbenoid Lewis structure of NY **4** in Fig. 2).

3.2. Analysis of the DFT reactivity indices of the reagents involved in the 32CA reactions of NY **4** with ethylene **2** and DCE **6**

Studies devoted to polar organic reactions have shown that the analysis of the reactivity indices defined within the conceptual DFT is a powerful tool to understand the reactivity in polar cycloadditions.^{12c,32} Global DFT indices, namely, the electronic chemical potential, μ , chemical hardness, η , electrophilicity, ω , and nucleophilicity, N , of AY **1**, NY **4**, ethylene **2** and DCE **6** are given in Table 1.

The electronic chemical potential of NY **4**, $\mu = -2.90$ eV, is higher than that of DCE **6**, $\mu = -5.64$, indicating that along a polar reaction the global electron density transfer (GEDT)¹⁰ will flux from the NY framework towards the electron-deficient (ED) ethylene one. It is worth to mention that the GEDT concept comes from the

Table 1
B3LYP/6-31G(d) electronic chemical potential, μ , chemical hardness, η , global electrophilicity, ω , and global nucleophilicity, N , in eV, of AY **1**, NY **4**, ethylene **2** and DCE **6**, and the *pseudodiradical* index,⁴ pr , of AY **1** and NY **4**

	μ	η	ω	N	pr
DCE 6	-5.64	5.65	2.82	0.65	
CY 9	-2.67	3.83	0.93	4.53	1.18
NY 4	-2.90	5.45	0.77	3.50	0.64
Ethylene 2	-3.37	7.77	0.73	1.86	
AY 1	-1.82	4.47	0.37	5.07	1.13

observation that the electron density transfer that takes place from a nucleophile to an electrophile along a polar reaction is not a local process, but a global one involving the two interacting molecules.¹⁰ In consequence, the entire system becomes a unique entity since the beginning of the reaction being, therefore, structurally indivisible. Thorough studies have permitted to establish good correlations between the increase of the polar character, measured by the GEDT at the TSs, and the feasibility of the reactions; the larger the GEDT at the TS is, the reaction more polar is.¹⁰ The GEDT at the TSs is computed by sharing the natural atomic charges at the TSs obtained by a NPA analysis between the nucleophilic and the electrophilic frameworks. Additionally, GEDT values have shown to be few dependent of the computational method used to obtain the atomic charges, due to these values come mainly from the integration of the electron density of two molecular frameworks that are usually not bound at the TSs yet.³³

The electrophilicity ω index of the simplest AY **1** is 0.37 eV, being classified as a marginal electrophile within the electrophilicity scale.³⁴ On the other hand, the nucleophilicity N index of AY **1** is 5.07 eV, being classified as a strong nucleophile within the nucleophilicity scale.³⁵

Likewise, the electrophilicity ω and nucleophilicity N indices of the simplest NY **4** are 0.77 eV and 3.50 eV, being classified as a marginal electrophile and a strong nucleophile, respectively, within the corresponding scales.

Ethylene **2** is one of the poorest electrophilic, $\omega=0.73$ eV, and nucleophilic, $N=1.86$ eV, species involved in organic reactions, being classified as a marginal electrophile³⁴ and a marginal nucleophile.³⁵ Therefore, it cannot participate in polar reactions.

Inclusion of two electron-withdrawing –CN groups at the C5 carbon (see Fig. 3 for atom numbering) of ethylene **2** drastically increases the electrophilicity ω index of DCE **6** to 2.82 eV, being classified as a strong electrophile. On the other hand, the nucleophilicity N index of DCE **6** is significantly decreased to 0.65 eV, being classified as a marginal nucleophile. Thus, NY **4** will participate as the nucleophilic species in polar 32CA reactions towards the electrophilic DCE **6**.

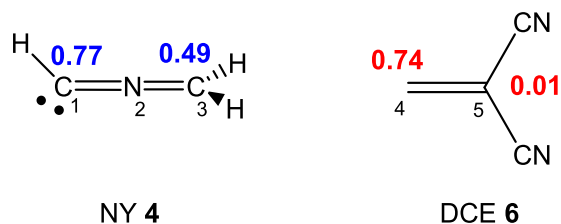


Fig. 3. Nucleophilic P_k^- Parr functions of NY **4** in blue, and electrophilic P_k^+ Parr functions of DCE **6**, in red.

In order to characterise the *pseudodiradical* reactivity of a TAC, the *pr* index, which comprises the hardness and the nucleophilicity index of the TAC, has recently been introduced as $pr=N/\eta$.⁴ A-TACs with *pr* values larger than 0.90 can be related to species having a very soft character, i.e., with low hardness η values, and low stabilised frontier electrons, i.e., with low ionisation potential, while P-TACs have low *pr* indices, showing a *zw-type* reactivity. Thus, the simplest AY **1** and CY **9** present high *pr* values, 1.13 and 1.18, respectively, in clear agreement with its *pseudodiradical* character, revealed by the topological analysis of the ELF (see AY **1** in Fig. 2) and their high reactivity towards non-activated ethylenes.³⁶ On the other hand, NY **4** has a *pr* value of 0.64, indicating that it will have low *pr-type* reactivity. Analysis of the global reactivity indices indicates that NY **4** will participate as the nucleophilic species in polar 32CA reactions towards electrophilic DCE **6**.

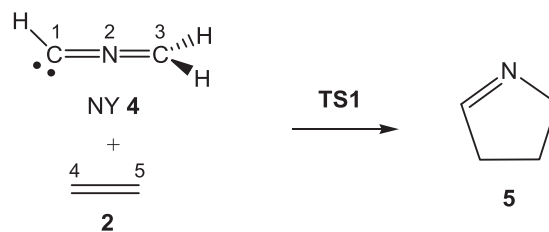
Along a polar reaction involving the participation of non-symmetric reagents, the most favourable reactive channel is that involving the initial two-centre interaction between the most electrophilic centre of the electrophile and the most nucleophilic centre of the nucleophile. Recently, we proposed the electrophilic P_k^+ and nucleophilic P_k^- Parr functions, derived from the changes of the electron density reached via the GEDT process¹⁰ from the nucleophile to the electrophile, as powerful tools in the study of the local reactivity in polar processes.²⁹ Analysis of these functions accounts for the most favourable single bond formation between the most electrophilic and nucleophilic centres of the reagents.¹⁰ Hence, in order to characterise the most nucleophilic and the most electrophilic centres of the species involved in this 32CA reaction, nucleophilic P_k^- Parr functions of NY **4** and electrophilic P_k^+ Parr functions of ED DCE **6** were analysed (see Fig. 3).

Analysis of the nucleophilic P_k^- Parr functions at the simplest NY **4** indicates that the carbenoid C1 carbon is the most nucleophilic centre of this species presenting the maximum value, $P_k^-=0.77$. Note that the C3 carbon also presents a strong nucleophilic activation, $P_k^-=0.49$. On the other hand, the electrophilic P_k^+ Parr functions of DCE **6** indicate that the non-substituted C4 carbon is the most electrophilic centre of this ED ethylene, $P_k^+=0.74$.

Therefore, in the 32CA reaction between NY **4** and DCE **6**, the most favourable electrophile-nucleophile interaction along the nucleophilic attack of NY **4** on DCE **6** will take place between the most nucleophilic centre of NY **4**, the carbenoid C1 carbon, and the most electrophilic centre of DCE **6**, the C4 carbon.

3.3. Analysis of the PESs of the 32CA reactions of NY **4** with ethylene **2** and DCE **6**

3.3.1. 32CA reaction between NY **4** and ethylene **2**. Analysis of the stationary points involved in the reaction between NY **4** and ethylene **2** indicates that this 32CA reaction takes place through a one-step mechanism. Consequently, the reagents, NY **4** and ethylene **2**, one TS, TS1, and pyrroline **5** were located and characterised (see Scheme 5). Gas phase total and relative electronic energies of the stationary points involved in this 32CA reaction are displayed in Table 2.



Scheme 5. 32CA reaction between NY **4** and ethylene **2**.

The activation energy associated with the 32CA reaction of NY **4** with ethylene **2** is 6.1 kcal mol⁻¹, the reaction being strongly exothermic, –87.0 kcal mol⁻¹. This activation energy is ca. 4 kcal mol⁻¹

Table 2
MPWB1K/6-31G(d) gas phase total (E, in a.u.) and relative^a (ΔE , in kcal mol⁻¹) electronic energies of the stationary points involved in the 32CA reaction of NY **4** with ethylene **2**

	E	ΔE
NY 4	–132.585923	
Ethylene 2	–78.529845	
TS1	–211.106042	6.1
5	–211.254344	–87.0

^a Relative to **4+2**.

higher than that of the 32CA reaction between the simplest AY **1** and ethylene **2**.

The geometry of **TS1** is given in Fig. 4. At **TS1**, the lengths of the two C–C forming bonds are 2.406 Å (C1–C4) and 2.449 Å (C3–C5). These large values indicate that this TS is very earlier.

The electronic nature of the 32CA reaction of NY **4** with ethylene **2** was analysed by computing the GEDT.¹⁰ The natural atomic charges, obtained through an NPA, were shared between the two frameworks involved in this 32CA reaction. At **TS1**, the GEDT that fluxes from the NY framework towards the ethylene one is 0.11e. Therefore, there is a slight GEDT from NY **4** to ethylene **2**. This GEDT value at the earlier **TS1**, which is similar to that found in the non-polar *pr*-type 32CA reaction between AY **1** and ethylene **2**,⁶ can be seen as some delocalisation of the electron density of the highly nucleophilic NY **4** into the ethylene fragment, instead of a GEDT process associated with a polar process.

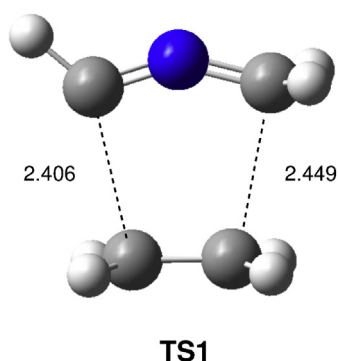


Fig. 4. Geometry of the TS involved in the 32CA reaction between NY **4** and ethylene **2**. Lengths are given in Angstroms.

3.3.2. 32CA reaction between NY **4 and DCE **6**.** Due to the non-symmetry of both reagents, the 32CA reaction between NY **4** and DCE **6** can take place through two regioisomeric channels: along the *r1* regioisomeric channel the reaction begins through the approach of the most nucleophilic centre of NY **4**, the C1 carbon, to the most electrophilic centre of DCE **6**, the C4 one, while along the *r2* regioisomeric channel, the C3 carbon of NY **4** approaches to the C4 carbon of DCE **6**. Analysis of the stationary points found along the two regioisomeric channels indicates that this 32CA reaction also takes place through a one-step mechanism. Calculation of the IRC from the TSs to the reagents stops in a molecular complex (MC), which is more stable than the separated reagents. Consequently, the reagents, two MCs, **MC2** and **MC3**, two TSs, **TS2** and **TS3**, and the corresponding pyrrolines, **7** and **8**, were located and characterised (see Scheme 6). Gas phase total and relative electronic energies of

Table 3
MPWB1K/6-31G(d) gas phase total (E, in a.u.) and relative^a (ΔE , in kcal·mol⁻¹) electronic energies of the stationary points involved in the 32CA reaction of NY **4** with ED DCE **6**

	E	ΔE
NY 4	-132.585923	
DCE 6	-262.926910	
MC2	-395.524741	-7.5
MC3	-395.520115	-4.6
TS2	-395.524616	-7.4
TS3	-395.517164	-2.7
7	-395.640171	-79.9
8	-395.636829	-77.8

^a Relative to **4+6**.

the stationary points involved in this 32CA reaction are displayed in Table 3.

The TSs associated with the two regioisomeric channels are located below the reagents, -7.5 (**TS2**) and -2.7 (**TS3**) kcal·mol⁻¹; however, if the formation of the corresponding MCs is considered, the activation energies become positive, 0.1 (**TS2**) and 1.9 (**TS3**) kcal·mol⁻¹. This 32CA is completely regioselective, the most favourable regioisomeric **TS2** being 4.7 kcal mol⁻¹ below **TS3**, and strongly exothermic, -79.9 (**7**) and -77.8 (**8**) kcal·mol⁻¹.

The geometries of **TS2** and **TS3** are given in Fig. 5. At **TS2**, the lengths of the two forming bonds are 2.377 Å (C1–C4) and 2.968 Å (C3–C5), while at the regioisomeric **TS3** these lengths are 2.372 Å (C3–C4) and 2.600 Å (C1–C5). From these geometrical parameters some significant behaviours should be remarked: *i*) these large C–C distances indicate that these TSs are earlier; *ii*) the difference between the two forming bonds shows that they correspond with asynchronous TSs. The most favourable **TS2** is more asynchronous than **TS3**; *iii*) the shortest C–C distance at both TSs corresponds with the C–C bond formation at the most electrophilic β -conjugated carbon of DCE **6**, i.e., the electrophilic species controls the asynchronicity of the formation of the two new C–C single bonds.

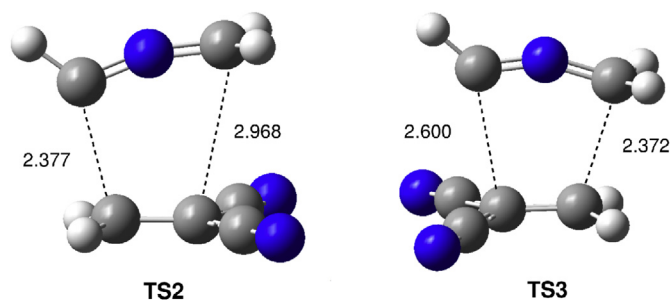
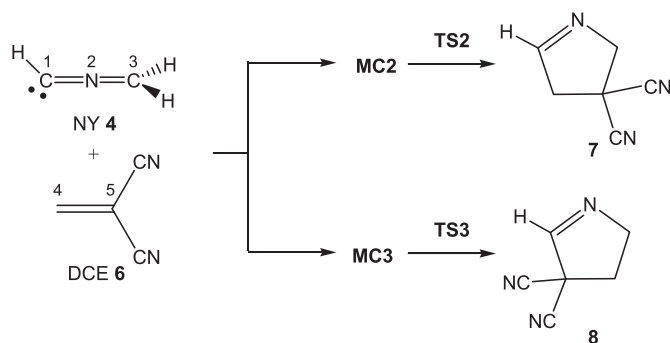


Fig. 5. Geometries of the two regioisomeric TSs involved in the 32CA reaction between NY **4** and DCE **6**. Lengths are given in Angstroms.

At the two regioisomeric TSs, the GEDT that fluxes from the NY framework toward the ED ethylene one is 0.24e (**TS2**) and 0.25e (**TS3**). Therefore, at these TSs there is a clear GEDT taking place from the nucleophilic NY **4** to the electrophilic DCE **6**, in agreement with a polar 32CA reaction and thereby with the lower activation energies found for the 32CA reaction with DCE **6** than that associated with the low polar process with ethylene **2**.

As was commented in the introduction section, 32CA reactions have been classified as *pr*-type and *zw*-type reactions depending on the electronic structure of the TACs. The topological analysis of the ELF and NPA of the simplest NY **4** indicate that this TAC has a carbenoid structure, being different from the *pseudodiradical* structure of the simplest AY **1** and the zwitterionic structure of nitron **10** (see Fig. 6).



Scheme 6. 32CA reaction between NY **4** and DCE **6**.

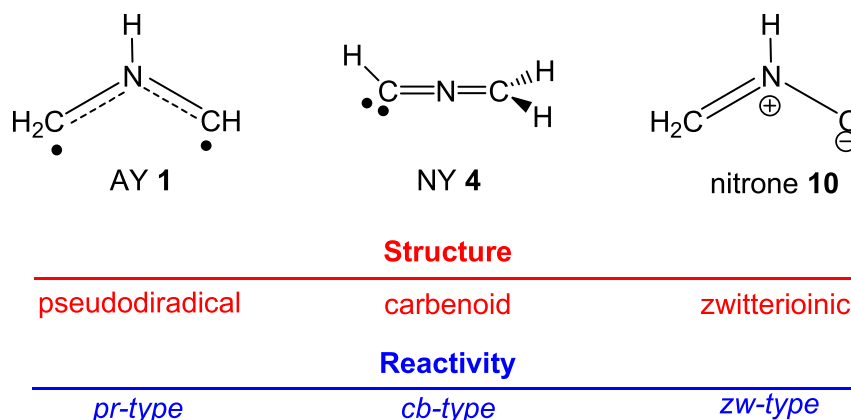


Fig. 6. Electronic structure of TACs and the proposed reactivity types in 32CA reactions.

Consequently, it is expected that carbenoid NY **4** presents a different reactivity than that of AY **1**, a *pr*-type reactivity, and that of nitrone **10**, a *zw*-type reactivity. This finding makes it possible to introduce in a new kind of 32CA reaction, carbenoid type (*cb*-type) that similar to *zw*-type 32CA reactions, the feasibility of the reaction depends on its polar character, i.e., the nucleophilic character of the carbenoid TAC and the electrophilic character of the ethylene derivative.

3.4. BET study of the molecular mechanisms of the 32CA reactions of NY **4** with ethylene **2** and DCE **6**

Herein, a BET study of the 32CA reaction of NY **4** with ethylene **2** and DCE **6** is performed to gain further insight into how the bonding changes take place along these cycloaddition reactions, and therefore, to establish the molecular mechanisms. First, a BET study of the 32CA reaction between NY **4** and ethylene **2** is performed. Later, a BET study of the two regioisomeric channels, *r1* and *r2*, associated with the polar *cb*-type 32CA reaction between NY **4** and DCE **6** is carried out. The corresponding BET studies are given in [Supplementary data](#).

3.4.1. BET study of the 32CA reaction between NY **4 and ethylene **2**.** Some appealing conclusions can be drawn from the BET study of the 32CA reaction between NY **4** and ethylene **2** (see [Supplementary data](#)): *i*) in this 32CA reaction, formation of two new C–C single bonds takes place almost synchronously at the beginning of the last part of *phase VI*, by means of two *C* catastrophes, but with different electron populations; *ii*) formation of the C1–C4 single bond begins at a distance of 2.01 Å by sharing the electron density of the non-bonding sp^2 hybridised lone pair present at the C1 carbon of NY **4** and that of the *pseudoradical* C4 carbon created at ethylene **2** along the reaction path, with an initial population of 1.76e; *iii*) this bonding pattern demands the depopulation of the C1 lone pair present in NY **4**, by 0.59e, in order to achieve the C–C formation with ethylene **2**; *iv*) formation of the C3–C5 single bond begins at a distance of 2.04 Å by the C-to-C coupling of two C3 and C5 *pseudoradical* centres with an initial population of 1.46e; *v*) in this low polar reaction, the two *pseudoradical* C4 and C5 centres generated in the ethylene framework, which are demanded for the formation of the two new C–C single bonds, come mainly from the depopulation of the C4–C5 double bond region of ethylene **2**.

3.4.2. BET study of the *r1* regioisomeric channel associated with the 32CA reaction between NY **4 and DCE **6**.** Some appealing

conclusions can be drawn from the BET study of the most favourable *r1* regioisomeric path associated with the 32CA reaction between NY **4** and DCE **6** (see [Supplementary data](#)): *i*) along the most favourable *r1* regioisomeric channel, formation of the two new C–C single bonds takes place at two well differentiated phases of the reaction; *ii*) formation of the first C1–C4 single bond begins in *phase II* at a distance of ca. 2.15 Å through a *C* catastrophe. Formation of this C–C single bond is achieved by the donation of the electron density of the non-bonding sp^2 hybridised lone pair present at the C1 carbon of NY **4** to the β -conjugated C4 carbon of the DCE moiety, with an initial population of 1.58e; *iii*) formation of the second C3–C5 single bond begins in the last part of *phase VIII* at a distance of ca. 2.19 Å by means of a *C* catastrophe. Formation of this C–C single bond is achieved by the C-to-C coupling of the two C3 and C5 *pseudoradical* centres, with an initial population of 1.13e; *iv*) consequently, this polar *cb*-type 32CA reaction presents a *two-stage one-step* mechanism, in which formation of the second C3–C5 begins in the last part of *phase VIII* after the complete formation of the first C1–C4 single bond.

3.4.3. BET study of the *r2* regioisomeric channel associated with the 32CA reaction between NY **4 and DCE **6**.** Some appealing conclusions can be drawn from the BET study of the *r2* regioisomeric path associated with the 32CA reaction between NY **4** and DCE **6** (see [Supplementary data](#)): *i*) along the least favourable *r2* regioisomeric path, formation of the two C–C single bonds takes place in a more synchronous manner; *ii*) formation of the first C3–C4 single bond ends in *phase V* at a distance of ca. 2.08 Å through a *C* catastrophe. Formation of this C–C single bond is achieved by a C-to-C coupling of the two *pseudoradical* centres generated at the C3 carbon of NY **4** and at the C4 carbon of DCE **6** in previous phases, with an initial population of 1.11e; *iii*) formation of the second C1–C5 single bond begins at the end of *phase VII* at a distance of ca. 1.96 Å also through a *C* catastrophe. Formation of this C–C single bond is reached by sharing the electron density proceeding from the sp^2 hybridised lone pair of the C1 carbon of NY **4** and that of the C5 *pseudoradical* centre generated at the DCE framework in the previous phase, with an initial population of 1.56e; *iv*) along the two regioisomeric channels, formation of the first C–C single bond begins at the β -conjugated C4 carbon of DCE **6**, which is the most electrophilic centre of this species; and finally, *v*) electrophilic DCE **6** shows two contrary compartments along the two regioisomeric channels; while along the least favourable *r2* regioisomeric channel, a new $V(C5)$ monosynaptic basin is created at the conjugated C5 carbon of DCE **6** in order to create the new C1–C5 single bond, along the most favourable *r1* regioisomeric channel, the conjugated C4 carbon

receives the electron density of the sp^2 hybridised lone pair of the C1 carbon of NY **4** during the formation of the C1–C5 single bond.

3.5. A new C–C bond formation model involving neutral sp^2 hybridised carbon lone pairs

Recently, a model for the C–C bond formation in organic reactions involving ethylene derivatives has been proposed.¹⁰ Topological analysis of the bonding changes along organic reactions involving unsaturated species made it possible to establish that the formation of a new C–C single bond is characterised by three consecutive events: *i*) depopulation of the C–C double bond regions in the two reactant species; *ii*) creation of two *pseudoradical* centres at the two interacting carbon atoms; and *iii*) a C-to-C coupling of these *pseudoradical* centres yielding the formation of the new C–C single bond. The last event takes place in the range of 2.0–1.9 Å, with an initial electron density of ca. 1.0 e. In polar reactions, these *pseudoradical* centres appear at the most nucleophilic and electrophilic centre of the two molecules. Analysis of the formation of the second C–C single bond along the most favourable *r1* regioisomeric channel and the first one along the least favourable *r2* regioisomeric channel indicates that the formation of the C3–C5 and C1–C5 single bonds follow this C–C bond formation model.

A different behaviour is found for the formation of the C1–C4 single bond along the most favourable *r1* regioisomeric channel. In this case, formation of the C1–C4 single bond takes place through the donation of the electron density of the non-bonding sp^2 hybridised lone pair present at the C1 carbon of NY **4** to the β -conjugated C4 carbon of the DCE moiety (see the conversion of the $V(C1)$ monosynaptic basin in red colour in **P1** into the $V(C1,C4)$ disynaptic basin in green colour in **P2** in Fig. 7). This event takes place at a distance of ca. 2.15 Å and with an initial population of 1.58e.

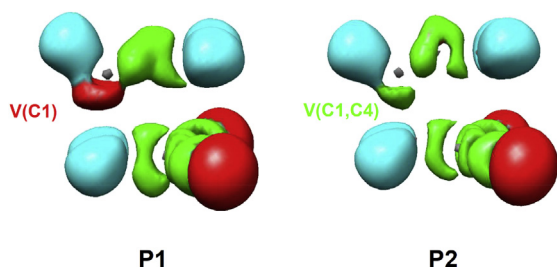


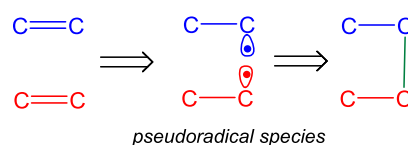
Fig. 7. Display of the ELF basins of selected points **P1** and **P2** associated with the formation of the C1–C4 single bond.

Very recently, we have studied the high reactivity of acetone **11** towards the carbenoid intermediate **IN**. This reaction is initialised by the nucleophilic attack of carbenoid intermediate **IN** on the carbonyl C5 carbon atom of acetone **11** (see Scheme 7). The topological analysis of the ELF associated with the formation of the C–C

single bond indicated that it takes place through the donation of the electron density of the carbenoid C4 non-bonding sp^2 hybridised lone pair of **IN** to the carbonyl C5 carbon of acetone **11**, at a C–C distance of 2.14 Å and with an initial population of 1.78e.

Consequently, the formation of C–C single bonds in organic reactions involving a nucleophilic species having a non-bonding sp^2 hybridised carbon lone pair and an electrophilic C–X double bond appears to follow a different pattern to that previously proposed (see Fig. 7). While in reactions involving ethylene derivatives, C–C bond formation takes place by the C-to-C coupling of two *pseudoradical* centres generated along the reaction (see Fig. 8a), in reactions involving nucleophilic carbenoids, the C–C bond is formed by donation of the electron density of a neutral non-bonding sp^2 hybridised carbon lone pair to an ED carbon atom (see Fig. 8b).

a) C–C bond formation involving nucleophilic ethylenes



b) C–C bond formation involving nucleophilic carbenoids

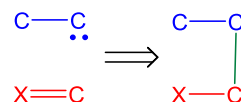


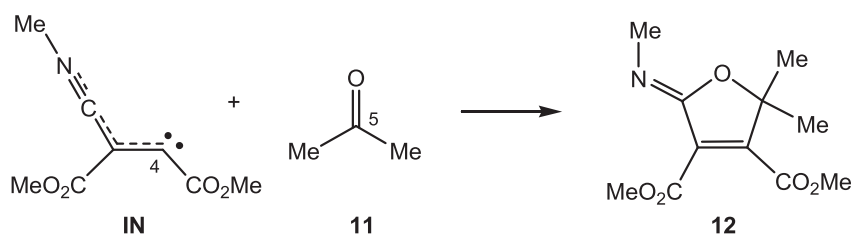
Fig. 8. Two models of the formation of C–C single bonds.

Analysis of the nucleophilic P_k^- Parr functions in carbenoid intermediate **IN** and TAC NY **4** indicates that the carbon atom having the non-bonding sp^2 hybridised lone pair is the most nucleophilic centre of these species. Consequently, it is expected that in polar reactions involving these carbenoid species, the most favourable C–C single bond formation follows this new reactivity model.

4. Conclusions

The 32CA reactions of the simplest NY **4** with ethylene **2** and the electrophilic DCE **6** have been studied within the MEDT through DFT calculations at the MPWB1K/6-31G(d) computational level. The obtained results are supported by the combination of the analysis of the reactivity indices at the ground state of the reagents, derived from the conceptual DFT, the exploration and characterisation of the PESs associated with these 32CA reactions and the BET study of the corresponding reactive channels.

A geometrical and electronic structural analysis of the simplest NY **4** indicates that this TAC presents a carbenoid structure with a non-bonding sp^2 hybridised lone pair at the C1 carbon atom,



Scheme 7. Cycloaddition reaction between carbenoid intermediate **IN** and acetone **11**.

which has an unappreciable charge. Due to its high nucleophilicity N index, $N=3.50$ eV, it is expected that NY **4** participates easily in polar 32CA reactions towards electrophilic ethylenes such as DCE **6**. Analysis of the nucleophilic P_k^- Parr functions allows characterising the carbenoid C1 carbon atom as the most nucleophilic centre of NY **4**, in clear agreement with the regioselectivity found in the polar 32CA reaction with DCE **6**.

An exploration of the PESs associated with these 32CA reactions indicates that these cycloaddition reactions take place through a one-step mechanism. While the 32CA reaction of NY **4** with ethylene **2** presents relative low activation energy, $6.1 \text{ kcal mol}^{-1}$, the most favourable regioisomeric TS associated with the polar 32CA reaction of NY **4** with DCE **6** is located $7.5 \text{ kcal mol}^{-1}$ below the reagents, the reaction being completely regioselective. These 32CA reactions are strongly exothermic.

While the BET study of the low polar 32CA reaction of NY **4** with ethylene **2** indicates that the formation of the two C–C single bonds is an almost synchronous process, this study at the most favourable regioisomeric channel associated with the polar 32CA reaction of NY **4** with DCE **6** indicates that the C–C single bond formation takes place via a *two-stage one-step* mechanism initialised by the nucleophilic attack of the carbenoid C1 carbon of NY **4** on the β -conjugated position of DCE **6**.

The topological analysis of the bonding changes associated with the C–C single bond formation along the two regioisomeric channels associated with the polar 32CA reaction of NY **4** with DCE **6** makes it possible to characterise two dissimilar models for the C–C bond formation along these 32CA reactions. Along the most favourable *r1* regioisomeric channel, the formation of the first C–C single bond begins by the donation of the electron density of the C1 sp^2 hybridised lone pair of NY **4** to the β -conjugated carbon atom of DCE **6**, while along the least favourable *r2* reactive channel the formation of the first C–C single bond takes place through the C-to-C coupling of two *pseudoradical* centres generated along the reaction at the C3 carbon atom of NY **4** and at the β -conjugated carbon atom of DCE **6**. Along both regioisomeric paths, the asynchronicity in the C–C single bond formation is controlled by the electrophile DCE **6**; the C–C bond formation at the β -conjugation position is more advanced than at the α position.

Finally, the carbenoid character of the simplest NY **4** makes it possible to introduce a new type of 32CA reaction, named carbenoid-type (*cb-type*) reaction, in which similar to *zw-type* 32CA reactions, the feasibility of the reaction depends on the polar character of the reaction, i.e., it depends on the nucleophilic character of the carbenoid TAC and the electrophilic character of the ethylene derivative.

This current study emphasizes the idea that molecular mechanisms cannot be characterised only by a static energy and geometric study of the corresponding stationary points but by a rigorous analysis of the molecular electron density changes along the reaction path. This choice allows ruling out out-dated concepts introduced in the past half century and introducing new ones, making it possible to establish a modern rationalisation and to gain insight into molecular mechanisms and reactivity in organic chemistry. Thus, the MEDT is presented as a useful new theory in the study of organic reactions, stating that *while the distribution of the electron density is responsible for the molecular shape and physical properties, the capability for changes in electron density, and not molecular orbital interactions, is responsible for molecular reactivity.*

Acknowledgements

This work has been supported by the Ministerio de Economía y Competitividad of the Spanish Government, project CTQ2013-45646-P, by FONDECYT through Projects 1140341, by the Millennium Nucleus of Chemical Processes and Catalysis (CPC), grant

number NC120082 and the Universidad Andres Bello by DI-793-15/R. M.R.-G. also thanks the Ministerio de Economía y Competitividad (BES-2014-068258) for a pre-doctoral contract co-financed by the European Social Fund (BES-2014-068258).

Supplementary data

Supplementary data associated with this article can be found in the online version, at <http://dx.doi.org/10.1016/j.tet.2016.01.061>.

References and notes

- (a) Sperry, J. B.; Wright, D. L. *Curr. Opin. Drug Discov. Devel.* **2005**, *8*, 723–740; (b) De Luca, L. *Curr. Med. Chem.* **2006**, *13*, 1–23.
- (a) Carruthers, W. *Some Modern Methods of Organic Synthesis*, 2nd ed.; Cambridge University: Cambridge, 1978; (b) Carruthers, W. In *Cycloaddition Reactions in Organic Synthesis*; Baldwin, J. E., Magnus, P. D., Eds.; Pergamon: Oxford, 1990; (c) *Synthetic Applications of 1,3-Dipolar Cycloaddition Chemistry toward Heterocycles and Natural Products*; Padwa, A., Pearson, W. H., Eds.; John Wiley & Sons, Inc.: New York, 2002; Vol. 59.
- Gothelf, K. V.; Jorgensen, K. A. *Chem. Rev.* **1998**, *98*, 863–910.
- Domingo, L. R.; Emamian, S. R. *Tetrahedron* **2014**, *70*, 1267–1273.
- In 1960 Errede⁶ studied the high chemical reactivity of *p*-xylylene, which was attributed to its *pseudodiradical* character. The authors defined a *pseudodiradical* as a diamagnetic compound that behaves chemically as if were a diradical. We used the *pseudodiradical* concept to describe organic molecules or species generated along the reaction path having a pair number of electrons, in which the topological analysis of the ELF shows the presence of non-bonding regions at some carbon atoms.⁷
- Errede, L. A.; Hoyt, J. M.; Gregorian, R. S. *J. Am. Chem. Soc.* **1960**, *53*, 5224–5227.
- Domingo, L. R.; Chamorro, E.; Pérez, P. *Lett. Org. Chem.* **2010**, *7*, 432–439.
- (a) Bailly, C. *Curr. Med. Chem. AntiCancer Agents* **2004**, *4*, 364–378; (b) Bellina, F.; Rossi, R. *Tetrahedron* **2006**, *62*, 7213–7256.
- Becke, A. D.; Edgecombe, K. E. *J. Chem. Phys.* **1990**, *92*, 5397–5403.
- Domingo, L. R. *RSC Adv.* **2014**, *4*, 32415–32428.
- Ríos-Gutiérrez, M.; Domingo, L. R.; Pérez, P. *RSC Adv.* **2015**, *5*, 84797–84809.
- (a) Parr, R. G. *W. Annu. Rev. Phys. Chem.* **1995**, *46*, 701–728; (b) Chermette, H. *J. Comput. Chem.* **1999**, *20*, 129–154; (c) Geerlings, P.; De Proft, F.; Lange-naecker, W. *Chem. Rev.* **2003**, *103*, 1793–1874; (d) De Proft, F.; Geerlings, P. *Chem. Rev.* **2001**, *101*, 1451–1464; (e) Ayers, P. W.; Anderson, J. S. M.; Bartolotti, L. J. *Int. J. Quantum Chem.* **2005**, *101*, 520–534; (f) Gázquez, J. L. *J. Mex. Chem. Soc.* **2008**, *52*, 3–10; (g) Nalewajski, R. F.; Korchowiec, J.; Michalak, A. In *Density Functional Theory IV*; Nalewajski, R., Ed.; Topics in Current Chemistry; Springer: Berlin, Heidelberg, 1996; Vol. 183, pp 25–141; (h) Geerlings, P.; Fias, S.; Boisdenghien, Z.; De Proft, F. *Chem. Soc. Rev.* **2014**, *43*, 4989–5008.
- (a) Polo, V.; Andrés, J.; Berski, S.; Domingo, L. R.; Silvi, B. *J. Phys. Chem. A* **2008**, *112*, 7128–7134; (b) Andrés, J.; González-Navarrete, P.; Safont, V. S. *Int. J. Quantum Chem.* **2014**, *114*, 1239–1252; (c) Andrés, J.; Berski, S.; Domingo, L. R.; Polo, V.; Silvi, S. *Curr. Org. Chem.* **2011**, *15*, 3566–3575; (e) Andrés, J.; Gracia, L.; González-Navarrete, P.; Safont, V. S. *Comp. Theor. Chem.* **2015**, *1053*, 17–30; (f) Andrés, J.; Gracia, L.; González-Navarrete, P.; Safont, V. S. *Quantum Chemical Topology Approach for Dissecting Chemical Structure and Reactivity* (Springer book series: Challenges and Advances in Computational Chemistry and Physics) In *Applications of Topological Methods in Molecular Chemistry*; Alikhani, E., Chauvin, R., Lepetit, C., Silvi, B., Eds.; Springer: 2015.
- (a) Thom, R. *Structural Stability and Morphogenesis: An Outline of a General Theory of Models*; Reading: MA, 1976; (b) Woodcock, A. E. R.; Poston, T. *A Geometrical Study of Elementary Catastrophes*; Springer: Berlin, 1974; (c) Gilmore, R. *Catastrophe Theory for Scientists and Engineers*; New York: Dover, 1981.
- Krokidis, X.; Noury, S.; Silvi, B. *J. Phys. Chem. A* **1997**, *101*, 7277–7282.
- (a) Krokidis, X.; Goncalves, V.; Savin, A.; Silvi, B. *J. Phys. Chem. A* **1998**, *102*, 5065–5073; (b) Krokidis, X.; Moriarty, N. W.; Lester, W. A.; Frenklach, M. *Chem. Phys. Lett.* **1999**, *314*, 534–542; (c) Fourre, I.; Silvi, B.; Chaquin, P.; Sevin, A. *J. Comput. Chem.* **1999**, *20*, 897–910; (d) Chesnut, D. B.; Bartolotti, L. *J. Chem. Phys.* **2000**, *257*, 175–181; (e) Fuster, F.; Sevin, A.; Silvi, B. *J. Phys. Chem. A* **2000**, *104*, 852–858; (f) Chamorro, E.; Santos, J. C.; Gómez, B.; Contreras, R.; Fuentealba, P. *J. Phys. Chem. A* **2002**, *106*, 11533–11539; (g) Chaquin, P.; Scemama, A. *Chem. Phys. Lett.* **2004**, *394*, 244–249; (h) Polo, V.; Andrés, J.; Castillo, R.; Berski, S.; Silvi, B. *Chem.—Eur. J.* **2004**, *10*, 5165–5172; (i) Polo, V.; Andrés, J. *J. Comput. Chem.* **2005**, *26*, 1427–1437; (j) Santos, J. C.; Andrés, J.; Aizman, A.; Fuentealba, P.; Polo, V. *J. Phys. Chem. A* **2005**, *109*, 3687–3693; (k) Polo, V.; Andrés, J. *J. Chem. Theory Comput.* **2007**, *3*, 816–823; (l) Salinas-Olvera, J. P.; Gomez, R. M.; Cortes-Guzman, F. *J. Phys. Chem. A* **2008**, *112*, 2906–2912; (m) Ndassa, I. M.; Silvi, B.; Volatron, F. *J. Phys. Chem. A* **2010**, *114*, 12900–12906; (n) Gillet, N.; Chaudret, R.; Contreras-García, J.; Yang, W. T.; Silvi, B.; Piquemal, J. P. *J. Chem. Theory Comput.* **2012**, *8*, 3993–3997.
- (a) Jaque, P.; Correa, J. V.; De Proft, P.; Toro-Labbé, A.; Geerlings, P. *Can. J. Chem.* **2010**, *88*, 858–865; (b) Geerlings, P.; Ayers, P. W.; Toro-Labbé, A.; Chattaraj, P. K.; De Proft, P. *Acc. Chem. Res.* **2012**, *45*, 683–695.
- Ayers, P. W.; Morell, C.; De Proft, P.; Geerlings, P. *Chem.—Eur. J.* **2007**, *13*, 8240–8247.
- Zhao, Y.; Truhlar, D. G. *J. Phys. Chem. A* **2004**, *108*, 6908–6918.

20. Hehre, W. J.; Radom, L.; Schleyer, P. V. R.; Pople, J. A. *Ab initio Molecular Orbital Theory*; Wiley: New York, 1986.
21. (a) Schlegel, H. B. *J. Comput. Chem.* **1982**, *2*, 214–218; (b) Schlegel, H. B. In *Modern Electronic Structure Theory*; Yarkony, D. R., Ed.; World Scientific: Singapore, 1994.
22. Fukui, K. *J. Phys. Chem.* **1970**, *74*, 4161–4163.
23. (a) González, C.; Schlegel, H. B. *J. Phys. Chem.* **1990**, *94*, 5523–5527; (b) González, C.; Schlegel, H. B. *J. Chem. Phys.* **1991**, *95*, 5853–5860.
24. (a) Reed, A. E.; Weinstock, R. B.; Weinhold, F. *J. Chem. Phys.* **1985**, *83*, 735–746; (b) Reed, A. E.; Curtiss, L. A.; Weinhold, F. *Chem. Rev.* **1988**, *88*, 899–926.
25. Parr, R. G.; von Szentpály, L.; Liu, S. *J. Am. Chem. Soc.* **1999**, *121*, 1922–1924.
26. (a) Parr, R. G.; Pearson, R. G. *J. Am. Chem. Soc.* **1983**, *105*, 7512–7514; (b) Parr, R. G.; Yang, W. *Density Functional Theory of Atoms and Molecules*; Oxford University: New York, 1989.
27. (a) Domingo, L. R.; Chamorro, E.; Pérez, P. *J. Org. Chem.* **2008**, *73*, 4615–4624; (b) Domingo, L. R.; Pérez, P. *Org. Biomol. Chem.* **2011**, *9*, 7168–7175.
28. Kohn, W.; Sham, L. J. *Phys. Rev.* **1965**, *140*, 1133–1138.
29. Domingo, L. R.; Pérez, P.; Sáez, J. A. *RSC Adv.* **2013**, *3*, 1486–1494.
30. Noury, S.; Krokidis, K.; Fuster, F.; Silvi, B. *Comput. Chem.* **1999**, *23*, 597–604.
31. Frisch, M. J.; Trucks, G. W.; Schlegel, H. B.; Scuseria, G. E.; Robb, M. A.; Cheeseman, J. R.; Scalmani, G.; Barone, V.; Mennucci, B.; Petersson, G. A.; Nakatsuji, H.; Caricato, M.; Li, X.; Hratchian, H. P.; Izmaylov, A. F.; Bloino, J.; Zheng, G.; Sonnenberg, J. L.; Hada, M.; Ehara, M.; Toyota, K.; Fukuda, R.; Hasegawa, J.; Ishida, M.; Nakajima, T.; Honda, Y.; Kitao, O.; Nakai, H.; Vreven, T.; Montgomery, J. A., Jr.; Peralta, J. E.; Ogliaro, F.; Bearpark, M.; Heyd, J. J.; Brothers, E.; Kudin, K. N.; Staroverov, V. N.; Kobayashi, R.; Normand, J.; Raghavachari, K.; Rendell, A.; Burant, J. C.; Iyengar, S. S.; Tomasi, J.; Cossi, M.; Rega, N.; Millam, J. M.; Klene, M.; Knox, J. E.; Cross, J. B.; Bakken, V.; Adamo, C.; Jaramillo, J.; Gomperts, R.; Stratmann, R. E.; Yazyev, O.; Austin, A. J.; Cammi, R.; Pomelli, C.; Ochterski, J. W.; Martin, R. L.; Morokuma, K.; Zakrzewski, V. G.; Voth, G. A.; Salvador, P.; Dannenberg, J. J.; Dapprich, S.; Daniels, A. D.; Farkas, O.; Foresman, J. B.; Ortiz, J. V.; Cioslowski, J.; Fox, D. J. *Gaussian 09, Revision A.02*; Gaussian: Wallingford CT, 2009.
32. Ess, D. H.; Jones, G. O.; Houk, K. N. *Adv. Synth. Catal.* **2006**, *348*, 2337–2361.
33. Domingo, L. R.; Ríos-Gutiérrez, M.; Pérez, P.; Chamorro, E. *Mol. Phys.* **2016**, <http://dx.doi.org/10.1080/00268976.2016.1142127> in press.
34. Domingo, L. R.; Aurell, M. J.; Pérez, P.; Contreras, R. *Tetrahedron* **2002**, *58*, 4417–4423.
35. Jaramillo, P.; Domingo, L. R.; Chamorro, E.; Pérez, P. *J. Mol. Struct. (Theochem)* **2008**, *865*, 68–72.
36. Domingo, L. R.; Sáez, J. A. *J. Org. Chem.* **2011**, *76*, 373–379.



Cite this: *Org. Biomol. Chem.*, 2016, **14**, 10427

An MEDT study of the carbenoid-type [3 + 2] cycloaddition reactions of nitrile ylides with electron-deficient chiral oxazolidinones†

Luis R. Domingo,^{*a} Mar Ríos-Gutiérrez^a and Patricia Pérez^{*b}

The molecular mechanism of the carbenoid-type [3 + 2] cycloaddition (32CA) reactions of a nitrile ylide (NY) with a non-chiral and a chiral oxazolidinone has been studied within Molecular Electron Density Theory (MEDT) at the MPWB1K/6-31G(d) computational level. Topological analysis of the Electron Localisation Function (ELF) of the NY shows that it presents a carbenoid structure. The high nucleophilic character of the NY together with the electrophilic character of the non-chiral oxazolidinone favour a polar 32CA reaction with a very low activation energy, the reaction being completely *meta/endo* selective. A Bonding Evolution Theory (BET) study of the molecular mechanism makes it possible to characterise a two-stage one-step carbenoid-type mechanism. Non-Covalent Interactions (NCI) analysis of the 32CA reaction between the NY and chiral oxazolidinone correctly explains the diastereoselectivity experimentally observed.

Received 9th September 2016,

Accepted 11th October 2016

DOI: 10.1039/c6ob01989g

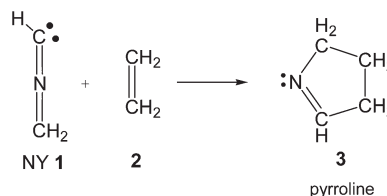
www.rsc.org/obc

1. Introduction

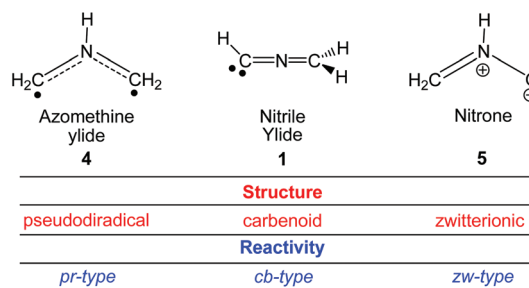
Pyrrolines are five-membered heterocyclic compounds of great pharmaceutical importance containing only one nitrogen atom.¹ They can be easily obtained through a [3 + 2] cycloaddition (32CA) reaction of a nitrile ylide (NY), acting as a three atom-component (TAC), with an ethylene derivative (see Scheme 1).²

Several Density Functional Theory (DFT) studies carried out within the Molecular Electron Density Theory (MEDT)^{3–5} devoted to the study of the reactivity of TACs in 32CA reactions have allowed establishing a useful classification of this class of cycloaddition reactions into pseudoradical-type (*pr-type*),^{6,7} carbenoid-type (*cb-type*)⁵ and zwitterionic-type (*zw-type*)^{6,8} reactions (see Scheme 2).

A recent comparative MEDT study of the 32CA reactions of the simplest NY **1** with ethylene **2** (see Scheme 1) and with the



Scheme 1 32CA reaction of the simplest NY **1** with ethylene **2**.



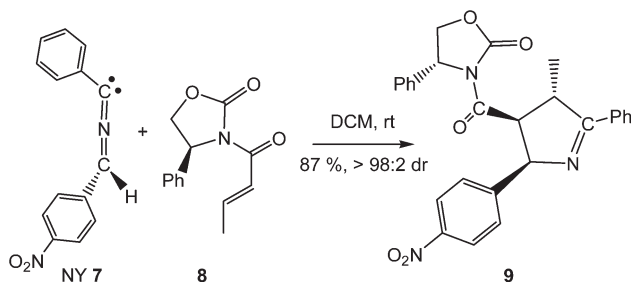
Scheme 2 Electronic structure of TACs and the proposed reactivity types in 32CA reactions.

electron-deficient (ED) dicyanoethylene (DCE) **6** allowed drawing two appealing conclusions:⁵ (i) the *cb-type* mechanism for these 32CA reactions was established, and (ii) due to the high nucleophilic character of NY **1**, a fast reaction with electrophilic ethylenes through a polar 32CA reaction was attained.

^aDepartment of Organic Chemistry, University of Valencia, Dr. Moliner 50, E-46100 Burjassot, Valencia, Spain. E-mail: domingo@utopia.uv.es

^bUniversidad Andres Bello, Facultad de Ciencias Exactas, Departamento de Ciencias Químicas, Millennium Nucleus Chemical Processes and Catalysis (CPC), Av. República 498, 8370146 Santiago, Chile. E-mail: p.perez@unab.cl; http://www.luisrdomingo.com

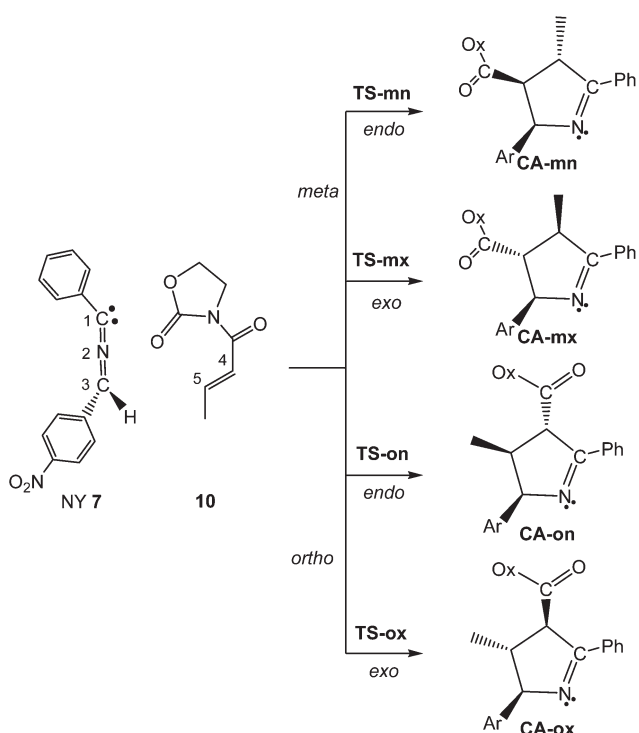
† Electronic supplementary information (ESI) available: ELF topological analysis along the *meta/endo* reaction channel associated with the 32CA reaction of NY **7** with oxazolidinone **10**. MPWB1K/6-31G(d) total and relative electronic energies in the gas phase and in DCM, as well as absolute enthalpies, entropies and Gibbs free energies at 25 °C and 1 atm in DCM, of the stationary points involved in the 32CA reaction of NY **7** with oxazolidinone **10**. See DOI: 10.1039/c6ob01989g



Scheme 3 32CA reaction of NY 7 with the chiral oxazolidinone **8** yielding pyrrolines **9**.

NYs, initially described over 50 years ago by Huisgen *et al.*,⁹ are some of the most reactive TACs. In 2009, Sibi *et al.*¹⁰ showed that the 32CA reaction of NY 7 with ED ethylene **8**, possessing a chiral auxiliary, takes place in high yield and stereoselectivity (see Scheme 3).

In order to characterise experimental *cb-type* 32CA reactions, an MEDT study of the 32CA reaction of NY 7 with 3-(*E*-but-2-enoyl)oxazolidin-2-one **8** yielding pyrroline **9**, experimentally studied by Sibi *et al.*,¹⁰ is performed herein at the MPWB1K/6-31G(d) computational level (see Scheme 3). The regio-, *endo/exo* stereo- and *syn/anti* diastereoselectivity experimentally found in this *cb-type* 32CA reaction is analysed. To this end, the molecular mechanism, and the regio- and *endo/exo* stereoselectivity of the 32CA reaction of NY 7 with the non-chiral oxazolidinone **10** are first studied (see Scheme 4). Then,



Scheme 4 Competitive *meta/ortho* regio- and *endo/exo* stereoselective reaction channels associated with the 32CA reaction between NY 7 and the non-chiral oxazolidinone **10**.

the diastereoselectivity along the most favourable *meta/endo* reaction channels of the 32CA reaction of NY 7 with the chiral oxazolidinone **8** is analysed.

2. Computational methods

Full geometry optimisations of the stationary points were carried out using the MPWB1K¹¹ exchange–correlation functional, together with the standard 6-31G(d) basis set.¹² The stationary points were also characterised by frequency computations in order to verify that TSs have one and only one imaginary frequency. Intrinsic reaction coordinate (IRC)¹³ pathways were traced to verify the connectivity between the minima and associated TSs. Solvent effects of dichloromethane (DCM) were taken into account by full optimization of the gas phase structures at the MPWB1K/6-31G(d) computational level using the polarisable continuum model (PCM) developed by Tomasi's group¹⁴ in the framework of the self-consistent reaction field (SCRF).¹⁵ Values of enthalpies, entropies and Gibbs free energies in DCM were calculated with the standard statistical thermodynamics at 25 °C and 1 atm.¹² The electronic structures of critical points were analysed by the natural bond orbital (NBO) method.¹⁶ The electron localisation function (ELF) topological analysis, $\eta(r)$,¹⁷ was performed with the TopMod program¹⁸ using the corresponding MPWB1K/6-31G(d) monodeterminantal wavefunctions of the selected structures of the IRC. Non-covalent interactions (NCIs) were computed by evaluating the promolecular density and using the methodology previously described.^{19,20} All computations were carried out with the Gaussian 09 suite of programs.²¹

The global electrophilicity index ω ,²² which measures the stabilisation in energy when the system acquires an additional electronic charge ΔN from the environment, is expressed by the following simple equation,²² $\omega = (\mu^2/2\eta)$, in terms of the electronic chemical potential, μ , and the chemical hardness, η . Both quantities may be approached in terms of the one electron energies of the frontier molecular orbitals HOMO and LUMO, ϵ_H and ϵ_L , as $\mu \approx (\epsilon_H + \epsilon_L)/2$ and $\eta = (\epsilon_L - \epsilon_H)$, respectively.²³ On the other hand, the nucleophilicity N index is defined as $N = \epsilon_{\text{HOMO}} - \epsilon_{\text{HOMO(TCE)}}$,²⁴ where ϵ_{HOMO} is the HOMO energy of the nucleophile and $\epsilon_{\text{HOMO(TCE)}}$ corresponds to the HOMO energy of tetracyanoethylene (TCE), taken as a reference. The electrophilic, P_k^+ , and nucleophilic, P_k^- , Parr functions²⁵ were obtained through the analysis of the Mulliken atomic spin densities of the corresponding radical anion and radical cation by single-point energy calculations over the optimised neutral geometries.

3. Results and discussion

The present MEDT study is organised as follows: in section 3.1, an analysis of the electronic structure of the experimental NY 7 is performed in order to understand its *cb-type* reactivity in 32CA reactions. Section 3.2 contains an analysis of the

conceptual DFT reactivity indices of the reagents involved in the 32CA reactions of NY 7 with oxazolidinones **8** and **10**. In section 3.3, the potential energy surfaces (PESSs) associated with the regio- and *endo/exo* stereoisomeric channels of the 32CA reaction of NY 7 with non-chiral oxazolidinone **10** are explored and characterised. Section 3.4 includes the discussion of the diastereoselectivity along the most favourable *meta/endo* approach modes of NY 7 towards the chiral oxazolidinone **8**, whereas section 3.5 discusses a BET study characterising the bonding changes along the most favourable *meta/endo* reaction channel associated with these 32CA reactions. Finally, in section 3.6 an NCI analysis is performed with the aim of rationalising the origin of the *endo* and *anti* stereoselectivities in the 32CA reactions of NY 7 with oxazolidinones **8** and **10**.

3.1 Analysis of the electronic structure of NY 7

In order to understand the *cb-type* reactivity of the experimental NY 7, an analysis of its electronic structure is performed. The representation of ELF attractors, natural atomic charges, obtained through population analysis (NPA), ELF basins and valence basin populations, and the proposed Lewis structures of NYs **1** and **7** are shown in Fig. 1.

Similar to the simplest NY **1**,⁵ ELF topological analysis of the experimental NY 7 shows the presence of one V(C1) monosynaptic basin associated with a non-bonding sp² hybridised lone pair with a population of 1.72e, two disynaptic basins, V(C1,N2) and V'(C1,N2), which integrate 2.20e and 2.11e, and one V(N2,C3) disynaptic basin integrating a population of 2.81e. This bonding pattern indicates that NY 7 has a linear allenic structure rather than a linear propargylic one. Interestingly, NY 7 also presents two monosynaptic basins, V(C3) and V'(C3), integrating 0.36e and 0.29e each one, suggesting that the C3 carbon of NY 7 could also have some

pseudoradical character (see Fig. 1). NPA of NY 7 indicates that the presence of the phenyl and aryl substituents at the C1 and C3 carbons decreases the electron density of these atoms by 0.27e and 0.12e, with respect to those in the simplest NY **1**.⁵ Analysis of the natural charges of the atoms belonging to the C–N–C framework does not allow assigning any zwitterionic structure to the simplest NY **1**, as has been proposed.²⁶

3.2 Analysis of the DFT reactivity indices of the reagents involved in the 32CA reactions of NY 7 with oxazolidinones **8** and **10**

Studies devoted to polar organic reactions have shown that the analysis of the reactivity indices defined within conceptual DFT is a powerful tool to understand the reactivity in polar cycloadditions.²⁷ Global DFT indices, namely, the electronic chemical potential, μ , chemical hardness, η , electrophilicity, ω , and nucleophilicity, N , at the ground state of the reagents involved in these 32CA reactions are given in Table 1.

The electronic chemical potential of experimental NY 7, $\mu = -3.86$ eV, is higher than those of oxazolidinones **8** and **10**, -4.07 (**8**) and -4.28 (**10**) eV, indicating that along with polar reactions the global electron density transfer (GEDT)⁴ will flux from the NY framework towards these oxazolidinones.

The electrophilicity ω and nucleophilicity N indices of the simplest NY **1** are 0.77 eV and 3.50 eV,⁵ being classified on the borderline of marginal electrophiles and as a strong nucleophile within the electrophilicity²⁸ and nucleophilicity²⁹ scales. Inclusion of one phenyl group at C1 and a *p*-NO₂-phenyl group at C3 of NY **1** notably increases both the electrophilicity ω and nucleophilicity N index of NY 7 to 2.33 eV and 3.67 eV, being classified as a strong electrophile but remaining a strong nucleophile. Thus, the similar nucleophilicity N indices computed for NYs **1** and **7** indicate that the presence of the nitro group in NY **1** will hardly affect the reactivity of NY 7 as a nucleophile towards ED oxazolidinones **8** and **10**.

Polar *cb-type* 32CA reactions require the participation of good electrophiles. Ethylene **2** is one of the poorest electrophilic species, $\omega = 0.73$ eV, and nucleophilic ones, $N = 1.86$ eV, being classified as a marginal electrophile and a marginal nucleophile and therefore it cannot participate in polar reactions. When an acetyl-oxazolidinone and a methyl group are added at each carbon atom of ethylene **2** resulting in oxazolidinone **10**, the electrophilicity ω and nucleophilicity N indices markedly increase to 1.56 eV and 1.90 eV, which allow **10** to be classified on the borderline of strong electrophiles and as a

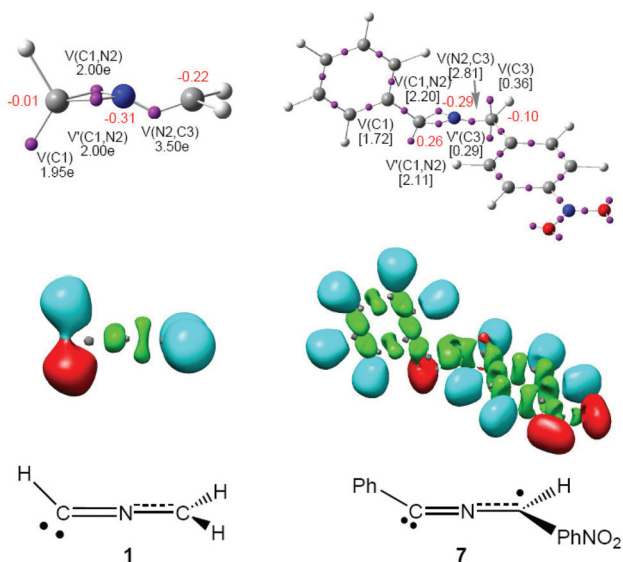


Fig. 1 Representation of ELF attractors and valence basin populations, natural atomic charges, in red, ELF basins and proposed carbenoid Lewis structures of NYs **1**⁵ and **7**.

Table 1 B3LYP/6-31G(d) electronic chemical potential, μ , chemical hardness, η , electrophilicity, ω , and nucleophilicity, N , in eV, of NYs **1** and **7**, ethylene **2** and oxazolidinones **8** and **10**

	μ	η	ω	N
NY 7	-3.86	3.20	2.33	3.67
Oxazolidinone 10	-4.28	5.88	1.56	1.90
Oxazolidinone 8	-4.07	5.51	1.50	2.30
NY 1	-2.90	5.46	0.77	3.50
Ethylene 2	-3.37	7.77	0.73	1.86

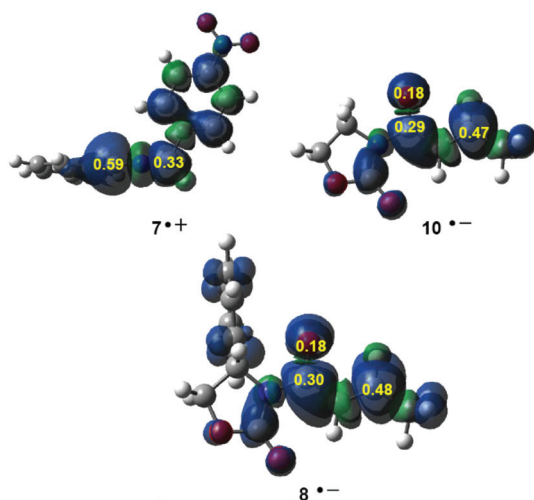


Fig. 2 3D representations of the ASD of the radical cation $7^{\bullet+}$ and the radical anions $8^{\bullet-}$ and $10^{\bullet-}$, and the nucleophilic P_k^- Parr functions of NY 7 and the electrophilic P_k^+ Parr functions of oxazolidinones **8** and **10**.

moderate nucleophile. The inclusion of the phenyl substituent present in chiral oxazolidinone **8** slightly decreases the electrophilicity, $\omega = 1.50$ eV, however, it increases the nucleophilicity of experimental oxazolidinone **8** to $N = 2.30$ eV. Consequently, it is expected that oxazolidinones **8** and **10** present similar reactivity in polar processes towards good nucleophiles.

Local reactivity, *i.e.* regioselectivity, is studied analysing the nucleophilic P_k^- Parr functions of NY 7 and the electrophilic P_k^+ Parr functions of oxazolidinones **8** and **10** (see Fig. 2).

Analysis of the nucleophilic P_k^- Parr functions of NYs 7 indicates that the carbenoid C1 carbon is the most nucleophilic center of this species presenting the maximum value, $P_k^- = 0.59$. Note that the C3 carbon is half as nucleophilically activated as the carbenoid C1 carbon, also presenting a considerable nucleophilic activation, $P_k^- = 0.33$. On the other hand, the electrophilic P_k^+ Parr functions of oxazolidinones **8** and **10** indicate that the β -conjugated C5 carbon is the most electrophilic center of these molecules, $P_k^+ = 0.48$ (**8**) and 0.47 (**10**), while the carbonyl carbon atom is somewhat electrophilically activated, presenting a significant P_k^+ value of 0.30 (**8**) and 0.29 (**10**). The α -conjugated C4 carbon has a negligible P_k^+ value (see Fig. 2). Interestingly, the carbonyl oxygen atom also presents a slight electrophilic activation, $P_k^+ = 0.18$. Consequently, in the 32CA reactions of NY 7 with oxazolidinones **8** and **10**, the most favourable electrophile–nucleophile interaction along this polar reaction will take place between the most nucleophilic center of NY 7, the carbenoid C1 carbon, and the most electrophilic center of oxazolidinones **8** and **10**, the β -conjugated C5 carbon, in clear agreement with the experimental outcomes.

3.3 Analysis of the PESs of the 32CA reaction of NY 7 with oxazolidinone **10**

Due to the non-symmetry of both reagents, the 32CA reaction between NY 7 and the non-chiral oxazolidinone **10** can take

place through four competitive reaction channels, which are related to the two regioisomeric approach modes of oxazolidinone **10** towards NY 7, namely, *meta* and *ortho*, and the two possible stereoisomeric approach modes, namely *endo* and *exo* (see Scheme 4). The *meta* and *ortho* reaction channels are associated with the formation of the C1–C4 or C1–C5 single bonds, respectively, while the *endo* and *exo* ones are related to the relative position of the carbonyl group of oxazolidinone **10** with respect to the position of the phenyl substituent present at the C3 carbon of NY 7 (see Scheme 4).

As a consequence of the free C–C and C–N single bond rotation in oxazolidinones **8** and **10**, several conformations are feasible. The most favourable one corresponds to the *s-trans* conformation, in which the two carbonyl oxygen atoms are on the same plane, in an *anti* rearrangement (see Fig. 3). For the two oxazolidinones, the *s-cis* conformation is found to be 7.1 (**8**) and 8.7 (**10**) kcal mol $^{-1}$ more unfavourable than the *s-trans* one in the gas phase (see later). Consequently, the *s-trans* conformation of **10** was selected for this study.

Analysis of the stationary points involved in the 32CA reaction between NY 7 and oxazolidinone **10** indicates that this 32CA reaction takes place through a one-step mechanism. Accordingly, the reagents, NY 7 and oxazolidinone **10**, four TSs, **TS-mn**, **TS-mx**, **TS-on**, and **TS-ox**, and the corresponding pyrrolines, **CA-mn**, **CA-mx**, **CA-on**, and **CA-ox**, were located and characterised (see Scheme 4). Relative energies, in the gas phase and in DCM, of the stationary points involved in this 32CA reaction are displayed in Table 2. Total energies are given in Table S2 in the ESI.†

The relative energies of the TSs with respect to the separated reagents are: -3.8 (**TS-mn**), 2.5 (**TS-mx**), 2.7 (**TS-on**) and 2.5 (**TS-ox**) kcal mol $^{-1}$. The most favourable **TS-mn** is located below the reagents; however, if the formation of the molecular complex **MC-mn** is considered, the activation energy of **TS-mn** becomes positive, 4.8 kcal mol $^{-1}$. These 32CA reactions are strongly exothermic, between 70 and 73 kcal mol $^{-1}$. From these energy parameters some significant conclusions can be drawn: (i) this 32CA reaction is completely *endo* stereoselective as **TS-mn** is 6.3 kcal mol $^{-1}$ lower in energy than **TS-mx**; (ii) this 32CA reaction is also completely *meta* regioselective as **TS-mn** is 6.3 kcal mol $^{-1}$ lower in energy than **TS-ox**. These behaviours

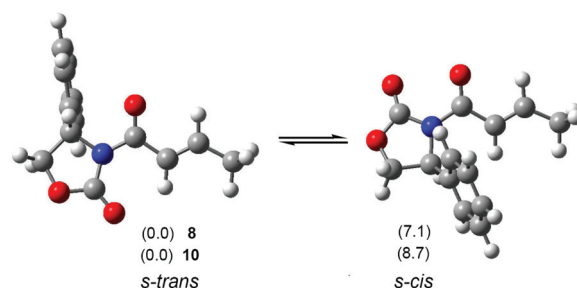


Fig. 3 MPWB1K/6-31G(d) gas phase *s-cis* and *s-trans* conformations of chiral oxazolidinone **8**. In parenthesis, relative energies for oxazolidinones **8** and **10** in kcal mol $^{-1}$.

Table 2 MPWB1K/6-31G(d) relative energies (relative to NY 7 plus **10**, in kcal mol⁻¹) in the gas phase and in DCM, of the stationary points involved in the 32CA reaction of NY 7 with the non-chiral oxazolidinone **10**

	Gas phase	DCM
MC-mn	-8.6	-6.5
TS-mn	-3.8	-1.7
TS-mx	2.5	2.5
TS-on	2.7	4.4
TS-ox	2.5	4.4
CA-mn	-72.6	-70.3
CA-mx	-70.9	-69.2
CA-on	-70.5	-69.2
CA-ox	-70.7	-69.2

are in agreement with the experimental results in which only the *meta/endo* oxazolidinone **8** is obtained; (iii) the strong exothermic character of these 32CA reactions makes them irreversible.

Inclusion of DCM solvent effects slightly increases the activation energies and decreases the exothermic character of the reaction with respect to the reagents as a consequence of a better solvation of NY 7 and oxazolidinone **10** than TSs and CAs.³⁰ In spite of this behaviour, the relative energy of **TS-mx** remains unchanged. In DCM, **TS-mn** remains 4.2 kcal mol⁻¹ below **TS-mx**.

Values of relative enthalpies, entropies and Gibbs free energies, in DCM, of the stationary points involved in the 32CA reaction of NY 7 with the non-chiral oxazolidinone **10** are summarised in Table 3. Absolute values are given in Table S3 in the ESI.† Inclusion of thermal corrections to the electronic energies increases activation enthalpies by between 1.0 and 1.6 kcal mol⁻¹ and reaction enthalpies by between 4.2 and 4.5 kcal mol⁻¹ (see Table 3). **TS-mn** remains 4.3 kcal mol⁻¹ lower in enthalpy than **TS-mx**, and **TS-mn** is 6.2 kcal mol⁻¹ lower in enthalpy than **TS-ox**. Addition of the entropic contribution to enthalpies increases the Gibbs free energies to 17.1, 19.2, 21.6 and 21.5 kcal mol⁻¹ for **TS-mn**, **TS-mx**, **TS-on** and **TS-ox**, respectively, due to the unfavourable activation entropy

Table 3 MPWB1K/6-31G(d) relative enthalpies (ΔH , in kcal mol⁻¹), entropies (ΔS , in cal mol⁻¹ K⁻¹) and Gibbs free energies (ΔG , in kcal mol⁻¹), computed at 25 °C and 1 atm in DCM, of the stationary points involved in the 32CA reaction of NY 7 with the non-chiral oxazolidinone **10**

	ΔH	ΔS	ΔG
MC	-4.9	-48.6	9.6
TS-mn	-0.7	-59.8	17.1
TS-mx	3.6	-52.2	19.2
TS-on	5.5	-54.2	21.6
TS-ox	5.5	-53.6	21.5
CA-mn	-65.8	-62.8	-47.1
CA-mx	-64.7	-60.1	-46.8
CA-on	-64.8	-58.5	-47.3
CA-ox	-65.0	-56.0	-48.3

associated with these bimolecular processes, between -53.5 and -59.8 kcal mol⁻¹ K⁻¹. Considering the Gibbs free activation energies, the *endo* selectivity decreases to 2.1 kcal mol⁻¹, while the reaction remains completely regioselective as **TS-mn** is 4.4 kcal mol⁻¹ lower in Gibbs free energy than **TS-ox**. Finally, this 32CA is strongly exergonic by *ca.* 47 kcal mol⁻¹. This decrease in relative Gibbs free activation energies, $\Delta\Delta G$, is a consequence of the higher activation entropy associated with the most favourable **TS-mn** (-59.8 kcal mol⁻¹ K⁻¹) than those corresponding to the other three TSs (see Table 3).

The geometries of the TSs involved in the four competitive reaction channels are given in Fig. 4. At the *meta* TSs the lengths of the C1-C4 and C3-C5 forming bonds are 2.249 and 2.775 Å (**TS-mn**) and 2.267 and 2.706 Å (**TS-mx**), while at the *ortho* TSs the lengths of the C1-C5 and C3-C4 forming bonds are 2.454 and 2.335 Å (**TS-on**) and 2.408 and 2.364 Å (**TS-ox**). Some appealing conclusions can be drawn from these geometrical parameters: (i) the TSs related to the *meta* reaction channels are more asynchronous than those related to the *ortho* ones; (ii) at the TSs associated with the more favourable *meta* reaction channels, the C-C bond formation involving the carbenoid C1 carbon and the β -conjugated position of oxazolidinone **10** is more advanced than the other, in clear agreement with the previous analysis of the Parr functions; (iii) at the synchronous *ortho* TSs, the C-C bond formation involving the carbenoid C1 carbon is slightly more advanced than that of the β -conjugated position of oxazolidinone **10**.

Inclusion of DCM solvent effects in the optimisation does not significantly modify the geometries of the TSs (see Fig. 4). Along the most favourable *meta* TSs, formation of the C1-C5 single bond is slightly more advanced than that in the gas phase, while the formation of the C3-C4 one is slightly more delayed. Consequently, in DCM, the 32CA reaction becomes slightly more asynchronous.³¹

The electronic nature of the 32CA reaction of NY 7 with oxazolidinone **10** was analysed by computing the GEDT at the four TSs.⁴ The values of the GEDT at the gas phase TSs, which fluxes from NY 7 toward oxazolidinone **10**, are 0.20e at **TS-mn**, 0.19e at **TS-mx**, 0.18e at **TS-on** and 0.16e at **TS-mx**. These values indicate that this 32CA reaction has some polar character. The GEDT at the more favourable *meta* TSs is slightly higher than that at the *ortho* ones, and slightly lower than that computed at the *meta* TS associated with the 32CA reaction between the simplest NY **1** and DCE **6** (0.24e).⁵

3.4 Study of the *anti/syn* diastereoselectivity along the *meta/endo* approach modes of NY 7 towards chiral oxazolidinone **8**

The chiral character of oxazolidinone **8** makes it possible that the approach of NY 7 towards the two diastereotopic faces of oxazolidinone **8** could result in two pyrrolines. Due to the high *meta/endo* selectivity found in the 32CA reaction of non-chiral oxazolidinone **10**, only the *anti* and *syn* approach modes of NY 7 to the diastereotopic faces of **8**, yielding pyrrolines **9** and **11**, have been studied (see Scheme 5). The geometries of the two diastereoisomeric TSs and their relative energies are given in Fig. 5.

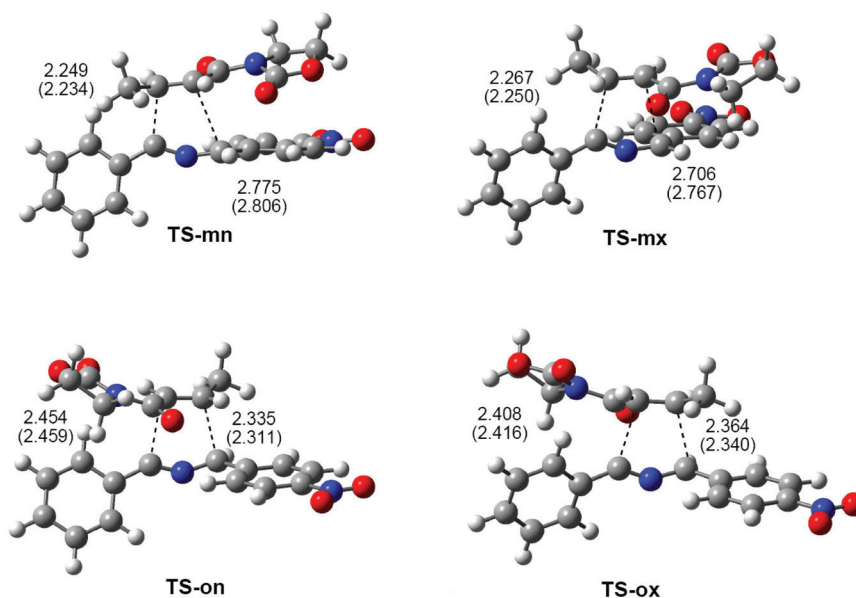
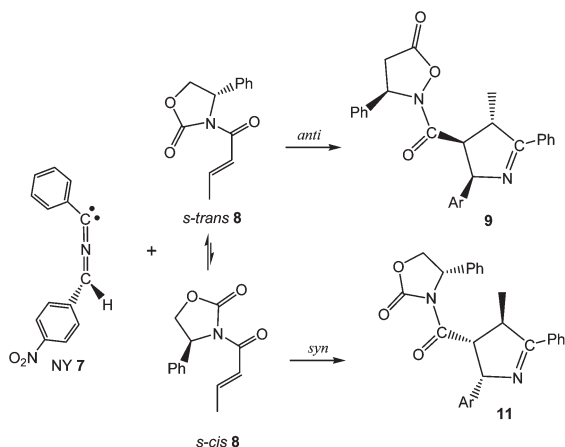


Fig. 4 MPWB1K/6-31G(d) geometries of the TSs involved in the 32CA reaction of NY 7 with oxazolidinone 10. Distances are given in Angstroms. Values in DCM are given in parentheses.



Scheme 5 *anti/syn* diastereoisomeric reaction channels along the *meta/endo* reactive approach mode of NY 7 towards the *s-trans* and *s-cis* conformation of chiral oxazolidinone 8.

Analysis of the relative energies in DCM shows that *anti* **TS-mna** is 5.8 kcal mol⁻¹ lower in energy than *syn* **TS-mns**, presenting a complete diastereoselectivity, in agreement with the experimental outcomes (see Fig. 5). At **TS-mna**, the phenyl substituent in chiral oxazolidinone 8 is located away from NY 7, not causing any steric hindrance. Although the phenyl substituent in the most favourable *s-trans* conformation of chiral oxazolidinone 8 prevents the *syn* approach of NY 7, the C–N single bond rotation in oxazolidinone 8 makes it possible that the phenyl substituent could also be located away from NY 7. However, this steric demand makes chiral oxazolidinone 8 to

adopt the more unfavourable *s-cis* conformation, thus increasing the relative energy of **TS-mns**.

The distances of the C1–C4 and C3–C5 forming bonds at **TS-mna** and **TS-mns**, 2.236 and 2.799 Å, and 2.239 and 2.809 Å, respectively, are closer to those found at **TS2-mn**. Consequently, the inclusion of the phenyl substituent in oxazolidinone 10 does not excessively modify the TS geometries. This behaviour is a consequence of the fact that in both TSs the phenyl substituent is located away from NY 7.

3.5 BET study characterising the C–C single bond formations along the most favourable *meta/endo* reaction channel associated with the 32CA reaction of NY 7 with oxazolidinone 10

Within MEDT, the study of the molecular mechanism of an organic reaction comprises the BET characterisation of the bonding changes along the reaction path together with the analysis of the energies associated with these changes. The BET study along the most favourable *meta/endo* reaction channel of the 32CA reaction between NY 7 and oxazolidinone 10 is given in the ESI.† The populations of the most significant valence basins of the selected points of the IRC are included in Table S1† and pictures of the attractor positions of the ELF for the points involved in the bond formation processes are displayed in Fig. S1.†

From the MEDT analysis of the electron density changes along the IRC associated with the most favourable *meta/endo* reaction channel some appealing conclusions can be drawn:

(i) the *meta/endo* IRC is topologically characterised by ten differentiated phases associated with the rupture and for-

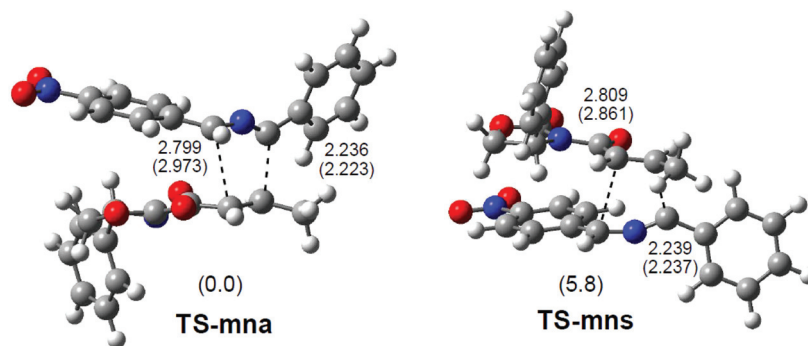


Fig. 5 MPWB1K/6-31G(d) gas phase geometries of the *anti/syn* diastereoisomeric TSs involved along the *meta/endo* reaction channels associated with the 32CA reaction of NY 7 with chiral oxazolidinone 8. Distances are given in Angstroms. Relative energies in kcal mol⁻¹ and distances in DCM are given parenthesis.

mation of double and single bonds. Consequently, this 32CA reaction is a non-concerted process;

(ii) formation of the first C1–C5 single bond takes place at a C–C distance of 2.04 Å with an initial electron density of 1.71e. This population is achieved through the donation of the electron density of the carbenoid C1 lone pair present in NY 7 to the β -conjugated position of the oxazolidinone moiety (see P7 in Fig. S1†);⁷

(iii) formation of the second C3–C4 single bond takes place at a C–C distance of 2.05 Å by a C-to-C coupling of two C3 and C4 *pseudoradical* centers generated along the IRC (see P8 in Fig. S1†);⁴

(iv) formation of the C3–C4 single bond begins when the C1–C5 single bond has already reached an electron density of 2.00e. This behaviour characterises the reaction mechanism as a non-concerted *two-stage one-step* mechanism.³² In this mechanism, the first C1–C5 single bond is completely formed along the first stage of the reaction through the nucleophilic attack of the carbenoid C1 carbon of NY 7 on the β -conjugated position of oxazolidinone 10, while the formation of the second C3–C4 single bond takes place at the second stage of the reaction through the coupling of two *pseudoradical* centers. This behaviour, which is similar to that found in the 32CA reaction between the simplest NY 1 and DCE 6, characterises the *cb-type* mechanism;

(v) and finally, the changes in electron density required for the formation of the first C1–C5 single bond, which are mainly associated with the depopulation of the C4–C5 double bond, present a low energy cost, 5.0 kcal mol⁻¹, as a consequence of the electrophilic character of oxazolidinone 10.

3.6 NCI analysis of the origin of the *endo* and *anti* selectivities in the 32CA reactions of NY 7 with chiral oxazolidinones 8 and 10

As commented on in the previous section, the 32CA reaction of NY 7 with oxazolidinone 10 yields the pyrroline CA-mn, resulting from a *meta/endo* approach mode of 10 as the single product. In addition, when chiral oxazolidinone 8 is used, pyrroline 9 is experimentally obtained with $a > 98 : 2$ dr.¹⁰

Analysis of the MWB1K/6-31G(d) relative energies in DCM of *meta/endo* TS-mn and *meta/exo* TS-mx gives a $\Delta\Delta E^\ddagger = 6.3$ kcal mol⁻¹, while the $\Delta\Delta E^\ddagger$ between *meta/endo/anti* TS-mna and *meta/endo/syn* TS-mns is 5.8 kcal mol⁻¹, in complete agreement with the experimental outcomes.

In order to explain the high *endo* and *anti* stereoselectivities along the 32CA reactions of NY 7 with oxazolidinones 8 and 10, a detailed analysis of the geometries of TS-mn, TS-mx, TS-mna and TS-mns was performed. Fig. 6 shows the top views of these TSs. As can be seen, while along the *exo* stereoisomeric approach mode the oxazolidinone ring of 8 is positioned away from the aryl substituent at TS-mx, the former ring is precisely above the aryl substituent and parallel at *endo* TS-mn, TS-mna and TS-mns (see Fig. 6). Therefore, this geometrical arrangement at the *meta/endo* TSs allows generating some type of favourable electronic interactions between the oxazolidinone and the aryl groups, justifying the preference of *endo* TS-mn over *exo* TS-mx. On the other hand, analysis of the geometries of the TSs associated with the *ortho* regioisomeric approach mode, TS-on and TS-ox, indicates that the phenyl ring of oxazolidinone 8 is positioned orthogonally to the molecular plane, thus preventing any interaction with the oxazolidinone ring neither in the *endo* stereoisomeric channel nor in the *exo* one (see Fig. 4). Consequently, favourable interactions are only feasible along the *meta/endo* reactive pathway.

In order to characterise the favourable interactions appearing between the oxazolidinone and the aryl substituents at the *meta/endo* and *meta/endo/anti* TSs, an NCI analysis¹⁹ of the electron density of TS-mn, TS-mx, TS-mna and TS-mns, as well as of the two conformations of oxazolidinone 8 is performed. NCI low-gradient isosurfaces for these *meta* TSs are displayed in Fig. 7, while those for *s-trans* and *s-cis* conformations of oxazolidinone 8 are shown in Fig. 8.

The most appreciable difference revealed from Fig. 7 is the presence of a larger green surface between the oxazolidinone ring of oxazolidinones 8 and 10 and the aryl group of NY 7 in the *endo* TSs than in the *exo* one. This larger green surface, associated with weak attractive van der Waals (VdW) interactions, accounts for the larger stabilisation of *endo* TS-mn

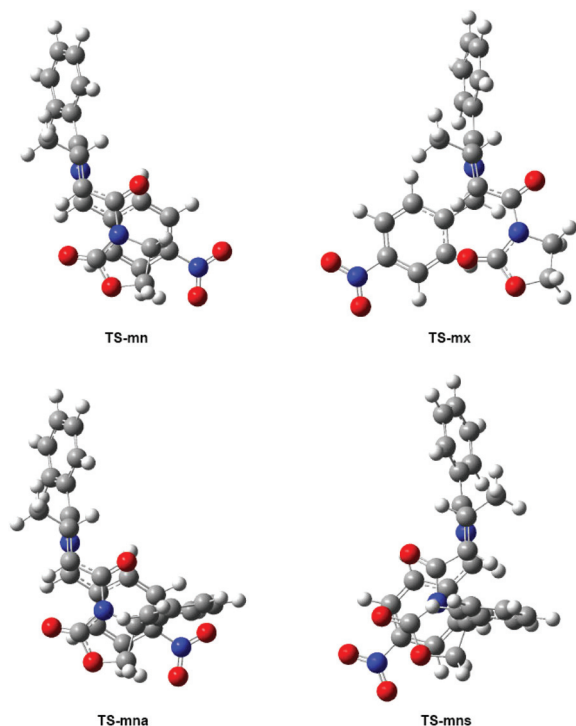


Fig. 6 Top view of the geometries of TS-mn, TS-mx, TS-mna and TS-mns.

with respect to *exo* TS-mx. In addition, it is noteworthy that while TS-mna presents a turquoise surface between the α -hydrogen and the carbonyl oxygen of the oxazolidinone ring,

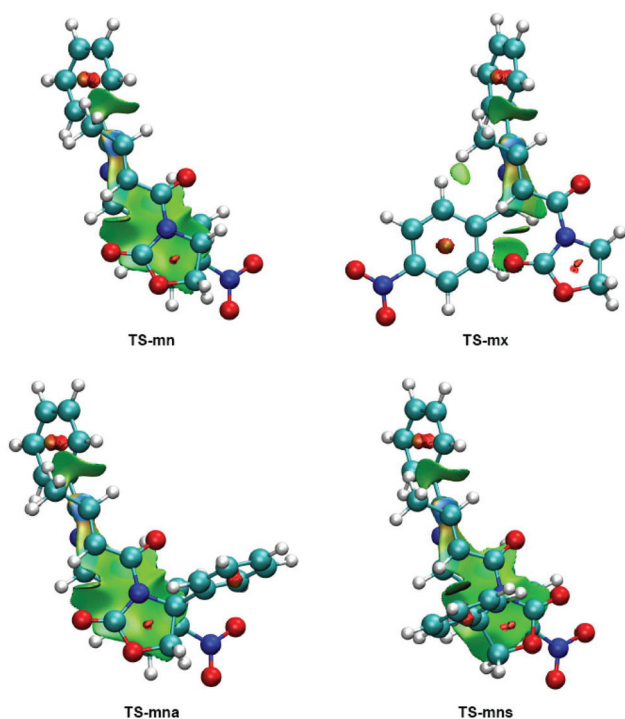


Fig. 7 NCI gradient isosurfaces of TS-mn and TS-mx, and of TS-mna and TS-mns. Green surfaces indicate weak attractive VdW interactions.

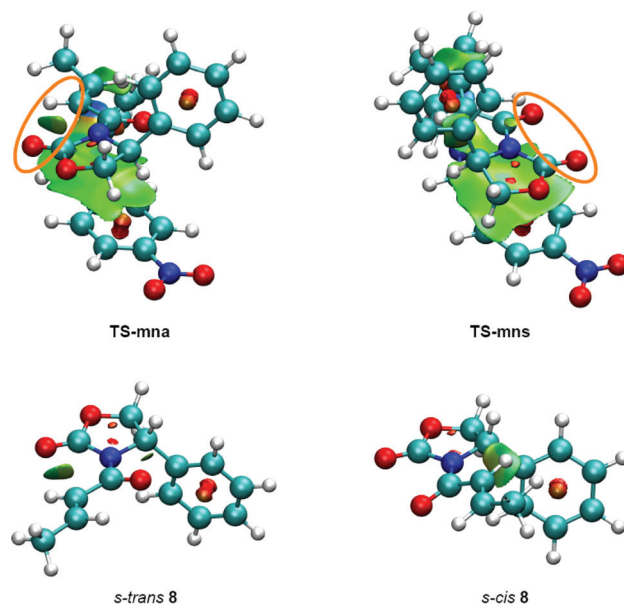


Fig. 8 NCI gradient isosurfaces of TS-mna and TS-mns and of *s-trans* and *s-cis* conformations of chiral oxazolidinone **8**. NCI gradient isosurfaces of TS-mna and *s-trans* **8** present the favourable intramolecular O–H hydrogen bond.

indicating a strong favourable hydrogen bond between them, no NCI surface is observed between the two carbonyl oxygen atoms in TS-mns (see Fig. 8). Consequently, this topological characteristic accounts for the stronger stabilisation of *anti* TS-mna than *syn* TS-mns. Note that although the *s-trans* conformation of **8** is more stable than the *s-cis* one, the very high steric hindrance between the phenyl substituent of the oxazolidinone group of *s-cis* **8** and the aryl ring of NY **7** along the *syn* diastereoisomeric approach mode forces the rotation around the C–N bond, so that the hydrogen bond interaction, which is present at *s-trans* **8**, is prevented at TS-mns.

The present NCI topological analysis allows concluding that, although weak attractive VdW interactions are appreciable in the TSs associated with the more favourable *meta* regioisomeric channels, the stronger VdW interactions taking place between the oxazolidinone ring of **8** and **10** and the aryl group of NY **7** along the *meta/endo* approach could be responsible for the regio- and stereoselectivities experimentally found in the 32CA reactions of NY **7** with oxazolidinone **8**.¹⁰ Interestingly, despite the similar NCI profiles of the *anti/syn* diastereoisomeric *meta/endo* TSs, the presence of a hydrogen-bond between the α -hydrogen and the carbonyl oxygen of the oxazolidinone ring in oxazolidinone *s-trans* **8** appears to be responsible for the high diastereoisomeric excess experimentally obtained in the 32CA reaction of NY **7** with oxazolidinone **8**.

4. Conclusions

The molecular mechanism of the *cb-type* 32CA reaction of NY **7** with non-chiral oxazolidinone **10** and chiral oxazolidinone **8**,

experimentally studied by Sibi *et al.*,¹⁰ has been studied within the MEDT at the MPWB1K/6-31G(d) computational level. ELF topological analysis of the electronic structure of NY 7 shows that this TAC presents a carbenoid structure similar to that found for the simplest NY 1; *i.e.* the C1 carbon presents an sp^2 lone pair with a high electron density, 1.72e.

Analysis of the conceptual DFT reactivity indices indicates that in spite of the high electrophilic character of NY 7, $\omega = 2.33$ eV, it also presents a high nucleophilic character, $N = 3.67$ eV, similar to that for the simplest NY 1, $N = 3.50$ eV. On the other hand, oxazolidinones 8 and 10 can participate as strong electrophiles in polar reactions. Analysis of the nucleophilic Parr functions in NY 7 and electrophilic Parr functions in oxazolidinone 8 correctly predicts the *meta* regioselectivity of this polar *cb-type* 32CA reaction.

Due to the non-symmetry of the reagents, the 32CA reaction between NY 7 and non-chiral oxazolidinone 10 can take place through four competitive reaction channels: the *meta* and *ortho* regioisomeric and the *endo* and *exo* stereoisomeric ones. Analysis of the stationary points involved in this 32CA reaction indicates that it takes place through a one-step mechanism. The 32CA reaction of the nucleophilic NY 7 with the electrophilic oxazolidinone 10 presents a very low activation energy. In fact, the most favourable **TS-mn** is found below the separated reagents. Analysis of the relative energies associated with the four competitive TSs indicates that this 32CA reaction is completely *meta* regioselective and completely *endo* stereoselective, in complete agreement with the experimental outcomes.

Analysis of the TS geometries indicates that at the more favourable *meta* regioisomeric TSs, the C–C bond formation involving the carbenoid C1 carbon and the β -conjugated position of the oxazolidinone 10 is more advanced than the other C–C bond formation.

Inclusion of DCM solvent effects does not substantially modify the selectivities or the TS geometries. Solvent effects slightly increase the relative energies as a consequence of a better solvation of the reagents than TSs and CAs.

A study of the *anti/syn* diastereoselectivity along the *meta/endo* approach modes associated with the 32CA reactions of NY 7 with the chiral oxazolidinone 8 shows that *meta/endo/anti TS-mna* is 5.8 kcal mol⁻¹ lower in energy than the *meta/endo/syn TS-mns*, showing complete diastereoselectivity, in good agreement with the experimental outcomes.

BET analysis of the molecular mechanism along the most favourable *meta/endo* reaction channel associated with the 32CA reaction of NY 7 with oxazolidinone 10 indicates that it takes place through a non-concerted *two-stage one-step* mechanism, which is initialised by the nucleophilic attack of the carbenoid C1 carbon of NY 7 on the β -conjugated position of oxazolidinone 10. BET analysis makes the characterisation of the *cb-type* mechanism possible.

NCI analysis of the *meta* TSs shows that the favourable VdW interactions that appear at the *endo TS-mn* and **TS-mna** together with the presence of an intramolecular hydrogen bond in the *s-trans* conformation of the chiral oxazolidinone 8,

which remains at **TS-mna**, are responsible for the complete diastereoselectivity experimentally found.

Acknowledgements

This work has been supported by the Ministry of Economy and Competitiveness of the Spanish Government, project CTQ2013-45646-P, by FONDECYT through Projects 1140341, by the Millennium Nucleus Chemical Processes and Catalysis (CPC), grant number NC120082 and the Universidad Andres Bello by DI-793-15/R. M. R.-G. also thanks the Ministry of Economy and Competitiveness for a pre-doctoral contract co-financed by the European Social Fund (BES-2014-068258).

References

- (a) C. Bailly, *Curr. Med. Chem.: Anti-Cancer Agents*, 2004, **4**, 364–378; (b) F. Bellina and R. Rossi, *Tetrahedron*, 2006, **62**, 7213.
- Synthetic Applications of 1,3-Dipolar Cycloaddition Chemistry Toward Heterocycles and Natural Products*, ed. A. Padwa and W. H. Pearson, John Wiley & Sons, Inc., 2002, vol. 59.
- L. R. Domingo, *Molecules*, 2016, **21**, 1319.
- L. R. Domingo, *RSC Adv.*, 2014, **4**, 32415.
- L. R. Domingo, M. Ríos-Gutiérrez and P. Pérez, *Tetrahedron*, 2016, **72**, 1524.
- L. R. Domingo and S. R. Emamian, *Tetrahedron*, 2014, **70**, 1267.
- L. R. Domingo, M. J. Aurell and P. Pérez, *Tetrahedron*, 2015, **71**, 1050.
- L. R. Domingo, M. J. Aurell and P. Pérez, *Tetrahedron*, 2014, **70**, 4519.
- (a) R. Huisgen, H. Stangl, H. J. Sturm and H. Wagenhofer, *Angew. Chem., Int. Ed. Engl.*, 1962, **74**, 3; (b) K. Bunge, R. Huisgen, R. Raab and H. Stangl, *Chem. Ber.*, 1972, **105**, 1279.
- M. P. Sibi, T. Soeta and C. P. Jasperse, *Org. Lett.*, 2009, **11**, 5366.
- Y. Zhao and D. G. Truhlar, *J. Phys. Chem. A*, 2004, **108**, 6908.
- W. J. Hehre, L. Radom, P. V. R. Schleyer and J. A. Pople, *Ab initio Molecular Orbital Theory*, Wiley, New York, 1986.
- K. Fukui, *J. Phys. Chem.*, 1970, **74**, 4161.
- (a) J. Tomasi and M. Persico, *Chem. Rev.*, 1994, **94**, 2027; (b) B. Y. Simkin and I. Sheikhet, *Quantum Chemical and Statistical Theory of Solutions-A Computational Approach*, Ellis Horwood, London, 1995.
- (a) E. Cances, B. Mennucci and J. Tomasi, *J. Chem. Phys.*, 1997, **107**, 3032; (b) M. Cossi, V. Barone, R. Cammi and J. Tomasi, *Chem. Phys. Lett.*, 1996, **255**, 327; (c) V. Barone, M. Cossi and J. Tomasi, *J. Comput. Chem.*, 1998, **19**, 404.
- (a) A. E. Reed, R. B. Weinstock and F. Weinhold, *J. Chem. Phys.*, 1985, **83**, 735; (b) A. E. Reed, L. A. Curtiss and F. Weinhold, *Chem. Rev.*, 1988, **88**, 899.

- 17 A. D. Becke and K. E. Edgecombe, *J. Chem. Phys.*, 1990, **92**, 5397.
- 18 S. Noury, X. Krokidis, F. Fuster and B. Silvi, *Comput. Chem.*, 1999, **23**, 597.
- 19 E. R. Johnson, S. Keinan, P. Mori-Sanchez, J. Contreras-Garcia, J. Cohen and A. W. Yang, *J. Am. Chem. Soc.*, 2010, **132**, 6498.
- 20 (a) J. R. Lane, J. Contreras-Garcia, J.-P. Piquemal, B. J. Miller and H. G. Kjaergaard, *J. Chem. Theory Comput.*, 2013, **9**, 3263; (b) J. Contreras-Garcia, E. R. Johnson, S. Keinan, R. Chaudret, J.-P. Piquemal, D. N. Beratan and W. Yang, *J. Chem. Theory Comput.*, 2011, **7**, 625.
- 21 M. J. Frisch, *et al.*, *Gaussian 09, Revision A.02*, Gaussian Inc., Wallingford CT, 2009.
- 22 R. G. Parr, L. von Szentpaly and S. Liu, *J. Am. Chem. Soc.*, 1999, **121**, 1922.
- 23 (a) R. G. Parr and R. G. Pearson, *J. Am. Chem. Soc.*, 1983, **105**, 7512; (b) R. G. Parr and W. Yang, *Density Functional Theory of Atoms and Molecules*, Oxford University Press, New York, 1989.
- 24 (a) L. R. Domingo, E. Chamorro and P. Pérez, *J. Org. Chem.*, 2008, **73**, 4615; (b) L. R. Domingo and P. Pérez, *Org. Biomol. Chem.*, 2011, **9**, 7168.
- 25 L. R. Domingo, P. Pérez and J. A. Sáez, *RSC Adv.*, 2013, **3**, 1486.
- 26 (a) D. H. Ess and K. N. Houk, *J. Am. Chem. Soc.*, 2007, **129**, 10646; (b) D. H. Ess and K. N. Houk, *J. Am. Chem. Soc.*, 2008, **130**, 10187.
- 27 (a) P. Geerlings, F. De Proft and W. Langenaeker, *Chem. Rev.*, 2003, **103**, 1793; (b) L. R. Domingo, M. Ríos-Gutiérrez and P. Pérez, *Molecules*, 2016, **21**, 748.
- 28 L. R. Domingo, M. J. Aurell, P. Pérez and R. Contreras, *Tetrahedron*, 2002, **58**, 4417.
- 29 P. Jaramillo, L. R. Domingo, E. Chamorro and P. Pérez, *J. Mol. Struct. (THEOCHEM)*, 2008, **865**, 68.
- 30 W. Benchouk, S. M. Mekelleche, B. Silvi, M. J. Aurell and L. R. Domingo, *J. Phys. Org. Chem.*, 2011, **24**, 611.
- 31 M. F. Ruiz-López, X. Assfeld, J. I. Garcia, J. A. Mayoral and L. Salvatella, *J. Am. Chem. Soc.*, 1993, **115**, 8780.
- 32 L. R. Domingo, J. A. Sáez, R. J. Zaragozá and M. Arnó, *J. Org. Chem.*, 2008, **73**, 8791.


 CrossMark
 click for updates

 Cite this: *RSC Adv.*, 2017, 7, 15586

Understanding the domino reaction between 1-diazopropan-2-one and 1,1-dinitroethylene. A molecular electron density theory study of the [3 + 2] cycloaddition reactions of diazoalkanes with electron-deficient ethylenes†

 Luis R. Domingo,^{*a} Mar Ríos-Gutiérrez^a and Saeedreza Emamian^b

The reaction between 1-diazopropan-2-one and 1,1-dinitroethylene has been studied using the Molecular Electron Density Theory (MEDT) at the B3LYP/6-31G(d,p) computational level. This reaction comprises two domino processes initialised by a common [3 + 2] cycloaddition (32CA) reaction yielding a 1-pyrazoline, which participates in two competitive reaction channels. Along channel I, 1-pyrazoline firstly tautomerises to a 2-pyrazoline, which by a proton abstraction and spontaneous loss of nitrite anion yields the final pyrazole, while along channel II, the thermal extrusion of the nitrogen molecule in 1-pyrazoline gives a very reactive diradical intermediate which quickly yields the final *gem*-dinitrocyclopropane. Analysis of the conceptual DFT reactivity indices permits an explanation of the participation of 1-diazopropan-2-one in polar 32CA reactions. A Bonding Evolution Theory (BET) study along the more favourable regioisomeric reaction path associated to the 32CA reaction allows an explanation of its molecular mechanism. The present MEDT study sheds light on these complex domino reactions as well as on the participation of diazoalkanes in polar 32CA reactions towards strong electrophilic ethylenes *via* a two-stage one-step mechanism.

 Received 13th January 2017
 Accepted 28th February 2017

DOI: 10.1039/c7ra00544j

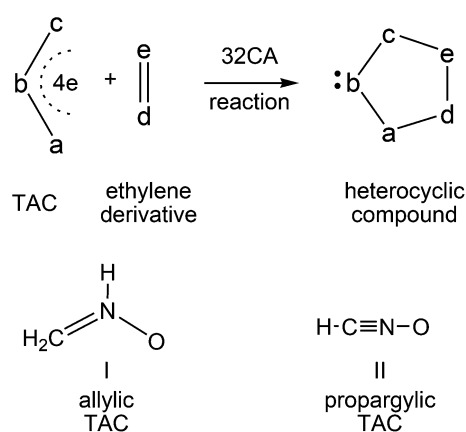
rsc.li/rsc-advances

1. Introduction

Heterocyclic compounds are easily synthesised in a highly regio- and stereoselective fashion by a [3 + 2] cycloaddition (32CA) reaction between a three atom-component (TAC) and an ethylene derivative (see Scheme 1).¹ Substitution of a, b and c in the TAC, and d and e in the ethylene by C, N, O, P or S atoms has proven to be a powerful synthetic tool in the construction of a great diversity of five-membered heterocyclic compounds.¹ TACs can be structurally classified into two categories: allylic type (A-TAC) and propargylic type (P-TAC) structures.² While A-TACs such as nitron I are bent, P-TACs such as nitrile oxide II have a linear structure (see Scheme 1).

Diazoalkanes (DAAs) are P-TACs in which four electrons are distributed in a linear C–N–N structure. After reporting the

cycloadditions of diazoacetate and diazomethane toward C–C multiple bonds by Buchner and von Pechmann in the 1890s,³ many 32CA reactions of DAAs have been reported. In contrast to many TACs which are generated as transient species in the reaction medium, mono- and di-substituted DAAs have been extensively prepared and isolated in pure form.^{1c} The participation of DAA **1** in a 32CA reaction toward non-symmetrically

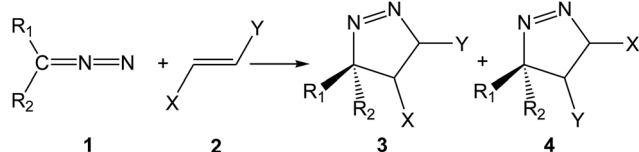


Scheme 1 Construction of five-membered heterocyclic compounds by a 32CA reaction and structural classification of TACs.

^aDepartment of Organic Chemistry, University of Valencia, Dr. Moliner 50, E-46100 Burjassot, Valencia, Spain. E-mail: domingo@utopia.uv.es; Web: <http://www.luisrdomingo.com>

^bChemistry Department, Shahrood Branch, Islamic Azad University, Shahrood, Iran

† Electronic supplementary information (ESI) available: Theoretical background of the topological analysis of ELF and the BET. BET study of the 32CA reaction between DAA **10** and DNE **11**. Geometry of **TS6**. B3LYP/6-31G(d,p) total electronic energies of the stationary points involved in the domino process between DAA **10** and DNE **11**, in gas phase and in the presence of benzene. See DOI: 10.1039/c7ra00544j

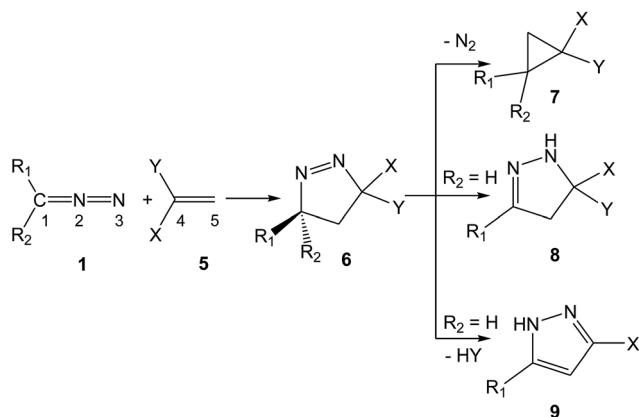


Scheme 2 Participation of DAAs in 32CA reactions toward non-symmetrically substituted ethylenes to generate two regioisomeric 1-pyrazolines.

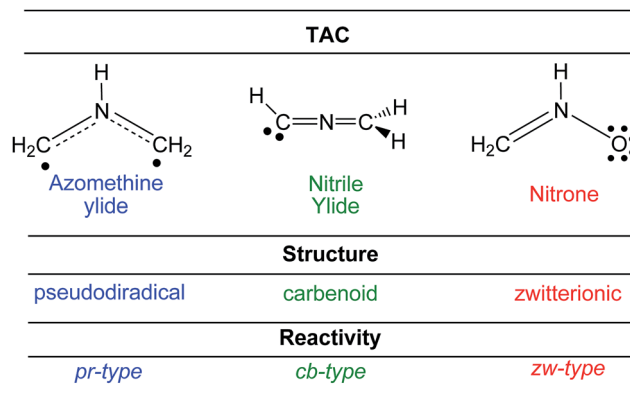
substituted ethylene **2** yields two regioisomeric 1-pyrazolines, **3** and **4**, depending on the approach mode of the reagents (see Scheme 2).

Pyrazolines play a key role in medicinal and agricultural chemistry due to their potent biological activities. Antimicrobial, anticancer, anti-tubercular, anti-inflammatory, antiviral, antitumor and antiangiogenic activities turn the synthesis of pyrazolines into an attractive and valued research area.⁴ Due to the strong repulsion caused by the lone pairs of two adjacent sp² hybridised nitrogen atoms, 1-pyrazolines potentially tend to lose a nitrogen molecule.⁵ In addition, 1-pyrazolines resulting from a 32CA reaction between DAAs **1** and electron-deficient (ED) ethylenes **5** can experience different subsequent transformations, depending on the electronic nature of the substituents present in the DAA and the ethylene. As shown in Scheme 3, cyclopropanes **7**, 2-pyrazolines **8** or pyrazoles (PYZ) **9** can be obtained, respectively, *via* the extrusion of the nitrogen molecule, tautomerisation or HY elimination at the resulting 1-pyrazolines **6**.

Establishing a relationship between the molecular electronic structure and reactivity is the main goal of theoretical organic chemistry. In this sense, very recently, Domingo proposed a new reactivity model in organic chemistry named Molecular Electron Density Theory (MEDT),⁶ in which changes in the electron density along an organic reaction, and not molecular orbital interactions, are responsible for its feasibility. Various MEDT studies devoted to the understanding of the relationship between the electronic structure of TACs and



Scheme 3 Transformation of 1-pyrazolines **6** into cyclopropanes **7**, 2-pyrazolines **8** or PYZs **9** when appropriate substitutions are present in DAAs **1** and ethylenes **5**.

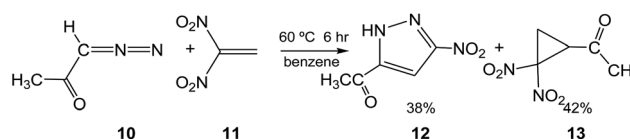


Scheme 4 Electronic structure of TACs and the proposed reactivity types in 32CA reactions.

their reactivity in 32CA reactions have allowed establishing a useful classification of these cycloaddition reactions into pseudodiradical-type⁷ (pr-type), carbenoid-type⁸ (cb-type) and zwitterionic-type⁷ (zw-type) reactions (see Scheme 4). TACs with a pseudodiradical character participate in pr-type 32CA reactions taking place easily through earlier transition state structures (TSs) with very low activation energies and even non-polar character,⁷ while TACs with a carbenoid or zwitterionic character participate in cb- or zw-type 32CA reactions whose feasibility depends on the polar character of the reaction, *i.e.* the nucleophilic character of the TAC and the electrophilic character of the ethylene derivative, or *vice versa*.^{7,8}

Recently, Ivanova *et al.*⁹ experimentally studied some 32CA reactions of various DAAs containing an α -hydrogen atom with 1,1-dinitroethylene (DNE) **11**, an ED ethylene, in the presence as well as in the absence of hexacarbonylmolybdenum, Mo(CO)₆. Thus, when DAA **10**, 1-diazopropan-2-one, was treated with DNE **11** in benzene at 60 °C for 6 h, a mixture of PYZ **12** and *gem*-dinitrocyclopropane (DNCP) **13** was obtained in 38% and 42% yields, respectively (see Scheme 5). Similar results were obtained in the presence of the Mo(CO)₆ complex.⁹

Herein, an MEDT study of the reaction of DAA **10** with DNE **11** yielding PYZ **12** and DNCP **13**, experimentally reported by Ivanova *et al.*,⁹ is carried out using quantum chemical procedures at the B3LYP/6-31G(d,p) computational level in order to understand this complex process. A Bonding Evolution Theory¹⁰ (BET) study of the more favourable regioisomeric channel associated with the 32CA reaction between DAA **10** and DNE **11** is performed in order to characterise the bonding changes along the studied 32CA reaction, and thus to establish the molecular mechanism of the reaction.



Scheme 5 Generation of PYZ **12** and DNCP **13** via the 32CA reaction of DAA **10** with DNE **11** experimentally studied by Ivanova *et al.*⁹

2. Computational details

All stationary points were optimised using the B3LYP functional¹¹ together with the 6-31G(d,p) basis set.¹² The Berny analytical gradient optimisation method¹³ was employed in geometry optimisation steps. The stationary points were characterised by frequency calculations in order to verify that TSs have one and only one imaginary frequency. Intrinsic Reaction Coordinate (IRC) curves¹⁴ were traced in order to check the energy profiles connecting each TS to the two associated minima of the proposed mechanism using the second order González-Schlegel integration method.¹⁵ Solvent effects of benzene were taken into account through single point energy computations at the gas phase optimised stationary points using the Polarizable Continuum Model (PCM) developed by Tomasi's group¹⁶ in the framework of the Self-Consistent Reaction Field (SCRF).¹⁷ The electronic structures of the stationary points were analysed by a Natural Population Analysis (NPA) within the Natural Bond Orbital (NBO) method.¹⁸ The global electron density transfer¹⁹ (GEDT) is computed by the sum of the natural atomic charges (q) of the atoms belonging to each framework (f) at the TSs; $\text{GEDT} = \sum q_f$. The sign indicates the direction of the electron density flux in such a manner that positive values mean a flux from the considered framework to the other one. All computations were carried out with the Gaussian 09 suite of programs.²⁰

The global electrophilicity ω index²¹ is given by the following expression, $\omega = \mu^2/2\eta$, based on the electronic chemical potential, μ , and the chemical hardness, η . Both quantities may be approached in terms of the one-electron energies of the frontier molecular orbitals HOMO and LUMO, ϵ_H and ϵ_L , such as $\mu \approx (\epsilon_H + \epsilon_L)/2$ and $\eta \approx (\epsilon_L - \epsilon_H)$.²² The global nucleophilicity N index²³ based on the HOMO energies obtained within the Kohn–Sham scheme²⁴ is defined as $N = \epsilon_{\text{HOMO}}(\text{Nu}) - \epsilon_{\text{HOMO}}(\text{TCE})$, in which Nu denotes the given nucleophile. This relative nucleophilicity N index is referenced to tetracyanoethylene (TCE). The pr index, which has recently been introduced in order to characterise the participation of pseudodiradical TACs in a pr-type 32CA reaction,⁷ comprises the chemical hardness η and the nucleophilicity N index of the TAC, as $\text{pr} = N/\eta$. Electrophilic P_k^+ and nucleophilic P_k^- Parr functions²⁵ were obtained through the analysis of the Mulliken atomic spin densities (ASD) of the radical anion of DNE 11 and the radical cation of DAA 10. DFT reactivity indices were computed at the B3LYP/6-31G(d) level.

The topological analysis of the Electron Localisation Function (ELF), $\eta(\mathbf{r})$,²⁶ was performed with the TopMod program²⁷ using the corresponding B3LYP/6-31G(d,p) monodeterminantal wavefunctions. For the BET study,¹⁰ the reaction paths were followed using the IRC procedure in mass-weighted internals. Steps of 0.1 [amu^{1/2} bohr] along the IRCs were assumed. A total of 300 points along each side of the IRC was analysed.

3. Results and discussion

The present theoretical study is divided into four parts: (i) first, an analysis of the electronic structure of experimental DAA 10 and the simplest DAA 14 is performed; (ii) then, an analysis of

Conceptual DFT (CDFT) reactivity indices at the ground state of the reagents involved in the 32CA reaction between DAA 10 and DNE 11 is performed in order to predict the reactivity and regioselectivity in this 32CA reaction; (iii) next, the reaction paths involved in these domino processes initialised by the 32CA reaction between DAA 10 and DNE 11 yielding PYZ 12 and DNCP 13 are studied; and (iv) finally, a BET study along the more favourable regioisomeric channel associated with the 32CA reaction of DAA 10 with DNE 11 is carried out in order to characterise the molecular mechanism of this cycloaddition.

3.1. Analysis of the electronic structures of DAAs 10 and 14

As commented in the Introduction, the reactivity of TACs can be correlated with their electronic structure. Consequently, first, an ELF topological analysis of the experimental DAA 10 and the simplest DAA 14 was performed. The representation of ELF attractors, natural atomic charges, obtained through an NPA, ELF valence basins and the proposed Lewis structures for DAAs 10 and 14 are shown in Fig. 1.

As can be seen in Fig. 1, ELF topology of the simplest DAA 14 shows the presence of two monosynaptic basins, $V(\text{C}1)$ and $V'(\text{C}1)$, integrating a total of 1.04 e, at the sp^2 hybridised C1 carbon. The C1–N2 bonding region appears characterised by the presence of one $V(\text{C}1, \text{N}2)$ disynaptic basin integrating 3.06 e, while the presence of two disynaptic basins, $V(\text{N}2, \text{N}3)$ and $V'(\text{N}2, \text{N}3)$, integrating 1.80 e each one, suggests the existence of a N2–N3 double bond according to the Lewis bonding model. Finally, ELF topology of DAA 14 shows the presence of two monosynaptic basins, $V(\text{N}3)$ and $V'(\text{N}3)$, with a total electron density of 3.90 e, associated with two lone pairs at the N3 nitrogen also according to the Lewis bonding model.

ELF topology of the experimental DAA 10 shows a very similar electronic structure to that found in the simplest DAA 14 (see Fig. 1). In this TAC, the two monosynaptic basins, $V(\text{C}1)$ and $V'(\text{C}1)$, present a population of 0.50 e each one. On the other hand, the C1–N2–N3 bonding region shows a similar bonding pattern than that in DAA 14. The only topological difference between the two DAAs is that at DAA 10 the non-bonding electron density associated to the N3 nitrogen atom is represented by one single $V(\text{N}3)$ monosynaptic basin integrating 3.76 e.

According to the Lewis structures, $V(\text{C})$ monosynaptic basins integrating *ca.* 1 e are associated to pseudoradical centers,^{28,29} while those integrating *ca.* 2 e in neutral molecules are associated to carbenoid centers.³⁰ TACs presenting two pseudoradical centers have been classified as pseudodiradical TACs,⁷ while those presenting a carbenoid center have been classified as carbenoid TACs.⁸ Finally, TACs that neither present pseudoradical nor carbenoid centers have been classified as zwitterionic TACs.⁷ Consequently, ELF topology of the experimental DAA 10 and simplest DAA 14 indicates that these TACs neither presents a pseudodiradical,⁷ nor a carbenoid⁸ nor a zwitterionic⁷ electronic structure that would enable them to participate in pr-, cb- or zw-type 32CA reactions (see Scheme 4),^{7,8} but they have a pseudoradical structure.

Although the ELF topological analysis of DAAs 10 and 14 allows establishing a similar bonding pattern in these TACs,

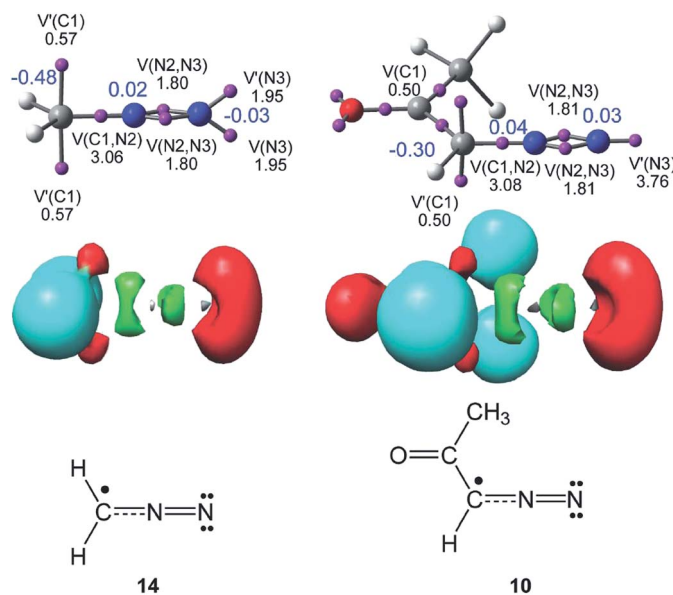


Fig. 1 Representation of ELF attractors, valence basin populations, in e, natural atomic charges, in e and in blue, ELF valence basins and proposed pseudoradical Lewis structures for DAAs **10** and **14**.

NPA does not allow characterising any zwitterionic structure for these two DAAs. It is noteworthy that the C1 carbon has a high negative charge, $-0.48 e$ (**14**) and $-0.30 e$ (**10**), while the N2 and N3 nitrogen atoms have a negligible charge. These findings disagree with the commonly accepted Lewis structure of DAAs represented by a 1,2-zwitterionic structure.

3.2. Analysis of the global and local CDFT reactivity indices at the ground state of the reagents involved in the 32CA reaction

Global reactivity indices defined within CDFT³¹ are powerful tools to explain the reactivity in cycloaddition reactions. Since the global electrophilicity and nucleophilicity scales are given at the B3LYP/6-31G(d) level, the present analysis has been performed at this computational level. The global indices, namely, electronic chemical potential (μ), chemical hardness (η), global electrophilicity (ω) and global nucleophilicity (N) for DAAs **10** and **14** and DNE **11**, and the pr index of DAAs **10** and **14**, are presented in Table 1.

As shown in Table 1, the electronic chemical potential of DAA **10**, $-4.40 eV$, is higher than that of DNE **11**, $-5.98 eV$. Consequently, along the polar 32CA reaction of DAA **10** with DNE **11**, the GEDT¹⁹ will take place from DAA **10** toward ED DNE **11**.

Table 1 B3LYP/6-31G(d) electronic chemical potential, μ , chemical hardness, η , global electrophilicity, ω , and global nucleophilicity, N , indices, in eV, for DAAs **10** and **14**, and DNE **11**, and the pr index of DAAs **10** and **14**

	μ	η	ω	N	pr
DNE 11	-5.98	5.03	3.56	0.62	
DAA 14	-3.64	4.73	1.40	3.11	0.66
DAA 10	-4.40	4.66	2.07	2.39	0.51

Along a polar reaction, there is an electron density transfer from the nucleophilic to the electrophilic species, which is measured by the GEDT¹⁹ value computed at the TS of the reaction; the larger the GEDT at the TS, the more polar the reaction. Note that the GEDT concept comes from the observation that the electron density transfer taking place from the nucleophile to the electrophile along a polar reaction is not a local process, but a global one involving the two interacting frameworks and depending on the electrophilic/nucleophilic interactions taking place between them.¹⁹

The simplest DAA **14** has an electrophilicity ω index of 1.40 eV and a nucleophilicity N index of 3.11 eV, being classified on the borderline of strong electrophiles³² and as a strong nucleophile.³³ Inclusion of a carbonyl group at the C1 carbon atom of the simplest DAA **14** increases the electrophilicity ω index of the experimental DAA **10** to 2.07 eV and decreases the nucleophilicity N index to 2.39 eV, being classified as a strong electrophile and as a moderate nucleophile. Note that most TACs are strong nucleophilic species.³⁴ Consequently, DAA **10** will participate as a strong electrophile or as a moderate nucleophile in polar 32CA reactions.

On the other hand, DNE **11** has a global electrophilicity ω index of 3.56 eV and a nucleophilicity N index of 0.62 eV, being classified as a strong electrophile and as a marginal nucleophile.

In order to characterise the participation of pseudoradical TACs in a pr-type 32CA reaction, the pr index has recently been introduced.⁷ A-TACs with pr values larger than 0.90 can be related to species having a very soft character, *i.e.* with low hardness η values, and low stabilised frontier electrons, *i.e.* with low ionisation potential, participating in pr-type 32CA reactions, while P-TACs with low pr values should participate in zw-type 32CA reactions. P-TACs **10** and **14** have pr values of 0.51 and 0.66, indicating that in spite of their pseudoradical

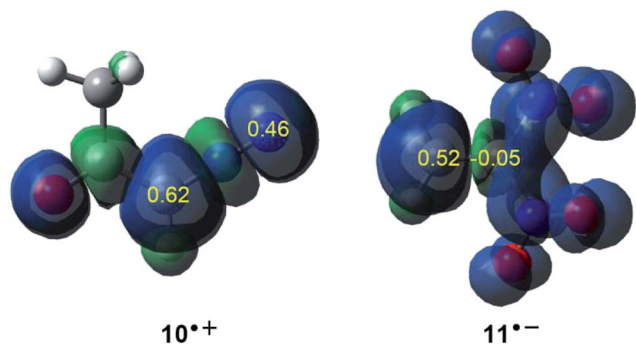


Fig. 2 3D representations of the ASD of the radical cation $10^{\bullet+}$ and the radical anion $11^{\bullet-}$, together with the nucleophilic P_k^- Parr functions of DAA **10** and the electrophilic P_k^+ Parr functions of DNE **11**.

structure they will have a low pr-type reactivity.⁷ This analysis is in clear agreement with the high activation energy found in the 32CA reaction between the simplest DAA **14** and ethylene **17**, $16.6 \text{ kcal mol}^{-1}$.³⁴ Consequently, DAA **10** will not be able to participate in pr-type 32CA reactions, and will thus participate as a strong electrophile or as a moderate nucleophile in polar 32CA reactions.

By approaching a non-symmetric electrophilic/nucleophilic pair along a polar or ionic process, the most favourable reactive channel is that associated with the initial two-center interaction between the most electrophilic center of the electrophile and the most nucleophilic center of the nucleophile. Recently, Domingo proposed the nucleophilic P_k^- and electrophilic P_k^+ Parr functions,²⁵ derived from the changes of spin electron-density reached *via* the GEDT process from the nucleophile to the electrophile, as a powerful tool in the study of the local reactivity in polar or ionic processes.

Accordingly, the nucleophilic P_k^- Parr functions of DAA **10** as well as the electrophilic P_k^+ Parr functions of DNE **11** were analysed in order to characterise the most nucleophilic and electrophilic centers of the species involved in this 32CA reaction (see Fig. 2).

Analysis of the nucleophilic P_k^- Parr functions at the reactive sites of DAA **10** indicates that the C1 carbon atom, with a maximum P_k^- value of 0.62, is the most nucleophilic center. On the other hand, the electrophilic P_k^+ Parr functions at the

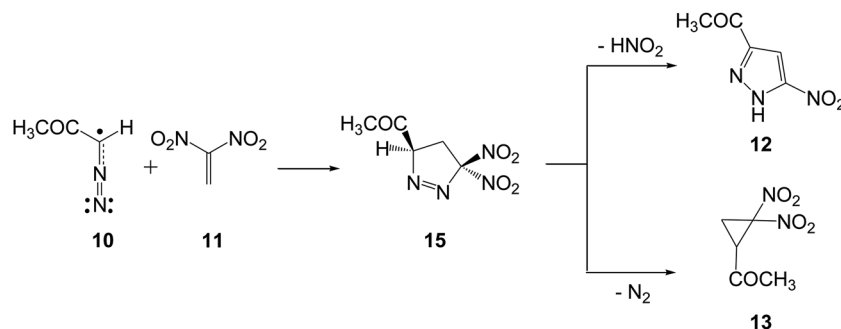
reactive sites of DNE **11** indicate that the most electrophilic center is the C5 carbon atom, possessing the maximum value of $P_k^+ = 0.52$. Note that the C4 carbon atom is electrophilically deactivated, possessing a negative P_k^+ value of -0.05 . Therefore, it is predictable that the most favourable electrophile-nucleophile interaction along the nucleophilic attack of DAA **10** on DNE **11** in a polar process will take place between the most nucleophilic center of DAA **10**, the C1 carbon atom, and the most electrophilic center of DNE **11**, the C5 carbon atom. This prediction is in complete agreement with the experimental outcomes⁹ favouring the formation of 1-pyrazoline **15** which, in turn, participates in the subsequent reactions to generate PYZ **12** and DNCP **13** (see Scheme 6).

3.3. Study of the domino reaction between DAA **10** and DNE **11** giving PYZ **12** and DNCP **13**

The reaction between DAA **10** and DNE **11** giving PYZ **12** and DNCP **13** is a domino process that comprises several consecutive reactions (see Scheme 6). The first one is a 32CA reaction between DAA **10** and DNE **11** yielding 1-pyrazoline **15**. Then, **15** may experience two competitive reactions: (i) a tautomerisation and the subsequent loss of nitrous acid to yield PYZ **12**; or (ii) the extrusion the nitrogen molecule and a rapid ring closure resulting in DNCP **13**.

The first reaction of these domino processes is a 32CA reaction between DAA **10** and DNE **11** yielding 1-pyrazolines **15** and/or **16**. Formation of these pyrazolines depends on the regioisomeric approach mode of the reagents, *i.e.* the initial formation of the C1–C5 or C1–C4 single bonds. An analysis of the stationary points involved in the two regioisomeric paths indicates that this 32CA reaction takes place through a one-step mechanism. Consequently, two reactive molecular complexes (MCs), **MC1** and **MC2**, two regioisomeric TSs, **TS1** and **TS2**, and the two corresponding 1-pyrazolines **15** and **16**, were located and characterised (see Scheme 7). B3LYP/6-31G(d,p) relative energies in gas phase and in benzene for the 32CA reaction between DAA **10** and DNE **11** are given in Scheme 7, while total energies are given in the ESI.†

When DAA **10** and DNE **11** gradually approach each other, the energy is reduced until the formation of two MCs located 1.4 (**MC1**) and 1.5 (**MC2**) kcal mol^{-1} below the separated reagents takes place. Further approach of the two DAA and DNE



Scheme 6 Domino reactions between DAA **10** and DNE **11** yielding PYZ **12** and DNCP **13**.

frameworks leads to the formation of the TSs, which are located 9.4 (**TS1**) and 16.7 (**TS2**) kcal mol⁻¹ above the corresponding MCs. Moreover, formation of 1-pyrazolines **15** and **16** becomes exothermic by 23.2 and 19.5 kcal mol⁻¹, respectively. Some appealing conclusions can be drawn from these energy results: (i) the activation energy associated with **TS1** is 7.4 kcal mol⁻¹ lower in energy than that associated with the 32CA reaction of the simplest DAA **14** with ethylene **17**; 16.6 kcal mol⁻¹.³⁴ It is interesting to note that in spite of the pseudoradical structure of DAAs **10** and **14** (see Fig. 1), the low pr index of these TACs (see Table 1) together with the very high activation energy of the 32CA reaction of DAA **14** with ethylene **17** indicates that they do not participate in pr-type 32CA reactions; (ii) this 32CA reaction is completely regioselective, **TS2** being 7.9 kcal mol⁻¹ above **TS1**, in complete agreement with the experimentally observed regioselectivity; and (iii) the strong exothermic character of this reaction makes the formation of 1-pyrazolines **15** and **16** irreversible. Consequently, 1-pyrazoline **15** is obtained through the kinetic control of the reaction.

Inclusion of the solvent effects of benzene does not significantly modify the relative gas phase energies (see Scheme 7). In benzene, the activation energy of the reaction slightly decreases to 8.1 kcal mol⁻¹, while the 32CA reaction remains completely regioselective.

After the formation of 1-pyrazoline **15**, this species can participate in the competitive reaction channels I and II (see Scheme 8). Along channel I, 1-pyrazoline **15** first tautomerises to 2-pyrazoline **18**, which by a loss of nitrous acid yields PYZ **12**, while along channel II, the thermal extrusion of the nitrogen molecule in 1-pyrazoline **15** gives the diradical intermediate **IN2**, which quickly yields the final DNCP **13**. (U)B3LYP/6-31G(d,p) relative energies in gas phase and in benzene for the competitive reactions of 1-pyrazoline **15** are given in Scheme 8, while total energies are given in the ESI.†

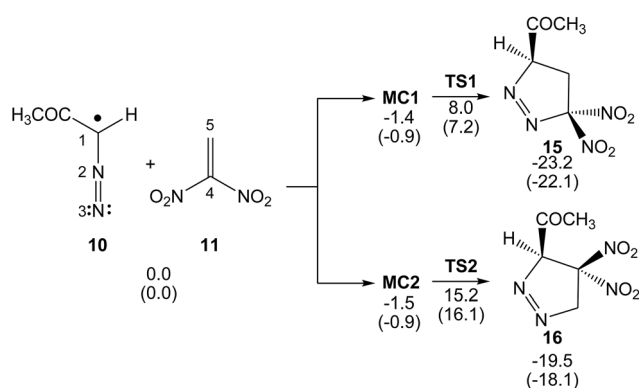
The two consecutive reactions involved in channel I can be promoted by any acid/basic species present in the reaction medium. In this study, the HNO₂/NO₂⁻ pair was selected as the acid/basic species since nitrous acid is a reaction product. Conversion of 1-pyrazoline **15** into 2-pyrazoline **18** is

a tautomerisation process associated to a 1,3-hydrogen shift. Several studies have shown that the direct 1,3-hydrogen shift is energetically very unfavourable due to the formation of a strained four-membered cyclic TS.³⁵ Consequently, the tautomerisation should take place through a stepwise mechanism. The first step consists in the H1 proton abstraction by the nitrite anion acting as a base yielding anionic intermediate **IN1**. From **MC3**, in which the nitrite anion forms a hydrogen-bond with the H1 hydrogen atom, this step has a very low activation energy, 1.3 kcal mol⁻¹ (**TS3**); formation of intermediate **IN1** is slightly exothermic by 0.6 kcal mol⁻¹. The subsequent proton transfer from nitrous acid to the N3 nitrogen atom has no activation barrier, formation of 2-pyrazoline **18** being exothermic by 16.3 kcal mol⁻¹; note that this step is a thermodynamically controlled acid/base process (since the nitrite anion is involved in some steps of channel I, relative energies in benzene are discussed). Conversion of 1-pyrazoline **15** into 2-pyrazoline **18** is thermodynamically very favourable as it is exothermic by 16.3 kcal mol⁻¹. This finding is in agreement with the experimental observation that in 32CA reactions involving DAAs containing an α -hydrogen atom, 2-pyrazolines are obtained as a reaction product (see 2-pyrazolines **8** in Scheme 3).

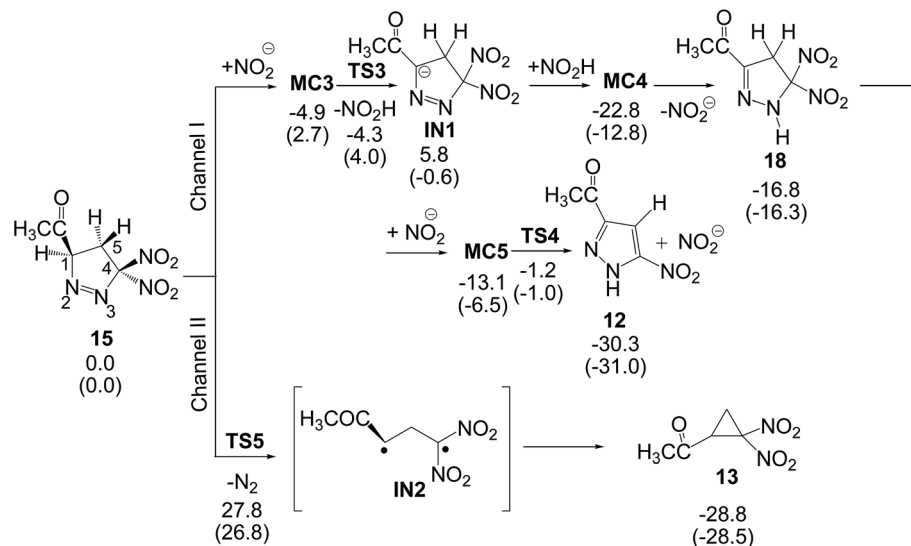
Due to the relative acid character of the H5 hydrogen atoms of 2-pyrazoline **18**, the corresponding proton abstraction process from C5 by the nitrite anion presents a low activation energy of 7.5 kcal mol⁻¹. Interestingly, after the H5 proton abstraction, the subsequent loss of the nitrite anion has not activation energy; this last step being exothermic by 24.5 kcal mol⁻¹. Along channel I, formation of final PYZ **12** plus nitrous acid from 1-pyrazoline **15** is exothermic by 31.0 kcal mol⁻¹. Consequently, conversion of 1-pyrazoline **15** into final PYZ **12** through the studied reaction channel I can be considered irreversible.

Along channel II, the thermal extrusion of the nitrogen molecule at 1-pyrazoline **15** gives a diradical intermediate **IN2**, which is quickly converted into the final DNCP **13** by a ring closure through a C-to-C coupling of the C1 and C4 radical centers present in intermediate **IN2**. Due to the diradical structure of intermediate **IN2**, channel II was studied using unrestricted UB3LYP calculations. The activation energy associated with the extrusion of the nitrogen molecule *via* **TS5** is 26.8 kcal mol⁻¹. In spite of this high activation energy, this unimolecular process is not entropically unfavourable. The IRC from **TS5** to products discontinues at species **19**, which is 17.0 kcal mol⁻¹ higher in energy than 1-pyrazoline **15**. However, full optimisation of this species yields the final DNCP **13** in a straightforward manner, and the extrusion of the nitrogen molecule and subsequent ring closure being exothermic by 28.5 kcal mol⁻¹. Consequently, the strong exothermic character of the formation of DNCP **13** as well as PYZ **12** makes these domino reactions irreversible.

In 1978, Engel studied the extrusion of the nitrogen molecule from cyclic and bicyclic azo compounds.³⁶ For the extrusion of the nitrogen molecule from cyclic azo compound **20** yielding cyclopropane **21**, an activation enthalpy of 39.0 kcal mol⁻¹ was experimentally estimated (see Scheme 9). Interestingly, a relatively similar gas phase activation energy of 42.1 kcal mol⁻¹ has



Scheme 7 32CA reaction between DAA **10** and DNE **11**. Relative energies are given in kcal mol⁻¹. Energies in benzene are given in parentheses.



Scheme 8 Proposed reaction channels for the conversion of 1-pyrazoline **15** into PYZ **12** and DNCP **13**. Relative energies are given in kcal mol⁻¹. Energies in benzene are given in parentheses.

been obtained at the UB3LYP/6-31G(d,p) level, asserting our computational level to study this reaction channel. In spite of this high activation enthalpy, the favourable activation entropy experimentally estimated for this extrusion reaction, 8.8 cal mol⁻¹ K, favours this thermal reaction.

Gas-phase optimised TSs involved in the domino reactions between DAA **10** and DNE **11** (see Schemes 7 and 8), including some selected distances, are given in Fig. 3. At the TSs associated with the 32CA reaction between DAA **10** and DNE **11**, the distances between the atoms involved in the formation of the C–C and C–N single bonds are: 2.025 Å (C1–C5) and 2.653 Å (N3–C4) at **TS1**, and 1.941 Å (N3–C5) and 2.369 Å (C1–C4) at **TS2**. Some appealing conclusions can be drawn from these geometrical parameters; (i) the more favourable **TS1** is associated with a highly asynchronous bond-formation process; (ii) this 32CA reaction takes place *via* a two-stage one-step mechanism³⁷ (see below). Thus, **TS1** is associated with the nucleophilic attack of the C1 carbon of DAA **10** on the β-conjugated position of DNE **11**, in clear agreement with the analysis of the Parr functions; and (iii) at the two regioisomeric TSs, the single-bond formation involving the most electrophilic center of DNE **11**, the C5 carbon, is more advanced than that involving the C4 carbon.

At **TS3**, associated with the proton abstraction at 1-pyrazole **15**, the length of the C1–H1 breaking bond is 1.294 Å, while the length of the H1–O forming bond is 1.381 Å. At **TS4**, associated with the proton abstraction at 2-pyrazoline **18**, the length of the

C5–H5 breaking bond is 1.422 Å, while the length of the H5–O forming bond is 1.240 Å. Finally, at **TS5**, associated with the extrusion of the nitrogen molecule in 1-pyrazole **15**, the lengths of the C1–N2 and N2–C3 breaking bonds are 2.052 Å and 2.294 Å, respectively. These lengths are relatively similar to those obtained at **TS6**, associated to the extrusion of the nitrogen

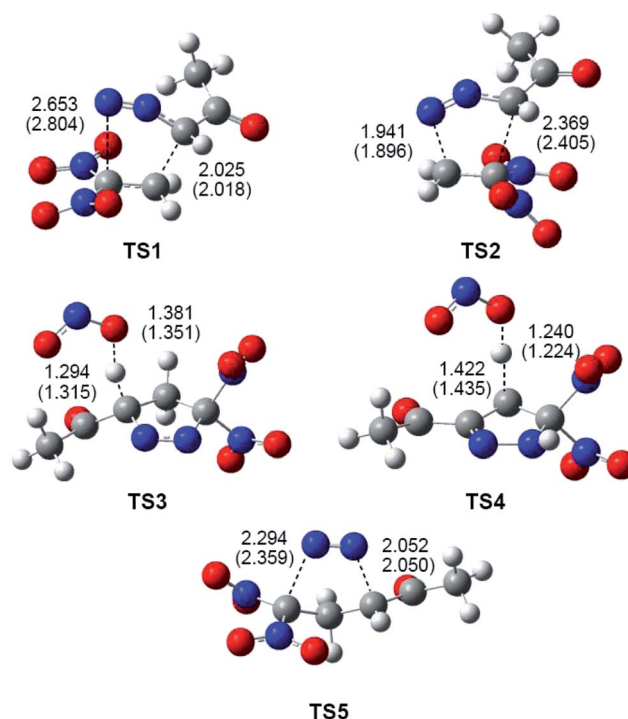
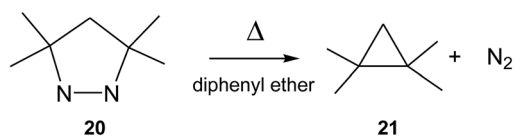


Fig. 3 B3LYP/6-31G(d,p) optimised geometries of the TSs involved in the domino reaction between DAA **10** and DNE **11**, see Schemes 7 and 8. Distances are given in Angstroms. Distances in benzene are given in parentheses.



Scheme 9 Thermal extrusion of the nitrogen molecule from cyclic azo compound **20**.

molecule from cyclic azo compound **20**, namely 2.23 Å (see **TS6** in the ESI†).

The inclusion of the solvent effects of benzene does not substantially modify the TS geometries. At the most favourable regioisomeric **TS1** associated with the 32CA reaction, benzene slightly increases the asynchronicity as the C3–N4 distance is increased, but this change has no chemical significance.

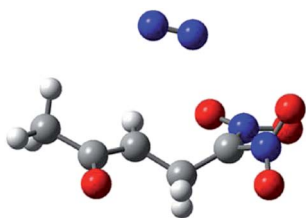
Both, the single imaginary frequency associated to **TS4**, -1005.6 cm^{-1} , and the atomic movements associated to this imaginary frequency, indicate that this TS is mainly associated with the H5 proton abstraction. However, the IRC from **TS4** towards the products shows that the extrusion of nitrite anion takes place in the same elementary step after the complete proton abstraction. On the other hand, as commented before, the IRC from **TS5** towards the products discontinues at species **19** (see Fig. 4). After removing the nitrogen molecule, full UB3LYP/6-31G(d,p) optimisation of a feasible diradical intermediate yields DNCP **13** in a straightforward manner.

The polar nature of the 32CA reaction between DAA **10** and DNE **11** was analysed by computing the GEDT¹⁹ at the corresponding TSS. In order to calculate the GEDT, the natural atomic charges, obtained through an NPA, at **TS1** and **TS2**, involved in the studied 32CA reaction, were computed at the ethylene as well as the DAA frameworks. In gas phase, the GEDT that fluxes from the DAA moiety toward the ED ethylene one is 0.34 e at **TS1** and 0.24 e at **TS2**. These values indicate that this 32CA reaction has a strong polar character. The higher GEDT value found at the more favourable regioisomeric **TS1** is in clear agreement with the relative low activation energy associated with this 32CA reaction (see Scheme 7).³⁸ This high polar character arises from the strong electrophilic character of DNE **11**, in spite of the moderate nucleophilic character of DAA **10** (see Section 3.2).

3.4. BET study of the 32CA reaction between DAA **10** and DNE **11**

In order to understand the molecular mechanism of the 32CA reaction between DAA **10** and DNE **11**, a BET study of the more favourable C1–C5 regioisomeric channel was performed. The complete BET study is given in the ESI.†

Some appealing conclusions can be drawn from this BET study: (i) ten differentiated phases associated with the creation or disappearance of valence basins are distinguished along the



19

Fig. 4 Diradical species **19** resulting from the IRC from **TS5** towards the products.

C1–C5 regioisomeric reaction channel (see Fig. 5); (ii) **TS1** is found in the very short phase VI presenting a bonding pattern similar to that found at **P5** (see ELF valence basins of **P5** in Fig. 6). **TS1** is characterised by the presence of three monosynaptic basins, V(C1), V(C4) and V(C5). While the V(C1) monosynaptic basin was already present at DAA **10**, the V(C4) and V(C5) monosynaptic basins present at the DNE **11** framework are formed along the reaction path on going from **MC1** to **TS1**. A significant amount of the electron density of these monosynaptic basins comes from the high GEDT that takes place at **TS1**, 0.35 e.³⁸ (iii) formation of the C1–C5 single bond begins at phase VII at a C1–C5 distance of 2.01 Å, following the recently proposed pattern:¹⁹ (a) depopulation of the C1–N2 and C4–C5 bonding regions, (b) formation of two non-bonding V(C1) and V(C5) monosynaptic basins (see **P5** in Fig. 6), and (c) formation of a new V(C1,C5) disynaptic basin through the merger of the electron density of the aforementioned monosynaptic basins (see the V(C1,C5) disynaptic basin at **P6** in Fig. 6); (iv) a different behaviour is found for the formation of the N3–C4 single bond. Formation of the N3–C4 single bond begins with the creation of a new V(N3,C4) disynaptic basin at the last phase X at the very short N3–C4 distance of 1.69 Å (see V(N3,C5) disynaptic basin at **P9** in Fig. 6). The electron population of this new disynaptic basin proceeds from the electron density of one V(C4) monosynaptic basin created at the α position of the two nitro groups and one V(N3) monosynaptic basin associated with a N3 pseudoradical center (see **P8** in Fig. 6); (v) at **P9**, the V(C1,C5) disynaptic basin has reached 97% of its population in 1-pyrazoline **15**. This behaviour indicates that this 32CA reaction takes place through a two-stage one-step mechanism;³⁷ and (vi) along the more favourable regioisomeric channel, formation of the first C1–C5 single bond takes place through a two-center interaction involving the most nucleophilic center of DAA **10**, the C1 carbon, and the most electrophilic center of DNE **11**, the C5 carbon, a behaviour anticipated by the analysis of the electrophilic and nucleophilic Parr functions.²⁵

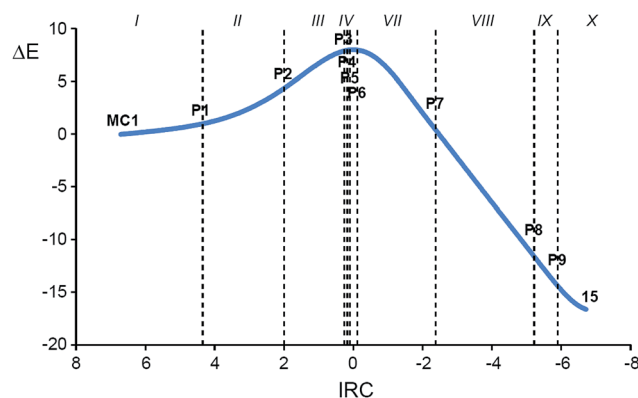


Fig. 5 Relative energy (ΔE , in kcal mol^{-1}) variations along the IRC ($\text{amu}^{1/2}\text{ bohr}$) associated with the 32CA reaction between DAA **10** with DNE **11** showing the relative positions of the selected points separating the ten topological phases along the reaction path.

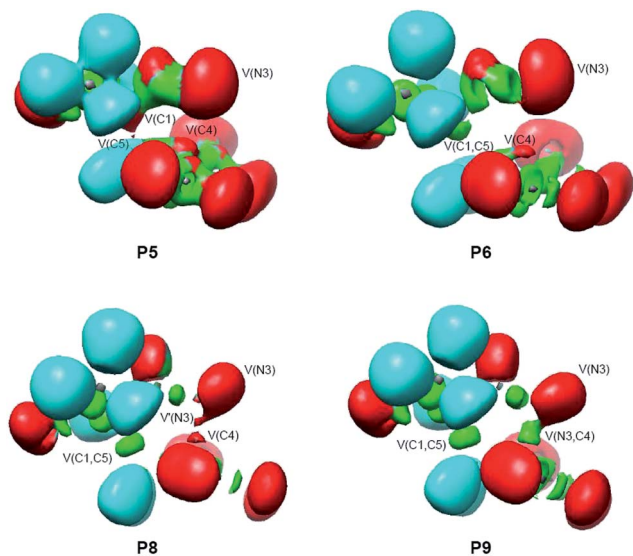


Fig. 6 ELF valence basin representations of selected points involved in the C1–C5 and N3–C4 single bond formation processes along the IRC path of the 32CA reaction between DAA 10 with DNE 11.

4. Conclusions

The reaction between DAA 10 and DNE 11 yielding PYZ 12 and DNCP 13 has been theoretically studied using the MEDT at the B3LYP/6-31G(d,p) computational level. Formation of PYZ 12 and DNCP 13 takes place through two domino processes initialised by a polar 32CA reaction between DAA 10 and DNE 11 yielding 1-pyrazoline 15, which experiences two successive competitive reactions. Along channel I, 1-pyrazoline 15 first tautomerises to 2-pyrazoline 18, which by a proton abstraction and spontaneous loss of nitrite anion yields PYZ 12, while along channel II, the thermal extrusion of the nitrogen molecule in 1-pyrazoline 15 gives a diradical intermediate IN2, which quickly closes yielding the final DNCP 13. Although the activation energies of the two competitive channels are not comparable, due to the need to model the corresponding acid/basic species demanded for the tautomerisation of 1-pyrazolines into 2-pyrazolines, and the further conversion of those into PYZs (see Scheme 8), the present MEDT study makes it possible to understand the chemical conversion of 1-pyrazolines obtained from a 32CA reaction of DAAs with ED ethylenes into the different reaction products experimentally observed.

ELF analysis of the electronic structures of DAAs 10 and 14 shows that they have a pseudoradical structure. Analysis of the CDFT reactivity indices indicates that although DAA 10 is not a strong nucleophile, the strong electrophilic character of DNE 11 favours the 32CA reaction to take place through a polar mechanism with high polar character and with relatively low activation energy, 9.4 kcal mol⁻¹. Note that the low pr index of these TACs together with the high activation energy associated with the non-polar 32CA reaction of the simplest DAA 14 with ethylene 17, 15.4 kcal mol⁻¹,³⁴ indicate that these pseudoradical TACs do not participate in pr-type 32CA reactions.

A BET study of the bonding changes along the more favourable regioisomeric channel associated with the 32CA reaction

between DAA 10 and DNE 11 allows concluding that: (i) formation of the first C1–C5 single bond takes place at a C1–C5 distance of 2.01 Å by a C-to-C coupling of two pseudoradical centers, one already present in DAA 10 and another generated at the most electrophilic center of DNE 11 as a consequence of the high GEDT taking place in this polar process;³⁸ (ii) formation of the second N3–C4 single bond begins at the end of the reaction path at the very short N3–C4 distance of 1.69 Å through sharing the electron density of two N3 and C4 pseudoradical centers. This model for the formation of carbon–heteroatom single bonds is similar to that found for the C–O single bond formation in the second stage of the cycloaddition reactions of carbenoid intermediates with CO₂;³⁹ and (iii) the high asynchronicity found in the formation of the C–C and C–N single bonds indicates that this polar 32CA reaction takes place through a two-stage one-step mechanism.³⁷

The present MEDT study sheds light on these complex domino reactions as well as on the participation of DAAs in polar 32CA reactions. The electronic structures of the studied DAAs as well as their reactivity towards ethylene do not permit the classification of these TACs into one of the three groups in which TACs are currently classified in Scheme 4. Currently, further studies devoted to the reactivity of pseudoradical TACs are being carried out by our group.

Acknowledgements

This research was supported by the Ministry of Economy and Competitiveness (MINECO) of the Spanish Government, project CTQ2016-78669-P. M. R.-G. also thanks MINECO for a pre-doctoral contract co-financed by the European Social Fund (BES-2014-068258).

References

- (a) W. Carruthers, *Some Modern Methods of Organic Synthesis*, Cambridge University Press, Cambridge, 2nd edn, 1978; (b) W. Carruthers, *Cycloaddition Reactions in Organic Synthesis*, ed. J. E. Baldwin and P. D. Magnus, Pergamon, Oxford, 1990; (c) *Synthetic Applications of 1,3-Dipolar Cycloaddition Chemistry Toward Heterocycles and Natural Products*, ed. A. Padwa and W. H. Pearson, John Wiley & Sons, Inc, 2002, vol. 59.
- K. V. Gothelf and K. A. Jorgensen, *Chem. Rev.*, 1998, **98**, 863.
- (a) E. Buchner, *Ber. Dtsch. Chem. Ges.*, 1888, **21**, 2637; (b) H. von Pechmann, *Ber. Dtsch. Chem. Ges.*, 1898, **31**, 2950.
- (a) J. V. Mehta, S. B. Gajera, P. Thakor, V. R. Thakkar and M. N. Patel, *RSC Adv.*, 2015, **5**, 85350; (b) K. A. Kumar and M. Govindaraju, *Int. J. ChemTech Res.*, 2015, **8**, 313.
- P. S. Engel, *Chem. Rev.*, 1980, **80**, 99.
- L. R. Domingo, *Molecules*, 2016, **21**, 1319.
- L. R. Domingo and S. R. Emamian, *Tetrahedron*, 2014, **70**, 1267.
- L. R. Domingo, M. Ríos-Gutiérrez and P. Pérez, *Tetrahedron*, 2016, **72**, 1524.
- O. Ivanova, E. M. Budynina, E. B. Averina, T. S. Kuznetsova, Y. K. Grishin and N. S. Zefirov, *Synthesis*, 2007, **13**, 2009.
- X. Krokidis, S. Noury and B. Silvi, *J. Phys. Chem. A*, 1997, **101**, 7277.

- 11 (a) C. Lee, W. Yang and R. G. Parr, *Phys. Rev. B: Condens. Matter Mater. Phys.*, 1988, **37**, 785; (b) A. D. Becke, *J. Chem. Phys.*, 1993, **98**, 5648.
- 12 W. J. Hehre, L. Radom, P. v. R. Schleyer and J. A. Pople, *Ab initio Molecular Orbital Theory*, Wiley, New York, 1986.
- 13 X. Li and M. J. Frisch, *J. Chem. Theory Comput.*, 2006, **2**, 835.
- 14 K. Fukui, *J. Phys. Chem.*, 1970, **74**, 4161.
- 15 (a) H. B. Schlegel, *J. Comput. Chem.*, 1982, **2**, 214; (b) H. B. Schlegel, in *Modern Electronic Structure Theory*, ed. D. R. Yarkony, World Scientific Publishing, Singapore, 1994.
- 16 (a) J. Tomasi and M. Persico, *Chem. Rev.*, 1994, **94**, 2027; (b) B. Y. Simkin and I. Sheikhet, *Quantum Chemical and Statistical Theory of Solutions – Computational Approach*, Ellis Horwood, London, 1995.
- 17 (a) E. Cancès, B. Mennucci and J. Tomasi, *J. Chem. Phys.*, 1997, **107**, 3032; (b) M. Cossi, V. Barone, R. Cammi and J. Tomasi, *Chem. Phys. Lett.*, 1996, **255**, 327; (c) V. Barone, M. Cossi and J. Tomasi, *J. Comput. Chem.*, 1998, **19**, 404.
- 18 (a) A. E. Reed, R. B. Weinstock and F. Weinhold, *J. Chem. Phys.*, 1985, **83**, 735; (b) A. E. Reed, L. A. Curtiss and F. Weinhold, *Chem. Rev.*, 1988, **88**, 899.
- 19 L. R. Domingo, *RSC Adv.*, 2014, **4**, 32415.
- 20 M. J. Frisch, *et al.*, *Gaussian 09, Revision A.02*, Gaussian, Inc., Wallingford CT, 2009.
- 21 R. G. Parr, L. von Szentpaly and S. Liu, *J. Am. Chem. Soc.*, 1999, **121**, 1922.
- 22 (a) R. G. Parr and R. G. Pearson, *J. Am. Chem. Soc.*, 1983, **105**, 7512; (b) R. G. Parr and W. Yang, *Density Functional Theory of Atoms and Molecules*, Oxford University Press, New York, 1989.
- 23 (a) L. R. Domingo, E. Chamorro and P. Pérez, *J. Org. Chem.*, 2008, **73**, 4615; (b) L. R. Domingo and P. Pérez, *Org. Biomol. Chem.*, 2011, **9**, 7168.
- 24 W. Kohn and L. J. Sham, *Phys. Rev.*, 1965, **140**, 1133.
- 25 L. R. Domingo, P. Pérez and J. A. Sáez, *RSC Adv.*, 2013, **3**, 1486.
- 26 A. D. Becke and K. E. Edgecombe, *J. Chem. Phys.*, 1990, **92**, 5397.
- 27 S. Noury, K. Krokidis, F. Fuster and B. Silvi, *Comput. Chem.*, 1999, **23**, 597.
- 28 L. R. Domingo, E. Chamorro and P. Pérez, *Lett. Org. Chem.*, 2010, **7**, 432.
- 29 L. R. Domingo and J. A. Sáez, *J. Org. Chem.*, 2011, **76**, 373.
- 30 M. Ríos-Gutiérrez, L. R. Domingo and P. Pérez, *RSC Adv.*, 2015, **5**, 84797.
- 31 (a) P. Geerlings, F. De Proft and W. Langenaeker, *Chem. Rev.*, 2003, **103**, 1793; (b) L. R. Domingo, M. Ríos-Gutiérrez and P. Pérez, *Molecules*, 2016, **21**, 748.
- 32 L. R. Domingo, M. J. Aurell, P. Pérez and R. Contreras, *Tetrahedron*, 2002, **58**, 4417.
- 33 P. Jaramillo, L. R. Domingo, E. Chamorro and P. Pérez, *J. Mol. Struct.: THEOCHEM*, 2008, **865**, 68.
- 34 L. R. Domingo, M. J. Aurell and P. Pérez, *Tetrahedron*, 2014, **70**, 4519.
- 35 S. R. Emamian, L. R. Domingo and S. F. Tayyari, *J. Mol. Graphics Modell.*, 2014, **49**, 47.
- 36 P. S. Engel, R. A. Hayes, L. Keifer, S. Szilagyí and J. W. Timberlake, *J. Am. Chem. Soc.*, 1978, **100**, 1876.
- 37 L. R. Domingo, J. A. Sáez, R. J. Zaragoza and M. Arnó, *J. Org. Chem.*, 2008, **73**, 8791.
- 38 L. R. Domingo, M. Ríos-Gutiérrez and P. Pérez, *Tetrahedron*, 2017, DOI: 10.1016/j.tet.2017.02.012.
- 39 L. R. Domingo, M. Ríos-Gutiérrez, E. Chamorro and P. Pérez, *Theor. Chem. Acc.*, 2017, **136**, 1.

Article

A Molecular Electron Density Theory Study of the Reactivity of Azomethine Imine in [3+2] Cycloaddition Reactions

Luis R. Domingo* and Mar Ríos-Gutiérrez

Department of Organic Chemistry, University of Valencia, Dr. Moliner 50, E-46100 Burjassot, Valencia, Spain; rios@utopia.uv.es

* Correspondence: domingo@utopia.uv.es; Tel.: +34-963-543-106

Academic Editor: Derek J. McPhee

Received: 10 April 2017; Accepted: 30 April 2017; Published: 6 May 2017

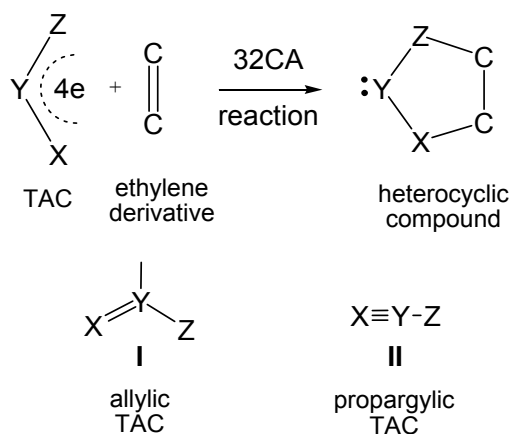
Abstract: The electronic structure and the participation of the simplest azomethine imine (AI) in [3+2] cycloaddition (32CA) reactions have been analysed within the Molecular Electron Density Theory (MEDT) using Density Functional Theory (DFT) calculations at the MPWB1K/6-311G(d) level. Topological analysis of the electron localisation function reveals that AI has a *pseudoradical* structure, while the conceptual DFT reactivity indices characterises this three-atom-component (TAC) as a moderate electrophile and a good nucleophile. The non-polar 32CA reaction of AI with ethylene takes place through a one-step mechanism with moderate activation energy, 8.7 kcal·mol⁻¹. A bonding evolution theory study indicates that this reaction takes place through a non-concerted [2n + 2 τ] mechanism in which the C–C bond formation is clearly anticipated prior to the C–N one. On the other hand, the polar 32CA reaction of AI with dicyanoethylene takes place through a *two-stage one-step* mechanism. Now, the activation energy is only 0.4 kcal·mol⁻¹, in complete agreement with the high polar character of the more favourable regioisomeric transition state structure. The current MEDT study makes it possible to extend Domingo's classification of 32CA reactions to a new *pseudo(mono)radical* type (*pmr-type*) of reactivity.

Keywords: azomethine imine; [3+2] cycloaddition reactions; molecular electron density theory; conceptual density functional theory; electron localisation function; bonding evolution theory; electron density; molecular mechanisms; chemical reactivity

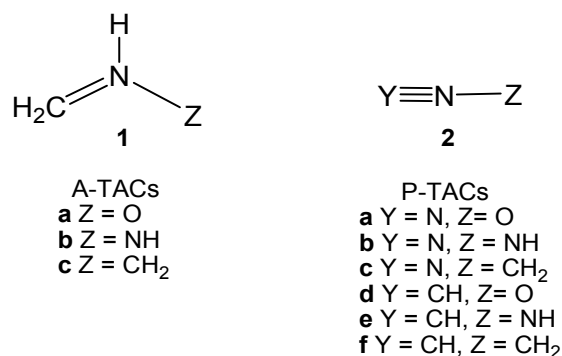
1. Introduction

[3+2] cycloaddition (32CA) reactions emerged as a powerful synthetic tool for the construction of five-membered heterocyclic compounds [1,2]. Although these reactions have been experimentally known since the end of the 19th century, it was Huisgen who, in 1961, defined them as “1,3-dipolar cycloadditions” [3,4]. These reactions are bimolecular in nature and involve the 1,3-addition of an ethylene derivative to a three-atom-component (TAC) (see Scheme 1). TACs can be structurally classified into two categories: allylic type (A-TAC) and propargylic type (P-TAC) structures [5,6]. While A-TACs such as **I** are bent, P-TACs such as **II** have a linear structure (see Scheme 1).

To explain the reactivity of TACs in 32CA reactions, Houk introduced, in 2007, a distortion/interaction energy model (DIEM) in which the activation barrier is divided into two additive terms: ΔE_d^\ddagger , called *distortion* energy, and ΔE_i^\ddagger , called *interaction* energy [7,8]. The applicability of this model was checked in 32CA reactions of nine different TACs, three A-TACs **1a–c** and six P-TACs **2a–f**, with ethylene **3** and acetylene **4** (see Scheme 2) [7,8].



Scheme 1. Construction of five-membered heterocyclic compounds by a 32CA reaction, and classification of TACs by structure.



Scheme 2. Nine TACs studied by Houk [7,8].

Houk found that the computed B3LYP/6-31G(d) activation enthalpies correlated very nicely with the distortion energies: $\Delta E^\ddagger = 0.74 \times \Delta E_d^\ddagger - 0.78 \text{ kcal}\cdot\text{mol}^{-1}$ ($R^2 = 0.97$) (see Figure 1). He concluded that the *distortion energy* of the reagents towards the transition state structure (TS) is the major factor controlling the reactivity differences of TACs. This finding, which can be considered a computational assertion of Hammond's postulate established in 1955 [9], does not resolve the question why activation energies depend on geometries, which are the result of the distribution of the molecular electron density. In addition, the partition of the TS geometries into two separated fragments has no physical significance within Density Functional Theory [10] (DFT), since in this quantum chemical theory the energy is a functional of the electron density and the external potential, i.e., the nuclei positions. Consequently, the energy of the two separated fragments cannot be correlated with the energy of the TS because each of them loses the external potential created by the other fragment [11].

Very recently, Domingo has proposed a new reactivity theory in organic chemistry, namely, Molecular Electron Density Theory [12] (MEDT), in which changes in the electron density along an organic reaction, and not molecular orbital (MOs) interactions as proposed by the Frontier Molecular Orbital (FMO) theory [13], are responsible for its feasibility.

Several MEDT studies devoted to understanding the reactivity of TACs participating in 32CA reactions have allowed establishing a very good correlation between their electronic structures and reactivities. Accordingly, depending on the electronic structure of the TAC, i.e., *pseudodiradical* (typically an azomethine ylide (AY) **1a**) [14], *carbenoid* (typically a nitrile ylide **2f**) [15] or *zwitterionic* (typically a nitron (Ni) **1c**), the 32CA reactions towards ethylene **3** have been classified into *pseudodiradical-type* (*pr-type*) [16], *carbenoid-type* (*cb-type*) [17] and *zwitterionic-type* (*zw-type*) [16] reactions (Scheme 3). The reactivity trend decreases in the order

pseudodiradical > carbenoid > zwitterionic, in such a manner that while *pr*-type 32CA reactions take place easily through earlier TSs even with a very low polar character [16,18], *zw*-type 32CA reactions demand the adequate nucleophilic/electrophilic activations to take place [16,17,19]. Note that the feasibility of the three reactivity types depends on the polar character of the reaction, i.e., the nucleophilic/electrophilic interactions taking place at the TSs; the more polar the reaction, the faster the reaction.

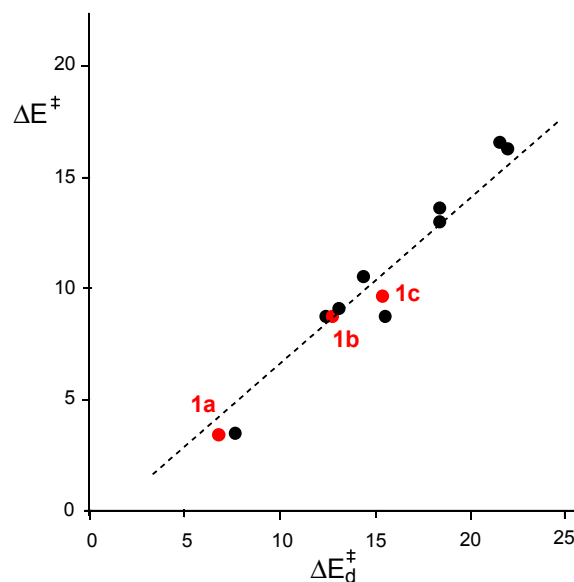
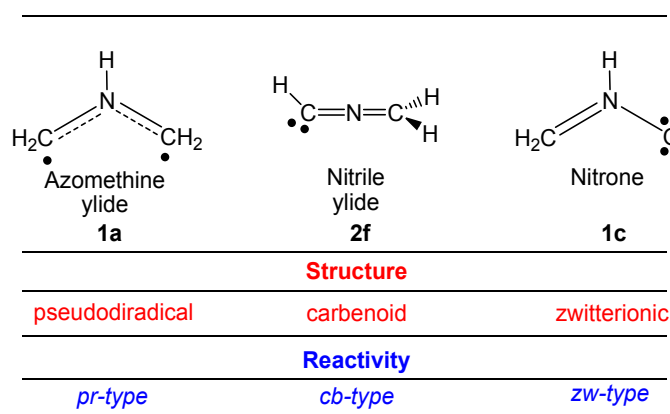


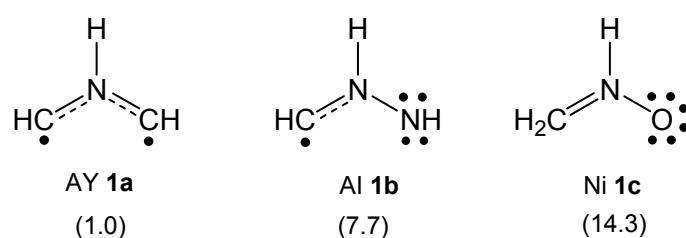
Figure 1. Plot of B3LYP/6-31G(d) activation energies ΔE^\ddagger vs. distortion energies: ΔE_d^\ddagger , in kcal·mol⁻¹, for Houk's 32CA reactions of TACs 1 and 2 with ethylene 3 and acetylene 4 [7,8]. The position of TACs 1a–c is marked in red (see Scheme 4).



Scheme 3. Electronic structure of TACs and the proposed reactivity types in 32CA reactions.

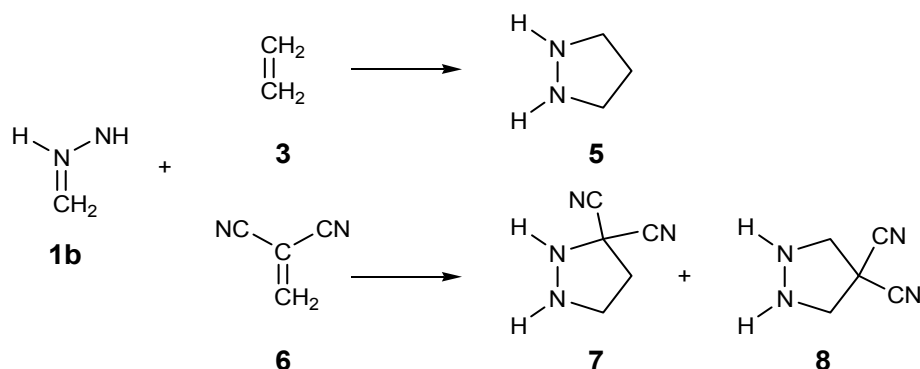
AY **1a**, azomethine imine (AI) **1b** and Ni **1c** constitute a series of three CH₂=NH–X (X = CH₂, NH, O) A-TACs in which the terminal X atom changes along the C, N, and O elements of the second arrow (see Scheme 4). In this short series of TACs, the activation energy associated with the 32CA reactions with ethylene **3** increases as the electronegativity of the atom X increases in the following order C < N < O (see Scheme 4) [16]. Interestingly, while the simplest AY **1a** has a *pseudodiradical* structure, [14] Ni **1c** has a zwitterionic one [20] (see Scheme 3). This behaviour causes these TACs to have a different reactivity towards ethylene **3** in 32CA reactions, i.e., the 32CA reaction involving AY **1a** is a *pr*-type reaction presenting a very low activation energy, 1.0 kcal·mol⁻¹, while that involving Ni **1c** is a *zw*-type reaction with a high activation energy of 14.3 kcal·mol⁻¹ (see Scheme 4). Note that

it is expected that the reactivity of AI **1b**, which presents an activation energy towards ethylene **3** of $7.7 \text{ kcal}\cdot\text{mol}^{-1}$, will be different to that of AY **1a** and Ni **1c**.



Scheme 4. Series of $\text{CH}_2=\text{NH}-\text{X}$ ($\text{X} = \text{CH}_2, \text{NH}, \text{O}$) A-TACs **1a–c**. In parentheses, MPWB1K/6-311G(d) activation energies, in $\text{kcal}\cdot\text{mol}^{-1}$ and with respect to the corresponding molecular complexes (MCs), associated with the 32CA reactions with ethylene **3**.

Considering that the simplest AI **1b** has a different activation energy towards ethylene **3** from that shown by AY **1a** and Ni **1c**, two TACs with a different electronic structure (see Scheme 3), an MEDT study of the 32CA reactions of the simplest AI **1b** with ethylene **3** and with electron-deficient (ED) dicyanoethylene (DCE) **6**, a strongly electrophilic ethylene, is herein carried out to establish the structure and reactivity of this TAC (see Scheme 5). Together with an electron localisation function (ELF) characterisation of the electronic structure of the simplest AI **1b**, a Bonding Evolution Theory [21] (BET) study of both reactions is performed in order to characterise the molecular mechanisms and to explain the activation energies implied in these cycloadditions.



Scheme 5. 32CA reactions of AI **1b** with ethylene **3** and DCE **6**.

2. Results and Discussion

The present theoretical study is divided into six parts: (i) an analysis of the electronic structure of AI **1b** is performed; (ii) the Conceptual DFT (CDFT) reactivity indices at the ground state (GS) of the reagents are analysed in order to predict the reactivity and regioselectivity in these 32CA reactions; (iii) the energy profiles associated with the 32CA reactions of AI **1b** with ethylene **3** and DCE **6** are studied; (iv) a BET study of the 32CA reaction of AI **1b** with ethylene **3** is performed to characterise the molecular mechanism of this cycloaddition; (v) an ELF topological analysis of the C–C and N–C bond formation processes along the polar 32CA reaction between AI **1b** and DCE **6** is carried out; and (vi) based on the electronic structure of AI **1b** and its reactivity towards ethylene **3**, a new type of reactivity in 32CA reactions is proposed.

2.1. ELF Topological Analysis and Natural Population Analysis (NPA) of AI **1b**

As the reactivity of the TACs has been correlated with their electronic structure [16,17], an ELF topological analysis of the simplest AI **1b** was first performed in order to characterise the electronic

structure of this TAC and thus, to predict its reactivity in 32CA reactions. ELF attractors, including the valence basin populations, the natural atomic charges of C and N atoms, ELF localisation domains and the proposed Lewis structure arising from the ELF topological analysis for AI **1b**, are shown in Figure 2.

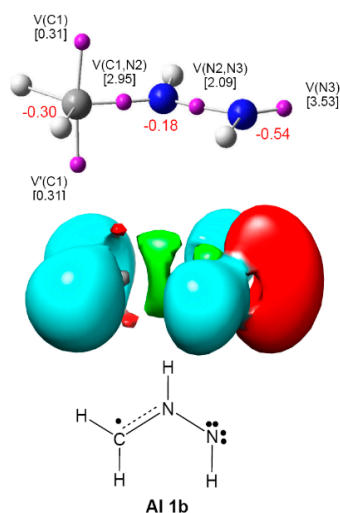


Figure 2. Representation of ELF attractors together with valence basin populations, natural atomic charges (in red) in average number of electrons (e), ELF localisation domains and the proposed Lewis structure for AI **1b**.

ELF topological analysis of the simplest AI **1b** shows the presence of two monosynaptic basins, V(C1) and V'(C1), integrating a total electron density of 0.62 e, two disynaptic basins, V(C1,N2) and V(N2,N3), with electron populations of 2.95 e and 2.09 e, and one V(N3) monosynaptic basin integrating 3.53 e. These ELF basins are related with the presence of a C1 *pseudoradical* centre, a C1–N2 bonding region integrating ca. 3 e, an N2–N3 single bond and an N3 non-bonding electron density (see the ELF-based Lewis structure of AI **1b** in Figure 2).

According to the Lewis structures, V(C) monosynaptic basins integrating ca. 1 e are associated to *pseudoradical* centres [14,18], while those integrating ca. 2 e in neutral molecules are associated to carbenoid centres [17]. TACs presenting two *pseudoradical* centres have been classified as *pseudodiradical* TACs [16], while those presenting a carbenoid centre have been classified as carbenoid TACs [17]. Finally, TACs that neither present *pseudoradical* nor carbenoid centres have been classified as zwitterionic TACs [16]. Consequently, ELF topological analysis of the electronic structure of the simplest AI **1b** indicates that this TAC, which presents a *pseudoradical* structure, does not have the electronic structure of any of the three representative *pseudodiradical*, carbenoid and zwitterionic TACs given in Scheme 3.

After the establishment of the bonding pattern of AI **1b** based on the ELF topological analysis, the charge distribution was analysed. The natural atomic charges, obtained through an NPA, are shown in Figure 2. As can be observed, the three atoms belonging to this TAC present negative charges: -0.30 e (C1), -0.18 e (N2) and -0.54 e (N3), while the hydrogen atoms support the positive charges. This charge distribution is in complete disagreement with the commonly accepted 1,2-zwitterionic structure given for AIs in which a positive charge and a negative charge are entirely located at the N2 and N3 nitrogen atoms [3,22].

Thus, while NPA reveals that this TAC does not have a 1,2-zwitterionic Lewis structure, ELF topological analysis of the electron density of AI **1b** permits establishing a *pseudoradical* electronic structure with a *pseudoradical* centre at the C1 carbon atom. The distinct electronic structure of AI **1b** with respect to that of the *pseudodiradical*, carbenoid and zwitterionic structures given in Scheme 3

justifies the different reactivity of these TACs (see Scheme 4), and therefore, the establishment of a new reactivity model in 32CA reactions.

2.2. Analysis of the CDFT Reactivity Indices at the GS of the Reagents

Global reactivity indices defined within CDFT [23,24] are powerful tools to explain the reactivity in cycloaddition reactions. Since the global electrophilicity and nucleophilicity scales are given at the B3LYP/6-31G(d) level, the present analysis has been performed at this computational level. The global indices, namely, the electronic chemical potential (μ), the chemical hardness (η), the electrophilicity (ω) and the nucleophilicity (N), for AI **1b**, ethylene **3** and DCE **6**, as well as the *pr* index of A-TACs **1a–c**, are presented in Table 1.

Table 1. B3LYP/6-31G(d) electronic chemical potential, μ , chemical hardness, η , electrophilicity, ω , and nucleophilicity, N , in eV, for A-TACs **1a–c**, ethylene **3** and DCE **6**, and the *pr* index of **1a–c**.

	μ	η	ω	N	<i>pr</i>
AY 1a	−1.82	4.47	0.37	5.07	1.13
AI 1b	−2.70	5.02	0.72	3.92	0.78
Ni 1c	−3.43	5.55	1.06	2.92	0.53
Ethylene 3	−3.37	7.77	0.73	1.86	
DCE 6	−5.64	5.64	2.82	0.65	

As shown in Table 1, the electronic chemical potential μ of AI **1b**, −2.70 eV, is higher than that of ethylene **3**, −3.37 eV, and DCE **6**, −5.64 eV. Consequently, along polar 32CA reactions, the global electron density transfer [25] (GEDT) will take place from AI **1b** toward ethylene **3** or DCE **6**; however, note that ethylene **3** has no tendency to participate in polar processes.

Along a polar reaction, there is an electron density transfer from the nucleophilic to the electrophilic species, which is measured by the GEDT [25] value computed at the TS of the reaction; the larger the GEDT at the TS, the more polar the reaction. Note that the GEDT concept comes from the observation that the electron density transfer taking place from the nucleophile to the electrophile along a polar reaction is not a local process, but a global one involving the two interacting frameworks and depending on the electrophilic/nucleophilic interactions taking place between them [25]. It should be emphasised here that this global property is lost with the molecular fragmentation carried out in Houk's DIEM [11].

The simplest AI **1b** has an electrophilicity ω index of 0.72 eV and a nucleophilicity N index of 3.92 eV, being classified as a marginal electrophile [26] and as a strong nucleophile [27]. The high electron density accumulated in the three heavy atoms belonging to AI **1b** could account for the high nucleophilic character of this TAC (see NPA in Section 2.1). Consequently, AI **1b** will participate only as a strong nucleophile in polar 32CA reactions.

Analysis of the reactivity indices of the three A-TACs given in Scheme 4 shows that the electrophilicity ω index increases and the nucleophilicity N index decreases as the electronegativity of the terminal X atom increases in the following order C < N < O; in any case, the three A-TACs are strong nucleophiles.

In order to characterise the participation of TACs in a *pr-type* 32CA reaction, the *pseudodiradical* (*pr*) index, has recently been introduced [16]. A-TACs with *pr* values larger than 0.90 can be related to species having a very soft character, i.e., with low hardness η values, and low stabilised frontier electrons, i.e., low ionisation potential, participating in *pr-type* 32CA reactions, while A-TACs with low *pr* values should participate in *zw-type* 32CA reactions. A-TACs AY **1a**, AI **1b** and Ni **1c** have *pr* values of 1.13, 0.78 and 0.53 (see Table 1), indicating that AI **1b** will not present a *pr-type* reactivity in 32CA reactions.

Polar cycloaddition reactions require the participation of good electrophiles and good nucleophiles. Ethylene **3** is one of the poorest electrophilic, $\omega = 0.73$ eV, and nucleophilic, $N = 1.86$ eV, species involved

in cycloaddition reactions, being classified as a marginal electrophile and as a marginal nucleophile. Consequently, ethylene **3** cannot participate in polar reactions. Substitution of two gem hydrogen atoms in ethylene **3** by two electron-withdrawing $-\text{CN}$ groups in DCE **6** considerably increases the electrophilicity ω index to 2.82 eV and decreases the nucleophilicity N index to 0.65 eV. Consequently, DCE **6** will participate only as a strong electrophile in polar 32CA reactions. Given the high nucleophilic character of AI **1b** and the strong electrophilic character of DCE **6**, it is expected that the 32CA reaction between AI **1b** and DCE **6** will have a high polar character.

By approaching a non-symmetric electrophilic/nucleophilic pair along a polar or ionic process, the most favourable reactive channel is that associated with the initial two-centre interaction between the most electrophilic centre of the electrophile and the most nucleophilic centre of the nucleophile. Recently, Domingo proposed the nucleophilic P_k^- and electrophilic P_k^+ Parr functions [28], derived from the changes of spin electron-density reached via the GEDT process from the nucleophile to the electrophile, as a powerful tool in the study of the local reactivity in polar or ionic processes. Accordingly, the nucleophilic P_k^- Parr functions of AI **1b** and the electrophilic P_k^+ Parr functions of DCE **6** were analysed in order to characterise the most nucleophilic and electrophilic centres of the species involved in this polar 32CA reaction (see Figure 3).

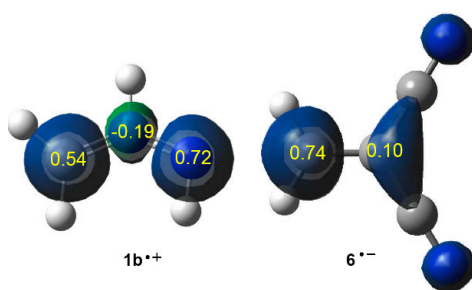


Figure 3. Three-dimensional (3D) representations of the atomic spin densities (ASD) of the radical cation $1b^{\bullet+}$ and the radical anion $6^{\bullet-}$, together with the nucleophilic P_k^- Parr functions of AI **1b** and the electrophilic P_k^+ Parr functions of DCE **6**.

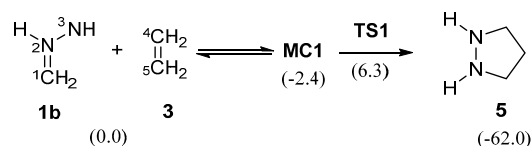
Analysis of the nucleophilic P_k^- Parr functions at the reactive sites of AI **1b** indicates that both the C1 carbon atom, with a P_k^- value of 0.54, and the N3 nitrogen atom, with a P_k^- value of 0.72, are nucleophilically activated, the latter more than the former. Note that the N2 nitrogen atom is nucleophilically deactivated, possessing a negative P_k^- value of -0.19 . On the other hand, the electrophilic P_k^+ Parr functions at the reactive sites of DCE **6** indicate that the more electrophilic centre is the C4 carbon atom, possessing the maximum value of $P_k^+ = 0.74$.

Therefore, it can be predicted that along a polar reaction the most favourable electrophile-nucleophile interaction along the nucleophilic attack of AI **1b** on DCE **6** will take place between the most nucleophilic centre of AI **1b**, the N3 nitrogen atom, and the most electrophilic centre of DCE **6**, the C4 carbon atom.

2.3. Study of the Reaction Channels Associated with the 32CA Reactions of AI **1b** with Ethylene **3** and DCE **6**

2.3.1. 32CA Reaction Involving Ethylene **3**

Due to the symmetry of ethylene **3**, the reagents, **1b** and **3**, one MC, **MC1**, only one TS, **TS1**, and the corresponding pyrazolidinone **5** were located and characterised; consequently, the 32CA reaction takes place through a one-step mechanism (see Scheme 6). The MPWB1K/6-311G(d) total and relative energies of the stationary points involved in the 32CA reaction of AI **1b** with ethylene **3** are given in Table S1 of the Supplementary Materials and Scheme 6, respectively, while the energy profile is graphically represented in red in Figure 4.



Scheme 6. 32CA reaction between AI **1b** and ethylene **3**. MPWB1K/6-311G(d) relative energies, in kcal·mol⁻¹, are given in parentheses.

The reaction between AI **1b** and ethylene **3** begins with the formation of **MC1**, which is slightly stabilised by only 2.4 kcal·mol⁻¹ with respect to the separated reagents (see Figure 4). From **MC1**, the activation energy associated with **TS1** is 8.7 kcal·mol⁻¹, the reaction being exothermic by 59.6 kcal·mol⁻¹. This activation energy is found between that associated with the non-polar 32CA reaction of AY **1a** with ethylene **3**, 1.0 kcal·mol⁻¹, a *pr-type* reaction, and that associated with the non-polar 32CA reaction of Ni **1c** with ethylene **3**, a *zw-type* reaction, 14.3 kcal·mol⁻¹ (see Scheme 4).

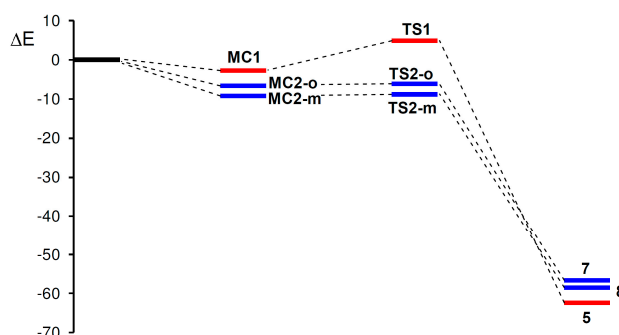


Figure 4. Energy profile (ΔE , in kcal·mol⁻¹) of the 32CA reaction of AI **1b** with ethylene **3**, in red, and with DCE **6**, in blue.

The geometry of **TS1** is displayed in Figure 5. At **TS1**, the distances between the C1 and C5, and the N3 and C4 interacting atoms are 2.272 and 2.289 Å, respectively. It has been well established that the formation of C–C single bonds takes place in the short distance range of ca. 1.9–2.0 Å [25], while several studies have shown that formation of C–N single bonds begins at shorter distances, ca. 1.7 Å [29]. Therefore, despite the geometrical symmetry of **TS1**, these parameters suggest an asynchronous bond formation process in which the C1–C5 bond formation is more advanced than the N3–C4 one.

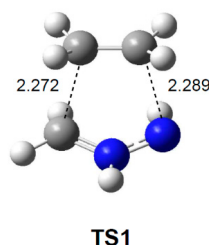


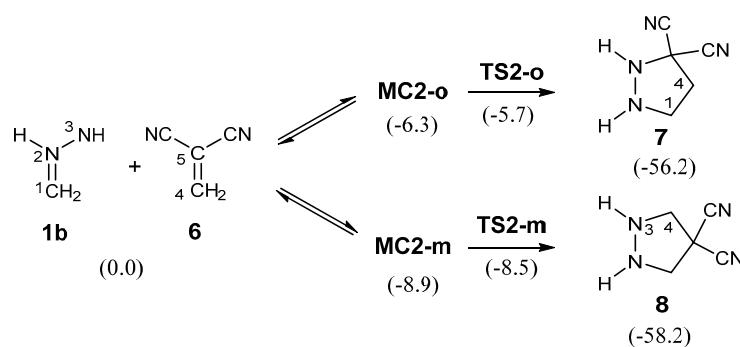
Figure 5. MPWB1K/6-311G(d) geometry of the TS associated with the 32CA reaction between AI **1b** and ethylene **3**. Distances are given in Angstroms, Å.

The electronic nature of the 32CA reaction between AI **1b** and ethylene **3** was analysed by computing the GEDT [25] at the corresponding TS. Cycloadditions with GEDT values near 0.0 e correspond to non-polar processes, whereas values higher than 0.2 e correspond to polar processes. In gas phase, the GEDT that fluxes from the AI moiety towards the ethylene one is 0.10 e at **TS1**. This value indicates that this 32CA reaction has a low polar character. Interestingly, the slight GEDT

computed at **TS1**, whose direction is in agreement with the analysis of the corresponding electronic chemical potential μ indices, can be rationalised as a delocalisation of the energetically destabilised electron density of the AI framework into the ethylene one, rather than a GEDT associated to a polar process [14]. Note that ethylene **2** has neither electrophilic nor nucleophilic character.

2.3.2. 32CA Reaction Involving DCE **6**

Due to the non-symmetry of AI **1b** and DCE **6**, this 32CA reaction can take place through two regioisomeric channels, the *ortho* and the *meta* (see Scheme 7), i.e., those associated with the initial formation of the C1–C4 and N3–C4 single bonds, respectively. A search for the stationary points involved in the two regioisomeric pathways allowed finding two MCs, **MC2-o** and **MC2-m**, two regioisomeric TSs, **TS2-o** and **TS2-m**, and the corresponding pyrazolidines **7** and **8**, which were properly characterised; consequently, the 32CA reaction takes place through a one-step mechanism (see Scheme 7). The MPWB1K/6-311G(d) total and relative energies of the stationary points involved in the 32CA reaction of AI **1b** with DCE **6** are given in Table S2 of the Supplementary Materials and Scheme 7, respectively, while the energy profile is graphically represented in blue in Figure 4.



Scheme 7. 32CA reaction between AI **1b** and DCE **6**.

When AI **1b** and DCE **6** gradually approach each other, the energy is reduced until the formation of two MCs located 6.3 (**MC2-o**) and 8.9 (**MC2-m**) kcal·mol⁻¹ below the separated reagents takes place (see Figure 4). Further approach of both the AI and the DCE frameworks leads to the formation of the TSs, which are found 3.2 (**TS2-o**) and 0.4 (**TS2-m**) kcal·mol⁻¹ above the more stable **MC2-m**. Note that both MCs are in thermodynamic equilibrium. Moreover, formation of pyrazolidines **7** and **8** from **MC2-m** becomes strongly exothermic by 47.3 and 49.3 kcal·mol⁻¹, respectively. Some appealing conclusions can be drawn from these energy results: (i) the activation barrier associated to the more favourable **TS2-m** is 8.3 kcal·mol⁻¹ lower than that associated to **TS1**, 8.7 kcal·mol⁻¹; (ii) this 32CA reaction is highly regioselective, **TS2-o** being 2.8 kcal·mol⁻¹ above **TS2-m**; and (iii) the strong exothermic character of this reaction makes the formation of pyrazolidines **7** and **8** irreversible.

The geometries of the TSs associated with the 32CA reaction between AI **1b** and DCE **6** are displayed in Figure 6. At the *ortho* **TS2-o**, the distances between the C1 and C4, and the N3 and C5 interacting atoms are 2.311 and 2.625 Å, while at the *meta* **TS2-m**, the distances between the N3 and C4, and the C1 and C5 interacting atoms are 2.142 and 2.796 Å. Some appealing conclusions can be drawn from these geometrical parameters: (i) both TSs correspond to highly asynchronous single bond formation processes in which the formation at the β conjugated position of DCE **6** is more advanced than that at the α one; (ii) geometrically, the more favourable **TS2-m** is more advanced and more asynchronous than **TS2-o**; and (iii) the more favourable **TS2-m** is associated to the two-centre interaction between the most nucleophilic centre of AI **1b** and the most electrophilic centre of DCE **6**, in complete agreement with the analysis of the Parr functions (see Section 2.2).

In gas phase, the GEDT that fluxes from the AI framework towards the ethylene one is 0.25 e at **TS2-o** and 0.27 e at **TS2-m**. The GEDT at the more favourable **TS2-m** is slightly higher than that at

TS2-o. These high values indicate that this 32CA reaction has a high polar character, in clear agreement with the very high nucleophilic character of AI **1b** and the high electrophilic character of DCE **6**, and account for the large decrease of the activation energy with respect to the non-polar 32CA reaction involving ethylene **3** via **TS1**.

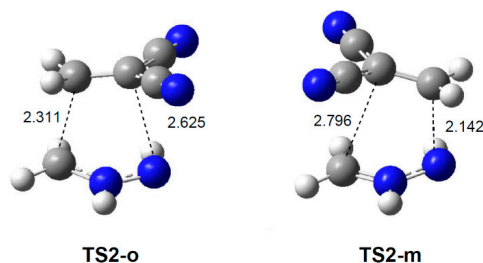


Figure 6. MPWB1K/6-311G(d) geometries of the TSs associated with the 32CA reaction between AI **1b** and DCE **6**. Distances are given in Angstroms, Å.

2.4. BET Study of the 32CA Reaction of AI **1b** with ethylene **3**

When trying to achieve a better understanding of bonding changes in organic reactions, the so-called BET [21] has proven to be a very useful methodological tool. This quantum-chemical methodology makes it possible to understand the bonding changes along a reaction path and, thus, to establish the nature of the electronic rearrangement associated with a given molecular mechanism [30].

In order to characterise the molecular mechanism of the non-polar 32CA reaction of AI **1b** with ethylene **3**, a BET study along the cycloaddition reaction was carried out. The complete BET study is provided in the Supplementary Materials. Some appealing conclusions can be drawn from this BET study: (i) the intrinsic reaction coordinate (IRC) associated with the 32CA reaction of the simplest AI **1b** with ethylene **3** is divided in nine differentiated phases, a behaviour that clearly indicates that the bonding changes along this one-step mechanism are non-concerted (see Figure 7); (ii) ELF topological analysis of **TS1** indicates that there is no bonding region between the N1 and C4, and the C3 and C4 interacting atoms, respectively; (iii) the moderate activation energy associated with this reaction, $8.7 \text{ kcal}\cdot\text{mol}^{-1}$, can be mainly associated with the rehybridisation of the C1 carbon from sp^2 to sp^3 ; (iii) formation of the first C3–C4 single bond takes place at a C–C distance of 2.03 Å through the C-to-C coupling of two C3 and C4 *pseudoradical* centres [25] (see points **P5** and **P6** in Figure 8); (iv) interestingly, while the C4 *pseudoradical* centre is generated along the reaction path through the depopulation of the C4–C5 double bond of ethylene **3**, the C3 *pseudoradical* centre is already present at the simplest AI **1b**; (v) formation of the second N1–C4 single bond takes place at an N–C distance of 1.92 Å through the C-to-N coupling of two N1 and C5 *pseudoradical* centres (see points **P7** and **P8** in Figure 7); (vi) formation of this C–N single bond is thus different to that found in the ketene-imine Staudinger reaction in which the first C–N single bond is formed through the donation of the electron density of the imine nitrogen lone pair to the ketene carbonyl carbon [29]; and (vii) the present BET study allows establishing the molecular mechanism of the non-polar 32CA reaction between the simplest AI **1b** and ethylene **3** and characterising it as a $[2n + 2\tau]$ process. The non-bonding $2n$ electrons involved in this 32CA reaction can be associated with the *pseudoradical* centre present at the C1 carbon and part of the electron density of the N3 nitrogen lone pairs of the simplest AI **1b**, while the 2τ electrons come from the C4–C5 double bond of ethylene **3**. Note that, in 1931, first Pauling [31] and later Slater [32] proposed that the C–C bonding region of ethylene **3** can be represented by two equivalent bonds named τ bonds. This electronic representation of C–C double bonds is in complete agreement with the ELF topological analysis of ethylene **3** in which the corresponding C–C bonding region is characterised by the presence of two equivalent $V(C,C)$ disynaptic basins integrating ca. 2 e each one (see the Supplementary Materials).

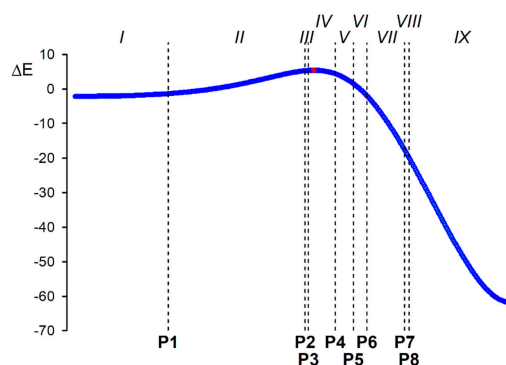


Figure 7. The nine phases, separated by black dashed lines, in which the IRC (in $\text{amu}^{1/2}\cdot\text{Bohr}$) associated with the non-polar 32CA reaction between AI **1b** and ethylene **3** is topologically divided. Relative energy variations, ΔE , with respect to the separated reagents, are given in $\text{kcal}\cdot\text{mol}^{-1}$. The red point indicates the position of **TS1**.

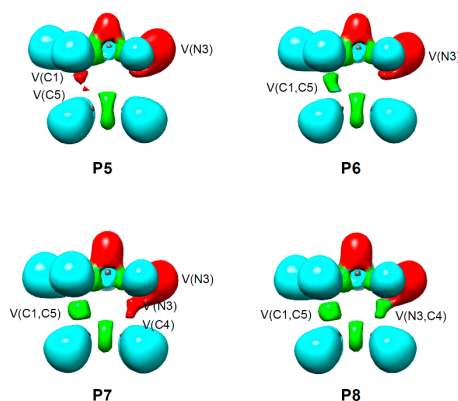


Figure 8. ELF localisation domains, represented at an isovalue of 0.74, for the points of the IRC defining Phases VI–IX involved in the formation of the C1–C5 and N3–C4 single bonds along the non-32CA reaction between AI **1b** and ethylene **3**.

2.5. ELF Topological Analysis of the C–C and N–C Bond Formation Processes along the Polar 32CA Reaction between AI **1b** and DCE **6**. Understanding the Role of the GEDT

Recently, an ELF topological analysis of some relevant points involved in the formation of the new single bonds along the IRC associated with the experimental 32CA reaction of an AI derivative with *N*-vinyl tetrahydroindole allowed establishing that this reaction takes place through a *two-stage one-step* mechanism [33]. Herein, in order to investigate the bond formation processes along the polar 32CA reaction of AI **1b** with DCE **6** and to understand the low activation energies associated with the two *meta/ortho* regioisomeric channels, an ELF topological analysis of the corresponding stationary points and some relevant points along the IRC involved in the formation of the new C–C and N–C single bonds was performed. Note that these points were selected by a similar procedure to that used in the previous BET study (see Computational Methods). The complete ELF topological analysis is provided in the Supplementary Materials, while a summary of the most appealing conclusions is reported herein.

Some appealing conclusions can be drawn from this ELF topological analysis along both *meta/ortho* regioisomeric channels: (i) in both reaction channels, the formation of the first single bond involves the most electrophilic centre of DCE **6**, the C4 carbon (see Figure 9); (ii) formation of the C–C single bonds along the two channels begins at C–C distances of 2.14 Å (*meta*) and 2.05 Å (*ortho*) through the C-to-C coupling of two C1 and C4/C5 *pseudoradical* centres (see **P1-o** and **P2-o** in Figure 9) [29]; (iii) interestingly, while along the more favourable *meta* channel the two C1 and C5 *pseudoradical* centres

are created as the reaction progresses, the C1 *pseudoradical* centre is already present at *ortho* **MC2-o**; (iv) while along the more favourable *meta* channel the C5 *pseudoradical* centre created at the DCE framework participates more than the C1 one created at the AI moiety in the C–C bond formation process, along the *ortho* channel the C1 *pseudoradical* centre already present at **MC2-o** contributes more to the C–C bond formation; (v) conversely, the N–C bond formation takes place differently along both channels. Formation of the N–C single bond begins at N–C distances of 1.81 Å (*meta*) and 1.84 Å (*ortho*) through the donation of part of the non-bonding electron density of the N3 nitrogen to the C4 carbon along the *meta* channel (see **P1-m** and **P2-m** in Figure 9) or through the C-to-N coupling of two C5 and N3 *pseudoradical* centres along the *ortho* channel; (vi) both reaction channels present highly asynchronous bond formation processes, in agreement with the previous geometry analysis. The polar 32CA reaction between AI **1b** and DCE **6** proceeds through a *two-stage one-step* mechanism [33] in which the formation of the second bond begins when the first one is already formed by up to 95%; (vii) the bonding patterns of **TS2-o** and **TS2-m** are very similar to those of the corresponding MCs and, accordingly, the very low energy barriers relative to the corresponding MCs, 0.6 (**TS2-o**) and 0.4 (**TS2-m**) kcal·mol^{−1}, can mainly be associated with slight electron density variations within the molecular system; (viii) therefore, these very low activation energies can be the consequence of the GEDT taking place at the polar TSs, which favours the polar 32CA reaction through an electronic stabilisation of both the nucleophile and electrophile frameworks; (ix) the energy difference between **TS2-o** and **TS2-m**, 2.8 kcal·mol^{−1}, is likely to be associated to the higher stability of the electron density distribution at **TS2-m** than that at the *pseudoradical* structure of **TS2-o**.

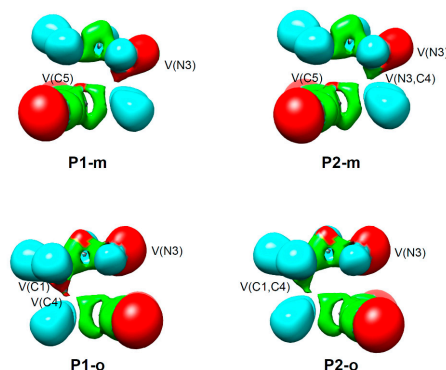


Figure 9. ELF localisation domains, represented at an isovalue of 0.68, for the selected points of the IRC involved in the formation of the first N3–C5 (*meta*) and C1–C4 (*ortho*) single bonds along the two *meta/ortho* reactive channel associated with the polar 32CA reaction between AI **1b** and DCE **6**.

The GEDT taking place at the TSs of the polar 32CA reaction between AI **1b** and DCE **6** does not only decrease the activation energy associated with the non-polar 32CA reaction involving ethylene **3**, but also modifies the molecular mechanism of the polar reaction making the most favourable reaction channel that involving the first N–C bond formation instead of the C–C one, in agreement with the analysis of the Parr functions. Note that, despite the *pseudoradical* character of the C1 carbon, the N3 nitrogen is the most nucleophilic centre of AI **1b** (see Section 2.2).

A comparative analysis between the BET study of the non-polar 32CA reaction involving ethylene **3** and the ELF topological analysis of the bond formation processes along the polar 32CA reaction involving DCE **6** makes it possible to understand the role of the GEDT in the polar process. Some appealing conclusions emerge from the corresponding comparative analysis: (i) while along the non-polar 32CA reaction of AI **1b** with ethylene **3** and the less favourable *ortho* channel of the polar 32CA reaction between AI **1b** and DCE **6** the most favourable interaction is that involving the C1 *pseudoradical* centre, along the more favourable *meta* channel of the polar 32CA reaction between AI **1b** and DCE **6** is that involving the interaction between the most nucleophilic and electrophilic centres of the reagents; (ii) thus, while the non-polar cycloaddition and the *ortho* channel of the polar reaction

begin with the initial formation of the C–C single bond, the *meta* channel of the polar reaction begins with the initial formation of the N–C single bond. Consequently, both mechanisms are different; (iii) formation of the new single bonds is slightly asynchronous in the non-polar reaction but highly asynchronous in the polar reaction; (iv) unlike polar Diels–Alder reactions and polar *zw-type* 32CA reactions in which the GEDT favours the bonding changes at the reagents, i.e., the rupture of the double bonds [34], in the polar 32CA reaction between AI **1b** and DCE **6**, the GEDT provokes an electronic stabilisation of both the nucleophilic and the electrophilic frameworks at the TSs, decreasing the activation energies from 8.7 kcal·mol⁻¹ (**TS1**) to 0.4 (**TS2-o**) and 3.2 (**TS2-m**) kcal·mol⁻¹.

2.6. Understanding the Reactivity of AI **1b** Possessing a Carbon Pseudoradical Centre

ELF topological analysis of several TACs have shown that unlike butadiene **9**, which presents a conjugated C–C double bond Lewis structure, TACs have very complex electronic structures that cannot be usually represented by a simple Lewis structure. On the other hand, unlike the non-polar Diels–Alder reaction between butadiene **9** and ethylene **3**, which has a high activation energy of ca. 25 kcal·mol⁻¹ [35], the non-polar 32CA reactions between TACs and ethylene **3** have activation energies that range from 1 to 15 kcal·mol⁻¹ [7,8]. Note that ethylene **3** is a poor electrophile and a poor nucleophile that cannot participate in polar reactions.

As has been aforementioned in the Introduction, a good correlation between the electronic structures of TACs and the activation energies involved in the non-polar 32CA reactions towards ethylene **3**, i.e., their reactivity, has been found [16,17]. Thus, while zwitterionic TACs such as Ni **1c**, which must break the C–N double bond before the creation of the carbon *pseudoradical* centre demanded for the subsequent C–C bond formation, present high activation energies towards ethylene **3** (14.3 kcal·mol⁻¹ for the reaction of Ni **1c** with ethylene **3**), *pseudodiradical* TACs such as AY **1a**, which already has the two required carbon *pseudoradical* centres in the structure, present unappreciable activation energies (1.0 kcal·mol⁻¹ for the reaction of AY **1a** with ethylene **3**). Note that AY **1a** and Ni **1c** are located at the extremes of the series given in Figure 10.

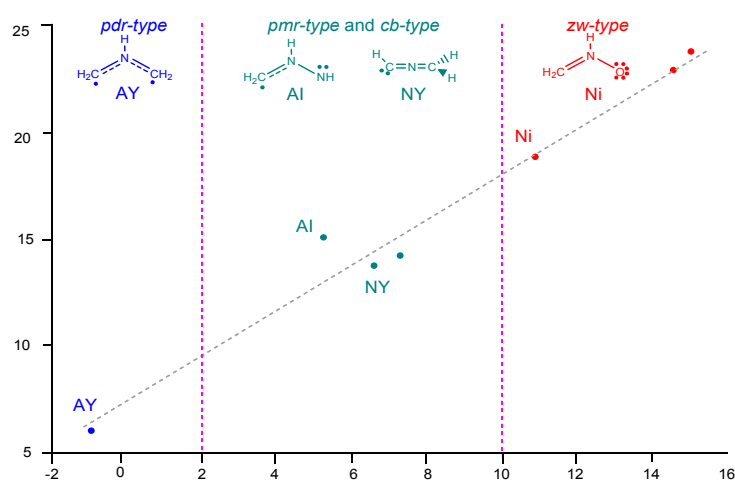


Figure 10. Plot of the MPWB1K/6-311G(d) relative energies ΔE^\ddagger vs. the distortion energies ΔE_d^\ddagger , in kcal·mol⁻¹, for Houk's 32CA reactions of TACs **1** and **2**, having at least one carbon atom, with ethylene **3** [7,8].

Very recently, the 32CA reactions of diazoalkanes (DAAs) with ED ethylenes have been studied [36]. ELF topological analysis of the simplest DAA **2c** showed that, similar to AI **1b**, this TAC also has a *pseudoradical* structure (see Figure 11) [36]. However, despite its *pseudoradical* structure, the 32CA reaction of DAA **2c** with ethylene **3** presents a high activation energy, 16.6 kcal·mol⁻¹, as a consequence of its lineal P-TAC structure [19].

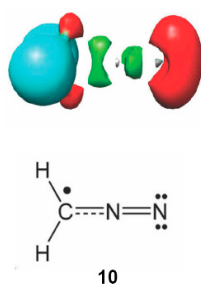


Figure 11. Representation of the ELF localisation domains and the proposed Lewis structure for DAA **2c**.

Why AI **1b** having one *pseudoradical* centre presents a different reactivity than AY **1a** having a *pseudodiradical* structure? Figure **12** shows how the two *pseudoradical* centres present in the simplest AY **1a** favour the synchronous C–C single bond formation process through an homolytic rupture of the C–C double bond of the ethylene framework [14], a behaviour that is not feasible in the 32CA reactions of *pseudoradical* AI **1b** and DAA **2c**. Note that, in these TACs, the non-bonding electron density present at the nitrogen atom is associated to the nitrogen sp^2 lone pairs, which must be redistributed before the creation of the nitrogen *pseudoradical* centre demanded for the C–N single bond formation.

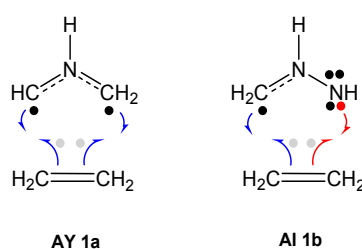
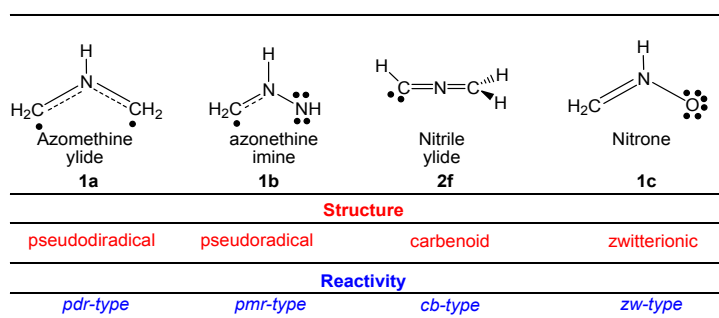


Figure 12. Bonding changes demanded for the C–C bond formation in the *pdr-type* 32CA reaction between AY **1a** and ethylene **3**, and for the C–C and C–N bond formation in *pmr-type* 32CA reaction between AI **1b** and ethylene **3**.

Consequently, from the comparison of the electronic structure and the reactivity of AI **1b** in the non-polar 32CA reaction with ethylene **3** with those of the three TACs given in Scheme **3**, a new type of 32CA reaction model should be considered. This new type, called *pseudo(mono)radical* type (*pmr-type*) 32CA reaction, is associated with TACs such as AI **1b** and DAA **2c** having only one *pseudoradical* carbon centre, i.e., a *pseudoradical* electronic structure (see Scheme **8**). In order to clearly differentiate the reactivity of *pseudodiradical* species from *pseudoradical* ones, we propose to change the original name of *pr-type* (see Scheme **3**) to *pdr-type* (see Scheme **8**).



Scheme 8. Electronic structure of TACs and the proposed reactivity types in the non-polar 32CA reactions towards ethylene **3**.

Thus, unlike symmetric *pseudodiradical* TACs such as AY **1a**, carbonyl ylides and thiocarbonyl ylides, which induce a symmetric depopulation of the C–C double bond of ethylene **3**, non-symmetric *pseudoradical* TACs such as AIs **1b** and DAAs **2c** are not able to induce an effective symmetric electron density depopulation of the C–C bonding region in the ethylene framework since the electron density demanded for the formation of the new C–N single bonds is at first being part of the non-bonding electron density of the nitrogen sp^2 lone pairs.

The present theoretical study emphasises how MEDT studies are able to rationalise the reactivity of organic compounds based on a rigorous analysis of the changes of the electron density along organic reactions [12]. Conversely, Houk's DIEM only permits to establish a good relationship between the *distortion* energy and the activation energy in the series of non-polar 32CA reactions given in Scheme 2, i.e., when more distorted the TS is with respect to the separated reagents, higher the activation energy. This finding, which is a computational assertion of Hammond's postulate [9], does not resolve the question *why the activation energies of these 32CA reactions depend on the geometry deformations* [7,8].

The molecular geometry is the result of the energy minimisation, which, within the DFT, is a functional of the electron density [10]. Consequently, activation energies, which are the difference in energies between the GS and the TS, should be understood as the energy involved in the changes in electron density demanded to reach the TS. Since the electron density in a molecule and its associated energy depends on the total electrons and the external potential, i.e., the nuclei positions [10], the geometry of any species involved in a reaction path cannot be divided into separated fragments because they lose the information of the whole molecular system.

On the other hand, we have proposed that the GEDT taking place at the TSs is one of the more relevant factors controlling activation energies; the larger GEDT, the lower the activation energy [34]. Such as the non-polar DA reaction between butadiene and ethylene **3** that has a negligible GEDT, the 32CA reactions towards ethylene **3** also do not have any polar character. Consequently, the activation energies implied in these non-polar 32CA reactions are mainly associated to the energy required for the changes in the GS electron density, and not to the geometry deformation such as Houk proposed [7,8], which is a consequence of the former.

3. Conclusions

The electronic structure and chemical properties of the simplest AI **1b** as well as its participation in 32CA reactions towards ethylene **3** and ED DCE **6** have been analysed within MEDT using DFT calculations at the MPWB1K/6-311G(d) level.

Analysis of the electron density pattern of the simplest AI **1b** reveals that this TAC presents a *pseudoradical* structure, characterised by the presence of a V(C1) monosynaptic basin integrating 0.62 e at the C1 carbon atom. The charge distribution at AI **1b** does not permit to assign any zwitterionic structure for this TAC, ruling out the common representation of this TAC as a 1,2-dipole.

CDFT analysis of AI **1b** indicates that this TAC is a moderate electrophile and a good nucleophile. Consequently, it is expected that AI **1b** will participate in polar 32CA reactions only towards electrophilically activated ethylenes. Analysis of the nucleophilic P_k^- indicates that the N3 nitrogen atom is more nucleophilically activated than the C1 carbon.

The 32CA reaction of AI **1b** with ethylene **3** takes place through a one-step mechanism with moderate activation energy, $8.7 \text{ kcal}\cdot\text{mol}^{-1}$, the reaction being strongly exothermic, $-62.0 \text{ kcal}\cdot\text{mol}^{-1}$. Analysis of the TS geometry shows a high symmetry in the lengths of the two C–C and C–N forming bonds. The GEDT at **TS1**, 0.10 e, indicates that this reaction has a low polar character.

BET analysis of this non-polar 32CA reaction indicates that in spite of the geometrical symmetry found at **TS1**, this one-step mechanism takes place through a non-concerted mechanism in which the C–C bond formation is clearly anticipated prior to the C–N one. Formation of the first C–C single bond takes place at a distance of 2.03 Å through the C-to-C coupling of two carbon *pseudoradical* centres [25], while formation of the second N–C single bond takes place at a distance of 1.92 Å through the C-to-N

coupling of two carbon and nitrogen *pseudoradical* centres. Consequently, at **TS1** the formation of the two single bonds has not yet begun.

BET analysis allows the molecular mechanism of the non-polar 32CA reaction to be characterised as a $[2n + 2\tau]$ process. This MEDT study makes it possible to reject the concept of *pericyclic mechanism*, since the bonding changes are neither concerted nor do they take place in a cyclic movement. In addition, ELF topological analysis of the structures involved in the formation of the two C–C and C–N single bonds indicates that the C1 *pseudoradical* and N3 non-bonding electron density belonging to AI **1b** and that belonging to the τ bond of ethylene **3** participate in the reaction. This behaviour, which indicates that only two electrons of the TAC and two electrons of the ethylene participate in this reaction, allows rejecting the classification of these reactions as $[4\pi + 2\pi]$ processes, and, consequently, the Woodward–Hoffmann rules of the conservation of orbital symmetry [37], according to which this thermal 32CA reactions should be forbidden by the MO symmetry.

The polar 32CA reaction of AI **1b** with DCE **6** also takes place through a one-step mechanism. However, the electrophilic activation of ethylene **3** provokes some remarkable changes in the 32CA reactions of AI **1b** towards ED ethylenes. Now, due to the non-symmetry of both reagents, two regioisomeric channels are feasible. **TS2-m**, associated with the initial C–N bond formation, is found $2.8 \text{ kcal}\cdot\text{mol}^{-1}$ below **TS2-o**, associated with the initial C–C bond formation; this polar 32CA reaction is highly regioselective, in clear agreement with the CDFT analysis of the Parr functions at the GS of the reagents. The activation barrier of the more favourable **TS2-m** is $8.3 \text{ kcal}\cdot\text{mol}^{-1}$ lower than that of **TS1**, associated with the non-polar 32CA reaction of AI **1b** with ethylene **3**. This large acceleration is in complete agreement with the high GEDT found at the polar **TS2-m**, 0.25 e, which provokes an electronic stabilisation of the both the nucleophilic and the electrophilic frameworks at the TSs. These behaviours are the consequence of the high nucleophilic character of AI **1b** and the high electrophilic character of DCE **6**.

Interestingly, ELF analysis of the bonding changes along the two regioisomeric channels indicates that the electrophilic activation of the ethylene compound does not only accelerate the reaction, but also changes the mechanism; the non-polar 32CA reaction begins with the C–C single bond formation, while the more favourable channel associated with the polar 32CA reaction starts with the C–N bond formation due to the favourable two-centre interaction between the most nucleophilic centre of AI **1b** and the most electrophilic centre of DCE **6** taking place in a polar process. In addition, while the non-polar reaction is only slightly asynchronous, the polar process takes place through a non-concerted *two-stage one-step* mechanism [33].

Analysis of the electronic structure of AI **1b** and its reactivity towards ethylene **3** indicates that this TAC is different to those previously studied. The *pseudoradical* structure and reactivity of the simplest AI **1b** towards ethylene **3**, such as those of the simplest DAA **10** [36], which are different to the *pseudodiradical* structure and *pdr-type* reactivity of AY **1a**, make it possible to extend Domingo's classification to a new type of *pseudoradical* TACs and *pmr-type* reactivity.

The present theoretical study emphasises how MEDT is able to rationalise the reactivity of the organic compounds based on a rigorous analysis of the changes of the electron density along organic reactions, thus rejecting obsolete concepts and models developed in the last century through the analysis of MOs [12,25].

4. Computational Methods

DFT calculations were performed using the MPWB1K functional [38] together with the 6–311G(d,p) basis set [39]. Optimisations were carried out using the Berny analytical gradient optimisation method [40,41]. The stationary points were characterised by frequency computations in order to verify that TSs have one and only one imaginary frequency. The IRC paths [42] were traced in order to check the energy profiles connecting each TS to the two associated minima of the proposed mechanism using the second order González-Schlegel integration method [43,44]. GEDT [25] is computed by the sum of the natural atomic charges (q), obtained by NPA [45,46], of the atoms

belonging to each framework (f) at the TSs; $GEDT = \sum q_f$. The sign indicates the direction of the electron density flux in such a manner that positive values mean a flux from the considered framework to the other one. All computations were carried out with the Gaussian 09 suite of programs [47].

CDFT [23,24] provides different indices to rationalise and understand chemical structure and reactivity. The global electrophilicity index [48] ω , is given by the following expression, $\omega = (\mu^2/2\eta)$, in terms of the electronic chemical potential μ and the chemical hardness η . Both quantities may be approached in terms of the one-electron energies of the frontier MOs HOMO and LUMO, ϵ_H and ϵ_L , as $\mu \approx (\epsilon_H + \epsilon_L)/2$ and $\eta \approx (\epsilon_L - \epsilon_H)$, respectively [49,50]. The global nucleophilicity index [51,52], N , based on the HOMO energies obtained within the Kohn-Sham scheme [53], is defined as $N = E_{HOMO}(\text{Nu}) - E_{HOMO}(\text{TCE})$, where tetracyanoethylene (TCE) is the reference. The *pr* index, which has recently been introduced in order to characterise the participation of *pseudodiradical* TACs in *pdr-type* 32CA reactions [16], comprises the chemical hardness η and the nucleophilicity N index of the TAC, as $pr = N/\eta$. Electrophilic P_k^- and nucleophilic P_k^- Parr functions [28] were obtained through the analysis of the Mulliken atomic spin densities (ASD) of the radical anion of DCE **6** and the radical cation of AI **1b** by single point calculations from the neutral species. DFT reactivity indices were computed at the B3LYP/6-31G(d) level.

ELF [54] studies were performed with the TopMod [55] program and using the corresponding B3LYP/6-311G(d,p) monodeterminantal wavefunctions over a grid spacing of 0.1 a.u.. For the BET study, the corresponding reaction channel was followed by performing the topological analysis of the ELF for 862 nuclear configurations along the IRC path. A BET procedure was used for the characterisation of the bond formation processes along the two *meta/ortho* regioisomeric channels associated to the polar reaction by performing the topological analysis of the ELF for 198 (*meta*) and 472 (*ortho*) nuclear configurations.

Supplementary Materials: Supplementary materials are available online. BET study of the non-polar 32CA reaction between AI **1b** and ethylene **3**. ELF topological analysis of the C–C and N–C bond formation processes along the *meta* and *ortho* regioisomeric channel associated with the polar 32CA reaction between AI **1b** and DCE **6**.

Acknowledgments: This research was supported by the Ministry of Economy and Competitiveness (MINECO) of the Spanish Government, project CTQ2016-78669-P (AEI/FEDER, UE). M. R.-G. also thanks MINECO for a pre-doctoral contract co-financed by the European Social Fund (BES-2014-068258).

Author Contributions: L.R.D. headed the subject and he and M.R.-G. performed the calculations, collected the literature and participated in the writing of the manuscript.

Conflicts of Interest: The author declares no conflict of interest.

Abbreviations

The following abbreviations are used in this manuscript:

32CA	[3+2] cycloaddition
AI	azomethine imine
ASD	atomic spin densities
A-TAC	allylic-type TAC
BET	Bonding Evolution Theory
<i>cb-type</i>	carbenoid-type
CDFT	Conceptual DFT
DAA	diazoalkanes
DCE	dicyanoethylene
DFT	Density Functional Theory
DIEM	Distortion/Interaction Energy Model
ED	electron-deficient
ELF	electron localisation function
FMO	Frontier Molecular Orbital
GEDT	global electron density transfer
GS	ground state

MC	molecular complex
MEDT	Molecular Electron Density Theory
MO	molecular orbital
Ni	nitrene
<i>pdr-type</i>	<i>pseudodiradical-type</i>
<i>pmr-type</i>	<i>pseudoradical-type</i>
P-TAC	propargylic-type TAC
TAC	three-atom-component
TCE	tetracyanoethylene
TS	transition state structure
<i>zw-type</i>	zwitterionic-type

References

1. Padwa, A. *1,3-Dipolar Cycloaddition Chemistry*; Wiley-Interscience: New York, NY, USA, 1984.
2. Padwa, A.; Pearson, W.H. *Synthetic Applications of 1,3-Dipolar Cycloaddition Chemistry Toward Heterocycles and Natural Products*; John Wiley & Sons, Inc.: New York, NY, USA, 2002.
3. Huisgen, R. 1,3-dipolar cycloadditions. *Proc. Chem. Soc.* **1961**, *33*, 357–396.
4. Huisgen, R. Kinetics and Mechanism of 1,3-Dipolar Cycloadditions. *Angew. Chem. Int. Ed. Engl.* **1963**, *2*, 633–696. [[CrossRef](#)]
5. Huisgen, R. The Concerted Nature of 1,3-Dipolar Cycloadditions and the Question of Diradical Intermediates. *J. Org. Chem.* **1976**, *41*, 403–419. [[CrossRef](#)]
6. Gothelf, K.V.; Jorgensen, K.A. Asymmetric 1,3-Dipolar Cycloaddition Reactions. *Chem. Rev.* **1998**, *98*, 863–909. [[CrossRef](#)] [[PubMed](#)]
7. Ess, D.H.; Houk, K.N. Distortion/Interaction energy control of 1,3-dipolar cycloaddition reactivity. *J. Am. Chem. Soc.* **2007**, *129*, 10646–10647. [[CrossRef](#)] [[PubMed](#)]
8. Ess, D.H.; Houk, K.N. Theory of 1,3-Dipolar Cycloadditions: Distortion/Interaction and Frontier Molecular Orbital Models. *J. Am. Chem. Soc.* **2008**, *130*, 10187–10198. [[CrossRef](#)] [[PubMed](#)]
9. Hammond, G.S. A Correlation of Reaction Rates. *J. Am. Chem. Soc.* **1955**, *77*, 334–338. [[CrossRef](#)]
10. Hohenberg, P.; Kohn, W. In homogeneous electron gas. *Phys. Rev.* **1964**, *136*, B864–B871. [[CrossRef](#)]
11. Domingo, L.R.; Ríos-Gutiérrez, M.; Duque-Noreña, M.; Chamorro, E.; Pérez, P. Understanding the carbenoid-type reactivity of nitrile ylides in [3+2] cycloaddition reactions towards electron-deficient ethylenes. A molecular electron density theory study. *Theor. Chem. Acc.* **2016**, *135*, 160. [[CrossRef](#)]
12. Domingo, L.R. The Molecular Electron Density Theory: A Modern View of Molecular Reactivity in Organic Chemistry. *Molecules* **2016**, *21*, 1319. [[CrossRef](#)] [[PubMed](#)]
13. Fukui, K. *Molecular Orbitals in Chemistry, Physics, and Biology*; Academic Press: New York, NY, USA, 1964.
14. Domingo, L.R.; Chamorro, E.; Pérez, P. Understanding the High Reactivity of the Azomethine Ylides in [3+2] Cycloaddition Reactions. *Lett. Org. Chem.* **2010**, *7*, 432–439. [[CrossRef](#)]
15. Domingo, L.R.; Ríos-Gutiérrez, M.; Pérez, P. An MEDT study of the carbenoid-type [3+2] cycloaddition reactions of nitrile ylides with electron-deficient chiral oxazolid. *Org. Biomol. Chem.* **2016**, *14*, 10427–10436. [[CrossRef](#)] [[PubMed](#)]
16. Domingo, L.R.; Emamian, S.R. Understanding the mechanisms of [3+2] cycloaddition reactions. The pseudoradical versus the zwitterionic mechanism. *Tetrahedron* **2014**, *70*, 1267–1273. [[CrossRef](#)]
17. Domingo, L.R.; Ríos-Gutiérrez, M.; Pérez, P. A new model for C-C bond formation processes derived from the Molecular Electron-Density Theory in the study of the mechanism of [3+2] cycloaddition reactions of carbenoid nitrile ylides with electron-deficient ethylenes. *Tetrahedron* **2016**, *72*, 1524–1532. [[CrossRef](#)]
18. Domingo, L.R.; Saez, J.A. Understanding the Electronic Reorganization along the Nonpolar [3+2] Cycloaddition Reactions of Carbonyl Ylides. *J. Org. Chem.* **2011**, *76*, 373–379. [[CrossRef](#)] [[PubMed](#)]
19. Domingo, L.R.; Aurell, M.J.; Pérez, P. A DFT analysis of the participation of TACs in *zw-type* [3+2] Cycloaddition Reactions. *Tetrahedron* **2014**, *70*, 4519–4525. [[CrossRef](#)]
20. Ríos-Gutiérrez, M.; Pérez, P.; Domingo, L.R. A bonding evolution theory study of the mechanism of [3+2] cycloaddition reactions of nitrenes with electron-deficient ethylenes. *RSC Adv.* **2015**, *5*, 58464–58477. [[CrossRef](#)]

21. Krokidis, X.; Noury, S.; Silvi, B. Characterization of elementary chemical processes by catastrophe theory. *J. Phys. Chem. A* **1997**, *101*, 7277–7282. [[CrossRef](#)]
22. Houk, K.N.; Sims, J.; Duke, R.E.; Strozier, R.W.; George, J.K. Frontier molecular orbitals of 1,3 dipoles and dipolarophiles. *J. Am. Chem. Soc.* **1973**, *95*, 7287–7301. [[CrossRef](#)]
23. Geerlings, P.; De Proft, F.; Langenaeker, W. Conceptual density functional theory. *Chem. Rev.* **2003**, *103*, 1793–1873. [[CrossRef](#)] [[PubMed](#)]
24. Domingo, L.R.; Ríos-Gutiérrez, M.; Pérez, P. Applications of the Conceptual Density Functional Theory Indices to Organic Chemistry Reactivity. *Molecules* **2016**, *21*, 748. [[CrossRef](#)] [[PubMed](#)]
25. Domingo, L.R. A New C-C Bond Formation Model Based on the Quantum Chemical Topology of Electron Density. *RSC Adv.* **2014**, *4*, 32415–32428. [[CrossRef](#)]
26. Domingo, L.R.; Aurell, M.J.; Perez, P.; Contreras, R. Quantitative characterization of the global electrophilicity power of common diene/dienophile pairs in Diels-Alder reactions. *Tetrahedron* **2002**, *58*, 4417–4423. [[CrossRef](#)]
27. Jaramillo, P.; Domingo, L.R.; Chamorro, E.; Perez, P. A further exploration of a nucleophilicity index based on the gas-phase ionization potentials. *J. Mol. Struct.* **2008**, *865*, 68–72. [[CrossRef](#)]
28. Domingo, L.R.; Pérez, P.; Sáez, J.A. Understanding the local reactivity in polar organic reactions through electrophilic and nucleophilic Parr functions. *RSC Adv.* **2013**, *3*, 1486–1494. [[CrossRef](#)]
29. Domingo, L.R.; Ríos-Gutiérrez, M.; Sáez, J.A. Unravelling the Mechanism of the Ketene-Imine Staudinger Reaction. An ELF Quantum Topological Analysis. *RSC Adv.* **2015**, *5*, 37119–37129. [[CrossRef](#)]
30. Polo, V.; Andrés, J.; Berskit, S.; Domingo, L.R.; Silvi, B. Understanding reaction mechanisms in organic chemistry from catastrophe theory applied to the electron localization function topology. *J. Phys. Chem. A* **2008**, *112*, 7128–7136. [[CrossRef](#)] [[PubMed](#)]
31. Pauling, L. The nature of the chemical bond. Application of results obtained from the quantum mechanics and from a theory of paramagnetic susceptibility to the structure of molecules. *J. Am. Chem. Soc.* **1931**, *53*, 1367–1400. [[CrossRef](#)]
32. Slater, J.C. Directed Valence in Polyatomic Molecules. *Phys. Rev.* **1931**, *37*, 481–489. [[CrossRef](#)]
33. Domingo, L.R.; Saéz, J.A.; Zaragoza, R.J.; Arnó, M. Understanding the Participation of Quadricyclane as Nucleophile in Polar $[2\sigma + 2\sigma + 2\sigma]$ Cycloadditions toward Electrophilic σ Molecules. *J. Org. Chem.* **2008**, *73*, 8791–8799. [[CrossRef](#)] [[PubMed](#)]
34. Domingo, L.R.; Ríos-Gutiérrez, M.; Pérez, P. How does the global electron density transfer diminish activation energies in polar cycloaddition reactions? A Molecular Electron Density Theory study. *Tetrahedron* **2017**, *73*, 1718–1724. [[CrossRef](#)]
35. Goldstein, E.; Beno, B.; Houk, K.N. Density functional theory prediction of the relative energies and isotope effects for the concerted and stepwise mechanisms of the Diels-Alder reaction of butadiene and ethylene. *J. Am. Chem. Soc.* **1996**, *118*, 6036–6043. [[CrossRef](#)]
36. Domingo, L.R.; Ríos-Gutiérrez, M.; Emamian, S. Understanding the domino reactions between 1-diazopropan-2-one and 1,1-dinitroethylene. A molecular electron density theory study of the $[3+2]$ cycloaddition reactions of diazoalkanes with electron-deficient ethylenes. *RSC Adv.* **2017**, *7*, 15586–15595.
37. Woodward, R.B.; Hoffmann, R. The conservation of orbital symmetry. *Angew. Chem. Int. Ed. Engl.* **1969**, *8*, 781–853. [[CrossRef](#)]
38. Zhao, Y.; Truhlar, G.D. Hybrid Meta Density Functional Theory Methods for Thermochemistry, Thermochemical Kinetics, and Noncovalent Interactions: The MPW1B95 and MPWB1K Models and Comparative Assessments for Hydrogen Bonding and van der Waals Interactions. *J. Phys. Chem. A* **2004**, *108*, 6908–6918. [[CrossRef](#)]
39. Hehre, W.J.; Radom, L.; Schleyer, P.V.R.; Pople, J.A. *Ab initio Molecular Orbital Theory*; Wiley: New York, NY, USA, 1986.
40. Schlegel, H.B. Optimization of equilibrium geometries and transition structures. *J. Comput. Chem.* **1982**, *3*, 214–218. [[CrossRef](#)]
41. Schlegel, H.B. *Modern Electronic Structure Theory*; Yarkony, D.R., Ed.; World Scientific Publishing: Singapore, 1994.
42. Fukui, K. Formulation of the reaction coordinate. *J. Phys. Chem.* **1970**, *74*, 4161–4163. [[CrossRef](#)]
43. González, C.; Schlegel, H.B. Reaction path following in mass-weighted internal coordinates. *J. Phys. Chem.* **1990**, *94*, 5523–5527. [[CrossRef](#)]

44. González, C.; Schlegel, H.B. Improved algorithms for reaction path following: Higher-order implicit algorithms. *J. Chem. Phys.* **1991**, *95*, 5853–5860. [[CrossRef](#)]
45. Reed, A.E.; Weinstock, R.B.; Weinhold, F. Natural-population analysis. *J. Chem. Phys.* **1985**, *83*, 735–7465. [[CrossRef](#)]
46. Reed, A.E.; Curtiss, L.A.; Weinhold, F. Intermolecular interactions from a natural bond orbital, donor-acceptor viewpoint. *Chem. Rev.* **1988**, *88*, 899–926. [[CrossRef](#)]
47. Frisch, M.J.; Trucks, G.W.; Schlegel, H.B.; Scuseria, G.E.; Robb, M.A.; Cheeseman, J.R.; Scalmani, G.; Barone, V.; Mennucci, B.; Petersson, G.A.; et al. *Gaussian 09, Revision D.01*; Gaussian, Inc.: Wallingford, CT, USA, 2013.
48. Parr, R.G.; von Szentpaly, L.; Liu, S. Electrophilicity index. *J. Am. Chem. Soc.* **1999**, *121*, 1922–1924. [[CrossRef](#)]
49. Parr, R.G.; Pearson, R.G. Absolute hardness—Companion parameter to absolute electronegativity. *J. Am. Chem. Soc.* **1983**, *105*, 7512–75162. [[CrossRef](#)]
50. Parr, R.G.; Yang, W. *Density Functional Theory of Atoms and Molecules*; Oxford University Press: New York, NY, USA, 1989.
51. Domingo, L.R.; Chamorro, E.; Pérez, P. Understanding the Reactivity of Captodative Ethylenes in Polar Cycloaddition Reactions. A Theoretical Study. *J. Org. Chem.* **2008**, *73*, 4615–4624. [[CrossRef](#)] [[PubMed](#)]
52. Domingo, L.R.; Pérez, P. The nucleophilicity N index in organic chemistry. *Org. Biomol. Chem.* **2011**, *9*, 7168–7175. [[CrossRef](#)] [[PubMed](#)]
53. Kohn, W.; Sham, L.J. Self-consistent equations including exchange and correlation effects. *Phys. Rev.* **1965**, *140*, 1133–1138. [[CrossRef](#)]
54. Becke, A.D.; Edgecombe, K.E. A simple measure of electron localization in atomic and molecular systems. *J. Chem. Phys.* **1990**, *92*, 5397–5403. [[CrossRef](#)]
55. Noury, S.; Krokidis, X.; Fuster, F.; Silvi, B. Computational tools for the electron localization function topological analysis. *Comput. Chem.* **1999**, *23*, 597–604. [[CrossRef](#)]

Sample Availability: Not Available



© 2017 by the authors. Licensee MDPI, Basel, Switzerland. This article is an open access article distributed under the terms and conditions of the Creative Commons Attribution (CC BY) license (<http://creativecommons.org/licenses/by/4.0/>).

